Removal of Arsenic from Water using Hybrid SLM-Electrocoagulation Technique

A
Thesis Submitted
in Partial Fulfillment of the Requirements
for the Degree of
DOCTOR OF PHILOSOPHY
By

SOUMI SARKAR
(Roll No. 156107008)

Under the Supervision of
Prof. PRABIRKUMAR SAHA

Department of Chemical Engineering
Indian Institute of Technology Guwahati
October 2024

Declaration

This is to certify that the thesis entitled "**Removal of Arsenic from Water using Hybrid SLM-Electrocoagulation Technique**", submitted by me to the *Indian Institute of Technology Guwahati*, for the award of the degree of Doctor of Philosophy, is a bonafide work carried out by me under the supervision of Prof. Prabirkumar Saha. The content of this thesis, in full or in parts, have not been submitted to any other University or Institute for the award of any degree or diploma. I also wish to state that to the best of my knowledge and understanding nothing in this report amounts to plagiarism.

Signed: Soumi Sarkar

Soumi Sarkar
Department of Chemical Engineering,
Indian Institute of Technology Guwahati,
Guwahati-781039, Assam, India.

Date: October 2024

I dedicate this thesis to the unwavering support and boundless love of my family. To my parents, whose sacrifices, support, and encouragement have been the driving force behind my academic pursuits. To my husband, for his constant support, encouragement, understanding, and shared laughter that made the challenging moments bearable. Their belief in my potential has been my greatest inspiration. Their presence has been a pillar of strength throughout this journey.

Soumi Sarkar.

Soumi Sarkar

Certificate

This is to certify that the thesis entitled "**Removal of Arsenic from Water using Hybrid SLM-Electrocoagulation Technique**", submitted by Soumi Sarkar (Roll no. 156107008), a research scholar in the *Department of Chemical Engineering, Indian Institute of Technology Guwahati*, for the award of the degree of Doctor of Philosophy, is a record of an original research work carried out by her under my supervision and guidance. The thesis has fulfilled all requirements as per the regulations of the institute and in my opinion has reached the standard needed for submission. The results embodied in this thesis have not been submitted to any other University or Institute for the award of any degree or diploma.

Signed: Saha

Prof. Prabirkumar Saha
Department of Chemical Engineering,
Indian Institute of Technology Guwahati,
Guwahati-781039, Assam, India.

Date: October 2024

Acknowledgements

The realization of my dream to conduct research at IIT Guwahati became possible when Prof. Prabirkumar Saha, my thesis supervisor, provided me with the opportunity to work under his guidance at the Department of Chemical Engineering. I am grateful to him for his invaluable guidance, unwavering support, and insightful feedback throughout the entire research process. His expertise and encouragement have been instrumental in shaping the direction of this thesis. I am also thankful to him, for his thoughtful comments and suggestions that greatly contributed to the refinement of this work.

I take this opportunity to extend my sincere gratitude to my Doctoral Committee members, Prof. Pranab K. Ghosh, Department of Civil Engineering, Prof. Mihir K. Purkait, and Prof. Chandan Das, Department of Chemical Engineering, for their valuable inputs, insightful suggestions and comments which helped me a lot to improve the quality of my research.

As is widely acknowledged, an academic journey remains incomplete without essential theoretical knowledge, which was generously provided to me by my course instructors, Prof. Mohammad Jawed, Department of Civil Engineering, Prof. Pranab Goswami, Department of Biosciences & Bioengineering, Prof. Mahuya De, Prof. Dipankar Bandyopadhyay, and Prof. Kaustubha Mohanty, Department of Chemical Engineering. I am grateful to them for their dedicated guidance, insightful teaching, and support throughout my academic journey.

I am grateful to the Head of the Department of Chemical Engineering, IIT Guwahati for the constant support I had received for the entire period. I express my gratitude to the faculty members of our department for providing the essential resources and a conducive environment for conducting this research. Additionally, I am thankful to the Central Instruments Facility, Centre for the Environment, and North East Centre for Biological Sciences and Healthcare Engineering at our institute for granting me access to their instruments for various experimental purposes. In this context, I wish to express my appreciation for the valuable assistance rendered by individuals from various departments: Dr. Dolly Gogoi, Dr. Kula K. Senapati, and Mr. Sujit Deb from the Central Instruments Facility; Dr. Deepmoni Deka and Dr. Partha Protim Bakal from the Centre for the Environment; and Dr. Moumita Das, Mr. Jitumoni Sarma, and

Mr. Purna Chetry from the North East Centre for Biological Sciences and Healthcare Engineering. They have played a crucial role in handling instruments related to the analysis and characterization of the samples for my research work.

Helen Keller's quote, "Alone we can do so little; together we can do so much," holds profound meaning in light of the indispensable support and assistance I have received from the dedicated staff members of our department. I extend my sincere appreciation to Dr. Lukumoni Borah, Mr. Harsaraj Biswanath, Ms. Ritumoni Kalita, Mr. Pankaj Kumar, Mr. Prasun K. Bhattacharjee, Mr. Balen C. Mahanta, Mr. Dipak K. Barman, Mr. Debajit Borah, Mr. Saiful Alam, and Dr. Kaustavmoni Deka for their invaluable analytical support in connection with my experimental work. Additionally, I appreciate their encouragement and assistance in fulfilling my responsibilities as a Research Assistant. My heartfelt thanks to Mr. Jayanta K. Mout and Mr. Ariful Hoque for their technical support throughout this journey. I express gratitude to Ms. Chinmayee Pathak, Mr. Deep J. Sinha, Mr. Sailen Das, Mr. Pankaj S. Baruah, and Mr. Bhagya Boro for their indispensable help with official paperwork and documentation.

I consider myself fortunate to be surrounded by a wonderful group of diligent and supportive seniors. Special thanks are due to all my co-workers at the Separation Science Lab for their camaraderie and collaborative spirit. I want to express my gratitude to Dr. Supriyo K. Mondal for his genuine cooperation, assistance, valuable suggestions, and guidance during our collaboration in the same research lab. Additionally, I extend my thanks to Dr. Mriganka S. Manna, Dr. Kamal K. Bhatluri, Dr. Atanu K. Pal, Dr. Abhik Bhattacharya, Dr. Papu K. Naik, Dr. Rupak Kishor, Dr. Shounak Chakraborty, Dr. Nilanjan Mandal, Dr. Murchana Changmai, Dr. Sanhita Das, and Dr. Sushma Chakraborty for their unwavering support, motivational talks, and assistance in various forms throughout this journey.

I would also like to acknowledge the support of Anwesan, Aviti, Thangsei, Niladri, Prabhakar, and Kapil during this journey. A special thanks goes to the interns Soumendu, Kaushik, Ananya, and Akash for their hard work, dedication, and assistance in experimental tasks. I extend my heartfelt appreciation to all the laboratory associates in the department, including both past and present Master's and Doctoral students, for their love and unconditional assistance throughout this journey.

In addition to research and experimental endeavours, I extend my gratitude to my violin guru, Dr. Devanand Pathak, my Sattriya dance teacher, Dr. Anwesa Mahanta, and my counselor, Mrs. Pallabita B. Chowdhury, for serving as my guides, supporters, teachers, and philosophers throughout this journey. I wish to convey my sincere appreciation to the members of our Hindustani Classical music group, our Sattriya dance team, and our Bird-Watchers' group for their unwavering support and encouragement.

My deepest gratitude goes to Hitesh Ramrakhiyani, Debasis Maharana, Remya Kommadath, Dr. Sayantan Chakraborty, and Dr. Rhythm Grover for their assistance, support, and care during times when I needed it the most. I extend my thanks to all my friends and well-wishers for their constant support, wisdom, and inspiration, which played a significant role, whether directly or indirectly, in the completion of my doctoral study.

I express my gratitude to the Ministry of Human Resource Development (MHRD), Department of Science and Technology (DST), and IIT Guwahati for their continuous fellowship support throughout my Ph.D. program. I appreciate the NPTEL-MOOCs for compensating me for fulfilling my responsibilities as a Teaching Assistant.

I would like to seize this moment to express my heartfelt thanks to the pillars of strength in my life: my grandmother, Ms. Purnima Das; my parents, Mrs. Shovona Sarkar & Mr. Asok K. Sarkar; and my parents-in-law, Mrs. Manideepa Banerjee and Mr. Jasho P. Banerjee. Their unwavering love, support, encouragement, patience, tolerance, and faith have been my guiding lights throughout this journey. A special note of appreciation goes to my sisters, Aradhana Banerjee and Sudeshna Das, for their consistent support, encouragement, and uplifting my spirit. I extend my gratitude to my loyal companions, Nemo, Shiro, and Bruno, for providing me with emotional support during this significant phase of my life.

I would like to convey my deepest appreciation to my beloved husband, Dr. Arunabha Banerjee, for his unwavering love, continual support, motivating presence, and remarkable patience and tolerance, which proved instrumental during my time at IIT Guwahati. Finally, I express my thanks to the Almighty for granting me the strength to successfully complete this endeavour.

Soumi Sarkar.

Soumi Sarkar

Abstract

In this research, a thorough study on liquid membrane based separation of arsenic has been conducted and a hybrid SLM-electrocoagulation technique has been developed for the removal of arsenic from water using environmentally and physiologically benign solvent, viz. sesame oil. The application of sesame oil for removal of arsenic is itself a novel approach as it is being reported for the first time in scientific community.

In this work, the liquid membrane is composed of a pseudo-binary mixture of sesame oil and Aliquat® 336 as they are procedurally identified as best solvent-extractant combo. A thorough study on the properties of the said pseudo-binary mixture has been conducted to understand their molecular interactions and transport properties by determining the surface tension (at 25°C), density and viscosity over a temperature range of 25°C – 60°C under atmospheric pressure. The experimental data have been fitted into various equations and empirical relations to understand the trend of the data. An observed negative trend in most cases indicates that the components of the mixtures form a strong bond which is difficult to dissociate. In addition, a new relation is established between density, surface tension, viscosity and intermolecular free length that is linear in nature. This pseudo-binary mixture fits well into this relation with R^2 value in the range of 0.9709 and the slope is negative, which is in corroboration with the findings obtained from the spectroscopic, thermodynamic and ultrasonic properties of the pseudo-binary mixture.

As arsenic mostly occurs in inorganic oxyanions of trivalent arsenite, $As^{(III)}$, and/or pentavalent arsenate, $As^{(V)}$; two-phase equilibrium study has been conducted for the extraction of $As^{(III)}$, $As^{(V)}$and combined $As^{(III)}$-$As^{(V)}$in ratios of (1:1), (1:2), and (2:1). From the distribution coefficient data, it is concluded that all the species of arsenic form complex with Aliquat® 336 in the stoichiometric ratio of 1:1. The extraction equilibrium constant reveals $As^{(V)}$to be most favourable for extraction into organic phase. The statistical and machine learned modelling approach are implemented in predicting the optimum process condition that would ensure highest yield in terms of optimum extraction%. The experimentally observed optimum extraction efficiency of the process is compared with the statistical model and machine learned model. Genetic Algorithm based optimization tool with Artificial Neural Network (ANN) is useful for this purpose.

Three-phase flat-sheet supported liquid membrane (FSSLM) based separation technique have been applied for simultaneous separation and recovery of individual arsenic species and combined arsenic species of $As^{(III)}$and $As^{(V)}$in three different ratios of (1:1), (1:2) and (2:1). The parameters studied in this work include concentration of receiving phase, extractant concentration, pH of receiving phase and stirring speed. The experimentally observed optimum extraction and recovery efficiency of the process are compared with the statistical and machine learned models. ANN and Genetic Algorithm are applied here as well. The mathematical modelling further provides insight into the transport mechanism of arsenic through the phases. Formation of different complexes between arsenic and Aliquat® 336 have been detected from this study. The extraction equilibrium constant and the permeability coefficients imply that the transport efficiency of $As^{(V)}$is better than that of $As^{(III)}$. The error percentage of statistical approach is in the range of 0.45 to 2.47 and ML based analysis is in the range of 0.21 to 11.9 for extraction and recovery of all the arsenic species.

In the hybrid SLM-electrocoagulation setup, a pair of iron and graphite electrodes have been augmented within FSSLM setup where the electrodes are placed in the receiving phase for electrocoagulation to occur that leads to the formation of iron-arsenic complex. This technique has been employed for the first time in arsenic contaminated drinking water. The removal mechanism of arsenic is two-fold with concentration gradient across the interphases followed by co-precipitation and adsorption by iron hydroxide/oxide formed in the electrocoagulation process. It is revealed that pH of the feed and receiving phases play significant roles in enhancing the removal efficiency of the combined arsenic species in an effort to reduce the arsenic concentration below 10 ppb in the treated water as per WHO guidelines on drinking water. The iron-arsenic complex characterized by SEM-EDX, TEM-EDX, FTIR and XRD indicated the formation of various phases of iron hydroxide/oxide such as goethite, hematite, lepidocrocite and magnetite. Further, the FTIR spectra stipulated the conversion of $As^{(III)}$to $As^{(V)}$due to oxidation reactions occurring during electrocoagulation process.

Nine adsorption isotherm models viz. Langmuir model, Freundlich model, Redlich-Peterson model, Sips isotherm, Temkin model, Dubinin-Radushkevich isotherm, Jovanovic model, Halsey isotherm and Harkins-Jura model and six adsorption kinetic models viz. pseudo first order, pseudo second order, Elovich model, fractional power function, intraparticle diffusion and liquid film diffusion model have been explored to

understand the adsorption phenomenon in depth. Dubinin-Radushkevich model and Freundlich isotherm model fits well with the adsorption data that suggests a heterogeneous and physical adsorption process occurring in all the combined ratios of arsenic ions. The Temkin model fits well with the adsorption data of combined $As^{(III)}$-$As^{(V)}$in the ratio of (1:2) predicting that the binding energies decrease linearly with the surface coverage due to indirect interactions between the adsorbate-adsorbent in the adsorption process and the positive variation in adsorption energy points to an exothermic physical adsorption process. However, the same isotherm model does not support either of the arsenic adsorption data of $As^{(III)}$& $As^{(V)}$indicating that the adsorption is characterized by a non-uniform distribution of binding energies. All the adsorption modelling has been validated through statistical error analysis. On the other hand, pseudo first order model is found to fit the kinetic data for all based on the statistical error analysis. The final iron-arsenic precipitate is a saleable value-added product and has found its application in construction material as well as an insecticide.

The hybrid SLM-electrocoagulation technique has been repeated on real groundwater samples collected from various locations of the Indian states of Assam (above 100 ppb) and West Bengal (below 100 ppb), viz. Jorhat, Mariani and Titabor in Assam; and from Bardhaman and Baruipur in West Bengal. The said nine adsorption isotherm models and six adsorption kinetics models were tested on them. Characterization of iron-arsenic complex has also been carried out. Results have been discussed.

All the experimentations in this research work have been conducted following response surface methodology (RSM) using face-centred central composite design.

Contents

List of Figures

List of Tables

Chapter 1

Introduction and Literature Review

THIS chapter navigates the complexities of arsenic contamination, spanning from its occurrence and conventional removal techniques to the innovative realm of liquid membrane-based separation and a proposed hybrid technique. The integration of experimental design, statistical analysis, and machine learning underscores the research's contemporary significance. Readers are invited to explore the chapter's relevance, objectives, and the promise it holds for addressing environmental challenges, encapsulating a compelling journey through arsenic removal methodologies and a forward-looking approach to sustainable solutions.

1.1 Occurrence of arsenic and its impacts

The occurrence of arsenic in various environments, both natural and human-influenced, can have significant impacts on human health and the ecosystem. Here are some key points regarding the occurrence of arsenic:

Geogenic sources: Arsenic occurs naturally in the Earth's crust and is often associated with rocks and sediments. It can be released into the environment through natural processes such as weathering of rocks [1, 2].

Anthropogenic sources: Human activities contribute significantly to arsenic contamination. Industries like mining, smelting plants, and the burning of fossil fuels release arsenic into the air and water. Pesticide application, especially historical practices, has led to the presence of arsenic in soil and water. The use of arsenic in wood preservatives and other products has contributed to its dispersion in the environment [3].

Occurrence in Various Deposits: Alluvial lacustrine deposits, volcanic deposits, geothermal sources, mining wastes, and landfills may contain elevated levels of arsenic [4, 5].

Association with Minerals: Arsenic is a constituent of over 300 minerals and is commonly found in ores of metals such as copper, lead, zinc, gold, and uranium [6].

The occurrence of arsenic from both natural and human-induced sources poses significant challenges to environmental and human health. Arsenic has a history of use in various products including, medicines for treating ailments like ulcers, tuberculosis, and syphilis. It was also used in insecticides, fungicides, rodenticides, wood preservatives, desiccants, glass, alloys, semiconductors, pigments, and pharmaceuticals [7]. Efforts to mitigate arsenic contamination involve regulatory measures, remediation strategies, and a shift away from the use of arsenic-containing products. However, due to extensive research revealing its toxic impacts, recent investigations have prompted the discontinuation of manufacturing, production, or utilization of arsenic in any consumable form, marking a pivotal shift in mitigating its adverse effects on human health and the environment. Arsenic is highly toxic to humans and animals, even in trace amounts. Chronic exposure to arsenic is associated with various health issues, including skin lesions, cancers (skin, lung, bladder), cardiovascular diseases, and neurological effects. Due to its health hazards, regulatory bodies in many countries have established limits for arsenic levels in drinking water and food products. Furthermore, being a metalloid, arsenic is challenging to eliminate completely, leading to efforts to transform it into insoluble forms by combining it with metals such as iron as many impurities of lead, iron, and

selenium are found to have traces of arsenic [7]. This process helps reduce the mobility of arsenic in the environment.

The natural contamination of arsenic in water especially groundwater is reported worldwide with maximum reports from Asia and Europe along with Africa, and parts of North America, South America and Australia [8]. The African nations are severely affected by arsenic as both surface and groundwater are contaminated. The African nations affected by arsenic are Botswana, Burkina Faso, Ethiopia, Ghana, Morocco, Nigeria, South Africa, Tanzania, Togo, and, Zimbabwe [9]. In Australia, the source of arsenic is reported to be pyrite sediments containing hydroxides and iron oxyhydroxides and gold mines in parts of Victoria region and New South Wales [10–12]. European countries that reported high arsenic concentrations in groundwater are Greece, Hungary, Romania, Croatia, Serbia, Turkey, and Spain [13]. Recently a study by Zuzolo et al. [14] reported arsenic contamination of groundwater sources in the central parts of Italy. In parts of the USA, the main sources of arsenic contamination in groundwater are geothermal fluids and volcanic activities [15]. In Mexico, groundwater is the main source of drinking water, and high arsenic concentration is reported in groundwater in different parts of Mexico [16, 17]. A new study by Alarcon-Herrera et al. [16] suggested that 8.81 million people are now exposed to high arsenic groundwater. Similarly, regions of Guatemala El Salvador also have high arsenic content that is volcanogenic [18, 19]. High concentrations of arsenic in the groundwater of Bolivia are due to the volcanic formations in the Neogene period [20]. Similarly, the source of arsenic in the groundwaters of the Argentinian Chaco-Pampean plain [21] are the tertiary aeolian loess-type deposits in the Pampean plain and fluvial sediments of tertiary and quaternary age maybe the source [20].

The developed nations including USA and Canada have lower levels of arsenic contamination in groundwater compared to the Asian countries [22]. It has also been reported that the arsenic pollution-prone zones are mostly located in the sedimentary basins close to the modern mountain belts and deltaic areas [8]. Moreover, tropical climate regions experience more arsenic contamination due to the climate that aids the release of arsenic from arsenic compounds [23]. Asian countries mostly affected by groundwater arsenic contamination include Afghanistan, Armenia, Azerbaijan, Bangladesh, Cambodia, China, Georgia, India, Indonesia, Iran, Iraq, Japan, Jordan, Kazakhstan, Kyrgyzstan, Laos, Malaysia, Mongolia, Myanmar, Nepal, Pakistan, Philippines, Russia, Saudi

Arabia, Sri Lanka, Thailand, Turkey, Turkmenistan, Uzbekistan, Vietnam, Tajikistan, and Korea. The significantly arsenic-affected countries are India, Bangladesh, China, Pakistan, and Vietnam [8]. The source of arsenic in these countries is Holocene alluvial sediments consisting of floodplain and deltaic sediments containing organic matter with high alkalinity arsenic-rich sediments [8], whereas in Japan the source of arsenic is volcanic sediments, Holocene coastal sands, and quaternary alluvium aquifer [24–26].

In India, a population of over 50 million people is reported to be at risk from groundwater arsenic contamination. Currently, the river Ganga is reported to be one of the world's most polluted rivers, containing a number of toxins, and toxic heavy metals including arsenic, chromium, cadmium, lead, copper, and mercury, as well as pesticides and pathogenic microbes [27]. Around 20 states including West Bengal, Jharkhand, Bihar, Uttar Pradesh, Assam, Gujarat, Haryana, Madhya Pradesh, Punjab, Arunachal Pradesh, Karnataka, Tamil Nadu, Himachal Pradesh, Telangana, Andhra Pradesh, Odisha, Nagaland, Tripura, Manipur, and Chhattisgarh are now affected by arsenic contamination [8]. A few of the union territories such as Delhi, Daman and Diu, Puducherry, and Jammu and Kashmir are also reported to be affected by arsenic [8]. On the basis of the source of arsenic, contaminated groundwater can be classified into alluvial terrain and hard rock terrain. Alluvial aquifers are the primary source of arsenic consisting of 90% of the groundwaters in India occurring in the states of Assam, Bihar, Jharkhand, Manipur, Uttar Pradesh, and West Bengal. While hard rock aquifers consist of only 10% which includes the states of Karnataka and Chattisgarh. In Karnataka, arsenic is found to be associated with sulfide mineralization, especially arsenopyrite and mainly restricted to the gold mineralized areas covering parts of Raichur and Yadgir districts. In Chattisgarh, it has been reported from the acid volcanic associated with Kotri lineament [8].

Based on the chemical properties of water such as pH, redox potential, and presence of other contaminants, arsenic can be found to be present in the organic and/or inorganic form in water. In the environment, arsenic can occur in different oxidation states (-III, 0, +III, and +V). In natural water or surface water, arsenic mostly occurs in inorganic form as oxyanions of trivalent arsenite, $As^{(III)}$, or pentavalent arsenate, $As^{(V)}$. Biological activity in surface waters significantly polluted by industrial wastes often leads to the production of organic arsenic such as monomethylarsonous acid and dimethylarsinous acid, $As^{(III)}$, or monomethylarsonic acid, dimethylarsinic acid, and arsanilic acid,

$As^{(V)}$[21]. Trivalent arsenic has been reported to be more harmful and toxic than the pentavalent form due to its reactivity with sulphur-containing compounds and generation of reactive oxygen species [28]. Inorganic forms of arsenic are found to be potent toxins [7].

Diseases caused by arsenic poisoning have been reported worldwide with over 12% of the population in Chile exhibiting dermatological manifestations due to consumption of high arsenic-containing drinking water [29]. Exposure to arsenic via drinking water (groundwater) has been reported to cause "blackfoot disease" in Taiwan [30]. The first case of arsenic-induced skin lesions was reported at the Department of Dermatology, School of Tropical Medicine, West Bengal, India in 1983 [31], as this place was suffering from the problem of arsenic-contaminated groundwater for decades [32–34]. Other minor incidents of arsenic poisoning from groundwater have also been reported from Minnesota, USA [35], Millard County, Utah [36, 37], Ontario, Canada [38], Nova Scotia, Canada [39], New Zealand [40], and Nakajo, Japan [41]. It was observed and reported by Karim [42] that there was a high concentration of arsenic in the urine, hair, and nails of the affected people in different arsenic-contaminated water in Bangladesh.

The toxicological impact of arsenic can be broadly classified into acute and sub-acute types. Acute arsenic poisoning might occur due to ingestion of contaminated food or drink and requires prompt medical attention [43]. The early symptoms of acute arsenic poisoning are burning and dryness of the mouth and throat, dysphasia, abnormal pain, nausea, diarrhea, and hematuria. Muscular cramps, facial edema, cardiac abnormalities, and shock can develop rapidly as a result of dehydration [44]. The illness occurring from chronic arsenic exposure is known as "arsenicosis" and in 1996, it was first reported in Bangladesh [45]. The four stages of arsenicosis, or chronic arsenic poisoning that have been recognized are as follows: [46, 47]

Preclinical: The presence of arsenic in the body that can be detected in urine or body tissue samples with no symptoms.

Clinical: Various effects on the skin such as darkening of the skin (melanosis) often observed on the palms. Even dark spots on the chest, back, limbs, or gums have been reported to be observed in patients. Oedema (swelling of hands and feet) is often seen. A more serious symptom is keratosis, or hardening of skin into nodules, often on palms and soles as shown in Fig. 1.1. World Health Organization (WHO)

FIGURE 1.1: Images of patients' palms and soles suffering from severe arsenic poisoning [53, 54].

has estimated that 5–10 years of exposure to arsenic may lead the affected person to this stage.

Complications: Clinical symptoms become more prominent and internal organs are affected including enlargement of the liver, kidneys, and spleen have been reported. Some research indicates that the occurrence of conjunctivitis, bronchitis, and diabetes may be linked to arsenic exposure at this stage.

Malignancy: Formation of tumours or cancer affecting the skin or other organs, and may develop gangrene as well.

Arsenic poisoning has also been reported to affect children by causing infant mortality, impaired intellect, and motor dysfunction [48–52]. The toxicological effects of arsenic have led to an exponential rise in scientific research for its removal in the past few decades.

1.2 Conventional techniques for removal of arsenic

Over the years, arsenic removal techniques have been thoroughly explored, and the prime factors for removal depended on the pH, redox state, cost, and availability. Some of the commonly used techniques include co-precipitation, oxidation, sorption and ion exchange, electrochemical and membrane-based.

The co-precipitation technique involves the addition of coagulants such as ferric chloride and aluminium sulphate to form hydroxide complexes that flocculate as agglomerates and adsorb arsenic especially $As^{(V)}$. This leads to the formation of arsenic-based wet

sludge that needs to be disposed off. Moreover, it requires the oxidation of $As^{(III)}$to $As^{(V)}$as precipitated $As^{(V)}$has been reported to be more stable than $As^{(III)}$[55]. Further, lime softening of water with calcium carbonate, magnesium hydroxide, and or ferric hydroxide has been found to remove arsenate through adsorption [56]. Palfy et al. [57] investigated the treatment of arsenic with hydrogen peroxide, calcium oxide, ferric sulphate, and Portland cement as precipitation agents for removal and waste neutralization of arsenic. The addition of these chemicals increased the solubility of arsenic and from the leachate analysis, it was found that lime precipitation in combination with cement solidification provided a safe material. A combination of lime and ferric compounds used in the treatment of arsenic via precipitation are also reported by Shi [58], Tahija and Huang [59], Meng et al. [60] and Wang and Reardon [61]. Other precipitation agents including lanthanum salt [62], Fenton's reagent [63], and bacterial strains [64] are also available in the published literatures.

The oxidation method involves the usage of oxidizing agents such as ozone, chlorine, hydrogen peroxide, and permanganate to oxidize the impurities along with arsenic to form non-toxic compounds that are later removed through filtration. Ozone may readily convert $As^{(III)}$to $As^{(V)}$but it leads to the formation of additional disinfectant byproducts [65]. Further, assimilable organic carbon (AOC), often formed along with other disinfectant byproducts, may pass through membrane processes such as nanofiltration due to its low molecular weight and small size [66–68]. Chlorine is a good oxidant for $As^{(III)}$[69]. Hydrogen peroxide is another oxidant that is limited by reactions with calcium hydroxide [70–72]. Permanganate is another oxidant that has been reported to work better than chlorine. However, this technique requires the addition of oxidants, and after oxidation, these processes require the addition of salts such as ferric sulfate to stabilize the arsenate complex generated [7]. Another alternative oxidation technique for arsenic treatment explored by Garcia et al. [73] is a photochemical oxidation process to convert $As^{(III)}$into $As^{(V)}$along with precipitation or filtration of $As^{(V)}$adsorbed on $Fe^{(III)}$ oxides. This technique was further developed and tested by a Swiss Federal Institute of Aquatic Science and Technology in a partnership project with Bangladesh [74]. However, the underlying chemistry is found to be very complex, and the removal efficiency is reported to be affected by the changes in the chemical matrix, or by changes in the operative conditions.

Sorption and ion exchange technologies involve the use of activated alumina, iron-coated

compounds, and ion exchange resins by passing the water through an in-line column containing solid active media that removes arsenic by sorption. This solid media could be activated alumina, granular activated carbon, granular ferric hydroxide, iron oxide-coated sand, and iron filings or ion exchange resin. Though activated alumina is readily and commercially available, it is reported to be less efficient and tends to generate arsenic-rich wastes during backwashing for regeneration. Further, regeneration of activated alumina requires the use of strong chemicals adding to the cost and toxicity. Moreover, the presence of iron and manganese in water requires pretreatment. Iron-coated compounds such as iron-coated sand are inexpensive and capable of removing both $As^{(III)}$and $As^{(V)}$. However, it requires standardization and produces toxic by-products. Similarly, ion exchange resins can be used for arsenic removal as they have high adsorption capacity, independent of pH, and specific arsenic removal resin is also available. However, ion exchange resins are highly expensive and the presence of sulphate and total dissolved solids might interfere with the process [75]. Other major limitation of these processes is the generation of both liquid and solid residuals through regeneration streams, spent backwash, spent regenerant, spent rinse streams, and/or spent resins that are disposed off in sanitary sewers, evaporation ponds/lagoons, and hazardous waste landfill [7].

Other affordable approaches employing electrochemical methods include electrocoagulation. Kumar et al. [76] found that anodic oxidation and in-situ generation of adsorbents (such as hydrous ferric oxides and hydroxides of aluminium) during electrolysis lead to the removal of arsenic while working with iron, aluminium, and titanium anodes. A review by Hansen et al. [77] elaborated on the available technologies for electrocoagulation of arsenic from solution comparing continuous-flow reactors with turbulent flow and airlift reactors using sacrificial anodes. It has been observed that increasing the current density beyond a maximum value did not improve the process further due to the passivation of the anode. Further, few researchers have explored the electrochemical reduction of inorganic $As^{(III)}$and $As^{(V)}$in aqueous solutions to maximize the yield of elemental arsenic at the cost of the highly toxic arsine gas [78–81]. Twardowski [7] reported a method for $As^{(III)}$removal from mineral acids by electrochemical reduction to arsenic. This was deposited on a three-dimensional carbon cathode, using a divided cell and cathode potentials that prevented the further reduction of arsenic to arsine gas. Bejan and Bunce [80] found that $As^{(V)}$was inactive and could be removed via the electrochemical method by prior chemical reduction to $As^{(III)}$in the system using a carbon

cathode and IrO_2/Ti anode to study the electrochemical reduction of $As^{(III)}$and $As^{(V)}$in acidic and basic solutions.

Amongst the membrane-based methods, nanofiltration is one of the methods that can be used to meet regulations for lowered arsenic concentrations in drinking water with low pressure [82]. Waypa et al. [83] studied the removal of both $As^{(V)}$and $As^{(III)}$from synthetic freshwater and from surface water sources using nanofiltration and reverse osmosis over a range of operational conditions. Urase et al. [84] further studied the effect of pH on the rejection generated from these membrane processes. Vrijenhoek and Waypa [85] investigated the behavior of the membrane and found that the separation of arsenic species was due to a combination of size exclusion, preferential passage of more mobile ions, and charge exclusion. Saitúa et al. [86] studied the impacts of operating conditions in arsenic removal by nanofiltration and observed that the arsenic rejection was independent of transmembrane pressure, crossflow velocity, and temperature. The presence of other inorganic contaminants had an insignificant influence on arsenic rejection. Seidel et al. [87] used porous nanofiltration membranes to study the difference in rejection between $As^{(V)}$and $As^{(III)}$. The rejection of $As^{(III)}$was less than the rejection of $As^{(V)}$and the removal of $As^{(V)}$varied between 60% and 90%. Oh et al. [88] studied the feasibility of removing the arsenic by low-pressure nanofiltration that was applied in rural areas with an electricity supply shortage using a manually operated bicycle pump. Sato et al. [89] also explored the efficiency of nanofiltration for arsenic removal and found that 95% of $As^{(V)}$and 75% of $As^{(III)}$could be removed without any modifications to the source water chemical compositions and without any chemical additives.

Reverse osmosis membranes are another alternative for arsenic removal in water. Kang et al. [90] studied the effect of pH on arsenic removal using reverse osmosis and concluded that arsenic removal is almost proportional to the removal efficiency of NaCl. Further, the removal of $As^{(V)}$is much higher than $As^{(III)}$over the pH range of 3–10 and the pH of the solution plays a significant role in arsenic removal, especially for $As^{(III)}$. In a study conducted by Ning [91], the efficacy of arsenic removal through reverse osmosis was examined. The results indicated highly effective removal of $As^{(V)}$. Additionally, successful removal of $As^{(III)}$was observed at high pH levels with the application of anti-scalants. Brandhuber and Amy [92] extensively studied arsenic removal from drinking water using several membrane filtration methods via bench and pilot testing. They summarized that reverse osmosis or nanofiltration membranes are capable of sustaining high

rates of arsenic. Coagulation could be used as a pretreatment when membranes of relatively large pore size such as microfiltration or ultrafiltration are applied for substantial arsenic removal. Moreover, preoxidation of $As^{(III)}$to $As^{(V)}$followed by nanofiltration may increase the efficiency of arsenic removal. However, the limitations of using membranes for arsenic removal are the cost-effectiveness of the treatment. Removal of a single contaminant such as arsenic makes it an expensive affair. The application of membrane technology is justified when the removal of total dissolved solids is essential due to the presence of contaminants such as sulphates, nitrates, carbonates, and requires treatment. In addition, the discharge of the concentrate can be a problem and the water loss associated with the concentrate stream lead to membrane fouling and reduction in flux.

On the other hand, liquid membrane-based separation processes [93] offer a compelling alternative to their solid membrane counterparts, particularly in scenarios demanding selective separation of solutes present in trace quantities within a solution. Unlike traditional solid membranes, liquid membranes demonstrate enhanced flexibility and adaptability, enabling precise control over the separation process. Notably, the ability of liquid membranes to selectively transport solutes uphill, even in the presence of minimal concentrations, enhances their applicability for challenging separation tasks [94]. The findings underscore the potential of liquid membrane-based approaches as a promising avenue for advancing separation technologies, offering a versatile solution for scenarios where stringent selectivity and uphill transport are imperative.

1.3 Liquid membrane-based separation technique

A membrane is a physical, semipermeable barrier that allows single or selected multiple species to pass through between two phases. These barriers are usually inorganic solids or polymers, used for the purification of gas, water, and particle filtration. However, in a liquid membrane-based system, a liquid barrier is used that is usually an organic phase immiscible with water and separates the two aqueous phases. Two phase liquid-liquid extraction based study forms the stepping stone towards liquid membrane based separation technique, that is often used because of its simplicity, low cost and selective separation. Liquid-liquid extraction consists of two different immiscible liquids, usually polar and non-polar solvent, for separation of compounds or metal complexes based on the relative solubility. There is a transfer of the analytes from one liquid phase

to another, usually from aqueous to organic phase due to differences in their chemical potentials. Liquid-liquid extraction (*a.k.a* solvent extraction) is based on the ability of the target species to distribute itself in different ratios between the two immiscible liquid phases. This distribution ratio is the ratio of the concentration of the solute in the organic phase to the concentration of the solute in the aqueous phase.

The configuration of a typical liquid membrane-based system is a feed (or source) phase containing the target component (or solute), an organic liquid phase (*a.k.a* liquid membrane) containing an complexing agent (*a.k.a* extractant) that selectively and temporarily binds itself to the target element, and a stripping or sink phase (*a.k.a.* receiving phase). Often, the liquid membrane is an organic solvent dividing the two aqueous solutions or vice versa. Based on the nature of the application, the source and receiving phase may be aqueous with the organic phase in between like aqueous/organic/aqueous or it can be an organic/aqueous/organic combination.

During diffusion, the target component is bound to the extractant, forms a complex, and is transferred through the liquid membrane into the receiving phase where the solute is released due to decoupling off the complex. Thus, the target element can be extracted and recovered simultaneously in a single step. Since the process is based on concentration difference it does not require pressure or voltage for separation. Hence the liquid membrane-based separation technique is an arrangement of two liquid-liquid extraction units in series innovated for the separation of hydrocarbons [95], extraction of copper [96] and removal of phenolic compounds and organic acids [97]. Another advantage is that the diffusion coefficients of the solutes in liquids are larger in magnitude than in solids. Separation based on liquid membrane has found its application in the following:

- Separation of aromatic hydrocarbons [98],
- Removal of heavy metals [99–102],
- Extraction of plant metabolites [94], and
- Separation of trace compounds such as amino acids [103, 104].

Traditionally the chemical solvents such as kerosene [105] and toluene [106] are used as solvents which build the framework of liquid membranes. However they introduce potential risk of toxicity, rendering them unsuitable for various applications, particularly in contexts such as drinking water purification. In contrast, natural solvents like vegetable oils exhibit a safer profile, making them more suitable alternatives in situations where potential human exposure is a critical concern. Bhatluri et al. [107] studied the liquid membrane-based simultaneous separation of cadmium and lead from wastewater using coconut oil as solvent. Similarly, Chakrabarty et al. [108] worked on the separation of mercury using coconut oil as the environmentally benign solvent . Secondary metabolite of plant like catechin have been extracted from tea leaves by Manna et al. [109] using sunflower oil as liquid membrane. Further, transport of textile dyes [110] and phenolic wastewater treatment by extraction of phenols using sesame oil have also been reported elsewhere [111]. Extractants (*a.k.a* carriers) are added to bind themselves to the target component and increase the efficiency of the liquid membrane in transporting the target species from one phase to another. Several organic extractants have been reported to have the capability of removing arsenic from its solution. These include acidic extractant such as bis(2,4,4-trimethylpentyl) dithiophosphinic acid (Cyanex 301) [112], neutral extractants viz, trioctylphosphine oxide (Cyanex 923) [106] and tributyl phosphate (TBP) [113], and basic extractants such as trioctylamine (TOA) [114] and methyltrioctylamonium chloride (Aliquat 336) [115–118].

1.3.1 Physical properties of liquid membrane

The measurement and analysis of volumetric (density) transport (viscosity) and thermodynamic properties (excess Gibbs' energy, change in enthalpy and entropy) of liquid membrane or pseudo-binary mixtures of diluent and extractant helps in understanding the intermolecular forces acting within them. This in turn throws light upon the bulk behaviour of the mixtures.

Excess molar volume and viscosity deviation derived from density and viscosity data, respectively provide an understanding of solute-solvent interaction and find extensive application in solution theory and molecular dynamics. Prior arts of density and viscosity studies on pseudo-binary mixtures of a few extractants with conventional organic solvents such as benzene, chlorobenzene, heptane, hexane have been found elsewhere

[109, 111, 119–136]. Srirachat et.al. [119] studied the effects of polarity and temperature on the pseudo-binary mixtures of D2EHPA and organic solvents. Similarly, Koekemoer et.al. [120] determined the density and viscosity of pseudo-binary mixture of D2EHPA and aliphatic kerosene. Litaiem and Dhahbi [121, 122] studied the physicochemical properties of Aliquat 336 with formamide [121] and Aliquat 336 with dimethyl carbonate [122]. The densities and viscosities of pseudo-binary mixtures of TBP with cyclohexane and n-heptane was studied over a temperature range of 15-35 ℃ by Fang et.al.[123]. Similar research work on TBP was reported elsewhere [124–128]. Density, viscosity, and excess molar volume of pseudo-binary mixtures were extensively studied by Oswal and Patel [129] (TOA with cyclohexane), Yamamoto et.al.[130] (TOA with propionic acid) and Fang et.al. [131] (diluent TOA with n-heptane, n-octane, n-nonane, and n-decane) who conducted the experiments at various temperatures.

In order to reduce the level of toxicity, these organic chemical solvents were replaced by environmentally benign diluent such as vegetable oils in this study. Extensive research has been carried out by Keshav et. al. [132] and Manna et.al. [109] using sunflower oil as a diluent. Similarly, sesame oil mixed with TBP has been used by Kazemi et.al. [111] as liquid membrane in wastewater treatment. Moreover, several research works have been carried out on the properties of vegetable oils [133–136]. However, studies on the pseudo-binary mixtures of vegetable oil and these extractants are rarely found.

Further, the surface tension is also an important physicochemical property that reveals the information about the bulk behaviour of the mixtures and their surface structure that might affect heat and mass transfer at the interface. It is the attractive force that acts upon the surface layer by the molecules of a liquid to draw the surface molecules towards the bulk of the liquid which leads to minimum surface area. Li et al. [137] studied the variation of surface tension and deviation of excess surface tension of pseudo-binary mixtures of ionic liquids and TBP for the temperature range of 20-50°C under atmospheric pressure. Khattab et.al. [138] studied the variation in density, viscosity, surface tension and molar volume of mixture of water and propylene glycol within a temperature range of 20-50°C under atmospheric pressure.

The ultrasonic velocity, isentropic compressibility, intermolecular free length and acoustic impedance are calculated from the experimental data of density, viscosity and surface tension at 25℃. These derived parameters are correlated and thereby provide a better

understanding of the intermolecular interactions in the pseudo-binary mixtures [139]. The ultrasonic velocity is related to the surface tension and density of the mixtures (based on Auerbach's relation[140]) and inversely proportional to the intermolecular free length and isentropic compressibility. Isentropic compressibility is a density response function which actually is the change in volume caused by mechanical pressure occurring at constant entropy. It is a measure of intermolecular interactions and determines the orientation and structural arrangement of the liquid molecules. Molecules are loosely packed, in liquid state, with intermolecular spaces between them. As the name suggests, intermolecular free length is the distance between the surfaces of the neighbouring molecules. Thus, it indicates the interaction between the extractant and solvent based on the distance between them due to which the structural arrangement of the neighbouring molecules get transformed. Acoustic impedance is the obstruction exerted by the mixture to the acoustic flow through the particles caused by pressure (acoustic) applied to it. It helps in determining acoustic transmission, reflection and absorption of sound at the boundary of two different liquids in a mixture.

1.3.2 Transport mechanism in liquid membrane

The mass transfer in the liquid membrane-based separation technique is based upon the mechanism of solution-diffusion through the membrane. The transport mechanism of arsenic ions from feed phase to receiving phase via membrane phase is shown in Fig. 1.2. The different transport mechanisms based on the diffusional modes through a liquid membrane are passive transport, facilitated transport (vide Fig. 1.2b), and coupled transport (active transport). In passive transport, the solute simply diffuses from the feed to receiving phase along their concentration gradient, and the rate of transport is limited by the equilibrium condition between the feed and strip phase. It is preferred to use when only one species is soluble in the organic phase. In facilitated transport, the target solute undergoes a reaction with the extractant to form an extractant-solute complex that diffuses through the membrane. Although the resistance to diffusion is greater for the complex, the phase equilibrium shifts forward by several orders of magnitude that ultimately leads to an increase in overall mass flux. However, there are some criteria to be fulfilled by this type of system i.e., the extractant should only be miscible in the organic phase and not in the aqueous phases and also, the complex formation rate should not be too high, as backward extraction reaction

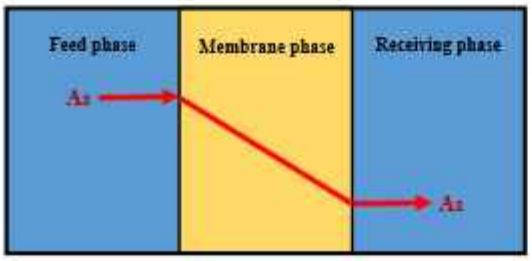

(A) Ordinary diffusive transport of component, As through LM

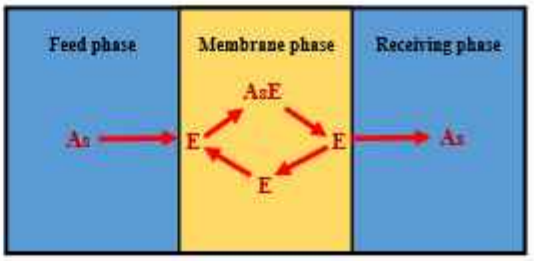

(B) Mechanism of carrier mediated (or facilitated) transport in LM with mobile carrier

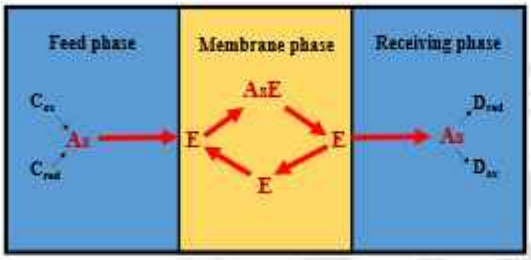

(C) Mechanism of carrier mediated transport in LM with mobile carrier-oxidation and reduction

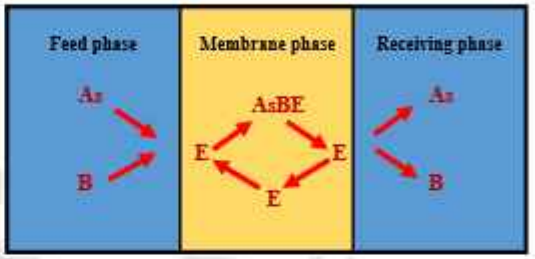

(D) Mechanism of coupled co-transport of arsenic in LM.

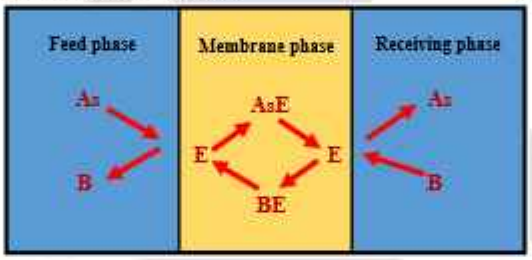

(E) Mechanism of coupled counter transport of arsenic in LM.

FIGURE 1.2: Schematic of transport mechanism - arsenic ions (As) coupled with extractants (E).

at the strip phase interface could become the rate-limiting step. In coupled transport, the extractant couples the transport of two species through the liquid membrane. When both the species undergo diffusion in the same direction from feed to receiving phase it is coupled co-transport (vide Fig. 1.2d), whereas when they diffuse in opposite directions, it is coupled counter-transport (vide Fig. 1.2e). The main advantage of this mode of transport is that one species can diffuse against its concentration gradient (uphill transport).

1.3.3 Types of liquid membrane

Based on the configuration, there are mainly three different types of liquid membrane-based separation processes, viz. bulk liquid membrane (BLM), supported (or immobilized) liquid membrane (SLM), and emulsion liquid membrane (ELM) [141]. BLM

comprises of feed and receiving aqueous phases divided by a barrier and a bulk organic liquid phase on top of both the aqueous phases or vice versa as shown in Fig. 1.3. BLMs have a very simple design for carrying out liquid membrane operations, but there are a few limitations such as small membrane surface, and bulk amount of liquid membrane required that limits its application at an industrial scale [142].

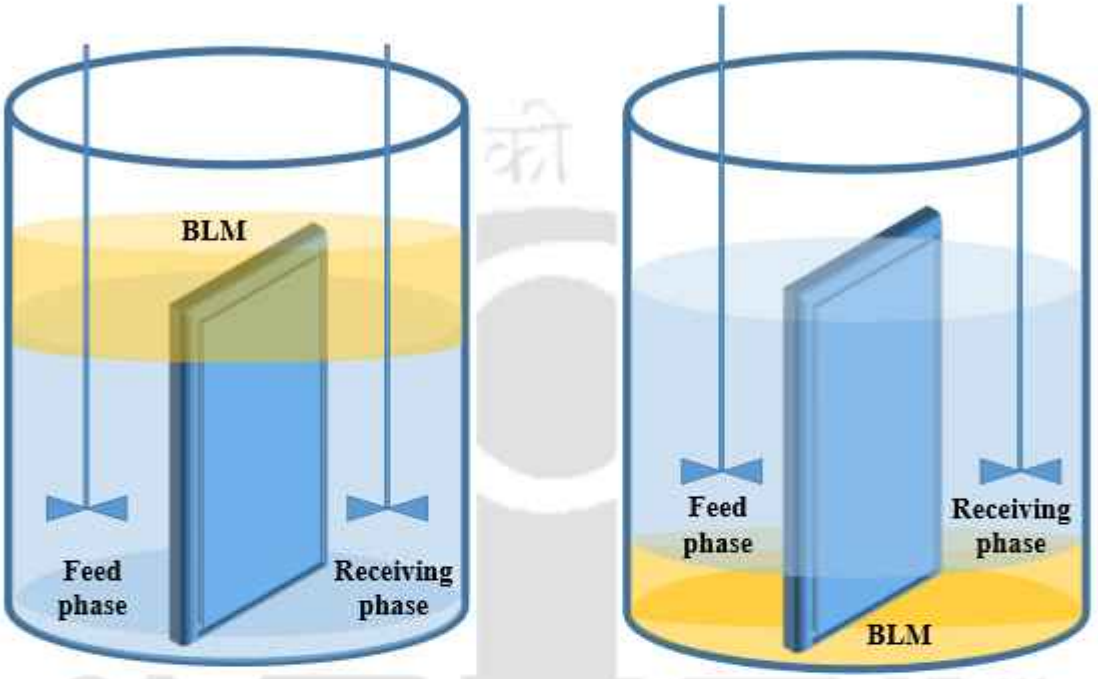

(A) Organic phase lighter than aqueous phase (B) Organic phase heavier than aqueous phase

FIGURE 1.3: Schematic of Bulk Liquid Membrane (BLM) setup

As the name suggests SLMs contain solid support that might be porous, polymeric, or ceramic in nature comprising the organic phase and dividing the feed phase and the receiving phase aqueous solutions. The pores of the solid membrane are completely filled with the organic phase by capillarity, making it a relatively stable and heterogeneous solid-liquid membrane. This solid support makes the configuration very stable and highly resistant to mechanical forces. The SLM system can be further classified into thin flat-sheet supports(FSSLM) as shown in Fig. 1.4a, hollow fibers (HFSLM) as shown in Fig. 1.4b, and spiral wound modules depending on the type of solid support used for the liquid membrane [143].

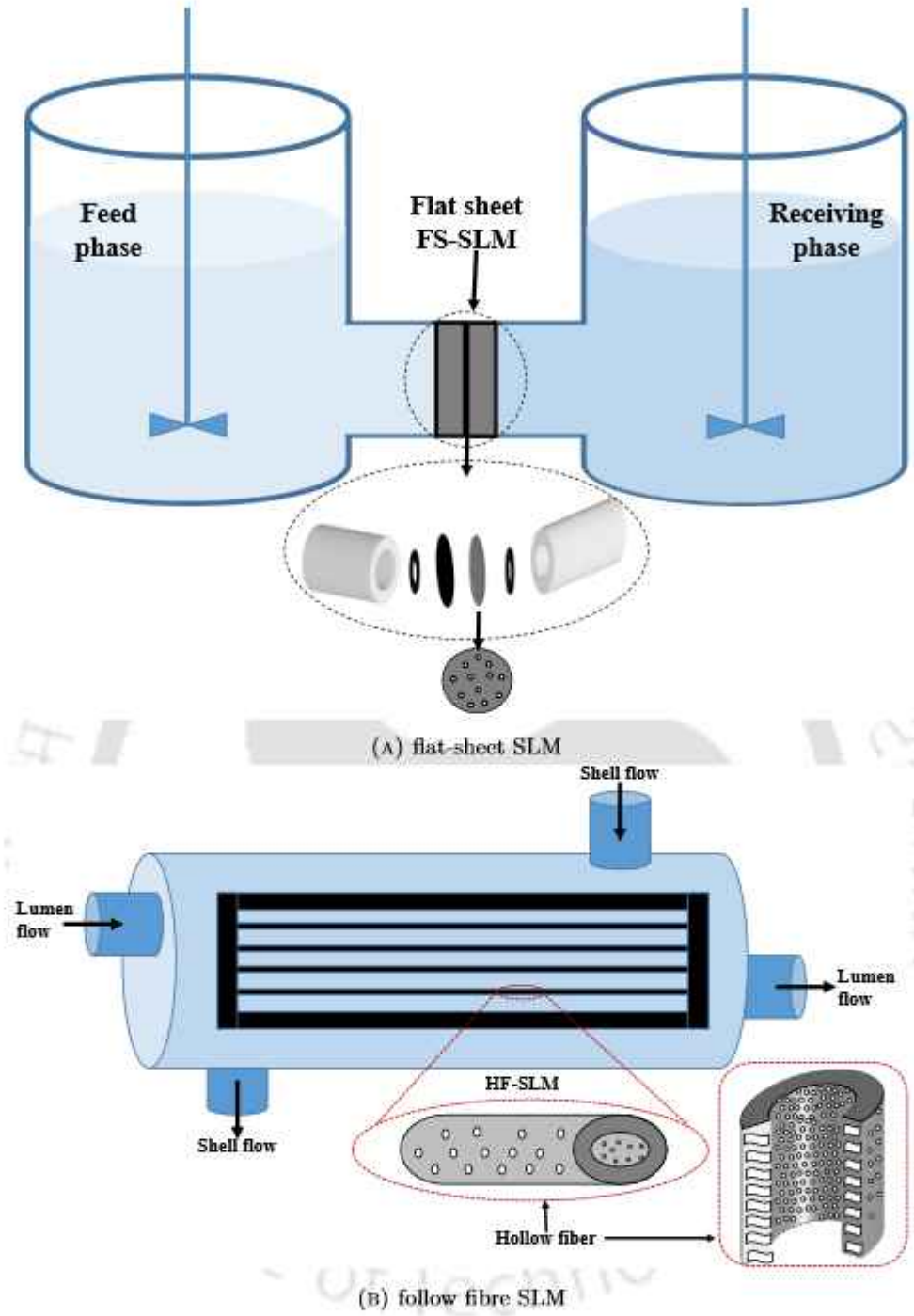

(A) flat-sheet SLM

(B) follow fibre SLM

FIGURE 1.4: Supported Liquid Membrane

The configuration of ELMs is the feed phase or the source containing an internal receiving aqueous phase coated by an outer layer of organic liquid membrane stabilized with surfactants as shown in Fig. 1.5. These are dispersed as very small droplets having a size of $1-10\mu$m. This water/oil emulsion highly increases the surface area and improves the transport rate of target species through the membrane [141].

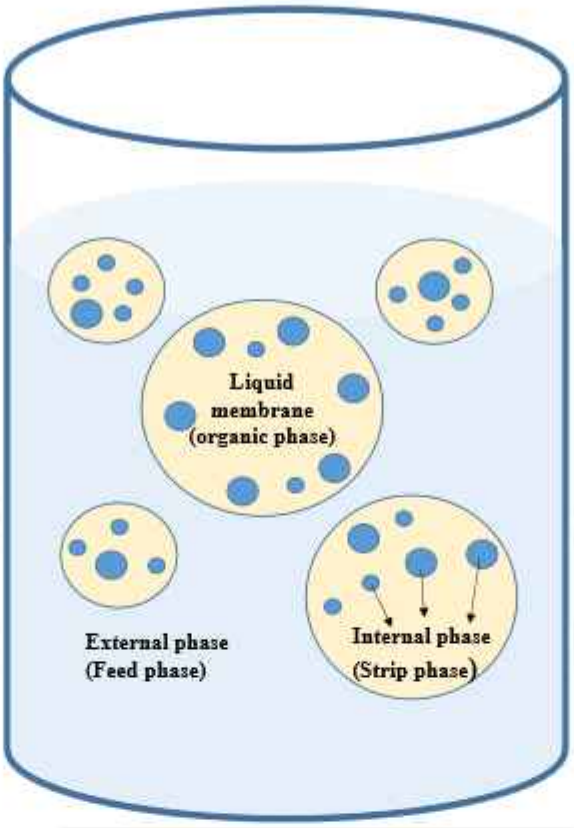

FIGURE 1.5: Schematic of Emulsion Liquid Membrane (ELM) setup.

1.3.4 Applications of liquid membrane

Any liquid membrane based separation technique is first initiated with a two-phase separation/extraction procedure.

Numerous published works exist that detail the separation of diverse metallic and non-metallic solutes, viz. arsenic [115], copper [144], cobalt, nickel, iron, cadmium, mercury [145, 146] and biomolecules [147]. Similar liquid-liquid extraction-based studies for the removal of arsenic have been carried out by multiple research groups to investigate the behavior of both organic and inorganic arsenic from various systems [148, 149]; to understand the removal of arsenic from sulphuric acid solution[150] and for determination and speciation analysis of inorganic arsenic[151]. SLM system for the removal of $As^{(V)}$and $As^{(III)}$was developed by Guell et al. [115], who used 0.1 M HCl solution as the receiving phase, Aliquat 336 as the extractant and a mixture of dodecane/dodecanol at pH 13 as the organic solvent. This SLM system was used to separate $As^{(V)}$from $As^{(III)}$and 44% recovery was obtained with real tap water due to the presence of other chemical compounds

that could negatively influence the $As^{(V)}$recovery. This led to a comparison between two membrane-based systems [152] using natural water and operating at neutral pH values. The performance of two anion-exchange membranes (AEMs) was compared to that of the SLM previously described [152]. Moreover, a study on the $As^{(III)}$ions transport under the optimal operational conditions for $As^{(V)}$at pH 7 was observed. The particular SLM system developed with Aliquat 336 as extractant and NaCl solution as receiving phase efficiently separated $As^{(III)}$and $As^{(V)}$. $As^{(V)}$removal from sulfuric acid solutions was studied using Cyanex 921(trioctylphosphine oxide) and sodium sulfate as the extractant and the receiving phase and flat commercial polyvinylidene fluoride (PVDF) membrane as support for the SLM system [105]. Through this SLM system, Perez et al. [105] established the steps of transportation occurring in SLM. Firstly, the metal ions propagated from the feed to the non-stirred boundary layer of the membrane. Then, the formation of the complex $As^{(V)}$-extractant took place at the feed solution–SLM interface. The $As^{(V)}$-Cyanex 921 complex diffused through the SLM, $As^{(V)}$was stripped at the SLM–stripping solution interface, and, finally, arsenic ions spread in the non-stirred boundary layer at the strip membrane interface. The experimental system showed good selectivity in arsenic removal, thus opening new prospects for wastewater purification from $As^{(V)}$ions. Another arsenic-separating SLM system was studied by Tsai et al. [153] to remove $As^{(III)}$and $Ga^{(III)}$ using ethylhexylphosphonic acid mono 2-ethylhexyl ester and a hydrophobic polytetrafluoroethylene (PTFE) membrane as the solid support. In the patent of Takigawa et al. [154] an SLM system was developed with a polybenzimidazole membrane using extractant mixture in its pores for the separation of hazardous metal ions such as arsenic, cadmium, antimony, palladium, etc. Thioxine was proposed as a complexing agent for some of the preselected toxic chemical ions, including arsenic.

HFSLM based studies have been done by Lothongkum et al. [116] for the removal of arsenic and mercury from natural-gas-co-produced water from the Gulf of Thailand. Toluene was used as the diluent and several extractant compounds were investigated that include Aliquat 336, Cyanex 923, and Cyanex 471 (tri-isobutylphosphine sulphide). The influence of sulphuric acid as a co-extractant on the concentration in the feed solution as well as that of the receiving solution (NaOH, distilled water, HNO_3, H_2SO_4, and thiourea) was also studied [116]. Pancharoen et al. [118] also worked on HFSLM based treatment of arsenic ions from produced water. Similarly, Prapaswat et al.[106] studied

the separation of $As^{(III)}$and $As^{(V)}$based on mass transfer theory. In another work, Sangtumrong et al.[114] separated $Hg^{(II)}$ and $As^{(III)}$ions from chloride media with HFSLM system by using tri-n-octylamine triocthyamine (TOA) dissolved in toluene as an extractant compound. NaOH was used in the stripping solution and HCl in the feed phase. Commercial microporous polypropylene fibers were used as support in the HFSLM system. The fabrication of a microfluidic membrane extraction system incorporating hollow fiber membranes for the continuous micro-scale extraction of arsenic was proposed by Hylton et al.[155]. Polymethyl methacrylate (PMMA) was used as the material for device assembly and commercial polypropylene was used as a solid membrane for the hollow fiber. The selective organic liquid (dibutyl butylphosphonate (DBBP)/tributyl phosphate (TBP) mixture) was fixed within the pores of the hydrophobic membrane to form the liquid membrane. In this way, a cost-effective real-time monitoring device could be developed for arsenic detection in water using HFSLM.

ELM studies have been conducted for the separation of $As^{(III)}$and $As^{(V)}$by Li et al. [156] using a system formed by monosuccimide L113A, liquid paraffin, and kerosene as surfactant, stabilizer, and solvent, respectively. The external phase was HCl solution, while the internal phase was KOH solution. This system promoted the permeation of $As^{(III)}$through the membrane into the internal phase by the $AsCl_3$ formation [157], where it was hydrolyzed to $AsO_3{}^{3-}$. Around 95% of $As^{(III)}$was recovered at optimum conditions. Similarly, Mousavi et al. [158] studied the extraction of $As^{(V)}$from water with a laboratory-scale ELM. The constituents of the experimentation included an aqueous solution of sodium sulphate used as internal phase, Span 80 (sorbitan mono-oleate) as emulsifier, 0.1M Cyanex 921 as carrier, paraffin as membrane solvent, and water containing 50 ppm $As^{(V)}$and 1.5 M sulphuric acid at different concentrations as the feed phase. 1.5 M reagent concentrations were used at a stirring speed of 500 rpm. This resulted in extraction of about 40% of arsenic [158]. Kiani et al. [159] presented research on the ultrasound-assisted preparation of stable water in an oil emulsion. The influence of different parameters, such as the surfactant type on droplet dimension, extraction amount, emulsifier content, and sonication time, was investigated for the removal of $As^{(V)}$oxide by oxidation of $As^{(III)}$oxide. Sulphuric acid was used as the feed phase, with sodium sulphate as the internal phase reagent, Cyanex 921 as carrier, Span 80 (sorbitan mono-oletae) as lipophilic emulsifier, Tween 20 (polyoxyethylene (20) sorbitan mono-laurate) as hydrophilic surfactant, and liquid paraffin as membrane solvent.

1.4 Proposed hybrid technique for arsenic removal

Multi-component separation by supported liquid membrane (SLM) process is an added advantage that led to extensive research work done by Chakrabarty et al. [160], Bhatluri et al. [107], and Mondal et al. [101] for simultaneous separation of mercury and lignosulfonate, cadmium and lead, nickel and zinc, respectively. Extraction of nickel through SLM was also carried out by Sulaiman et al. [161, 162]. Further, the electrocoagulation process is another efficient technique for the separation of heavy metals. This has been thoroughly researched for the removal of toxic metals/pollutants including arsenic from water [163] and iron electrodes have been reported to give maximum efficiency in the removal of $As^{(III)}$and $As^{(V)}$through oxidation and adsorption [76]. Based on the literature review, it has been found that the transport efficiency of $As^{(III)}$is low in comparison to $As^{(V)}$by the FSSLM technique. In a novel approach, as intended in this research, the FSSLM in combination with electrocoagulation provides selective uphill extraction and recovery of low concentrations of arsenic ions by creating an ever-unsaturated condition in the receiving phase. Removal efficiency is thus improved without the addition of any chemical coagulant or adsorbent which makes it a simple cost effective process. The additional advantage of the combinatorial usage of two techniques is selective electrocoagulation which would otherwise be impossible in electrocoagulation alone. Due to the structural limitations, FSSLM is preferred over HFSLM while integrating it with electrocoagulation. This research work incorporates the said combinatorial process for removal of arsenic by hybrid process, viz. liquid membrane-based separation technique coupled with electrocoagulation method. The optimization of the parameters affecting the removal efficiency of arsenic and different adsorption isotherm and kinetic models are intended to be studied to understand the removal mechanism of arsenic by this technique. To the best of the authors' knowledge, such a hybrid technique has not been reported for the removal of arsenic ions from water.

After the recovery of arsenic as an arsenic-iron precipitate, it is inevitable to conscientiously dispose of this complex which is also sustainable. One of the disposal techniques suggested by Mudgal was mixing with livestock waste such as cow dung [164]. This lead to the biological degradation of dissolved arsenic species into arsine gas, generating a more toxic product through this process. Another disposal technique includes drying the raw sludge followed by dumping it in small pits or sanitary landfills [165]. Both

these disposal techniques are unsustainable as it leads to further contamination through leaching or generation of even more toxic gases by biodegradation. A sustainable way of disposing of arsenic-based sludge is to stabilize and solidify it in a calcium silicate hydrate matrix forming cement [166] or in Portland cement [167]. The arsenic ions are adsorbed by calcium and silicon compounds leading to a homogeneous dispersion of As ions in the formed matrix [166]. It has been reviewed that for the past few years, industries have been favoring the formation of insoluble iron-arsenic complexes and allowing it to sediment at the bottom of residue ponds for arsenic disposal due to the complexes' long-term stability in acidic pH and oxidizing conditions [168]. A preliminary literature survey reveals that the arsenic-iron complex may be expected to precipitate once an iron electrode is employed. This complex has been reported to be a non-hazardous stable compound with long-term stability due to the ability of iron oxyhydroxides to trap arsenic [169] for years over acidic conditions and oxidizing environment [55]. It finds its application in construction materials [170]. This itself is a novel approach to gathering this value-added by-product.

1.5 Arsenic-Infested Groundwater: Locations for Sample Collection

It has been found that arsenic is naturally present in the groundwater of Indo-Ganga plains and West Bengal lies in the lower part of the Ganga basin where 9 out of 18 districts have been reported to have arsenic concentrations above 50 ppb [171]. In 1983, arsenic was first detected in Bardhaman. The blocks of Purbasthali, Kalna, and Katwa in this district were identified to contain arsenic-contaminated groundwater. On further investigation, it was found that high concentrations of arsenic were found in the villages of Mandra, Srirampur, Chandpur of Purbasthali-I, Phaleya village of Purbasthali-II, Dainhat municipality of Katwa-II and Atkatia mouza of Kalna-II. It was reported that people residing in Purbasthali blocks were most affected by arsenic [172]. This block contains 13 villages and all the villages were reported to be severely affected by arsenic. As Purbasthali is surrounded by the Bhagirathi, Ajay, and Damodar rivers, its underground water tables were reported to be contaminated with arsenic. This region was found to be extremely rich in alluvial soil content and the depth of the contaminated aquifers was in the range of 15-82 meters with thickness in the range of 40-60 meters

[173]. Hence this block is the focus of this study. The source of arsenic in this region is geogenic and it was further established that this natural contaminant gets distributed around the major flood plains as a result of the sedimentation processes [174]. The awareness created by researchers and scientists lead to active water testing in this region for which most of the arsenic-contaminated tube wells and hand pumps have been marked and most of them are not in use anymore. Though Mandra village was severely affected by arsenic [174], a groundwater sample was collected from Srirampur village as arsenic-contaminated water is still available here even at a depth of 50 meters. This particular source was not used for drinking purposes as the presence of arsenic in it was known by the local users.

Another worst arsenic-affected area to be reported in West Bengal is the Ramnagar block of Baruipur in South 24 Paraganas district [175]. The arsenic origin was related to the sediments deposited in the late Holocene that consisted of clay, peat, sand, and silt in this location. The clay and peat layer were reported to contain more arsenic than the sand and silt layer. Further, the constituents of the sand layer were concluded to be the cause of arsenic contamination of groundwater as its components included coated iron oxy-hydroxides with residual magnetite, ilmenite, illite, chlorite, biotite, and siderite, storing varied concentrations of arsenic in it [175]. The mobilization of arsenic from these minerals into the aquifers was attributed to the microbial activity in the sediments that changed the pH leading to redox reactions for which desorption of arsenic from these minerals and contamination of groundwater occurred [175].

Recently, Jorhat has been the focus of many researchers as it is an important academic and business center for North East India with the presence of the oil and tea industry. The rapid growth and development have transformed the region to contain a mix of rural, semi-urban, and urban localities where the majority of the population depends on groundwater for drinking and other domestic purposes [176]. A group of researchers investigated the groundwater system of the entire Jorhat district to understand the geochemical associations and measure the quantity of arsenic and fluoride in the system [177]. The pH varied from 6-10 within the area studied by Saikia et al. [177] and the groundwater was reported to have high iron content with arsenic in the range of 0.5-162 ppb [177]. Titabor and Majuli regions within the Jorhat district were said to contain maximum arsenic concentrations [177]. The pH in the western part of Jorhat district was reported to be in the range of 5.2-7.7 with high iron content and arsenic concentration

varying from 4.7-70 ppb [176]. Further, a group of scientists led by Ghosh[178] explored the presence of arsenic-resistant bacteria in contaminated sites of Northeast India that lie in the Ganga-Brahmaputra-Meghna delta. This research work highlighted the role of bacteria in arsenic mobilization through the scavenging of iron from siderophore. The bacteria present in the sediments depend on iron and acquire it from a siderophore. This leads to the release of arsenate as the iron gets dislodged from the mineral. The arsenate gets converted to arsenite either through anaerobic respiration or aerobic detoxification reactions by the resistant microbes. This leads to the dissemination of $As^{(III)}$into the groundwater [178]. This was later confirmed by Das et al. [179] to be the primary cause that exacerbated arsenic contamination in the Titabor region of the Jorhat district. The reported arsenic concentration range of 50-356 ppb found in the Titabor subdivision is in accordance with this study. The common and primary mechanism for arsenic mobilization is the reductive dissolution of iron oxides/hydroxides coupled with microbial degradation of organic matter in the sediments. Often, anionic competition for adsorption sites between phosphate and arsenate leads to the precipitation of minerals with phosphorus (in the form of phosphate) and the enrichment of arsenic by dissolution in groundwater [180]. Various research works and studies conducted so far exhibit the intertwined relationship of iron with arsenic which has been explored in the hybrid technique.

A part of this research work involves two case studies based on the application of the hybrid technique for arsenic removal from groundwater samples. These samples were collected from two states of India, namely, West Bengal and Assam, in order to determine the efficiency of this hybrid technique in arsenic removal from groundwater samples. A thorough study by Nickson et al. [181] emphasized the spread of arsenic in several districts of Assam including Barpeta, Bongaigaon, Cachar, Darrang, Dhemaji, Dhubri, Goalpara, Golaghat, Hailakandi, Jorhat, Kamrup, Karimganj, Lakhimpur, Marigaon, Nagaon, Nalbari, Sibsagar, and Sonitpur. The percentage of arsenic source $> 50\mu g\ L^{-1}$ was reported to be 28% in Cachar and 23% in Jorhat [181]. It was later established by Shah et al. [182] that the lowland valley areas covered with Holocene newer alluvium deposits were mostly affected by arsenic. Later, the arsenic contamination was further confirmed in Barpeta, Dhemaji, Darrang, Karimganj, and Sonitpur [183]. The source of arsenic established by researchers in these provinces were reductive dissolution [184]; reducing conditions due to heavy sediment load and presence of organic matter[185];

heavy deposition of sediments caused by surface erosion of surrounding hills and creating aquifers [186]; transportation by the nearby river [187]; and natural deposits in the earth along with industrial and agricultural pollution [188].

1.6 Application of experimental design

The COST approach often overlooks parameter interactions, reducing optimization chances. Experimental design involves randomly varying parameters, predicting interactions among variables for a cost-effective approach. This method facilitates variable modification, enabling cause-and-effect relationship identification, serving as a basis for developing new research objectives. The main concepts for developing an experimental design include:

Blocking: Process of restricting random trials by performing experiments with one setting of the factor and then all the experiments with the other setting.

Randomization: The order of the experiments to be performed to eliminate unknown effects or uncontrolled variables.

Replication: The repetition of the experiments to be able to reproduce precise results and overcome biases/errors.

Hence the Design of Experiment (DOE) is a tool for planning, conducting, and analyzing controlled tests to evaluate the effects of multiple input factors on parameters. It efficiently identifies interactions compared to the one factor at a time (OFAT) approach. DOE is performed through the following steps:

- Screening a design to narrow the field of variables under assessment by acquiring an understanding of the inputs and outputs being investigated through process flowchart.
- Developing a design to study the response of a combination of factors and factor levels to determine the appropriate measure for the output and identify a region of values where the process is close to optimization.

- Creating a design matrix for the factors being investigated to generate a model for the responses that would contain all the possible combinations of high and low levels for each input factor for the corresponding responses.
- Ensuring the stability and repeatability of the whole system.

DOE can be applied when more than one input factor is found to influence output(s). It can also be used to figure input(s)/output(s) relationships and develop a predictive equation for further analysis.

By employing the design of experiments:

- Identification of the key factors in a process is possible.
- Exploration of settings that would ensure acceptable performance for the process can be conducted.
- Investigation into the key, main, and interaction effects in the process is facilitated.
- Identification of settings that result in reduced variation in the output becomes achievable.

DOE can be classified into four main types:

- Factorial designs are the preliminary designs often used to identify the important factors for a process/experiment by screening for the important factors, and/or by characterizing how the known factors interact and affect the process. There are full factorial and fractional factorial designs with different resolutions including Plackett-Burman and Taguchi designs. These designs are often used as a starting point for more complex response surface modeling.
- Response surfaces are randomized designs classified into central composite design, Box-Behnken design, one-factor, and miscellaneous is a collection of designs including 3-level factorial, hybrid, pentagonal, and hexagonal designs.
- Mixture designs are when there are variations in the relative proportions of components in the experiment affecting the response of the system. This design is classified into lattice, centroid, screening, and optimal designs.

- Custom designs are created according to the requirements of the experiments especially when the standard designs cannot be accommodated to the experimental data. The different types of this design include optimal, user-defined, historical, and simple sample.

Full factorial designs encompass all main and interaction effects, while fractional factorial designs reduce sample size, compromising statistical analysis. Plackett-Burman designs lack variable interactions, Taguchi designs offer flexibility with simpler structures, and Box-Behnken designs predict with precision at the center of the factor space.

TABLE 1.1: List of few DOE applications related to arsenic removal and liquid membrane from the literature review

Authors (year)	DOE applied	Research work	Ref.
Bayuo et al.(2023)	RSM-CCD	As(III) removal using activated carbon from maize plant	[189]
Zialame et al. (2023)	RSM-CCD	As(III) removal using nanomagnetic compound	[190]
A.Theam & S. Bun (2023)	RSM-CCD	As(III) removal in airlift reactor with Fe^{+2}	[191]
Irshad et al. (2023)	RSM-CCD	As removal by *Bacillus* XZM Composite	[192]
Moghanjooghi et al. (2023)	RSM-CCD	Arsenic Removal by CTAB-modified Zeolite	[193]
Lie et al. (2023)	Box-Behnken	As(V) removal by Ti electrocoagulation	[194]
S.K.Mondal & P. Saha (2018)	RSM-CCD	Separation of Cr^{+6} using liquid membrane	[100]
Mondal et al.(2019)	RSM-CCD	SLM based separation and recovery of Ni & Zn	[101]
Traiwongsa et al.(2023)	RSM-CCD	Hg ions separation by non-toxic organic liquid membrane	[195]
Part of this work (2023)	RSM-CCD	Hybrid technique for removal of As(III) & As(V)	[196]

One-factor response surface designs focus on a single continuous factor. Miscellaneous response surface designs are discouraged due to limitations. Mixture designs analyze

component proportions, and screening/optimal designs are for formulation work. Custom designs suit higher-order models, spreading replication throughout. When standard designs yield excessive runs, custom designs are preferred for existing data analysis. Central Composite Design (CCD) of Response Surface Methodology, also known as the Box-Wilson design, is chosen for this study due to its advantages over other designs. Based on factorial designs with center and axial points, CCD fits quadratic models, offering 3-5 levels for each factor. Face-centered CCD, with 3 levels for each factor, employs a systematic approach to generate an empirical model, predicting the interaction effects of independent variables. The number of levels is a crucial criterion, and face-centered CCD is selected for its efficiency. This cost-effective, high-resolution, saturated design provides valuable insights into variable roles, optimizing experiments for comprehensive understanding and effective parameter estimation [197]. Table1.1 enlists the applications of DOE from the literature review.

1.7 Significance of statistical analysis and machine learning based approach

Statistical analysis helps to understand the trend and pattern of the data obtained from the experiments by adding meaning and justification to the research work. It is an essential tool for scientific research that is used for planning, designing, collecting data, analysing, interpreting, and reporting research findings with experimental biases and errors. It provides an objective approach to relate the independent variable(s) to the dependent variable(s) through cause-effect relationships. Statistics help one to make sense of and gather large amounts of information by identifying patterns and trends in data. This further aids in making predictions and informed decisions related to experiments. However, statistical analysis can be complex and difficult to understand, and even skewed to support a particular viewpoint or agenda. Moreover, it can provide an inference regarding a particular situation or phenomenon, and may not be representative of the larger picture, leading to an illusion of precision and accuracy, even when the data is uncertain or inconclusive.

The statistical approach can be broadly classified into three categories: descriptive, correlational, and inferential analyses. Descriptive statistical analysis mainly quantifies and

characterizes the unknown data at the very beginning of an analysis by measuring central tendency and variability. Measures of central tendency include the mean, median, and mode that highlight the performance level of a group of scores, and measures of variability including the range, variance, and standard deviation summarize the spread of scores among participants. Through measures of central tendency, information on the level of performance is obtained, while measures of variability disclose the consistency of that performance. Correlational analysis expresses the extent of the relationship between the input and output variables without establishing about cause and effect. Pearson or Spearman's coefficient is used to quantify the strength of the relationship with statistical significance. Correlational analysis mostly predicts a linear relationship between the process parameters and the response. In addition, it cannot be accurately applied to predict curvilinear relationships. So inferential statistical analysis is incorporated to make predictions and draw conclusions based on the descriptive summary and correlation between the data obtained from the analyses. This analysis can be classified into hypothesis testing through Z-test, t-test, F-test, Mann-Whitney test, and analysis of variance (ANOVA) test and regression analysis including linear regression, nominal regression, logistic, and ordinal regression. The standard flowchart for statistical analysis is illustrated in Fig. 1.6.

A few of the recent works related to arsenic removal incorporating statistical analysis are mentioned here. Statistical analysis has been performed by a group of researchers to explore the impact of different modified biochars on the rice and paddy soil containing arsenic, cadmium, and lead [198]. Normality and homogeneity of the data were first checked, followed by a one-way analysis of variance along with Tukey's multiple comparison test. Further, correlational analysis was carried out with redundancy analysis. In addition, principal component analysis was done to determine the statistical correlations between the parameters studied [198]. A group of scientists implemented statistical analysis to study the removal of arsenic from water by adsorption using iron-coated adsorbents. These adsorbents were produced by the hydrothermal carbonization of olive pomace. The optimization of the process parameters for better efficiency was performed through statistical analysis that included the Shapiro-Wilk test to check normality, Levene's test to check the homogeneity of variances, one-way and two-way analysis of variance followed by Tukey post hoc test [199]. Moreover, rice bran composition and its nutritional aspects were explored to remove arsenic content by percolating

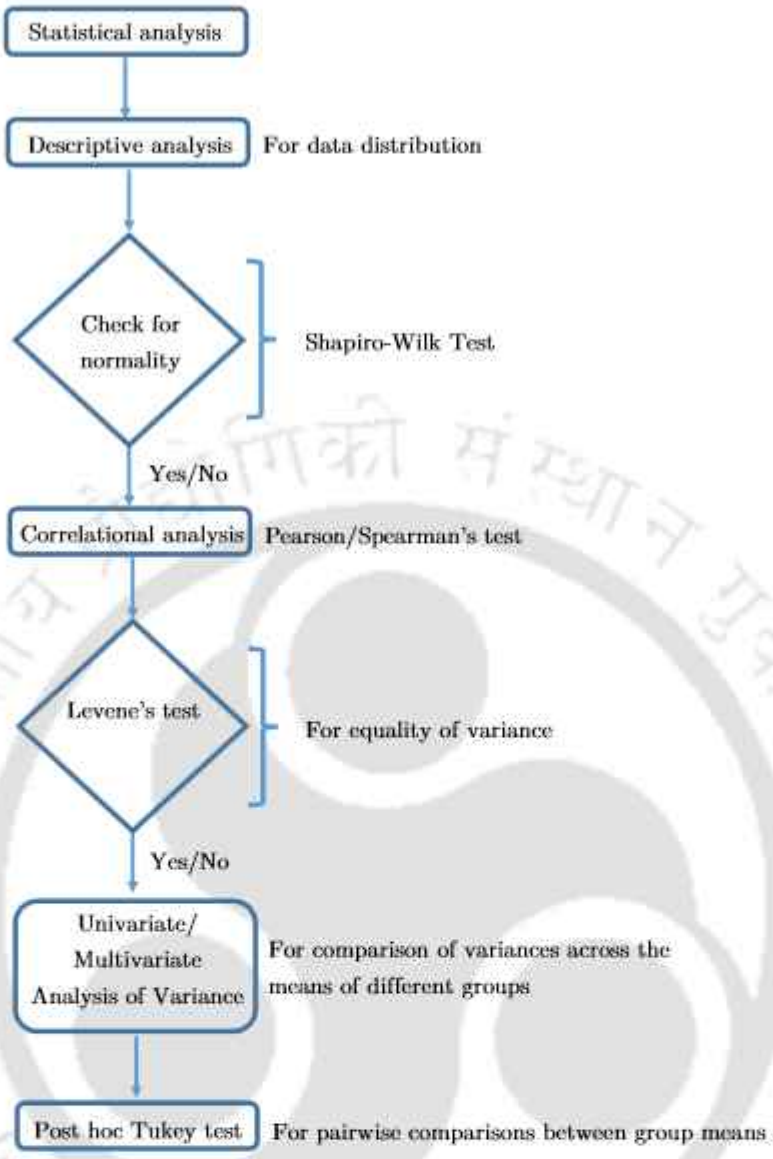

FIGURE 1.6: A flowchart for statistical analysis.

cooking water through statistical analysis [200]. The median and range of the data were determined with analysis of variance and Tukey's test of the studied variables. Through the mean and the standard deviation data, the limit of detection was also established [200]. Various kinds of research work have been carried out following the same protocol of standard statistical analysis. Another research work includes the evaluation of arsenic removal plants placed in parts of West Bengal [201]. Simple analysis of variance, paired t-test and independent t-test have been performed in this work to investigate the efficiency of the arsenic removal plants [201].

Machine learning (ML), on the other hand, is an approach for analysing data that automates the construction of analytical models. As a subset of artificial intelligence, it

asserts that models have the capability to self-learn from data with minimal human intervention. In case of data analysis, it is possible to employ machine learning techniques to the experimental results and obtain a black-box model that maps independent variables to the dependent variable(s). The significance of such a model is the fact that the machine-learned model is an ever-evolving model which can take a new set of experimental results at a future time and capture the alterations in the process behavior, if any. The machine learning approach employs a set of computational tools that can recognize the pattern of a process given a particular dataset.

Artificial Neural Network (ANN) is one such tool that can map a relationship between inputs and outputs of a process and then use it to anticipate the process behaviour[202]. ANN comprises of input, hidden, and output layers as shown in Fig. 1.7. These layers are interconnected to each other by functions $\phi(\cdot)$ that mimic neurons. Each neuron consists of an activation function [202] followed by a summing junction. The inputs u_i, assigned weight w_i, and bias b_i are combined into an argument that is fed into the activation function. There are various options for activation functions, and the best fitting function depends upon the type of dataset which needs to be detected through trials. These neurons act on the data and extract useful information from the dataset [202, 203]. A mean squared error (MSE) function yields the error between the experimental and

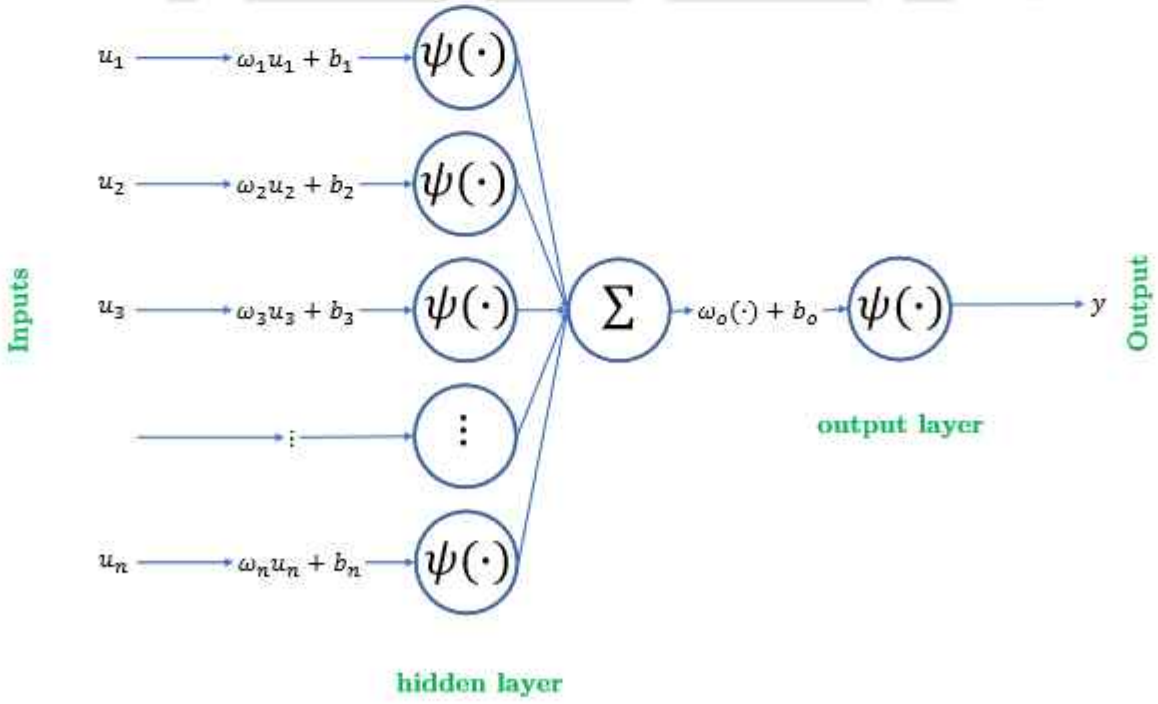

FIGURE 1.7: Various layers of ANN.

predicted values and helps to predict the accuracy of the model,

$$MSE = \frac{\sum_{i=1}^{m}\sum_{j=1}^{n}(y_{e^j{}_i} - y_{p^j{}_i})}{mn} \tag{1.1}$$

where m is the number of input datasets, n is the number of output nodes, y is the value of the output with subscripts e and p referring to experimental and predicted respectively. The number of nodes in the hidden layer is optimized to minimize the MSE.

Further, different techniques are available for nonlinear optimization, such as Nelder-Mead simplex Method, Trust-Region method, interior search Method, and genetic algorithm (GA) method[204]. Since ANN is not necessarily a differentiable function and it can predict the value of the objective function in a constrained region, the GA fulfills both requirements as it is a non-derivative constrained optimization technique.

A genetic algorithm (GA) is based on the natural selection theory of biological evaluation [203]. In GA, a problem is initiated with a given population group, which evaluates based on the fitness function towards the optimum solution. GA-based optimization involves several steps such as selection (selecting the number of individuals based on fitness function from population to breed the new population), crossover (generating the new data point by combining the information of two data points from selected data), and mutation (random change in the information of a new data point similar to the mutation in the biological world). As the simulation proceeds, the GA converges in the more suitable population (set of data points) and eventually leads to the optimum solution based on the fitness functions.

The convenience of reviewing large volumes of data and discovering specific trends and patterns is one of the advantages of wide applications of ML-based analysis. In addition, ML-based algorithms are good at managing multi-dimensional and multi-variety data in a dynamic environment. As ML algorithms gain experience, it improves their accuracy and efficiency. This leads to better predictions and optimization of the model with the increase in the volume of the data. However, the limitations of the ML-based approach include huge data acquisition as massive data sets are required to train and test models, which should be unbiased and of good quality. Another major challenge is the selection of necessary algorithms for the specific study and the ability to precisely interpret the results generated by the algorithms. Further, ML is highly susceptible to errors if small

data sets are used for training a model. As this would lead to biased predictions coming from a biased training set which might be difficult to detect.

A few of the recent arsenic removal research work implementing machine learning are stated here. $As^{(V)}$removal efficiency from wastewater using various metal-organic frameworks (MOFs) were predicted through Light Gradient Boosting Machine Learning, Extreme Gradient Boosting, Gradient Boosting Decision Tree, and Random Forest approaches [205]. A group of scientists developed an ANN model to predict the efficiency of arsenic removal by different adsorbents [206]. A few statistical evaluation metrics such as mean square error, root-mean-square error, Pearson's correlation coefficient, and determination coefficient were used to identify the best-performing model [206]. The level of arsenic contamination in the groundwaters of Jharkhand, India was assessed using various machine learning models including decision trees, random forests, multilayer perceptrons, and Naive Bayes algorithms [207]. Further, the Pearson correlation was applied to find a relationship between arsenic occurrence and considered parameters [207]. Two advanced machine learning algorithms (boosted regression trees and random forests) were implemented to understand the factors influencing surface water vulnerability towards arsenic pollution by Mohammadi et al. [208]. In another research work based on As removal by Roy et al. [209], an ANN model developed from batch experimental data sets provided reasonable predictive performance of arsenic adsorption. The model with high accuracy had an ANN architecture consisting of 7-3-2 neurons in the input, hidden, and output layers including the bias in the first two layers [209].

Statistical analysis and ML-based approaches are both data-dependent methods but there are a few fundamental differences between the two.

- Statistical analysis has more of a numerical approach based on mathematical and statistical information, whereas, ML is mostly automated through algorithms that self-comprehend and train itself using the provided data without much human intervention.
- Statistical analysis is primarily based on the concepts of probability and derivatives while ML is involved with the concepts of genetic algorithms and artificial neural networks.

- Statistical analysis is divided into descriptive, correlational, and inferential analyses. ML is classified into supervised, unsupervised, and reinforcement learning.
- Statistical analysis is mainly used to find the distribution pattern, characterize the data, investigate the correlation between variables, and explore the cause-and-effect relationship between them. However, the ML-based approach primarily focuses on prediction by generating a model from trained and tested datasets.
- The different approaches of statistical analysis function on the basis of assumptions related to the data including normality, homogeneity, homoscedasticity, multicollinearity, etc, but, ML-based approaches are not dependent on any such assumptions.

Combining both approaches for data analysis helps to overcome the limitations of individual statistical and machine learning-based approaches and these analyses have been performed in this research work.

1.8 Relevance and objective of the thesis work

Though there are several traditional methods for the removal of arsenic from water, there are some limitations in each method. In recent times, the membrane-based process has become an efficient method to concentrate or remove pollutants from the source. The solid membrane-based methods have certain disadvantages such as membrane fouling leading to low flux rates and low selectivity. While liquid membrane-based technique being highly selective, provides a large surface area in small-sized equipment and reduces the separation time as extraction and recovery processes occur simultaneously. Moreover, the diffusivity of solute in liquids is several orders of magnitude higher than polymeric membranes which results in the requirement of less number of separation stages, saving of reagents, and overall reduction of costs. Further, the use of extractants increases the mass transfer rate leading to very high separation factors. Based on the literature survey presented, the following unfulfilled areas were observed.

- Environmentally benign solvent as the liquid membrane for the extraction and recovery of arsenic is yet to be explored especially when the treated water may be used for drinking purposes.

- Recovery and reuse of arsenic removed from water is yet to be explored.

The main aim of this research is to study the application of a liquid membrane-based separation technique for the removal of arsenic from water which could be achieved through the following measurable objectives:

- ✓ Identification of environmentally benign solvent, extractant, and strippant for maximum extraction and recovery of $As^{(III)}$, $As^{(V)}$, and combination of $As^{(III)}$and $As^{(V)}$in various ratios (viz. 1:1, 1:2, and 2:1) by two-phase equilibrium and three-phase FSSLM study.
- ✓ To study the volumetric, acoustic, thermodynamic and spectroscopic properties of combinations of identified solvent and extractant under regular experimental conditions, i.e. within a temperature range of 25-60°C under atmospheric pressure.
- ✓ Study the effects of various parameters such as extractant concentration, receiving phase concentration, pH, temperature, and stirring speed on extraction and recovery of arsenic in two-phase equilibrium and three-phase FSSLM experimentation, and analyze the results through statistical and ML-based approaches.
- ✓ Development of a mathematical model for simulating the solute transport mechanism through the liquid membrane that can be used for performing initial calculations for any scalability measures.
- ✓ Development of a hybrid technique by integrating FSSLM with electrocoagulation techniques to enhance the recovery efficiency of arsenic species and to gain insights into the interactions occurring among the arsenic species for complex formation through adsorption isotherm and kinetics modelling.
- ✓ Case studies with application of the proposed technique on real groundwater samples from arsenic prone areas of eastern and north-eastern India.

Chapter 2

Theoretical Background

This chapter elucidates the principle concepts of liquid membrane-based methodologies utilized for selectively transporting arsenic between phases. It emphasizes the crucial role of equations governing the modelling of liquid membrane properties in comprehending and enhancing the separation process. The significance of understanding the reaction mechanisms between arsenic and Aliquat 336, as well as arsenic and iron, is underscored in the context of transport and separation mechanisms. Mathematical modelling in this chapter plays a pivotal role in exploring arsenic transport and permeation across phases, particularly in the context of two-phase equilibrium studies and three-phase FSSLM studies. Equations that delineate mass transfer, diffusion, and other pertinent parameters contribute to predicting and optimizing separation efficiency. Furthermore, arsenic removal methodologies extend to FSSLM-electrocoagulation based hybrid technique, where mathematical models based on adsorption isotherms and kinetics aid in comprehending the removal mechanism. These models facilitate predictions of arsenic removal efficiency under various conditions and offer insights into the adsorption behaviour and kinetics inherent in the process.

2.1 Transport methodology

Arsenic present in the aqueous feed phase binds to the extractant present in the organic phase to form a complex, which leads to the transport of arsenic ions from the feed to the organic phase. The extractants may be dissolved in any one of the environmentally benign diluents, viz. vegetable oils such as coconut oil, mustard oil, sesame oil, soyabean oil and sunflower oil, that has maximum extraction efficiency. Environmental benignity is emphasized in order to reduce the toxicity of the organic phase. Various types of extractants including acidic, basic and neutral have been studied to find the one that shows better binding affinity with arsenic ions. These include acidic extractant such as bis(2,4,4-trimethylpentyl) dithiophosphinic acid (Cyanex 301) [112], neutral extractants viz, trioctylphosphine oxide (Cyanex 923) [106] and tributyl phosphate (TBP) [113], and basic extractants such as trioctylamine (TOA) [114] and methyltrioctylamonium chloride (Aliquat 336) [115–118]. Di-(2-ethylhexyl) phosphoric acid (D2EHPA) is an acidic organophosphoric extractant with a tendency to form dimers. This anionic ligand finds its application in the extraction of divalent metals [210, 211], lanthanide[212] and arsenic[213]. TBP is efficient in forming complex with arsenic ions. It has mostly been applied for the extraction of rare earth elements[214], metals[215] including arsenic[155]. However, Aliquat 336 is preferred in this work for its ability to react with both dissociated and undissociated arsenic ions present in the feed phase.

Fig.2.1 shows the extraction efficiency of the aforementioned diluents and extractants. Mustard oil is highly viscous and showed poor extraction efficiency. Though coconut oil shows a good extraction percentage for arsenic ions, it has not been used due to its tendency to change its state with temperature. Sesame, soybean, and sunflower oils were highly efficient in extracting arsenic ions. Sesame oil was observed to give the maximum extraction of around 50% for the arsenic species. So, sesame oil was selected for further studies as it was found to be the most effective environmentally benign diluent for arsenic extraction. On the other hand, Aliquat 336 showed a maximum extraction of approximately 80% for both the arsenic ions. Though TOA is a basic extractant, it cannot bind with neutral arsenic species and requires protonation to be able to bind with anions[114]. TBP and D2EHPA have a tendency to form dimers and transform from α to β multimers causing low extraction efficiency of arsenic species. However, TBP showed better extraction than D2EHPA owing to its small hydrocarbon chain in comparison to

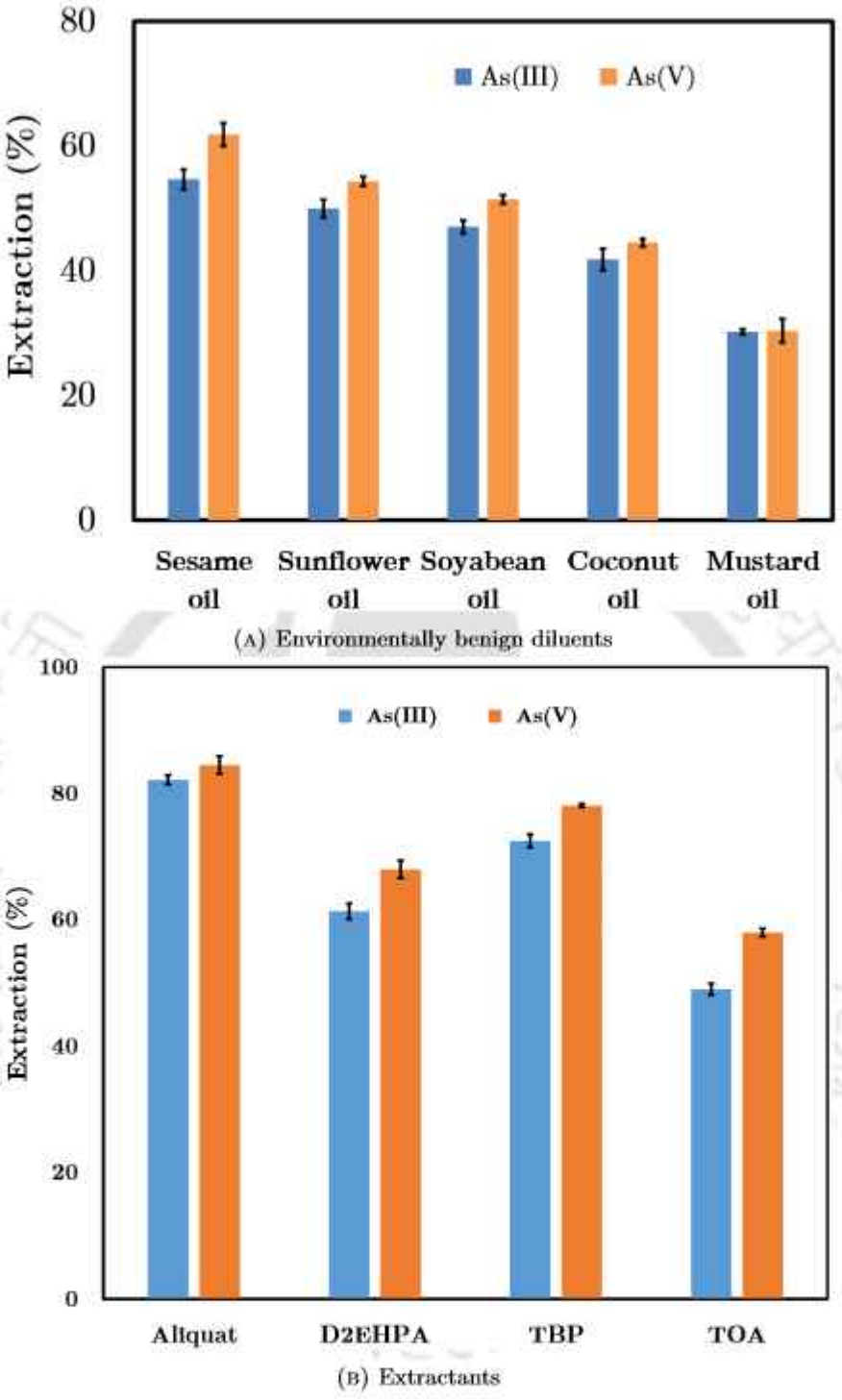

(A) Environmentally benign diluents

(B) Extractants

FIGURE 2.1: Extraction efficiency of various components

the long-branched chain of D2EHPA molecule[216]. The plausible cause of arsenic ions transport in the case of TOA, TBP, and D2EHPA is due to the concentration gradient across the two phases. Due to a strong intermolecular interaction between sesame oil and Aliquat 336, the later is immobilized within the organic phase without being adversely affected to perform its function as an extractant [216]. Hence an organic phase consisting

of a mixture of sesame oil and Aliquat 336 performs best in extraction of arsenic from aqueous phase.

In three phase SLM, one of the aqueous phases is the feed phase acting as the source of arsenic and the other aqueous phase is the receiving (or recovery) phase. A solid membrane dipped in liquid organic phase is placed in between the two aqueous phases viz, the feed phase and the recovery phase. The feed phase is the source of the arsenic ions where interaction between arsenic ions and the extractant leads to the extraction of arsenic from the feed into the membrane phase. The receiving phase is the other aqueous phase where re-extraction or recovery of arsenic takes place due to concentration gradient.

In the novel SLM-electrocoagulation hybrid technique, electrocoagulation is conducted using electrodes for simultaneous extraction and recovery of arsenic as precipitates. The electrocoagulation process in the receiving phase is carried out to remove arsenic ions using iron electrode as the sacrificial anode and graphite rod as the cathode. Iron has been reported to be highly efficient in arsenic removal by forming iron-arsenic complexes[217]. The anodic iron plate diminishes as ferrous ions dissolve into the receiving phase followed by the release of hydrogen gas at the cathode. The overall reactions in both the phases is given in the Fig. 2.2. The SLM technique involves selective uphill extraction

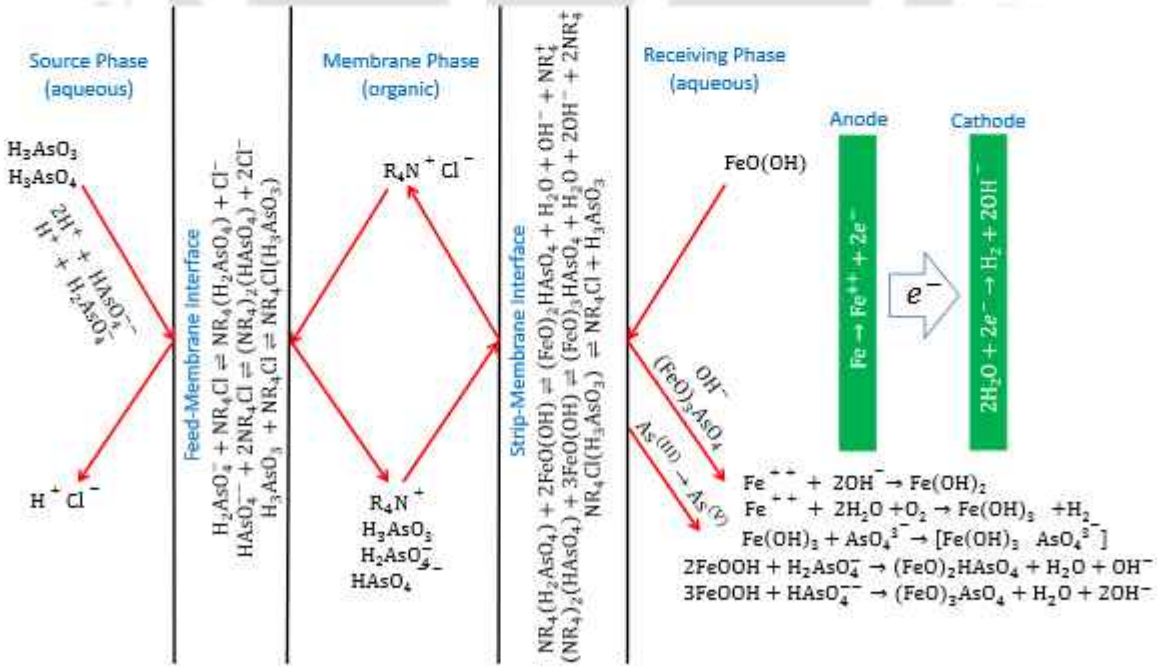

FIGURE 2.2: Reactions occurring in the hybrid process

and recovery of low concentrations of arsenic ions, whereas electrocoagulation technique creates an ever-unsaturated condition in the receiving phase. Removal efficiency is thus improved without addition of any chemical coagulant or adsorbent that makes it a simple cost effective process. The additional advantage of the combinatorial usage of two techniques is selective electrocoagulation which would otherwise be impossible in electrocoagulation alone. Interested readers may refer elsewhere[99, 101, 218] to know the process better.

It has been intended to study the extraction of $As^{(III)}$and $As^{(V)}$when they are present in water as single components, as well as when they are present in combinations with various ratios such as $As^{(III)}$:$As^{(V)}$:: 1 : 1 , $As^{(III)}$:$As^{(V)}$:: 1 : 2 , and $As^{(III)}$:$As^{(V)}$:: 2 : 1 .

2.2 Equations for the modeling of properties of liquid membrane

Hereafter M, S, U, η and ρ refer to the molecular weight, surface tension, ultrasonic velocity, viscosity and density of a liquid and the subscripts m, c and s of any variable refer to mixture, extractant and solvent respectively. x_i, $\eta_{i,T}$ and $\rho_{i,T}$ refer to the mole fraction of the component i and its density and viscosity at temperature T. The experimentally obtained viscosity data are correlated with temperature through four model equations, viz.

Vogel-Fulcher-Tammann model [219]: Hereafter this is abbreviated as VFT model [220–222]

$$\eta_m = A_\eta \exp\left(\frac{B_\eta}{T - C_\eta}\right) \tag{2.1}$$

where A_η, B_η and C_η are adjustable parameters.

Jouyban-Acree model [138, 223]:

$$\ln \eta_m = x_c \ln \eta_{c,T} + x_s \ln \eta_{s,T} + \frac{x_c x_s}{T} \sum_{j=0}^{5} A_{\eta,j} \left(x_c - x_s\right)^j \tag{2.2}$$

where $A_{\eta,j}$ for $j = 0$ to 5 are model constants.

Gruenberg-Nissan model [224, 225]:

$$\ln \eta_m = x_c \ln \eta_c + x_s \ln \eta_s + x_c x_s G_{cs} \tag{2.3}$$

where G_{cs} is a parameter proportional to the internal change in energy and approximately measures the strength of interaction between the components.

Hind et. al. [226]:

$$\eta_m = x_c^2 \eta_c + x_s^2 \eta_s + 2 x_c x_s H_{cs} \tag{2.4}$$

where H_{cs} is related to unlike pair interactions.

The viscosity deviation, $\Delta\eta$, is calculated as the following [225]:

$$\Delta\eta = \eta_m - x_c \eta_c - x_s \eta_s \tag{2.5}$$

The experimentally obtained density data are correlated through two model equations, viz.

Parthasarathy and Bakhshi [227]

$$\rho_m = A + \frac{B}{{\eta_m}^{1/2}} \tag{2.6}$$

where A and B are adjustable parameters.

Jouyban-Acree model [138, 223]: Jouyban-Acree model is also used to fit the density data as the following:

$$\ln \rho_m = x_c \ln \rho_{c,T} + x_s \ln \rho_{s,T} + \frac{x_c x_s}{T} \sum_{j=0}^{7} A_{\rho,j} \left(x_c - x_s\right)^j \tag{2.7}$$

where $A_{\rho j}$ for $j = 0$ to 7 are model constants.

The excess molar volume, V^E, is a non-additive property of mixture and calculated as[225],

$$V^E = \left(\frac{x_c M_c + x_s M_s}{\rho_m}\right) - \left(\frac{x_c M_c}{\rho_c}\right) - \left(\frac{x_s M_s}{\rho_s}\right) \tag{2.8}$$

It is assumed that the surface tension of a pseudo-binary liquid mixture is a linear function of the surface layer mole fraction. The liquid mixture is assumed to be in

equilibrium with its own vapour. The condition for equilibrium between the surface layer and the bulk liquid phase yields an equation involving the surface and the bulk compositions that leads to [228].

$$S_m = \frac{x_c S_c K + x_s S_s}{x_c K + x_s} \tag{2.9}$$

where K is called separation factor which is a function of temperature that shows the extent of surface layer enrichment in the component of lower surface tension. The experimental values of surface tension of the mixtures may be correlated with the mole fractions to find the value of K. The deviation in surface tension of the pseudo-binary mixtures, S^E, is calculated as

$$S^E = S_m - (x_c S_c + x_s S_s) \tag{2.10}$$

The ultrasonic velocity, U in m s^{-1}, through a liquid is calculated using the Auerbach's equation [139, 140]

$$U = \left(\frac{S \times 10^{10}}{6.33 \times \rho}\right)^{2/3} \tag{2.11}$$

The deviation in ultrasonic velocity of the pseudo-binary mixtures, U^E, is calculated [229] as

$$U^E = U_m - (x_c U_c + x_s U_s) \tag{2.12}$$

Isentropic compressibility, K_s, of a liquid is reciprocal of elastic bulk modulus and it is obtained through Newton Laplace equation for prediction of the speed of sound though a medium of solid, liquid, or gas. The compressibility is expressed as [139]

$$K_s = \frac{1}{\rho U^2} \tag{2.13}$$

The isentropic compressibility increases with the temperature. The evolution of the K_s (in Pa^{-1}) with temperature (in °C) was modelled by Oroian and Gutt[139] using a polynomial model as

$$K_{s,\text{sesame oil}} = 8.33 \times 10^{-15} T^2 + 1.76 \times 10^{-12} T + 4.80 \times 10^{-10} \tag{2.14}$$

The deviation in isentropic compressibility of the pseudo-binary mixtures, K_s^E, is calculated by the following equation [229].

$$K_s^E = K_{s,m} - (x_c K_{s,c} + x_s K_{s,s}) \tag{2.15}$$

Kalidoss-Jacobson relation is employed to calculate the intermolecular free length, L_f, [139, 230, 231]

$$L_f = k_L \sqrt{K_s} \tag{2.16}$$

where k_L is a temperature dependent term. The intermolecular free length increases with the temperature. The evolution of the L_f (in m) with temperature (in ℃) was modelled by Oroian and Gutt[139] using a polynomial model as

$$L_{f,\text{sesame oil}} = 3.45 \times 10^{-16} T^2 + 1.17 \times 10^{-13} T + 2.06 \times 10^{-11} \tag{2.17}$$

The deviation in intermolecular free length of the pseudo-binary mixtures, L_f^E, is calculated as [229]

$$L_f^E = L_{f,m} - (x_c L_{f,c} + x_s L_{f,s}) \tag{2.18}$$

Acoustic impedance, Z, is calculated as [139].

$$Z = \rho U \tag{2.19}$$

The acoustic impedance increases with temperature. The evolution of the Z (in kg $m^{-2}s^{-1}$) with temperature (in ℃) was modelled by Oroian and Gutt[139] using a linear model as

$$Z_{\text{sesame oil}} = 1 \times 10^6 T - 3136 \tag{2.20}$$

The deviation in acoustic impedance of the pseudo-binary mixtures, Z^E, is calculated as [229]

$$Z^E = Z_m - (x_c Z_c + x_s Z_s) \tag{2.21}$$

The values of viscosity deviation, excess molar volume, surface tension, ultrasonic velocity and acoustic impedance for each mixture have been fitted to Redlich-Kister polynomial (hereafter referred to as RKP) function equation[119, 225, 232–234] through

least-squares method by taking the limits $i = 0$ to n.

$$f = x_c(1 - x_c)\sum_{i=0}^{n} A_i(2x_c - 1)^i \tag{2.22}$$

where f refers to $\Delta\eta$, V^E, S^E, U^E or Z^E and A_i is the regression coefficient of the ith term. The correlation of the experimental data with the calculated values of each of the model Eq.(2.1) to Eq.(2.22) is tested by calculating the standard deviation, σ, as [225]

$$\sigma = \sqrt{\frac{1}{n-k}\sum\left(\frac{E-C}{E}\right)^2} \tag{2.23}$$

where E stands for experimental values, C refers to calculated values, n is the number of data points and k represents the number of numerical coefficients given in Tables 4.2 – 4.9. An exponential model is proposed using the aforementioned parameters as

$$\eta^2 = ae^{b\left(\rho S_m L_f\right)} \tag{2.24}$$

where a and b are constants which can further be represented in linear form as

$$\ln\eta^2 = c + b\left(\rho S_m L_f\right) \tag{2.25}$$

where $c = \ln a$ is the revised parameter of the proposed model. Apparent molar volume of the extractants and solvents in the mixtures are calculated as [119]

$$V_{\phi 1} = \left(\frac{x_s M_s}{x_c}\right)\left(\frac{\rho_s - \rho_m}{\rho_s\rho_m}\right) + \frac{M_c}{\rho_m} \tag{2.26}$$

$$V_{\phi 2} = \left(\frac{x_c M_c}{x_s}\right)\left(\frac{\rho_c - \rho_m}{\rho_c\rho_m}\right) + \frac{M_s}{\rho_m} \tag{2.27}$$

The volumetric thermal expansion coefficient shows the change in the volume of the liquid with a change in temperature at constant pressure. The thermal expansion coefficient, α, is calculated as [119]

$$\alpha = \frac{1}{\rho}\left(\frac{\partial\rho}{\partial T}\right)_p \tag{2.28}$$

The Gibbs' energy of a real mixture varies from that of a hypothetical ideal mixture having the same constituents. The difference between the two is the excess Gibbs' energy. The excess thermodynamic properties play an important role in studying the behaviour of pseudo-binary mixtures. By definition, the excess Gibbs' energy (ΔG^E) consists of

enthalpy of mixing which depicts the intermolecular forces between the molecules due to the mixing process and entropy that reflects the state of disorder or random behaviour of particles in the mixture. Eq.(2.29) is used to calculate excess Gibbs' energy for the pseudo-binary mixtures. Excess Gibbs' free energy of the pseudo-binary mixtures is calculated as [119]

$$\frac{\Delta G^E}{RT} = \ln(\eta_m V_m) - \{x_c \ln(\eta_c V_c) + x_s \ln(\eta_s V_s)\} \tag{2.29}$$

The enthapy (ΔH) and entropy (ΔS) of activation are calculated by Eyring's approach [235, 236] to Andrade's theory [237] with the viscosity expressed in the form [238, 239].

$$\nu = \frac{hN_A}{M_{av}} \exp\left(\frac{\Delta G^E}{RT}\right) \tag{2.30}$$

where $M_{av} = \sum_i x_i M_i$ is the average molar mass, ν is kinematic viscosity, h is Planck's constant, N_A is the Avogradro number, R is the gas constant, and T is the absolute temperature. By applying the stadard thermodynamic equation

$$\Delta G^E = \Delta H - T\Delta S \tag{2.31}$$

It is possible to write

$$R \ln\left(\frac{\eta M}{\rho h N_A}\right) = \frac{\Delta H}{T} - \Delta S \tag{2.32}$$

2.3 Reaction mechanism

The arsenic ions present in the feed phase are either in the dissociated state such as $H_2AsO_3^-$ (in case of $As^{(III)}$), $H_2AsO_4^-$, $HAsO_4^{2-}$, AsO_4^{3-} (in case of $As^{(V)}$) or in the undissociated forms of H_3AsO_3 (in case of $As^{(III)}$) and H_3AsO_4 (in case of $As^{(V)}$) depending on the pH of the feed phase[106]. The pH of the feed phase in the experiments have been varied from 3 [240] to 9 [241] imitating the groundwater conditions of Digboi Refinery area in India [242]. The pH of the recovery phase was varied between 3 and 7 as ferric hydroxide precipitation starts in this pH range [243]. In the explored pH range for this study, $As^{(III)}$is present in the undissociated form of H_3AsO_3 and $As^{(V)}$in dissociated species of $H_2AsO_4^-$, and they are abundant compared to other ions. It is to be noted that H_3AsO_3 is the predominant form of $As^{(III)}$in the pH range of 2-9. Any change

in pH within this range will not affect the extraction of $As^{(III)}$. Whereas $H_2AsO_4^-$ is the dominant form of $As^{(V)}$in the pH range of 2-7. An increase in pH beyond 7 would lead to the formation and presence of $HAsO_4^{2-}$. In that case the stoichiometric ratio of arsenic-aliquat would also change for the two phase study. However, not much change in initial feed phase pH was observed in two phase study.

The interactions between Aliquat 336 and the arsenic ions have been studied here owing to its ability to react with both dissociated and undissociated arsenic ions[118] as given below.

$$H_3AsO_3 + nNR_4Cl \leftrightharpoons (NR_4Cl)_n(H_3AsO_3) \tag{2.33}$$

$$H_2AsO_4^- + nNR_4Cl \leftrightharpoons (NR_4)_n(H_2AsO_4) + nCl^- \tag{2.34}$$

where R≡$(C_8H_{17})_3CH_3$ denotes methyltrioctyl and n denotes the number of Aliquat 336 molecules to be associated with one molecule of arsenic salt to form the desired complex. In addition, the pKa values of inorganic $As^{(III)}$are reported to be pKa^1 = 9.23, pKa^2 = 12.13 & pKa^3 = 13.4 [244] and that of $As^{(V)}$are pKa^1 = 2.2, pKa^2 = 7 & pKa^3 = 11.5 [245]. This indicates that $As^{(V)}$is a stronger acid and H_3AsO_3 and $H_2AsO_4^-$ are the prevalent species of $As^{(III)}$and $As^{(V)}$, respectively, within the studied pH range of groundwater[246]. From this, it can be inferred that $As^{(III)}$is thermodynamically stable and most abundant in anoxic conditions or lower pH range; whereas, $As^{(V)}$is most stable and abundant under oxic conditions; and under suboxic conditions at intermediate pH range, both the arsenic species may possibly coexist for which combined $As^{(III)}$and $As^{(V)}$in various ratios may be studied[246].

In the three phase SLM, the reactions occurring between arsenic ions and Aliquat 336 at the feed-membrane interface are Eq.(2.33), Eq.(2.34) and

$$HAsO_4^{2-} + 2NR_4Cl \leftrightharpoons (NR_4)_2(HAsO_4) + 2Cl^- \tag{2.35}$$

whereas the reactions occurring in the membrane-strip interface is as mentioned below[118]

$$NR_4Cl(H_3AsO_3) \leftrightharpoons NR_4Cl + H_3AsO_3 \tag{2.36}$$

$$NR_4(H_2AsO_4) \leftrightharpoons NR_4^+ + H_2AsO_4^- \tag{2.37}$$

$$(NR_4)_2(HAsO_4) \leftrightharpoons 2NR_4^+ + HAsO_4^{2-} \tag{2.38}$$

Further, arsenic is naturally found in iron based minerals. Iron is abundant and readily reacts with arsenic so it finds its application in arsenic remediation. Hence ferric chloride has often been used as a coagulant for arsenic removal[247, 248]. In this study, ferric chloride solution has been used as the strippant. In the receiving phase, iron hydroxides are formed from ferric chloride based on the pH as in Eq.(2.46) which then reacts with $As^{(III)}$as in Eq.(2.50)[249] and $As^{(V)}$as in Eq.(2.51) and Eq.(2.52)[250].

$$FeCl_3 + 3H_2O \longrightarrow Fe(OH)_3 + 3HCl \tag{2.39}$$

$$Fe(OH)_3 + 3H_3AsO_3 \longrightarrow Fe(H_2AsO_3)_3 + 3H_2O \tag{2.40}$$

$$2Fe(OH)_n + H_2AsO_4^- \longrightarrow Fe_2O_{10}H_{15} \cdot H_2AsO_4 \longrightarrow Fe_2AsO_{13}H_{15} + H_2O \tag{2.41}$$

$$4Fe(OH)_n + 2HAsO_4^{2-} \longrightarrow 2Fe_2O_{10}H_{15} \cdot 2HAsO_4 \longrightarrow 2Fe_2AsO_{13}H_{15} + H_2O \tag{2.42}$$

In the SLM-electrocoagulation hybrid technique, the reactions occurring at the electrodes are given in the equations Eqs.(2.43)-(2.45). At cathode:

$$2H_2O + 2e^- \longrightarrow H_2(g) + 2OH^- \tag{2.43}$$

At anode:

$$Fe(s) \longrightarrow Fe^{++} + 2e^- \tag{2.44}$$

$$Fe^{++} \longrightarrow Fe^{+++} + e^- \tag{2.45}$$

The ferric ions get hydrolysed by the hydroxide ion forming iron oxyhydroxides Eq.(2.46).

$$Fe^{+++} + 3OH^- \longrightarrow Fe(OH)_3(s) \tag{2.46}$$

The polymerization of iron oxyhydroxides lead to the generation of different phases of iron oxides/hydroxides such as goethite, hematite, lepidocrocite, maghemite, magnetite that form the electrocoagulation floc as given in the following Eqs.(2.47)-(2.49) [243].

$$2Fe(OH)_3 \longrightarrow Fe_2O_3 + 3H_2O(\text{hematite, maghemite}) \tag{2.47}$$

$$6Fe(OH)_3 \longrightarrow 2Fe(OH)_2O_3 + Fe_3O_4 + 6H_2O + O_2(\text{hematite, maghemite}) \tag{2.48}$$

$$Fe(OH)_3 \longrightarrow FeO(OH) + H_2O(\text{goethite,lepidocrocite}) \tag{2.49}$$

The affinity of arsenic towards iron in the receiving phase leads to the disruption of the extractant-arsenic complex formed at the feed-membrane interphase and the arsenic ions form an insoluble complex with the iron oxyhydroxide by displacing a hydroxyl group from it through ligand exchange [105]. The reactions at membrane-receiving interphase is represented in the Eqs.(2.50)-(2.51). The reaction mechanism for $As^{(III)}$with iron includes the release of H_3AsO_3 at the membrane-receiving interphase, as in Eq.(2.52) [118], followed by the oxidation of $As^{(III)}$to $As^{(V)}$to form ${AsO_4}^{3-}$, ${HAsO_4}^{2-}$ or ${H_2AsO_4}^{-}$ anions [77]. The reactions between these anions and iron oxyhydroxides through ligand exchange are as given in the Eqs.(2.53)-(2.55) [251]. Eq.(2.56) gives the resultant reaction.

$$NR_4(H_2AsO_4) + 2FeO(OH)(s) \longrightarrow (FeO)_2HAsO_4 + H_2O + OH^- + NR_4^+ \tag{2.50}$$

$$(NR_4)_2(HAsO_4) + 3FeO(OH)(s) \longrightarrow (FeO)_3AsO_4 + H_2O + 2OH^- + 2NR_4^+ \tag{2.51}$$

$$NR_4Cl(H_3AsO_3) \longrightarrow NR_4Cl + H_3AsO_3 \tag{2.52}$$

$$2FeO(OH)(s) + H_2AsO_4^- \longrightarrow (FeO)_2HAsO_4 + H_2O + OH^- \tag{2.53}$$

$$3FeO(OH)(s) + HAsO_4^{2-} \longrightarrow (FeO)_3AsO_4(s) + H_2O + 2OH^- \tag{2.54}$$

$$Fe(OH)_3(s) + AsO_4^{3-} \longrightarrow [Fe(OH)_3AsO_4](s) \tag{2.55}$$

$$Fe^{+++} + AsO_4^{2-} + 2H_2O \longrightarrow FeAsO_4 \cdot 2H_2O \tag{2.56}$$

2.4 Mathematical modelling

The distribution (*a.k.a.* partition) coefficient, $D_{(\cdot)}$, for arsenic ions is the ratio of concentration of arsenic ions in the organic phase (C_{org}) to the concentration of arsenic ions in the aqueous phase (C_{aq}) as in

$$D_{(\cdot)} = \frac{C_{org}}{C_{aq}} \tag{2.57}$$

whereas the magnitude of extraction (%Extraction) may be expressed as

$$\%\text{Extraction} = \frac{C_0 - C_t}{C_0} \times 100 \tag{2.58}$$

where C_t is the concentration of arsenic ions in the feed phase at time t and C_0 is the initial concentration of arsenic ions in the aqueous feed phase. Based on the two phase equilibrium study, the extraction equilibrium constant and the mole balance of

the reacting arsenic species and Aliquat 336 can be obtained from the Eq.(2.33) and Eq.(2.34). And the extraction equilibrium constants for $As^{(III)}$and $As^{(V)}$can be expressed as

$$K_{III} = \frac{[(NR_4Cl)_n(H_3AsO_3)]_{fm}}{[H_3AsO_3]_{fm}[NR_4Cl]^n} = D_{III}\frac{1}{[NR_4Cl]^n} \tag{2.59}$$

$$K_V = \frac{[(NR_4)_n(H_2AsO_4)]_{fm}[Cl^-]^n}{[H_2AsO_4^-]_{fm}[NR_4Cl]^n} = D_V\frac{[Cl^-]^n}{[NR_4Cl]^n} \tag{2.60}$$

where suffix fm refers to "feed-membrane interface", and D_{III} and D_V are the distribution coefficients of $As^{(III)}$and $As^{(V)}$respectively. The magnitude of $[Cl^-]$ in the Eq.(2.60) is surmised to be negligible in comparison to $[NR_4Cl]$. Hence Eq.(2.86) and Eq.(2.60) may be re-written as

$$D_i = K_i[NR_4Cl]^n \tag{2.61}$$

or

$$\ln D_i = n\ln[NR_4Cl] + \ln K_i \tag{2.62}$$

where i denotes III and/or V as the case may be. The experimental data may be plotted as per Eq.(2.62) whose slope and the intercept would yield the values of n and the equilibrium constant.

Further the rate of complex formation between arsenic ions and Aliquat 336 and the nature of the diffusional process through the membrane may also be modelled through steady-state diffusion based modelling approach with the following few assumptions:

- The direction of mass flow of arsenic is from the feed phase to the organic phase in two-phase, and additionally from the organic membrane phase to the receiving phase in three phase SLM. So the molar flux in the feed phase decreases with time.
- The complex formation reactions between arsenic ions and aliquat 336 are fast and reversible at both the interfaces.
- The complex formation reactions occur at the interface only and not in the bulk aqueous or organic phases.
- The extraction of arsenic ions into the receiving phase is fast, after their diffusion through the membrane into the receiving phase.

According to Fick's law of diffusion

$$J = -D\frac{dC_x}{dx} \tag{2.63}$$

where J is the molar flux of arsenic (in mol·m^{-2}s^{-1}), D is the diffusion coefficient (in m^{2}s^{-1}) and C_x is the concentration of arsenic (in mol·m^{-3}) at a distance x (in m). Upon discretizing Eq.(2.63) one obtains

$$J = -D\frac{\Delta C_x}{\Delta x} \tag{2.64}$$

Further the rate of change of arsenic inside the feed cell may be related to mass flow of arsenic transferred to the receiving phase as

$$\frac{d\left(C_l V\right)}{dt} = J(A\epsilon) \tag{2.65}$$

where V is the volume (in m^3) of feed phase, A is the membrane area (in m^2) and ϵ is the porosity of the membrane. Using Eq.(2.64), the Eq.(2.65) may further be simplified into

$$\frac{dC_l}{dt} = -D\frac{A\epsilon}{V}\frac{\Delta C_x}{\delta\tau} = -D\frac{\epsilon}{\delta\tau}\frac{A}{V}\left(C_{x,f} - C_{x,s}\right) \tag{2.66}$$

where $C_{x,f}$ and $C_{x,s}$ are the concentration of arsenic at the feed-membrane and membrane-strip interfaces, and τ and δ are the tortuosity of membrane pores and the thickness (in m) of membrane, respectively. The arsenic concentration in the membrane-strip interface is considered to be negligible, i.e. $C_{x,s} = 0$, because it is turned into ferric-arsenite coagulation. Further, it is possible to correlate the concentrations of arsenic in membrane/feed interface as

$$K_x = \frac{C_{x,f}}{C_l C_c} \tag{2.67}$$

where K_x is the equlibrium extractant constant and C_c is the concentration of the carrier element (if any). Combining Eq.(2.66) and Eq.(2.67) one obtains

$$\frac{dC_l}{dt} = -D\frac{\epsilon}{\delta\tau}\frac{A}{V}K_x C_c C_l \tag{2.68}$$

The Eq.(2.68) may further be expressed as

$$\frac{dC_l}{dt} = -P\frac{A}{V}C_l \tag{2.69}$$

where $P = D\frac{\epsilon}{\delta\tau}K_x C_c$ is termed as permeability coefficient (expressed in unit of velocity) whose value refers to the speed with which the arsenic from the feed phase are transported to the stripping phase. It is reported[252] that the diffusion coefficient (D) and the viscosity (μ) are the parameters which control the transport through the membranes and they can be related as $D\mu^{\alpha} = K'(\text{constant})$, where $0.5 < \alpha < 1$ is a coefficient for this kind of liquid media[253, 254]. In case of present work with Aliquat 336 it is observed that $\alpha = 2/3$. Hence, $P = K''\mu^{-2/3}C_c$ where all the constant terms are assimilated into $K'' = K'\frac{\epsilon}{\delta\tau}K_x$. The Eq.(2.69) may be integrated to obtain

$$\ln\frac{C_t}{C_0} = \left(-P\frac{A}{V}\right)t \tag{2.70}$$

A simple kinetic study would reveal the value of permeability of the transport process. The mass transfer coefficients for aqueous and organic phases can thereby be calculated from aqueous and organic phase resistances. From Eq.(2.64)

$$J_{aq} = \frac{1}{\Delta_{aq}}\left\{[\mathrm{H_3AsO_3}]_f - [\mathrm{H_3AsO_3}]_{fm}\right\} \tag{2.71}$$

$$\Delta_{aq}^{-1} = \frac{D_{aq}}{\Delta x_{aq}} \tag{2.72}$$

where suffix aq, f, and fm refer to "aqueous","feed" and "feed-membrane interface" respectively, whereas Δ_{aq} refers to the aqueous phase resistance term and Δx_{aq} refers to the thickness of aqueous film. Similarly diffusion of Aliquat-Arsenic complex through the membrane phase can be written as

$$J_{org} = \frac{1}{\Delta_{org}}\left\{[(\mathrm{NR_4Cl})_n(\mathrm{H_3AsO_3})]_{fm} - [(\mathrm{NR_4Cl})_n(\mathrm{H_3AsO_3})]_{ms}\right\} \tag{2.73}$$

$$\Delta_{org}^{-1} = \frac{\epsilon D_{org}}{\delta\tau^2} \tag{2.74}$$

where suffix org and ms refer to "organic" and "membrane-strip interface" respectively, whereas Δ_{org} refers to the membrane phase resistance term. The Aliquat-arsenic complex gets dissociated very fast at the membrane-strip interface and hence its concentration is negligible as compared to that at feed-membrane interface, i.e. Eq.(2.73) becomes

$$J_{org} = \frac{1}{\Delta_{org}}[(\mathrm{NR_4Cl})_n(\mathrm{H_3AsO_3})]_{fm} \tag{2.75}$$

Moreover at steady state

$$J_{aq} = J_{org} = J \tag{2.76}$$

Using Eq.(2.86), Eq.(2.61), Eq.(2.71), Eq.(2.75) and Eq.(2.76) one obtains

$$J = \frac{D_{III}\left[\mathrm{H_3AsO_3}\right]_f}{\Delta_{org} + D_{III}\Delta_{aq}}$$

The permeability coefficient can be defined as flux of solute per unit of its concentration in the feed phase, i.e.

$$P = \frac{J}{\left[\mathrm{H_3AsO_3}\right]_f} = \frac{D_{III}}{\Delta_{org} + D_{III}\Delta_{aq}} \tag{2.77}$$

or

$$\left(\frac{1}{P}\right) = \Delta_{aq} + \left(\frac{1}{D_{III}}\right)\Delta_{org} \tag{2.78}$$

The above formulation may be extended for $As^{(V)}$as well. Hence the Eq.(2.78) may be re-written for both $As^{(III)}$and $As^{(V)}$as

$$\left(\frac{1}{P}\right) = \Delta_{aq} + \left(\frac{1}{D_i}\right)\Delta_{org} \tag{2.79}$$

where i denotes III and/or V as the case may be. The value of D_i will be different for different concentration of NR_4Cl. By plotting P^{-1} versus D_i^{-1} of the Eq.(2.79) for various $[NR_4Cl]$ at constant pH a straight line with slope Δ_{org} and intercept Δ_{aq} would be obtained. The mass transfer coefficients for aqueous and organic phases can thereby be found from Eq.(2.74) and Eq.(2.72).

2.5 Arsenic removal by electrocoagulation

In the receiving phase, the amount of iron liberated from the anode theoretically can be calculated by the Faraday's law, as in Eq.(2.80).

$$A_{Fe} = \frac{ItM}{vzF} \tag{2.80}$$

where, A_{Fe} (in g·mL^{-1}) is the amount of iron liberated from the anode, I is the applied current (in A or C·s^{-1}), t is the treatment time (in s), M is the atomic weight of iron (in g·mol^{-1}), v is the volume of the reactor (in mL), z is the number of electrons transferred

in the reaction and F is the Faraday's constant (96485 C·mol^{-1})[217]. Arsenic removal (in %) is calculated from the Eq.(2.81).

$$Re_{As} = 100\frac{C_i - C_f}{C_i} \tag{2.81}$$

Arsenic removal capacity per dissolved iron anode is given by Eq.(2.82) [105].

$$q = \frac{C_i - C_f}{A_{Fe}} \tag{2.82}$$

where, Re_{As} (in %) is the arsenic removal efficiency, C_i and C_f are the initial and final arsenic concentrations (both in mg·L^{-1}) in the receiving phase and q is the arsenic removal capacity per dissolved iron anode. And the magnitude of recovery (%Recovery) may be expressed as

$$\%\text{Recovery} = \frac{C_f}{C_0} \times 100 \tag{2.83}$$

It is only used in three phase FSSLM study.

2.6 Adsorption modeling

As iron is highly reactive, it keeps producing new adsorption sites for arsenic ions and subsequent co-precipitation.

2.6.1 Isotherms

The equilibrium removal of arsenic can be mathematically expressed in terms of the adsorption isotherms. To understand the adsorption isotherm process, various model isotherms have been studied.

Assuming a mono-molecular layer of arsenic adsorption occurring on the sites of iron oxyhydroxides that is homogeneous in nature, Langmuir model predicts the surface coverage. The functionality is as given in Eq.(2.84)

$$q_e = \frac{q_{max} K_L C_e}{1 + K_L C_e} \tag{2.84}$$

$$\frac{1}{q_e} = \left(\frac{1}{q_{max} K_L}\right)\frac{1}{C_e} + \frac{1}{q_{max}} \tag{2.85}$$

where, q_e is the amount of adsorbate on the adsorbent at equilibrium in (mg·g^{-1}), C_e is the equilibrium concentration of adsorbate in the aqueous phase in (mg·L^{-1}), K_L is the Langmuir's binding constant in (L·mg^{-1}) and q_{max} is the maximum sorbent capacity (mg·g^{-1}).

The Freundlich isotherm equation attributes to the change in the equilibrium constant of the binding process to the heterogeneity of the surface. The empirical equation gives the relation between the amount adsorbed per unit mass of adsorbate. The relation is represented in Eq.(2.86) as

$$q_e = K_F C_e^{1/n} \tag{2.86}$$

where K_F and $1/n$ are the constants for adsorption capacity and intensity, respectively.

By combining these two models, Redlich-Peterson, i.e. Eq.(2.87), and Sips i.e. Eq.(2.88), models are developed to apply them over a wide range of adsorbate concentrations in either homogeneous or heterogeneous systems.

$$\ln \frac{C_e}{q_e} = R_P \ln C_e - \ln A \tag{2.87}$$

$$\ln \frac{1}{q_e} = (-K_s) \ln C_e + \ln a_s \tag{2.88}$$

where q_e is the amount of adsorbate at equilibrium (in mg·g^{-1}), C_e is the equilibrium concentration of adsorbate on the adsorbent (in mg·g^{-1}), R_P and A are constants, values of which are obtained from the slope and intercept, K_s and a_s are constants.

The direct and indirect adsorbate-adsorbent interactions leading to adsorption energy generation are evaluated through the Dubinin-Radushkevich model Eq.(2.89) and the Temkin isotherm model Eq.(2.91),

The Dubinin-Radushkevich model is a two parameter isotherm that differentiates between physical and chemical adsorption mechanism on heterogeneous surfaces with Gaussian energy distribution [255]. Dubinin-Radushkevich model is expressed as in Eq.(2.89) [256–258].

$$\ln q_e = \ln q_{max} - \beta \epsilon^2 \tag{2.89}$$

$$\epsilon = RT \ln \left(1 + \frac{1}{C_e}\right) \tag{2.90}$$

where R is gas constant (8.314×10^{-3} kJ·mol^{-1}K^{-1}) and T is temperature (in K). β is the activity coefficient (in mol^{2}kJ^{-2}) related to mean free energy of adsorption which is also called Dubinin-Radushkevich constant and ϵ is termed as Polanyi potential (in kJ·mol^{-1}). The mean adsorption energy (in J·mol^{-1}) may be expressed as $(2\beta)^{-0.5}$.

The Temkin isotherm model helps to predict the interactions between the adsorbate [259] and the energy released based on the assumption that the heat of adsorption of all molecules in the layer decreases linearly with the increase in surface coverage [260]. The experimental data has been fitted to this model given by Eq.(2.91).

$$q_e = \frac{RT}{b} \ln\left(K_T C_e\right) \tag{2.91}$$

where b is Temkin constant associated with the heat of sorption (in J·mol^{-1}) and K_T is Temkin isotherm constant (in L·mg^{-1}) [261].

For multilayer adsorption processes on heterogeneous surfaces, Halsey isotherm [262] and Harkins-Jura models as expressed in Eq.(2.92) & Eq.(2.93) respectively are given below.

$$q_e = \exp\left(\frac{\ln K_H - \ln C_e}{n_H}\right)$$

$$\text{or} \qquad \ln q_e = \left(-\frac{1}{n_H}\right)\ln C_e + \frac{1}{n_H}\ln K_H \tag{2.92}$$

$$\frac{1}{q_e^2} = \left(-\frac{1}{H_J}\right)\ln C_e + \frac{B}{H_J} \tag{2.93}$$

where q_e is the amount of adsorbate at equilibrium (in mg·g^{-1}), C_e is the equilibrium concentration of adsorbate on the adsorbent (in mg·g^{-1}), K_H, n_H, H_J and B are the constants. The Jovanovic model [256] is a modified version of the Langmuir model that includes adsorption interactions and is used for both mobile and monolayer adsorption processes. The linearized expression of the model is given as

$$\ln q_e = \left(-K_J\right) C_e + \ln q_{max} \tag{2.94}$$

where q_e is the amount of adsorbate at equilibrium (in mg·g^{-1}), C_e is the equilibrium concentration of adsorbate on the adsorbent (in mg·g^{-1}), K_J and q_{max} are constants.

2.6.2 Kinetics

The adsorption kinetics modelling is performed to analyze the kinetics data in order to estimate the equilibrium adsorption amount and the rate at which the adsorption equilibrium is achieved by the following empirical models. The pseudo first-order model was proposed by Lagergren[263] and its linearized form is given as [264]

$$\ln(q_e - q_t) = (-k_1)\, t + \ln q_e \tag{2.95}$$

where q_e is the quantity of adsorbate at equilibrium per unit weight of the adsorbent ($mg{\cdot}g^{-1}$), q_t is the amount adsorbed at any time t ($mg{\cdot}g^{-1}$), t is time in minutes, k_1 is the pseudo first-order rate constant (min^{-1}). The linearized form of the pseudo second-order kinetics model as represented by [265]

$$\frac{t}{q_t} = \left(\frac{1}{q_e}\right) t + \frac{1}{k_2 q_e^2} \tag{2.96}$$

where k_2 is the pseudo second order rate constant ($g{\cdot}mg^{-1}min^{-1}$). The Elovich kinetics is an empirical model based on the assumption that the adsorption energy increases with time and the adsorbent has a heterogeneous surface coverage. The linear expression is given as [264]

$$q_t = \frac{1}{\beta} \ln t + \frac{1}{\beta} \ln(\alpha\beta) \tag{2.97}$$

where α is the initial adsorption rate constant (in $mg{\cdot}g^{-1}min^{-1}$), β is the desorption constant (in $g{\cdot}mg^{-1}$). The linear form of the fractional power function is [266]

$$\ln q_t = \nu \ln t + \ln k_3 \tag{2.98}$$

where k_3 is a fractional power constant (in $mg{\cdot}g^{-1}$) and ν is a positive constant (in min^{-1}). The intraparticle diffusion model was described by [267] and its linear expression is presented as

$$q_t = k_{id} t^{0.5} + c \tag{2.99}$$

where k_{id} is the intraparticle diffusion rate constant ($mg{\cdot}g^{-1}min^{-0.5}$) and c is the thickness of the adsorbent. This model is used to deduce the rate-controlling step when the intraparticle diffusion process occurs [264] and the thickness of the adsorbent [266]. The liquid film diffusion model denotes the rate coefficient based on the particle size of

the adsorbent for the particle-diffusion controlled process and establishes the fractional attainment to equilibrium. The linear form of the model is given as [266]

$$\ln\left(1-\frac{q_t}{q_e}\right) = -k_{lfd}.t \tag{2.100}$$

where k_{lfd} is the rate coefficient for particle-diffusion controlled process corresponding to the particle size of the adsorbent (min^{-1}) and q_t/q_e is the fractional attainment to equilibrium.

2.6.3 Statistical error analysis for adsorption models

The best fitting adsorption isotherm model with the experimental data is often determined by the coefficient of correlation (R^2) values.

$$R^2 = 1 - \frac{\sum_{i=1}^{n}(Y_i - y_i)^2}{\sum_{i=1}^{n}(Y_i - Y)^2} \tag{2.101}$$

But, the transformation of non-linear models to linear expressions lead to biasness in the data. In order to overcome this, few statistical error functions have been calculated to predict the best fit adsorption model based on the error values obtained. Few of the error functions included in this study are namely, root mean square error (RMSE), chi-square test (χ^2) and hybrid fractional error function (HFEF) as follows:

$$\text{RMSE} = \sqrt{\frac{1}{n}\sum_{i=1}^{n}(Y_i - y_i)^2} \tag{2.102}$$

$$\chi^2 = \sum_{i=1}^{n}\frac{(Y_i - y_i)^2}{y_i} \tag{2.103}$$

$$\text{HFEF} = \left(\frac{100}{n-p}\right)\sum_{i=1}^{n}\frac{(Y_i - y_i)^2}{y_i} \tag{2.104}$$

where, Y_i is the obtained amount of adsorbate of sample observation i at equilibrium from the batch experiments, y_i is the estimated (calculated) amount of adsorbate of sample observation i from the isotherm models for corresponding Y_i, Y is the mean of samples, n is the number of observations and p is the number of parameters within the isotherm equation. Both isotherm and kinetics data are validated with the values from the statistical error analysis.

Summary of the Theoretical Background

- An organic phase consisting of a pseudo-binary mixture of sesame oil and Aliquat 336 performs best in extraction of arsenic from aqueous phase.
- The important equations in modelling of liquid membrane properties for understanding and enhancing separation processes are emphasized.
- The reaction mechanisms between arsenic and Aliquat 336, as well as arsenic and iron, are elaborated in transport and separation mechanisms.
- Equations covering extraction equilibrium, mass transfer, diffusion, and relevant parameters contributing to predicting and optimizing separation efficiency are further discussed.
- Arsenic removal methodologies extended to FSSLM-electrocoagulation hybrid technique, incorporating mathematical models based on adsorption isotherms and kinetics are incorporated.

Abbreviation

Cyanex 301 Bis(2,4,4-trimethylpentyl) dithiophosphinic acid

Cyanex 923 Trioctylphosphine oxide

TBP Tributyl phosphate

TOA Trioctylamine

Aliquat 336 Methyltrioctylammonium chloride

D2EHPA Di-(2-ethylhexyl) phosphoric acid

HFEF Hybrid Fractional Error Function

RKP Redlich-Kister Polynomial

RMSE Root Mean Square Error

SLM Supported Liquid Membrane

VFT Vogel-Fulcher-Tammann model

Nomenclature

η_m	viscosity of mixture
η_c	viscosity of extractant
η_s	viscosity of solvent
$\Delta\eta$	excess viscosity of mixture
A_η	adjustable parameter in VFT model
B_η	adjustable parameter in VFT model
C_η	adjustable parameter in VFT model
T	absolute temperature
x_c	mole fraction of extractant
x_s	mole fraction of solvent
G_{cs}	Gruenberg-Nissan constant
H_{cs}	Hind constant
ρ_m	density of mixture
ρ_c	density of extractant
ρ_s	density of solvent
ρ_E	excess density of mixture
A	adjustable parameter of Parthasarathy and Bakshi model [227]
B	adjustable parameter of Parthasarathy and Bakshi model [227]
M_c	Molecular weight of extractant
M_s	Molecular weight of solvent
V_E	excess molar volume of mixture
V_m	molar volume of mixture
V_c	molar volume of extractant
V_s	molar volume of solvent
S_m	surface tension of the mixture
S_c	surface tension of extractant
S_s	surface tension of solvent
S^E	excess surface tension of mixture
K	separation factor for surface layer
U	ultrasonic velocity
U^E	excess ultrasonic velocity of mixture
U_c	ultrasonic velocity of extractant

U_s	ultrasonic velocity of solvent
U_m	ultrasonic velocity of mixture
K_s	isentropic compressibility
K_s^E	excess isentropic compressibility of mixture
$K_{s,m}$	isentropic compressibility of mixture
$K_{s,c}$	isentropic compressibility of extractant
$K_{s,s}$	isentropic compressibility of solvent
L_f	intermolecular free length
L_f^E	excess intermolecular free length
$L_{f,m}$	intermolecular free length of mixture
$L_{f,c}$	intermolecular free length of extractant
$L_{f,s}$	intermolecular free length of solvent
k_L	temperature dependent term related to intermolecular free length and isentropic compressibility
Z	acoustic impedance
Z^E	excess acoustic impedance of mixture
Z_m	acoustic impedance of mixture
Z_c	acoustic impedance of extractant
Z_s	acoustic impedance of solvent
a	constant of equation
b	constant of an equation
c	equal to $\ln(a)$
σ	standard deviation
n	data points
k	number of numerical coefficients
E	experimental values of properties
C	calculated values of properties
α	thermal expansion coefficient
$V_{\Phi 1}$	apparent molar volume of extractants
$V_{\Phi 2}$	apparent molar volume of solvents
ΔG^E	excess Gibbs' free energy
ΔH	excess enthalpy
ΔS	excess entropy

R	gas constant
ν	kinematic viscosity
h	Planck's constant
N_A	Avogadro's number
$D_{(\cdot)}$	distribution or partition coefficient
C_{org}	concentration of arsenic ions in the organic phase
C_{aq}	concentration of arsenic ions in the aqueous phase
C_0	initial concentration of arsenic in feed phase
C_t	concentration of arsenic ions in the feed phase at time t
D_{III}	distribution coefficient of $As^{(III)}$
D_V	distribution coefficient of $As^{(V)}$
K_{III}	extraction equilibrium constant for $As^{(III)}$
K_V	extraction equilibrium constant for $As^{(V)}$
K_x	equilibrium extractant constant
n	stoichiometric ratio obtained from the distribution plot
J	molar flux of arsenic
D	diffusion coefficient
C_x	concentration of arsenic (in mol-m^{-3}) at a distance x (in m)
V	volume of feed phase (in m^3)
A	membrane area (in m^2)
P	permeability coefficient
ϵ	porosity of the membrane
δ	thickness of membrane (in m)
τ	tortuosity of membrane pore
C_c	concentration of the extractant
$C_{x,f}$	concentration of arsenic at the feed-membrane interface
$C_{x,s}$	concentration of arsenic at the membrane-strip interface
J_{aq}	molar flux in aqueous phase
D_{aq}	diffusion coefficient in aqueous phase
Δx_{aq}	thickness of the aqueous film
Δ_{aq}	aqueous phase resistance
J_{org}	molar flux in organic phase
D_{org}	diffusion coefficient in organic phase

Δx_{org}	thickness of the organic film
Δ_{org}	membrane phase resistance
A_{Fe}	amount of iron liberated from anode
I	applied current (in A)
t	treatment time (in s)
M	atomic weight of iron (in g·mol^{-1})
v	volume of the reactor (in mL)
z	number of electrons transferred in the reaction
F	Faraday's constant (96485 C·mol^{-1})
Re_{As}	arsenic removal (in %)
C_i	initial arsenic concentration in the receiving phase
C_f	final arsenic concentration in the receiving phase
q	arsenic removal capacity per dissolved iron anode
q_e	amount of adsorbate on the adsorbent at equilibrium (mg·g^{-1})
q_{max}	maximum sorbent capacity (mg·g^{-1})
K_L	Langmuir's binding constant (L·mg^{-1})
C_e	equilibrium concentration of adsorbate in the aqueous phase (mg·L^{-1})
K_F	adsorption capacity constant for Freundlich isotherm
n	adsorption intensity constant for Freundlich isotherm
R_P	Redlich-Peterson constant
A	constant parameter for Redlich-Peterson equation
K_s	Sips constant
a_s	intercept of Sips equation
β	activity coefficient (Dubinin-Radushkevich constant)
ϵ	Polanyi potential
b	Temkin constant associated with the heat of sorption
K_T	Temkin isotherm constant
K_H	Halsey isotherm constant
n_H	constant parameter of Halsey isotherm
H_J	Harkins-Jura isotherm constant
B	constant parameter for Harkins-Jura model
K_J	Jovanovic isotherm constant

q_t	amount adsorbed at any time t in $mg{\cdot}g^{-1}$
k_1	pseudo first order rate constant (min^{-1})
k_2	pseudo second order rate constant ($g{\cdot}mg^{-1}{\cdot}min^{-1}$)
α	initial adsorption rate constant ($mg{\cdot}g^{-1}{\cdot}min^{-1}$)
β	desorption constant ($g{\cdot}mg^{-1}$)
v	positive constant (min^{-1})
k_3	fractional power constant ($mg{\cdot}g^{-1}$)
k_{id}	intraparticle diffusion rate constant ($mg{\cdot}g^{-1}{\cdot}min^{-0.5}$)
c	thickness of the adsorbent
k_{lfd}	rate coefficient for particle-diffusion (min^{-1})
Y_i	obtained amount of adsorbate of sample observation I at equilibrium
y_i	estimated calculated amount of adsorbate of sample observation i
$\bar{Y}$	mean of the samples
n	number of observations
p	number of parameters within the isotherm equation

Chapter 3

Materials & Methods

This chapter outlines the details of the various chemicals and instruments utilized for carrying out the experiments. This chapter includes the description of the sources from where the materials are procured, details of the experimental procedure, and the characterization techniques applied in the experiments. Furthermore, the FSSLM setup is described here that is used for three-phase and hybrid studies.

3.1 Chemicals & Reagents

The simulated arsenic-contaminated water was prepared by using Sodium (meta)arsenite ($NaAsO_2$) and sodium arsenate dibasic heptahydrate ($Na_2HAsO_4{\cdot}7H_2O$) salts procured from Merck® India. The stock solutions (1000 ppm) were prepared by dissolving the required amount in Milli-Q® deionized water (Millipore, USA).

Refined vegetable oils of good quality (Fortune® , Adani Wilmer Limited) such as coconut oil, mustard oil, sunflower oil, soybean oil, and sesame oil of RRO PRIMIO brand (FSSAI approved) were used as green solvents. The molecular weight of sesame oil is 848[136]. The molecular weight of sunflower oil is 876.16[268]. Sodium chloride (NaCl)

and ferric chloride salts, procured from Merck® India, have been used for preparing the receiving phases in various SLM experimentations.

TABLE 3.1: Details of extractants used for this study

Extractant	Formula	CAS No.	Molar mass (g mol^{-1})	Purity (wt%)	Company
Aliquat	$C_{25}H_{54}ClN$	63393-96-4	404.16	⩾95%	Sigma-Aldrich
D2EHPA	$C_{16}H_{35}O_4P$	298-07-7	322.43	⩾95%	Merck
TBP	$C_{12}H_{27}O_4P$	126-73-8	266.32	⩾99%	Sigma-Aldrich
TOA	$C_{24}H_{51}N$	1116-76-3	353.67	98%	Sigma-Aldrich

The extractants used for experimentation include tributyl phosphate (TBP), trioctylamine (TOA), methyltrioctyl ammonium chloride (Aliquat® 336), and di-2-ethylhexyl phosphoric acid (D2EHPA) were procured from Sigma Aldrich India. The details of the extractants used in this thesis are given in Table 3.1.

The reagents required for analysis by atomic absorption spectrometer and for adjusting pH, namely, hydrochloric acid (HCl), sodium hydroxide (NaOH), potassium iodide (KI), and sodium borohydride ($NaBH_4$) were purchased from Merck® India. As a solid support, durapore membrane (0.45 micrometer PVDF membrane with porosity (ϵ), membrane thickness (δ) and tortuosity (τ) - 0.70, 125μm and 1.19, respectively) was used and impregnated with the organic phase. All the chemicals and reagents were of Guaranteed Reagents (GR) grade and used without further purification.

3.2 Analytical Instruments

3.2.1 Atomic Absorption Spectrometer

Atomic Absorption Spectrophotometer (AAS) (Make-Varian, Model-240FS AA, Agilent Technologies) was used for arsenic analysis. Samples were drawn from the feed and receiving phases and analyzed to measure the concentrations of arsenic ions in both phases using the vapor generation mode (VGA) of AAS at 193.7nm wavelength with a slit of 0.7, argon flow 50ml.min^{-1} and pump velocity of 120 rpm. The sample preparation

procedure for AAS consisted of standard solution preparation, reductant solution preparation, acid solution preparation, and finally sample preparation following the guidelines provided by the manual of AAS.

The standard solution was prepared by serial dilution from the stock solution of arsenic. The range of standard solutions prepared were 10-100 ppb and to this, KI was added followed by HCl. Similarly, for the sample preparation, KI was added along with HCl. This reaction was carried out for 45 minutes cautiously as the color development due to the reaction is time dependent [269]. The reductant solution was prepared by dissolving 0.6% $NaBH_4$ in 0.5% NaOH solution and 6M HCl solution was used as the acid solution. The concentration of the unknown sample was obtained through interpolation of the calibration curve generated prior to analysis using the standard solutions (vide Fig.A.1).

3.2.2 Viscosity measurement

The dynamic viscosity of the liquid samples were measured using an interfacial rheometer (Anton Paar, model Physica MCR 301) with parallel-disc configuration. A sufficient quantity of the mixture (~0.5-1 mL) was added with a micropipette on the base of the rheometer to avoid sample underfill errors. The viscosity of samples were measured in triplicates at a shear rate of 50 s^{-1}.

3.2.3 Density measurement

The density of the pure solvents and pseudo-binary mixtures were measured with a vibrating tube density-meter (Anton Paar, model DM 4500M). A small volume (~1-2 mL) of sample was injected into the tube using a syringe. The density was measured thrice with a repeatability of 0.1 kg m^{-3}. The temperature of the samples was varied from 25-60°C while measuring density.

3.2.4 Surface tension measurement

The surface tension of the pure solvents, extractants and pseudo-binary mixtures were measured at 25°C with a tensiometer (Kyowa, model DY300) by Wilhelmy plate method using a platinum plate of width 238.5 mm and thickness 1.5 mm. The plate was burned

in an alcohol burner each time after analysis till it turned red to clean and reuse for the next sample.

3.2.5 Fourier Transform Infrared Spectroscopy (FTIR) analysis with attenuated total reflection (ATR)

FTIR-ATR spectroscopy of pure solvents, extractants and equimolar pseudo-binary mixtures were carried out by the attenuated total reflectance (ATR) mode (Shimadzu, model IR Affinity - 1 and Make-PerkinELmer, Model-Spectrum two). The resolution of the sample analysis was 4.0 with number of scans set to 60 in the range of 700 - 4000 cm^{-1}. The precipitate for FTIR-ATR analysis was prepared by filtering the receiving phase and the residue was oven dried at 80°C for 2 hours to remove the moisture. After cooling to room temperature, the samples were ground into a fine powder using an agate mortar and pestle to increase the surface area and improve the signal quality. Before placing the sample, the ATR crystal was cleaned with ethanol to remove any contaminants. A small amount of the solid sample was placed directly onto the ATR crystal ensuring that the entire surface of the crystal was covered. This was done to ensure good contact between the sample and the crystal as it is crucial for obtaining a clear spectrum. Before measuring the sample, a background spectrum was taken into account for any atmospheric absorption or instrumental noise. This was done with a clean, empty ATR crystal. After placing the sample and ensuring good contact with the crystal, the FTIR spectrum was collected which showed characteristic absorption peaks corresponding to the functional groups present in the sample. After the measurement, the ATR crystal was cleaned again to remove any residual sample in order to prevent cross-contamination between samples. Gloves were worn during the handling of the samples and solvents. The FTIR spectra were recorded using the mode and the resolution of the sample analysis was 4 cm^{-1} with number of scans set to 60 to enhance the signal-to-noise ratio. The spectral range was set from 4000 cm^{-1} to 400 cm^{-1} to cover all relevant vibrational modes. Background spectra were recorded under the same conditions and subtracted from the sample spectra to correct for atmospheric and instrument-related interferences. The obtained spectra were analysed for the identification of characteristic peaks corresponding to different functional groups in the samples.

3.2.6 EDX coupled with SEM and/or TEM

The precipitate obtained due to the reactions between iron and arsenic species in the hybrid removal technique was characterized by Energy Dispersive X-ray Spectroscopy (EDX) coupled with Scanning Electron Microscope (SEM) (Make-Zeiss, Model-Sigma), Transmission Electron Microscope (TEM) (Make-Jeol, Model-2100F). The sample for EDX analysis is prepared by the drop cast technique. In this technique, the residue obtained after filtering the receiving phase is dissolved in 20 ml of ethanol followed by sonication for 5 minutes. After the sample is dispersed well and forms a solution in ethanol, a drop of ~0.2 ml of sample is taken and placed on a small piece of glass slide covered by aluminium foil. This is placed in the hot air oven at 100°C for 24 hours to evaporate the ethanol. The samples were thoroughly washed with deionized water to remove any surface contaminants. The sample for EDX analysis was prepared by the drop cast technique. In this technique, the residue obtained after filtering the receiving phase was dissolved in 20 mL of ethanol followed by sonication for 5 minutes. After the sample was dispersed well and formed a solution in ethanol, a drop of ~0.2 mL of sample was taken and placed on a small piece of glass slide covered by aluminium foil. This was placed in the hot air oven at 100°C for 24 hours to evaporate the ethanol. The dried samples were then mounted on aluminium stubs using carbon tape to ensure proper conductivity and were coated with a thin layer of gold using a sputter coater to prevent charging during analysis. The precipitate obtained due to the reactions between iron and arsenic species in the hybrid removal technique was characterized by EDX coupled with SEM and/or TEM. The accelerating voltage was set to 20 kV to obtain a clear and detailed spectrum. The analysis was performed under high vacuum conditions to improve the resolution and accuracy of the measurements. The spectra were collected from multiple points on each sample to ensure representativeness and consistency in the elemental composition analysis. The analysed data provided qualitative and quantitative information on the elemental composition of the samples.

3.2.7 X-Ray Diffractometer (XRD)

XRD (Make-Rigaku, Model-SmartLab 9kW) were also used for the characterization of the precipitate. The diffractometer was equipped with a Copper K-alpha source having

a wavelength of 1.54 angstrom for XRD analysis. The sample analysis was done at a scanning rate of 6° min^{-1} with 2θ in the range of 20-80°.

3.2.8 Other information

A digital pH meter (Make-Eutech Instruments, Model-EUTECH pH700) was used to measure the pH of the aqueous phases. The precipitate for FTIR and XRD analysis was prepared by filtering the receiving phase and the residue was oven dried at 80°C for 2 hours to remove the moisture. The dried product was cooled to room temperature and calcined at 500°C for 4 hours [270].

3.3 Experimental procedures

3.3.1 Estimation of physical properties of organic phase

Pseudo-binary mixture of identified solvent and extractant was prepared in 25 mL glass beaker by weight percentage in the range of 10-90% covered with paraffin film as given in Table B.1. The samples were prepared by measuring the weight using an electronic balance (Citizen, model CX 220) with a precision range of ± 0.0001 g and stirred with a magnetic stirrer (Tarsons, digital spinot) for 30-60 min at 300 rpm. The samples were then stored in airtight tubes to avoid contamination and evaporation. The density and viscosity measurements were done immediately after sample preparation. A sufficient quantity of the mixture (~0.5-1 mL) was added with a micropipette on the base of the rheometer to avoid sample underfill errors. The viscosity of samples was measured in triplicates at a shear rate of 50 s^{-1}. A small volume (~1-2 mL) of the sample was injected into the tube using a syringe. The density values were measured thrice with a repeatability of 0.1 kg m^{-3}. The temperature of the sample was varied from 25-60°C while measuring density.

3.3.2 Groundwater sample collection from arsenic prone areas

A groundwater sample was obtained from a school located in the Kobla Chak region of Purbasthali - I, Madhya Srirampur, in the Purba Bardhaman district of West Bengal.

This sample has been referred to as "WB1" in the rest of the thesis. Prior testing of local water samples had indicated the presence of arsenic in the water sample collected from the school, so the students and staff refrained from drinking water from the hand pump at that location. The second groundwater sample was taken from a private hand pump near Canning Road, Ramnagar in Baruipur, which is situated in the South 24 Parganas district of West Bengal. This hand pump was recently constructed and is utilized on a daily basis by the family. This groundwater samples are referred to as "WB2" in this thesis. Third groundwater sample was collected from a private well that is being used daily by the family residing near Bamungaon in Jorhat. This is referred to as "AS1" in this thesis. Fourth groundwater sample was collected from a well in Mariani, near Kenedy Park close to a temple. This is referred to as "AS2" in this thesis. The fifth groundwater sample was collected from a private well near Bogagaon in Titabor. This is referred to as "AS3" in this thesis.

Clean, acid-resistant polyethylene bottles were used to directly collect groundwater samples, and clean gloves made of inert materials were worn during the collection process. Gloves were replaced between sampling locations to prevent cross-contamination. To preserve the water samples for transportation and experimentation, 3 ml of 6M HCl per liter of sample was added. The collected groundwater samples were sealed in the bottles to avoid cross-contamination and transported in dark boxes to avoid exposure to direct sunlight. The bottles were not placed on or near uncovered ground, vehicle exhaust, or contaminated areas before or after the collection to prevent cross-contamination. These groundwater samples were utilized as the feed phase in the experiments.

3.3.3 Two-phase equilibrium study

The aqueous feed phase was synthesized by diluting the stock solution to make 100 ppb concentration of $As^{(III)}$, $As^{(V)}$and combined $As^{(III)}$-$As^{(V)}$solutions in three different ratios of $As^{(III)}$:$As^{(V)}$:: 1 : 1 , $As^{(III)}$:$As^{(V)}$:: 1 : 2 and $As^{(III)}$:$As^{(V)}$:: 2 : 1 . The organic phase was prepared by dissolving the desired amount of extractant in the required amount of environmentally benign diluent (vegetable oil). An equal volume (20ml each) of feed and organic phases were poured cautiously into a conical flask without forming any emulsions. This was placed in the shaking incubator for mixing at a particular stirring rate for the said duration as shown in Fig. 3.1. The mixture was then kept

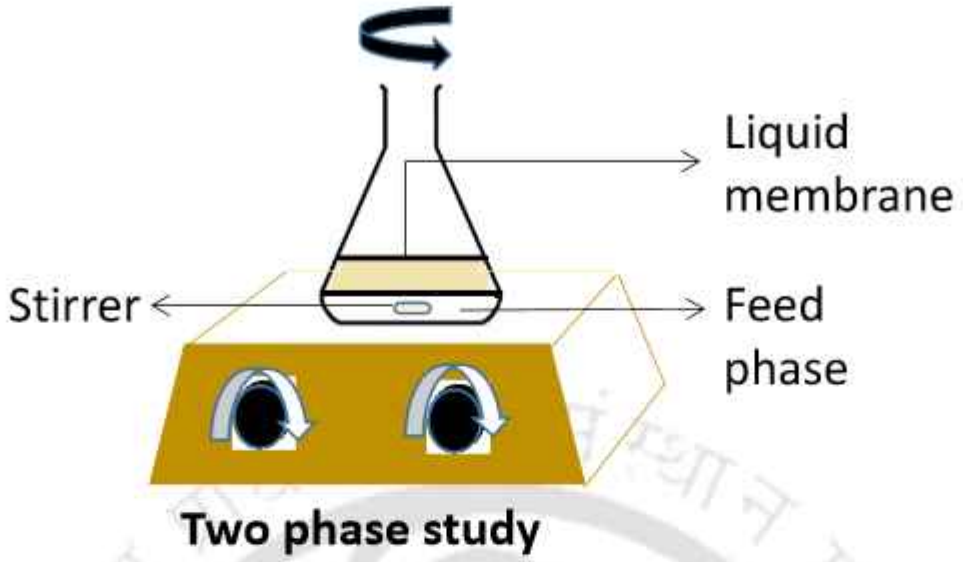

FIGURE 3.1: Two-phase experimental study

undisturbed for 8 hours until the aqueous and organic phases were separated into two distinct layers due to the variation in their densities. The samples were collected from the aqueous phase to analyze the total concentration of arsenic ions by AAS. The amount of arsenic ions extracted into the organic phase was calculated by mass balance. Based on the optimum conditions obtained, the two-phase study was conducted (in triplicate) by varying the extractant concentration to evaluate the distribution coefficient in order to estimate the extraction equilibrium constant.

3.3.4 Three-phase FSSLM study

The experimental setup as shown in Fig. 3.2 comprised of two cells, an extension connecting the cells and supporting the membrane in between them. The membrane phase was prepared by completely immersing the laminar microporous polyvinylidene fluoride (PVDF) membrane into the pseudo-binary mixture of sesame oil and Aliquat® 336 (v/v) (a.k.a. liquid membrane) for 24 hours. After the pores of the membrane were filled, it was allowed to dry for 2 hours to drip off the excess liquid from the surface of the solid membrane. The excess liquid on the surface was wiped off gently with a tissue. This solid membrane impregnated with the organic mixture acted as the SLM. The SLM was carefully placed between two membrane discs with latex support to prevent any leakage. An equal volume of feed and receiving phases were poured into the setup.

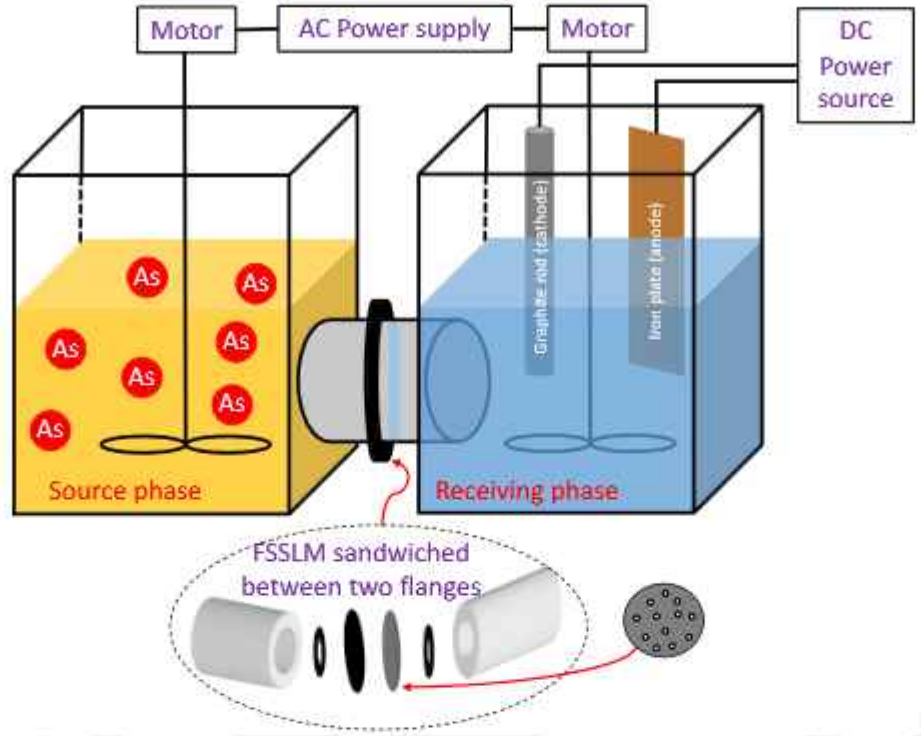

(A) Schematic

(B) Actual

FIGURE 3.2: Experimental setup for three-phase FSSLM and hybrid technique

The volume of the aqueous phases was 200 ml. In addition, to avoid the influence of residence interface films, two impellers (Make-REMI Model-RQG 121/D) in both the feed and receiving phases were kept in the center of the SLM cells for continuous stirring without touching the walls of the setup.

In case of hybrid SLM-electrocoagulation process, a sacrificial iron plate is used as the

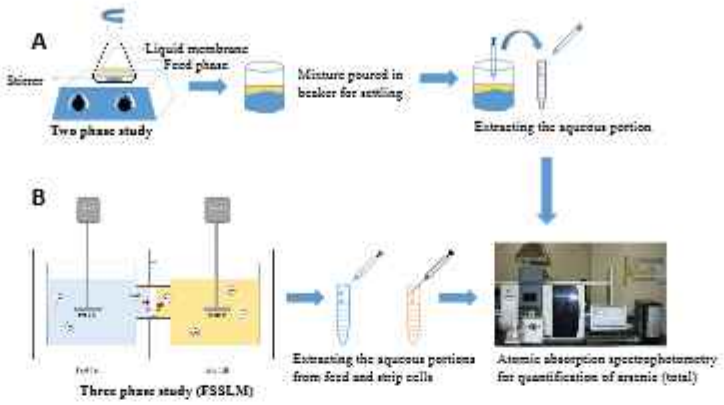

FIGURE 3.3: Experimental procedure followed for quantification of arsenic.

anode due to its reactive nature with arsenic while a graphite rod has been used as cathode. Graphite rod doesn't easily react with the hydrogen gas evolved at the cathode. Further, the structural properties of graphite enables it to be a good conductor so it is used as the cathode. They are connected to a DC power supply and placed inside the receiving phase cell of the SLM apparatus. The electroplating accessories are removed during simple SLM experimentations without electrocoagulation.

To ensure that the setup is leak proof, a test was done with colored water prior to the three phase experimentation. Stability of SLM setup was observed to be 120 hours. Samples were drawn from the feed and receiving phases at specific time intervals and analyzed to measure the concentrations of arsenic ions in AAS. Further experiments were conducted with the optimized conditions to determine the permeation coefficient and transport percentage.

The experimental procedure for quantification of arsenic in two and three phase studies is illustrated in Fig. 3.3.

3.4 Design of experiment

The response surface methodology (RSM) incorporates a randomly designed group of experiments by varying the parameters simultaneously to generate an empirical model for optimization. This increases the efficiency by doing the least amount of experiments

for optimization. Design expert® 13 was used in this thesis work for designing the experiments, plotting the figures, and optimization. The number of experiments in this design was determined by the following:

$$N = 2^x + 2x + c \tag{3.1}$$

where N is the total number of experimental runs, x is the number of parameters being optimized, c is the number of center points, 2^x determines the number of factorial runs and $2x$ gives the number of axial points.

It is revealed from elsewhere[94, 100, 271] that the extraction in two-phase equilibrium depends mainly on 5 parameters viz.

A: pH of the feed phase

B: %Extractant concentration (vol/vol)

C: Duration (hours)

D: Temperature (°C)

E: Stirring speed (rpm)

The parameters studied and their operational range for both the arsenic ions are listed in Table 3.2. Hence, in this study, face-centered design of central composite design has been used to conduct 50 experiments each for $As^{(III)}$, $As^{(V)}$, $As^{(III)}$:$As^{(V)}$:: 1 : 1 , $As^{(III)}$:$As^{(V)}$:: 1 : 2 , $As^{(III)}$:$As^{(V)}$:: 2 : 1 , that comprised of $2^5 = 32$ factorial runs, $2 \times 5 = 10$ axial points and 8 centre points, by varying following above 5 parameters to detect the optimum level for maximum extraction of arsenic ions.

In a similar manner the extraction and recovery in three-phase SLM depends mainly on 3 parameters viz.

F: Concentration of receiving phase

G: pH of the receiving phase

H1: Stirring speed (rpm) or

H2: Extractant concentration (%)

It would further be revealed from hybrid study of SLM and electrocoagulation in Chapter 7 (and published elsewhere [218]) that the optimum extractant concentration was obtained for individual arsenic ions in the three-phase SLM study. Assuming that the same concentration would not apply to the combined arsenic study, the extractant concentration (**H2**) was varied in those cases instead of stirring speed (**H1**). Further, in most of the experiments conducted, the extractant concentration has turned out to be a significant parameter. The parameters studied and their operational range for both the arsenic ions are listed in Table 3.2.

TABLE 3.2: Summary of variable range studied for optimization

Type	Factor	Name	Min.	Max.	Mean
Two phase	A	pH of feed phase	4	10	7
	B	Extractant concentration (%)	2	10	6
	C	Duration (hours)	2	12	7
	D	Temperature (°C)	25	55	40
	E	Stirrer speed (rpm)	50	250	150
Three phase	F	Concentration of receiving phase (ppm)	1	3	2
	G	pH of receiving phase	3	7	5
	H1	Stirrer speed (rpm)	200	300	250
	H2	Extractant concentration (%)	10	40	25

Hence, in this study, face-centered design of central composite design has been used to conduct 15 experiments each for $As^{(III)}$, $As^{(V)}$, $As^{(III)}$:$As^{(V)}$:: 1 : 1 , $As^{(III)}$:$As^{(V)}$:: 1 : 2 , $As^{(III)}$:$As^{(V)}$:: 2 : 1 , that comprised of $2^3 = 8$ factorial runs, $2 \times 3 = 6$ axial points and 1 centre point, by varying following above 3 parameters to detect the optimum level for maximum extraction and recovery of arsenic ions.

3.5 Statistical and machine learning based analysis

In two-phase equilibrium studies, there were five independent variables and one dependent variable for all the single and mixed arsenic species. The independent variables were further subdivided into three levels based on their range. The mean, median, variance, standard deviation, range, interquartile range, skewness, and kurtosis were calculated

for each level of the independent variables for the dependent variable from the descriptive analysis. Kolmogorov-Smirnov and Shapiro-Wilk models were used to assess the normality of the data. Based on the normality test, correlational analysis was performed to find the relationship between the independent and dependent variables. Then, a five-way analysis of variance (ANOVA) test was carried out to find the differences between five independent variables with respect to one dependent variable.

In three phase SLM study, there are three independent variables namely, the concentration of receiving phase, pH of receiving phase, and stirring speed for $As^{(III)}$, $As^{(V)}$and extractant concentration for three different ratios of combined $As^{(III)}$-$As^{(V)}$. Each of the independent variables had three levels. The extraction and recovery (%) of arsenic ions were the dependent variables. From the descriptive analysis, the mean, median, variance, standard deviation, range, interquartile range, skewness, and kurtosis were obtained for each level of the independent variables with respect to the dependent variables. Then the test for normality was done using two models, Kolmogorov-Smirnov and Shapiro-Wilk. On the basis of the normality test, Pearson correlation analysis was performed to find the relationship between the independent and dependent variables. Multivariate Analysis of Variance (MANOVA) test was done for analyzing differences between groups as there were two dependent variables and three independent variables. The multivariate analysis predicted the individual or combined significant effect of independent variables on the dependent variables. On the basis of the significant main effect, the tests of between-subjects effects were investigated. This indicated the impact of individual or combined independent variables on each dependent variable. Then the post hoc Tukey test was carried out to further understand the significant main effect.

The machine learning toolbox in MATLAB offers a comprehensive set of tools that were effectively employed for modeling and optimizing LM process based on experimental results. MATLAB's rich library of machine learning algorithms, including regression, classification, clustering, and ensemble methods, were used to develop reasonably accurate models that capture the intricate relationships within experimental data. The toolbox facilitates the preprocessing of data, feature selection, and model evaluation. For optimization, MATLAB provides optimization algorithms that can be seamlessly integrated with machine learning models. By leveraging this toolbox, parameter tuning and optimization were conducted to identify the optimal conditions for a given process,

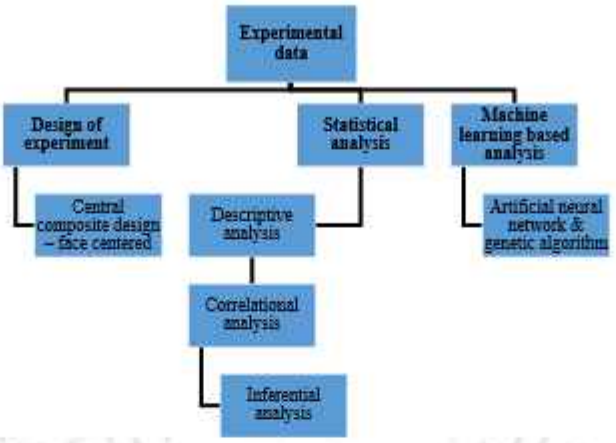

FIGURE 3.4: Data optimization approaches followed in two and three phase studies.

maximizing efficiency or minimizing costs. The scheme followed for data optimization in two and three phase studies is as given in Fig. 3.4.

Summary of Materials & Methods

- This chapter details chemicals and instruments used in experiments.
- The sources of materials, experimental procedures, and characterization techniques are described here.
- The information on the procurement of materials and their sources are provided.
- A comprehensive description of the experimental procedures employed are included with an outline of the FSSLM setup used for three-phase and hybrid studies.
- The characterization techniques applied during the experiments are highlighted.

Abbreviation

ANN Artificial neural network

ANOVA Analysis of variance

FCCCD Face-centered central composite design

FSSLM Flat sheet supported liquid membrane

GA Genetic algorithm

MANOVA Multiple analysis of variance

ML Machine learning

MSE Mean squared error

RSM Response surface methodology

VGA Vapor generation mode

Nomenclature

$\Psi(\cdot)$ Functions which mimic neurons

u_i Inputs

ω_i Assigned weight

b_i Bias

m Number of input datasets

n Number of output nodes

y_e Experimental output values

y_p Predicted output values

Chapter 4

Properties of liquid membrane

This chapter outlines the molecular interactions and transport properties of a pseudo-binary mixture of sesame oil and Aliquat® 336 by determining the surface tension (at 25°C), density, and viscosity over a temperature range of 25°C – 60°C under atmospheric pressure. The obtained viscosity data were fitted into the Vogel-Fulcher-Tammann equation [219], Gruenberg-Nissan equation [224, 225], and an equation proposed by Hind et al. [226]. An empirical relation given by Parthasarathy and Bakshi [227] was validated on the experimental data of density. The Jouyban-Acree model [138, 223] was used to correlate both viscosity and density data. Data on excess molar volume and viscosity deviation derived from the density and viscosity of mixtures led to an understanding of solute-solvent interactions. The surface tension of the mixture was validated by a modified ideal mixing rule equation. The excess properties were fitted into the Redlich-Kister polynomial equation [232]. Further, the volumetric thermal expansion coefficient, excess Gibbs free energy, change in enthalpy of mixing, and entropy of activation of the liquids were calculated. Analysis of FTIR studies further illustrated the intermolecular interactions in this pseudo-binary mixture.

4.1 Viscosity and viscosity deviation

The experimental data of viscosity (η) and the derived viscosity deviation ($\Delta\eta$) of the pseudo-binary mixture (comprising of sesame oil and Aliquat® 336) are reported in Table 4.1.

TABLE 4.1: Viscosity and viscosity deviation of pseudo-binary mixture for varying mole fractions of extractant (x_e) at different temperature (T in ℃) range under atmospheric pressure

	η (Pa s)					$\Delta\eta$ (Pa s)				
T / x	25	30	40	50	60	25	30	40	50	60
0.000	0.039	0.031	0.022	0.016	0.012					
0.099	0.044	0.036	0.024	0.018	0.013	-0.095	-0.069	-0.035	-0.018	-0.010
0.189	0.050	0.041	0.028	0.020	0.015	-0.180	-0.130	-0.065	-0.034	-0.019
0.344	0.071	0.057	0.038	0.026	0.019	-0.315	-0.230	-0.113	-0.059	-0.032
0.473	0.103	0.081	0.051	0.034	0.024	-0.414	-0.302	-0.148	-0.076	-0.042
0.583	0.149	0.113	0.070	0.045	0.032	-0.478	-0.351	-0.170	-0.088	-0.047
0.677	0.207	0.161	0.097	0.060	0.040	-0.515	-0.372	-0.179	-0.092	-0.049
0.759	0.286	0.215	0.125	0.075	0.049	-0.519	-0.379	-0.181	-0.093	-0.050
0.830	0.363	0.275	0.152	0.090	0.062	-0.514	-0.372	-0.181	-0.093	-0.045
0.894	0.535	0.396	0.214	0.122	0.076	-0.405	-0.298	-0.143	-0.073	-0.038
0.950	0.709	0.527	0.278	0.156	0.095	-0.289	-0.209	-0.100	-0.050	-0.026
1.000	1.048	0.773	0.397	0.217	0.126					

Viscosity of pure extractant and solvent are plotted against temperature in Fig. 4.1a. Depending on the experimental viscosity data, pure sesame oil exhibits lower viscosity in comparison to pure Aliquat® 336. Viscosity of pseudo-binary mixture versus mole fraction of the extractant are given in Fig. 4.2. Viscosities of all the pure extractant and solvent as well as their mixture decrease with increase in temperature. The viscosity was measured at a shear rate of 50 s^{-1}($\sim$ 29 rpm $\sim$ 0.5 Hz). Its uncertainty in measurement is $\pm$0.05 m Pa s. As the temperature increases the kinetic energy of the molecules increases, thereby weakens the intermolecular interactions resulting in the

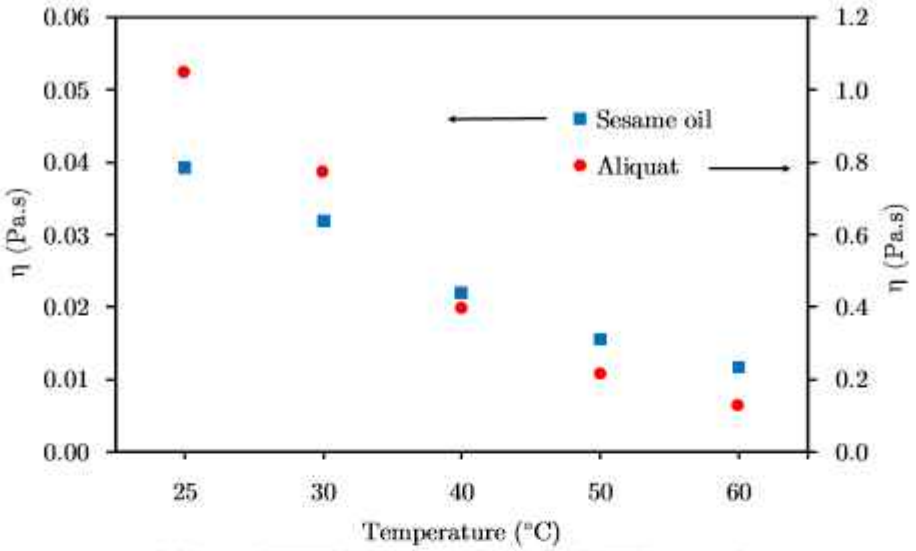

(A) Change in viscosity of pure liquids (extractants and solvents) with temperature

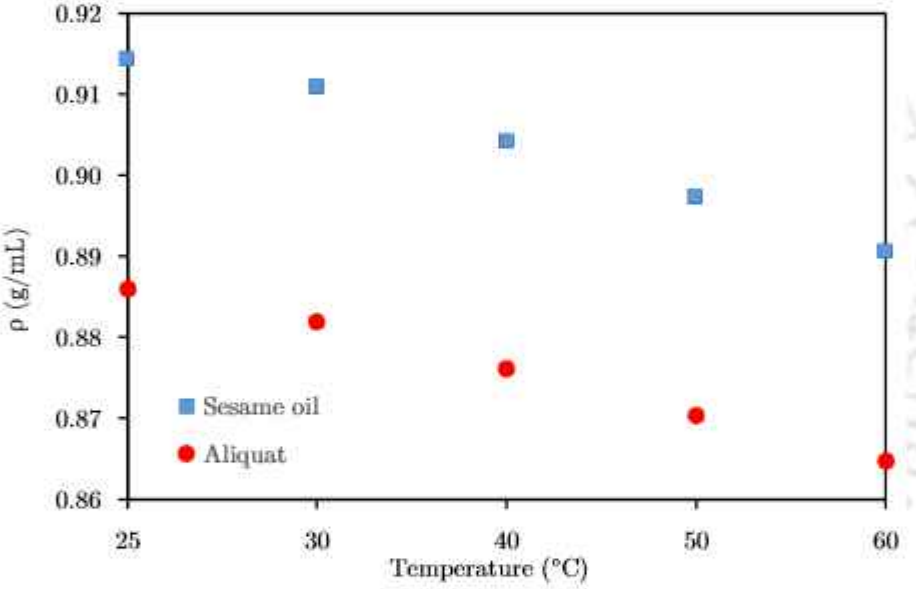

(B) Density variation with temperature for extractants

FIGURE 4.1: Variation of fluid properties with change in temperature

decrease of viscosity. The viscosity of pseudo-binary mixture increases with increase in mole fraction of Aliquat. Pseudo-binary mixture consists of sesame oil and Aliquat which is highly viscous. This is due to the size and nature of the molecules of Aliquat. The hydrocarbon chain in Aliquat is quite long which experiences van der Waals force of interactions [122]. Further, it behaves as a cationic surfactant that forms structural micelle aggregates [121]. This leads to the increase in viscosity with increase in concentration of Aliquat in pseudo-binary mixture. The experimental data of viscosity are correlated (vide Fig. 4.2) with VFT model (Eq. 2.1), Jouyban-Acree model (Eq. 2.2),

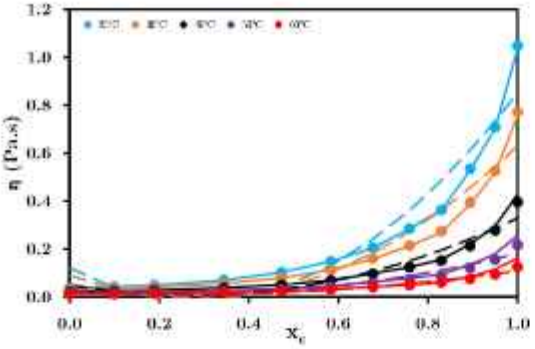

(A) The experimental values (indicated by markers) are fitted with VFT model[219] (solid lines) and the model developed by Hind et.al. [226] (broken lines)

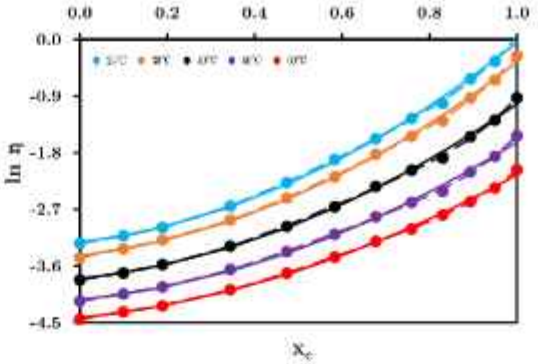

(B) The experimental values (indicated by markers) are fitted with Gruenberg-Nissan model [224, 225] (solid lines) and the Jouyban-Acree model [138, 223] (broken lines)

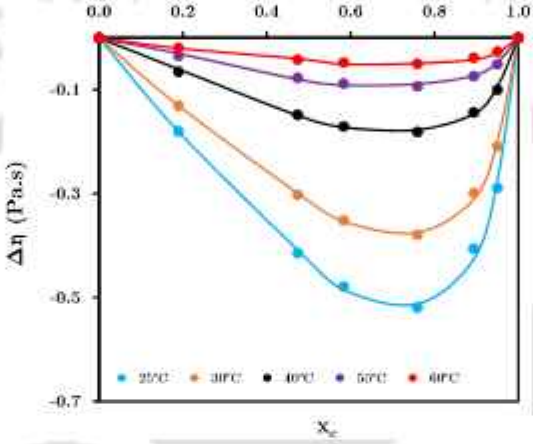

(C) The calculated values (vide Table 4.3) from experimental data (indicated by markers) are fitted with fourth order Redlich-Kister polynomial equation[232] (solid lines)

FIGURE 4.2: Viscosity/Deviation of viscosity of pseudo-binary mixtures with mole fraction over a temperature range of 25 to 60 °C

Gruenberg-Nissan model (Eq. 2.3) and the model (Eq. 2.4) proposed by Hind et al. [226]. VFT model fits well with standard deviation in the range of 0.115 - 0.291 (vide Table 4.2).

TABLE 4.2: Parameters to VFT model and standard deviation of experimetal data of viscosity of pure components

Extractants/Solvents	Parameters of VFT model			σ
	A_η	B_η	C_η	
Aliquat	4.32×10^{-5}	1573	-131	0.291
Sesame oil	0.0006	411.6	-75.6	0.115

As viscosity increases in a non-linear manner in mixture, the model proposed by Hind et al.[226] does not fit well. Standard deviation is quite high for this model (σ_{max} =

0.914) as compared to other models used for correlation of the experimental data (vide Table 4.6).

As the number of parameters increases, the model fits well with the experimental data as is evident in the Jouyban-Acree model ($\sigma_{max} = 0.049$ from Table 4.6). The G_{cs} parameter of the Gruenberg-Nissan model throws some important insights into the molecular interactions in the mixtures. The negative G_{cs} values indicate interactions caused by van der Waals force of attraction in mixture [225].

When a solution or mixture is produced by mixing an extractant and a solvent, it deviates from the ideal behaviour of the pure components. This deviation can be understood in terms of molecular interactions and their effect on viscosity. In a pure fluid, molecules are generally in a state of equilibrium, where they experience balanced forces from neighbouring molecules. When the fluid flows, molecules move from these equilibrium positions. Viscosity is a measure of a fluid's resistance to deformation or flow. It reflects how much internal friction exists when molecules move past each other. In mixture, these movements of molecules are strongly affected by intermolecular forces viz, dipole-dipole interactions, hydrogen bonding and van der Waals forces, that causes deviation in viscosity, $\Delta\eta$, which is computed using Eq. 2.5. Fig. 4.2 show that the deviation in viscosity increases with temperature. Furthermore, $\Delta\eta$ is always negative for mixture. A negative value of $\Delta\eta$ indicates a strong intermolecular interaction between Aliquat and sesame oil (Fig. 4.2). On the other hand, a shift in the value of $\Delta\eta$ from negative to positive indicates that after a certain limit (mole fraction of the extractant) the interactions between the molecules of the extractant and solvent changes to being repulsive in nature. The RKP function (Eq. 2.22) demonstrates a good fit (vide Fig. 4.2) for $\Delta\eta$ with standard deviation in the range of 0.034 - 0.097 (vide Table 4.3).

Trend of $\Delta\eta$ depends on the size, shape and intermolecular interactions of the components in the mixture. A negative trend in $\Delta\eta$ is attributed to the van der Waals interactions. This validates the strong ionic interactions in mixture that shows a negative trend in $\Delta\eta$ values. The dipole moment of Aliquat is as high as 26.63 D (i.e. debye, a unit used to express electric dipole moments of molecules. 1 D = 3.336×10^{-30}

coulomb metre) [272] that results in strong dipole-dipole interactions with the triglyceride molecules of sesame oil in mixture. The values of $\Delta\eta$ is optimum at $x_{\text{Aliquat}} \approx 0.75$, irrespective of the change in temperature.

TABLE 4.3: Coefficients of RKP function developed for viscosity deviation , $\Delta\eta = x_c(1 - x_c)\left\{a_0 + a_1(2x_c - 1) + a_2(2x_c - 1)^2 + a_3(2x_c - 1)^3 + a_4(2x_c - 1)^4\right\}$ of pseudo-binary mixture and their standard deviation, σ

Temp (℃)	a_0	a_1	a_2	a_3	a_4	σ
25	-1.726	-1.658	0.386	-0.067	-4.316	0.041
30	-1.261	-1.172	0.205	-0.179	-2.934	0.034
40	-0.626	-0.505	0.176	-0.220	-1.345	0.055
50	-0.334	-0.266	0.210	-0.067	-0.831	0.087
60	-0.173	-0.246	0.215	0.265	-0.869	0.097

$\Delta\eta$ values become less negative with rise in temperature due to the reduction of intermolecular interactions caused by collisions of molecules caused by increase in kinetic energy. The increase in temperature breaks the existing bonds to form new intermolecular interactions as is evident from the fall in positive trend of the $\Delta\eta$ values. The uncertainties in the viscosity deviation has been shown in the Table 4.4.

TABLE 4.4: Uncertainty in the derived properties

Derived properties	Deviations in pseudo-binary mixtures
Viscosity deviation	0.060
Excess molar volume	0.110
Surface tension deviation	0.110
Deviation in ultrasonic velocity	0.001
Deviation in acoustic impedance	0.090

4.2 Density and excess molar volume

The measured data of density and calculated values of excess molar volume of pseudo-binary mixture are given in Table 4.7. The variation in the data of experimental density for all the pure extractant and solvent with temperature is reported in Fig. 4.1b.

TABLE 4.5: Thermal expansion coefficient, $\alpha \times 10^4$ (in $^{\circ}C^{-1}$), of the pseudo-binary mixture

T	x_c											
	0.000	0.099	0.189	0.344	0.473	0.583	0.677	0.759	0.830	0.894	0.950	1.000
30	7.003	7.215	7.277	7.263	7.231	7.136	7.153	6.660	7.062	6.929	6.882	6.298
40	7.517	7.490	7.330	7.346	7.325	7.195	7.182	7.101	7.044	7.023	7.010	6.563
50	7.596	7.457	7.546	7.182	7.349	7.341	7.222	7.163	7.105	6.981	6.921	6.641
60	7.541	7.475	7.456	7.616	7.361	7.320	7.240	7.181	7.144	6.995	7.000	6.406

TABLE 4.6: Coefficients of models for fitting data of viscosity of pseudo-binary mixture and their standard deviations in the temperature range of 25-60°C at atmospheric pressure

Temp (°C)	Jouyban-Acree							Gruenberg-Nissan		Hind et al.[226]	
	$A_{\eta,1}$	$A_{\eta,2}$	$A_{\eta,3}$	$A_{\eta,4}$	$A_{\eta,5}$	$A_{\eta,6}$	σ	G_{cs}	σ	H_{cs}	σ
25	0.043	-3.238	-2.334	-0.043	-1.122	-1.418	0.049	-2.33	0.664	-0.368	0.914
30	-0.262	-3.467	-2.269	-0.149	-0.881	-1.591	0.021	-2.27	0.131	-0.262	0.837
40	-0.929	-3.823	-2.027	-0.069	-1.055	-1.569	0.014	-2.024	0.041	-0.114	0.577
50	-1.531	-4.161	-1.806	-0.158	-1.051	-1.566	0.009	-1.808	0.028	-0.051	0.427
60	-2.078	-4.441	-1.557	-0.032	-0.768	-1.27	0.004	-1.553	0.016	-0.021	0.287

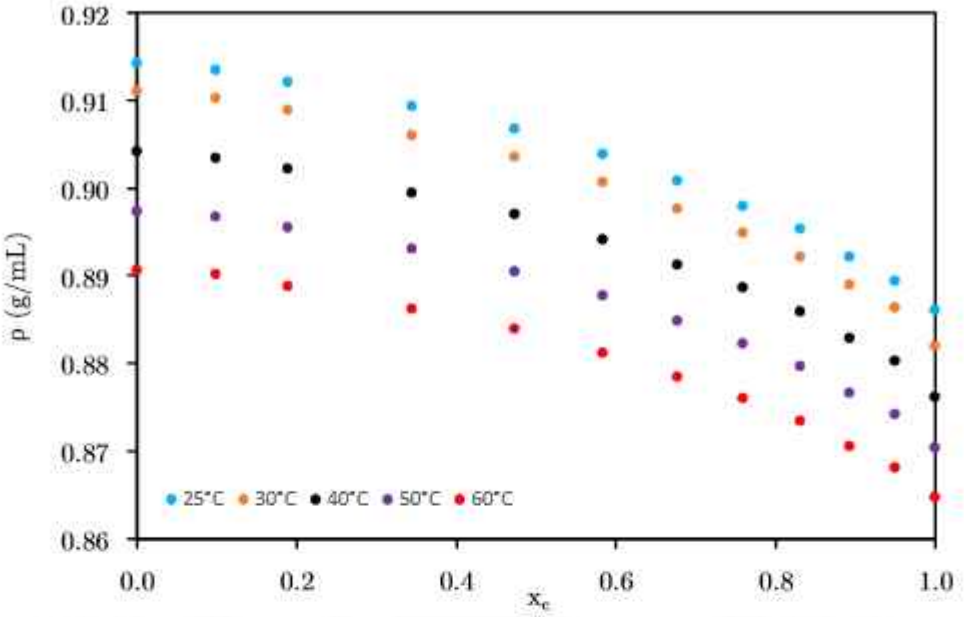

FIGURE 4.3: Density of pseudo-binary mixture at different mole fractions of extractants and temperatures

The uncertainty in the measurement of density is ± 0.001 g cm^{-3}. As the temperature increases, the kinetic energy of the molecules increase that leads to an increase in the collision between the molecules. This in turn increases the intermolecular spaces in the mixture leading to a decrease in density. The densities of all the extractant and solvent decrease with increase in temperature. The change in density of the pseudo-binary mixture with temperature and mole fraction is given in Fig. 4.3.

TABLE 4.7: Density and excess molar volume of pseudo-binary mixture for varying mole fractions of extractants (x_c) at different temperature (T in °C) under atmospheric pressure

	ρ(g cm^3)					V^E(cm^3 mol^{-1})				
T / x_c	25	30	40	50	60	25	30	40	50	60
0.000	0.914	0.911	0.904	0.897	0.891					
0.099	0.913	0.910	0.903	0.897	0.890	-0.876	-0.659	-0.847	-1.121	-0.420
0.189	0.912	0.909	0.902	0.895	0.889	-0.919	-0.740	-1.015	-1.163	-0.471
0.344	0.909	0.906	0.899	0.893	0.886	-0.985	-0.824	-0.995	-1.339	-0.509
0.473	0.907	0.904	0.897	0.890	0.884	-1.075	-1.120	-1.231	-1.366	-0.716
0.583	0.904	0.901	0.894	0.888	0.881	-0.883	-1.037	-1.165	-1.235	-0.596
0.677	0.901	0.898	0.891	0.885	0.878	-0.660	-0.874	-0.946	-1.027	-0.421

Continued on the next page

Table 4.7 – continued from the previous page

	ρ(g cm^3)					V^E(cm^3 mol^{-1})				
T / x_c	25	30	40	50	60	25	30	40	50	60
0.759	0.898	0.895	0.889	0.882	0.876	-0.564	-0.975	-1.038	-1.097	-0.510
0.830	0.895	0.892	0.886	0.880	0.873	-0.454	-0.999	-1.043	-1.082	-0.497
0.894	0.892	0.889	0.883	0.877	0.871	-0.334	-0.754	-0.760	-0.812	-0.287
0.950	0.889	0.886	0.880	0.874	0.868	-0.276	-0.845	-0.815	-0.852	-0.307
1.000	0.886	0.882	0.876	0.870	0.865					

The density of mixture decreases with mole fraction of extractant because the density of Aliquat is less than sesame oil. At room temperature Aliquat is an ionic liquid [121, 273] that consists of quarternary ammonium cation and chloride anion.

As the concentration of Aliquat increases in the mixture, the number of ions increases as well. These cations and anions interact strongly with the fatty acids of vegetable oil but cause repulsion as well that reduces the density of the mixture. Further, the density decreases with increase in temperature. This is due to the fact that increase in temperature increases the kinetic energy causing the molecules to move apart. This increases the volume leading to expansion due to weak bonding. The empirical relation (Eq.(2.6) by Parthasarathy and Bakshi [227]) between viscosity and density has been fitted with the experimental values (vide Fig. 4.3, Table 4.8, Fig. 4.4a and Fig. 4.4b). The standard deviation lies in the range of 0.0021-0.0028. However, this model is not reliable as the viscosity of the mixture increases exponentially with concentration of extractants and the model fails at the higher concentration level. Nevertheless Jouyban-Acree model is reliable at all temperature and concentrations of extractant (vide Table 4.8 and Fig. 4.4). In fact Jouyban-Acree model fits better (σ in the range of 0.0036-0.0047) than the model proposed by Parthasarathy and Bakshi [227].

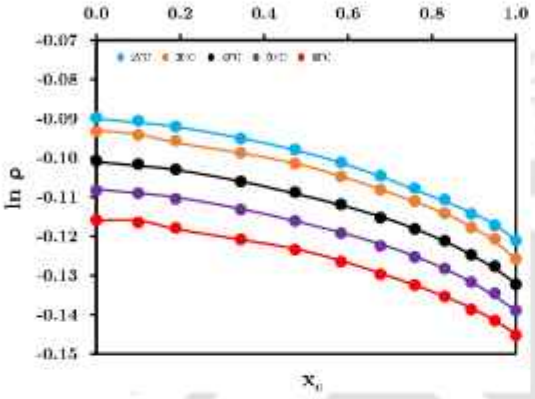

(A) The experimental data (indicated by markers) are fitted with Jouyban-Acree model [138, 223] (solid lines)

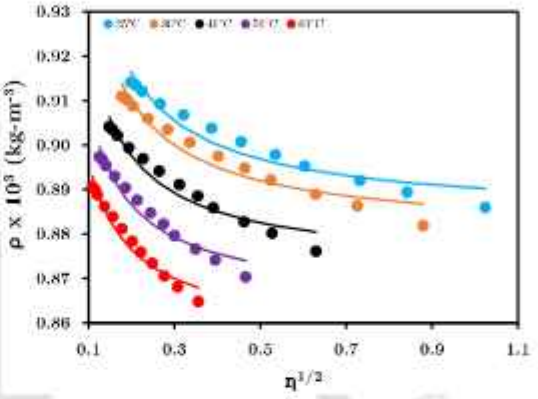

(B) The experimental data (indicated by markers) are fitted with model proposed by Parthasarathy and Bakshi [227] (solid lines)

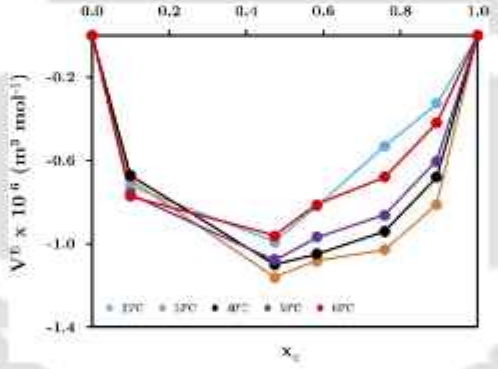

(C) The calculated values (vide Table 4.7) from experimental data (indicated by markers) are fitted with fourth order Redlich-Kister polynomial equation[232] (solid lines)

FIGURE 4.4: Density and excess molar volume of the pseudo-binary mixtures at diffrerent mole fractions of extractants within a temperature range of 25 to 60 °C .

TABLE 4.8: Coefficients of Jouyban-Acree model and a model proposed by Parthasarathy and Bakhshi[227] as fitted on the experimental data of density and viscosity of pseudo-binary mixture; including their standard deviations, σ

Temp (°C)	Jouyban-Acree									Parthasarathy-Bakshi		
	$A_{\rho,1}$	$A_{\rho,2}$	$A_{\rho,3}$	$A_{\rho,4}$	$A_{\rho,5}$	$A_{\rho,6}$	$A_{\rho,7}$	$A_{\rho,8}$	σ	A	B	σ
25	-0.121	-0.090	0.027	0.006	-0.005	-0.017	0.021	0.037	0.0047	0.884	0.0065	0.0027
30	-0.126	-0.093	0.029	0.010	-0.013	0.028	0.045	-0.028	0.0044	0.88	0.0060	0.0028
40	-0.132	-0.101	0.027	0.010	0.015	-0.004	-0.008	0.011	0.0043	0.872	0.0050	0.0026
50	-0.139	-0.108	0.027	0.010	0.015	-0.004	-0.008	0.011	0.0043	0.865	0.0044	0.0023
60	-0.145	-0.116	0.026	0.007	-0.018	0.016	0.049	-0.035	0.0036	0.857	0.0039	0.0021

There is no change in volume if ideal mixture is formed. However, real mixture undergoes either an increase or decrease in volume due to molecular interactions between components of mixture. Excess molar volume indicates the changes or differences in the pseudo-binary mixture and specific interactions between their components. The calculated values of V^E from experimental data of densities of pseudo-binary mixtures (vide Table 4.7) are fitted using the fourth order Redlich-Kister polynomial (RKP) function [274, 275] as given by Eq.(2.22) and are plotted in Fig. 4.4.

A positive trend in V^E depicts expansion of volume on mixing; thus repulsive interactions or weaker interactions act between the components of the mixture, whereas a negative V^E shows ionic interactions of molecules in the mixture stronger than individual components prior to mixing. V^E, similar to $\Delta\eta$, is negative for mixture as in Fig. 4.4. Sesame oil mainly consists of monosaturated oleic acid [276]. As the temperature increases, the molar volume of the components increases. The molar volume of sesame oil varies from 0.927 to 0.952 m^3kmol^{-1} with rise in temperature. As the molar volume increases, the expansion results in weakening of the intermolecular interactions.

The calculated data using RKP model (Eq. 2.22) is in good agreement with the experimental values with standard deviation in the range of 0.077-0.165 (vide Table 4.9).

TABLE 4.9: Coefficients of RKP function developed for excess molar volume, $V^E = x_c(1-x_c)\left\{a_0 + a_1(2x_c-1) + a_2(2x_c-1)^2 + a_3(2x_c-1)^3 + a_4(2x_c-1)^4\right\}$ of pseudo-binary mixture and their standard deviation, σ

Temp (°C)	a_0	a_1	a_2	a_3	a_4	σ
25	-3.811	2.890	-1.404	-0.110	-2.652	0.165
30	-4.553	1.596	-4.974	-3.476	-1.199	0.077
40	-4.358	0.833	-3.348	-1.120	-2.197	0.110
50	-4.197	2.218	-5.648	-1.433	0.844	0.103
60	-3.663	3.124	-6.764	-0.813	3.547	0.117

4.3 Surface tension

The chief constituent of sesame oil is triacylglycerides with long chain unsaturated hydrocarbons. The intramolecular hydrogen bonding between –O–H groups in triacylglycerides and van der Waals forces exerted by the long chain unsaturated hydrocarbon tail

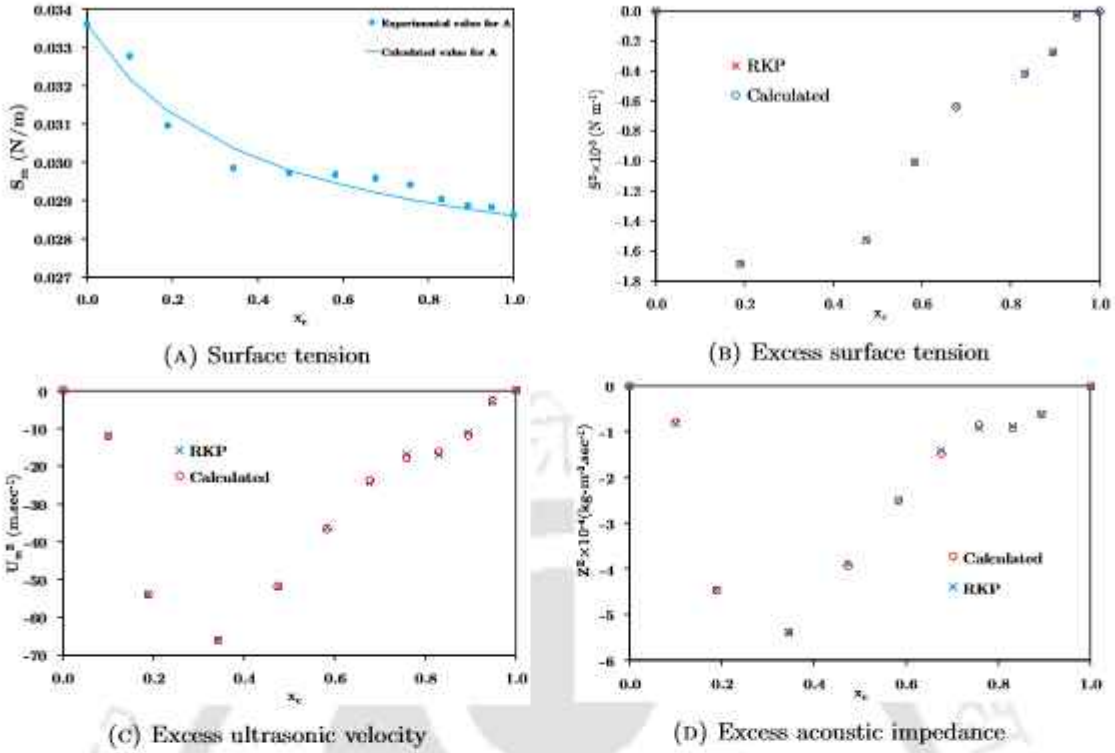

(A) Surface tension (B) Excess surface tension

(C) Excess ultrasonic velocity (D) Excess acoustic impedance

FIGURE 4.5: Various properties of pseudo-binary mixtures at 25 °C against mole fraction

leads to strong cohesive forces between the molecules of the oil. Hence, the surface tension of the oil is more than that of the extractant. If written in the increasing order, the surface tension of the pure components can be arranged in the following way –Aliquat 336<sesame oil [277, 278].

The surface tension was measured using Wilhelmy plate method whose accuracy is 0.1%. We have obtained an uncertainty of ± 0.001 m N m^{-1}. The surface tension of the mixture decreases with the increase in the concentration of the extractant. Aliquat has been used as surfactant and phase transfer catalyst by Dutta and Patil [279]. Being a cationic surfactant, Aliquat reduces the surface tension in mixture [122]. The decrease in surface tension with mole fraction of Aliquat in mixture is non-linear as seen in Fig. 4.5a.

The pure extractant, when added to the oil to form the solution, tend to disrupt the strong cohesive forces. The reduction in surface tension increases the surface area. This in turn favours the application of the pseudo-binary mixture in removal, extraction or separation of metals as more exposed surface area increases the scope of intermolecular interactions. In Table 4.10, the experimental values of viscosity, density and surface

tension are compared with the values obtained from various literatures and their average absolute deviation (AAD) values are also given.

TABLE 4.10: Comparison of experimental data of viscosity, density and surface tension of pure extractants and solvents with those in the published literature

Properties	Aliquat 336			Sesame oil		
	Expt.	Lit.	AAD	Expt.	Lit.	AAD
η (Pa s)	1.048	1.5020[122]	0.43	0.039	0.065 (293.15K)[280]	0.67
ρ (kg m^3)	886	887.5[122]	0.0017	914	914-919[281]	0.0055
S_m (mN m^{-1})	28.603	28[122]	0.021	33.58	30.29[277]	0.098

The surface tension of mixture (S_m) and its deviation (S^E) are given in Table 4.11.

TABLE 4.11: Surface tension and its deviation for all the pseudo-binary mixtures (BM) at 25℃

x_c	S_m (mN m^{-1})	S^E (mN m^{-1})
0.000	33.58	0.000
0.099	32.75	-0.338
0.189	30.95	-1.689
0.344	29.84	-2.033
0.473	29.70	-1.522
0.583	29.67	-1.013
0.677	29.57	-0.637
0.759	29.40	-0.407
0.830	29.03	-0.415
0.894	28.86	-0.274
0.950	28.82	-0.034
1.000	28.60	0.000

The RKP model (Eq. 2.22) is in good agreement with the experimental values with standard deviation of 0.11(vide Eq.(4.1)).

$$S^E = x_c(1-x_c)\{-5.61 + 9.44(2x_c-1) - 3.41(2x_c-1)^2 + 1.95(2x_c-1)^3 - 16.91(2x_c-1)^4 - 24.24(2x_c-1)^5 + 43.4(2x_c-1)^6\} \quad (4.1)$$

The uncertainties in the surface tension deviation has been shown in the Table 4.4.

4.4 Acoustic properties

The ultrasonic velocity, isentropic compressibility, intermolecular free length and acoustic impedance of the mixtures are derived from the Eqs. 2.11, 2.13, 2.16, and 2.19 respectively using the experimental values of surface tension and density as given in Table 4.12 and Fig. A.2.

TABLE 4.12: The calculated data for ultrasonic velocity, isentropic compressibility, intermolecular free length and acoustic impedance for all the pseudo-binary mixture

x_c	U_m (m sec^{-1})	K_s (Pa^{-1})	L_f (m)	Z (kg m^{-2} sec)
0.000	1498.98	4.87×10^{-10}	2.01×10^{-11}	1.37×10^{6}
0.099	1474.83	5.03×10^{-10}	2.05×10^{-11}	1.35×10^{6}
0.189	1421.79	5.42×10^{-10}	2.13×10^{-11}	1.30×10^{6}
0.344	1390.24	5.69×10^{-10}	2.18×10^{-11}	1.26×10^{6}
0.473	1388.65	5.72×10^{-10}	2.18×10^{-11}	1.26×10^{6}
0.583	1390.56	5.72×10^{-10}	2.18×10^{-11}	1.26×10^{6}
0.677	1390.78	5.74×10^{-10}	2.19×10^{-11}	1.25×10^{6}
0.759	1388.20	5.78×10^{-10}	2.19×10^{-11}	1.25×10^{6}
0.830	1379.37	5.87×10^{-10}	2.21×10^{-11}	1.23×10^{6}
0.894	1377.22	5.91×10^{-10}	2.22×10^{-11}	1.23×10^{6}
0.950	1378.65	5.92×10^{-10}	2.22×10^{-11}	1.23×10^{6}
1.000	1375.28	5.97×10^{-10}	2.23×10^{-11}	1.22×10^{6}

The ultrasonic velocity (speed of sound) is empirical and derived from the experimental values of surface tension and density at 25 °C . It is an approximation of the behavior and the correlation was developed considering the room temperature only (25 °C).

Surface tension is high in sesame oil due to strong cohesive forces (hydrogen bonding and van der Waals forces), which is reduced by the addition of the cationic surfactant, Aliquat 336. So, there is a decrease in surface tension with increasing mole fraction of Aliquat 336. The reduction in surface tension increases surface area, enhancing the mixture's effectiveness in applications involving metal removal, extraction, or separation. The ultrasonic velocity initially falls and then becomes nearly constant in mixture (vide Table 4.12). The initial decrease signifies the disruption of strong cohesive forces within the oil, leading to increased molecular mobility. The subsequent stabilization indicates a new equilibrium where the mixture's structure is stable, providing insights into the optimal conditions. The isentropic compressibility K_s increases gradually after $x_{\text{Aliquat}} = 0.4$ (vide Table 4.12). Isentropic compressibility measures a fluid's ability to be compressed under adiabatic conditions, inversely related to the fluid's bulk modulus. As the mole fraction of Aliquat 336 increases, isentropic compressibility also rises. At lower concentrations, Aliquat 336 disrupts the strong cohesive forces in sesame oil (such as hydrogen bonding and van der Waals interactions), increasing the free volume and molecular mobility. Around a mole fraction of 0.4, significant structural changes occur, creating a more open, less densely packed mixture. The weakened intermolecular forces make the mixture more compressible, marking a critical point where the surfactant's effects are most pronounced. The intermolecular free length versus mole fraction follows a similar trend with a gradual change as observed in Table 4.12. Intermolecular free length refers to the average distance between molecules in a fluid, influenced by intermolecular forces and molecular packing. As the mole fraction of Aliquat 336 increases, the cohesive forces in sesame oil weaken, leading to a gradual increase in intermolecular free length. Rather than causing a sudden disruption, Aliquat 336 slowly inserts itself between oil molecules, progressively altering the molecular arrangement. Each addition of Aliquat 336 results in a dynamic equilibrium with a new balance of forces. This controlled, gradual change in intermolecular free length allows for predictable modifications in fluid properties, which is crucial for precise applications. The acoustic impedence decreases with mole fraction of extractant (vide Table 4.12). Acoustic impedance measures the resistance an acoustic wave faces as it travels through a medium, determined by the product of the medium's density and sound speed. As the concentration of Aliquat 336

increases, acoustic impedance decreases. This cationic surfactant weakens intermolecular forces (e.g., hydrogen bonding and van der Waals forces) in sesame oil, increasing free volume and reducing density. The disruption also lowers the mixture's stiffness, decreasing sound speed. The combination of reduced density and sound speed leads to lower acoustic impedance, meaning the mixture becomes easier for sound waves to pass through-a key factor in applications like ultrasonic imaging.

Fig. 4.5b shows deviation in excess surface tension of the mixture against the concentration of extractant. The calculated values (vide Table 4.12) are fitted with sixth order Redlich-Kister polynomial equation. Mixture shows negative deviation. This is quite similar to the excess molar volume trend. The excess properties of the ultrasonic velocity, isentropic compressibility, intermolecular free length and acoustic impedance of the mixture are calculated and showed in Table 4.13.

TABLE 4.13: The deviation data for excess properties of ultrasonic velocity, isentropic compressibility, intermolecular free length and acoustic impedance for all the pseudo-binary mixture

x_c	U_m^E (m sec^{-1})	K_s^E (Pa^{-1})	L_f^E (m)	Z^E (kg m^{-2} sec)
0.099	-11.85	5.5×10^{-12}	1.2×10^{-13}	-8.01×10^{3}
0.189	-53.81	3.5×10^{-11}	7.1×10^{-13}	-4.48×10^{4}
0.344	-66.18	4.4×10^{-11}	8.9×10^{-13}	-5.39×10^{4}
0.473	-51.76	3.3×10^{-11}	6.7×10^{-13}	-3.92×10^{4}
0.583	-36.29	2.1×10^{-11}	4.4×10^{-13}	-2.50×10^{4}
0.677	-24.43	1.3×10^{-11}	2.7×10^{-13}	-1.47×10^{4}
0.759	-16.92	7.7×10^{-12}	1.7×10^{-13}	-8.65×10^{3}
0.830	-16.89	8.9×10^{-12}	1.8×10^{-13}	-9.27×10^{3}
0.894	-11.24	6.0×10^{-12}	1.2×10^{-13}	-6.09×10^{3}
0.950	-2.85	3.2×10^{-13}	1.1×10^{-14}	91.7

U_m^E shows negative deviation for mixture as shown in Fig. 4.5c. The calculated values (vide Table 4.12) are fitted with seventh order Redlich-Kister polynomial equation. As K_s and L_f are inversely proportional to the U_m, their excess deviation curves are opposite to that of U_m^E (vide Table 4.13). The positive deviation of L_f^E in mixture indicates that the intermolecular free length of the mixture increases compared to the free length of the individual pure components due to electrostatic repulsion or van der Waals forces.

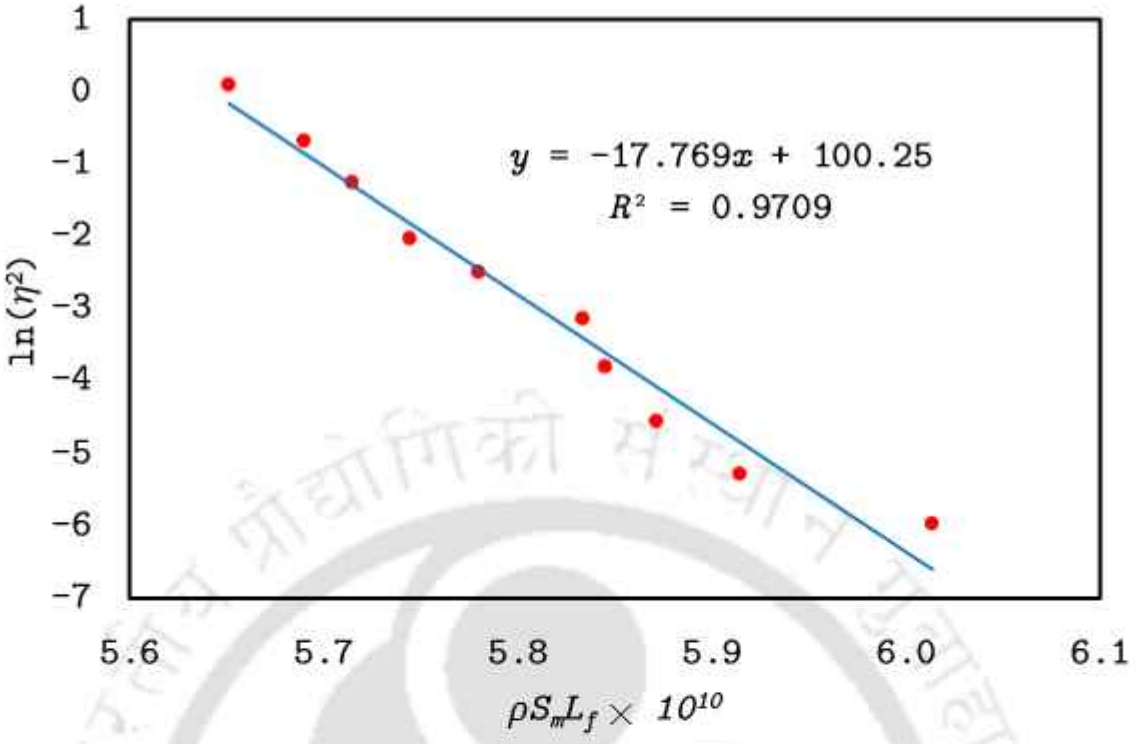

FIGURE 4.6: Graphical interpretation of the proposed model (Eq.(2.25))

The acoustic impedance is a product of density and ultrasonic velocity. Z^E is negative for mixture owing to fall in density and a very gradual change in ultrasonic velocity.

A new model is being proposed through Eq.(2.25) in this work relating the surface tension and intermolecular free length to the viscosity of the mixture at 25℃. As observed in Fig. 4.6, the data yield linear fit having R^2 value in the range of 0.9709 for pseudo-binary mixture.

A negative deviation in the pseudo-binary mixture indicates a decrease in viscosity with increase in intermolecular free length. The uncertainties of the deviation in ultrasonic velocity and acoustic impedance have been shown in the Table 4.4.

4.5 Apparent molar volume

Apparent molar volume shows the change in the property of the pseudo-binary mixture when the extractant is added to the solvent on a molar basis, and it is usually less than the molar volume. The apparent molar volume of pseudo-binary mixture at different temperature has been calculated and reported in Table 4.14.

TABLE 4.14: Apparent molar volumes of pseudo-binary mixture at atmospheric pressure

	$V_{\phi 1}$ (cm^3 mol^{-1})					$V_{\phi 2}$ (cm^3 mol^{-1})				
x \ T	25	30	40	50	60	25	30	40	50	60
0.000						928	931	938	945	952
0.099	449	452	453	453	463	927	930	937	944	951
0.189	452	454	456	458	465	927	930	937	944	951
0.344	454	456	458	461	466	926	930	937	943	951
0.473	454	456	459	462	466	926	929	936	943	950
0.583	455	456	459	462	466	926	928	935	942	950
0.677	455	457	460	463	467	926	928	935	942	950
0.759	455	457	460	463	467	925	927	934	941	950
0.830	455	457	460	463	467	924	925	932	939	949
0.894	456	457	461	464	467	925	924	931	938	949
0.950	456	457	461	464	467	920	914	922	928	946
1.000	456	458	461	464	467					

The change in apparent molar volume of the mixture is almost constant with increase in mole fraction for the extractant. This indicates that the intermolecular and intramolecular interactions occur as the concentration of the extractant increases. Table 4.13 shows the apparent molar volume of the pseudo-binary mixture at 25°C .

4.6 Thermal expansion coefficient

The thermal expansion coefficient (α) is a measure of how much a material's volume changes with a change in temperature as given by Eq.(2.28). The Table 4.5 lists the values of α for the pseudo-binary mixture being studied. The value of the thermal expansion coefficient decreases as bond energy increases. This means that materials with stronger intermolecular bonds will have lower thermal expansion coefficients. Sesame oil has the highest thermal expansion coefficient (0.0008) compared to Aliquat 336 (0.0007),

as the temperature changes from 30°C to 60°C under atmospheric pressure. An increasing trend in α values indicates that the bonding between molecules in the pseudo-binary mixture becomes weaker, allowing for greater expansion. While a decreasing trend in the values of α suggests that the intermolecular forces in the mixture are stronger than in the pure solvent and extractant. In other words, when the components are mixed, the interactions between different molecules result in a mixture that expands less compared to the pure substances.

TABLE 4.15: Excess Gibbs' free energy (ΔG^{*E}) of the pseudo-binary mixture

x_e \ T	25	30	40	50	60
0.1	349	431	414	467	564
0.2	376	498	542	609	726
0.3	402	488	605	744	922
0.5	406	462	598	758	959
0.6	400	393	545	700	931
0.7	315	398	545	642	859
0.8	242	246	383	461	636
0.9	113	98	142	183	314

4.7 Excess Gibbs energy, enthalpy and entropy

As observed in Fig. 4.7 and Table 4.15, excess Gibbs' free energy for the pseudo-binary mixture increases with temperature. However it increases upto a certain point and then decreases with increase in concentration of the extractant. A positive excess Gibbs' free energy means the pure components are unable to mix well while a negative excess Gibbs' free energy indicates that there is a driving force for mixing to occur. Therefore, as the concentration of extractant increases the strong intermolecular interactions in the mixture causes a negative deviation of excess Gibbs' free energy. The excess Gibbs' free energy increases with temperature as the interactions between the components weaken with the rise in temperature. Initially as the concentration of the extractant increase, repulsive forces dominate the intermolecular interactions causing the positive deviation.

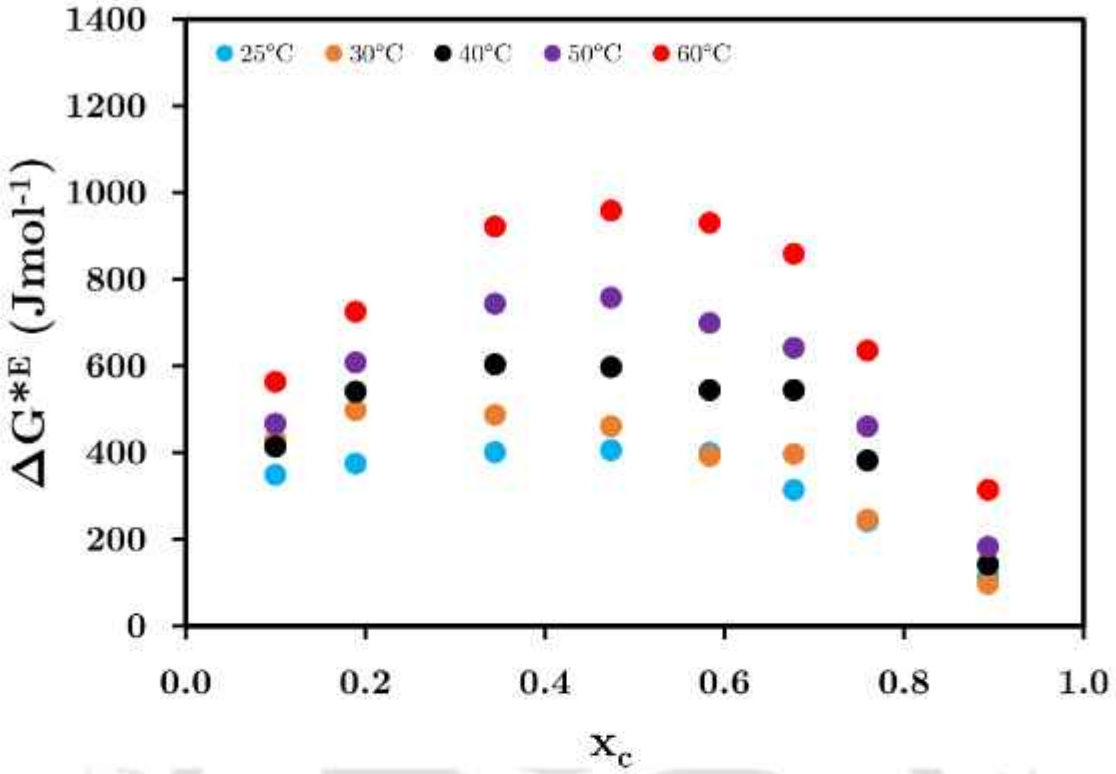

FIGURE 4.7: Excess Gibbs' free energy of pseudo-binary mixture with mole fraction over the temperature range of 25 to 60 °C

However, beyond a certain mole fraction, there is a negative deviation observed due to the strong inter and intra molecular interactions occurring with the increase in concentration of the extractant in the pseudo-binary mixture.

Changes in enthalpy (ΔH) and entropy (ΔS) can be obtained by plotting the left hand side of Eq.(2.31) against T^{-1} for pseudo-binary mixture.

As the graphs are linear (vide Fig. 4.8), the slope is the value of ΔH while the intercept is the value of ΔS. The enthalpy of the pseudo-binary mixture increases while the entropy of the mixture decreases with mole fraction as shown in Fig. 4.8.

A positive deviation in enthalpy indicates that heat is absorbed upon mixing (endothermic) while a negative trend in entropy indicates that the components of the mixture form a strong bond which is difficult to dissociate. As a result of the interactions, the extractant in the pseudo-binary mixture gets immobilized to the organic phase and does not easily dissociate into the aqueous phase as evident from the trends of ΔH and ΔS; thus, finding its application as liquid membrane.

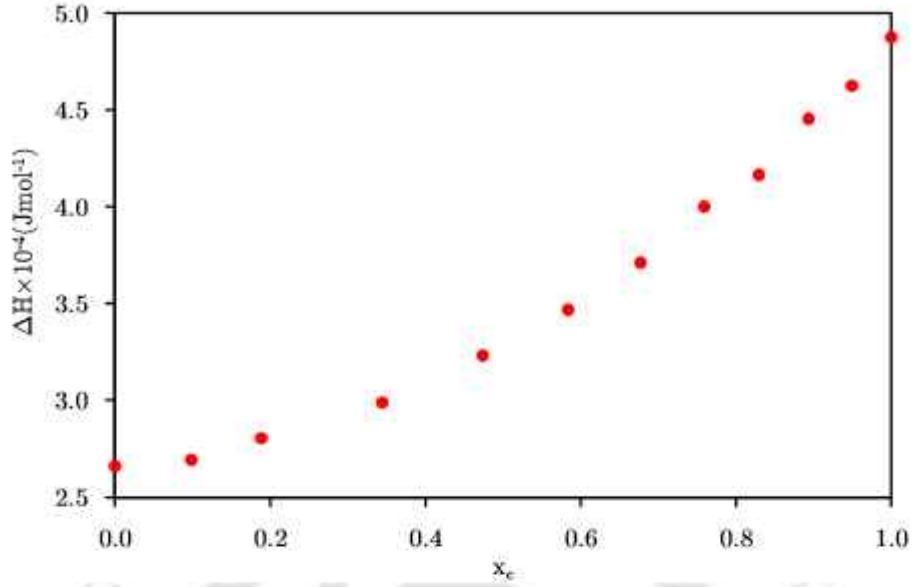

(A) Change in enthalpy

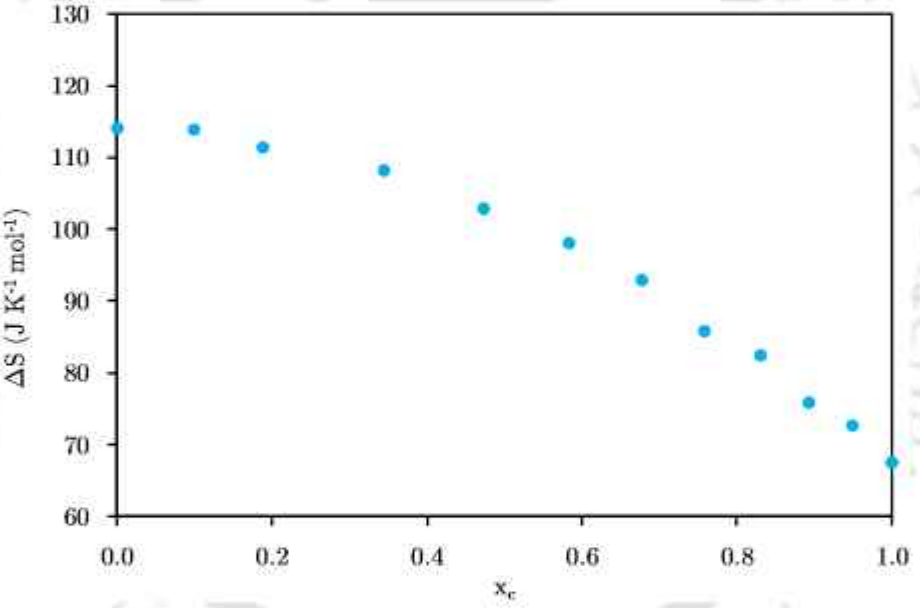

(B) Change in entropy

FIGURE 4.8: Change in enthalpy and entropy of activation of pseudo-binary mixture of sesame oil and Aliquat® 336

4.8 FTIR results

The FTIR spectra of the pseudo-binary mixture and its components are shown in Fig. 4.9. In Aliquat, the peaks in the range of 721-1465 cm^{-1} indicates the out of plane =C—H(sp^2) bending while the peaks at 2852 and 2920 cm^{-1} corresponds to —C—H (sp^3) stretch. The absence of these peaks indicates the intermolecular interaction of sesame oil with Aliquat. The peak at 1456 cm^{-1} present in pseudo-binary mixture

interpret a sharp C-H bend. The shift in peaks at 1238, 1163 and 1095 cm^{-1} in the mixture (close to 1236, 1159 and 1097 cm^{-1} in sesame oil) indicate the interaction between the alkyl group of aliquat with =C—O—C group of ether, C—O group of alcohol and —C—O—C group of ether, respectively, present in sesame oil.

Summary of the properties of liquid membrane

- The viscosity and density of the pseudo-binary mixture increased and decreased respectively with increase in mole fraction of Aliquat® 336.

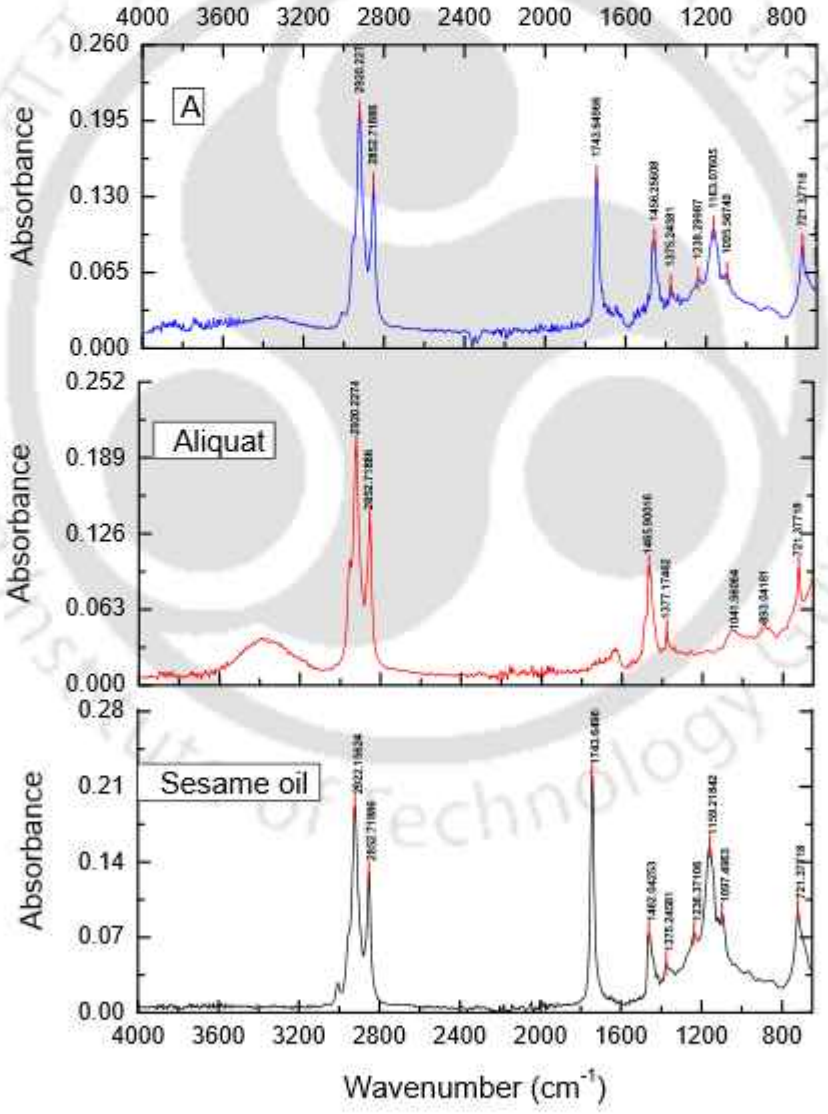

FIGURE 4.9: FTIR spectra of pseudo-binary mixture

- Both the density and viscosity of the pseudo-binary mixture decreased with increase of temperature.
- Viscosity deviation and excess molar volume of the pseudo-binary mixture were negative that indicates strong molecular interactions.
- The surface tension of the pseudo-binary mixture decreased with the increase in the concentration of the Aliquat® 336.
- Aliquat® 336 disrupts the strong cohesive force when it is added to the sesame oil.
- The reduction in surface tension increases the surface area, which increases the scope of intermolecular interactions.
- In the pseudo-binary mixture, the excess Gibb's free energy first increases and then decreases with increase in mole fraction of Aliquat® 336. This can be related to the interactions between the molecules in the mixture which is repulsive at low mole fraction and favourable in high mole fraction.
- The change in enthalpy of the pseudo-binary mixture increased with mole fraction. A positive deviation in enthalpy indicated that heat was absorbed upon mixing (endothermic).
- The change in entropy linearly decreased with mole fraction for sesame oil and Aliquat® 336 mixture. A negative trend meant that entropy decreased on forming the mixture indicating that the components of the mixtures formed a strong bond which would be difficult to dissociate.
- A new relation is obtained between density, surface tension, viscosity, and intermolecular free length that is linear in nature. The pseudo-binary mixture fits well into this relation with R^2 value in the range of 0.96 and the slope is negative, which is in corroboration with the findings obtained from the properties of the pseudo-binary mixture.
- A comparison of the FTIR analysis of pure sesame oil, Aliquat® 336, and the pseudo-binary mixture further justified the observations of the liquid membrane properties.

Nomenclature

BM Binary Mixture

M Molecular weight

M_{av} Average molar mass

x Mole fraction

m,c,s subscripts of any variable that refer to mixture, extractant, and solvent respectively.

η Viscosity

$\Delta\eta$ Viscosity deviation

ρ Density

V^E Excess molar volume

S Surface tension

S^E Excess surface tension

U Ultrasonic velocity

U^E Excess ultrasonic velocity

K_s Isentropic compressibility

K_s^E Excess isentropic compressibility

L_f Intermolecular free length

L_f^E Excess intermolecular free length

Z Acoustic impedance

Z_E Excess acoustic impedance

σ Standard deviation

$V_{\phi 1}$ Apparent molar volume of extractants

$V_{\phi 2}$ Apparent molar volume of solvents

α Thermal expansion coefficient

ΔG^E Excess Gibbs' free energy

ΔH Change in enthalpy

ΔS Change in entropy

ν Kinematic viscosity

h Planck's constant

N_A Avogadro number

R Gas constant

T Absolute temperature

Chapter 5

Two-phase equilibrium study

This chapter outlines the two-phase equilibrium study for the removal of arsenic species and combined arsenic species from water. The optimization of the operational parameters for maximum removal efficiency has been followed through response surface methodology (RSM) using a face-centered central composite design (FCCCD) approach. The distribution coefficient and extraction equilibrium constant are determined. The statistical and machine-learned modelling approaches are implemented in predicting the optimum process condition that would ensure the highest yield in terms of optimum extraction%. The experimentally observed optimum extraction efficiency of the process is compared with the statistical model and machine-learned model. The utilization of Genetic Algorithm (GA) based optimization tool in conjunction with Artificial Neural Network (ANN) is a widely accepted approach that has been followed here for achieving this objective.

5.1 Experimental observations and inferences

The experiments have been carried out as per the DoE given in Sec 3.4 and the results are recorded in Table 5.1. All 5 factors, viz. feed phase pH, extractant concentration, duration of experiment, temperature, and stirring speed were varied in the same manner

for 5 cases viz. $As^{(III)}$, $As^{(V)}$, $As^{(III)}$:$As^{(V)}$:: 1 : 1 , $As^{(III)}$:$As^{(V)}$:: 1 : 2 and $As^{(III)}$:$As^{(V)}$:: 2 : 1 , and the corresponding extraction% has been mentioned. $As^{(III)}$:$As^{(V)}$:: 1 : 1 , $As^{(III)}$:$As^{(V)}$:: 1 : 2 and $As^{(III)}$:$As^{(V)}$:: 2 : 1 have been referred to as AS11, AS12 and AS21 in Table 5.1

TABLE 5.1: Experimental design with factors and response for two-phase extraction of arsenic

Run	Factors					Extraction (%) of				
	A	B	C	D	E	$As^{(III)}$	$As^{(V)}$	As11	As12	As21
1	4	2	2	25	250	50.74	45	63.1	64.58	60.11
2	7	6	7	40	150	62.98	73	77.18	81.15	75.39
3	7	6	2	40	150	60.22	70	69.16	79.56	72.83
4	10	10	12	25	250	57.47	50	60.61	63.39	70.67
5	7	6	7	40	50	51.65	72	70.71	78.49	74.9
6	7	6	7	40	250	75.05	78	82.13	83.47	79.84
7	7	6	7	40	150	72.9	74	79.69	80.45	78.98
8	4	2	12	55	50	53.28	53	65.93	68.22	66.74
9	4	2	2	25	50	48.88	43	62.39	64.2	63.61
10	7	6	7	40	150	70.65	75	85.12	79.65	77.95
11	10	2	12	25	250	48.42	41	54.43	56.98	54.12
12	7	6	12	40	150	78.19	81	82.6	83.91	80.71
13	4	10	12	25	50	59.98	63	72.67	77.21	73.65
14	4	10	2	55	50	58.36	60	68.41	71.45	70.96
15	10	10	12	25	50	54.22	49	60.32	61.47	60.42
16	10	2	12	55	50	46.51	42	48.64	58.02	54.6
17	7	6	7	55	150	80.56	79	83.78	85.17	81.38
18	4	2	12	55	250	54.39	55	66.4	68.65	67.87
19	10	2	2	25	50	25.49	30	25.94	41.51	36.93
20	4	2	2	55	250	51.21	49	65.3	65.25	64.73
21	4	10	12	55	50	60.13	67	73.97	77.91	74.57
22	7	6	7	40	150	75.78	76	80.34	82.64	78.63
23	4	2	12	25	250	53.82	51	65.8	66.85	65.29
24	10	2	2	55	50	29.47	36	30.65	47.05	40.31
25	10	6	7	40	150	53.99	43	60.12	61.6	60.89

Continued on next page

Table 5.1 – continued from previous page

Run	Factors					Extraction (%) of				
	A	B	C	D	E	$As^{(III)}$	$As^{(V)}$	As11	As12	As21
26	10	10	2	55	50	53.09	47	57.52	60.6	59.48
27	7	6	7	40	150	76.71	75	80.85	83.52	77.13
28	7	6	7	40	150	68	73	81.59	80.23	76.71
29	10	2	2	55	250	35.67	37	40.23	49.24	45.54
30	10	10	12	55	250	57.6	52	62.21	63.45	62.6
31	10	10	2	25	50	52.11	45	55.7	59.47	56.19
32	4	10	12	55	250	65.67	68	75.21	78.15	74.76
33	10	2	2	25	250	32.58	31	35.98	46.66	38.15
34	7	2	7	40	150	71.17	65	75.24	78.39	74.82
35	4	10	2	25	50	58.59	58	66.67	68.85	68.63
36	7	6	7	40	150	72.4	73	81.94	80.82	79.15
37	10	2	12	55	250	51.97	44	55.68	58.96	52.85
38	7	6	7	40	150	73.94	72	82.97	83.82	80.83
39	10	10	2	25	250	52.94	46	55.97	60.27	56.89
40	7	6	7	25	150	51.15	72	78.83	79.17	75.03
41	4	6	7	40	150	61.78	62	68.09	69.96	70.3
42	7	10	7	40	150	80.86	84	84.89	85.13	84.1
43	4	10	12	25	250	60.64	66	73.27	77.83	73.8
44	10	10	12	55	50	54.63	51	62.19	61.68	60.93
45	4	10	2	55	250	62.95	61	71.15	72.1	70.47
46	4	2	2	55	50	49.59	47	63.88	65.05	64.17
47	4	10	2	25	250	59.38	59	67.84	69.65	68.96
48	10	2	12	25	50	39.43	39	43.14	53.41	54.11
49	4	2	12	25	50	51.96	50	65.7	65.39	64.93
50	10	10	2	55	250	56.5	48	58.76	60.61	59.73

The impact of the parameters on the extraction efficiency of $As^{(III)}$is given in Fig. 5.1. Similarly impact of the parameters on the extraction efficiency of $As^{(V)}$, $As^{(III)}$:$As^{(V)}$:: 1 : 1 , $As^{(III)}$:$As^{(V)}$:: 1 : 2 and $As^{(III)}$:$As^{(V)}$:: 2 : 1 , are given in Fig. A.3-A.6.

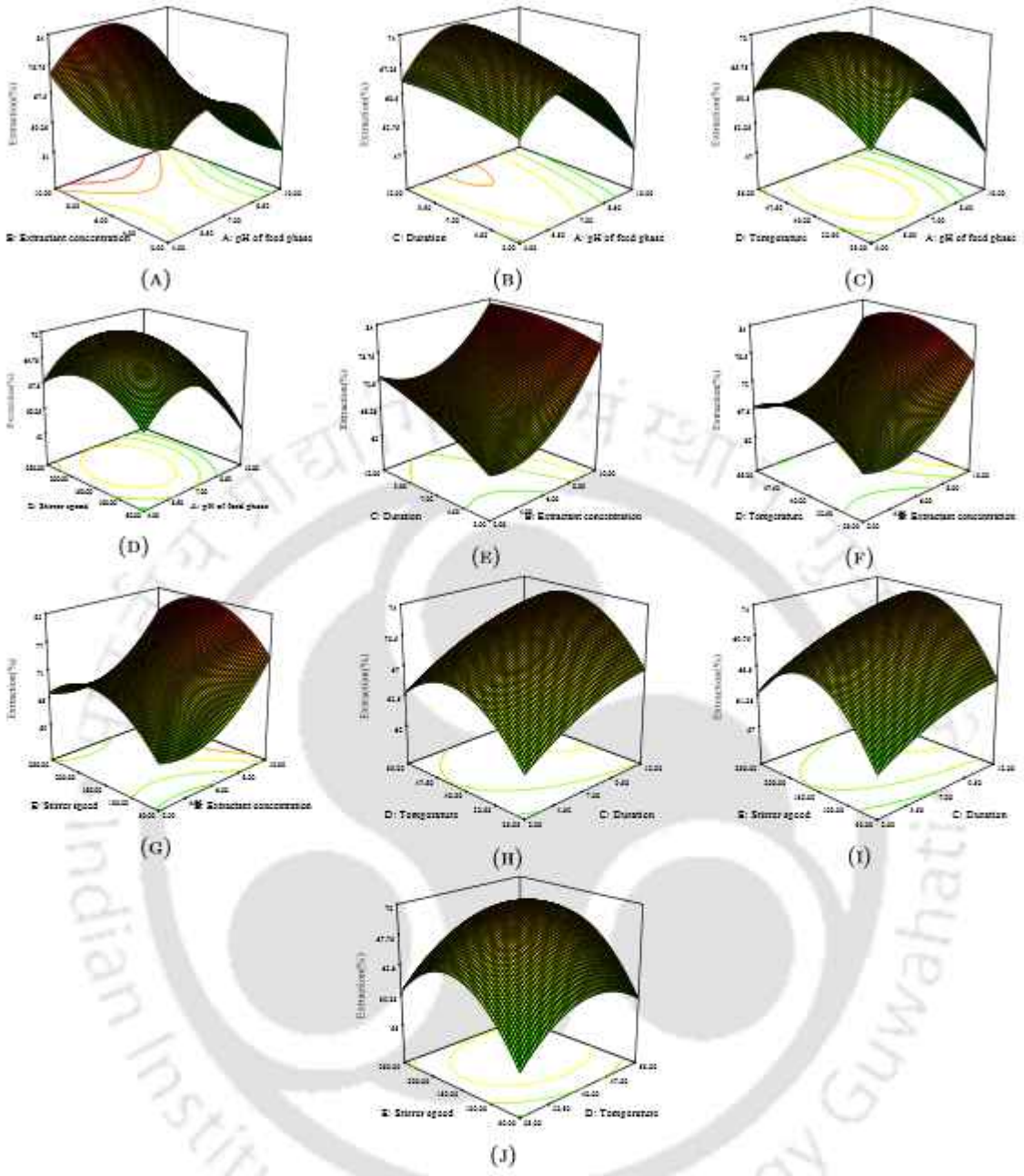

FIGURE 5.1: Effect of parameters on the extraction of $As^{(III)}$in two phase study

5.1.1 Effect of pH of the feed phase

The pH of the feed phase was varied from 4 to 10 based on the pH reported for contaminated waters in Digboi[242] and Kamrup district of Assam [282]. The optimum pH for $As^{(III)}$is 6.8 for extraction of 84%. $As^{(III)}$exists as H_3AsO_3 at $pH < 9$ [283]. Aliquat 336 is an ionic liquid comprising of quarternary ammonium cation and chloride anion that interacts with both undissociated and dissociated forms of arsenic ions favoring the

removal of arsenic within this pH range. The optimum pH for $As^{(V)}$is ~6.7 for extraction of 86% and in this pH, $As^{(V)}$is present in the form of $H_2AsO_4^-$ dissociated ions. The optimum pH for combined $As^{(III)}$-$As^{(V)}$lies in the range of 6.3-6.65 indicating the presence of both H_3AsO_3 and $H_2AsO_4^-$ at intermediate pH range.

5.1.2 Effect of extractant concentration

Aliquat 336 is a highly viscous cationic surfactant forming structural micelle aggregates owing to its long hydrocarbon chain. The bulk amount of organic phase utilized in this two-phase study further increases the viscosity. So, the extractant concentration in the organic phase was varied from 2 to 10% (v/v) based on the viscosity of the organic phase, because extractant concentration more than 10% (v/v) could increase the viscosity of the organic phase, causing intense emulsification. The optimum extractant concentration for both the arsenic ions and combined species was found to be ~10% (v/v).

5.1.3 Effect of duration of experiment

The duration of this study was varied from 2 to 12 hours [110]. The optimum duration for combined $As^{(III)}$-$As^{(V)}$in three different ratios was in the range of 7-12 hours; for $As^{(III)}$, significant extraction efficiency (84%) was achieved at 9 hours. However, for $As^{(V)}$, the extraction efficiency reached 86% at 12 hours. This difference of three hours could be attributed to the presence of uncharged and charged ions in the case of $As^{(III)}$and $As^{(V)}$, respectively. Although 9 hours was identified as the point where significant extraction for $As^{(III)}$occurred, to ensure uniformity in the experimental procedure and to accommodate the longer duration required for $As^{(V)}$, the study was conducted up to 12 hours. This extended duration ensured consistency across all conditions, as not much variation in results was observed beyond 9 hours for $As^{(III)}$.

5.1.4 Effect of temperature

The variation in temperature was studied over the range of 25°C to 55°C [284]. The optimum temperature for $As^{(III)}$was 37°C for extraction of 84% and 55°C for 86% extraction of $As^{(V)}$. This could possibly be due to the presence of H_3AsO_3 in the case of $As^{(III)}$that interacted by disrupting the strong ionic interactions between Aliquat 336

and sesame oil at 37°C . While $H_2AsO_4^-$ being an anion requires a higher temperature of 55°C to interact with the ionic interactions of the extractant and diluent. Thus, the intermediate temperature range lying between 35°C -47°C was found to be optimum for combined arsenic species indicating synergistic interactions between the arsenic species.

TABLE 5.2: Experimentally found distribution coefficients of various arsenic species and/or their combinations in two phase studies

Arsenic species/combinations	Extractant concentration (%)	Distribution coefficient		
		Run I	Run II	Run III
$As^{(III)}$	2	0.647	0.638	0.63
	4	1.146	1.065	1.092
	6	1.536	1.614	1.423
	8	1.935	1.923	1.963
	10	2.231	2.393	2.433
$As^{(V)}$	2	0.235	0.266	0.282
	4	0.658	0.633	0.731
	6	1.19	1.21	1.241
	8	1.827	1.878	1.817
	10	2.533	2.581	2.483
$As^{(III)}$:$As^{(V)}$:: 1 : 1	2	0.149	0.119	0.129
	4	0.296	0.286	0.276
	6	0.446	0.459	0.466
	8	0.63	0.66	0.67
	10	0.831	0.842	0.824
$As^{(III)}$:$As^{(V)}$:: 1 : 2	2	0.175	0.193	0.212
	4	0.5	0.475	0.466
	6	0.852	0.814	0.755
	8	1.125	1.143	1.112
	10	1.491	1.471	1.492
$As^{(III)}$:$As^{(V)}$:: 2 : 1	2	0.189	0.229	0.237
	4	0.577	0.528	0.493
	6	0.879	0.844	0.836
	8	1.25	1.275	1.292
	10	1.708	1.69	1.621

5.1.5 Effect of stirring speed

Stirring enhances the mass transfer of arsenic species through the liquid membrane. The variation in stirring speed was observed over a range of 50 to 250 rpm [100], and the optimum stirring speed for both the arsenic species was found to be ~ 170 rpm. While the optimum stirring speed was found to vary from 143-196 rpm for different ratios of $As^{(III)}$-$As^{(V)}$. At an optimum stirring speed, the mixing is vigorous enough to ensure that arsenic molecules are efficiently transported from the bulk solution to the organic phase without causing excessive turbulence that might lead to the formation of stable emulsions. The boundary layer formed between the aqueous phase and the organic phase, where the concentration gradient is significant, is minimized at this stirring speed. An optimum stirring speed provides the right balance between reducing the thickness of the boundary layer and maintaining steady transfer of arsenic species from the bulk feed phase to the organic phase.

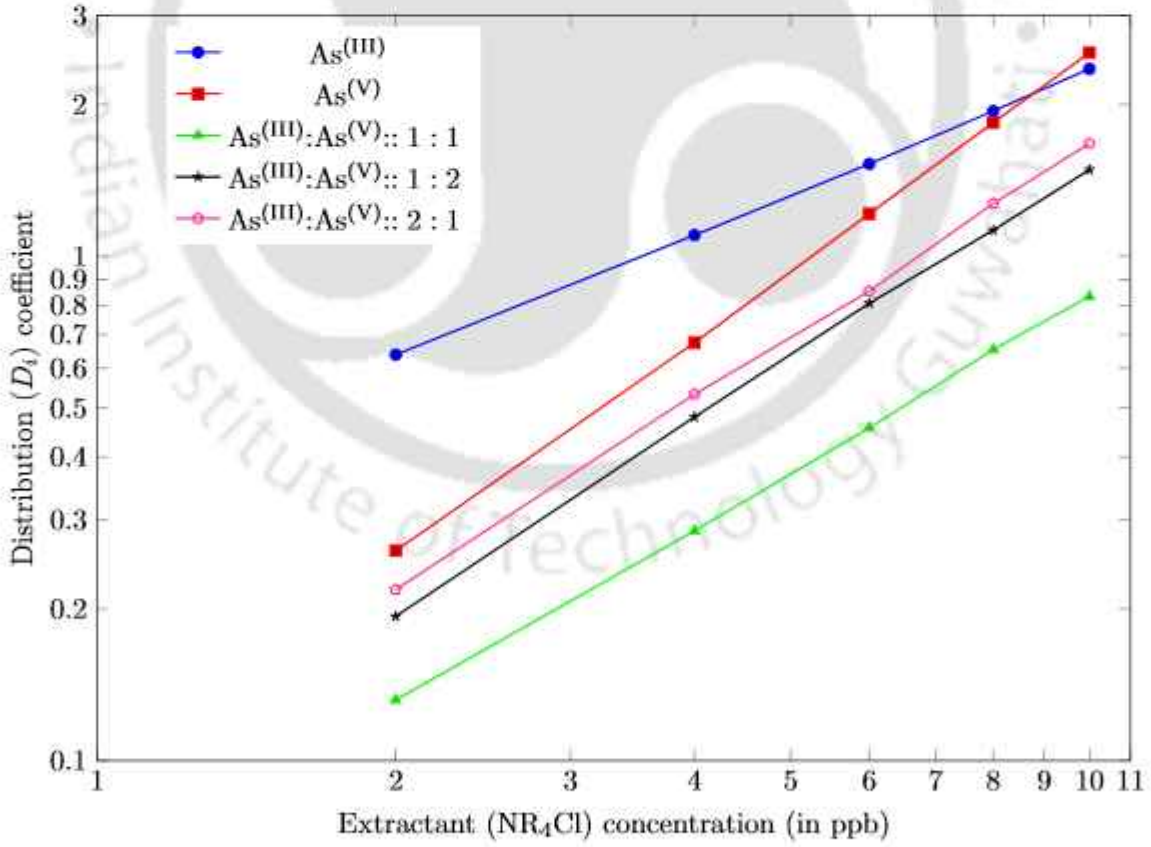

FIGURE 5.2: Distribution coefficient vs. extractant concentration for single and mixed arsenic species in two-phase extraction study

5.2 Mathematical modelling

The extraction equilibrium and the moles of extractant reacting with arsenic species were determined from the distribution data of distribution coefficient versus extractant concentration for single and mixed species of arsenic, as recorded in Table 5.2. A very dilute concentration of Aliquat 336 (2-10% vol/vol) had been employed for this study. Therefore, it can be assumed that a monomer form of the extractant predominates in the organic phase instead of micellar aggregates. The graphical representation of the distribution coefficient (D_i) against the Aliquat 336 concentration in the logarithmic scale is given in Fig.5.2. A linear relationship was obtained for all the arsenic species. Table 5.3 shows the model parameters (n and K) as referred to in Eq.(2.62).

TABLE 5.3: Extraction equilibrium model parameters for various arsenic species and/or their combinations in two phase study

Arsenic species/combinations	Model parameters	
	n	K
$As^{(III)}$	0.8	4.5
$As^{(V)}$	1.4	8.2
$As^{(III)}$:$As^{(V)}$:: 1 : 1	1.15	2.16
$As^{(III)}$:$As^{(V)}$:: 1 : 2	1.27	4.31
$As^{(III)}$:$As^{(V)}$:: 2 : 1	1.26	4.76

The slope, n, is in the range of 0.8-1.4 for all the arsenic species; the minimum being 0.8 for $As^{(III)}$, a maximum of 1.4 for $As^{(V)}$, and the mixed species lying in between this range. This implies that the formation of the arsenic-Aliquat 336 complex in the organic phase predominantly follows the stoichiometric ratio of 1:1. The slope values close to 1 suggest that each mole of arsenic species interacts with approximately one mole of Aliquat 336, forming a 1:1 complex. The equilibrium constant K, being highest for $As^{(V)}$, indicates that the extraction of $As^{(V)}$into the organic phase is more favourable compared to $As^{(III)}$and combined arsenic species. This supports the understanding that the interaction strength and stability of the complex are highest for $As^{(V)}$.

5.3 Statistical analysis

The equations of the quadratic models are used to make predictions about the response for given levels of each factor. These equations in terms of coded factors for extraction of $As^{(III)}$, $As^{(V)}$, $As^{(III)}$: $As^{(V)}$:: 1:1, $As^{(III)}$: $As^{(V)}$:: 1:2, and $As^{(III)}$: $As^{(V)}$:: 2:1 are given in the following equations:

$$\begin{aligned} Y_{As^{(III)}} = {} & 71.02 - 4.68A + 6.19B + 3.25C + 1.88D + 2.34E + 1.79AB + 1.63AC \\ & + 0.3497AD + 0.6303AE - 1.87BC - 0.2241BD - 0.3797BE + 0.0659CD \\ & + 0.1078CE + 0.1741DE - 12.49A^2 + 5.64B^2 - 1.17C^2 - 4.52D^2 - 7.03E^2 \end{aligned} \tag{5.1}$$

$$\begin{aligned} Y_{As^{(V)}} = {} & 74.76 - 6.65A + 6.35B + 3.24C + 1.71D + 0.8529E - 0.6563AB - 0.0937AC \\ & + 0.0312AD - 0.0937AE - 0.4687BC - 0.4687BD - 0.0937BE - 0.1562CD \\ & + 0.0938CE - 0.0313DE - 23.15A^2 - 1.15B^2 - 0.1474C^2 - 0.1474D^2 - 0.6474E^2 \end{aligned} \tag{5.2}$$

$$\begin{aligned} Y_{As^{(III)}:\ As^{(V)}::\ 1:1} = {} & 80.51 - 8.46A + 5.85B + 3.83C + 1.22D + 1.75E + 2.75AB \\ & + 1.76AC + 0.3431AD + 0.9788AE - 1.24BC - 0.1206BD - 1.03BE \\ & - 0.2506CD - 0.1912CE - 0.0225DE - 15.71A^2 + 0.2463B^2 - 3.94C^2 \\ & + 1.49D^2 - 3.4E^2 \end{aligned} \tag{5.3}$$

$$\begin{aligned} Y_{As^{(III)}:\ As^{(V)}::\ 1:2} = {} & 81.87 - 6.67A + 4.44B + 2.81C + 1.02D + 0.7679E + 0.4422AB \\ & + 0.4022AC + 0.1322AD + 0.3616AE - 0.4641BC - 0.4078BD \\ & - 0.2347BE - 0.1141CD + 0.0241CE - 0.2584DE - 16.42A^2 \\ & - 0.444B^2 - 0.469C^2 - 0.034D^2 - 1.22E^2 \end{aligned} \tag{5.4}$$

$$Y_{As^{(III)}:\ As^{(V)}::\ 2:1} = 78.52 - 7.03A + 5.23B + 3.38C + 0.8882D + 0.625E + 1.62AB + 1.47AC - 0.2103AD + 0.5891AE - 0.8397BC - 0.4772BD + 0.2409CE - 0.0853DE - 13.35A^2 + 0.5106B^2 - 2.18C^2 - 0.7444D^2 + 0.3059BE - 0.8747CD - 1.58E^2 \quad (5.5)$$

Their analysis of variance is tabulated in Table 5.4 and Table B.2 through Table B.5.

TABLE 5.4: Analysis of variance for two-phase extraction of $As^{(III)}$

Source	Sum of squares	df	Mean square	F-value	p-value
Model	6958.94	20	347.95	11.55	<0.0001
A	745.99	1	745.99	24.76	<0.0001
B	1303.74	1	1303.74	43.27	<0.0001
C	359.39	1	359.39	11.93	0.0017
D	119.64	1	119.64	3.97	0.0558
E	186.5	1	186.5	6.19	0.0188
AB	102.21	1	102.21	3.39	0.0758
AC	85.25	1	85.25	2.83	0.1033
AD	3.91	1	3.91	0.13	0.7212
AE	12.71	1	12.71	0.42	0.5211
BC	111.49	1	111.49	3.7	0.0643
BD	1.61	1	1.61	0.053	0.819
BE	4.61	1	4.61	0.15	0.6984
CD	0.14	1	0.14	4.617×10^{-3}	0.9463
CE	0.37	1	0.37	0.012	0.9123
DE	0.97	1	0.97	0.032	0.8589
A^2	385.96	1	385.96	12.81	0.0012
B^2	78.63	1	78.63	2.61	0.1171
C^2	3.4	1	3.4	0.11	0.7395
D^2	50.57	1	50.57	1.68	0.2054
E^2	122.12	1	122.12	4.05	0.0535
Residual	873.8	29	30.13		
Lack of fit	734.28	22	33.38	1.67	0.2485
Pure error	139.52	7	19.93		
Total	7832.74	49			

TABLE 5.5: Optimization and error analysis for two-phase extraction of arsenic ions

Model parameters	$As^{(III)}$		$As^{(V)}$		$As^{(III)}$:$As^{(V)}$:: 1 : 1		$As^{(III)}$:$As^{(V)}$:: 1 : 2		$As^{(III)}$:$As^{(V)}$:: 2 : 1	
	Stats	ML	Stats	ML	Stats	ML	Stats	ML	Stats	ML
R^2	0.8884	...	0.9893	...	0.966	...	0.976	...	0.974	...
Adjusted R^2	0.8115	...	0.9819	...	0.942	...	0.959	...	0.956	...
Predicted R^2	0.6368	...	0.9655	...	0.882	...	0.916	...	0.909	...
Adequate precision	15.818	...	39.394	...	26.14	...	27.63	...	28.94	...
pH of feed phase	6.81	6.91	6.65	7.63	6.59	7.18	6.65	7.50	6.26	6.48
Extractant concentration % (vol/vol)	10	10	10	7.784	10	10	10	8.717	10	10
Duration (hours)	9	12	12	12	7	7.9	12	8.8	9	5.5
Temperature (°C)	37	48.94	55	37.87	47	35.33	35	41.89	45	55
Stirring speed (rpm)	176	161.43	170	154.7	196	202.95	173	245.39	143	158.17
Predicted extraction (%)	82.37	87.82	84.15	83.13	87.03	85.56	87.59	86.39	85.1	85.94
Obtained extraction (%)	84		86		85.5		86		84.5	
Error (%)	1.94	4.54	2.15	3.33	1.79	0.07	1.85	0.45	0.71	1.7

The Table 5.5 presents the optimum conditions obtained for maximum extraction of arsenic ions. The "Stats" and "ML" columns of Table 5.5 refer to "Statistical" and "Machine Learning" respectively. The results of statistical modelling is being discussed in this section, while the simulation results of machine learned model would be discussed in Sec 5.4. The predicted maximum extraction of $As^{(III)}$and $As^{(V)}$are 82.37% and 84.15%, as opposed to 84% and 86% respectively obtained through experimentations. On the other hand, the predicted maximum extraction of combined $As^{(III)}$:$As^{(V)}$:: 1 : 1 ,$As^{(III)}$:$As^{(V)}$:: 1 : 2 and $As^{(III)}$:$As^{(V)}$:: 2 : 1 are 87.03%, 87.59% and 85.1% as opposed to 85.5%, 86% and 84.5% respectively obtained through experimentations, as given in Table 5.5.

A significant model with F-value of 11.55 (vide Table 5.4) is obtained for $As^{(III)}$. The feed phase pH and extractant concentration are found to be the most significant parameters as the p-value is < 0.0001 in both the cases (vide Table 5.4). The F-value for lack of fit is 1.67, implying it to be not significant; and there is 24.85% chance that a value this large could occur due to noise. The coefficient of determination (R^2) is found to be 0.8884 with adjusted R^2 value to be 0.8115 and the predicted R^2 value is 0.6368. The predicted R^2 value is in agreement to the adjusted R^2 value. Further, a ratio of 15.818 is obtained for adequate precision indicating a desirable signal to noise ratio. The quadratic model obtained for $As^{(V)}$is found to be significant with F-value equal to 134.26 (vide Table B.2). In this case, the pH of the feed phase, extractant concentration, duration and temperature are found to be the significant parameters as reported in Table B.2. A non-significant lack of fit value of 2.38 is obtained with 12.06% chances of occurrence of this value due to noise. A high value of the coefficient of determination (R^2) (0.9893) indicates this model to be significant. The predicted R^2 (0.9655) is in close agreement with the adjusted R^2 value (0.9819). Additionally, the adequate precision value of 39.394 indicates an adequate signal with a very high signal to noise ratio. The significant F-values of the models for $As^{(III)}$-$As^{(V)}$combined in different ratios are 40.77 (for $As^{(III)}$:$As^{(V)}$:: 1 : 1), 58.44 (for $As^{(III)}$:$As^{(V)}$:: 1 : 2) and 53.75 (for $As^{(III)}$:$As^{(V)}$:: 2 : 1) with a non significant lack of fit values as given in Table B.3, Table B.4 and Table B.5, respectively. The pH of the feed phase, extractant concentration and duration are found to be the significant parameters for all the three combined ratios of $As^{(III)}$-$As^{(V)}$. The high values of R^2 stipulates the models to be significant. The reasonable agreement between adjusted R^2 and predicted R^2 values with a difference less than 0.2 and high adequate precision

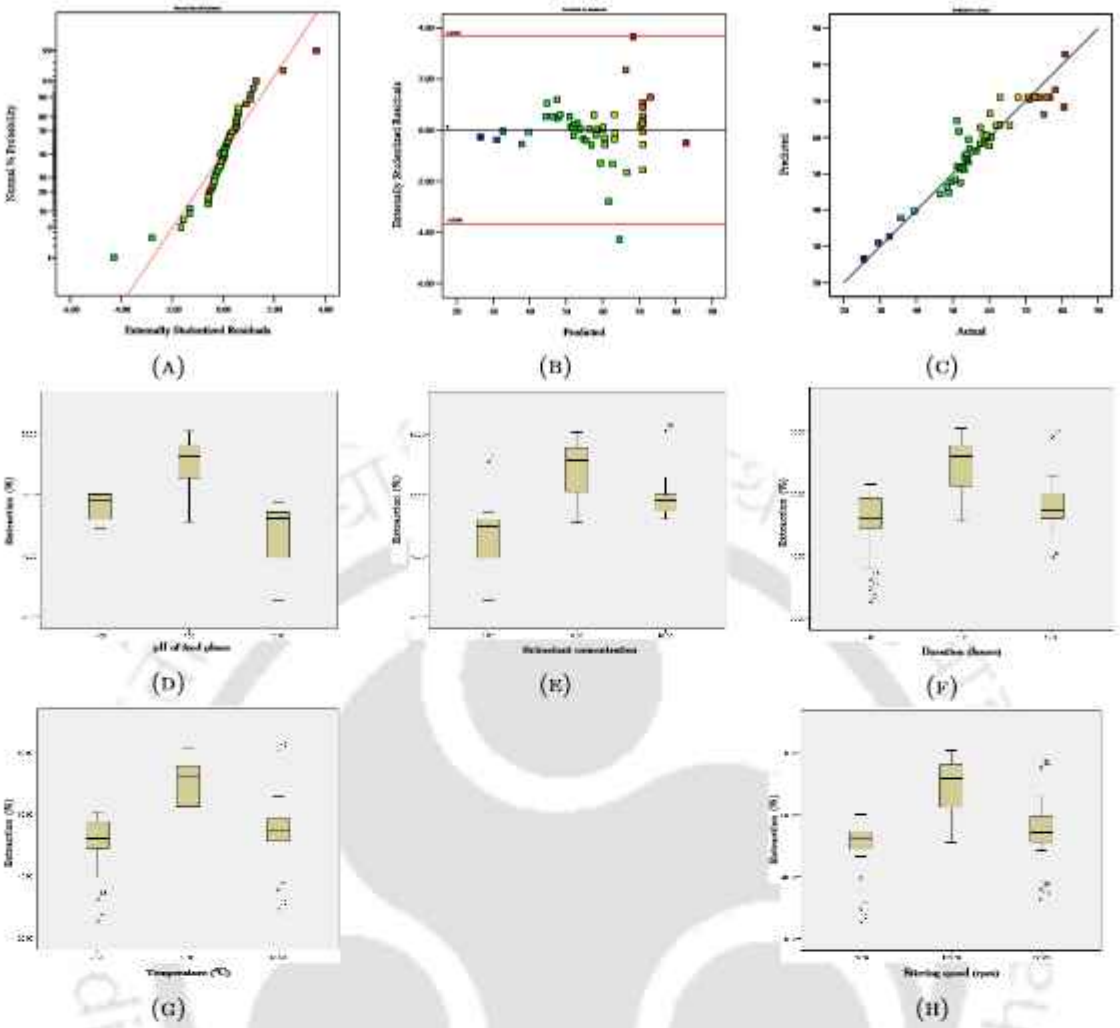

FIGURE 5.3: Statistical analysis of the quadratic model predicted and box plots for extraction of $As^{(III)}$

values further corroborates the significance of the models. Fig. 5.3 and Fig. A.7 show the minimum, maximum, lower quartile, median and upper quartile with outliers obtained from the descriptive statistical analysis.

The box plots, ie. Fig. 5.3 and Fig. A.12 through Fig. A.13 help to visualize the interquartile range in order to understand the distributions of the different levels of independent variables with respect to the dependent variable. The length of the box indicates the variation of the data. In case of $As^{(III)}$, the median lies close to the lower quartile or upper quartile indicating a non-normal skewed distribution as shown in Fig. 5.3. Again Fig. A.7a through Fig. A.7c for $As^{(V)}$shows the spread of the data set that is similar to $As^{(III)}$, with mild and strong outliers lying beyond the minimum and maximum values. For $As^{(III)}$-$As^{(V)}$combinations, as given in Fig. A.7d through Fig. A.7l, the distribution appears to be either left-skewed or right skewed.

TABLE 5.6: Normality test for the extraction of arsenic ions using Shapiro-Wilk model

Independent variables	Range	df	$As^{(III)}$		$As^{(V)}$		$As^{(III)}$:$As^{(V)}$:: 1 : 1		$As^{(III)}$:$As^{(V)}$:: 1 : 2		$As^{(III)}$:$As^{(V)}$:: 2 : 1	
			Stat.	Signific.	Stat.	Signific.	Stat.	Signific.	Stat.	Signific.	Stat.	Signific.
A	4	17	0.94	0.348	0.956	0.556	0.928	0.201	0.874	0.025	0.956	0.560
	7	16	0.88	0.039	0.959	0.640	0.875	0.032	0.918	0.159	0.977	0.934
	10	17	0.84	0.007	0.947	0.406	0.842	0.008	0.838	0.007	0.912	0.110
B	2	17	0.913	0.113	0.98	0.96	0.896	0.057	0.949	0.445	0.920	0.147
	6	16	0.907	0.103	0.701	0.001	0.825	0.006	0.726	0.001	0.812	0.004
	10	17	0.781	0.001	0.909	0.096	0.942	0.337	0.890	0.046	0.933	0.245
C	2	17	0.861	0.016	0.957	0.571	0.834	0.006	0.945	0.376	0.884	0.036
	7	16	0.894	0.064	0.772	0.001	0.835	0.008	0.753	0.001	0.850	0.013
	12	17	0.929	0.208	0.923	0.166	0.977	0.930	0.937	0.284	0.946	0.392
D	25	17	0.839	0.007	0.972	0.851	0.910	0.100	0.960	0.627	0.903	0.077
	40	16	0.922	0.18	0.802	0.003	0.857	0.017	0.735	0.001	0.868	0.025
	55	17	0.934	0.256	0.956	0.564	0.945	0.382	0.978	0.934	0.975	0.905
E	50	17	0.827	0.005	0.984	0.986	0.859	0.015	0.958	0.593	0.914	0.119
	150	16	0.929	0.233	0.806	0.003	0.831	0.007	0.743	0.001	0.875	0.033
	250	17	0.939	0.311	0.978	0.931	0.950	0.460	0.978	0.933	0.967	0.763

"Stat." referes to Statistic and "Signific." refers to Significance

Shapiro-Wilk test is preferred over the Kolmogorov-Smirnov test for assessing the normality of the data as it is more appropriate for small sample size ($\leqslant 50$). Table 5.6 shows the normality test results for the extraction of arsenic ions using Shapiro-Wilk model.

TABLE 5.7: Spearman's correlational analysis for the extraction of single arsenic ions

Type	Variables	Parameters	A	B	C	D	E	%Ex
$As^{(III)}$	A	Corr. Coeff.	1	0	0	0	0	-0.284
		Signific.(2-tailed)	-	1	1	1	1	0.046
	B	Corr. Coeff.	0	1	0	0	0	0.477
		Signific.(2-tailed)	1	-	1	1	1	0.000
	C	Corr. Coeff.	0	0	1	0	0	0.185
		Signific.(2-tailed)	1	1	-	1	1	0.199
	D	Corr. Coeff.	0	0	0	1	0	0.139
		Signific.(2-tailed)	1	1	1	-	1	0.334
	E	Corr. Coeff.	0	0	0	0	1	0.160
		Signific.(2-tailed)	1	1	1	1	-	0.268
	%Ex	Corr. Coeff.	-0.284	0.477	0.185	0.139	0.160	1
		Signific.(2-tailed)	0.046	0.000	0.199	0.334	0.268	-
$As^{(V)}$	A	Corr. Coeff.	1	0	0	0	0	-0.390
		Signific.(2-tailed)	-	1	1	1	1	0.005
	B	Corr. Coeff.	0	1	0	0	0	0.366
		Signific.(2-tailed)	1	-	1	1	1	0.009
	C	Corr. Coeff.	0	0	1	0	0	0.199
		Signific.(2-tailed)	1	1	-	1	1	0.165
	D	Corr. Coeff.	0	0	0	1	0	0.105
		Signific.(2-tailed)	1	1	1	-	1	0.468
	E	Corr. Coeff.	0	0	0	0	1	0.060
		Signific.(2-tailed)	1	1	1	1	-	0.681
	%Ex	Corr. Coeff.	-0.390	0.366	0.199	0.105	0.060	1
		Signific.(2-tailed)	0.005	0.009	0.165	0.468	0.681	-

"Corr. Coeff." refers to Correlation Coefficient and "Signific." refers to Significance

Based on the Shapiro-Wilk test and the skewed distribution of the data, Spearmann

correlation analysis has been carried out to evaluate the relationship between the dependent variable (extraction) and each independent variable as shown in the Table 5.7 and Table B.6. As is evident from the data, the extraction of arsenic have a significant correlation with pH of the feed phase and the extractant concentration.

The correlation coefficients are consistently negative for the case of pH of feed phase while it is consistently positive for extractant concentration. A negative value suggests that a monotonic relationship exists where the extraction efficiency increases with the decrease in feed phase pH while the reverse is true in case of extractant concentration.

The Levene's test of equality of error variances for $As^{(III)}$, $As^{(V)}$and combinations of $As^{(III)}$-$As^{(V)}$is performed to check the homogeneity of variances of the dependent variable with respect to the independent variable (vide Table 5.8).

TABLE 5.8: Levene's Test of Equality of Error Variances in two phase

Type of arsenic species	F	df1	df2	Sig.
$As^{(III)}$	0.251	42	7	0.998
$As^{(V)}$	0.515	42	7	0.913
$As^{(III)}$:$As^{(V)}$:: 1 : 1	0.207	42	7	1
$As^{(III)}$:$As^{(V)}$:: 1 : 2	0.667	42	7	0.806
$As^{(III)}$:$As^{(V)}$:: 2 : 1	0.301	42	7	0.993

The p-value for $As^{(III)}$(0.998), $As^{(V)}$(0.913), $As^{(III)}$:$As^{(V)}$:: 1 : 1 (1), $As^{(III)}$:$As^{(V)}$:: 1 : 2 (0.806) and $As^{(III)}$:$As^{(V)}$:: 2 : 1 (0.993) are found to be more than the significance level, testing the null hypothesis to be true. This implies that the error variance of the dependent variable is equal across the groups of independent variable.

In the univariate analysis of variance, the significance column in Table 5.9 and Table B.7 through Table B.10 refers to the p-values for each tested difference of means pertaining to the independent and dependent variables. In this analysis, the p-values pertaining to the independent variables lying below the standard α of 0.05 indicates that their means differ significantly. In case of $As^{(III)}$, the means of all the five independent variables differ significantly. While for $As^{(V)}$, the means of the combined factor of feed phase pH-extractant concentration along with the five independent variables differ significantly.

TABLE 5.9: Univariate analysis of variance for extraction of $As^{(III)}$

Source	Type III Sum of Squares	df	Mean Square	F	Significance
Corrected model	7693.223	42	183.172	9.190	0.003
Intercept	65896.978	1	65896.978	3306.237	0.000
A	797.301	2	398.651	20.001	0.001
B	878.036	2	439.018	22.027	0.001
C	427.371	2	213.685	10.721	0.007
D	430.544	2	215.272	10.801	0.007
E	467.984	2	233.992	11.74	0.006
AB	102.209	1	102.209	5.128	0.058
AC	85.249	1	85.249	4.277	0.077
AD	3.913	1	3.913	0.196	0.671
AE	12.713	1	12.713	0.638	0.451
BC	111.49	1	111.49	5.594	0.05
BD	1.607	1	1.607	0.081	0.785
BE	4.613	1	4.613	0.231	0.645
CD	0.139	1	0.139	0.007	0.936
CE	0.372	1	0.372	0.019	0.895
DE	0.97	1	0.97	0.049	0.832
ABC	71.85	1	71.85	3.605	0.099
ABD	10.204	1	10.204	0.512	0.497
ABE	15.694	1	15.694	0.787	0.404
ACD	0.279	1	0.279	0.014	0.909
ACE	0.25	1	0.25	0.013	0.914
ADE	3.007	1	3.007	0.151	0.709
BCD	1.292	1	1.292	0.065	0.806
BCE	0.144	1	0.144	0.007	0.935
BDE	8.395	1	8.395	0.421	0.537
CDE	0.76	1	0.76	0.038	0.851
ABCD	2.36	1	2.360	0.118	0.741
ABCE	0.008	1	0.008	0.000	0.984
ABDE	0.272	1	0.272	0.014	0.910
ACDE	1.151	1	1.151	0.058	0.817
BCDE	0.059	1	0.059	0.003	0.958
ABCDE	0.102	1	0.102	0.005	0.945
Error	139.518	7	19.931		
Total	174372.259	50			
Corrected total	7832.741	49			

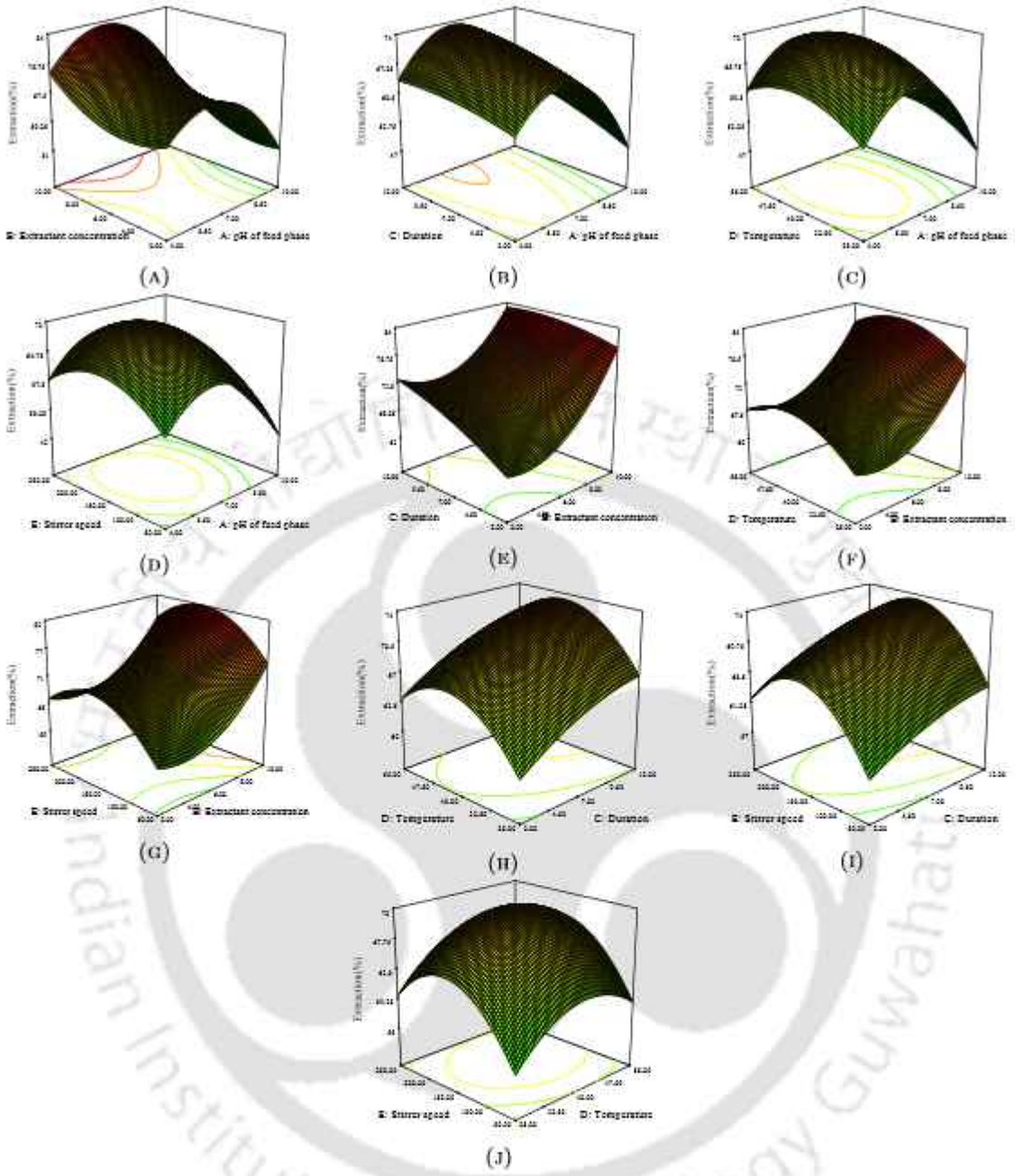

FIGURE 5.4: Variation of %extraction in two phase with various combinations of factors for $As^{(III)}$using statistical model

Similarly, for different ratios of $As^{(III)}$-$As^{(V)}$species, pH of the feed phase, extractant concentration, time and the combination of extractant concentration-time are the common factors whose means vary significantly. Fig. 5.4 and Fig. A.8 through Fig. A.11 represent the variation of %extraction with various combinations of factors for $As^{(III)}$, $As^{(V)}$, $As^{(III)}$:$As^{(V)}$:: 1 : 1 , $As^{(III)}$:$As^{(V)}$:: 1 : 2 , and $As^{(III)}$:$As^{(V)}$:: 2 : 1 using statistical model. The observations noted in Sec. 5.1 are found to be corroborated through these plots.

5.4 Machine learned analysis

Fifty data points from Table 5.1 are used to train, validate and test the ANN for each arsenic species. Initially, simulations were performed to optimize the number of neurons in the hidden layer. Fig. 5.5a shows the MSE with the different number of neurons in the hidden layer. The minimum MSE was achieved with 6 neurons in the hidden layer. Thus, the same number of neurons has been selected for further simulations. Fig. 5.5b compares the model predictions with all data points with experimental results. The regression curve shows that model predictions are sufficiently fitting with the model predictions on all data points, which confirms the authenticity of the training.

The trained ANN was used to study the effects of various operating conditions and membrane parameters on the transport of the arsenic ions. Global optimization of the ANN model has also been done to detect the best operating condition to achieve maximum %extraction. The results of the said best operating condition will be revealed later. In these simulations, the effects of variations of two input parameters were analyzed simultaneously through surface graphs, while values of other input parameters were kept constant at the best condition. The range of input parameters was kept the same as reported in Table 3.2.

Fig. 5.5c and Fig. 5.5l present variation of %extraction with various combinations of factors. It is revealed from Fig. 5.5c through Fig. 5.5f that neither high nor low pH is suitable for good extraction. At pH 6.7-6.8, the extraction of the arsenic ions into the organic phase is highly favoured. The interaction between aliquat and arsenic ions is maximum forming arsenic-aliquat complexes; favouring the extraction of arsenic ions from the aqueous phase into the organic phase. The presence of H^+ ions at lower pH range and OH^- ions at higher pH range possibly interferes with the complex formation of arsenic-aliquat leading to lower extraction of arsenic ions at extreme pH conditions[151]. Same is true for stirring speed. The variation in stirring speed was observed over a range of 50 to 250 rpm and the optimum stirring speed for both the arsenic species is found to be 170 rpm. While, the stirring speed varies from 143-196 rpm for different ratios of $As^{(III)}$and $As^{(V)}$. The minimum thickness of the diffusion layer is obtained at the optimum stirring rate[285]. At lower stirring speed the accumulation of arsenic-aliquat complex forms a boundary layer at the interphases leading to lower extraction efficiencies. While at higher stirring speed, the extraction decreases owing to turbulences that lead

to less interfacial contact time for complex formation[286]. Thus, optimum stirring speed provides effective time for interaction. However, the %extraction increases with increase in extractant concentration, duration and temperature. It is further established from Fig. 5.5g, Fig. 5.5h and Fig. 5.5i that higher concentration of extractant always favours the %extraction. Aliquat 336 is a highly viscous cationic surfactant forming structural micelle aggregates owing to its long hydrocarbon chain. The bulk amount of organic phase utilized in this two-phase study further increases the viscosity. Maximum extractant concentration of 10% is optimum for arsenic extraction. Beyond this the viscosity of the liquid membrane increases which in turn impacts the diffusion of the arsenic ions through the organic phase. Fig. 5.5j and Fig. 5.5k show the relationship of duration with temperature and stirring speed respectively. The surf figures reiterate the earlier revealed facts too. Fig. 5.5l shows that a combination of high temperature and high stirring speed and/or a combination of low temperature and low stirring speed is not good for effective %extraction. The optimum duration for $As^{(III)}$is 9 hours to obtain an extraction of 84%. While, the optimum duration for $As^{(V)}$is 12 hours for an extraction of 86%. This difference of three hours could be attributed to the presence of uncharged and charged ions in case of $As^{(III)}$and $As^{(V)}$, respectively. The variation in temperature was studied over the range of 25°C to 55°C . The optimum temperature for $As^{(III)}$is 37°C for an extraction of 84% and 55°C for 86% extraction of $As^{(V)}$. This could possibly be due to the presence of H_3AsO_3 in case of $As^{(III)}$that interacts by disrupting the strong ionic interactions between aliquat 336 and sesame oil at 37°C . While $H_2AsO_4^-$ being an anion, requires higher temperature of 55°C to interact with the ionic interactions of the extractant and diluent. Thus, intermediate temperature range lying between 35°C -47°C is found to be optimum for combined arsenic species indicating synergistic interactions between the arsenic species.

Moreover, Sec.5.3 has already demonstrates that the transport of the arsenic ions across the membrane strongly depends on the operating parameters tabulated in Table 3.2. Fig. 5.5 also indicates that these parameters have coupled effects on the transport as the optimum value of a parameter where maximum transport was found to vary with other parameters.

Thus, global optimization is required to determine the optimum parameters where maximum transport could be achieved. In this study, a genetic algorithm is used for constrained global optimization. MATLAB Genetic Algorithm solver "ga" was linked with

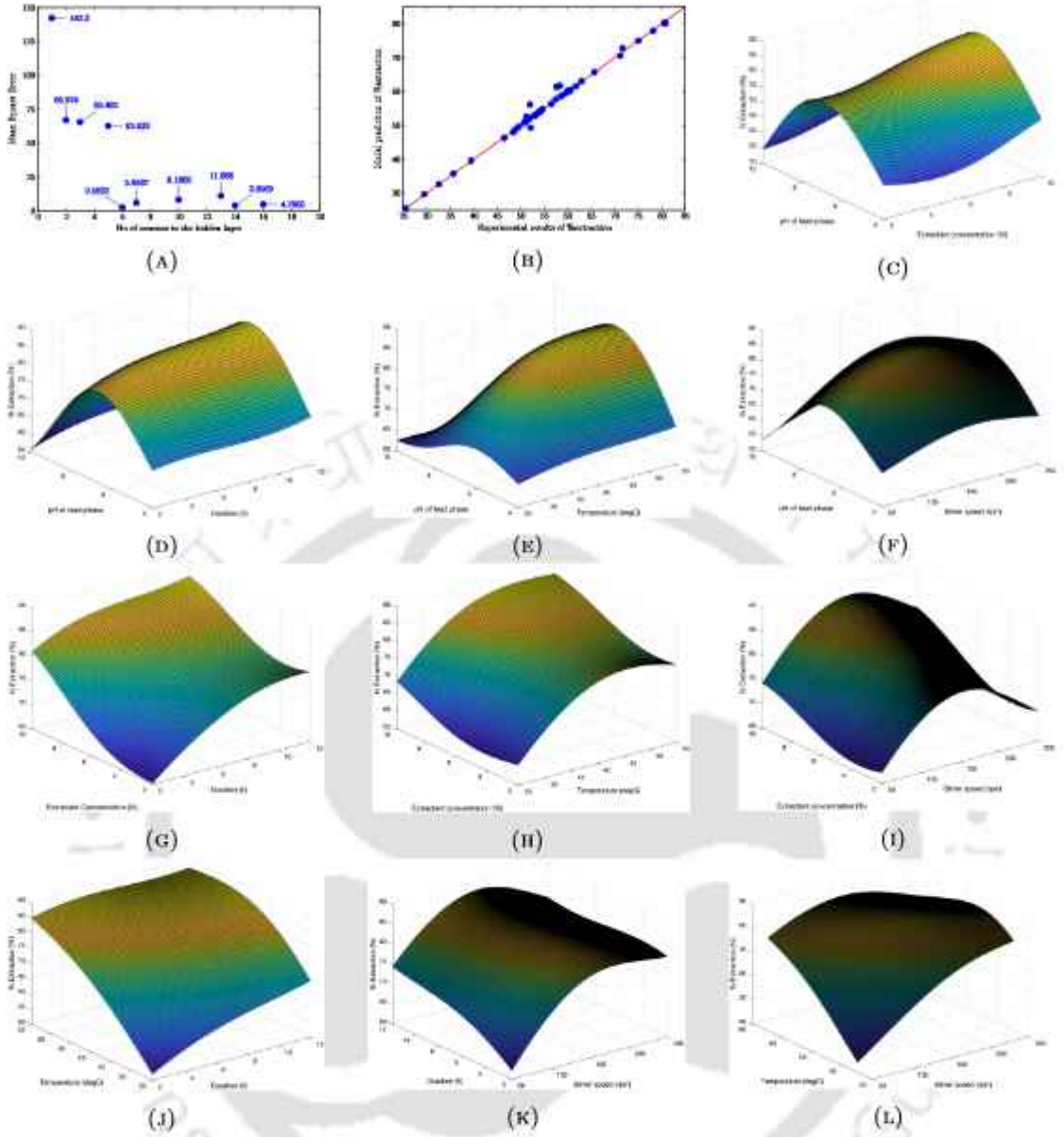

FIGURE 5.5: Various plots of two phase extraction for $As^{(III)}$using machine learning

the trained ANN to determine the optimum values of the five operating parameters stated in Table 3.2. In the genetic algorithm, the upper and lower limits of the different parameters were kept the same as given in the experimental study, of Table 3.2. Optimization was performed to maximize the %extraction of arsenic. After 124 generations and 5881 function counts the GA has arrived at the best value of %extraction at 87.82% at the optimum operating condition given in Table 5.5. The machine learned model predicts higher extraction percentage than the statistical model, however it uses higher duration, higher temperature and a lower stirring speed.

In the similar manner the datasets of $As^{(V)}$and 3 combinations of $As^{(III)}$-$As^{(V)}$have

been passed through machine learning algorithm. The results are given in Fig. A.14 through Fig. A.17, and their efficiencies are tabulated in Table 5.5. In all cases the minimum MSE was achieved with less than 8 neurons in the hidden layer. The variation of %extraction against the individual factors are also similar that have been observed in case of $As^{(III)}$, though at a different degree of variability. It is interesting to note that the %extraction of $As^{(III)}$is favoured by lowering the temperature, whereas %extraction of $As^{(V)}$is favoured at higher temeprature. For combined salt cases, the trend is favoured as per the salt which is at higher percentage in the combined species. Temperature has practically no effect on %extraction when $As^{(III)}$and $As^{(V)}$are at equal proportion, i.e. $As^{(III)}$:$As^{(V)}$:: 1 : 1 . The reason behind this phenomenon lies with the fact that $As^{(III)}$is present as an uncharged species in the particular pH range. Whereas, $As^{(V)}$is present in its anionic form that forms inter and/or intra molecular bonds for which higher temperature is required for maximum extraction of a $As^{(V)}$. The %extraction of arsenic, predicted through machine learned algorithm, is comparable to that obtained through statistical model (vide Table 5.5). In case of combined species, the error% is mostly less in case of machine learned model. The error percentage obtained from statistical analysis is in the range of 0.71-2.15 while from ML-based analysis, it is in the range of 0.07-4.54 for all the arsenic species (vide Table 5.5).

Summary of the two-phase equilibrium study

- The extractant concentration and the feed phase pH were found to be the most significant factors for the maximum extraction of arsenic species in this phase, which is in agreement with the statistical analysis.
- The maximum extraction obtained for $As^{(III)}$& $As^{(V)}$were 84% and 86%, respectively. While the extraction of combined $As^{(III)}$-$As^{(V)}$in various ratios were in the range of 84.5-86%.
- From the distribution coefficient data, it is proposed that all the species of arsenic form a complex with Aliquat® 336 in the stoichiometric ratio of 1:1.
- The extraction equilibrium constant obtained from the plot indicates $As^{(V)}$to be most favourable for extraction into the organic phase.

- Through statistical analysis it was inferred that the distribution of the data was skewed and the homogeneity of variances between the dependent and independent variables was confirmed.
- The extraction efficiency of arsenic in the two-phase study, predicted through the ML algorithm, is comparable to that obtained through the statistical model.
- The minimum mean square error in the ML-based approach was achieved with 6, 8, 8, 10, and 5 neurons in the hidden layer for $As^{(III)}$, $As^{(V)}$, and combined $As^{(III)}$-$As^{(V)}$ratios of (1:1), (1:2), and (2:1), respectively.
- The statistical analysis reveals an error percentage ranging from 0.71 to 2.15, whereas the ML-based analysis shows a range of 0.07 to 4.54 for all arsenic species.

Abbreviation

ANN Artificial neural network

D2EHPA Di-2-ethylhexylphosphoric acid

FCCCD Face-centered central composite design

GA Genetic algorithm

ML Machine learning

MSE Mean squared error

RSM Response surface methodology

TBP Tributyl phosphate

TOA Trioctylamine

Nomenclature

C_{aq} Concentration of arsenic ions in the aqueous phase

C_{org} Concentration of arsenic ions in the organic phase

C_i initial concentration of arsenic ions in the aqueous phase

C_t Concentration of arsenic ions in the aqueous phase at time t

$D_{(.)}$ Distribution coefficient

D_{III} Distribution coefficient for $As^{(III)}$ions

D_V Distribution coefficient for $As^{(V)}$ions

K_{III} Extraction equilibrium constant for $As^{(III)}$ions

K_V Extraction equilibrium constant for $As^{(V)}$ions

Chapter 6

Three-phase FSSLM study

This chapter outlines the simultaneous separation and recovery of individual arsenic species and combined arsenic species of $As^{(III)}$and $As^{(V)}$in three different ratios of (1:1), (1:2), and (2:1) using FSSLM technology. Mathematical modelling was carried out to determine the permeability coefficient, flux, and mass transfer coefficients for the transport of individual and combined arsenic species. The statistical and machine-learned modelling approaches were implemented to predict the optimum process condition that would ensure the highest yield in terms of optimum extraction% and recovery%. The experimentally observed optimum extraction and recovery efficiency of the process was compared with the statistical and machine-learned models. ANN and Genetic Algorithms were the tools applied for machine-learning based modelling.

6.1 Experimental observations and inferences

The experiments have been carried out as per the DoE given in Sec 3.4 (vide Table 3.2) and the results are recorded in Tables 6.1 & 6.2. Three factors viz. the receiving phase concentration (F), pH of receiving phase (G), and stirring speed (H1) were varied for $As^{(III)}$and $As^{(V)}$, whereas three factors viz. receiving phase concentration (F), pH of receiving phase (G), and extractant concentration (H2) were varied for the three cases of

$As^{(III)}$:$As^{(V)}$:: 1 : 1 , $As^{(III)}$:$As^{(V)}$:: 1 : 2 and $As^{(III)}$:$As^{(V)}$:: 2 : 1 , and the corresponding extraction% and recovery% were reported.

TABLE 6.1: Experimental design with factors and response for three-phase extraction and recovery of $As^{(III)}$and $As^{(V)}$individually

Run	Factors			$As^{(III)}$		$As^{(V)}$	
	F	G	H1	Ext. (%)	Rec. (%)	Ext. (%) of	Rec. (%)
1	1	3	200	35	26	35	25
2	1	3	300	32	22	31	15
3	1	5	250	53	44	40	26
4	1	7	200	44	30	35	20
5	1	7	300	42	29	32	18
6	2	3	250	40	33	53	44
7	2	5	200	55	43	58	43
8	2	5	250	62	50	65.5	48.5
9	2	5	300	51	37	55	39
10	2	7	250	48	39	69	40
11	3	3	200	37	29	55	30
12	3	3	300	35	24	49	24
13	3	5	250	55	45	60	35
14	3	7	200	47	36	54	30
15	3	7	300	43	34	52	28

"Ext." refers to Extraction and "Rec." refers to Recovery

TABLE 6.2: Experimental design with factors and response for three-phase extraction and recovery of various combinations of $As^{(III)}$and $As^{(V)}$

Run	Factors			$As^{(III)}$:$As^{(V)}$:: 1 : 1		$As^{(III)}$:$As^{(V)}$:: 1 : 2		$As^{(III)}$:$As^{(V)}$:: 2 : 1	
	F	G	H2	Ext (%)	Rec (%)	Ext (%)	Rec (%)	Ext (%)	Rec (%)
1	1	3	10	29.8	11.81	31.8	14.1	24.8	6.9
2	1	3	40	45.39	26.93	47.4	28.8	40.4	21.9
3	1	5	25	40.1	21.4	42.1	23.4	35.6	16.4
4	1	7	10	36.4	14.63	38.4	16.6	31.6	9.6
5	1	7	40	48.89	29.98	50.8	31.9	43.8	24.3

Continued on next page

Table 6.2 – continued from previous page

Run	Factors			$As^{(III)}$:$As^{(V)}$:: 1 : 1		$As^{(III)}$:$As^{(V)}$:: 1 : 2		$As^{(III)}$:$As^{(V)}$:: 2 : 1	
	F	G	H2	Ext (%)	Rec (%)	Ext (%)	Rec (%)	Ext (%)	Rec (%)
6	2	3	25	52.9	30.91	54.9	32.8	47.9	25.9
7	2	5	10	49.9	28.93	52.3	30.7	44.9	23.9
8	2	5	25	53.32	33.31	55.23	35.35	48.4	28.3
9	2	5	40	57.87	38.77	59.8	40.7	52.8	33.8
10	2	7	25	57.56	35.76	59.6	37.9	52.6	30.8
11	3	3	10	54.2	34.62	56.3	36.6	49.2	29.6
12	3	3	40	63.91	44.19	64.9	46.2	58.9	39.2
13	3	5	25	62.12	43.21	64.2	45.5	57.3	38.2
14	3	7	10	57.5	35.7	59.5	37.7	52.5	30.7
15	3	7	40	65.66	46.56	67.7	48.5	60.7	41.6

6.1.1 Effect of receiving phase concentration

The concentration of ferric chloride solution was varied from 1-3 ppm. The ratio of iron and arsenic was varied from 10:1 to 30:1. The ratio of iron and arsenic $\geqslant 50$ was reported for arsenic removal from groundwater using sand filters [287]. Such high content of iron was required due to the presence of other anions/contaminants that interfered with the iron-arsenic interactions in the groundwater. Furthermore, the iron-arsenic ratio of 10 was found to be optimum for the removal of arsenic [288]. In this study, the removal process included an anoxic stage, followed by aeration and sand filtration. In comparison to the literature, the 30:1 ratio is found to be the optimum for combined arsenic species in the present study (in between 10 and 50) and is attributed to the absence of additional oxygen supply and other interfering anions. This is based on sensitivity plots derived from the data obtained experimentally and presented in Table 6.1 and Table 6.2.

6.1.2 Effect of pH of the receiving phase

It has been reported that $FeCl_3$ shows poor adsorption capacity at pH$\geqslant 8$ so the studied pH range was $3-7$ for this work. However, the pH range $5-7$ has been found to be optimum for the removal of arsenic ions [247]. In the present work, the obtained

optimum pH 5 in the receiving phase in case of single-species experimentation, and optimum pH 7 in case of combined species of arsenic salts. These are in accordance with the reported pH range [247]. As it is evident from Pearson's correlational analysis, the recovery of arsenic ions is directly correlated to their extraction (%). Thus for both extraction and recovery of arsenic species, the pH values of 5 & 7 in the receiving phases were found to be the optimum in cases of single feed and mixed feed, respectively, as obtained in Table 6.1 and Table 6.2.

6.1.3 Effect of extractant concentration

Based on the previous research works [218], the extractant concentration for $As^{(III)}$and $As^{(V)}$was found to be 10% (v/v) and 30%(v/v), respectively. However, this parameter was studied for the combined arsenic species by varying from 10-40% (v/v) to find the optimum concentration for maximizing extraction and recovery. The extractant concentration is one of the significant parameters for the removal of all the single and mixed arsenic species. Forty percent of the pseudo-binary mixture (Aliquat 336-sesame oil) was found to yield the maximum extraction and recovery for the three different ratios of $As^{(III)}$and $As^{(V)}$, (vide Table 6.1 and Table 6.2.)

6.2 Mathematical Modelling

The value of permeability of the transport process was computed from the experimental results using Eq. 2.70, which is graphically shown in Fig. 6.1. It is observed that the permeability coefficients for the processes involving $As^{(III)}$, $As^{(V)}$, $As^{(III)}$:$As^{(V)}$:: 1 : 1 , $As^{(III)}$:$As^{(V)}$:: 1 : 2 , and $As^{(III)}$:$As^{(V)}$:: 2 : 1 are 0.8991, 1.025, 0.9396, 0.978, and 0.8205, respectively. It was obvious that permeation was favoured towards $As^{(V)}$, as opposed to $As^{(III)}$. Pentavalent arsenic had greater ionic size than trivalent one. As a result, $As^{(V)}$fits more easily into the crystal lattice of a material. Moreover, higher positive charge of $As^{(V)}$tends to enhance the mobility of ions. The above reasons facilitate faster diffusion through the crystal structure of the material.

The values of permeability, that are used in Eq. 2.77 to obtain the rate of flux of solute of transfer, are shown in Fig. 6.2. It was observed that the flux is higher for the cases where unequal combinations of mixed solutes were used. When there is an unequal proportion

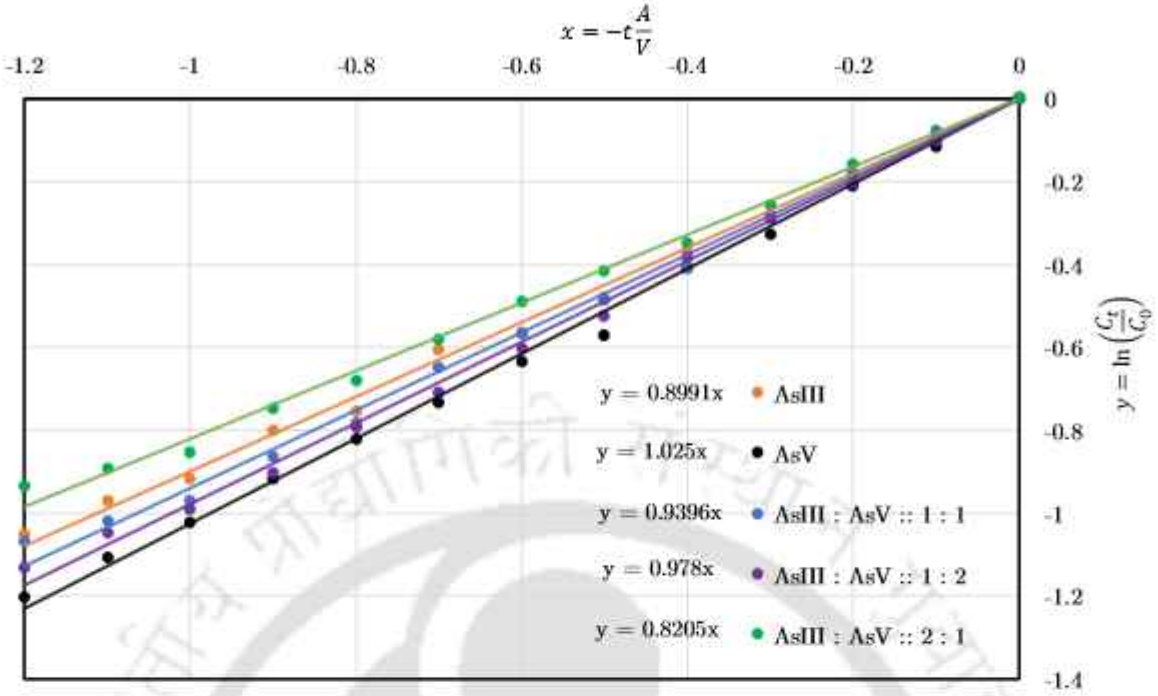

FIGURE 6.1: Graphical method of finding permeability coefficient as per Eq. 2.70.

of $As^{(V)}$and $As^{(III)}$ions, the presence of one type of ion in higher concentration creates vacancies in the crystal lattice to accommodate the other type of ion. Vacancies act as diffusion paths, facilitating the movement of ions. This increased vacancy formation leads to a higher flux of mass transfer. In certain cases, the presence of both $As^{(V)}$and

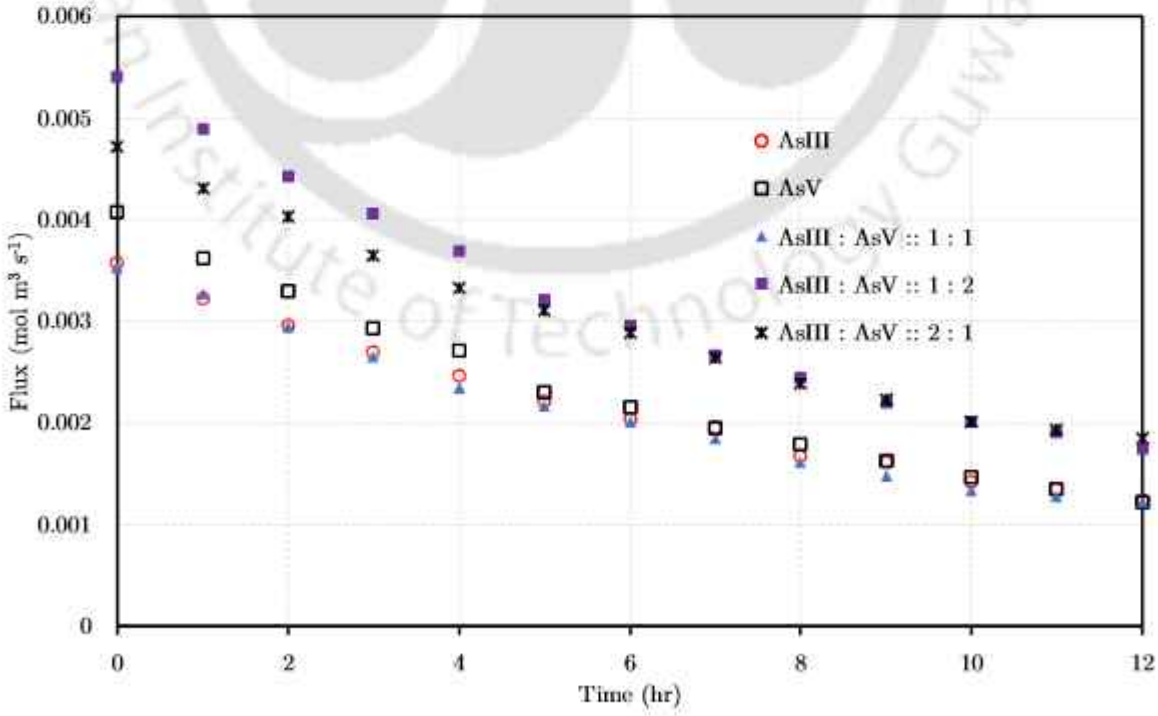

FIGURE 6.2: Rate of flux of solute as per Eq. 2.77.

$As^{(III)}$ions together may create synergistic effects, influencing the overall diffusivity. This could be due to complex interactions between the two ions and the material's crystal lattice, resulting in enhanced diffusion properties. As mentioned before, $As^{(V)}$ions are larger and carry a higher positive charge compared to $As^{(III)}$ions.

TABLE 6.3: Experimentally found distribution coefficients and permeability of various arsenic species and/or their combinations in three phase studies

Arsenic species/combinations	Extractant concentration (%)	Distribution coefficient	Permeability
$As^{(III)}$	10	2.178	0.8994
	20	3.42	0.8996
	25	4.145	0.8997
	30	4.886	0.8998
	40	6.001	0.8999
$As^{(V)}$	10	2.430	0.1388
	20	18.01	0.5588
	25	35.322	0.7436
	30	62.082	1.0242
	40	136.037	1.0242
$As^{(III)}$:$As^{(V)}$:: 1 : 1	10	1.073	0.0258
	20	12.368	0.2421
	25	30.207	0.5213
	30	54.026	0.7536
	40	154.952	0.9406
$As^{(III)}$:$As^{(V)}$:: 1 : 2	10	1.358	0.0395
	20	16.132	0.3536
	25	35.742	0.6294
	30	74.125	0.823
	40	236.5	0.9768
$As^{(III)}$:$As^{(V)}$:: 2 : 1	10	1.744	0.1258
	20	20.726	0.5612
	25	44.982	0.6631
	30	87.44	0.7643
	40	225.984	0.8215

When these ions are mixed in unequal proportions, the larger $As^{(V)}$ions tend to create more vacancies and provide more space for diffusion. Additionally, the higher charge of $As^{(V)}$ions enhances their mobility, leading to increased mass transfer flux.

The values of mass transfer resistances are obtained from the plot of $1/P$ vs. $1/D$ at various extractant concentrations as given by equation Fig. 2.79. The slope and intercept give the values of Δ_{org} and Δ_{aq}, respectively. The permeability, P and the distribution coefficient, D are tabulated for different concentrations of extractant in Table 6.3. From the Fig.6.3, Δ_{org} and Δ_{aq} for $As^{(III)}$, $As^{(V)}$, $As^{(III)}$:$As^{(V)}$:: 1 : 1 , $As^{(III)}$:$As^{(V)}$:: 1:2 and $As^{(III)}$:$As^{(V)}$:: 2 : 1 are {5.77,0.16}, {15.31,0.91}, {40.84,0.69}, {33.32,0.77}, and {11.77,1.20}, respectively. It is observed that the resistances in the phases (both organic and aqueous) are low for $As^{(III)}$than that for $As^{(V)}$. In case of combined salts of $As^{(III)}$and $As^{(V)}$, the said resistances decrease with an increase in ratio of $As^{(III)}$. The opposite phenomenon is observed in the event of an increase in $As^{(V)}$ratio. The elevated resistances encountered by $As^{(V)}$ions in both organic and aqueous phases can be attributed to the larger ionic size and higher positive charge compared to $As^{(III)}$. As resistances are inversely proportional to the diffusion coefficients, it may be argued that diffusion coefficients are lower for $As^{(V)}$than that for $As^{(III)}$. They

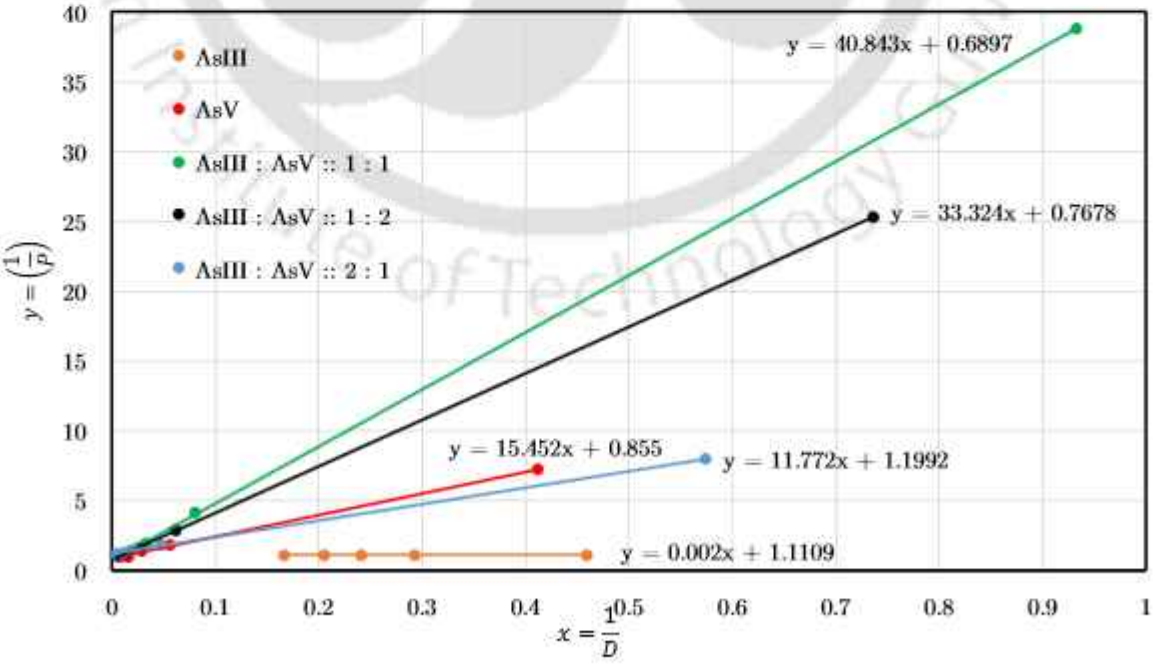

FIGURE 6.3: Plot for finding organic and aqueous phase resistances as per Eq. 2.79.

may further be calculated as follows. The mass transfer coefficients in aqueous phase (Δaq^{-1}) and organic phase (Δorg^{-1}) for $As^{(III)}$- $As^{(V)}$are calculated as 4.03×10^{-6} and 6.8×10^{-8} $m.s^{-1}$ for (1:1), 3.61×10^{-6} and 8.34×10^{-8} $m.s^{-1}$ for (1:2) and 2.33×10^{-6} and 2.36×10^{-7} $m.s^{-1}$ for (2:1), respectively. Reduced mass transfer resistance and increased mass transfer coefficients in the aqueous phase, as opposed to the organic phase, signify the ease of movement of arsenic ions from the membrane phase towards the aqueous strip phase.

6.3 Statistical analysis

A quadratic model obtained through DoE for prediction for extraction and recovery of arsenic species are given in the following equations:

$$Z^{E}_{As(III)} = 60.08 + 1.1F + 4.5G - 1.5H1 - 0.125FG - 0.125FH1 - 0.125GH1 - 3.45F^2 - 13.45G^2 - 4.45H1^2 \quad (6.1)$$

$$Z^{R}_{As(III)} = 48.45 + 1.7F + 3.4G - 1.8H1 + 0.75FG - 0.25FH1 + 0.75GH1 - 2.36F^2 - 10.86G^2 - 6.86H1^2 \quad (6.2)$$

$$Z^{E}_{As(V)} = 64.93 + 9.7F + 1.9G - 1.80H1 + 0.125FG - 0.125FH1 + 0.625GH1 - 13.32F^2 - 2.32G^2 - 6.82H1^2 \quad (6.3)$$

$$Z^{R}_{As(V)} = 47.92 + 4.27F - 0.2G - 2.34H1 + 0.75FG + 0.5FH1 + 1.5GH1 - 15.55F^2 - 4.05G^2 - 5.05H1^2 \quad (6.4)$$

Table B.11 presents ANOVA results of $As^{(III)}$in 3 phase SLM. The F-value of 23.14 implies the model for $As^{(III)}$is significant and there is only a 0.01% chance that a value this large could occur due to noise. In the extraction and recovery of $As^{(III)}$ions, pH of the receiving phase plays a significant role as indicated by the model given in Table B.11. The F-value of 0.84 for lack of fit implies that the value is not significant relative to the pure error and that there is a 57.36% chance that a value this large could not occur due to noise indicating this model to be a good fit. The predicted R^2 of 0.87 is in reasonable agreement with the adjusted R^2 of 0.91 (vide Table 6.4).

TABLE 6.4: Optimization and error analysis for three-phase SLM on individual arsenic ions

Model parameters	$As^{(III)}$				$As^{(V)}$			
	Statistics		ML		Statistics		ML	
	Extraction	Recovery	Extraction	Recovery	Extraction	Recovery	Extraction	Recovery
Standard deviation	2.97	3.46	...	...	2.64	2.64	...	...
Mean	49.05	38.23	...	...	48.88	35.6	...	...
R^2	0.95	0.93	...	...	0.97	0.97	...	...
Adjusted R^2	0.91	0.87	...	...	0.95	0.95	...	...
Predicted R^2	0.87	0.85	...	...	0.9	0.89	...	...
Adequate precision	12.8	10.53	...	...	16.14	17.3	...	...
Concentration of receiving phase (ppm)	2		4		2		2.13	
pH of receiving phase	5		5.18		5		7	
Stirrer speed (rpm)	250		200		250		250.72	
Extractant concentration % (v/v)	10		10		30		30	
Predicted (%)	61	49	59.1	48.5	67	48	68.5	42
Observed (%)	60	48	60	48	66.7	47	66.7	47
Error (%)	1.64	2.04	1.52	1.03	0.45	2.1	2.63	11.9

The adequate precision measures the signal to noise ratio and the value reported here in Table 6.4 is 12.802 (>4 desirable) that indicates it to be an adequate signal. Fig. A.18 shows the effect of interaction of parameters on the extraction and recovery of $As^{(III)}$. Further, the F-value of 15.41 for recovery of $As^{(III)}$ions implies that the model is significant with 0.01% chance that a value this large could occur due to noise as given in Table B.11. The lack of fit value reported in table is 0.30 with 89.67% chance that a value this large could not occur due to noise indicating this model to be a good fit. Further, the R^2 value is 0.93 with the predicted R^2 value in reasonable agreement with the adjusted R^2 value and the adequate precision value is 10.53 as shown in Table 6.4. In Fig. A.19 the effect of interaction of parameters on the extraction of $As^{(V)}$is observed. In case of $As^{(V)}$the F-value of 38.85 (vide Table B.12) with a 0.01% chance implies that the model is significant and that this value couldn't occur due to noise. In this case the concentration and pH of the receiving phase are suggested to be significant model terms for extraction and recovery of $As^{(V)}$ions. The lack of fit value is 2.12 that is insignificant relative to the pure error and there is a 21.51% chance that this value could occur due to noise as shown in Table B.12. Moreover, the R^2 value is 0.97 (vide Table 6.4) with the predicted R^2 value in reasonable agreement with the adjusted R^2 value and the adequate precision is 16.14 as given in Table 6.4. On the other hand, for recovery of $As^{(V)}$the F-value of 41.99 with 0.01% chance implies that the model is significant. The lack of fit value is 1.61 with 30.77% chance indicating that the value is not significant relative to the pure error and this value couldn't occur due to noise as shown in Table B.12. The R^2 value is 0.97 with the predicted R^2 value in reasonable agreement with the adjusted R^2 value and the adequate precision value is 17.3 as shown in Table 6.4. A normal distribution of the residuals have been observed from the plots for the extraction and recovery of $As^{(III)}$and $As^{(V)}$, as given in Fig. A.23.

The minimum, maximum, lower quartile, median and upper quartile with outliers is given in the box plots for descriptive statistical analysis (vide Fig. A.18 and Fig. A.19). As the mean is close to the median, the distribution of the data is symmetric with skewness $\leqslant 0.5$. The high variance and standard deviation indicates that the points of the data set are spread out and not close to the mean. While in certain data sets, median is more towards the first (lower) quartile or third (upper) quartile implying an asymmetrical frequency distribution. The box plots for concentration of receiving phase helps to visualize the differences in distribution between 1-3 ppm concentration range

for extraction and recovery of arsenic species in Fig. A.18 and Fig. A.19. The median is higher for 2 ppm in both the cases. The length of the box indicates the variation of the data which shows positive skewness. This further justifies that 2 ppm gives the maximum extraction and recovery for both the arsenic ions. Similarly, the data for the other two independent variables are fairly distributed with pH 5 giving the maximum extraction and recovery at 250 rpm. This is in tune with the optimum result obtained from the design of experiment (vide Table 6.4).

Shapiro-Wilk test is preferred over the Kolmogorov-Smirnov test for assessing the normality of the data as it is more appropriate for small sample size (< 50). The significance values of the Shapiro-Wilk test (vide Table B.16) are more than 0.05 indicating the data to be normally distributed. As the data set is found to be normal, Pearson's correlational analysis is carried out to identify the extent to which two variables are linearly related to each other. From the given Table B.18, it is evident that the dependent variables are linearly related to each other. The increase in extraction percentage of both the arsenic ions in turn increases the recovery percentage or vice versa at $\alpha = 0.01$ for 2-tailed significance analysis. In case of $As^{(V)}$, there is a significant correlation between the concentration of the receiving phase and the extraction percentage at $\alpha = 0.05$ for 2-tailed significance analysis.

The multivariate test tabulates the four tests of significance for each model effect as given in Table B.20 and Table B.21. Pillai's trace is more robust than the other statistical tests based on model assumptions [289]. On the basis of the Pillai's trace test shown in Table B.20, the significance values for all effects are greater than 0.1 except for concentration of receiving phase (p-value = 0.085) for $As^{(III)}$. This indicates that the receiving phase concentration has a significant main effect in the multivariate test. The tests of between-subjects effects was carried out as reported in Table B.25. The combined independent variables, concentration and pH of the receiving phase has a significant effect on the extraction percentage of $As^{(III)}$. And for $As^{(V)}$, all the three independent variables and the combined effect of stirring speed and pH of receiving phase are found to have a significant impact on the dependent variables that is obtained from the multivariate test reported in Table B.21. On this basis, the tests of between-subjects effects showed significant impact of the three individual independent variables on both the dependent variables for $As^{(V)}$as given in Table B.26.

Since there are significant main effects obtained for the variables, post hoc (Tukey HSD) analyses are calculated to explain the effect. The significant levels of the independent variables are obtained from this analysis as given in Table B.30 & Table B.31.

A quadratic model for prediction for extraction and recovery of mixed arsenic species are given in the following equations:

$$Z^{E}_{As^{(III)}:As^{(V)}::\,1:1} = 53.81 + 10.28F + 1.98G + 5.39H2 - 0.63FG - 1.28FH2 - 0.58GH2 - 3.43F^2 + 0.69G^2 - 0.66H2^2 \quad (6.5)$$

$$Z^{R}_{As^{(III)}:As^{(V)}::\,1:1} = 33.65 + 9.95F + 1.42G + 6.07H2 - 0.3FG - 1.25FH2 + 0.19GH2 - 1.85F^2 - 0.82G^2 - 0.3H2^2 \quad (6.6)$$

$$Z^{E}_{As^{(III)}:As^{(V)}::\,1:2} = 55.8 + 10.21F + 2.07G + 5.23H2 - 0.5FG - 1.4FH2 - 0.45GH2 - 3.5F^2 + 0.61G^2 - 0.6H2^2 \quad (6.7)$$

$$Z^{R}_{As^{(III)}:As^{(V)}::\,1:2} = 35.68 + 9.97F + 1.41G + 6.04H2 - 0.28FG - 1.2FH2 + 0.23GH2 - 1.72F^2 - 0.82G^2 - 0.47H2^2 \quad (6.8)$$

$$Z^{E}_{As^{(III)}:As^{(V)}::\,2:1} = 48.91 + 10.24F + 2G + 5.36H2 - 0.64FG - 1.24FH2 - 0.61GH2 - 3.23F^2 + 0.57G^2 - 0.83H2^2 \quad (6.9)$$

$$Z^{R}_{As^{(III)}:As^{(V)}::\,2:1} = 28.63 + 10.02F + 1.35G + 6.01H2 - 0.2FG - 1.15FH2 + 0.13GH2 - 1.87F^2 - 0.82G^2 - 0.32H2^2 \quad (6.10)$$

The statistical analysis of the extraction and recovery of mixed arsenic species would use similar statistical tools such as ANOVA, normality tests, Pearson's analysis etc. and their explanations would also be similar in nature. Thus only salient features are discussed over here in order to avoid repetitive statements. The following tables and figures show various statistical analysis data for mixed arsenic species $As^{(III)}$:$As^{(V)}$:: 1 : 1 , $As^{(III)}$:$As^{(V)}$:: 1 : 2 and $As^{(III)}$:$As^{(V)}$:: 2 : 1 .

The ANOVA analysis	Table B.13, Table B.14, and Table B.15
Normality test using Shapiro-Wilk model	Table B.17
Pearson's correlational analysis	Table B.19
The MANOVA analysis for combined arsenic species	Table B.22,Table B.23,Table B.24
Tests of between-subjects effects	Table B.27, Table B.28, and Table B.29

Post hoc (Tukey HSD) analyses	Table B.32, Table B.33, and Table B.34
Levene's test of homogeneity of error variances	Table B.35
Normal plot of residuals	Fig. A.23
Effect of interaction of parameters and box plot for statistical analysis	Fig. A.20, Fig. A.21, and Fig. A.22

The concentration of the receiving phase solution and extractant concentration are the significant terms of the model for both extraction and recovery of all the combined species of arsenic, as observed in Table B.13, Table B.14, and Table B.15. The R^2 values and the predicted R^2 values are in reasonable agreement with the adjusted R^2 value and the adequate precisions are between 35-40, as given in Table 6.6. The normal plot of residuals elucidates the normal distribution of the data as shown in Fig. A.23. The distribution of the data is symmetric with skewness $\leqslant 0.5$, while in certain data sets, median is more towards the first (lower) quartile or third (upper) quartile implying an asymmetrical frequency distribution. Box plots, Fig. A.20, Fig. A.21, and Fig. A.22, indicate that concentration of receiving phase at 2 ppm & 3 ppm yield maximum extraction and recovery for all the arsenic ions. The data for the other two independent variables are fairly distributed with pH 5 and pH 7 yielding maximum extraction and recovery at 250 rpm. Shapiro-Wilk test, in Table B.17, indicates the data to be normally distributed. From the Pearson's correlational analysis (vide Table B.19), it is evident that the dependent variables are linearly related to each other. As this indicates that the receiving phase concentration has a significant main effect in the multivariate test, the tests of between-subjects effects was carried out as reported in Table B.27, Table B.28, and Table B.29. Since there are significant main effects obtained for the variables, post hoc (Tukey HSD) analyses are calculated to explain the effect. The significant levels of the independent variables are obtained from this analysis as given in Table B.32, Table B.33, and Table B.34.

6.4 Machine learned analysis

Fifteen data sets, both from Table 6.1 and Table 6.2 are used to train, validate and test the ANN for each arsenic species. The entire operations are similar to that explained in

Sec.5.4.

TABLE 6.6: Optimization and error analysis for three-phase SLM on combined arsenic ions

Model parameters	$As^{(III)}$:$As^{(V)}$:: 1 : 1				$As^{(III)}$:$As^{(V)}$:: 1 : 2				$As^{(III)}$:$As^{(V)}$:: 2 : 1			
	Statistics		ML		Statistics		ML		Statistics		ML	
	Ext	Rec	Ext	Rec	Ext	Rec	Ext	Rec	Ext	Rec	Ext	Rec
Standard deviation	1.26	1.24	...	...	1.43	1.24	...	...	1.23	1.25	...	...
Mean	52.11	32.16	...	...	54.1	34.17	...	...	47.17	27.12	...	...
R^2	0.989	0.989	...	...	0.986	0.989	...	...	0.989	0.989	...	...
Adjusted R^2	0.98	0.98	...	...	0.97	0.98	...	...	0.98	0.98	...	...
Predicted R^2	0.94	0.94	...	...	0.92	0.94	...	...	0.94	0.94	...	...
Adequate precision	39.6	39.9	...	...	34.7	39.6	...	...	40.5	39.4	...	...
Concentration of receiving phase (ppm)	3		3		3		3		3		3	
pH of receiving phase	7		7		7		7		7		7	
Stirrer speed (rpm)	250		250		250		250		250		250	
Extractant concentration % (v/v)	40		38.1		40		36		40		40	
Predicted (%)	66	47	65.7	46.6	67.5	49	67.7	48.7	60.5	42	61.2	41.6
Observed (%)	65	46.5	65	46.5	66.5	48.5	66.5	48.5	59	41	59	41
Error (%)	1.5	1.1	1.07	0.21	1.48	1.02	1.77	0.41	2.47	2.4	3.6	1.44

Thus only salient features are discussed over here in order to avoid repeating statements. The following list of figures show various machine learned analysis for mixed arsenic species $As^{(III)}$:$As^{(V)}$:: 1 : 1 , $As^{(III)}$:$As^{(V)}$:: 1 : 2 and $As^{(III)}$:$As^{(V)}$:: 2 : 1 .

Mean Squared Error (MSE) with different numbers of neurons	Fig. A.24a, Fig. A.25a, Fig. A.26a, Fig. A.27a, and Fig. 6.4a
Comparative plots of experimental v/s model prediction of %extraction/%recovery	Fig. A.24b, Fig. A.25b, Fig. A.26b,Fig. A.27b, and Fig. 6.4b
Variation of %extraction/%recovery in three phase SLM with various combinations of factors	Fig. A.24, Fig. A.25, Fig. A.26, Fig. A.27, and Fig. 6.4

Initially, simulations were performed to optimize the number of neurons in the hidden layer. The minimum MSE was achieved with 4, 5, 27, 14, and 21 neurons in the hidden layer for $As^{(III)}$, $As^{(V)}$, $As^{(III)}$:$As^{(V)}$:: 1 : 1 , $As^{(III)}$:$As^{(V)}$:: 1 : 2 , and $As^{(III)}$:$As^{(V)}$:: 2 : 1 respectively. Global optimization of the ANN model yields the best operating condition to achieve maximum extraction and recovery. They are given in Table 6.6. The range of input parameters are maintained the same as reported in Table 3.2.

The machine learned results on the data of $As^{(III)}$and $As^{(V)}$are not up to the mark. There exists considerable process/model mismatch. It would be due to less number of neurons that needed to arrive at the MSE. And the value of MSE were high for $As^{(III)}$and $As^{(V)}$in comparison to that of mixed arsenic species. Thus optimization too was not successful. On the other hand, the machine learned results on the data of $As^{(III)}$:$As^{(V)}$:: 1 : 1 , $As^{(III)}$:$As^{(V)}$:: 1 : 2 , and $As^{(III)}$:$As^{(V)}$:: 2 : 1 were better than even the statistical model. The optimization results were almost perfect. Interestingly, concentration and pH of receiving phase were same for all three cases at 3 and 7 respectively. The differences in extractant concentration were very minimum. The predicted values of extraction and recovery based on the statistical approach were close to the experimental values and the error (%) is in the range of 0.45-2.47 for all the arsenic species (vide Table 6.4 and Table 6.6).

Summary of the three-phase FSSLM study

- The distribution plot against the concentration of the extractant suggested the formation of different complexes between arsenic and Aliquat 336.

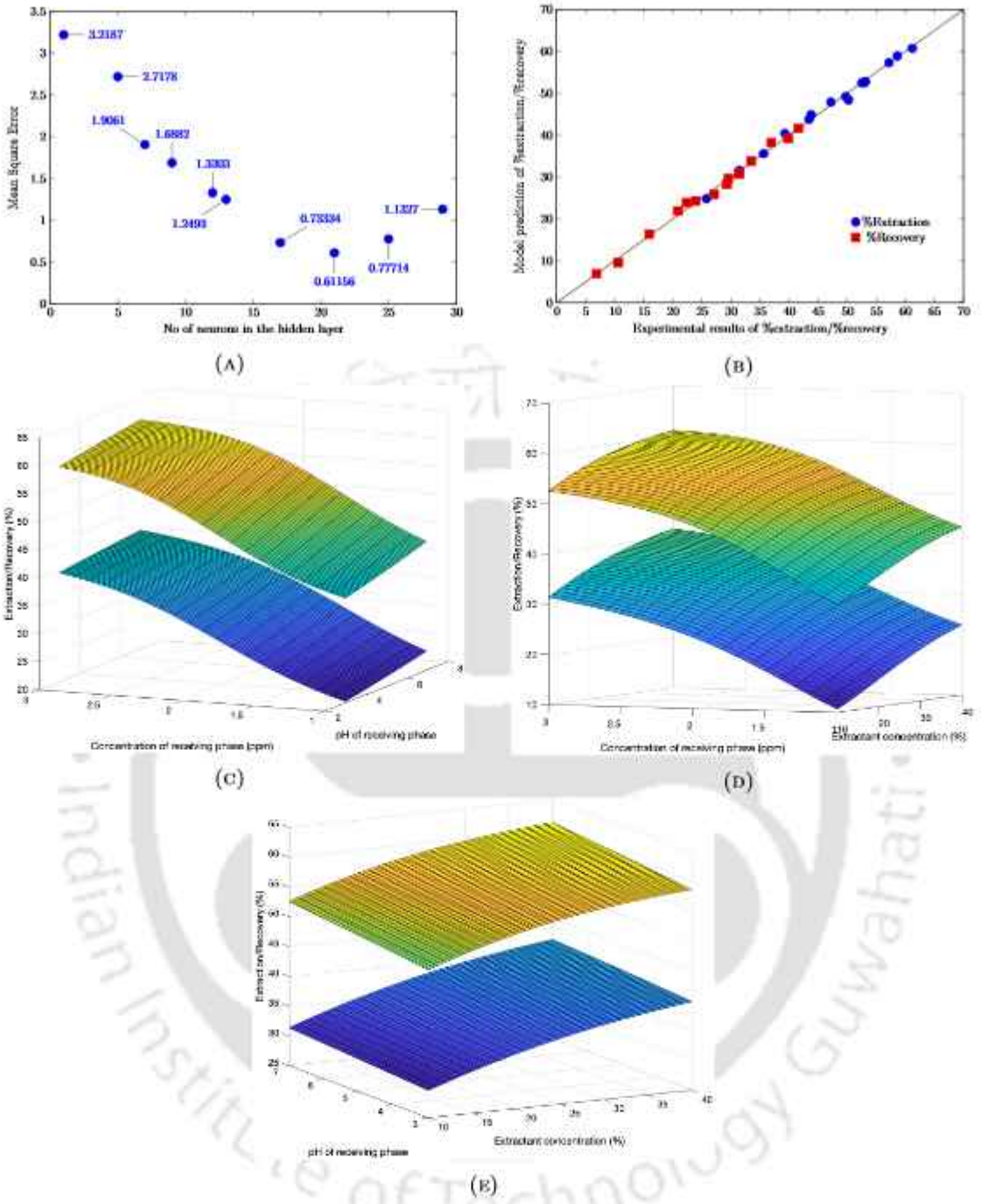

FIGURE 6.4: Various plots of three phase SLM for $As^{(III)}$:$As^{(V)}$:: 2 : 1 using machine learning

- The permeability coefficients suggests that the transport efficiency of $As^{(V)}$was better than that of $As^{(III)}$.

- Two ppm and 3 ppm were found to be the optimum conditions for the concentration of the receiving phase with pH 7 and 250 rpm stirring speed. However, the extractant concentration varied from 10% for $As^{(III)}$to 30% for $As^{(V)}$and 40% for combined arsenic ions in the ratio of (1:1), (1:2), and (2:1).

- The extraction efficiency varied from 59% - 66.5% while the recovery efficiency was found to be in the range of 41% - 48.5% for all the arsenic ions.
- The maximum permeability coefficient for $As^{(V)}$with 30% extractant is 1.0242 $cm.h^{-1}$. However, the mass transfer coefficient in the organic phase was found to be maximum for $As^{(III)}$having a value of 1.39×10^{-3} $m.s^{-1}$.
- The minimum MSE was achieved with 4, 5, 27, 14, and 21 neurons in the hidden layer for $As^{(III)}$, $As^{(V)}$, and combined $As^{(III)}$-$As^{(V)}$ratios of (1:1), (1:2), and (2:1), respectively.
- The machine-learned results on the experimental data of $As^{(III)}$and $As^{(V)}$were not up to the mark in the FSSLM study. There were considerable process/model mismatch. Thus optimization was not successful.
- While the machine-learned results on the SLM data of combined arsenic species were better than the statistical model, the predicted values of extraction and recovery were very close to the experimental values with less than 1.5% error in most cases.
- The error (%) of statistical approach is in the range of 0.45-2.47 and ML-based analysis is in the range of 0.21-11.9 for extraction and recovery of all the arsenic species.

Abbreviation

ANN Artificial neural network

FCCCD Face-centered central composite

FSSLM Flat sheet supported liquid membrane

GA Genetic algorithm

ML Machine learning

MSE Mean squared error

Stats Statistical analysis

Nomenclature

A Membrane area

C Concentration of arsenic

D Diffusion coefficient

F Concentration of receiving phase

G pH of receiving phase

$\mathbf{H_1}$ Stirring speed

$\mathbf{H_2}$ Extractant concentration

J Molar flux

K Equilibrium extraction constant

P Permeability coefficient

t Time

V Volume of feed phase

x Distance

$\mathbf{Z^{E/R}}$ Extraction or recovery efficiency of arsenic ions

Δ_{aq} Aqueous phase resistance

Δ_{org} Organic phase resistance

δ Thickness of membranes

ϵ Porosity of membrane

τ Tortuosity of membrane pores

Chapter 7

Removal of arsenic by the hybrid technique

This chapter describes the development of a hybrid technique which is a combination of FSSLM with electrocoagulation methods. The setup consists of an FSSLM setup with iron and graphite electrodes placed in the receiving phase for electrocoagulation to occur leading to the formation of an iron-arsenic complex. Sodium chloride (NaCl) solution was used as the receiving phase for the hybrid technique. The concentration of NaCl was varied from 0.1M to 1M to study its effect on the formation of the iron-arsenic complex. Different physicochemical parameters have been varied to optimize the transport and removal efficiency of arsenic species through RSM using face-centered central composite design. The chapter includes adsorption isotherm and kinetics modeling for the removal of arsenic from synthetic water samples containing arsenic in two different oxidation states, i.e., +3 and +5. Three different combinations of $As^{(III)}$and $As^{(V)}$in ratios of (1:1), (1:2), and (2:1) have also been studied here to better understand the removal process in such cases.

7.1 Development and validation of model through DOE

The experimental design includes sixteen factorial runs, eight axial runs and six centre points comprising of thirty experiments for $As^{(V)}$study. The variation of studied independent variables are as follows:

A concentration of sodium chloride in the receiving phase in the range of 0.1−1 M

B Concentration of extractant in the range of 10−40% (vol/vol)

C pH of receiving phase in the range of 3−7

D Voltage in the range of 1−2 V.

These have been depicted using both coded (-1 to +1) and actual values and the initial arsenic concentration is 100 ppb as reported in Table B.36. The experimental data was fitted based on sequential analysis of variance (ANOVA) modeling and predicted a quadratic model fitting has been reported in Table B.37. The quadratic equations in terms of coded factors for $As^{(V)}$ions is expressed as given in Eq.(7.1).

$$RE_1 = 81.33 + 12.06A + 7.67B + 5.72C + 3.44D - 2.06AB - 1.19AC - 0.69AD + 0.81BC + 0.063BD - 0.062CD - 9.50A^2 - 2.00B^2 + 0.50C^2 - 1.00D^2 \quad (7.1)$$

This was calculated using the significant p-value and non-significant lack of fit. A diagnostic study was done for the best model using the normal plot of residuals, with an actual vs. predicted plot to check the outliers. The model statistics like coefficient of determination (R^2), predicted residual error sum of squares (PRESS) and coefficient of variation (CV) has also been reported in Table B.38. Finally, the plots generated has been used to depict the optimum process conditions for maximum arsenic removal efficiency.

Based on the model for $As^{(V)}$, it was found that the pH and the extractant concentration played a significant role in the removal efficiency. Hence the independent variables for $As^{(III)}$study has been changed. The studied independent variables are as follows:

A pH of feed phase in the range of 3−9

B pH of receiving phase in the range of 3–7

C Concentration of extractant in the range of 10–40%.

In case of $As^{(III)}$, the model has eight factorial runs, six axial runs and six centre points to design twenty experiments to study the removal efficiency. The initial arsenic concentration is 100 ppb and based on the $As^{(V)}$model the optimum conditions for voltage (2 V) and concentration of sodium chloride in the receiving phase (1 M) has been used to perform the experiments. Table B.39 shows the experimental design, range of independent variables and their corresponding values of the dependent variable retrieved from the experiments. The experimental data was fitted based on sequential analysis of variance (ANOVA) modeling and predicted a quadratic model fitting has been reported in Table B.40. The quadratic equations in terms of coded factors for $As^{(III)}$ions is expressed as given in Eq.(7.2).

$$RE_2 = 76.76 - 0.86A + 0.59B - 10.39C - 0.18AB - 0.11AC - 0.051BC - 1.75A^2 + 1.04B^2 + 4.78C^2 \quad (7.2)$$

This was calculated using the significant p-value and non-significant lack of fit. The model statistics like coefficient of determination (R^2), predicted residual error sum of squares (PRESS) and coefficient of variation (CV) has also been reported in Table B.38.

The Model F-value for $As^{(V)}$is 32.57 that implies the model is significant. There is only a 0.01% chance that a value this large could occur due to noise as its corresponding p-value is less than 0.0001. The p-values of the coded factors A, B, C are less than 0.0001, indicating these variables to be significant. Thus, the extractant concentration and pH of the receiving phase are found to be the significant factors to maximize the removal efficiency. The lack of fit F-value of 2.89 implies that it is not significant relative to the pure error and there is a 12.67% chance that this value could occur due to noise. The R^2 value is 0.9681 and the predicted R^2 of 0.8722 is in reasonable agreement with the adjusted R^2 of 0.9384. The adequate precision value measures the signal to noise ratio. A ratio of 23.471 indicates an adequate signal. The statistical analysis of the quadratic model predicted for removal of $As^{(V)}$on the basis of normal plot of residuals, residuals versus predicted and predicted versus actual plots are given in Fig. A.28.

The F-value of the $As^{(III)}$model is 39.10 and its p-value is less than 0.0001 indicating it to be a significant model. In this case the coded factor C that is extractant concentration is found to be the significant model term. The F-value of the lack of fit is 3.30 that is insignificant relative to the pure error. Based on its p-value, there is a 10.81% chance that this F-value could occur due to noise. The R^2 value is 0.9724 and the predicted R^2 of 0.8613 is in reasonable agreement with the adjusted R^2 of 0.9475. The adequate precision value of 18.179 indicates an adequate signal. The normal plot of residuals follows a straight line indicating a normal distribution as shown in Fig. A.29a. While the residuals versus predicted plot is a random scatter within the outliers, the predicted versus actual plot is split by the 45 degree line indicating the model to be well predicted as given in Fig. A.29.

As pH is one of the significant factors for removal of arsenic, as observed in the individual arsenic cases, the study of combined $As^{(III)}$and $As^{(V)}$species focus primarily on it. Another significant factor, extractant concentration has already been established, hence it has not been repeated here. Moreover, the interactive effect of pH and extractant concentration in previous quadratic equations are not as prominent as the main effects, hence it has been neglected here to understand the effects of pH prominently. The experimental design consisted of 4 factorial runs, 4 axial runs and 5 centre points comprising of 13 experiments each for $As^{(III)}$-$As^{(V)}$in the ratios of $As^{(III)}$:$As^{(V)}$:: 1 : 1 , $As^{(III)}$:$As^{(V)}$:: 1 : 2 and $As^{(III)}$:$As^{(V)}$:: 2 : 1 . The studied independent variables include pH of feed phase (A) and pH of receiving phase (B) in the range of 3-9 & 3-7, respectively. Table B.43 show the experimental design with factors or independent variables and their corresponding values of the response or dependent variable retrieved from the experiments.

The optimum extractant concentration of 40% obtained from the supported liquid membrane study[218] has been applied here. Sodium chloride salt (1M) was used as the receiving phase solution and a potential difference of 2V was applied throughout the experiments. The experimental data was fitted based on sequential analysis of variance (ANOVA) modeling and predicted a quadratic model fitting as reported in Table B.44. The quadratic equations in terms of coded factors for the combined arsenic ions are

given as

$$Y_{As^{(III)}:As^{(V)}::\,1:1} = 84.23 + 1.9A + 6.19B - 1.72AB - 1.25A^2 + 4.09B^2 \quad (7.3)$$

$$Y_{As^{(III)}:As^{(V)}::\,1:2} = 83.64 + 2.02A + 5.79B - 1.45AB - 1.44A^2 + 3.97B^2 \quad (7.4)$$

$$Y_{As^{(III)}:As^{(V)}::\,2:1} = 83.63 + 2.37A + 5.29B - 1.36AB - 1.46A^2 + 3.79B^2 \quad (7.5)$$

This was calculated using the significant p-value of the quadratic model and non-significant lack of fit. A diagnostic study was done for the model using the normal plot of residuals, with an actual vs. predicted plot to check the outliers. The model statistics like coefficient of determination (R^2), predicted residual error sum of squares and coefficient of variation have also been reported in Table B.45. Finally, the plots generated, viz. Fig. A.32, have been used to depict the optimum process conditions for maximum arsenic removal efficiency.

The Model F-value of 126.85 for the case of $As^{(III)}$:$As^{(V)}$:: 1 : 1 implies the model is significant. There is only a 0.01% chance that a value this large could occur due to noise as its corresponding p-value is less than 0.0001. The p-Values of the coded factor B, B^2 are less than 0.0001, indicating that the variable pH of the receiving phase is significant in this case. In Fig. A.32a, the effect of the parameters on the removal efficiency is shown. The lack of fit F-value of 5.3 implies that it is not significant relative to the pure error and there is a 7.04% chance that a value this large could occur due to noise. The R^2 value is 0.9891 and the predicted R^2 of 0.9251 is in reasonable agreement with the adjusted R^2 of 0.9813. The adequate precision ratio of 36.347 indicates an adequate signal over signal to noise ratio. The quadratic model predicted on the basis of normal plot of residuals, residuals versus predicted and predicted versus actual plots are given in Fig. A.32d, Fig. A.32g and Fig. A.32j, respectively.

Fig. A.32b shows the effect of interaction of the parameters on the removal efficiency of combined arsenic species in $As^{(III)}$:$As^{(V)}$:: 1 : 2 ratio. The F-value is 163.37 and its p-value is less than 0.0001 indicating it to be a significant model. In this case the coded factors A, B and B^2 are found to be the significant model terms. Thus, pH of both the phases play an important role in enhancing the removal efficiency. The F-value of the lack of fit is 1.47 that is insignificant relative to the pure error. Based on its p-value, there is a 34.83% chance that this F-value could occur due to noise. The R^2 value is 0.9915 and the predicted R^2 of 0.9627 is in reasonable agreement with the adjusted R^2 of

0.9854. The adequate precision value of 41.65 indicates an adequate signal. The normal plot of residuals indicates a normal distribution as shown in Fig. A.32e. While the residuals versus predicted plot is a random scatter within the outliers, i.e. Fig. A.32h, and the predicted versus actual plot is split by the 45 degree line indicating the model to be well predicted as shown in Fig. A.32k.

In case of $As^{(III)}$:$As^{(V)}$:: 2 : 1 ratio of combined $As^{(III)}$-$As^{(V)}$species, the F-value of the model is 105.47 with p-value less than 0.0001. The model is significant with the coded factors A, B and B^2 as the significant model terms. The lack of fit F-value of 2.57 implies that it is not significant relative to the pure error and a p-value of 0.1916 elucidates that there is 19.16% chance of F-value this large that could occur due to noise. The impact of interaction of the parameters on the removal efficiency of combined arsenic species is given in Fig. A.32c. The R^2 value is 0.9869 and the predicted R^2 of 0.9277 is in reasonable agreement with the adjusted R^2 of 0.9775. The adequate precision value of 33.8 indicates it to be an adequate signal. The linear normal plot of residuals indicate a normal distribution as shown in Fig. A.32f. In Fig. A.32i the residuals versus predicted plot is a random scatter within the outliers. The predicted versus actual plot is split by the 45 degree line indicating the model to be well predicted similar to the other models as shown in Fig. A.32l. The Table B.45 shows the optimum conditions obtained from the quadratic modelling.

7.2 Effect of variables

The concentration of extractant is found to be a significant variable for the removal of both the arsenic ions. In the $As^{(V)}$model, the pH and concentration of the receiving phase was found to be the other significant parameters. The effect of the variables on the removal efficiency are plotted in Fig. A.30 and Fig. A.31 for $As^{(III)}$and $As^{(V)}$, respectively.

7.2.1 Variation of pH in feed phase

The pH of the feed phase was not varied for $As^{(V)}$salt. The experiments were performed at the reported pH of $As^{(V)}$salt solution (i.e. pH 5.68) in accordance with the water samples in Assam [290]. However, pH was varied for $As^{(III)}$solution in accordance with

the report on contaminated groundwater conditions of nearby areas of Digboi refinery in Upper Assam [242]. The minimum (pH=3) and maximum (pH=9) in that area were reported by Prakash et al. [240] and Bordoloh and Barua [241], respectively. However, the variation of pH in the range of 3−9 in the feed phase has little impact on the removal of $As^{(III)}$as arsenic exists as H_3AsO_3 while pH<9 [283]. Interactions between arsenic and Aliquat 336 takes place mainly in the feed-membrane interphase. The ability of Aliquat 336 to interact with undissociated forms of arsenic over a wide range of pH favours the removal of arsenic. This is further confirmed by the predicted model.

The pH 7 of the receiving phase is found to be favourable for maximum removal of the arsenic ions in all the three combined species as ferric hydroxide produced by the hydrolysis of the ferrous ions starts precipitating in this pH range[243]. This leads to the formation of flocs by polymerization of $Fe(OH)_n$ that causes the adsorption of arsenic ions. pH 6.5 of the feed phase was found to be favourable for maximum removal of combined arsenic ions. Interested readers may refer to the Table B.45 and Fig. A.31 for detailed data and graphical representation. However, in the case of $As^{(III)}$:$As^{(V)}$:: 1 : 1 ratio of $As^{(III)}$-$As^{(V)}$, pH of receiving phase plays a significant role in the removal efficiency as it favours the formation of iron oxyhydroxides from the ferrous ions and leads to the oxidation of $As^{(III)}$to $As^{(V)}$. In case of $As^{(III)}$:$As^{(V)}$:: 1 : 2 and $As^{(III)}$:$As^{(V)}$:: 2 : 1 ratios, pH of feed phase and pH of receiving phase are significant factors for maximum removal efficiency. In this range of feed phase pH, $As^{(III)}$exists as H_3AsO_3 and $As^{(V)}$exists as $H_2AsO_4^-$, $HAsO_4^{2-}$, that interacts with aliquat to form the complex at the feed-membrane interphase. When the ratio of $As^{(III)}$to $As^{(V)}$ions is either $As^{(III)}$:$As^{(V)}$:: 1 : 2 or $As^{(III)}$:$As^{(V)}$:: 2 : 1 , either of the arsenic ions compete with each other to form the aliquat-arsenic complex for which the feed phase pH becomes an important factor in comparison to $As^{(III)}$:$As^{(V)}$:: 1 : 1 ratio of arsenic species. While the pH of the receiving phase plays a dominant role in the removal of arsenic species in all the three ratios as the oxidation of $As^{(III)}$to $As^{(V)}$takes place that leads to the generation of $H_2AsO_4^-$, $HAsO_4^{2-}$ and AsO_4^{3-} anions[77].

7.2.2 Extractant concentration

The concentration of extractant plays an integral role in the extraction of arsenic ions as it binds with the arsenic species and transports them from one phase to another due

to concentration gradient. In the removal of $As^{(V)}$, around 30% of extractant is required due to the formation of $H_2AsO_4^-$ and $HAsO_4^{2-}$ dissociated ions based on the pH of the feed phase. This follows the reaction stoichiometry as given in reaction Eqs.(2.34)-(2.35), according to which total three moles of NR_4Cl reacts with $H_2AsO_4^-$ & $HAsO_4^{2-}$. The amount required for removal of $As^{(III)}$is less compared to that of $As^{(V)}$ions as reported in Table B.38. This is in accordance with the stoichiometry of the reactions mentioned in section 2.3. 10% of Aliquat 336 is found to be optimum for the removal of $As^{(III)}$owing to the presence of H_3AsO_3 as one mole of NR_4Cl reacts with one mole of H_3AsO_3. Interested readers may refer to the Table B.38 and Fig. A.29 for detailed data and trend analysis.

7.2.3 Variation of pH in the receiving phase

The pH of the receiving phase plays a dominant role in the removal of $As^{(V)}$. pH 7 is found to be favourable for maximum removal of the arsenic ions as ferric hydroxide generated by the hydrolysis of the ferrous ions starts precipitating at this pH [243]. This in turn leads to the formation of flocs by polymerization of $Fe(OH)_n$ that causes the adsorption of arsenic ions. The initial pH of the receiving phase was varied in the range of 3−7. But it was not found to be a significant variable for $As^{(III)}$in comparison to $As^{(V)}$as it exists as H_3AsO_3 at pH<9 [283]. Meanwhile, the oxidation of $As^{(III)}$to $As^{(V)}$takes place that leads to the generation of $H_2AsO_4^-$, $HAsO_4^{2-}$ and AsO_4^{3-} anions [77]. The pH in the receiving phase plays an important role in the formation of iron oxyhydroxides from the ferrous ions. This process in itself increases the pH of the aqueous solution favouring the oxidation of $As^{(III)}$to $As^{(V)}$.

7.2.4 Concentration of sodium chloride in the receiving phase

Sodium chloride solution plays the role of an electrolyte in the receiving solution that facilitates the conductivity in the solution and reduces the ohmic drop and energy consumption during electrocoagulation process. The conductivity in solution is reported to be maximum and the cell voltage correction for ohmic drop is minimum for sodium chloride compared to other sodium and potassium salts [291]. Sodium cations are reported to have no effect on the electrocoagualtion process. However, chloride ions in comparison to sulphate and nitrate ions are favourable for anodic dissolution due to its

corrosive nature that enhances the release of the iron from the anode. Further, these anions play a significant role in the chemical oxidation of the coagulant species during the electrocoagulation process [292]. Thus, sodium chloride is selected for the receiving phase and approximately 1.0 M sodium chloride solution is found to be optimum for the formation of iron-arsenic complexes in the receiving phase. Interested readers may refer to the Table B.38 and Fig. A.30 for detailed data and graphical representation. Based on the experiments and observations for $As^{(V)}$, 1.0 M sodium chloride was selected as the receiving phase for carrying out the removal of $As^{(III)}$. The role of NaCl is that of an electrolyte, acting as a medium to provide ion transport mechanism between the cathode and anode within the cell. Since, NaCl does not directly participate in the reactions for the removal of arsenic ions, the optimum condition obtained for $As^{(V)}$was applied to $As^{(III)}$, and combinations of $As^{(III)}$and $As^{(V)}$as well.

7.3 Characteristics of precipitate

EDX coupled with SEM and TEM have been employed for chemical characterization of the precipitate. The measured intensities provide quantitative information on the elemental composition and distribution. The EDX elemental analysis of precipitate obtained from the removal of $As^{(III)}$and $As^{(V)}$is given in Fig. 7.1 and Fig. 7.2. As

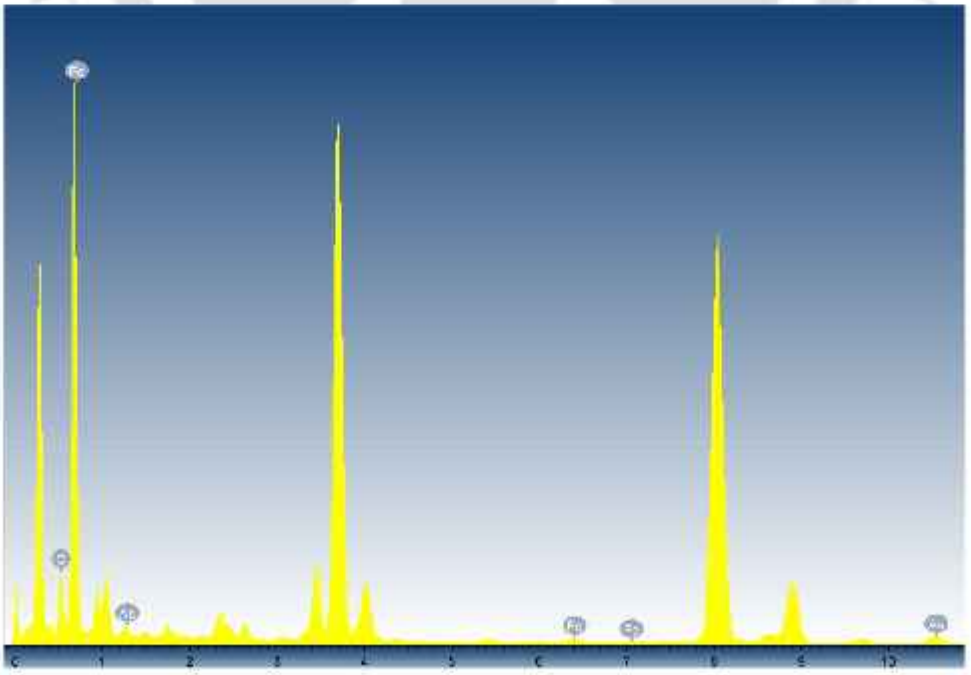

FIGURE 7.1: TEM-EDX analysis of the precipitate obtained from Fe-$As^{(III)}$interactions

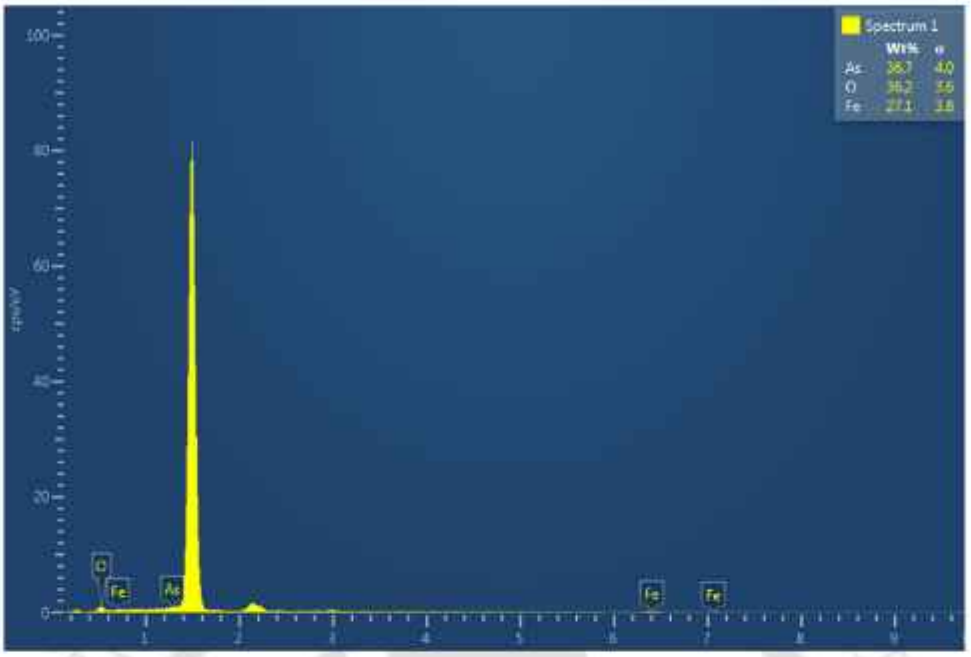

FIGURE 7.2: SEM-EDX analysis of the precipitate obtained from Fe-$As^{(V)}$interactions

the SEM-EDX analysis was inconclusive, TEM-EDX analysis was carried out to analyze the precipitate containing $As^{(III)}$. The maximum peak is of aluminium as aluminium foil has been used for the drop casting technique. The major elements include iron, arsenic and oxygen. The mapping of the elements as given in Fig. 7.3 and Fig. 7.4 confirms the distribution of iron, oxygen and arsenic in different colors as the main elements that constitute the precipitate. Several peaks for maghemite are observed in the range of 212-729 cm^{-1}. Similarly, for lepidocrocite the range of IR adsorption frequency bands lie in the range of 223-3400 cm^{-1}. In case of goethite, the IR adsorption range varies from 268-3400 cm^{-1}, while the range of IR adsorption peaks for hematite begins from 461 cm^{-1} and goes up to 3398.9 cm^{-1}. The analysis of the composition of the precipitate involving $As^{(III)}$and $As^{(V)}$is reported in Table 7.1.

TABLE 7.1: Analysis of the composition of the precipitate

Element	TEM-EDX for $As^{(III)}$		SEM-EDX for $As^{(V)}$
	Weight %	Atomic %	Weight %
Oxygen	79.11	94.3	36.2
Arsenic	16.53	4.21	36.7
Iron	4.36	1.49	27.1

The FTIR spectra of $As^{(III)}$and $As^{(V)}$are given in Fig. 7.5. The peak in the range of 1100-1700 cm^{-1} corresponds to $As^{(V)}$and the presence of a peak at 587 cm^{-1} in $As^{(III)}$indicates

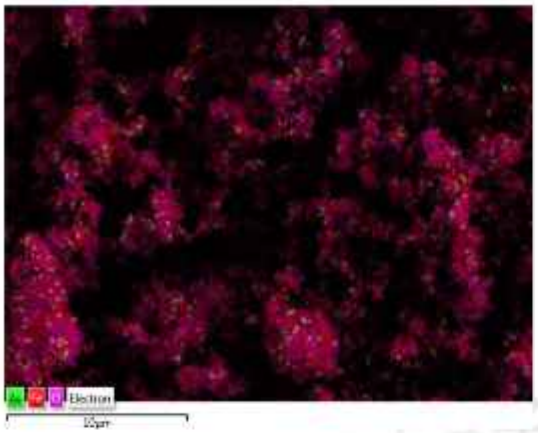

(A) Mapping of arsenic, iron and oxygen present in the precipitate

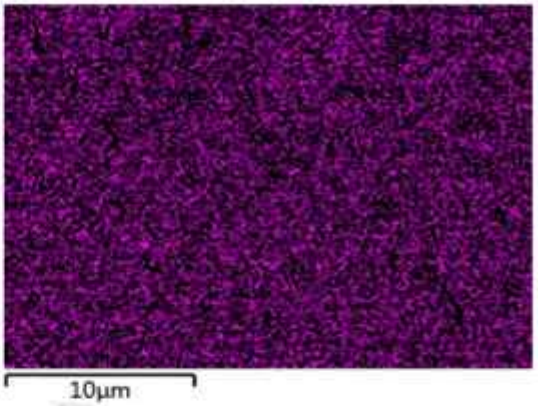

(B) Mapping of oxygen found in the precipitate

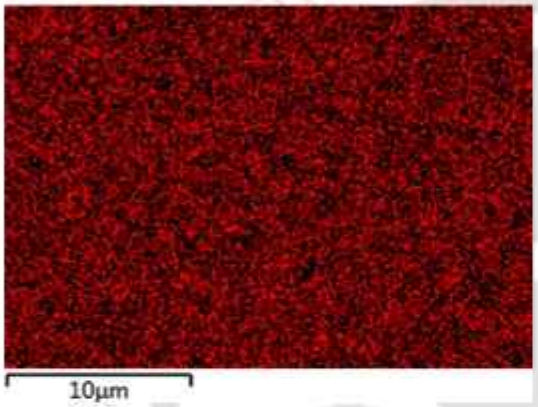

(C) Mapping of iron present in the precipitate

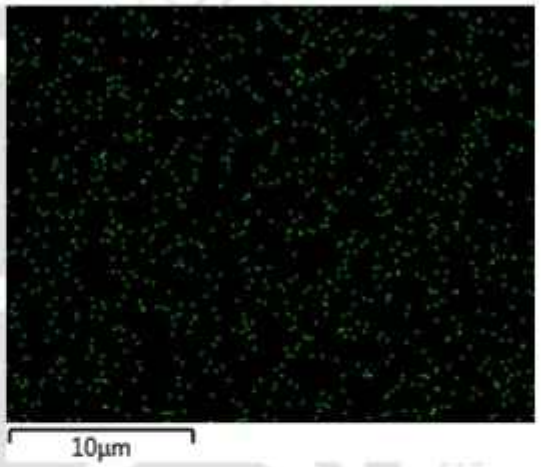

(D) Mapping of arsenic in the precipitate

FIGURE 7.3: Mapping of elements found in the Fe-$As^{(III)}$precipitate by SEM

the transformation of arsenic species from $As^{(III)}$to $As^{(V)}$[293]. FTIR spectra of pristine iron has been observed by several other researchers elsewhere[294–302].

The transformation of iron oxyhydroxides into four phases namely, hematite, maghemite, goethite and lepidocrocite have been observed in this study. Their corresponding IR adsorption bands in the absence of arsenic are listed in Table B.41. On the other hand, Table B.42 includes the list of IR adsorption frequency bands obtained due to the formation of iron-arsenic precipitate from the removal of arsenic species in the receiving phase by the hybrid technique. The transformation of different forms of iron oxides for adsorption of arsenic species are indicated by the peaks in the range of 523-1055 cm^{-1}. The peaks at 523 cm^{-1} and 554 cm^{-1} are ascribed to hematite (Fe_2O_3) whereas the peaks at 632 cm^{-1} and 659 cm^{-1} indicate the presence of goethite (α-FeOOH) [301]. The peak at 894 cm^{-1} is attributed to the Fe-O-As bending vibration in α-FeOOH [303]. The peak at 1000 cm^{-1} confirms the presence of lepidocrocite (β-FeOOH) in the

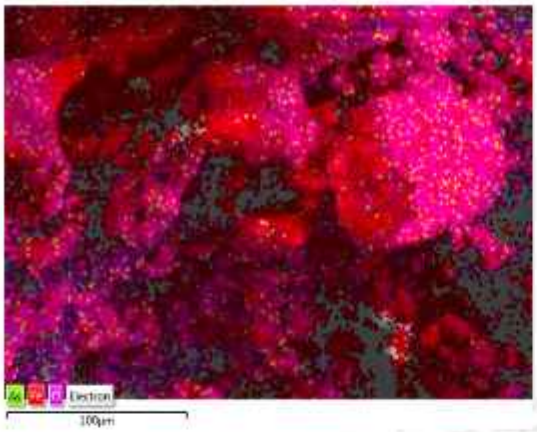

(A) Mapping of arsenic, iron and oxygen present in the precipitate

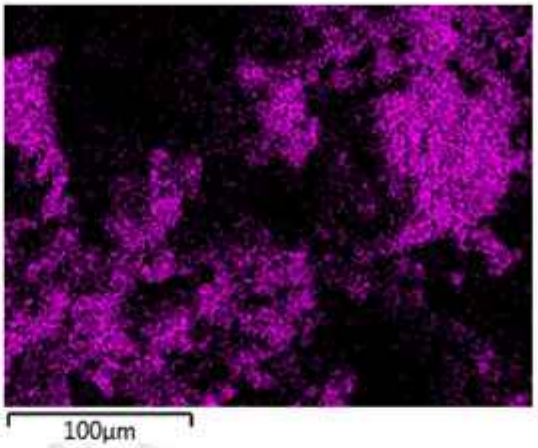

(B) Mapping of oxygen found in the precipitate

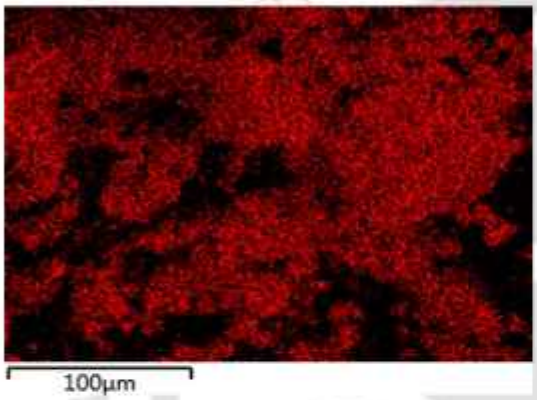

(C) Mapping of iron present in the precipitate

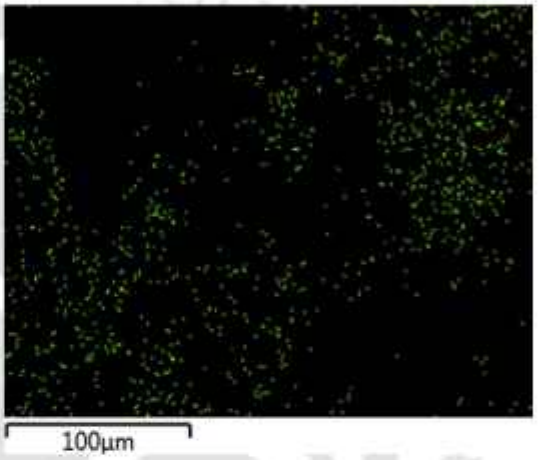

(D) Mapping of arsenic in the precipitate

FIGURE 7.4: Mapping of elements found in the Fe-$As^{(V)}$precipitate by SEM

precipitate [299]. The shift of the peak at 1029 cm^{-1} is caused by the bending vibration of Fe-O-OH bond present in β-FeOOH due to interactions with arsenic ions [304]. The shift in the peak at 1055 cm^{-1} indicates the presence and interaction of iron oxide in the maghemite phase [298]. Fig. 7.6 shows the XRD analysis of the calcined samples of $As^{(III)}$and $As^{(V)}$. The XRD pattern confirms the formation of ferric oxide in both the precipitates [305]. The peak positions obtained are 24.12 (012), 33.16 (104), 35.64 (110), 40.88 (113), 49.44 (024), 54.06 (116), 57.56 (018), 62.42 (214), 63.98 (300). This further corroborates with the formation of hematite phase of iron oxide in the precipitate [306]. α-Fe_2O_3 having a rhombohedral structure has been identified from all the peaks [307]. The size of the ferric oxide nanoparticle calculated from Debye–Scherrer equation is 11 nm [270].

The FTIR spectra of all the three combinations of arsenic species are given in Fig. 7.7a. The peaks in the range of 1100-1700 cm^{-1} corresponds to $As^{(V)}$indicating the conversion

of $As^{(III)}$to $As^{(V)}$[293]. The presence of iron oxides in different phases are indicated by the peaks at 879 cm^{-1}, 1045 cm^{-1} and 1087 cm^{-1}. The peak at 803 cm^{-1} is attributed to the arsenate adsorbed on iron oxide[303]. The peak at 879 cm^{-1} indicates the bending vibrations of Fe-O-OH in goethite[308].

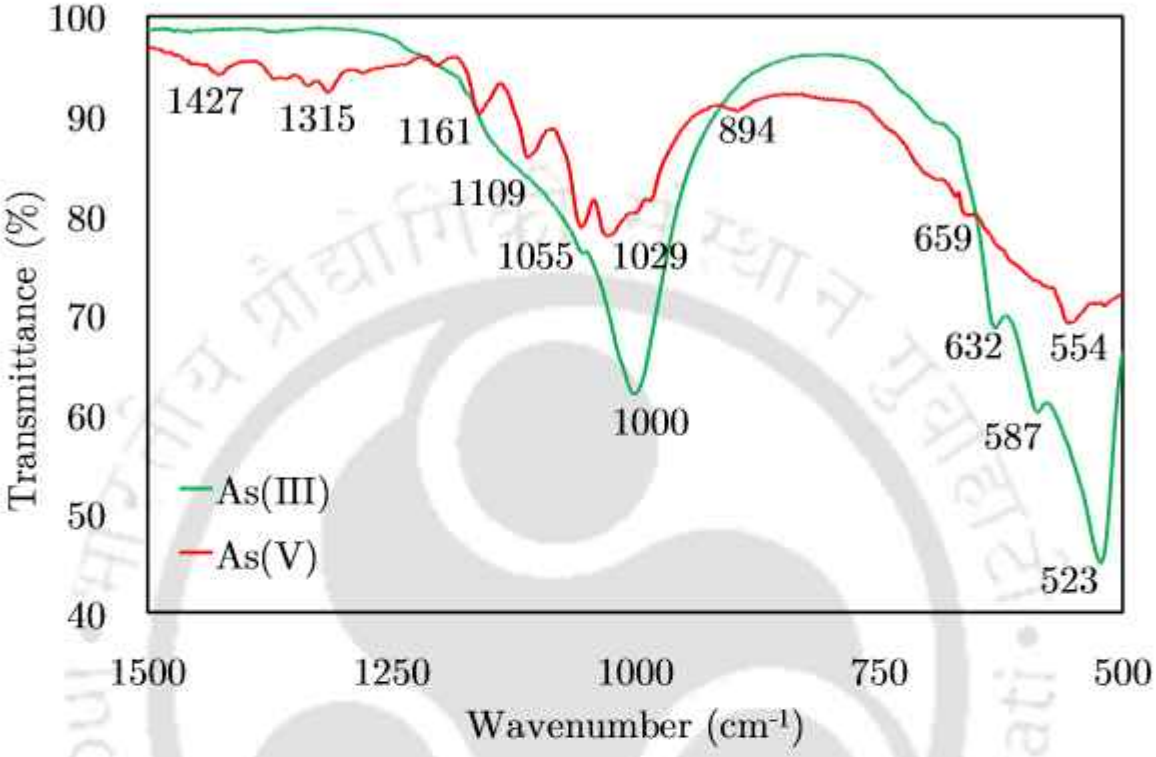

FIGURE 7.5: Plot of the FTIR data for the precipitate obtained from the removal of arsenic ions

The shift of the peak at 1045 cm^{-1} is due to the oscillatory vibrations in magnetite[299]. The peak at 1087 cm^{-1} further confirms the presence of iron oxide in the goethite phase[301]. Fig. 7.7b shows the XRD analysis of the calcined samples.

The XRD pattern confirms the presence of goethite, hematite and lepidocrocite in the precipitates[305]. The peak positions obtained are 27.25 (130)[307], 32.07 (104)[306], 35.64 (110), 45.36 (202)[307], 57.56 (018) and 62.42 (214). This further corroborates the formation of iron oxide in the precipitates[306]. The sizes of the ferric oxide nanoparticle calculated from Debye–Scherrer equation are 35, 38 and 47nm for cases $As^{(III)}$:$As^{(V)}$:: 1 : 1 , $As^{(III)}$:$As^{(V)}$:: 1 : 2 and $As^{(III)}$:$As^{(V)}$:: 2 : 1 combination of arsenic ions, respectively[270]. EDX coupled with SEM have been used to analyze the elements for chemical characterization of the precipitate. The measured intensities provide quantitative information on the elemental composition and distribution. The EDX elemental analysis of precipitate is given in Fig. 7.8.

The maximum peak is of aluminium as aluminium foil has been used for the drop casting technique. The major elements include iron, arsenic and oxygen. The mapping of the elements as given in Fig. 7.9a confirms the distribution of oxygen, iron and arsenic in different colors as the main elements that constitute the precipitate are shown in Fig. 7.9b, Fig. 7.9c and Fig. 7.9d respectively.

7.4 Adsorption isotherm modelling

The adsorption data of $As^{(III)}$, $As^{(V)}$and combined arsenic species were fitted into the isotherm models, viz. Eq.(2.84) through Eq.(2.94), as shown in the Fig. 7.10 and Fig. 7.11. The Freundlich isotherm shows that the adsorption for removal of the combined arsenic species fit well with R^2 varying from 0.9519 to 0.9759.

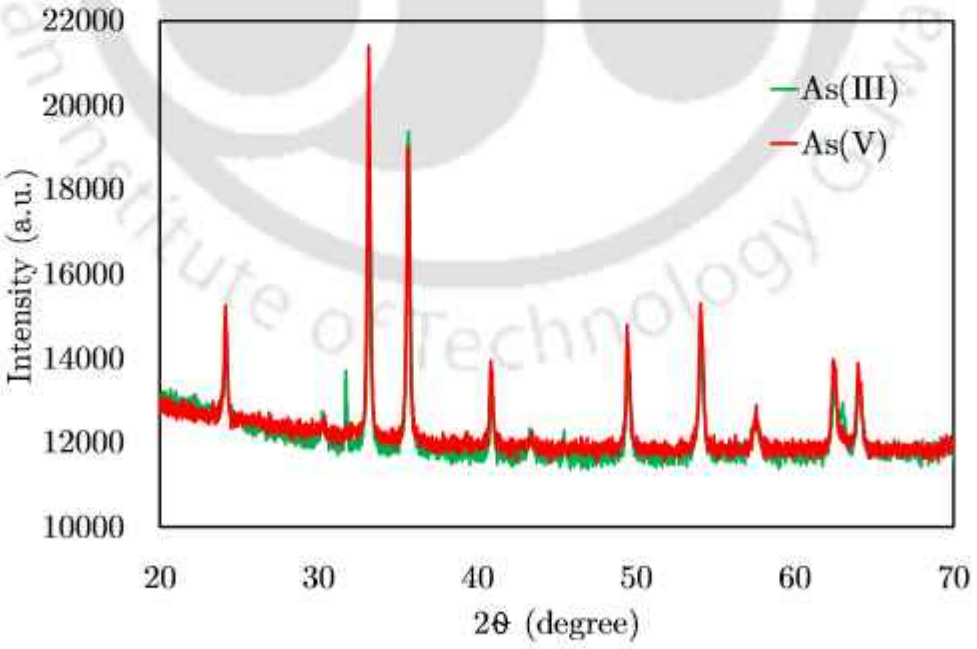

FIGURE 7.6: Plot of the XRD data for the precipitate obtained from the removal of arsenic ions

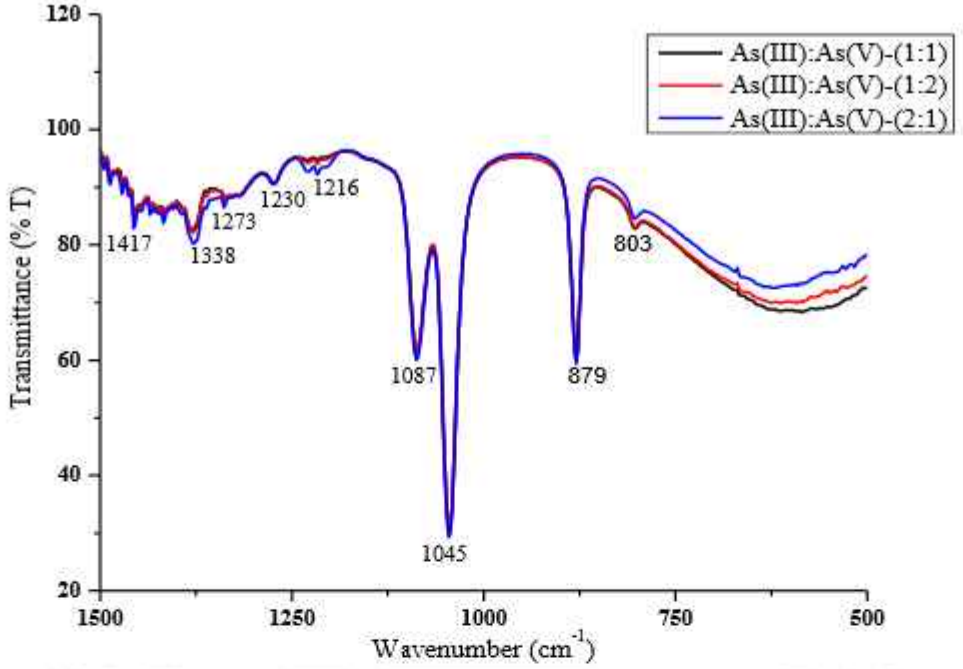

(A) Plot of the FTIR data

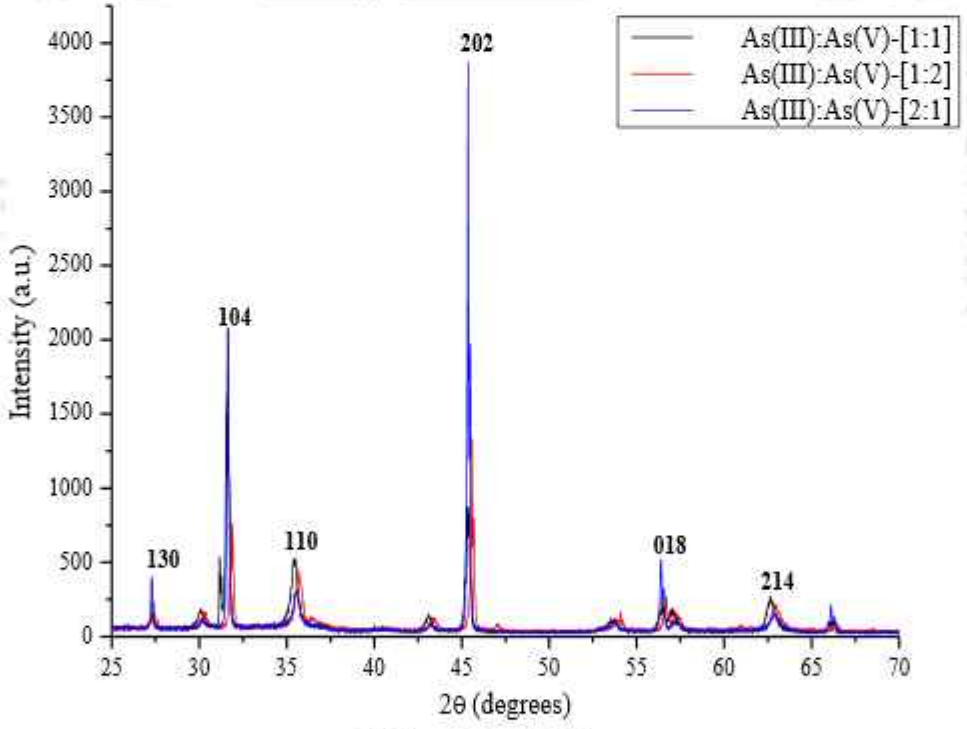

(B) Plot of the XRD data

FIGURE 7.7: Plots for the precipitate obtained from the removal of arsenic ions

TABLE 7.2: Coefficient of the isotherm models for all the arsenic ions

Model	Parameters	As(III)	As(V)	As(III):As(V) :: (1:1)	As(III):As(V) :: (1:2)	As(III):As(V) :: (2:1)
Langmuir	K_L	-106.57	-126.54	0.384	1.222	0.956

	R_L	-9.4 x 10^{-5}	-7.9 x 10^{-5}	0.025	0.0054	0.0069
	R^2	0.9772	0.9038	0.9125	0.9571	0.909
	RMSE	2.3683	12.09604	3.924	1.435	1.702
	χ^2	0.1613	4.09495	0.711	0.066	0.323
	HFEF	0.2511	0.53248	2.279	0.432	1.86
Freundlich	ln K_F	17.352	32.226	43.048	3.2724	19.944
	1/n	4.227	7.0588	11.143	1.6381	5.9635
	R^2	0.9594	0.9593	0.9759	0.9519	0.9688
	RMSE	0.0846	0.2197	0.2030	0.0524	0.1442
	χ^2	0.0020	0.0160	0.0170	0.0008	0.0061
	HFEF	0.0844	0.1243	0.004	0.149	0.661
Redlich-Peterson	R_P	-3.227	-6.059	-10.143	-0.6378	-4.9635
	ln A	17.352	32.226	43.048	3.2712	19.944
	R^2	0.9322	0.9455	0.9710	0.7517	0.9556
	RMSE	0.0846	0.2197	0.414	0.0522	0.1442
	χ^2	0.0053	0.0244	0.096	0.0041	0.012
	HFEF	0.2337	0.1939	32.329	0.861	0.82
Sips	K_S	4.227	7.059	0.92	0.56	0.85
	a_S	2.9 x 10^{-8}	1.0 x 10^{-14}	0.021	0.123	0.035
	R^2	0.9594	0.9593	0.976	0.952	0.969
	RMSE	0.0846	0.2197	0.018	0.0312	0.024
	χ^2	0.0020	0.0160	8E-5	0.00024	0.00015
	HFEF	0.0885	0.1272	12.14	0.0875	0.066
Temkin	b	1092.91	1050.15	1962.12	33480.7	1822.68
	K_T	156.34	176.39	66.72	92.11	45.65
	R^2	0.363	0.512	0.7678	0.9758	0.8909
	RMSE	0.34	0.42	0.055	0.0027	0.0511
	χ^2	0.0006	0.0578	0.03	0.00022	0.01242
	HFEF	0.45	1.24	497.33	0.589	2.475
Dubinin-Radushkevich	β	6.97 x 10^{-8}	1.15 x 10^{-7}	2.32 x 10^{-7}	3.34 x 10^{-8}	1.36 x 10^{-7}
	E	2677.62	2088.17	1469.65	3872.15	1916.86
	R^2	0.9573	0.956	0.9793	0.9487	0.9663
	RMSE	0.087	0.263	0.188	0.054	0.150

	χ^2	0.0021	0.0174	0.015	0.00086	0.012
	HFEF	0.0853	0.1298	0.002	0.155	0.00234
Jovanovic	q_{max}	0.0004	0.00003	4 x 10^{-5}	0.0043	0.0133
	K_J	-601.61	-1076.2	-585.13	-90.922	-65.439
	R^2	0.9668	0.9717	0.9779	0.948	0.9298
	RMSE	0.0764	0.1831	0.1552	0.0015	0.0066
	χ^2	0.0016	0.0111	0.1396	0.00097	0.0052
	HFEF	0.0815	0.1022	2.3263	0.0098	0.0871
Halsey	η_H	-0.2366	-0.1416	0.0785	0.6313	1.0758
	K_H	0.0165	0.0104	49.0149	5.089	1.915
	R^2	0.9594	0.9593	0.9842	0.9592	0.9564
	RMSE	0.0846	0.2197	0.0082	0.0011	0.0037
	χ^2	0.0020	0.0160	0.0048	0.00069	0.0015
	HFEF	0.0840	0.1242	0.0949	0.0069	0.0376
Harkin-Jura	H_J	1.10 x 10^{-4}	3.49 x 10^{-5}	0.000142	0.000346	0.001882
	B	-4.773	-4.895	-4.024	-3.728	-3.533
	R^2	0.9468	0.6266	0.935	0.9095	0.9668
	RMSE	213.91	3335.57	269.49	129.87	36.1
	χ^2	36.69	3977.95	72	16.35	8.43
	HFEF	0.621	1.756	0.05	1.2	2.45

Similarly, the Dubinin-Radushkevich model fits well with the data in accordance to the $As^{(III)}$, $As^{(V)}$data suggesting the adsorption process to be heterogeneous in nature. The mean adsorption energy calculated from the Dubinin-Radushkevich isotherm is in the range of 1.5 - 3.9 kJ·mol^{-1} indicating a physical process of adsorption occurring for the arsenic species as it is below 8kJ·mol^{-1} [309]. Langmuir model fits well with the experimental values for all the arsenic species (vide Table 7.2), however the regression produces unrealistic model parameters, and thus the isotherm is not reliable. The χ^2 test values are low in the range of 0.066-0.711 indicating there is not much difference between linear and non-linear regression analysis of this model. However, the high RMSE and HFEF values indicate that there are differences between the experimental and predicted data of the adsorption model. This strengthens our assessment about the adsorption being heterogeneous in nature instead of homogeneous. The Temkin isotherm

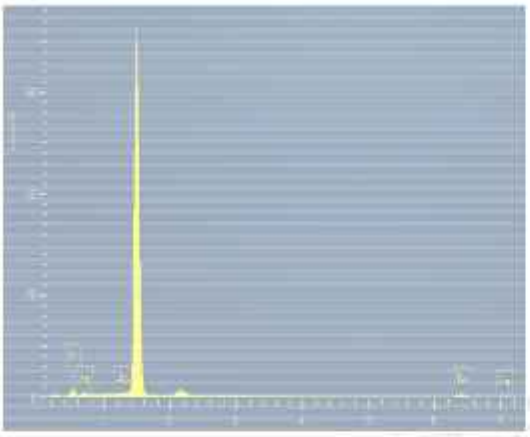

(A) $As^{(III)}$:$As^{(V)}$:: 1 : 1

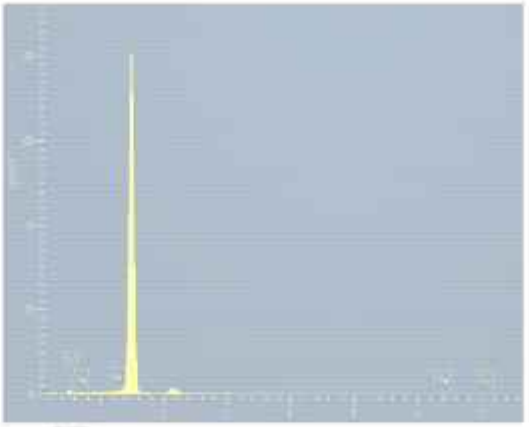

(B) $As^{(III)}$:$As^{(V)}$:: 1 : 2

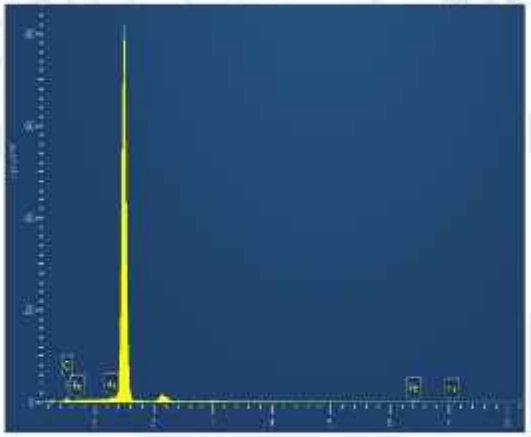

(C) $As^{(III)}$:$As^{(V)}$:: 2 : 1

FIGURE 7.8: FESEM-EDX analysis of the precipitate obtained from Fe-As interactions

model predicts that the binding energies decrease linearly with the surface coverage due to indirect interactions between the adsorbate-adsorbent in the adsorption process. However, the Temkin isotherm model fits well in case of (1:2) ratio of arsenic species. The heat of sorption equal to 1.96, 33.48 and 1.82 kJ·mol^{-1} for $As^{(III)}$-$As^{(V)}$in the ratio of (1:1), (1:2) and (2:1), respectively. The positive variation in adsorption energy (the value of b) indicates it to be a physical adsorption process [310] that is exothermic in nature [261]. The RMSE values in the range of 0.0027-0.055 and low χ^2 test values indicate that there is not much difference between the experimental and predicted data & between linear and non-linear regression analysis of this model. However, the high values of HFEF for $As^{(III)}$:$As^{(V)}$:: 1 : 1 and for $As^{(III)}$:$As^{(V)}$:: 2 : 1 further corroborates that this model fits well with the adsorption data of for $As^{(III)}$:$As^{(V)}$:: 1 : 2 .

Though the R^2 values are in the range of 0.9035-0.9668, the negative isotherm constants of Harkins-Jura model and high statistical error values of RMSE, χ^2 test and HFEF

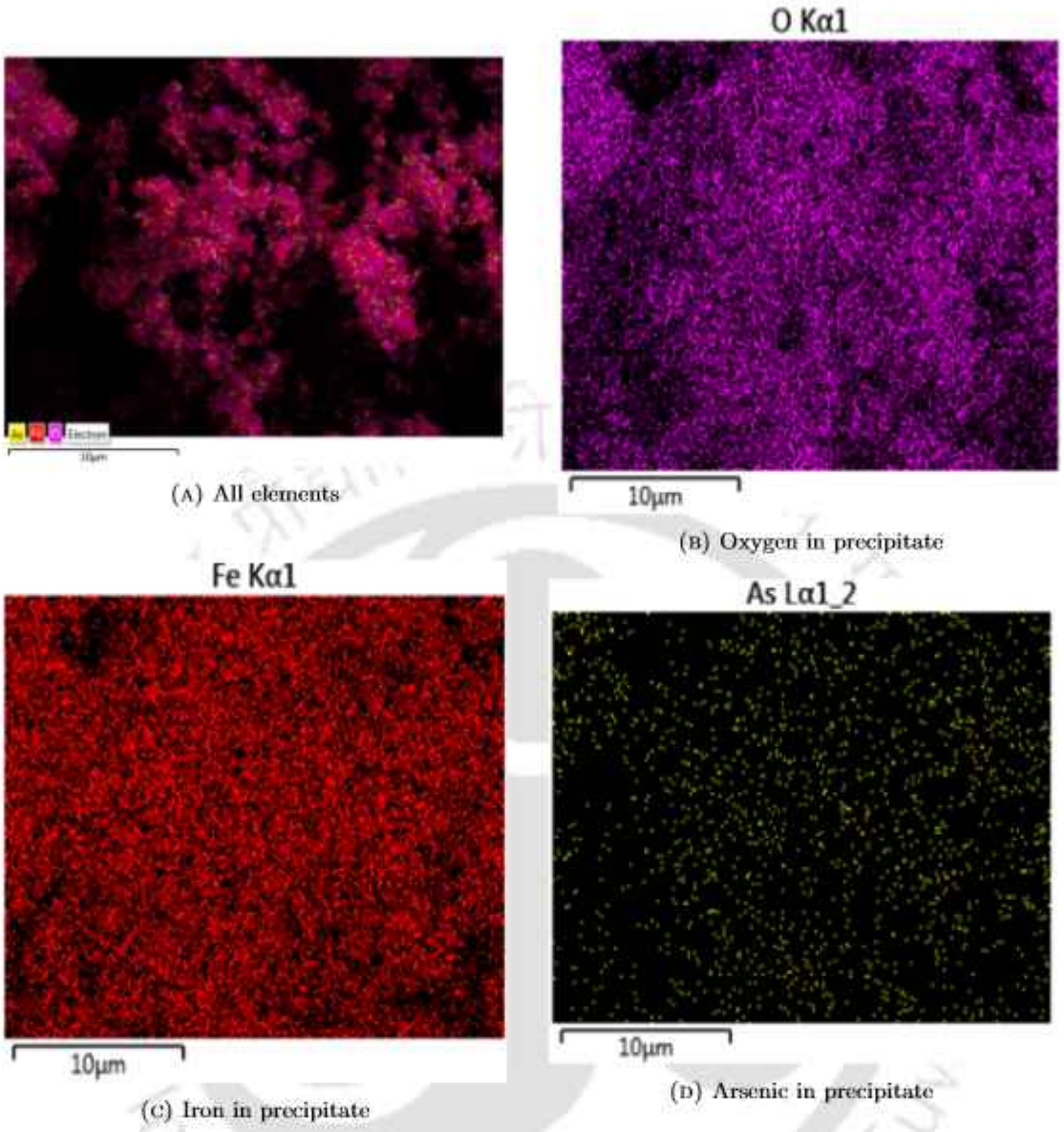

(A) All elements

(B) Oxygen in precipitate

(C) Iron in precipitate

(D) Arsenic in precipitate

FIGURE 7.9: Mapping of elements in the precipitate

renders this model to be a misfit for the adsorption data. Smaller statistical error values stipulate similarities between the calculated data obtained from the model and the experimental values. While larger values indicate the variation between the two sets of data. Based on this evaluation, Freundlich isotherm and Dubinin-Radushkevich model fits well with the adsorption data in comparison to the other two-parameter isotherm models. It is observed that the adsorption of combined arsenic species on iron complexes follow a pore filling exponential distribution that is heterogeneous in nature as suggested by the fitting of Freundlich and Dubinin-Radushkevich models. Moreover, indirect adsorbate-adsorbate interactions occur leading to the generation of adsorption energies in all the molecules of the layer, which is estimated through Temkin isotherm

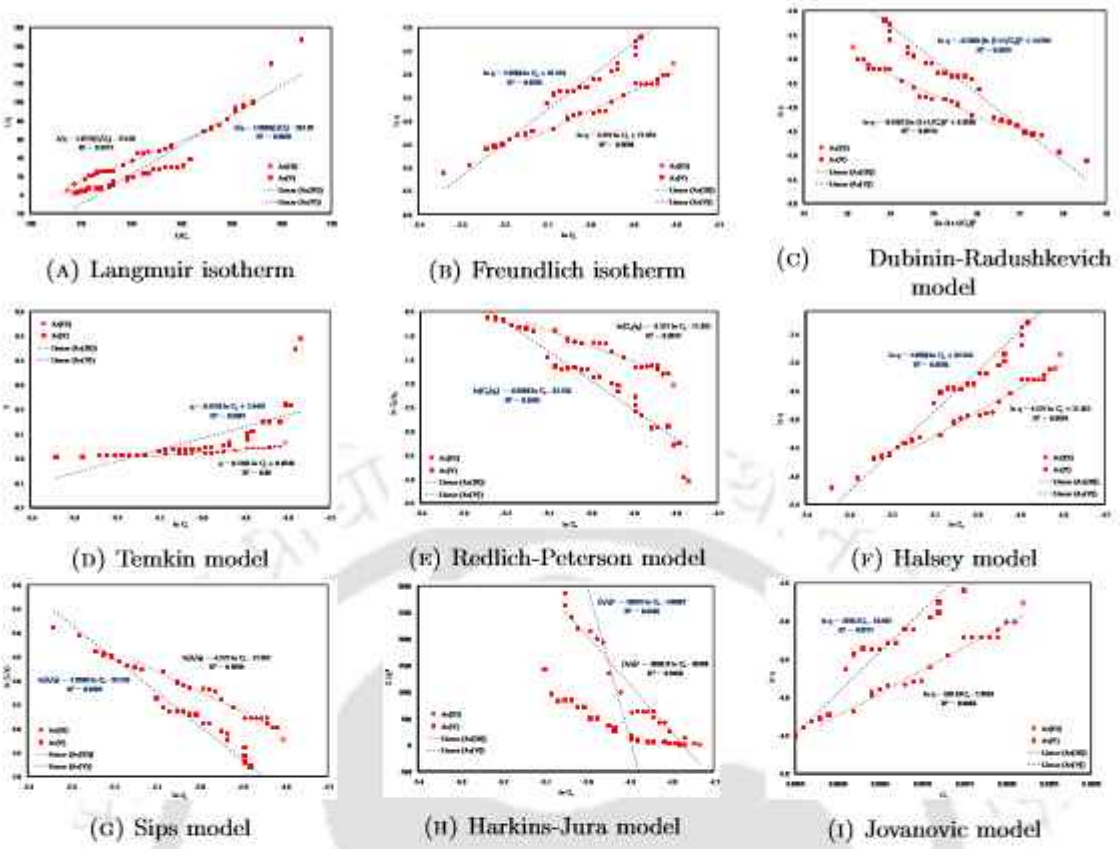

(A) Langmuir isotherm (B) Freundlich isotherm (C) Dubinin-Radushkevich model

(D) Temkin model (E) Redlich-Peterson model (F) Halsey model

(G) Sips model (H) Harkins-Jura model (I) Jovanovic model

FIGURE 7.10: Plot of isotherm models for $As^{(III)}$and $As^{(V)}$

model. However, neither monolayer homogeneous adsorption process nor multilayer adsorption with heterogeneous pore distribution on the surface of adsorbents occur in either of the arsenic species as assessed by the Langmuir and Harkins-Jura isotherm models. Since the Langmuir model doesn't fit the adsorption data, Redlich-Peterson model which has been developed by combining Langmuir and Freundlich models follows the same pattern for the experimental adsorption data. R^2 values of the Redlich-Peterson model are in the range of 0.7517-0.971 and smaller statistical error values shows that there are similarities between the experimental values and the predicted data obtained from the model. But the negative isotherm constants indicates that the data does not fit into this model.

In case of three-parameter isotherm models, Sips isotherm fits well with the data. Sips isotherm model is also a combination of Langmuir and Freundlich models but fits well with all the adsorption data. R^2 values of the Sips model are in the range of 0.952-0.976. Low values of RMSE and χ^2 test reflects that the model fits well with the adsorption data. Based on the HFEF values, the model fits well with the adsorption data of $As^{(III)}$:$As^{(V)}$:: 1 : 2 and $As^{(III)}$:$As^{(V)}$:: 2 : 1 . This diversion is due to a low concentration

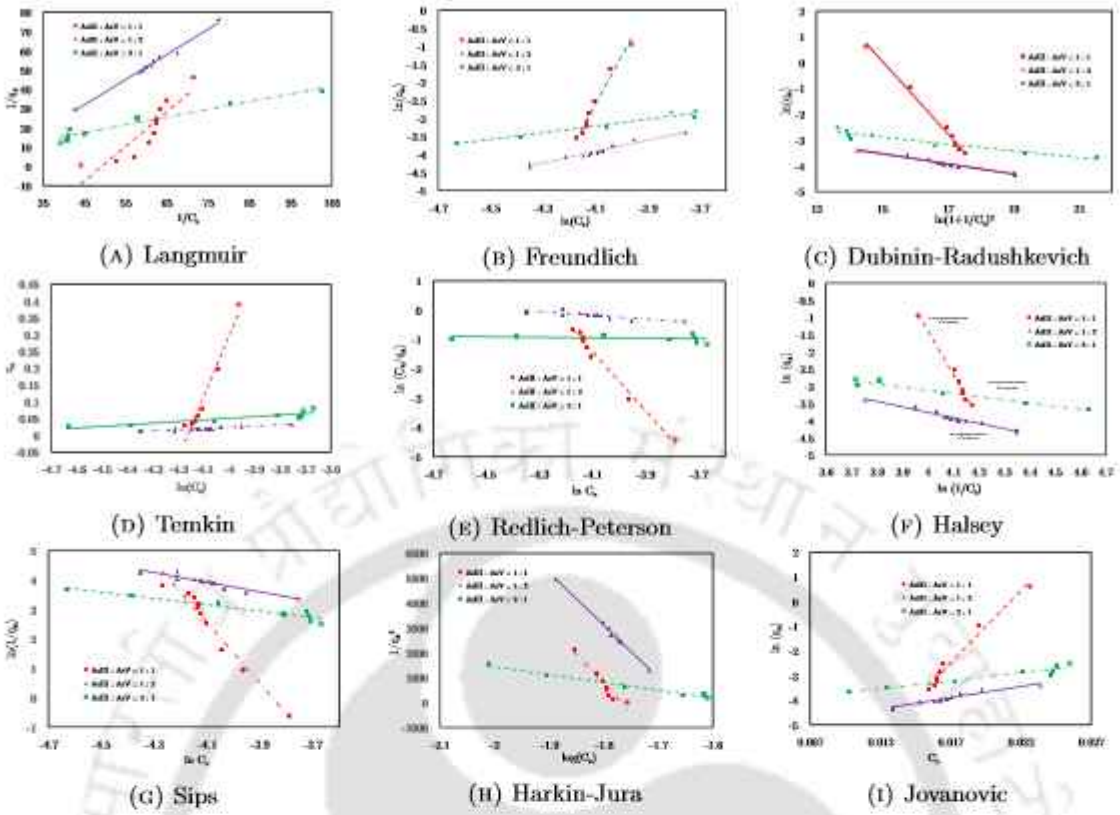

(A) Langmuir (B) Freundlich (C) Dubinin-Radushkevich

(D) Temkin (E) Redlich-Peterson (F) Halsey

(G) Sips (H) Harkin-Jura (I) Jovanovic

FIGURE 7.11: Plot of isotherm models for mixed arsenic species

of adsorbate in which this model transforms into the Freundlich model. Thus confirming the heterogeneous adsorption nature and exponential distribution of active sites in iron compounds for adsorption and removal of arsenic species through complex formation. Jovanovic model yields negative K_J and small q_{max} and hence it is not appropriate.

7.5 Adsorption kinetics modelling

Table 7.3 & Table 7.4 depict the adsorption kinetics models for individual and combined arsenic species. The PFO rate constant, k_1 values are in the range of 0.008-0.0241; k_1 being maximum for $As^{(V)}$and minimum for combined arsenic species in the ratio of (1:2). The adsorption rate values for PFO are low owing to the very low concentration of the adsorbent. The pseudo-first-order model is found to fit the data based on the consistency of the experimental adsorption capacity with the calculated adsorption capacity coupled with lower statistical error values as observed in RMSE, χ^2, and HFEF. Though the R^2 values of the PSO model is higher than the PFO model, the PFO model is a better

fit owing to the low statistical error values for all the individual and combined arsenic species.

TABLE 7.3: Coefficients of the adsorption kinetics models and statistical error functions for removal of $As^{(III)}$& $As^{(V)}$

Adsorption kinetics models	Parameters & statistical error functions	Values obtained for	
		$As^{(III)}$	$As^{(V)}$
	$q_{e,exp}$	0.0075	0.0054
	$q_{e,cal}$	0.0095	0.0058
Pseudo-first order	k_1	0.0138	0.0241
	PFO rate	0.0001	0.00013
	R^2	0.9975	0.9948
	RMSE	0.0546	0.12
	χ^2	0.0004	0.0017
	HFEF	0.0844	0.2001
Pseudo-second order	k_2	1.6825	0
	PSO rate	0.0126	0
	R^2	0.9982	1
	RMSE	396.4863	0.5878
	χ^2	6.245	0
	HFEF	0.1607	0.0002
Elovich model	α	0.0003	0.0009
	β	500	1000
	R^2	0.9861	0.9309
	RMSE	0.0003	0.0002
	χ^2	0.00001	0.00001
	HFEF	0.5242	0.4444
Fractional power function	k_3	0.0008	0.0015
	ν	0.4047	0.2343
	R^2	0.9819	0.9092
	RMSE	0.0559	0.0515
	χ^2	0.0006	0.00005

	HFEF	0.1224	0.1048
Intraparticle diffusion	k_{ipd}	0.0004	0.0002
	C	0.0014	0.0027
	R^2	0.9363	0.8317
	RMSE	0.00045	0.0004
	χ^2	0.00003	0.00003
	HFEF	0.7483	0.8388
Liquid film diffusion	k_{lfd}	0.0138	0.0241
	C	0.0009	0.0719
	R^2	0.9975	0.9948
	RMSE	0.0546	0.12
	χ^2	0.0014	0.0045
	HFEF	0.2205	0.5292

TABLE 7.4: Coefficients of the adsorption kinetics models and statistical error functions for removal of combined arsenic ions

Adsorption kinetics models	Parameters & statistical error functions	Values obtained for $As^{(III)}$and $As^{(V)}$in the ratio of		
		$As^{(III)}$:$As^{(V)}$:: 1 : 1	$As^{(III)}$:$As^{(V)}$:: 1 : 2	$As^{(III)}$:$As^{(V)}$:: 2 : 1
	$q_{e,exp}$	0.0051	0.0061	0.0066
	$q_{e,cal}$	0.0059	0.0068	0.0067
Pseudo-first order	k_1	0.0104	0.008	0.0098
	PFO rate	0.00005	0.000048	0.000065
	R^2	0.9933	0.9984	0.9985
	RMSE	0.0812	0.0371	0.0365
	χ^2	0.001	0.0002	0.0002
	HFEF	0.0928	0.0281	0.0484
Pseudo-second order	k_2	0.8016	1.3289	0.6317
	PSO rate	0.00416	0.0081	0.0042
	R^2	0.9688	0.9992	0.9723
	RMSE	2927	461	2114

	χ^2	161	4.8892	111
	HFEF	0.3639	0.0695	0.3121
Elovich model	α	0.0001	0.0002	0.00012
	β	588.24	588.24	454.55
	R^2	0.9669	0.9964	9971
	RMSE	0.00027	0.0002	0.0002
	χ^2	0.00002	0.00001	0.0001
	HFEF	0.44084	0.35795	0.35286
Fractional power function	k_3	0.0002	0.0004	0.0002
	ν	0.5686	0.4439	6483
	R^2	0.9528	0.9643	0.9284
	RMSE	0.0944	0.0637	0.1303
	χ^2	0.0016	0.0007	0.0031
	HFEF	0.1157	0.0827	0.2042
Intraparticle diffusion	k_{ipd}	0.0003	0.0003	0.0004
	C	-0.0004	0.0008	0.0001
	R^2	0.9612	0.9538	0.937
	RMSE	0.00027	0.0005	0.0008
	χ^2	0.00002	0.00005	0.00012
	HFEF	0.8827	0.6294	1.04857
Liquid film diffusion	k_{lfd}	0.0104	0.0079	0.0098
	C	0.2243	-0.1307	0.1183
	R^2	0.9933	0.9983	0.9985
	RMSE	0.0812	0.0399	0.0365
	χ^2	0.004	0.0009	0.0008
	HFEF	0.3911	0.1613	0.196

The adsorption and desorption constants are obtained from the alpha and beta values of the Elovich model. The adsorption value is found to be the minimum for combined arsenic species in the ratio of [1:1] having a value of 0.0001. The adsorption values arranged in ascending order is as follows $As^{(III)}$:$As^{(V)}$:: 1 : 1 <$As^{(III)}$:$As^{(V)}$:: 1 : 2 <$As^{(III)}$<$As^{(III)}$:$As^{(V)}$:: 2 : 1 <$As^{(V)}$as shown in Fig. 7.12c. The high R^2 values in the range of 0.9309 - 0.9971, and low statistical error values indicate that this model is a

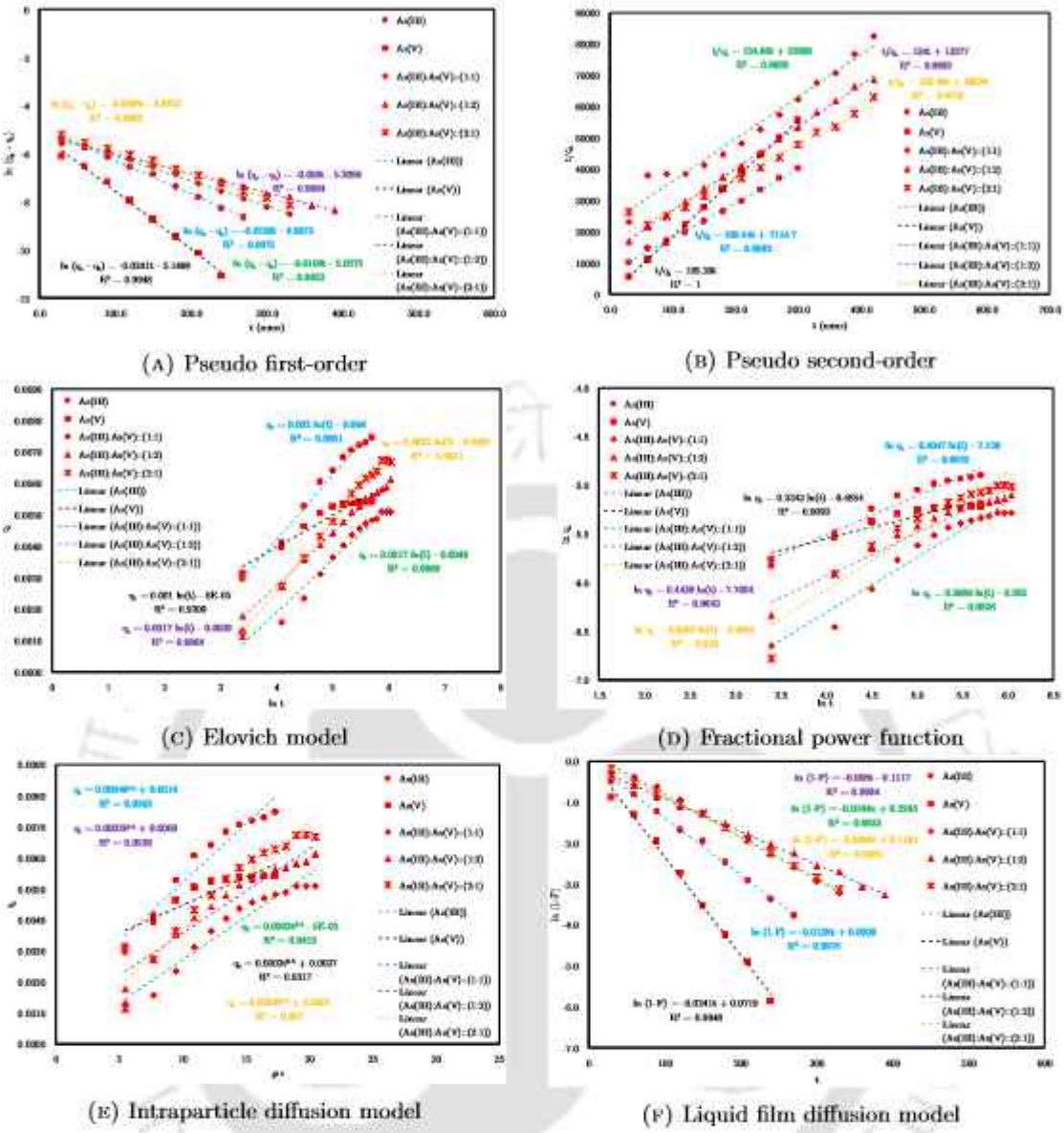

(A) Pseudo first-order

(B) Pseudo second-order

(C) Elovich model

(D) Fractional power function

(E) Intraparticle diffusion model

(F) Liquid film diffusion model

FIGURE 7.12: Adsorption kinetics modeling

good fit. The desorption value is found to be the maximum for $As^{(V)}$having a value of 1000 in comparison to $As^{(III)}$and $As^{(III)}$-$As^{(V)}$combined species in the ratio of (1:1) and (1:2). The minimum desorption value is found to be for $As^{(III)}$:$As^{(V)}$:: 2 : 1 . This shows that adsorbed $As^{(V)}$cannot be easily extracted from the iron-arsenic complex as shown in figure 7.12.

Further, the low adsorption constant indicates that a saturation level is almost achieved. While a high desorption value indicates that the arsenic is strongly entrapped into the iron complex and cannot be easily released into the bulk liquid phase. The fractional power function model also fits well with the data. The rate constant value is found to

be maximum for individual $As^{(V)}$, and $As^{(III)}$but it is minimum for combined arsenic species of (1:1) and (2:1) ratios. However, the values of the rate constant are too small, and ν is less than unity [266].

The intraparticle diffusion (IPD) and liquid film diffusion (LFD) models are investigated to determine the rate-controlling step and to further understand the diffusion mechanisms. The R^2 values of the IPD model is in the range of 0.8317-0.9612. Based on the R^2 values, this model is a good fit for the adsorption kinetics data of $As^{(III)}$:$As^{(V)}$:: 1 : 1 . While the R^2 values of the LFD model is in the range of 0.9948-0.9985, indicating that LFD model is a better fit in comparison to IPD model. But these models cannot be established as the only rate-determining step as all the plots have an intercept value $C \neq 0$. The value of C for individual arsenic ions is positive for both IPD and LFD models. The positive C values indicate that adsorbent boundary thickness and liquid film thickness participate in the adsorption process. The thickness in the case of $As^{(III)}$:$As^{(V)}$:: 1 : 1 is negative for the IPD model. Moreover the thickness of $As^{(III)}$:$As^{(V)}$:: 1 : 2 is also negative for the LFD model. This negative thickness is due to a combined effect of diffusion and surface reaction for which the boundary layer is negative [311]. The thickness for IPD and LFD models is minimum and positive in the case of $As^{(III)}$:$As^{(V)}$:: 2 : 1 .

7.6 Operational cost analysis

Operational cost analysis is a valuable tool to optimize the operations, enhance cost efficiency, and maintain financial sustainability. It provides a detailed understanding of the cost structure, enabling better-informed decision-making at both tactical and strategic levels. As this hybrid technique relies on an electric current to facilitate its processes, involving the release of ions within the electrocoagulation reactor during the treatment period, the expenses associated with operating this reactor are crucial. From an economic standpoint, the total operating cost of the electrocoagulation reactor has been assessed using the following Eq.(7.6) [312] .

$$OC = P_{ec} \times W_{ec} + P_{ee} \times E_{cons} \tag{7.6}$$

where

- OC is the total operational cost (INR.m^{-3}),
- P_{ec} is the price of unit weight of electrode (INR.mg^{-1}) [during the research period, the value equals to 15 x 10^{-6} INR.mg^{-1}],
- W_{ec} is the weight of actual electrode consumed (mg.m^{-3}),
- P_{ee} is the price of unit electrical energy (INR.kWh^{-1}) [during the research period, the value equals to 1.49 INR.kWh^{-1}],
- E_{cons} is the electrical energy in kWh.m^{-3} that is utilized for the process as calculated by the Eq.(7.7) [313]

$$E_{cons} = \frac{V.I.t}{v \times 1000} \tag{7.7}$$

where, V is the voltage applied (volt), I is the applied electric current (Amps.), t is the electrolysis time in hours, and v is the volume of the water treated in m^3.

The primary components of the operational expenses for the electrocoagulation system are predominantly associated with the electricity consumption. While the cost of dissolved metal is contingent on the chosen material, its significance in the context of electrocoagulation is minimal. It is noteworthy, however, that the costs of distinct systems do not exhibit direct proportionality due to variations in electrode materials, effluents, chemicals, and system configurations. The total cost estimated for arsenic removal by batch process of electrocoagulation systems are reported in Table 7.5.

Considering the average current and voltage, the electricity consumption per cubic meter of treated water amounted to 6.16 kWh.m^{-3} for $As^{(III)}$, 6.44 kWh.m^{-3} for $As^{(V)}$, 9.24 kWh.m^{-3} for $As^{(III)}$-$As^{(V)}$in the ratio of (1:1), 9.54 kWh.m^{-3} for $As^{(III)}$-$As^{(V)}$in the ratio of (1:2), and 9.66 kWh.m^{-3} for $As^{(III)}$-$As^{(V)}$in the ratio of (2:1) in the batch process.

The electrode material usage for the electrocoagulation process stood at 3.69 kg.m^{-3} for $As^{(III)}$, 3.36 kg.m^{-3} for $As^{(V)}$, 1.13 kg.m^{-3} for $As^{(III)}$-$As^{(V)}$in the ratio of (1:1), 1.39 kg.m^{-3} for $As^{(III)}$-$As^{(V)}$in the ratio of (1:2), and 4.19 kg.m^{-3} for $As^{(III)}$-$As^{(V)}$in the ratio of (2:1). Upon computation, the operational costs per million m^3 of drinking water were determined to be INR 64.5 for $As^{(III)}$and $As^{(V)}$, and in the range of INR 31- INR 77 for $As^{(III)}$-$As^{(V)}$combined ratios as given in Table 7.6. However, it is crucial to acknowledge that these costs are contingent on various factors, as indicated in Eq. 7.6, and thus cannot be directly compared with those of other systems as compiled in Table 7.5.

TABLE 7.5: Cost estimation for arsenic removal by electrocoagulation systems

Water treated	Reactor design & Anode material with electrode configuration	Energy consumption ($kWh \cdot m^{-3}$)	References
Tap water containing $As^{(V)}$	2 litre plastic reactor with 2-6 iron electrodes in monopolar parallel connection mode	0.45	[314]
Groundwater	~89 cc plastic reactor with 7 aluminium electrodes in monopolar parallel connection mode	3.9	[315]
Synthetic arsenic water	0.8 litre Plexiglas reactor with 4 iron electrodes	0.09	[316]
Groundwater	0.95 litre reactor with iron ball anode	0.015	[317]
Tap water	3 litre beaker with a pair of iron electrode in monopolar mode	8.33×10^{-3}	[318]
Synthetic water & groundwater	1 litre with stainless steel electrodes in monopolar parallel connection mode	0.9	[319]

TABLE 7.6: Economic analysis for the electrocoagulation part of the hybrid technique

Arsenic species	Electrical energy consumed (E_{cons}) ($kWh \cdot m^{-3}$)	Weight of actual electrode consumed (W_{ec}) ($mg \cdot m^{-3}$)	Total operational cost (OC) ($INR \cdot m^{-3} \times 10^{-6}$)
$As^{(III)}$	6.16	3.69	64.53
$As^{(V)}$	6.44	3.66	64.49
$As^{(III)}$:$As^{(V)}$:: 1 : 1	9.24	1.13	30.72
$As^{(III)}$:$As^{(V)}$:: 1 : 2	9.54	1.39	35.07
$As^{(III)}$:$As^{(V)}$:: 2 : 1	9.66	4.19	77.24

Summary of the removal of arsenic by the hybrid technique

- Hybrid technique method involving supported liquid membrane and electrocoagulation processes has been found to be an excellent technique for the removal of arsenic species from water by uphill transport of arsenic species against its concentration gradient along with coagulation and adsorption by iron oxyhydroxides.
- Optimum process conditions are pH 5 of the feed phase, pH 7 of receiving phase with 1M NaCl solution as the receiving phase using 2 volts for removal of $As^{(III)}$and $As^{(V)}$from the contaminated water. While pH 6.5 of the feed phase and pH 7 of the receiving phase play significant roles in enhancing the removal efficiency of the combined arsenic species.
- Almost 90% of the arsenic was removed after the treatment of the water by the hybrid technique.
- The iron-arsenic complex characterized by SEM-EDX, TEM-EDX, FTIR, and XRD indicated the formation of various phases of iron hydroxide/oxide such as goethite, hematite, lepidocrocite, and magnetite.
- Further, the FTIR spectra stipulated the conversion of $As^{(III)}$to $As^{(V)}$due to oxidation reactions occurring during the electrocoagulation process.
- Among the models, the Dubinin-Radushkevich model, and Freundlich isotherm model fit well with the adsorption data suggesting a heterogeneous and physical adsorption process occurring in all the combined ratios of arsenic ions.
- The Temkin model fits well with the adsorption data of (1:2) ratio predicting that the binding energies decrease linearly with the surface coverage due to indirect interactions between the adsorbate-adsorbent in the adsorption process and the positive variation in adsorption energy points to an exothermic physical adsorption process.
- However, the Temkin isotherm model does not support either of the arsenic adsorption data of $As^{(III)}$and $As^{(V)}$indicating that the adsorption is characterized by a non-uniform distribution of binding energies.
- Pseudo first-order model was found to fit the kinetic data for all based on the statistical error analysis.

- On evaluating the economic aspect of the electrocoagulation part of the hybrid technique, it was observed that the total operation cost was estimated to be in the range of 31-77 INR per cubic centimetre for removal of arsenic species.

Abbreviation

EDX Energy dispersive X-ray spectroscopy

FCCCD Face-centered central composite design

FTIR Fourier transform infrared spectroscopy

HFEF Hybrid fractional error function

IR Infrared radiation

RMSE Root mean square error

RSM Response surface methodology

SLM Supported liquid membrane

SEM Scanning electron microscopy

TEM Transmission electron microscopy

XRD X-ray diffraction

Nomenclature

A Redlich-Peterson constant

a_s Sips constant

A_{Fe} Amount of iron liberated from anode

B Harkins-Jura constant

b Temkin constant associated with the heat of sorption

C_i Initial concentration of arsenic in the aqueous phase

C_e Equilibrium concentration of arsenic in the aqueous phase

C_f Final concentration of arsenic in the aqueous phase

c Thickness of the adsorbent for adsorption kinetics

F Faraday's constant

H_J Harkins-Jura constant

I Applied current

K_F Freundlich constant for adsorption capacity

K_L Langmuir binding constant

K_H Halsey isotherm constant

K_J Jovanovic isotherm constant

K_S Sips constant for adsorption capacity

K_T Temkin isotherm constant for adsorption capacity

k_1 Pseudo-first order rate constant

k_2 Pseudo-second order rate constant

k_3 Fractional power constant

k_{id} Intraparticle diffusion rate constant

k_{lfd} Rate coefficient for particle-diffusion controlled process corresponding to the particle size of the adsorbent

M Atomic weight of iron

N Number of observations

n Freundlich constant for adsorption intensity

n_H Halsey isotherm constant

p Number of parameters

q Arsenic removal capacity per dissolved iron anode

q_e Quantity of adsorbate at equilibrium per unit weight of the adsorbent

q_t Quantity of adsorbate adsorbed at time t

q_{max} Maximum sorbent capacity

R Gas constant

R_L Langmuir's separation factor

R_P Redlich-Peterson constant

Re_{As} Arsenic removal efficiency

T Absolute temperature

t Treatment time

v Volume of the reactor

Y mean of the samples

Y_i Obtained amount of adsorbate of sample observation i at equilibrium from the batch experiments

y_i Estimated/calculated amount of adsorbate of sample observation i from the isotherm models for corresponding Y_i

z Number of electrons transferred in the reaction

α Initial adsorption rate constant

β Activity coefficient of Dubinin-Radushkevich model

β_k Desorption constant

ϵ Polanyi potential of Dubinin-Radushkevich model

ν Positive constant of fractional power function model for adsorption kinetics

Chapter 8

Case studies on the removal of arsenic by the hybrid technique

This chapter outlines the application of the hybrid technique on groundwater samples obtained from various regions of Assam and West Bengal, India. The arsenic removal mechanism by hybrid technique from five different groundwater samples was studied through nine adsorption isotherm models and six adsorption kinetics models as mentioned in the previous chapter. The nine adsorption isotherm models studied here include Langmuir model, Freundlich model, Redlich-Peterson model, Sips isotherm, Temkin model, Dubinin-Radushkevich isotherm, Jovanovic model, Halsey isotherm and Harkins-Jura model. Similarly, six adsorption kinetic models have been studied to understand the adsorption kinetics of the arsenic removal mechanism namely, pseudo first order, pseudo second order, Elovich model, fractional power function, intraparticle diffusion, and liquid film diffusion model. The adsorption isotherm and kinetic models have been validated through statistical error analysis. The validation of the modeling was investigated using statistical error analysis. The experimentations were conducted following RSM using a face-centered central composite design. Additionally, perception-based analysis had also been carried out to understand the status of groundwater contamination in Baruipur through the people living in arsenic-affected areas of West Bengal.

8.1 Study area

In Assam, India, three groundwater samples were gathered from distinct locations. The initial sample originated from a private well actively used by a family residing near Bamungaon in Jorhat. Another sample was obtained from a well located in Mariani, near Kenedy Park, adjacent to a temple and a nearby tea estate. The third sample was collected from a private well in close proximity to Bogagaon in Titabor. Fig. 8.1a illustrates the geographical distribution of these sample collection points. Fig. 8.1b provide information about the sampled locations in West Bengal. One of the samples was obtained from Vidyanagar School in the Kobla Chak region of Purbasthali-I, Madhya Srirampur, situated in the Purba Bardhaman district of West Bengal. Due to prior local water sample testing indicating arsenic contamination, the school children and staff refrained from consuming water from the specific hand pump. The second groundwater sample was collected from a recently installed private hand pump regularly used by a local family near Canning Road, Ramnagar in Baruipur, located in the South 24 Parganas district of West Bengal. Table 8.1 provide the GPS coordinates and initial characteristics of all the groundwater samples for further reference.

8.2 Design of questionnaire for perception-based analysis

Conducting perception-based surveys involving local communities allows for active engagement and inclusion of their perspectives [320]. It helps in understanding how residents perceive the quality of their water and contributes to a more comprehensive, community-oriented water quality assessment. Perception-based surveys and analysis can serve as an early warning system by identifying concerns or issues related to water quality that may not be immediately apparent through traditional testing methods [321]. Residents may notice changes in taste, color, or odour that could indicate potential problems. While scientific testing provides objective data on water quality, perception-based analysis offer a subjective dimension. Integrating both scientific measurements and community perceptions provides a more holistic view of the overall water quality situation. Perception-based analysis help identify localized concerns that may vary from one community to another. Understanding the specific water quality issues that residents perceive allows for targeted interventions and tailored solutions [322]. Perception-based

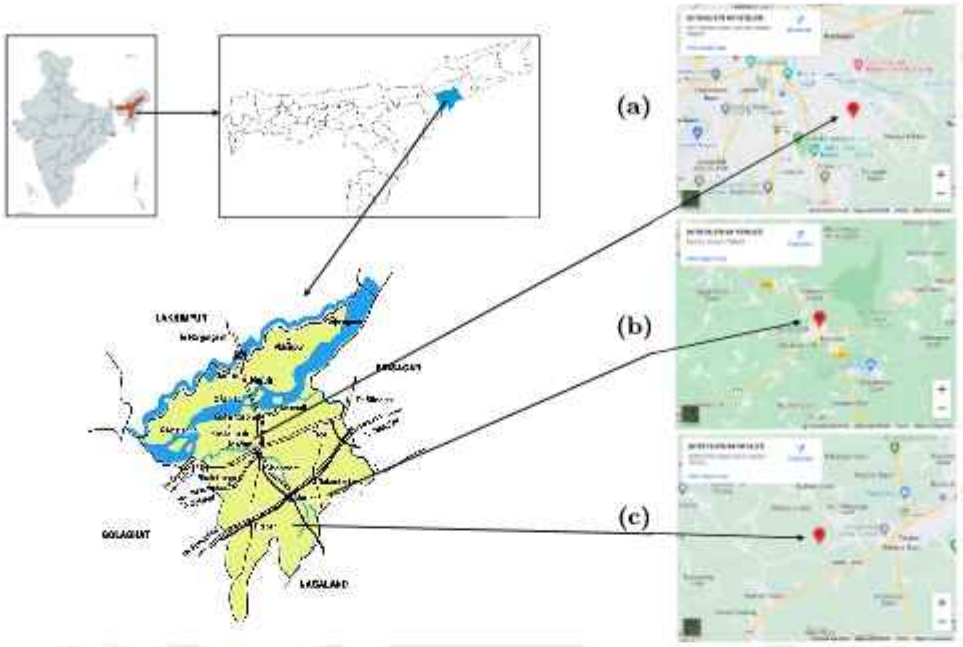

(A) in Assam (a) AS1 (b) AS2 (c) AS3

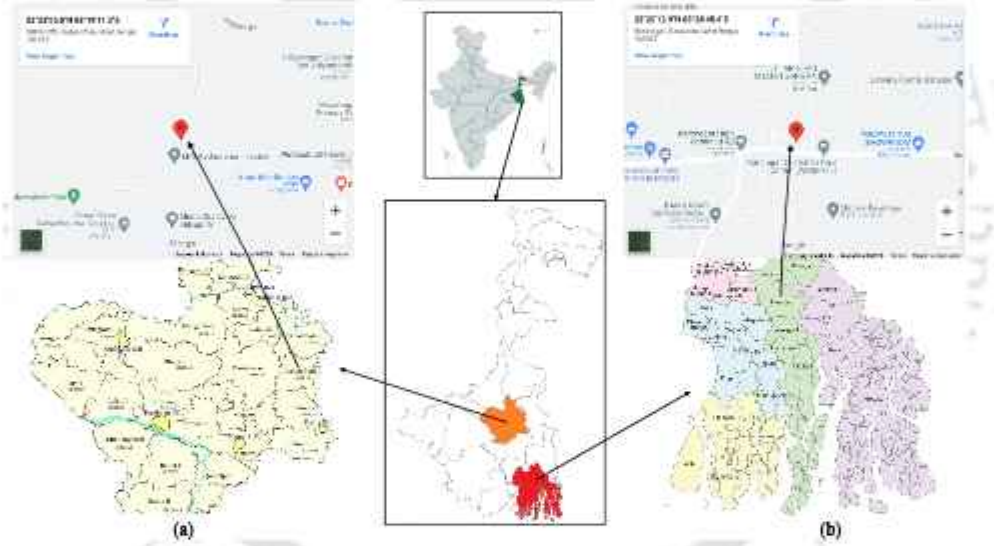

(B) in West Bengal (a) WB1 (b) WB2

FIGURE 8.1: Maps showing the districts in India from where groundwater samples were collected

surveys aid in effective risk communication. By understanding how people perceive water quality risks, authorities can communicate more effectively, providing information that addresses community concerns and dispels misconceptions. People's behaviours related to water use and consumption are influenced by their perceptions of water quality. Perception survey analysis can uncover these behaviours, helping to design interventions that encourage positive water-related practices. Assessing public perceptions contributes to public health awareness.

TABLE 8.1: Specifications of the groundwater samples before treatment

Samples	Location	Source	GPS coordinates (in degree)	pH	Temp (in °C)	As conc. (in ppb)	Fe conc. (in $mg.L^{-1}$)	Electrical conductivity
AS1	Jorhat	Private well	26.741896, 94.242294	6.8	25	150	5.4	221 μS/cm at 25°C
AS2	Mariani	Public well	26.659724, 94.316879	7.5	25	200	8.7	225 μS/cm at 25°C
AS3	Titabor	Private well	26.586123, 94.153930	7.9	25	300	15.4	268 μS/cm at 25°C
WB1	Bardhaman	Public well	23.3986112, 88.3197316	7.2	26	80	6.3	453 μS/cm at 26°C
WB2	Baruipur	Private well	22.3369259, 88.4792888	7.9	27	25	9.8	778 μS/cm at 27°C

If communities are aware of potential water quality issues and understand the importance of safe water practices, it can lead to improved public health outcomes. Policy makers can use perception survey data to inform the development of water quality policies. By aligning policies with community concerns and priorities, policy makers can ensure that regulatory frameworks address the most relevant issues [322]. Perception surveys provide insights for long-term planning. Understanding how communities perceive water quality allows for the development of sustainable and effective long-term strategies to address both current and future challenges. Involving communities in water quality assessments through perception surveys empowers them to take an active role in safeguarding their water resources. Empowered communities are more likely to participate in and support water quality improvement initiatives. Perception survey analysis supports adaptive management approaches. As water quality conditions change, the ongoing collection and analysis of community perceptions allow for flexible, adaptive responses to emerging issues. In summary, perception survey analysis is integral to a comprehensive water quality assessment strategy. By incorporating the community's perceptions alongside scientific data, authorities can develop more effective, community-driven, and sustainable solutions for maintaining and improving water quality.

While the emphasis on the necessity for safe and dependable potable water is paramount, various research endeavours are underway to identify contaminants and enhance water quality. This is particularly crucial as millions of individuals in rural areas continue to depend on untested and untreated water sources for consumption. This analysis intercepts the perceptions of local water users, considering the general demographics of the surveyed areas, to identify dependent water sources, water usage patterns, and water quality. Questionnaire surveys are employed in further investigations to comprehend the adopted water treatment methods and raise awareness about arsenic contamination and its impacts.

The questionnaire for this study is crafted following the template outlined by the WHO/UNICEF Joint Monitoring Programme for Water Supply and Sanitation (JMP), which furnishes essential inquiries regarding drinking water and sanitation for household surveys [323]. Additionally, insights from the Intellectual Property document of Public Affairs Centre (PAC) and relevant research articles on surveys, such as those by Gevera et al. [324] and Francis et al. [325], have been incorporated into the questionnaire design.

TABLE 8.2: Design of questionnaire survey for arsenic-contaminated areas

Section	Title	No. of questions	Description
Part I	General demographic questions	7	This consists of details related to location, GPS coordinates, gender, age, occupation, duration of residence in the community, and the number of members in the family.
Part II	Water use and organoleptic characteristics	16	This comprises of questions about the availability of water, available sources of water in the community and individual's house, consumption of water per day, and organoleptic characteristics such as color, odor, and taste of the consumed water.
Part III	Water quality and arsenic related questions	14	The third part has questions related to the quality of water, treatment of water before consumption, presence of arsenic in groundwater, permissible limit of arsenic in drinking water and its health impacts, number of people affected by consuming arsenic-contaminated water in a family and the community, and other water-related issues faced by the locality (if any).
Part IV	Bore well/-hand pump/open well usage	3	This concluding segment is specifically tailored for individuals who obtain water from a bore well, hand pump, or open well, as these sources are known to be associated with the potential presence of arsenic.

The questionnaire is structured into four segments (I-IV), encompassing a total of forty questions (vide Table 8.2). The initial section covers general demographic inquiries, including location details with GPS coordinates, gender, age, occupation, years of residency in the specific locality, and the number of family members in the household.

The second segment focuses on water usage and organoleptic analysis, probing into aspects like the odour, color, and taste of consumed water, as well as the availability, sources, and consumption patterns of water. The third set of questions delves into water quality, water treatment practices for consumption, and arsenic contamination in groundwater. These questions aim to assess the locals' awareness regarding the presence of arsenic, its permissible limit in drinking water, and the consequences of consuming arsenic-contaminated water. The fourth part of the questionnaire explores the source of consumed water, informing the design of the final section. This concluding segment is specifically tailored for individuals who obtain water from a bore well, hand pump, or open well, as these sources are known to be associated with the potential presence of arsenic. Fig. A.35 to Fig. A.38 show the prepared questionnaire for this study.

In West Bengal, a group of researchers examined over one lakh water samples to assess the status of groundwater arsenic contamination, understanding regional variability and temporal changes over a 20-year period [326]. The state is reported as an "arsenic-endemic" region of India [327], especially in the lower part of the Ganga basin where nine out of 18 districts have arsenic concentrations above 50 ppb [171]. The Bengal Delta plain's arsenic-affected areas are mainly concentrated in the eastern part of the Hooghly River, the lowermost western tributary of the Ganga. Due to severe arsenic contamination in South 24 Parganas, a study explored the seasonal variation of arsenic in tube wells in this region over a one-year period [171]. Given the Bengal Delta Plain's notorious status as the most arsenic-contaminated region [328], a case study in Baruipur and Sonarpur block of South 24 Paraganas district, West Bengal, aimed to determine groundwater arsenic concentration and its effects on children in the region [329]. Another study in Baruipur sought to identify the nature of arsenic pollutants in the Bengal basin's groundwater [175]. The persisting three-decade-long crisis of high arsenic contamination in West Bengal's drinking water has prompted researchers to consider policy modifications for effective implementation and a lasting solution to this issue [327].

Among the worst arsenic-affected areas in West Bengal is the Ramnagar block of Baruipur in the South 24 Parganas district [175]. Despite this, there is insufficient information regarding drinking water quality and arsenic contamination awareness among users in the rural region of Ramnagar block, which has a history of arsenic mass poisoning as established through literature review. Consequently, this study targets the local perception of water quality and awareness of arsenic contamination in the area. The key

objectives of this study include:

- to record the demographic traits of the residents living in the localities
- to identify the dependent water sources, water usage pattern, and understand the perceived water quality notions
- to investigate water treatment methods adopted,
- to create awareness about arsenic contamination and its health impacts

The survey aimed to collect information and insights regarding water quality and usage patterns in regions of Baruipur, West Bengal, where arsenic contamination is prevalent. This initiative sought to comprehend the perspectives of the local residents. The survey questions were verbally presented in the vernacular language (Bengali) and later translated for documentation. Participation was voluntary, with random interested individuals willingly taking part; no one was compelled to join. Participants were informed solely about the research purpose of the questionnaire survey, and their anonymity was preserved. They were encouraged to freely share their opinions and suggestions, resulting in each survey lasting approximately 15-30 minutes.

The research area is situated near Canning Road, Ramnagar, in Baruipur, within the South 24 Parganas district of West Bengal. The South 24 Parganas district is positioned in the lower Ganga basin, identified as part of the mature tract of the Gangetic plain. The district is covered by quaternary sediments, ranging in thickness from 15 to 75 meters, deposited by the river Ganga and its tributaries. Groundwater-bearing aquifers are located within these quaternary and Tertiary sediments, characterized by alluvium with a clayey nature, fine sand, and a silty-clay capping. The district experiences an average annual rainfall of approximately 1800 mm, with a hot and humid climate. The hottest month sees temperatures as high as 40 °C , while the coldest month typically has temperatures as low as 10 °C .

According to 2009 statistics, Ramnagar II is the gram panchayat of Ramnagar village, covering an estimated geographical area of 1364.2 hectares. The village comprises about 3,964 houses, with a total population of 17,053 people, including approximately 8,706 males and 8,347 females. The reported literacy rate for Ramnagar village is 67.78%, with 72.62% of males and 62.73% of females being literate. Groundwater resources from

shallow and deep tube wells serve as the primary sources for irrigation, supplemented by surface water from rivers, canals, and ponds.

The statistical analysis of the survey data includes descriptive statistics, incorporating mean, median, and standard deviation to describe the central tendency and dispersion of variable responses. A normality test assesses the distribution pattern of the data. The Kruskal-Wallis test examines statistically significant differences between groups, and the chi-square test determines the relationship or independence of categorical variables. Post hoc tests and variance analysis identify specific means that show differences. Additionally, multinomial logistic regression is employed to model nominal variables with more than two levels.

8.3 Perception analysis based on questionnaire survey

The participation rate was modest, with nearly 3 out of 10 locals engaging in the entire questionnaire survey, except for a few who abstained due to time constraints or lack of interest. Incomplete responses were excluded from the final survey. Over 30 individuals from three distinct locations in Ramnagar, Baruipur, took part, and a cumulative total of 97 participants from all locations provided responses to all survey questions.

8.3.1 Demographic characteristics

The demographic questions in the initial set of the survey consisted of gender, age, occupation, and residency in that particular location (vide Table 8.3 and Fig. 8.2).

TABLE 8.3: Demographic characteristics of the respondents (in %) based on gender and duration of residency

Location	Gender		Recidency period			
	Male	Female	< 5 years	5-10 years	10-50 years	> 50 years
1	46.88	53.13	18.75	34.38	25.00	21.88
2	48.39	51.61	12.90	41.94	35.48	9.68
3	47.06	52.94	17.65	23.53	29.41	29.41

Out of the total 97 participants, 47% were male and 53% were female respondents who completed the questionnaire survey as given in Fig.8.2. The age was categorized into six

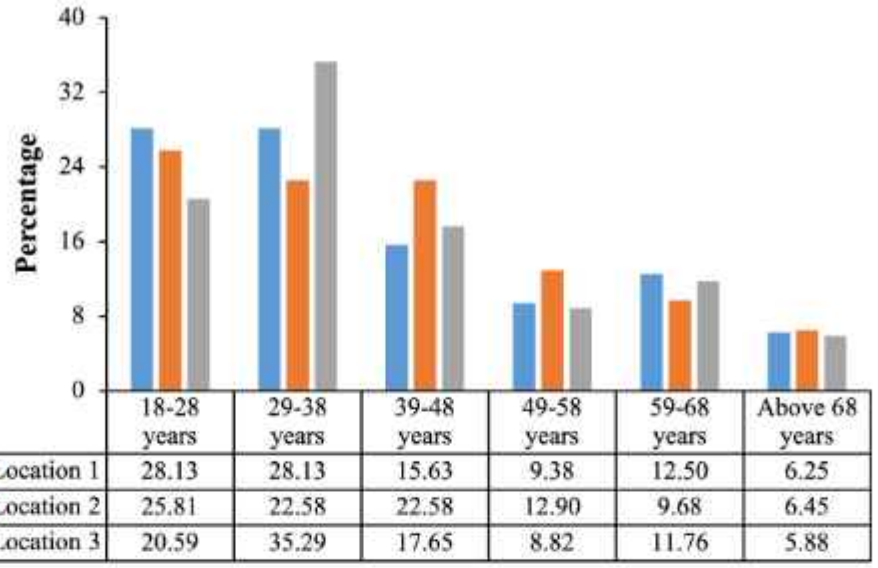

	18-28 years	29-38 years	39-48 years	49-58 years	59-68 years	Above 68 years
Location 1	28.13	28.13	15.63	9.38	12.50	6.25
Location 2	25.81	22.58	22.58	12.90	9.68	6.45
Location 3	20.59	35.29	17.65	8.82	11.76	5.88

Age

(A) Demographic analysis based on the age of the respondents

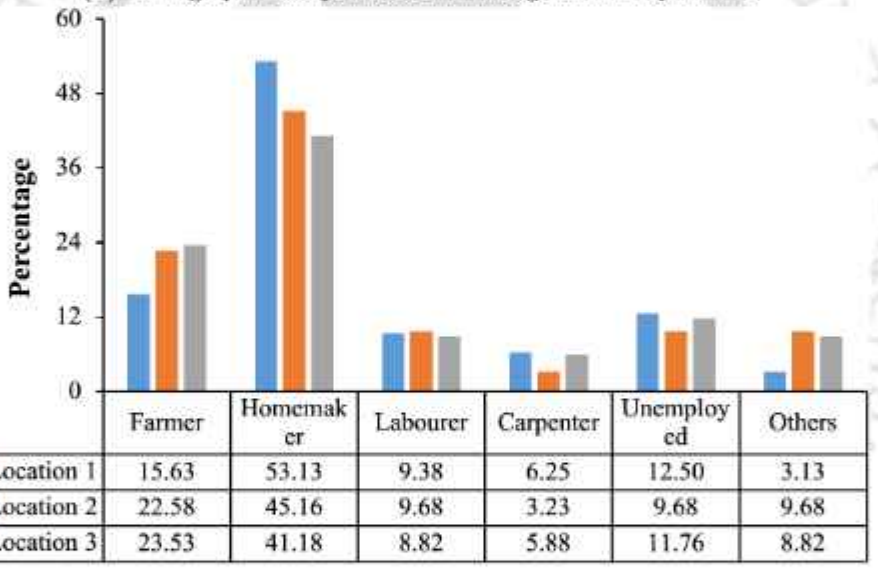

	Farmer	Homemaker	Labourer	Carpenter	Unemployed	Others
Location 1	15.63	53.13	9.38	6.25	12.50	3.13
Location 2	22.58	45.16	9.68	3.23	9.68	9.68
Location 3	23.53	41.18	8.82	5.88	11.76	8.82

Occupation

(B) Occupation-based classification of the respondents for demographic characterization

FIGURE 8.2: Demographic analysis of the questionnaire survey for characterization of the respondents

groups from 18 to above 68 years [330]. Fig.8.2 shows that around 29% of the respondents belonged to the age group of 29-38 years and 25% were from the age group of 18-28 years. Further, the occupation of participants was classified into farmer, homemaker, labourer, carpenter, unemployed, and others. It was noted that the occupation of most of the participants were homemakers and farmers as in Fig8.2. This could be due to the majority of respondents being females participating in the interview. Moreover, the

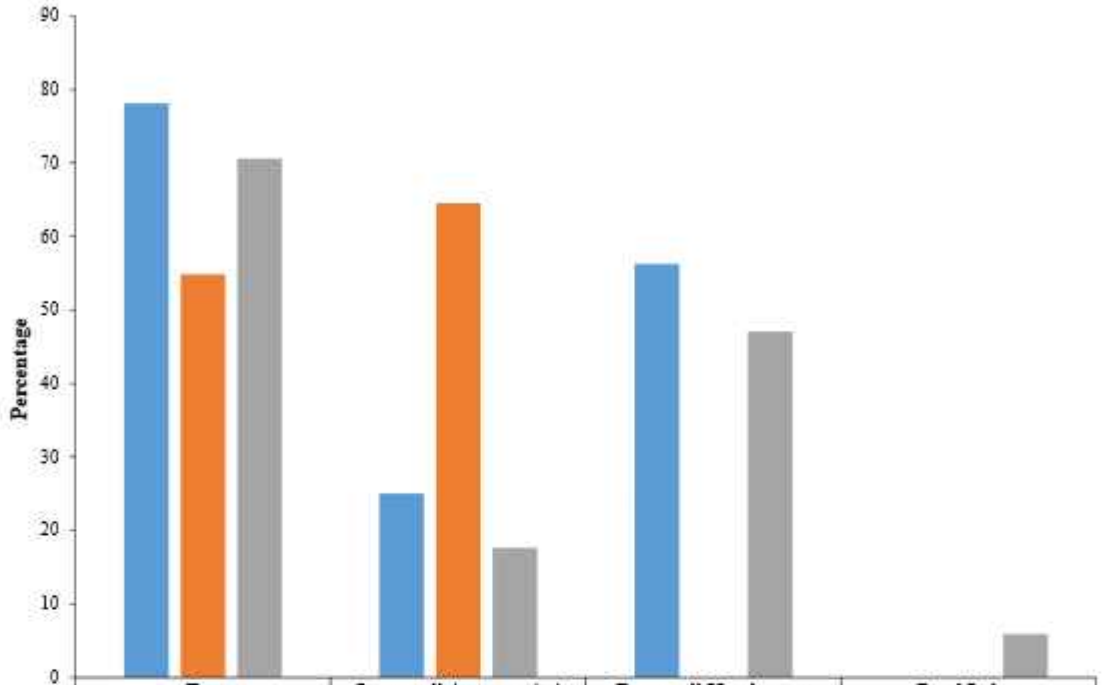

	Tap	Open well (community)	Bore well/Hand pump	Pond/Lakes
Location 1	78.13	25	56.25	0
Location2	54.84	64.52	0.00	0
Location 3	70.59	17.65	47.06	5.88

FIGURE 8.3: Water sources available for domestic purposes

years of residency in the particular area were asked to establish the duration of living in the same place along with the number of members living in the family. It was observed that most of the respondents have been living in the study area for more than five years with at least three to four members in their families as established from Fig.8.2.

8.3.2 Water usage pattern

Figure 8.3 illustrates the available water sources in the area, encompassing tap water supply, open wells, household bore wells or hand pumps, and nearby surface water resources like ponds. However, for drinking purposes, 78% of households in the first location and 71% in the third location primarily relied on tap water supply, while 65% of households in the second location depended on open wells within the community. Locals predominantly relied on tap water supply, open or bore wells, and hand pumps for various household water needs, including drinking and cooking.

In the first location, approximately 75% of respondents reported having a water source within their households. Conversely, in the second location, 74% lacked access to water

within their households and had to fetch water from within 50 meters of their homes. Similar to the first location, the third location heavily depended on tap water supply and bore wells, with 82% of participants reporting having water resources within their households. Approximately 62% of all participants acknowledged having a water source within their households, and 46% reported consuming more than 5 litres of water per day per individual.

8.3.3 Perceived water quality

Table 8.4 illustrates that the majority of participants did not report any noticeable changes in color, odor, or taste while consuming water from their respective sources. However, about 31% observed alterations in water color, and an even smaller percentage (12%) noted changes in food color when utilizing the same water for cooking. While this change in water color was observed across all three locations, alterations in food color were predominantly reported by respondents in the first and third locations.

Upon closer examination, it was determined that the change in water color occurred primarily during the summer or monsoon seasons. Participants described the altered water color as unclear, muddy, and reddish. This phenomenon is likely attributed to the presence of iron, which imparts color to both water and food (especially rice, a staple in this region) when cooked in it. This is particularly noticeable in the summer when more water is drawn from aquifers through bore wells or hand pumps. Additionally, the change in water color during the monsoon season could be linked to the mixing of sewage with potable water.

TABLE 8.4: Perceived water quality of all the respondents based on organoleptic characteristics

Location	Organoleptic characteristics			
	Odour	Taste	Colour	Cooked food colour change
1	0	0	21.88	12.5
2	0	0	32.26	9.68
3	5.88	0	38.24	14.71

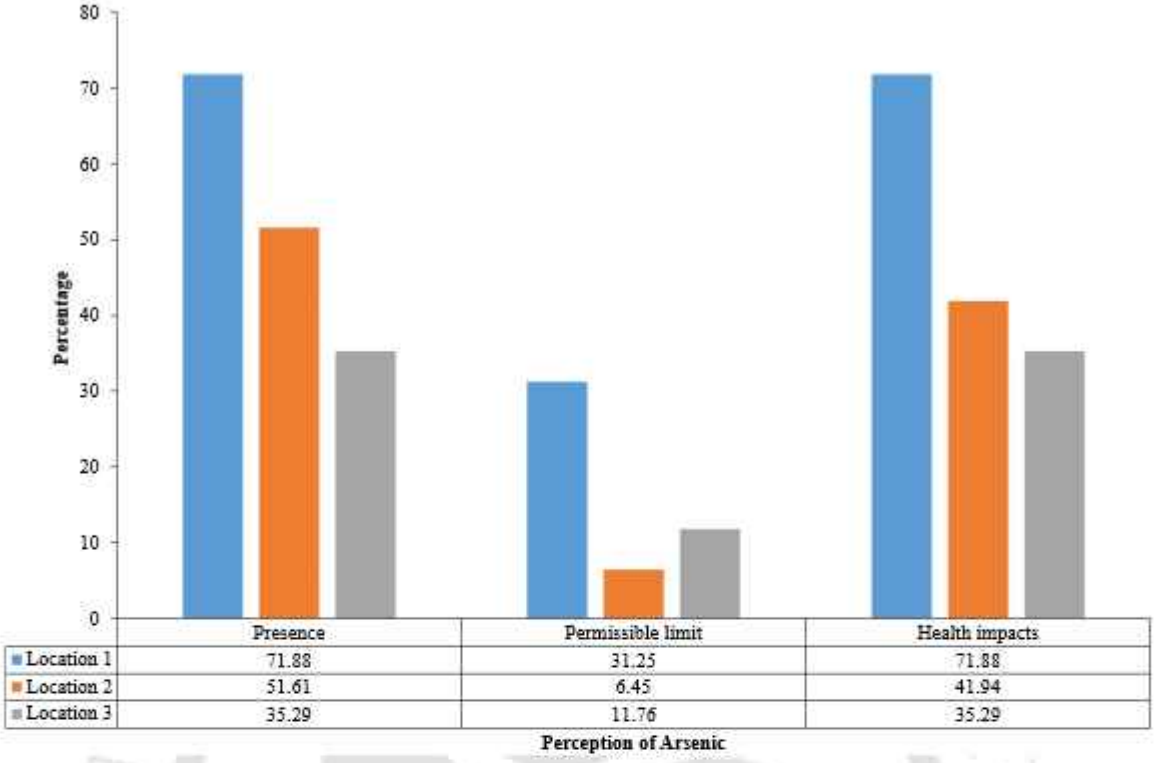

FIGURE 8.4: Perception of respondents about the presence of arsenic in groundwater

8.3.4 Arsenic based notions

The Fig. 8.4 shows that the majority of participants were aware of the presence of arsenic, with almost 53% acknowledging its existence in the groundwater. However, knowledge about the permissible limit of arsenic in drinking water was not widespread among the residents. Even though 60% of the participants were not familiar with the acceptable level of arsenic in drinking water, most were aware of the health impacts associated with consuming arsenic-contaminated water. This awareness stemmed from first-hand observations of neighbours or family members experiencing conditions such as melanosis and skin lesions.

Approximately 20% of the participants admitted to having at least one family member currently experiencing arsenic poisoning, while 54% stated that none of their family members were presently suffering from arsenic poisoning. In contrast, 23% of the total participants reported that 5-10 individuals in their locality had been severely affected by arsenic in the past. Some participants mentioned witnessing the unfortunate deaths of their neighbours due to arsenic poisoning, underscoring the serious health implications of

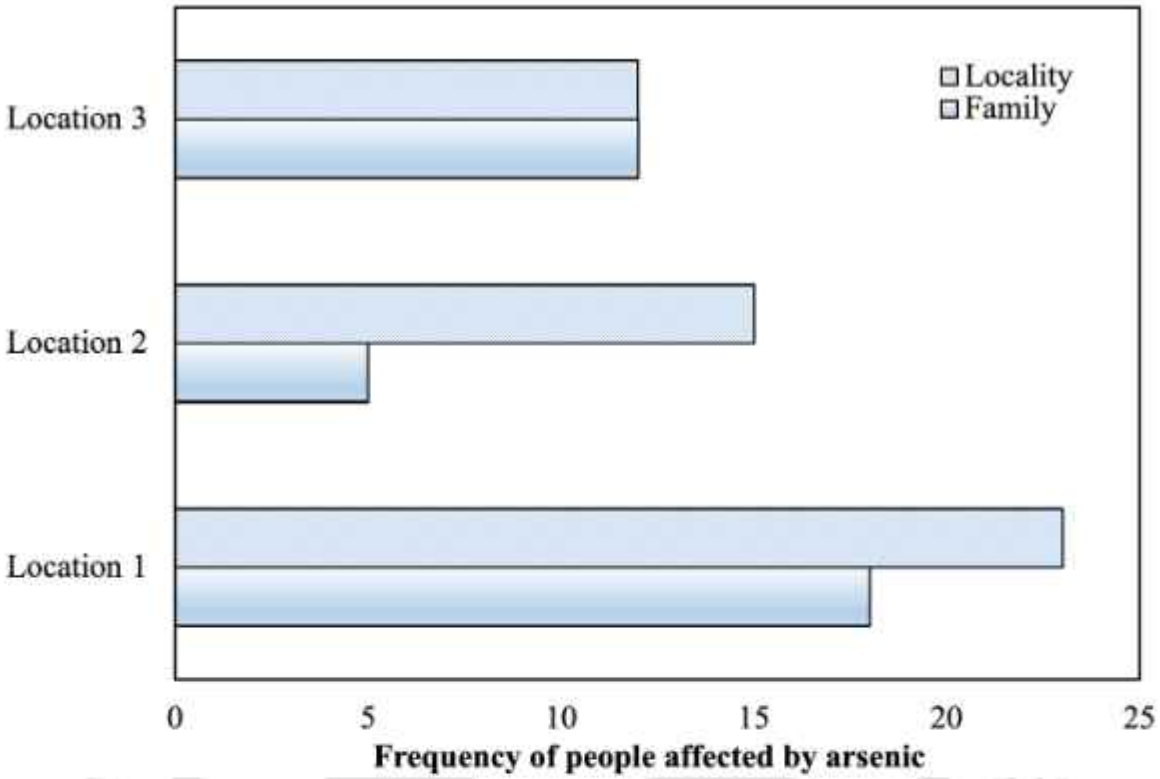

FIGURE 8.5: Participants' responses to the number of people affected by arsenic in their family and locality

arsenic contamination. The responses of participants affected by arsenic in their families and locality are depicted in Figure 8.5.

8.3.5 Water treatment

While the majority, comprising 59% of the participants, believed that they consumed safe water, and 29% rated the water quality as "very good," 40% of the total population took precautions by treating their water before consumption. The remaining 60% placed blind trust in and relied solely on their water sources, without adopting any water treatment methods, as depicted in Fig.8.6a. The accompanying Fig.8.6b illustrates the prevalent water treatment methods embraced by the locals, with boiling being the most commonly adopted approach. Among the 40% who treated their water, 21% resorted to boiling, 10% opted for filtration, and 9% utilized alum as a water treatment method before consumption.

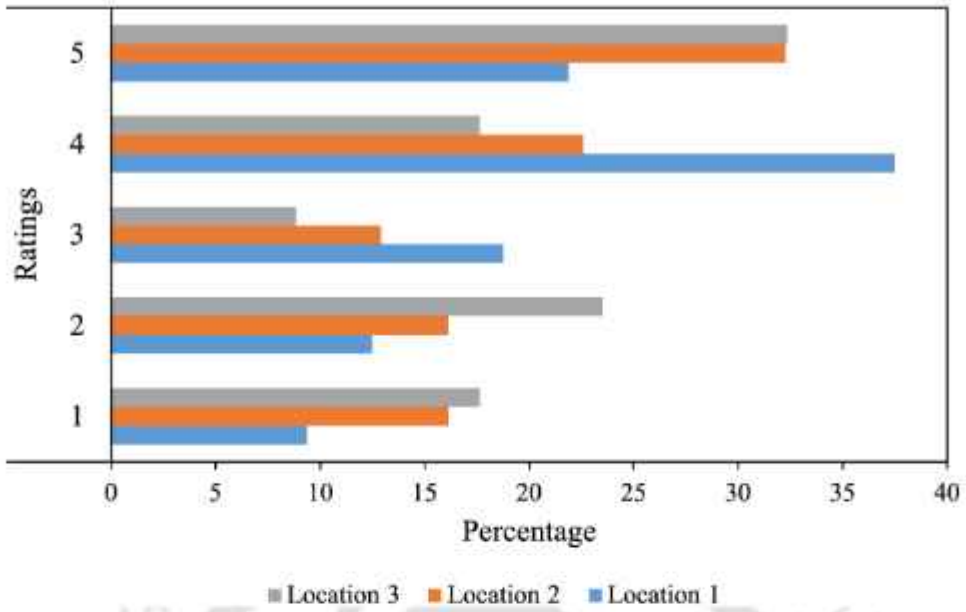

(A) Water quality ratings given by all the respondents. (Ratings in the range of 1-5, where 1 stands for very poor, 2 – poor, 3 – moderate, 4 – good, and 5 – very good.)

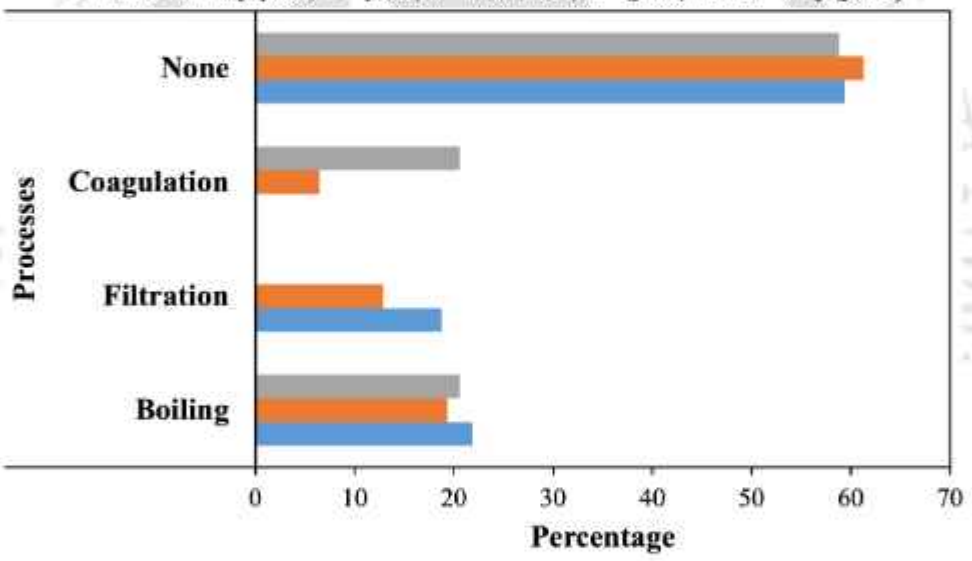

(B) Water treatment processes adopted by all the participants

FIGURE 8.6: Participants' responses to the water related matters

8.4 Statistical modelling

8.4.1 Normality and ANOVA test

To assess the normality of the data, Kolmogorov-Smirnov and Shapiro-Wilk tests were conducted, revealing significant differences from a normal distribution ($p < 0.05$). Consequently, the Kruskal-Wallis test was employed instead of a one-way analysis of variance.

Based on the Kruskal-Wallis test, several variables exhibited statistically significant differences among the three locations. Variables such as the distance covered by users to obtain water, awareness of arsenic, the presence of arsenic in groundwater, the permissible limit of arsenic in water, health impacts of arsenic, and the number of family members affected by arsenic consumption in a household displayed notable p values ($p < 0.05$). A higher Kruskal-Wallis H value indicates a more substantial difference, as detailed in Table 8.5.

TABLE 8.5: Test statistics of Kruskal-Wallis test with location as the grouping variable for statistically significant parameters

Parameters	Kruskal-Wallis H	df	Asymptomatic significance
Distance of water source from household	25.209	2	<0.001
Perception on arsenic	8.256	2	0.016
Presence of arsenic in groundwater	8.692	2	0.013
Permissible limit of arsenic for drinking water	7.436	2	0.024
Health impacts on consuming arsenic-contaminated water	7.460	2	0.024
No. of members affected by arsenic in the family	7.142	2	0.028

Among these variables with statistical significance, the distance traveled by users to obtain water exhibits a substantial Kruskal-Wallis H coefficient of 25.21, indicating a significant difference among the three locations. The chi-square test conducted for all locations indicates statistical significance ($p < 0.05$) for several variables, namely age, occupation, the number of family members residing, organoleptic characteristics of the consumed water, and water-related issues, along with perceptions of arsenic. This suggests an association between these variables and the locations. Conversely, gender, water quality rating, and the water treatment adopted (if any) by the users appear to be independent of the location. The Pearson chi-square coefficients for all the statistically significant variables across the three locations are presented in Table 8.6. The test of between-subjects effects in the multivariate analysis of variance test further substantiated the significance of parameters, including the distance travelled by users to obtain water, awareness of arsenic, the presence of arsenic in groundwater, the permissible limit

of arsenic in water, and the number of family members affected by arsenic consumption in a household ($p < 0.05$).

TABLE 8.6: Test statistics of the Chi-square test for statistically significant parameters associated with the locations

Parameters	Chi-square	df	Asymptomatic significance
Age	23.062	5	<0.001
Occupation	70.072	5	<0.001
No. of members in the family	22.124	4	<0.001
Water consumption	8.433	2	0.015
Distance of water source from household	5.454	1	0.020
Odor	96.515	2	<0.001
Taste	40.918	1	<0.001
Color	17.093	2	<0.001
Perception on safe water	34.412	2	<0.001
Process for water treatment	65.680	3	<0.001
Perception on arsenic	22.351	2	<0.001
Presence of arsenic in groundwater	25.072	2	<0.001
Permissible limit of arsenic in drinking water	31.320	2	<0.001
Health impacts of consuming arsenic-contaminated water	24.392	2	<0.001
Family members affected by arsenic	72.845	4	<0.001
No. of people affected by arsenic in the locality	84.546	5	<0.001
Other water-related issues	33.732	2	<0.001
Specific water-related issues	8.000	2	0.018

The multivariate tests revealed a significant main effect, as indicated by Hotelling's trace value and Roy's largest root for the locations, both with p-values < 0.05 (vide Table 8.7).

TABLE 8.7: Multivariate test statistics for all the locations.

Multivariate tests	Value	F	Hypothesis df	Error df	Significance
Pillai's Trace	0.773	1.890	48	144	0.002
Wilks' Lambda	0.359	1.979	48	142	0.001
Hotelling's Trace	1.418	2.068	48	140	<0.001
Roy's Largest Root	1.076	3.227	24	72	<0.001

The estimated marginal means provided in Table 8.8 illustrate the means and standard errors of the outcome for each location of the dependent variable.

TABLE 8.8: Estimated marginal means of statistically significant variables for all the locations from multivariate analysis of variance

Dependent variable	**Location**	**Mean**	**Standard error**	**95% confidence interval**	
				Lower bound	**Upper bound**
Perception on arsenic	1	1.375	0.123	1.131	1.619
	2	1.581	0.125	1.333	1.828
	3	1.853	0.119	1.617	2.089
Presence of arsenic in groundwater	1	1.344	0.118	1.110	1.578
	2	1.581	0.120	1.343	1.818
	3	1.824	0.114	1.597	2.050
Permissible limit of arsenic in drinking water	1	1.906	0.109	1.691	2.122
	2	2.323	0.110	2.103	2.542
	3	2.000	0.105	1.791	2.209
Health impacts on consuming arsenic-contaminated water	1	1.375	0.116	1.145	1.605
	2	1.710	0.118	1.476	1.944
	3	1.735	0.113	1.512	1.959
No. of family members affected by arsenic	1	2.875	0.228	2.422	3.328
	2	3.710	0.232	3.250	4.170
	3	3.265	0.221	2.825	3.704
No. of people affected by arsenic in the locality	1	3.438	0.370	2.702	4.173
	2	3.710	0.376	2.962	4.457
	3	4.471	0.359	3.757	5.184

8.4.2 Logistic Regression Analysis

The goodness-of-fit table within multinomial logistic regression presents two measures, Pearson and Deviance chi-square statistics, providing an assessment of how well the model aligns with the data for all the locations. The high value of the Pearson chi-square statistic (175.55), coupled with a statistically significant result ($p<0.05$), implies a poor fit of the model to the data. In contrast, the Deviance chi-square statistic (122.32) yields a p-value of 0.72, suggesting a better fit. The p-value for model fitting is <0.001, indicating that the full model is statistically significant, and it predicts the dependent variable more effectively than the intercept-only model. The pseudo R^2 measures, calculated by Cox and Snell, Nagelkerke, and McFadden, are reported in Table 8.9.

TABLE 8.9: Pseudo R^2 values for multinomial logistic regression modelling on statistically significant parameters for all the locations.

Multinomial Logistic Regression modelling for	Statistic	Coefficients
Respondents' perception of arsenic-related questions	Cox and Snell	0.534
	Nagelkerke	0.601
	McFadden	0.348
Water quality assessment based on participant's response	Cox and Snell	0.268
	Nagelkerke	0.302
	McFadden	0.142
Respondents' perception on water treatment	Cox and Snell	0.281
	Nagelkerke	0.317
	McFadden	0.151
Participants' water usage pattern	Cox and Snell	0.264
	Nagelkerke	0.297
	McFadden	0.139

The logistic regression model, focusing on users' perceptions of arsenic-related questions, highlights that variables such as the permissible limit of arsenic in drinking water and the number of people affected by consuming contaminated water are statistically significant across all locations (p-values of 0.048 and 0.040, respectively, from likelihood ratio

tests). However, the overall statistical significance value for the model's coefficients is not significant.

Similarly, a logistic regression model for water quality assessment indicates a well-fitting model with high Pearson and Deviance chi-square statistics (169.88 and 164.99), though the p-value for model fitting is 0.45, suggesting lack of statistical significance. Pseudo R^2 values are reported as 0.268, 0.302, and 0.142 for Cox and Snell, Nagelkerke, and McFadden, respectively. The users' perception of water safety emerges as a statistically significant variable for all locations (p-value = 0.027) from likelihood ratio tests.

In the third logistic regression model focused on water treatment, the model fits well according to low Pearson and Deviance chi-square statistics (83.22 and 97.55), both with non-statistically significant results (p = 0.624 and 0.228). However, the p-value for model fitting is 0.022, indicating overall statistical significance. Pseudo R^2 values are calculated as 0.281, 0.317, and 0.151 for Cox and Snell, Nagelkerke, and McFadden, respectively. The participants' response to water treatment processes is statistically significant (p-value = 0.002).

The final logistic regression model, focusing on water usage, indicates high Pearson and Deviance chi-square statistics (120.18 and 107.40) with non-statistically significant p-values (0.083 and 0.288), yet the model is statistically significant overall ($p<0.001$). Pseudo R^2 values are reported as 0.264, 0.297, and 0.139 for Cox and Snell, Nagelkerke, and McFadden, respectively. The distance traveled by locals to fetch water is a statistically significant parameter.

The overall conclusions emerging from this study include that people are well aware of arsenic contamination and its impacts. Other than arsenic there are a few upcoming water-related issues as complained about by the locals. Though there is an abundance of water resources available to the locals including tap water supply, open wells in the community, household bore wells, hand pumps, and surface water sources such as ponds, water scarcity is an upcoming water-related issue, especially in summer. Most of them are habituated to consuming water from bore wells and hand pumps increasing their dependency on groundwater. The majority of the respondents were females and homemakers with their ages ranging from 29-38 years. Consumption of safe water and arsenic contamination increased awareness amongst a few for which water treatment methods were followed by a few and reliability on tap water supply was observed. The

small number of respondents focussing on a particular block of an area is a limitation of this study. This work could be extended to other arsenic-impacted regions and a large mass of people could be approached for the survey. Further, a temporal variation could be recorded by conducting similar surveys for each season.

8.4.3 Design of Experimentation

Table B.46 shows the experimental design with responses for all the locations. The experimental design comprises thirteen experiments with four factorial runs, four axial runs, and five center points for samples from each location. The independent variables included in this study are extractant concentration (A) and pH of the receiving phase (B). The extractant concentration range has been studied within 10-40% (v/v). The receiving phase pH has been varied here from 3 to 7. Sodium chloride (1 M) salt has been used as the receiving phase solution and 2V potential difference has been applied in all the experiments conducted. The experimental data is plotted based on sequential analysis of variance modeling which is based on significant p-values and insignificant lack of fit F-values. A quadratic model is predicted and the contour plots are generated to investigate the optimum process conditions for the maximum removal of arsenic from all the different locations. The following are the quadratic equations in terms of coded factors for each location.

$$Y_{WB1} = 88.53 - 3.54A + 1.25B + 0.625AB + 2.00A^2 - 3.62B^2 \quad (8.1)$$

$$Y_{WB2} = 82.86 - 10.83A - 3.00B - 1.50AB + 6.98A^2 - 10.52B^2 \quad (8.2)$$

$$Y_{AS1} = 98.25 - 4.48A - 0.32B - 0.30AB - 3.42A^2 + 0.68B^2 \quad (8.3)$$

$$Y_{AS2} = 98.93 - 3.83A - 0.80B - 0.60AB - 3.12A^2 + 0.08B^2 \quad (8.4)$$

$$Y_{AS3} = 88.64 + 3.12A - 1.72B - 0.18AB + 1.31A^2 - 0.19B^2 \quad (8.5)$$

The model F-value of 145.62 for WB1 implies that the model is significant and there is only a 0.01% chance that an F-value this large could occur due to noise. Based on the p-values, it is evident that A, A^2 and B^2 are significant model terms. The lack of fit F-value of 1.2 indicates it to be not significant relative to the pure error. There is a 41.57% chance that a value this large could occur due to noise. Similarly, the model F-value for the second sample WB2 is found to be significant with an insignificant lack

of fit F-value of 1.2. P-values less than 0.01% indicate model terms to be significant on the basis of which A and B^2 are found to be significant model terms. The analysis of variance for the models is given in Table B.48. The normal probability plots in Fig. A.33 illustrate a normal distribution of the residuals with a moderate scattering of the data. The R^2 value obtained from the modeling of WB1 is 0.9905 and the predicted R^2 of 0.9479 is in reasonable agreement with the adjusted R^2 value of 0.9837. While the R^2 value is 0.983 for WB2. The predicted R^2 value of 0.907 has a difference of less than 0.2 with the adjusted R^2 value of 0.971. The adequate precision value compares the range of the predicted values at the design points to the average prediction error and gives a value of 32.75 for WB2. Further, the signal-to-noise ratio depicted by the adequate precision value is 44.93 for WB1. Table B.47 posits the optimum conditions obtained from the quadratic modeling. The coefficient of variation (C.V.) is a statistical measure depicting the relative dispersion of the data around the mean of the data series. In other words, it is the extent of variability expressed as a percentage of the ratio of standard deviation to mean. In ascending order, the C.V. values can be outlined as 0.47 for WB1 and 2.03 for WB2. The lower the value of C.V., the more precise is the estimate due to less dispersion of data around the mean. The model F-value of 40.96 for AS1 implies that the model is significant and there is only a 0.01% chance that an F-value this large could occur due to noise. Based on the p-values, it is evident that A and A^2 are significant model terms. The lack of fit F-value of 1.49 indicates it to be not significant relative to the pure error. There is a 34.4% chance that a value this large could occur due to noise. Similarly, the model F-value for the second sample AS2 is found to be significant with an insignificant lack of fit F-value of 1.64. There is a 31.4% chance that a value this large could occur due to noise. P-values less than 0.05 indicate model terms to be significant on the basis of which A, B, AB, and A^2 are found to be significant model terms. The model F-value of 76.38 for AS3 study is found to be significant with an insignificant lack of fit F-value of 1.08. The analysis of variance for the models is given in Table B.49. In Fig. A.33, a plot of observed response values vs. predicted response values is depicted to check the outliers. Further, the normal probability plot in Fig. A.33 shows a normal distribution of the residuals with a moderate scattering of the data. The R^2 value obtained from the modeling of AS1 is 0.9669 and the predicted R^2 of 0.8463 is in reasonable agreement with the adjusted R^2 value of 0.9433. While the R^2 value of 0.9931 for AS2 elucidates a better prediction of the model in comparison to AS1 and AS3. The predicted R^2 value of 0.9637 is much closer to the adjusted R^2 value of 0.9881. Further,

the signal-to-noise ratio depicted by the adequate precision value is maximum for AS2 (38.77) and minimum for AS1 (16.35). In the third case study of AS3, the R^2 value is 0.982. The predicted R^2 value is in reasonable agreement with the adjusted R^2 value. Table B.47 posits the optimum conditions obtained from the quadratic modeling. The adequate precision value compares the range of the predicted values at the design points to the average prediction error and gives a value of 30.88. The coefficient of variation (C.V.) is a statistical measure illustrating the relative dispersion of the data around the mean of the data series. In other words, it is the extent of variability and expressed as a percentage of the ratio of standard deviation to mean. In ascending order, the C.V. values can be outlined as 0.361 for AS2, 0.517 for AS3, and 0.897 for AS1. The lower the value of C.V., the more precise is the estimate due to less dispersion of data around the mean. On the basis of the coefficient of determination and the coefficient of variation values, the quadratic model fits and predicts better for AS2 in comparison to AS1 and AS3.

8.5 Effect of variables

8.5.1 Extractant concentration

Several organic extractants have been reported to have the capability of removing arsenic from their solution. These include acidic extractants such as bis(2,4,4-trimethylpentyl) dithiophosphinic acid (Cyanex 301), neutral extractants viz, trioctylphosphine oxide (Cyanex 923) and tributyl phosphate (TBP), and basic extractants such as trioctylamine (TOA) and methyltrioctylamonium chloride (Aliquat 336). However, Aliquat 336 is preferred for its ability to react with both dissociated and undissociated arsenic ions present in the feed phase. Based on these research works, the extractant applied for this study is aliquat 336 and the liquid membrane is a pseudo-binary mixture of sesame oil and aliquat 336. The extractant concentration is rendered to be a significant factor in all the case studies. The optimum concentration of aliquat 336 in the liquid membrane is found to be 10% for WB1, WB2, AS1 and AS2. This exhibits that $As^{(III)}$is the prominent arsenic species present in the groundwater samples of these places. As it has been established in the earlier research works that $As^{(III)}$is mostly present as H_3AsO_3 that forms complex with 10% (v/v) aliquat to extract arsenic from the feed phase into the

membrane phase[218]. The optimum extractant concentration is 40% for AS3. Aliquat is required to form complexes with combined arsenic species of $As^{(III)}$and $As^{(V)}$. This extends the presence of both $As^{(III)}$and $As^{(V)}$species in groundwater samples of AS3.

8.5.2 pH of the receiving phase

The initial pH of the receiving phase was varied between 3 and 7 as ferric hydroxide precipitation starts in this pH range[?]. The arsenic ions present in the feed phase are either in the dissociated state such as $H_2AsO_4^-$, $HAsO_4^{2-}$, AsO_4^{3-} (in case of $As^{(V)}$) or in the undissociated forms like H_3AsO_3 (in case of $As^{(III)}$) depending on the pH of the feed phase[106]. The initial pH of the groundwater sample which is used as the feed phase of AS1 is 6.8 while that for AS2 and AS3 is pH 7.9 and 7.7, respectively. On the basis of pH and the extractant concentration, H_3AsO_3 is the prevalent form of $As^{(III)}$found in AS1 and AS2. While H_3AsO_3, $H_2AsO_4^-$, and $HAsO_4^{2-}$ forms of $As^{(III)}$and $As^{(V)}$might be present in AS3. pH 5 is found to be favorable for the maximum removal of arsenic ions from the groundwater samples of WB1 and WB2. The hydrolysis of the ferrous ions starts precipitation usually at around pH 7 which leads to the formation of flocs of $Fe(OH)_n$ by polymerization that causes the adsorption of arsenic ions. But the presence of iron and other pollutants in the groundwater samples accelerates this process for which the optimum pH is lower than the reported pH [218]. The optimum pH of the receiving phase is observed to be pH 3 so as to maintain a pH difference that would readily transport arsenic ions from the membrane phase to the receiving phase. Further, the pH of the receiving phase rises as the electrocoagulation process progresses and becomes highly alkaline with the liberation of hydrogen gas which leads to the transformation of ferrous to ferric ions and $As^{(III)}$to $As^{(V)}$ions. This difference in pH between the feed and the receiving phases leads to immediate reactions and interactions between iron and arsenic as is evident from the adsorption kinetics liquid diffusion model (explained in section 8.7).

8.6 Adsorption isotherms modelling

Nine isotherm models have been studied to fit the adsorption data as in Fig. 8.7. Assuming a mono-molecular layer of arsenic adsorption occurring on the sites of iron

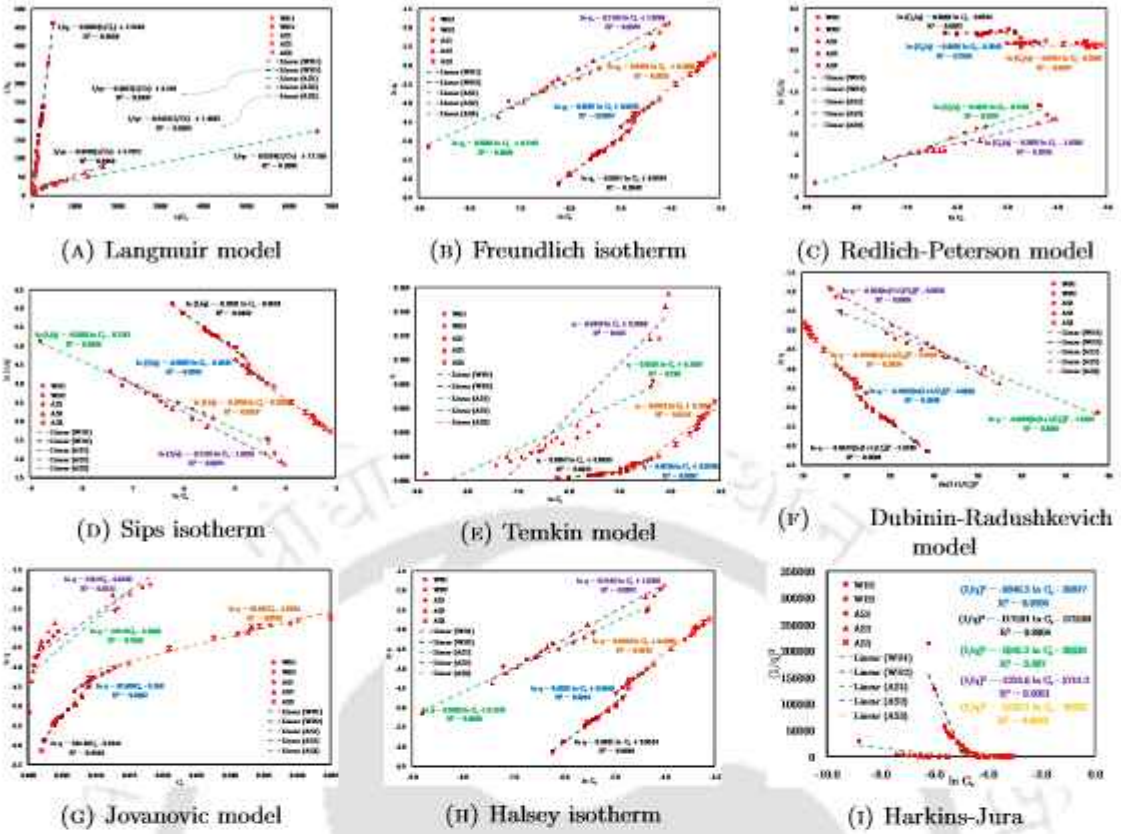

(A) Langmuir model (B) Freundlich isotherm (C) Redlich-Peterson model

(D) Sips isotherm (E) Temkin model (F) Dubinin-Radushkevich model

(G) Jovanovic model (H) Halsey isotherm (I) Harkins-Jura

FIGURE 8.7: Adsorption isotherm modeling

oxyhydroxides that are homogeneous in nature, the Langmuir model predicts the surface coverage. Langmuir isotherm model fits well with the data with R^2 values to be 0.99. This indicates that monolayer adsorption between adsorbate and adsorbent mostly occurs in all samples. The chi-square test values and the HFEF values are low and within the range of 0.01-0.56 and 0.12–0.32, respectively. But the RMSE values have a wide range of 1.1 for WB1, 7.7 for WB2, 0.88 for AS3, 1.41 for AS2, and 5.38 for AS1. This means that the average difference between the experimental and predicted data is low for samples obtained from WB1 and AS3; and high for the adsorption data obtained from WB2, AS1 and AS2. Based on the R^2 value and the statistical error function analysis, it can be predicted that the Langmuir model fits well with the data obtained from WB1 and AS3. Langmuir model can be expressed by a dimensionless constant known as the separation factor (R_L)[256]. R_L values are positive and less than 1 indicating that this is a favorable adsorption process[256]. Similarly the Freundlich isotherm model fits well with the R^2 value in the range of 0.985-0.9957. The RMSE values obtained are 0.016, 0.052, 0.095, 0.053 and 0.037 for WB1, WB2, AS1, AS2 and AS3 respectively. The chi-square test values are very low and in the range of 0.0001-0.0026. The HFEF values

are less than one and in the range of 0.03−0.15. Therefore, all the adsorption data fit well with the Freundlich isotherm model inferring that the adsorption is heterogeneous in nature as well.

Redlich-Peterson isotherm and Sips isotherm models are three-parameter empirical models developed by combining both Langmuir and Freundlich models. These models also validate the experimental data. The Sips isotherm model fits well with the data as this model transforms into the Freundlich isotherm model during low concentrations of adsorbate with respect to the concentrations of adsorbent. The R^2 values for this model are in the range of 0.985−0.9957. The statistical error analysis values are low indicating that the predicted model fits well with the experimental values. However, the Redlich-Peterson model doesn't fit well with the data obtained from WB1, WB2 and AS3 based on R^2 values. Though both Langmuir and Freundlich models are valid for all the sets of adsorption data, based on the R^2 value and the statistical error function analysis enlisted in Table 8.10, the Freundlich isotherm model predominates as affirmed by the Sips model.

TABLE 8.10: Coefficients of the adsorption isotherm models and statistical error functions

Isotherm models	Parameters & statistical error functions	Values obtained for				
		WB1	WB2	AS1	AS2	AS3
Langmuir	K_L	4.7419	2.8223	737.9	128.4	2.3
	R_L	0.0026	0.0139	0.065	0.199	0.91
	R^2	0.9937	0.9938	0.991	0.996	0.997
	RMSE	1.0931	7.6966	5.387	1.406	0.877
	χ^2	0.0163	0.2753	0.561	0.061	0.03
	HFEF	0.1229	0.3183	0.879	0.372	0.297
Freundlich	$\ln K_F$	0.0545	0.0534	0.1781	1.0206	0.2903
	$1/n$	0.9397	0.9931	0.5983	0.7145	0.9759
	R^2	0.9932	0.9849	0.9889	0.9957	0.9913
	RMSE	0.0157	0.0520	0.0952	0.0531	0.0372
	χ^2	0.0001	0.0005	0.0026	0.0009	0.0004

	HFEF	0.0316	0.0763	0.0585	0.1525	0.1001
Redlich-Peterson	R_P	0.0603	0.0069	0.4017	0.2855	0.0241
	$\ln A$	0.0545	0.0534	0.1781	1.0206	0.2903
	R^2	0.3764	0.0032	0.9757	0.9735	0.0647
	RMSE	0.0157	0.0520	0.0952	0.0531	0.0372
	χ^2	0.0007	0.0298	0.0034	0.001	0.0037
	HFEF	0.4514	4.9370	0.3284	0.2002	0.93
Sips	K_S	0.9397	0.9931	0.5983	0.7145	0.9759
	a_S	0.9469	0.9480	0.8368	0.3604	0.748
	R^2	0.9932	0.9849	0.9889	0.9957	0.9913
	RMSE	0.0157	0.0520	0.0952	0.0531	0.0372
	χ^2	0.0001	0.0005	0.0026	0.0009	0.0004
	HFEF	0.0351	0.0848	0.2484	0.1695	0.1112
Temkin	b	1.82×10^5	4.76×10^5	129	58.6	79.2
	$\ln K_T$	5.6471	6.4038	8.369	7.253	4.994
	R^2	0.9901	0.8815	0.788	0.944	0.9118
	RMSE	0.0003	0.0008	0.015	0.0116	0.004
	χ^2	1×10^{-5}	0.0001	0.0053	0.0023	0.0003
	HFEF	0.1780	1.0151	2.866	1.7917	0.7515
Dubinin-Radushkevich	q_{max}	0.1274	0.0722	0.1881	0.414	0.2137
	β	1.69×10^{-8}	1.49×10^{-8}	0.0074	0.0104	0.0204
	E	5440.3	5801.1	8.2041	6.925	4.9472
	R^2	0.9948	0.9804	0.9805	0.9983	0.9824
	RMSE	0.0138	0.0591	0.1261	0.0329	0.0528
	χ^2	1×10^{-5}	0.0007	0.0045	0.0003	0.0009
	HFEF	0.0267	0.0758	0.2431	0.0952	0.1538
Jovanovic	q_{max}	0.0057	0.0018	0.015	0.0218	0.011
	K_J	-87.606	-204.36	-142.42	-118.2	-43.031
	R^2	0.9692	0.9464	0.7038	0.8511	0.9523
	RMSE	0.0335	0.0979	0.4919	0.3115	0.087
	χ^2	0.0003	0.0018	0.0691	0.0304	0.0024
	HFEF	0.0590	0.1559	1.1553	0.8317	0.2242

Halsey	η_H	-1.0641	-1.0069	-1.6714	-1.399	-1.025
	K_H	0.9436	0.9476	0.7425	0.2397	0.7427
	R^2	0.9932	0.9849	0.9889	0.9957	0.9913
	RMSE	0.0157	0.0520	0.0952	0.0531	0.0372
	χ^2	0.0001	0.0005	0.0026	0.0009	0.0004
	HFEF	0.0316	0.0763	0.2235	0.1525	0.1001
Harkins-Jura	H_J	100×10^{-6}	8.5×10^{-6}	170×10^{-6}	810×10^{-6}	320×10^{-6}
	B	-4.0439	-4.8946	-5.18	-4.63	-3.23
	R^2	0.9204	0.8004	0.687	0.6051	0.9043
	RMSE	586.44	24820	5998.71	1115.32	414.4
	χ^2	61.742	11015	6276.05	822.48	197.56
	HFEF	0.7780	3.628	9.487	6.11	3.73

The Temkin isotherm model establishes that direct and indirect intermolecular interactions occur during the complex formation. Additionally, it predicts that the binding energies decrease linearly with the surface coverage due to indirect interactions between the adsorbate-adsorbent in the adsorption process. The R^2 values for this isotherm are in the range of 0.788-0.99 indicating that the Temkin isotherm model fits well the adsorption data of all samples, especially in the case of AS2. The heat of sorption of 476 kJ·mol^{-1} is maximum for WB2 in comparison to WB1 (182 kJ·mol^{-1}), AS1 (129 kJ·mol^{-1}), AS2 (58.6 kJ·mol^{-1}) and AS3 (79.2 kJ·mol^{-1}). The positive variation in adsorption energy indicates it to be a physical adsorption process that is exothermic in nature. The high heat of adsorption suggests that the process could occur on or near the surface of the adsorption sites indicating surface coverage whose cumulative interactions lead to such a high energy generation, while the lower heat of adsorption for samples from AS2 and AS3 stipulates non-uniform heterogeneous interactions that occur during the adsorption process. The RMSE values in the range of 0.0003-0.015 indicate that there is not much difference between the experimental and predicted data. The low chi-square test values portray that there is not much difference between linear and non-linear regression analysis of this model. However, the high values of HFEF for WB2, AS1 and AS2 reflects that the linear expression of this model fits well with the adsorption data of WB1 and AS3.

The Dubinin-Radushkevich model is a two-parameter isotherm that differentiates between physical and chemical adsorption mechanisms on heterogeneous surfaces with Gaussian energy distribution [255]. The R^2 values for the Dubinin-Radushkevich model lie in the range of 0.9804–0.9983 suggesting that this model fits well with the data. The low statistical error values estimated for all three locations further confirm the goodness of the fit. The mean adsorption energy calculated from the model is in the range of 4.95-8.2 kJ·mol^{-1}. The mean adsorption energy for WB2 adsorption data is higher than WB1 but the model fits well with the data obtained from WB1 based on the R^2 value of 0.9948 and low statistical error values of RMSE (0.0138), chi-square test value (0.000) and HFEF (0.0267). The mean adsorption energy for AS1 adsorption data is high but the model fits well with the data obtained from AS2 based on the R^2 value of 0.9983 and low statistical error values of RMSE (0.0329), chi-square test value (0.0003) and HFEF (0.0952). Though the values of q_{max} and β obtained from the expression are very low, the heterogeneous adsorption process is affirmed through the coefficient values and error functions calculated.

Jovanovic isotherm model fits well with the adsorption data having R^2 values of 0.9692 for WB1 and 0.9464 for WB2, but the K_J constants are negative for both samples. Moreover, the statistical error values and q_{max} estimated are quite low, rendering it to be a misfit with the experimental data. Jovanovic isotherm model fits well with the adsorption data of AS3 having R^2 value 0.9523, whereas the R^2 values for AS1 and AS2 are 0.7038 and 0.8511, respectively. The RMSE values are in the range of 0.087-0.492 and the χ^2 test values are very low and in the range of 0.002-0.069. However, the HFEF values are low for AS2 (0.832) and AS3 (0.224) but high for AS1 (1.155). Since the Jovanovic model is based on the concepts of the Langmuir model, the adsorption data from AS3 fit this model better than the data obtained from AS1 and AS2, predicting that monolayer formation occurs during the adsorption process. However, the negative coefficients render it to be a misfit with the experimental data. Similarly, the Halsey isotherm model fits well with the data but the negative coefficients make it unsuitable to draw inferences about the removal mechanism of arsenic. Further, the Harkins-Jura model does not fit the data. This helps to rule out the multilayer adsorption process with heterogeneous pore distribution following a pore-filling mechanism.

8.7 Adsorption kinetics modelling

The rate of binding arsenic to the ferric hydroxides is determined through adsorption kinetics by determining the rate constant and the rate-controlling step. Researchers have identified three prominent steps in adsorption that includes adsorption on the interior regions of the adsorbent; pore or intraparticle diffusion in which the adsorbate percolates in the interior sites of the adsorbent particles; and surface or liquid film diffusion that involves the transportation of the adsorbate from the bulk solution to the external surface of the adsorbent[331]. Based on these steps, the following six models have been studied, pseudo-first order model (PFO), pseudo-second order model (PSO), Elovich model, fractional power function model, intraparticle diffusion model (IPD), and liquid film diffusion model (LFD). This provides insight into the mechanism of the adsorption process. Fig. 8.8 depicts the adsorption kinetics models for all the samples. Considering the R^2 values only it seems that the PSO model fits well but the statistical data values along with R^2 values presented in Table 8.11 suggest that the PFO model fits well with both WB1 and WB2 data. Though the rate constant values and PFO rate are low, the consistency of the experimental adsorption capacity with the calculated adsorption capacity coupled with lower statistical error values as observed in RMSE, χ^2 and HFEF supports PFO model as the best fitting kinetics model in comparison to PSO.

TABLE 8.11: Coefficients of the adsorption kinetics models with statistical validation

Kinetic models	Parameters & statistical error functions	Values obtained for				
		WB1	WB2	AS1	AS2	AS3
	$q_{e,exp}$	0.0050	0.0022	0.0056	0.007	0.0086
	$q_{e,cal}$	0.0053	0.0024	0.0058	0.0062	0.009
	k_1	0.0110	0.0079	0.0071	0.007	0.0103
	rate	5.84×10^{-5}	1.36×10^{-5}	3.98×10^{-5}	4.89×10^{-5}	6.94×10^{-5}
Pseudo first order	R^2	0.9942	0.9897	0.9915	0.9919	0.9938

	RMSE	0.0652	0.0625	0.0631	0.06	0.0771
	χ^2	0.0006	0.0005	0.0006	0.0006	0.0009
	HFEF	0.1157	0.0988	0.0872	0.0862	0.1067
Pseudo second order	k_2	1.3168	4.7613	3.0229	0.4556	1.7563
	rate	6.15×10^{-5}	3.26×10^{-5}	10×10^{-5}	5.16×10^{-5}	17×10^{-5}
	R^2	0.9966	0.9822	0.9937	0.9882	0.9972
	RMSE	739.12	4435.6	1550.4	1242.72	651.502
	χ^2	13.518	209.76	53.549	38.14	14.7994
	HFEF	0.1916	0.4591	0.2502	0.2276	0.1108
Elovich	α	0.00014	0.00067	0.0005	0.0001	0.00048
	β	625	1000	1000	434.78	526.32
	R^2	0.9919	0.9818	0.9814	0.99	0.971
	RMSE	0.0002	0.00019	0.00021	0.00018	0.00025
	χ^2	0.00001	0.00001	0.00001	0.00001	0.00001
	HFEF	0.6833	0.48307	0.31897	0.23441	0.22872
Fractional power function	k_3	0.0003	0.0002	0.0013	0.0002	0.0015
	ν	0.5137	0.3901	0.2409	0.6234	0.3023
	R^2	0.9831	0.9934	0.9947	0.9633	0.9617
	RMSE	0.0469	0.0222	0.01308	0.09079	0.04499
	χ^2	0.0004	0.00008	0.00003	0.00154	0.00041
	HFEF	0.0929	0.0336	0.01638	0.11127	0.06497
Intraparticle diffusion	k_{ID}	0.0003	0.0001	0.0002	0.0004	0.0003
	R^2	0.9770	0.9886	0.9883	0.9761	0.9268
	RMSE	0.0002	0.0001	0.00041	0.00036	0.00044
	χ^2	0.00001	0.00001	0.00004	0.00003	0.00003
	HFEF	0.5013	0.7051	0.68384	0.50275	0.42873
Liquid film diffusion	k_{LFD}	0.0110	0.0079	0.0071	0.007	0.0103
	R^2	0.9942	0.9897	0.9915	0.9919	0.9938
	RMSE	0.0652	0.0625	0.0631	0.06	0.0771
	χ^2	0.0027	0.0027	0.0022	0.0028	0.0028
	HFEF	0.3892	0.4076	0.3375	0.4248	0.3498

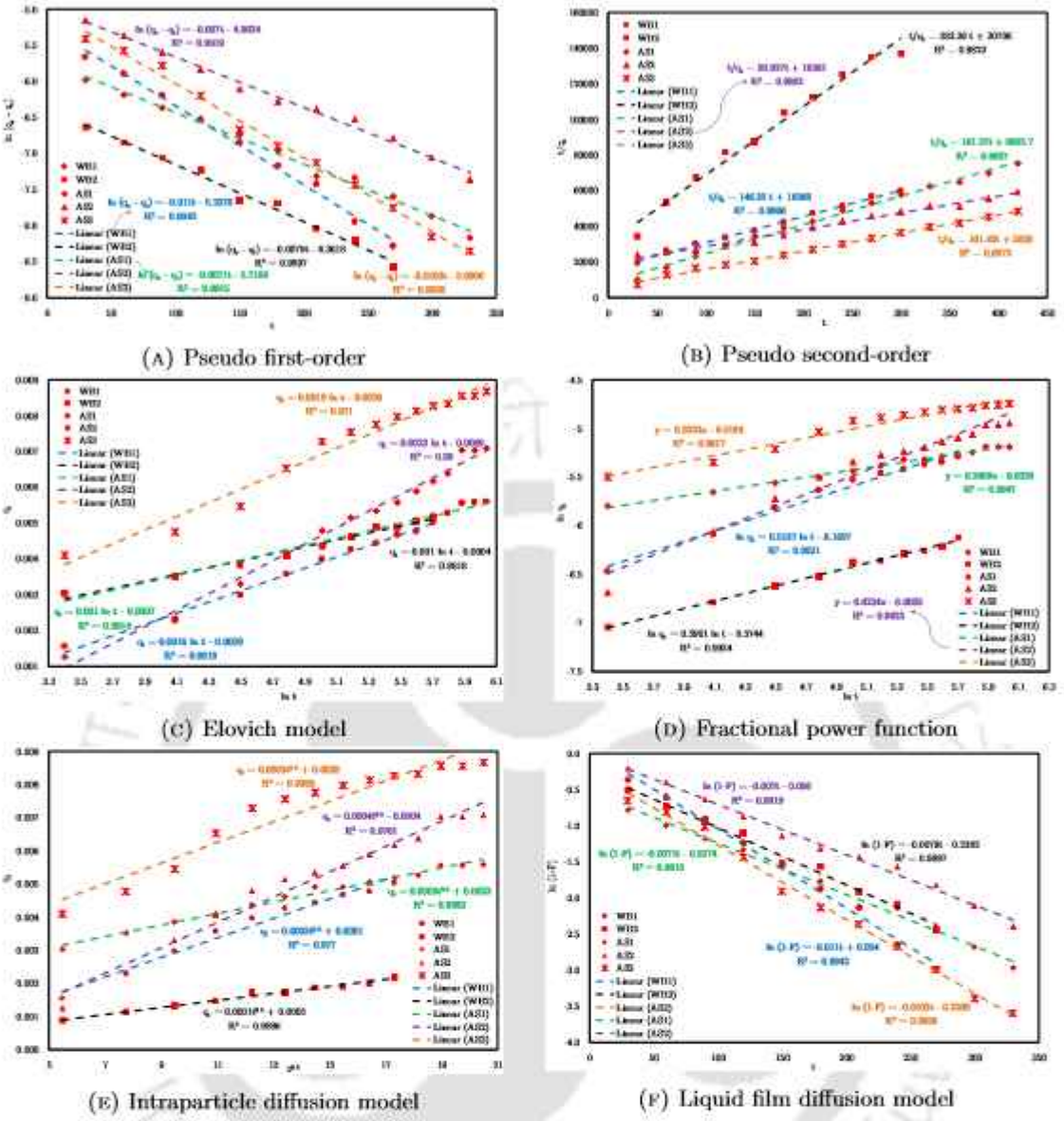

(A) Pseudo first-order

(B) Pseudo second-order

(C) Elovich model

(D) Fractional power function

(E) Intraparticle diffusion model

(F) Liquid film diffusion model

FIGURE 8.8: Adsorption kinetics modeling

The Elovich model elucidates the adsorption and desorption constants by α and β values based on the available concentrations of adsorbent and adsorbate. These values are positive for all samples with high R^2 values and low statistical error values. The low adsorption constant indicates that a saturation level is almost achieved whereas a high desorption value indicates that the arsenic is strongly entrapped into the iron complex and cannot be easily released into the bulk liquid phase. β value is the highest for AS1 in comparison to AS2 & AS3. The fractional power function model also fits well with the data but the values of the parameters are too small and less than unity[266].

The rate-controlling step and the diffusion mechanisms are explored through IPD and

LFD models. Linear plots are observed for both models with R^2 values of LFD model slightly greater than IPD model. These models can be established as the only rate-determining step if the plot begins from the origin. However, there is the thickness of the adsorbent, calculated from IPD as the value of $C \geqslant 0$ for both samples. The value of C for WB1, WB2, AS1 and AS3 are 0.0001, 0.0003, 0.0022 and 0.0028. The thickness in the case of AS2 is negative. The value of C estimated from LFD models are 0.054 for WB1 and -0.24 for WB2. The positive C values for WB1 in both IPD and LFD models indicate that a liquid film boundary and adsorbent boundary thicknesses participate in the adsorption process in which the liquid film boundary layer thickness is more than that of the adsorbent layer thickness. However, in WB2 there is a positive adsorbent layer of thickness 0.0003 (IPD) while a negative thickness in the case of liquid film diffusion. This exhibits the occurrence of a combined effect of diffusion and surface reaction for which the boundary layer is negative[311]. The value of C estimated from LFD models is negative for all three samples. The positive C values for AS1 and AS3 in the IPD model indicate that adsorbent boundary thicknesses participate in the adsorption process. However, in the case of AS2 in the IPD model and LFD models for AS1, AS2, and AS3, there is a negative thickness due to a combined effect of diffusion and surface reaction for which the boundary layer is negative[311].

8.8 Characteristics of precipitate

The FTIR spectra are given in Fig. 8.9. The peak at 437cm^{-1} is attributed to the stretching of Fe-O forming an octahedron shape[332].The presence of $As^{(III)}$species is indicated by peaks at 542cm^{-1} and 550 cm^{-1} that occur due to the As^{3+}-O bond stretching[332]. The shift in peak at 795cm^{-1} corresponds to the interaction of arsenic with α-FeOOH[333]. The peak at 890 cm^{-1} is attributed to the Fe-OH bending vibrations of goethite[334]. The peaks in the range of 1100-1700 cm^{-1} correspond to $As^{(V)}$[293]. The transformation of different forms of iron oxides for the adsorption of arsenic species is indicated by the peaks in the range of 879-1088 cm^{-1}. The peak at 879 cm^{-1} is attributed to the Fe-O-H bending vibrations in goethite[303].

The peaks at 1630 and 1640 cm^{-1} correspond to $As^{(V)}$[293]. This indicates that the $As^{(III)}$species is oxidized to $As^{(V)}$by the electrocoagulation process. Fig. 8.10 shows the XRD analysis of the calcined samples.

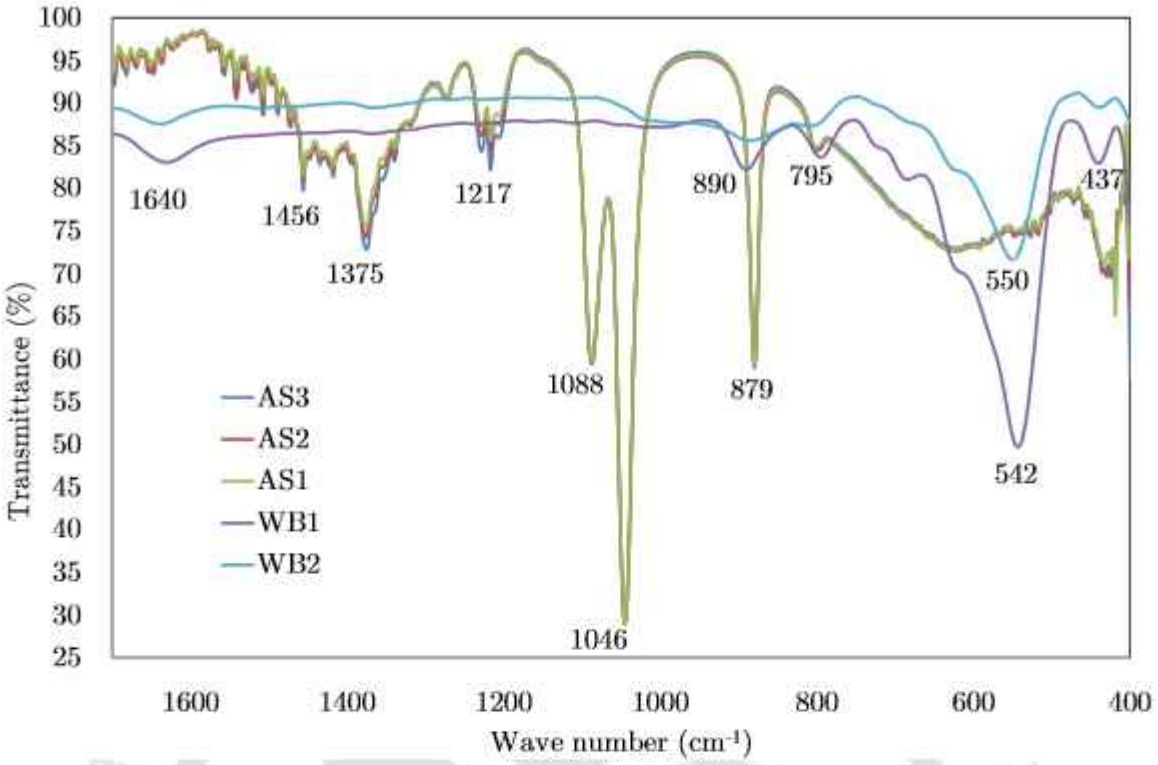

FIGURE 8.9: Plot of the FTIR data for the precipitate obtained from the removal of arsenic ions

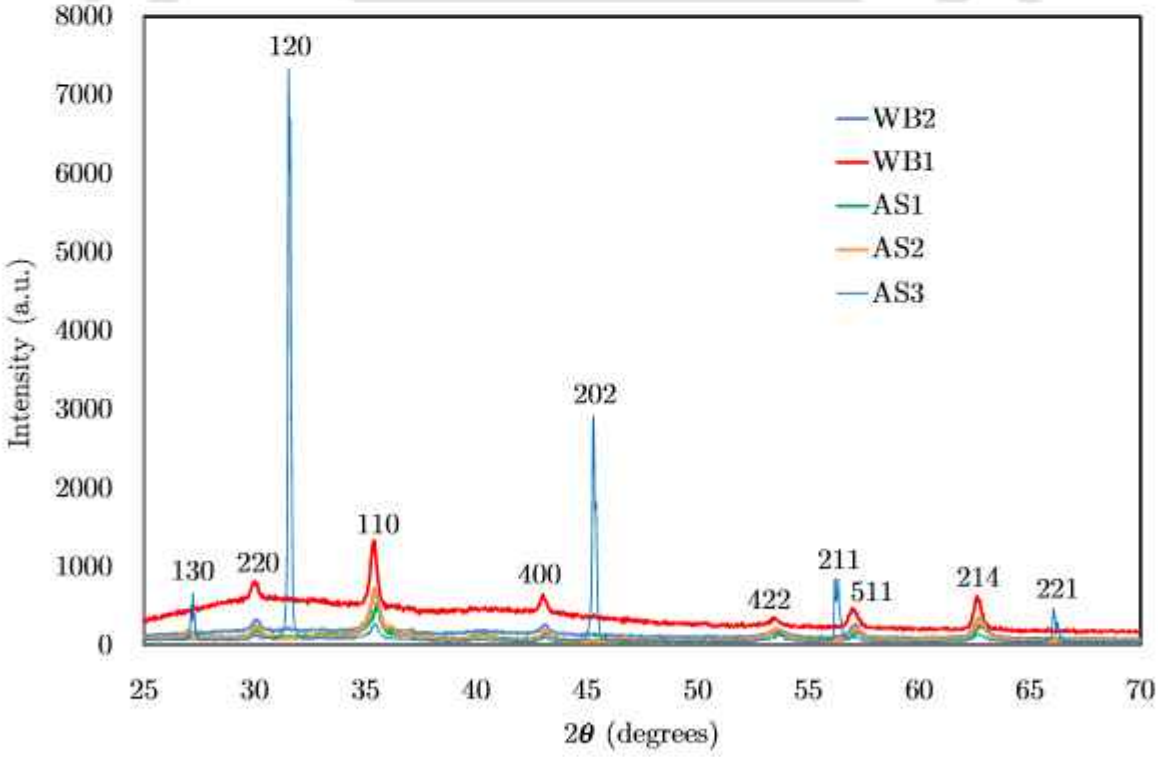

FIGURE 8.10: Plot of the XRD data for the precipitate obtained from the removal of arsenic ions

The XRD pattern confirms the formation of ferric oxide in both precipitates[305] as the peak positions obtained are 30.09(220), 35.42(311), 43.05(400), 53.39(422), 56.94(511), and 62.51(440)[335]. The size of the ferric oxide nanoparticle calculated from the Debye–Scherrer equation is 21 nm for WB1 and 19 nm for WB2[270]. The peak positions obtained are 27.25 (130), 31.54 (120), 35.64 (110), 45.36 (202), 56.23 (211), 62.42 (214), and 66.04 (221). This further corroborates the formation of the hematite and goethite phases of iron oxide in the precipitate[306]. The size of the ferric oxide nanoparticle calculated from the Debye–Scherrer equation is 24, 20, and 34 nm for AS1, AS2, and AS3, respectively[270].

Energy-dispersive X-ray spectroscopy (EDX) analyzes the elemental composition of the precipitate. The EDX elemental analysis of precipitate obtained from the removal of arsenic from the different areas for the case study is given in Fig. 8.11. The measured intensities manifest the presence of iron, oxygen, and arsenic as the main constituents of the precipitate. The presence of sodium, chloride, and silicon is attributed to the ions present in the receiving phase.

Summary of the case studies on the removal of arsenic by the hybrid technique

- Based on the perception study, it was observed that the people were well informed about the issue of arsenic contamination and its consequences. In addition to arsenic, locals had raised concerns about a few emerging water-related issues. Despite the availability of various water resources such as tap water supply, community wells, household bore wells, hand pumps, and surface water sources like ponds, water scarcity is becoming a noteworthy problem, especially during the summer months.

- The perception study revealed that the majority of respondents were females and homemakers aged between 29 and 38 years. A significant number of individuals had developed a reliance on groundwater, primarily from bore wells and hand pumps. However, increased awareness about safe water consumption and arsenic contamination had prompted some individuals to adopt water treatment methods, while others had shown a preference for tap water supply.

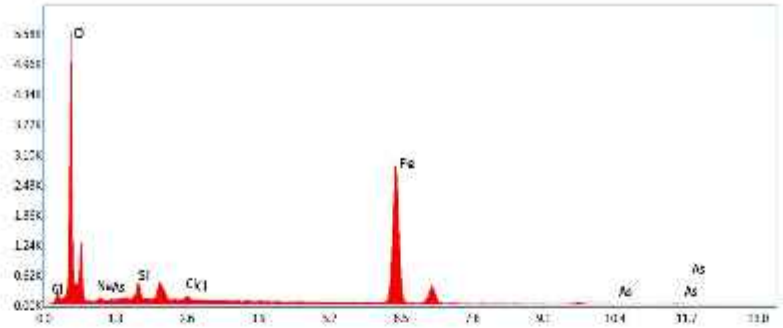

(A) Case study WB1

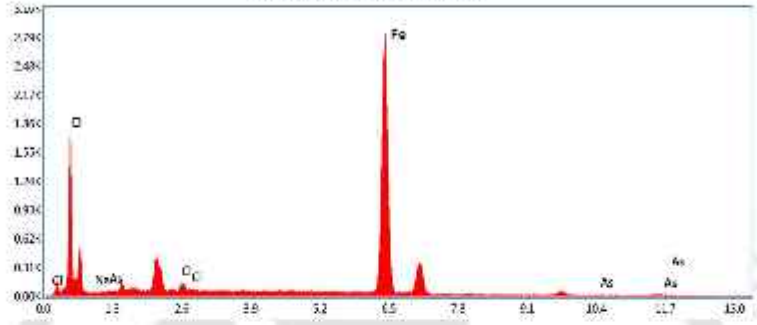

(B) Case study WB2

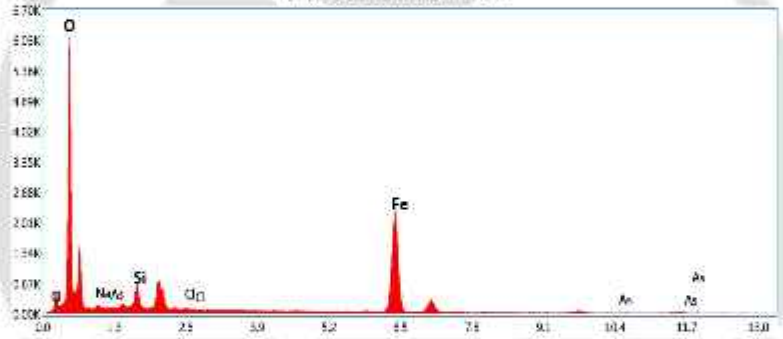

(C) Case study AS1

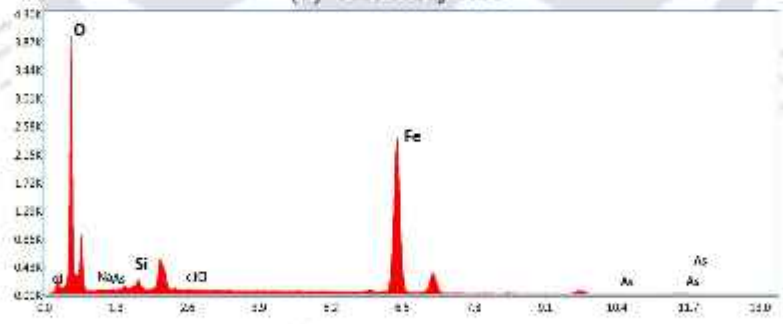

(D) Case study AS2

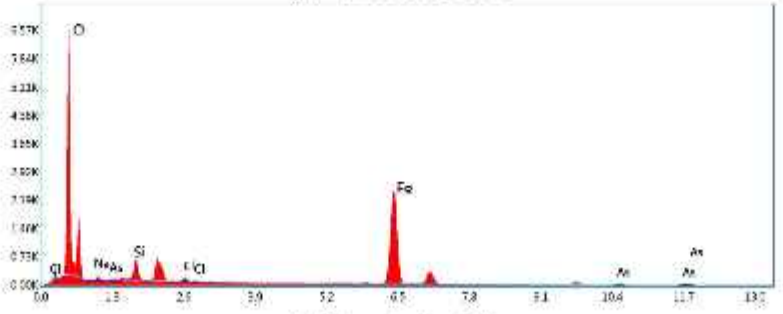

(E) Case study AS3

FIGURE 8.11: EDX analysis of the precipitate interactions

- The arsenic concentration in regions of Assam is above 100 ppb while in West Bengal it is well below 100 ppb.
- The application of the hybrid technique leads to the removal of arsenic below 10 ppb in accordance with the WHO guidelines for safe drinking water.
- Extractant concentration was found to be the most significant parameter for all the cases.
- The optimum concentration of Aliquat 336 in the liquid membrane is found to be 10% for AS1, AS2, WB1, and WB2. While the optimum extractant concentration is 40% for AS3.
- Receiving phase pH value less than 7 is found to be favourable for the maximum removal of arsenic ions due to the presence of iron in the groundwater samples that accelerates this process.
- The iron-arsenic complex was characterized by SEM-EDS, FTIR, and XRD confirming the formation of various phases of iron hydroxide/oxide such as goethite, hematite, lepidocrocite, and magnetite.
- Both Langmuir and Freundlich isotherm models were found to fit with the adsorption isotherm data.
- Pseudo first-order model was found to fit the kinetic data for all the groundwater samples.

Abbreviation

EDS Energy dispersive X-ray spectroscopy

FCCCD Face-centered central composite design

FTIR Fourier transform infrared spectroscopy

RSM Response surface methodology

SEM Scanning electron microscopy

XRD X-ray diffraction

Chapter 9

Conclusions

This concluding chapter summarizes the inferences drawn from the present research work, lists out its limitations, and provides recommendations towards future direction for removal of arsenic from water using hybrid FSSLM-electrocoagulation technique.

9.1 Concluding remarks on the salient research contributions of this study

In the present work, the performance of liquid membrane-based processes has been investigated for the removal of arsenic ions from water. Preliminary experimentations were done in a two-phase equilibrium study to identify the most effective environmentally benign diluent and extractant for arsenic extraction. The volumetric, acoustic, physicochemical, spectroscopic, and thermodynamic properties of the identified diluent-extractant pseudo-binary mixture were estimated thoroughly over a temperature range of 25-60°C . The extraction efficiency of individual and combined arsenic ions was explored through a variation of different parameters in two phase studies. The extraction equilibrium constants were estimated for application in a FSSLM using the identified diluent-extractant combo in the two phase study. Consequently, the three-phase FSSLM

study was performed using this selected liquid membrane (i.e. pseudo-binary mixture of diluent and extractant) to find the extraction% and recovery% of individual and mixed $As^{(III)}$and $As^{(V)}$species in water. As arsenic is naturally found to be adsorbed in iron minerals, ferric chloride solution was used as the receiving phase for the FSSLM study with PVDF as the solid support for the liquid membrane. The modeling of the arsenic transport process was explored through statistical and machine-learning approaches for both two-phase and three-phase studies in predicting the optimum process condition that would ensure the highest yield in terms of optimum extraction% and/or recovery%. ANN coupled with Genetic Algorithm based optimization tool was applied in machine learning algorithm.

To further improve the removal efficiency of arsenic below 10 ppb, a hybrid technique was applied which is a combination of FSSLM and electrocoagulation process with sacrificial iron anode and graphite cathode in its receiving phase. This led to the formation of an iron-arsenic complex that precipitated below during this process. Various characterization techniques were applied to identify the iron oxyhydroxides and also to confirm the formation of the said complex of iron-arsenic. Case studies were performed with this technique on the groundwater samples collected from various locations of the states of Assam and West Bengal, India. All the experimentations were performed by following the face-centered central composite design of the response surface methodology to randomly design a group of experiments by varying the parameters simultaneously and generate an empirical model for optimization.

This study makes significant contributions to the field of arsenic removal, offering a holistic and innovative approach to address the environmental and health challenges associated with arsenic contamination. The salient research findings and features of this study are presented as follows:

- Sesame oil is the most effective environmentally benign diluent for arsenic extraction, while Aliquat 336 is the preferred extractant due to its ability to react with both dissociated and undissociated ions of arsenic. They form pseudo-binary mixture, i.e. organic phase, which act as a good liquid membrane for FSSLM. The identification of vegetable oil as an environmentally benign diluent and the formulation of a liquid membrane using sesame oil and Aliquat 336 represent pioneering

steps towards more sustainable approach to arsenic removal methodologies than traditional solvents.

- The exploration of volumetric, acoustic, spectroscopic, and thermodynamic properties provides a thorough understanding of the liquid membrane system. For instance, negative excess molar volume indicates strong molecular interaction in the mixture. A new relation was obtained between density, surface tension, viscosity, and intermolecular free length based on the experimental findings of this study.

- Determination of equilibrium constants, permeability coefficients, and mass transfer coefficients for individual and combined arsenic species through two-phase and three-phase studies offers valuable insights into the efficiency of the removal process. For instance, it is revealed that the formation of Arsenic-Aliquat® 336 complex in the organic phase follows the stoichiometric ratio of 1 : 1, whereas the extraction of $As^{(V)}$into the organic phase is more favourable in comparison to $As^{(III)}$and combined arsenic species. It is further observed that mass transfer resistances are more during the transport of $As^{(V)}$than that of $As^{(III)}$.

- The implementation of statistical analysis and machine learning-based modeling not only optimizes conditions but also demonstrates a forward-looking, data-driven approach. For instance, the error percentage of statistical approach is in the range of 0.45 to 2.47 and ML based analysis is in the range of 0.21 to 11.9 for extraction and recovery of all the arsenic species. It is also revealed that the feed phase pH and extractant concentration are found to be the common significant parameters in most of the cases. Pillai's trace is more robust than the other statistical tests based on model assumptions, which indicates that the receiving phase concentration has a significant main effect in the multivariate test.

- The proposed hybrid technique, combining FSSLM and electrocoagulation processes, presents an innovative solution for achieving arsenic levels below 10 ppb. FTIR spectra stipulated the conversion of $As^{(III)}$to $As^{(V)}$due to oxidation reactions occurring during the electrocoagulation process. The precipitate indicates the formation and presence of different phases of iron oxide/hydroxides such as goethite, hematite, lepidocrocite, and magnetite. The size of the ferric oxide nanoparticle calculated from the Debye-Scherrer equation was 19 - 34 nm after treatment

of groundwater samples from various locations of Assam and West Bengal. The iron-arsenic precipitate is a saleable value-added product that has applications in construction materials as well as pesticides.

- The adsorption studies show that Dubinin-Radushkevich model and Freundlich isotherm model fits well with the adsorption data suggesting a heterogeneous and physical adsorption process occurring in both individual and combined ratios of arsenic ions. Temkin isotherm model does not support either of the $As^{(III)}/As^{(V)}$ adsorption data indicating that the adsorption is characterized by a non-uniform distribution of binding energies. While it fits well with the adsorption data for the case of $As^{(III)}$:$As^{(V)}$::1:2 ratio predicting that the binding energies decrease linearly with the surface coverage due to indirect interactions between the adsorbate-adsorbent in the adsorption process and the positive variation in adsorption energy points to an exothermic physical adsorption process.
- The inclusion of an arsenic-specific questionnaire survey for perception-based studies in contaminated areas of Assam and West Bengal adds a sociocultural dimension to the research, contributing to a comprehensive understanding of arsenic-related challenges in specific regions.
- Overall, this study stands as a multidimensional and impactful contribution to the ongoing efforts in arsenic remediation research.

In summary, the contributions cover a broad spectrum, from the choice of solvent and membrane preparation to in-depth analyses of properties, coefficients, and the development of a hybrid technique. The inclusion of statistical analysis, machine learning, and a survey adds a multidimensional aspect to the study, making it a comprehensive and impactful piece of research in the field of arsenic removal. The results of this work were compared to other recently-published works, as shown in Tables 9.1 and 9.2.

Despite the promising applications of the study in arsenic removal from drinking water, it is essential to acknowledge certain limitations. Firstly, the effectiveness of the proposed methods may vary under different environmental conditions, and the scalability of these approaches to diverse settings needs careful consideration.

TABLE 9.1: Comparison with literature for two phase study

Process	Arsenic species	Diluent	Extractant	Extraction%	References
Solvent extraction	$As^{(V)}$-3000 ppm	Kerosene	2M DBBP - 0.8M D2EHPA	50%	[213]
Liquid-liquid extraction	$As^{(III)}$- 10 mg·L^{-1}, $As^{(V)}$- 10 mg·L^{-1}	Dodecane modified with 4% dodecanol	0.5M Aliquat 336	$As^{(III)}$- 100%, $As^{(V)}$- 100%	[115]
Aqueous two phase system	$As^{(III)}$- 15 mg·kg^{-1}, $As^{(V)}$- 15 mg·kg^{-1}, DMA - 15 mg·kg^{-1}	Triton X - 100/165 +, Choline chloride + water	Ammonium pyrrolidine dithiocarbamate (APDC)	$As^{(III)}$- 69.02%, $As^{(V)}$- 92.99%, DMA - 90.05%	[149]
Liquid-liquid extraction	$As^{(III)}$- 2.5 g·dm^{-3}, $As^{(V)}$- 2.5 g·dm^{-3}	Toluene, Exxsol D 220/230, Octane	Cyanex® 923, Cyanex® 925, Cyanex® 301, Hydrophobic glycol, Hydroxamic acids	$As^{(III)}$- 98.7% with 50% v/v Cyanex® 301 in toluene, $As^{(V)}$- 60.6% with 50% v/v Cyanex® 925 in toluene	[150]
Aqueous two phase system	$As^{(III)}$-30 mg·kg^{-1}, $As^{(V)}$-30 mg·kg^{-1}	L64 +, Na2SO4 +, water	Ammonium pyrrolidine dithiocarbamate (APDC)	$As^{(III)}$- 98%, $As^{(V)}$- 18%	[151]
Liquid-liquid extraction	$As^{(III)}$-100 ppb, $As^{(V)}$-100 ppb, $As^{(III)}$:$As^{(V)}$:: 1 : 1 -100 ppb, $As^{(III)}$:$As^{(V)}$:: 1 : 2 -150 ppb, $As^{(III)}$:$As^{(V)}$:: 2 : 1 -150 ppb	Sesame oil	10% (v/v) Aliquat 336	$As^{(III)}$- 84%, $As^{(V)}$- 86%, $As^{(III)}$:$As^{(V)}$:: 1 : 1 - 85.5%, $As^{(III)}$:$As^{(V)}$:: 1 : 2 - 86%, $As^{(III)}$:$As^{(V)}$:: 2 : 1 - 84.5%	This work

TABLE 9.2: Comparison with literature for three phase study (FSSLM)

Removal process	Arsenic species	Diluent	Extractant	Receiving phase	Extraction%	Recovery%	Authors
FSSLM	$As^{(V)}$- 10^{-3} mol·L^{-1}	Kerosene	0.1M Cyanex® 921 in PVDF	2M Na_2SO_4	94%	94%	[285]
FSSLM	$As^{(V)}$- 10mg·L^{-1}	Dodecane modified with 4% dode-canol	0.5M Aliquat 336 in PVDF	0.1M NaCl	95%	95%	[152]
FSSLM	$As^{(III)}$- 100 ppb, $As^{(V)}$- 100 ppb, $As^{(III)}$:$As^{(V)}$:: 1 : 1 - 100 ppb, $As^{(III)}$:$As^{(V)}$:: 1 : 2 - 150 ppb, $As^{(III)}$:$As^{(V)}$:: 2 : 1 - 150 ppb	Sesame oil	10% - 40% (v/v) Aliquat 336 in PVDF	2-3ppm $FeCl_3$	$As^{(III)}$- 60%, $As^{(V)}$- 66.7%, $As^{(III)}$:$As^{(V)}$:: 1 : 1 - 65%, $As^{(III)}$:$As^{(V)}$:: 1 : 2 - 66.5%, $As^{(III)}$:$As^{(V)}$:: 2 : 1 - 59%	$As^{(III)}$- 48%,$As^{(V)}$- 47%,$As^{(III)}$:$As^{(V)}$:: 1 : 1 - 46.5%, $As^{(III)}$:$As^{(V)}$:: 1 : 2 - 48.5%, $As^{(III)}$:$As^{(V)}$:: 2 : 1 - 41%	This work

Additionally, the reliance on modelling approaches, whether mathematical, statistical, or machine learning, introduces inherent uncertainties and assumptions that may not fully capture the complexity of real-world scenarios. Practical implementation may encounter challenges related to the availability of resources, infrastructure, and community cooperation. Furthermore, while surveying provides valuable insights into public perceptions, it may not encompass the full spectrum of socio-cultural factors that influence community engagement. Understanding these limitations is crucial for refining and adapting the proposed arsenic removal strategies to ensure their practical viability and long-term success in diverse contexts.

9.2 Limitations of this study

This study has several notable limitations that should be acknowledged to provide a comprehensive understanding of its findings. Firstly, the exclusive focus on batch processes in contaminant removal restricts the generalizability of the results, as industrial operations often employ diverse processing modes. These findings may not fully capture the intricacies associated with continuous or hybrid processes, limiting the broader applicability of its conclusions. Furthermore, this study's concentration on specific contaminants may overlook the challenges posed by a wider range of pollutants prevalent in different industrial contexts. To enhance the scope of this work, future research should explore additional contaminants to offer a more holistic perspective on contaminant removal processes. Additionally, the reliance on localized surveys for the perception study introduces a potential bias, as the findings may not accurately represent the diverse viewpoints present in a global or more extensive demographic context. To overcome this limitation, future research should consider conducting perception studies on a more diverse and widespread scale. Lastly, incorporating case studies from various geographical regions and industrial sectors would provide a more comprehensive understanding of the challenges and solutions related to contaminant removal. While the study on batch process arsenic removal provides valuable insights, these limitations underscore the necessity for future research endeavours to broaden the scope, incorporate diverse case studies, and account for the nuanced variations in contaminant removal processes across different industries and regions.

9.3 Scope for further research work

Future research in the field of contaminant removal processes should aim to address the identified limitations and further advance our understanding of this critical area. Firstly, investigations should extend beyond the confines of batch processes to encompass continuous and hybrid systems, ensuring a comprehensive analysis of contaminant removal methods across diverse operational modes. Additionally, researchers should delve into a broader array of contaminants, recognizing the multifaceted challenges posed by different pollutants in varied industrial settings. To enhance the study's applicability, future research should incorporate extensive case studies representing various industries and geographical regions, accounting for the contextual variations that influence contaminant removal efficiency. Moreover, expanding perception studies on a global scale and across diverse demographics can provide a more inclusive understanding of stakeholders' perspectives. Future research offers several avenues for further research and exploration in the field of water treatment and analysis. Here are some potential areas for future investigation that can be further extended by studying:

- **Continuous mode experiments:** Evaluate the efficiency of the liquid membrane technique in continuous mode operations. This could involve designing and conducting experiments that simulate real-world scenarios, where water treatment processes typically operate continuously rather than in batch mode and include parameters related to scalability.
- **Cumulative impact of contaminants/ions:** Investigating the impact of multiple contaminants or ions present in water that affects the overall efficiency of the liquid membrane technique. This could involve studying synergistic or antagonistic effects between different pollutants and their impact on the removal of the target species.
- **Interaction of pollutants with arsenic:** Explore in-depth the interactions between various pollutants and arsenic in water. Understanding these interactions can provide insights into the selectivity and specificity of the liquid membrane technique for arsenic removal in the presence of other contaminants.
- **Application of this technique for removal of other contaminants:** Extend the liquid membrane-based separation technique to address the removal of other

contaminants beyond arsenic. Investigate its efficacy for the removal of different types of pollutants, broadening the application range of this technology.

- **Micro/Nano-sized sensing devices:** Explore the development of micro/nano-sized sensing devices based on liquid membrane technology. These devices could be designed for on-site and real-time monitoring of arsenic or other contaminants in groundwater or wastewater, providing a more dynamic and responsive approach to water quality analysis.

- **Environmental impact assessment:** Assess the environmental impact of the liquid membrane technique, considering factors such as waste generation, energy consumption, and the potential release of by-products. This will contribute to a comprehensive understanding of the sustainability and eco-friendliness of the technology.

Overall, the scope of future research should encompass a holistic and integrated approach, transcending the limitations identified in the current study, to offer more nuanced insights into contaminant removal processes and their real-world applications. By delving into these areas, researchers can contribute to the advancement of knowledge in water treatment and pave the way for the development of more effective and sustainable technologies for addressing water quality challenges.

Bibliography

[1] F. N. Robertson, "Arsenic in ground-water under oxidizing conditions, south-west United States," *Environmental geochemistry and Health*, vol. 11, pp. 171–185, 1989.

[2] J. Hering and M. Elimelech, "International perspective on arsenic in groundwater: problems and treatment strategies," in *Proc. AWWA, Annual Conference*, 1995.

[3] P. Bhattacharya, S. Nordqvist, and G. Jacks, "Status of arsenic contamination in the soils around a former wood preservation facility at Konsterud, Kristinehamns municipality, Varmlands county, western Sweden," in *Proc. 5th Seminar on Hydrogeology and Environment Geochemistry, Norges Geologiske Undersokelse, Report*, vol. 95, 1995, pp. 70–72.

[4] A. H. Welch, M. S. Lico, and J. L. Hughes, "Arsenic in ground water of the western United States," *Groundwater*, vol. 26, no. 3, pp. 333–347, 1988.

[5] N. E. Korte and Q. Fernando, "A review of arsenic (III) in groundwater," *Critical Reviews in Environmental Science and Technology*, vol. 21, no. 1, pp. 1–39, 1991.

[6] L. Lorenzen, J. Van Deventer, and W. Landi, "Factors affecting the mechanism of the adsorption of arsenic species on activated carbon," *Minerals Engineering*, vol. 8, no. 4-5, pp. 557–569, 1995.

[7] T. S. Choong, T. Chuah, Y. Robiah, F. G. Koay, and I. Azni, "Arsenic toxicity, health hazards and removal techniques from water: an overview," *Desalination*, vol. 217, no. 1-3, pp. 139–166, 2007.

[8] E. Shaji, M. Santosh, K. Sarath, P. Prakash, V. Deepchand, and B. Divya, "Arsenic contamination of groundwater: A global synopsis with focus on the Indian peninsula," *Geoscience Frontiers*, vol. 12, no. 3, p. 101079, 2021.

[9] G. Medunić, Ž. Fiket, and M. Ivanić, "Arsenic contamination status in Europe, Australia, and other parts of the world," *Arsenic in Drinking Water and Food*, pp. 183–233, 2020.

[10] S. Appleyard, J. Angeloni, and R. Watkins, "Arsenic-rich groundwater in an urban area experiencing drought and increasing population density, Perth, Australia," *Applied geochemistry*, vol. 21, no. 1, pp. 83–97, 2006.

[11] A. L. Hinwood, D. J. Jolley, and M. R. Sim, "Cancer incidence and high environmental arsenic concentrations in rural populations: results of an ecological study," *International Journal of Environmental Health Research*, vol. 9, no. 2, pp. 131–141, 1999.

[12] A. H. Smith and M. M. H. Smith, "Arsenic drinking water regulations in developing countries with extensive exposure," *Toxicology*, vol. 198, no. 1-3, pp. 39–44, 2004.

[13] I. A. Katsoyiannis, M. Mitrakas, and A. I. Zouboulis, "Arsenic occurrence in Europe: Emphasis in Greece and description of the applied full-scale treatment plants," *Desalination and Water Treatment*, vol. 54, no. 8, pp. 2100–2107, 2015.

[14] D. Zuzolo, D. Cicchella, A. Demetriades, M. Birke, S. Albanese, E. Dinelli, A. Lima, P. Valera, and B. De Vivo, "Arsenic: Geochemical distribution and age-related health risk in Italy," *Environmental Research*, vol. 182, p. 109076, 2020.

[15] N. Morales-Simfors, J. Bundschuh, I. Herath, C. Inguaggiato, A. T. Caselli, J. Tapia, F. E. A. Choquehuayta, M. A. Armienta, M. Ormachea, E. Joseph *et al.*, "Arsenic in Latin America: A critical overview on the geochemistry of arsenic originating from geothermal features and volcanic emissions for solving its environmental consequences," *Science of the Total Environment*, vol. 716, p. 135564, 2020.

[16] M. T. Alarcón-Herrera, D. A. Martin-Alarcon, M. Gutiérrez, L. Reynoso-Cuevas, A. Martín-Domínguez, M. A. Olmos-Márquez, and J. Bundschuh, "Co-occurrence, possible origin, and health-risk assessment of arsenic and fluoride in drinking water sources in Mexico: Geographical data visualization," *Science of the Total Environment*, vol. 698, p. 134168, 2020.

[17] J. Bundschuh, M. Armienta, P. Birkle, P. Bhattacharya, J. Matschullat, and A. Mukherjee, *Natural arsenic in groundwaters of Latin America*. CRC Press, 2008.

[18] M. A. Armienta and N. Segovia, "Arsenic and fluoride in the groundwater of Mexico," *Environmental Geochemistry and Health*, vol. 30, pp. 345–353, 2008.

[19] R. Libbey, A. Williams-Jones, B. Melosh, and N. Backeberg, "Characterization of geothermal activity along the North American–Caribbean plate boundary in Guatemala: The Joaquina geothermal field," *Geothermics*, vol. 56, pp. 17–34, 2015.

[20] A. A. Alcaine, C. Schulz, J. Bundschuh, G. Jacks, R. Thunvik, J.-P. Gustafsson, C.-M. Mörth, O. Sracek, A. Ahmad, and P. Bhattacharya, "Hydrogeochemical controls on the mobility of arsenic, fluoride and other geogenic co-contaminants in the shallow aquifers of northeastern La Pampa province in Argentina," *Science of the Total Environment*, vol. 715, p. 136671, 2020.

[21] P. L. Smedley and D. G. Kinniburgh, "A review of the source, behaviour and distribution of arsenic in natural waters," *Applied geochemistry*, vol. 17, no. 5, pp. 517–568, 2002.

[22] T. J. Sorg, A. S. Chen, and L. Wang, "Arsenic species in drinking water wells in the usa with high arsenic concentrations," *Water Research*, vol. 48, pp. 156–169, 2014.

[23] A. Ranjan, "Spatial analysis of arsenic contamination of groundwater around the world and India," *International Journal of Innovative Studies in Sociology and Humanities*, vol. 4, pp. 6–15, 2019.

[24] T. Tsuda, A. Babazono, E. Yamamoto, N. Kurumatani, Y. Mino, T. Ogawa, Y. Kishi, and H. Aoyama, "Ingested arsenic and internal cancer: a historical cohort study followed for 33 years," *American Journal of Epidemiology*, vol. 141, no. 3, pp. 198–209, 1995.

[25] S. Mitsunobu, N. Hamanura, T. Kataoka, and F. Shiraishi, "Arsenic attenuation in geothermal streamwater coupled with biogenic arsenic (III) oxidation," *Applied Geochemistry*, vol. 35, pp. 154–160, 2013.

[26] E. Even, H. Masuda, T. Shibata, A. Nojima, Y. Sakamoto, Y. Murasaki, and H. Chiba, "Geochemical distribution and fate of arsenic in water and sediments of rivers from the Hokusetsu area, Japan," *Journal of Hydrology: Regional Studies*, vol. 9, pp. 34–47, 2017.

[27] S. Tandon and R. Sinha, "The Ganga river: a summary view of a large river system of the Indian sub-continent," *The Indian rivers: scientific and socio-economic aspects*, pp. 61–73, 2018.

[28] M. F. Hughes, B. D. Beck, Y. Chen, A. S. Lewis, and D. J. Thomas, "Arsenic exposure and toxicology: a historical perspective," *Toxicological Sciences*, vol. 123, no. 2, pp. 305–332, 2011.

[29] J. Borgono and R. Greiber, "Epidemiological study of arsenicism in the city of Antofagasta," *Trace Substances in Environmental Health*, vol. 5, pp. 13–24, 1972.

[30] F.-J. Lu, "Fluorescent humic substances and blackfoot disease in Taiwan," *Applied Organometallic Chemistry*, vol. 4, no. 3, pp. 191–195, 1990.

[31] K. Saha, "Review of arsenicosis in West Bengal, India—a clinical perspective," *Critical Reviews in Environmental Science and Technology*, vol. 33, no. 2, pp. 127–163, 2003.

[32] D. Das, A. Chatterjee, G. Samanta, B. Mandal, T. R. Chowdhury, G. Samanta, P. P. Chowdhury, C. Chanda, G. Basu, D. Lodh *et al.*, "Report. arsenic contamination in groundwater in six districts of West Bengal, India: the biggest arsenic calamity in the world," *Analyst*, vol. 119, no. 12, pp. 168N–170N, 1994.

[33] D. Das, A. Chatterjee, B. K. Mandal, G. Samanta, D. Chakraborti, and B. Chanda, "Arsenic in groundwater in six districts of West Bengal, India: the biggest arsenic calamity in the world. part 2. arsenic concentration in drinking water, hair, nails, urine, skin-scale, and liver tissue (biopsy) of the affected people," *Analyst*, vol. 120, no. 3, pp. 917–924, 1995.

[34] A. Chatterjee, D. Das, B. K. Mandal, T. R. Chowdhury, G. Samanta, and D. Chakraborti, "Arsenic in groundwater in six districts of West Bengal, India: the biggest arsenic calamity in the world. Part I. arsenic species in drinking water and urine of the affected people," *Analyst*, vol. 120, no. 3, pp. 643–650, 1995.

[35] E. J. Feinglass, "Arsenic intoxication from well water in the United States," *New England Journal of Medicine*, vol. 288, no. 16, pp. 828–830, 1973.

[36] J. Southwick, A. Western, M. Beck, T. Whitley, R. Isaacs, J. Petajan, and C. Hansen, *An epidemiological study of arsenic in drinking water in Millard County, Utah.* Van Nostrand Reinhold Co, New York, NY, 1983.

[37] D. R. Lewis, J. W. Southwick, R. Ouellet-Hellstrom, J. Rench, and R. L. Calderon, "Drinking water arsenic in Utah: A cohort mortality study." *Environmental health perspectives*, vol. 107, no. 5, pp. 359–365, 1999.

[38] J. Wyllie, "An investigation of the source of arsenic in a well water," *Canadian Public Health Journal*, vol. 28, no. 3, pp. 128–135, 1937.

[39] D. A. Grantham and J. F. Jones, "Arsenic contamination of water wells in Nova Scotia," *Journal-American Water Works Association*, vol. 69, no. 12, pp. 653–657, 1977.

[40] J. Ritchie, "Arsenic and antimony in some New Zealand thermal waters. [Rotorua-Taupo region]," *New Zealand Journal of Science*, vol. 4, no. 2, 1961.

[41] H. Terade, K. Katsuta, T. Sasagawa, H. Saito, H. Shirata, K. Fukuchi, T. Sekiya, Y. Yokoyama, S. Hirokawa, Y. Watanabe, K. Hasegawa, T. Oshina, and T. Sekiguchi, "Clinical observations of chronic toxicosis by arsenic," *Nihon Rinsho*, vol. 118, pp. 2394–2403, 1960.

[42] M. M. Karim, "Arsenic in groundwater and health problems in Bangladesh," *Water Research*, vol. 34, no. 1, pp. 304–310, 2000.

[43] C. Jain and I. Ali, "Arsenic: occurrence, toxicity and speciation techniques," *Water research*, vol. 34, no. 17, pp. 4304–4312, 2000.

[44] A. K. Done and A. J. Peart, "Acute toxicities of arsenical herbicides," *Clinical toxicology*, vol. 4, no. 3, pp. 343–355, 1971.

[45] A. H. Smith, E. O. Lingas, and M. Rahman, "Contamination of drinking-water by arsenic in Bangladesh: a public health emergency," *Bulletin of the world health organization*, vol. 78, no. 9, pp. 1093–1103, 2000.

[46] H. Romero-Schmidt, A. Naranjo-Pulido, L. Mendez-Roclriguez, B. Acosta-Vargas, and A. Ortega-Rubio, "Environmental health risks by arsenic consumption in water wells in the Cape region, Mexico," *WIT Transactions on Biomedicine and Health*, vol. 5, 2001.

[47] N. R. Council, *Drinking Water and Health,: Volume 1*. Washington, DC: The National Academies Press, 1977.

[48] G. A. Wasserman, X. Liu, F. Parvez, H. Ahsan, P. Factor-Litvak, A. van Geen, V. Slavkovich, N. J. Lolacono, Z. Cheng, I. Hussain, H. Momotaj, and J. H. Graziano, "Water arsenic exposure and children's intellectual function in Araihazar, Bangladesh," *Environmental health perspectives*, vol. 112, no. 13, pp. 1329–1333, 2004.

[49] M. M. Rahman, J. C. Ng, and R. Naidu, "Chronic exposure of arsenic via drinking water and its adverse health impacts on humans," *Environmental geochemistry and health*, vol. 31, pp. 189–200, 2009.

[50] F. Parvez, G. A. Wasserman, P. Factor-Litvak, X. Liu, V. Slavkovich, A. B. Siddique, R. Sultana, R. Sultana, T. Islam, D. Levy, J. L. Mey, A. van Geen, K. Khan, J. Kline, H. Ahsan, and J. H. Graziano, "Arsenic exposure and motor function among children in Bangladesh," *Environmental health perspectives*, vol. 119, no. 11, pp. 1665–1670, 2011.

[51] S. Bhowmick, S. Pramanik, P. Singh, P. Mondal, D. Chatterjee, and J. Nriagu, "Arsenic in groundwater of West Bengal, India: a review of human health risks and assessment of possible intervention options," *Science of the Total Environment*, vol. 612, pp. 148–169, 2018.

[52] D. Saha and R. K. Ray, "Groundwater resources of India: potential, challenges and management," *Groundwater development and management: Issues and challenges in South Asia*, pp. 19–42, 2019.

[53] K. S. Subramanian and M. J. Kosnett, "Human exposures to arsenic from consumption of well water in West Bengal, India," *International journal of occupational and environmental health*, vol. 4, no. 4, pp. 217–230, 1998.

[54] A. for Toxic Substances and D. R. (ATSDR), *Arsenic Toxicity: Case Studies in Environmental Medicine*, revised october 2000 ed. Atlanta, GA: U.S. Department of Health and Human Services, Public Health Service, ATSDR, 2000, available from the ATSDR website: https://www.atsdr.cdc.gov/HEC/CSEM/, Course Number: SS3060, Expiration Date: October 30, 2006.

[55] C. Sullivan, M. Tyrer, C. R. Cheeseman, and N. J. Graham, "Disposal of water treatment wastes containing arsenic—a review," *Science of the total environment*, vol. 408, no. 8, pp. 1770–1778, 2010.

[56] K. A. Fields, A. H. Chen, and L. Wang, "Arsenic removal from drinking water by coagulation/filtration and lime softening plants," National Risk Management Research Laboratory, Cincinnati, OH 45268, Tech. Rep., 6 2000.

[57] P. Palfy, E. Vircikova, and L. Molnar, "Processing of arsenic waste by precipitation and solidification," *Waste Management*, vol. 19, no. 1, pp. 55–59, 1999.

[58] B. Shi, "Application of lime-ferric salt process to purification of waste water at shenyang smelter," *NONFERROUS METALS-BEIJING-*, vol. 50, pp. 137–140, 1998.

[59] D. Tahija and H.-H. Huang, "Factors influencing arsenic coprecipitation with ferric hydroxide," *Proceeding of Minor Elements*, pp. 149–155, 2000.

[60] X. Meng, G. P. Korfiatis, C. Christodoulatos, and S. Bang, "Treatment of arsenic in bangladesh well water using a household co-precipitation and filtration system," *Water research*, vol. 35, no. 12, pp. 2805–2810, 2001.

[61] Y. Wang and E. J. Reardon, "A siderite/limestone reactor to remove arsenic and cadmium from wastewaters," *Applied Geochemistry*, vol. 16, no. 9-10, pp. 1241–1249, 2001.

[62] S. Tokunaga, S. A. Wasay, and S.-W. Park, "Removal of arsenic (V) ion from aqueous solutions by lanthanum compounds," *Water Science and Technology*, vol. 35, no. 7, pp. 71–78, 1997.

[63] M. B. Krishna, K. Chandrasekaran, D. Karunasagar, and J. Arunachalam, "A combined treatment approach using fenton's reagent and zero valent iron for the removal of arsenic from drinking water," *Journal of Hazardous Materials*, vol. 84, no. 2-3, pp. 229–240, 2001.

[64] C. Casiot, G. Morin, F. Juillot, O. Bruneel, J.-C. Personné, M. Leblanc, K. Duquesne, V. Bonnefoy, and F. Elbaz-Poulichet, "Bacterial immobilization and oxidation of arsenic in acid mine drainage (Carnoulès creek, France)," *Water Research*, vol. 37, no. 12, pp. 2929–2936, 2003.

[65] R. Pulicharla, F. Proulx, S. Behmel, J.-B. Sérodes, and M. J. Rodriguez, "Trends in ozonation disinfection by-products—occurrence, analysis and toxicity of carboxylic acids," *Water*, vol. 12, no. 3, p. 756, 2020.

[66] M. K. Ramseier, A. Peter, J. Traber, and U. von Gunten, "Formation of assimilable organic carbon during oxidation of natural waters with ozone, chlorine dioxide, chlorine, permanganate, and ferrate," *Water Research*, vol. 45, no. 5, pp. 2002–2010, 2011.

[67] F. C. Pick, K. E. Fish, C. A. Biggs, J. P. Moses, G. Moore, and J. B. Boxall, "Application of enhanced assimilable organic carbon method across operational drinking water systems," *PLoS One*, vol. 14, no. 12, p. e0225477, 2019.

[68] Z. U. Rehman, B. Khojah, T. Leiknes, S. Alsogair, and M. Alsomali, "Removal of bacteria and organic carbon by an integrated ultrafiltration—nanofiltration desalination pilot plant," *Membranes*, vol. 10, no. 9, p. 223, 2020.

[69] M. C. Dodd, N. D. Vu, A. Ammann, V. C. Le, R. Kissner, H. V. Pham, T. H. Cao, M. Berg, and U. Von Gunten, "Kinetics and mechanistic aspects of As (III) oxidation by aqueous chlorine, chloramines, and ozone: relevance to drinking water treatment," *Environmental science & technology*, vol. 40, no. 10, pp. 3285–3292, 2006.

[70] S. Sorlini, F. Gialdini, and M. Stefan, "Arsenic oxidation by UV radiation combined with hydrogen peroxide," *Water Science and Technology*, vol. 61, no. 2, pp. 339–344, 2010.

[71] R. Li, Z. Yao, S. Yu, T.-a. Zhang, and D. Yang, "Surface modification of arsenic sulfide particles for their stabilization," *Journal of Cleaner Production*, vol. 398, p. 136491, 2023.

[72] M. Chen, Z. Chen, P. Wu, and J. P. Chen, "Simultaneous oxidation and removal of arsenite by Fe (III)/CaO_2 fenton-like technology," *Water Research*, vol. 201, p. 117312, 2021.

[73] M. G. García, J. d'Hiriart, J. Giullitti, H. Lin, G. Custo, M. d. V. Hidalgo, M. I. Litter, and M. A. Blesa, "Solar light induced removal of arsenic from contaminated groundwater: the interplay of solar energy and chemical variables," *Solar Energy*, vol. 77, no. 5, pp. 601–613, 2004.

[74] M. Wegelin, D. Gechter, S. Hug, A. Mahmud, and A. Motaleb, "Soras-a simple arsenic removal process," in *Water, sanitation and hygiene - Challenges of the Millennium: Proceedings of the 26th WEDC International Conference, 5-9 November 2000*, P. J., Ed., The organization. Dhaka, Bangladesh: Water, Engineering and Development Centre, Loughborough University, 11 2000, pp. 213–258.

[75] D. Saurav, B. S. Sudipta, L. P. Jyoti, B. Madhumita, R. Yadav, and C. Mridul, "Groundwater arsenic contamination in north eastern states of India," *Journal of Environmental Research and Development*, vol. 9, no. 3, p. 621, 2015.

[76] P. R. Kumar, S. Chaudhari, K. C. Khilar, and S. Mahajan, "Removal of arsenic from water by electrocoagulation," *Chemosphere*, vol. 55, no. 9, pp. 1245–1252, 2004.

[77] H. K. Hansen, P. Nunez, D. Raboy, I. Schippacasse, and R. Grandon, "Electrocoagulation in wastewater containing arsenic: Comparing different process designs," *Electrochimica Acta*, vol. 52, no. 10, pp. 3464–3470, 2007.

[78] H. Shen and P. K. Dasgupta, "Electrochemical arsine generators for arsenic determination," *Analytical chemistry*, vol. 86, no. 15, pp. 7705–7711, 2014.

[79] I. Chernykh, A. Tomilov, A. Smetanin, and A. Khudenko, "Electrochemical reduction of arsenic acid," *Russian journal of electrochemistry*, vol. 37, no. 9, pp. 942–946, 2001.

[80] D. Bejan and N. Bunce, "Electrochemical reduction of as (III) and As (V) in acidic and basic solutions," *Journal of applied electrochemistry*, vol. 33, pp. 483–489, 2003.

[81] M. Smirnov, V. Turygin, N. Shalashova, A. Khudenko, and A. Tomilov, "Electrochemical reduction of as (III) in acid media," *Inorganic Materials*, vol. 43, pp. 25–29, 2007.

[82] E. O. Kartinen Jr and C. J. Martin, "An overview of arsenic removal processes," *Desalination*, vol. 103, no. 1-2, pp. 79–88, 1995.

[83] J. J. Waypa, M. Elimelech, and J. G. Hering, "Arsenic removal by RO and NF membranes," *Journal-American Water Works Association*, vol. 89, no. 10, pp. 102–114, 1997.

[84] T. Urase, J.-i. Oh, and K. Yamamoto, "Effect of pH on rejection of different species of arsenic by nanofiltration," *Desalination*, vol. 117, no. 1-3, pp. 11–18, 1998.

[85] J. J. Waypa, *Separation of ionic species by polymeric nanofiltration membranes in crossflow membrane filtration: implications for arsenic removal*. University of California, Los Angeles, 1998.

[86] H. Saitúa, M. Campderrós, S. Cerutti, and A. P. Padilla, "Effect of operating conditions in removal of arsenic from water by nanofiltration membrane," *Desalination*, vol. 172, no. 2, pp. 173–180, 2005.

[87] A. Seidel, J. J. Waypa, and M. Elimelech, "Role of charge (donnan) exclusion in removal of arsenic from water by a negatively charged porous nanofiltration membrane," *Environmental engineering science*, vol. 18, no. 2, pp. 105–113, 2001.

[88] J. Oh, K. Yamamoto, H. Kitawaki, S. Nakao, T. Sugawara, M. Rahman, and M. Rahman, "Application of low-pressure nanofiltration coupled with a bicycle pump for the treatment of arsenic-contaminated groundwater," *Desalination*, vol. 132, no. 1-3, pp. 307–314, 2000.

[89] Y. Sato, M. Kang, T. Kamei, and Y. Magara, "Performance of nanofiltration for arsenic removal," *Water Research*, vol. 36, no. 13, pp. 3371–3377, 2002.

[90] M. Kang, M. Kawasaki, S. Tamada, T. Kamei, and Y. Magara, "Effect of pH on the removal of arsenic and antimony using reverse osmosis membranes," *Desalination*, vol. 131, no. 1-3, pp. 293–298, 2000.

[91] R. Y. Ning, "Arsenic removal by reverse osmosis," *Desalination*, vol. 143, no. 3, pp. 237–241, 2002.

[92] P. Brandhuber and G. Amy, "Alternative methods for membrane filtration of arsenic from drinking water," *Desalination*, vol. 117, no. 1-3, pp. 1–10, 1998.

[93] A. Shrier, N. Li, and R. Cahn, "Liquid membrane process for the separation of aqueous mixtures," Dec. 18 1973, uS Patent 3,779,907.

[94] M. S. Manna, K. K. Bhatluri, P. Saha, and A. K. Ghoshal, "Transportation of bioactive (+) catechin from its aqueous solution using flat sheet supported liquid membrane," *Journal of membrane science*, vol. 447, pp. 325–334, 2013.

[95] N. N. Li, "Separation of hydrocarbons by liquid membrane permeation," *Industrial & Engineering Chemistry Process Design and Development*, vol. 10, no. 2, pp. 215–221, 1971.

[96] J. W. Frankenfeld, R. P. Cahn, and N. N. Li, "Extraction of copper by liquid membranes," *Separation Science and Technology*, vol. 16, no. 4, pp. 385–402, 1981.

[97] R. E. Terry, N. N. Li, and W. Ho, "Extraction of phenolic compounds and organic acids by liquid membranes," *Journal of Membrane Science*, vol. 10, no. 2-3, pp. 305–323, 1982.

[98] M. Matsumoto, Y. Inomoto, and K. Kondo, "Selective separation of aromatic hydrocarbons through supported liquid membranes based on ionic liquids," *Journal of Membrane Science*, vol. 246, no. 1, pp. 77–81, 2005.

[99] K. K. Bhatluri, M. S. Manna, A. K. Ghoshal, and P. Saha, "Separation of cadmium and lead from wastewater using supported liquid membrane integrated with in-situ electrodeposition," *Electrochimica Acta*, vol. 229, pp. 1–7, 2017.

[100] S. K. Mondal and P. Saha, "Separation of hexavalent chromium from industrial effluent through liquid membrane using environmentally benign solvent: A study of experimental optimization through response surface methodology," *Chemical Engineering Research and Design*, vol. 132, pp. 564–583, 2018.

[101] S. K. Mondal, M. K. Beriya, and P. Saha, "Separation and recovery of nickel and zinc from synthetic wastewater using supported liquid membranes with in situ electrodeposition," *Industrial & Engineering Chemistry Research*, vol. 58, no. 23, pp. 9970–9987, 2019.

[102] S. K. Mondal and P. Saha, "Removal of hexavalent chromium from wastewater using supported liquid membrane: synthesis of chromium-iron complex through electrochemical reaction," *Water and Environment Journal*, vol. 34, pp. 753–771, 2020.

[103] P. Parhi *et al.*, "Supported liquid membrane principle and its practices: A short review," *Journal of Chemistry*, vol. 2013, 2013.

[104] H. Itoh, M. Thien, T. Hatton, and D. Wang, "A liquid emulsion membrane process for the separation of amino acids," *Biotechnology and bioengineering*, vol. 35, no. 9, pp. 853–860, 1990.

[105] J. Martinez-Villafane, C. Montero-Ocampo, and A. García-Lara, "Energy and electrode consumption analysis of electrocoagulation for the removal of arsenic from underground water," *Journal of Hazardous Materials*, vol. 172, no. 2-3, pp. 1617–1622, 2009.

[106] T. Prapasawat, P. Ramakul, C. Satayaprasert, U. Pancharoen, and A. W. Lothongkum, "Separation of as (III) and as (V) by hollow fiber supported liquid membrane based on the mass transfer theory," *Korean Journal of Chemical Engineering*, vol. 25, no. 1, pp. 158–163, 2008.

[107] K. K. Bhatluri, M. S. Manna, P. Saha, and A. K. Ghoshal, "Supported liquid membrane-based simultaneous separation of cadmium and lead from wastewater," *Journal of Membrane Science*, vol. 459, pp. 256–263, 2014.

[108] K. Chakrabarty, P. Saha, and A. K. Ghoshal, "Separation of mercury from its aqueous solution through supported liquid membrane using environmentally benign diluent," *Journal of Membrane Science*, vol. 350, no. 1-2, pp. 395–401, 2010.

[109] M. S. Manna, K. K. Bhatluri, P. Saha, and A. K. Ghoshal, "Transportation of catechin (C) using physiologically benign vegetable oil as liquid membrane," *Industrial & Engineering Chemistry Research*, vol. 51, no. 46, pp. 15 207–15 216, 2012.

[110] G. Muthuraman and K. Palanivelu, "Transport of textile dye in vegetable oils based supported liquid membrane," *Dyes and Pigments*, vol. 70, no. 2, pp. 99–104, 2006.

[111] P. Kazemi, M. Peydayesh, A. Bandegi, T. Mohammadi, and O. Bakhtiari, "Stability and extraction study of phenolic wastewater treatment by supported liquid membrane using tributyl phosphate and sesame oil as liquid membrane," *Chemical engineering research and design*, vol. 92, no. 2, pp. 375–383, 2014.

[112] L. Iberhan and M. Wiśniewski, "Extraction of arsenic (III) and arsenic (V) with Cyanex 925, Cyanex 301 and their mixtures," *Hydrometallurgy*, vol. 63, no. 1, pp. 23–30, 2002.

[113] P. Navarro and F. J. Alguacil, "Removal of arsenic from copper electrolytes by solvent extraction with tributylphosphate," *Canadian metallurgical quarterly*, vol. 35, no. 2, pp. 133–141, 1996.

[114] S. Sangtumrong, P. Ramakul, C. Satayaprasert, U. Pancharoen, and A. Lothongkum, "Purely separation of mixture of mercury and arsenic via hollow fiber supported liquid membrane," *Journal of Industrial and Engineering Chemistry*, vol. 13, no. 5, pp. 751–756, 2007.

[115] R. Güell, C. Fontàs, V. Salvadó, and E. Anticó, "Modelling of liquid-liquid extraction and liquid membrane separation of arsenic species in environmental matrices," *Separation and purification technology*, vol. 72, no. 3, pp. 319–325, 2010.

[116] A. W. Lothongkum, S. Suren, S. Chaturabul, N. Thamphiphit, and U. Pancharoen, "Simultaneous removal of arsenic and mercury from natural-gas-co-produced water from the Gulf of Thailand using synergistic extractant via HFSLM," *Journal of membrane science*, vol. 369, no. 1-2, pp. 350–358, 2011.

[117] L. D. Mafu, T. A. M. Msagati, and B. B. Mamba, "The simultaneous stripping of arsenic and selenium from wastewaters using hollow-fibre supported liquid membranes," *Environmental Monitoring and Assessment*, vol. 186, no. 12, pp. 8865–8874, 2014.

[118] U. Pancharoen, W. Poonkum, and A. W. Lothongkum, "Treatment of arsenic ions from produced water through hollow fiber supported liquid membrane," *Journal of alloys and compounds*, vol. 482, no. 1-2, pp. 328–334, 2009.

[119] W. Srirachat, T. Wannachod, U. Pancharoen, and S. Kheawhom, "Effect of polarity and temperature on the binary interaction between D2EHPA extractant and organic solvents (kerosene, n-heptane, chlorobenzene and 1-octanol): Experimental and thermodynamics," *Fluid Phase Equilibria*, vol. 434, pp. 117–129, 2017.

[120] L. R. Koekemoer, M. J. G. Badenhorst, and R. C. Everson, "Determination of viscosity and density of Di-(2-ethylhexyl) Phosphoric Acid + Aliphatic Kerosene," *Journal of Chemical & Engineering Data*, vol. 50, no. 2, pp. 587–590, 2005.

[121] Y. Litaiem and M. Dhahbi, "Physicochemical properties of an hydrophobic ionic liquid (Aliquat 336) in a polar protic solvent (Formamide) at different temperatures," *Journal of Dispersion Science and Technology*, vol. 36, no. 5, pp. 641–651, 2015.

[122] ——, "Measurements and correlations of viscosity, conductivity and density of an hydrophobic ionic liquid (Aliquat 336) mixtures with a non-associated dipolar aprotic solvent (DMC)," *Journal of Molecular Liquids*, vol. 169, pp. 54–62, May 2012.

[123] S. Fang, C. X. Zhao, and C. H. He, "Densities and viscosities of binary mixtures of tri-n-butyl phosphate + cyclohexane, + n-heptane at T = (288.15, 293.15, 298.15, 303.15, and 308.15) K," *Journal of Chemical & Engineering Data*, vol. 53, no. 9, pp. 2244–2246, 2008.

[124] B. K. Rout, N. C. Mishra, and V. Chakravortty, "Viscosity and density of binary liquid mixtures of tri-n-butyl phosphate+benzene,+carbon tetrachloride,+isobutyl methyl ketone and +acetylacetone at 25, 30, 35,40 and 45 °C," *Indian Journal of Chemical Technology*, vol. 1, pp. 347–350, 1994.

[125] N. Swain, D. Panda, S. K. Singh, and V. Chakravortty, "Viscosity and density of tri-n-butyl phosphate + benzene + toluene from 30°c to 45°c," *Journal of Chemical & Engineering Data*, vol. 44, no. 1, pp. 32–34, 1999.

[126] ——, "Viscosity and density of tri-n-butyl phosphate + benzene + o-xylene from 30°c to 45°c," *Journal of Chemical & Engineering Data*, vol. 42, no. 6, pp. 1235–1237, 1997.

[127] Q. Tian and H. Liu, "Densities and viscosities of binary mixtures of tributyl phosphate with hexane and dodecane from (298.15 to 328.15) K," *Journal of Chemical & Engineering Data*, vol. 52, no. 3, pp. 892–897, 2007.

[128] K. Tiwari, C. Patra, S. Padhy, and V. Chakravortty, "Molecular interaction study on binary mixtures of dimethyl sulphoxide + isobutyl methyl ketone (IBMK), + acetylacetone and + tri-n-butylphosphate (TBP) from the excess properties of ultrasonic velocity, viscosity and density," *Physics and Chemistry of Liquids*, vol. 32, no. 3, pp. 149–157, 1996.

[129] S. L. Oswal and A. T. Patel, "Viscosity of binary mixtures. I. mono-, di-, and tri-n-butyl and -n-octylamine with cyclohexane," *International Journal of Thermophysics*, vol. 12, no. 5, pp. 821–835, Sep 1991.

[130] H. Yamamoto, K. Sakamoto, Y. Bando, S. Matsumoto, and J. Shibata, "Density and excess molar volume of tri-n-octylamine + propionic acid + diluent at 298.15K," *Journal of Chemical & Engineering Data*, vol. 42, no. 2, pp. 238–242, 1997.

[131] S. Fang, X. B. Zuo, X. J. Xu, and D. H. Ren, "Density, viscosity and excess molar volume of binary mixtures of tri-n-octylamine+diluents (n-heptane, n-octane, n-nonane, and n-decane) at various temperatures," *The Journal of Chemical Thermodynamics*, vol. 68, pp. 281–287, 2014.

[132] A. Keshav, K. L. Wasewar, and S. Chand, "Reactive extraction of propionic acid using tri-n-octylamine, tri-n-butyl phosphate and aliquat 336 in sunflower oil as diluent," *Journal of Chemical Technology & Biotechnology*, vol. 84, no. 4, pp. 484–489, 2008.

[133] R. M. Davies, "Effect of the temperature on dynamic viscosity, density and flow rate of some vegetable oils," *Journal of Scientific Research in Engineering & Technology*, vol. 1, pp. 14–24, 2016.

[134] L. M. Diamante and T. Lan, "Absolute viscosities of vegetable oils at different temperatures and shear rate range of 64.5 to 4835 s^{-1}," *Journal of Food Processing*, vol. 2014, pp. 1–6, 2014.

[135] B. Esteban, J. R. Riba, G. Baquero, A. Rius, and R. Puig, "Temperature dependence of density and viscosity of vegetable oils," *Biomass and Bioenergy*, vol. 42, pp. 164–171, 2012.

[136] G. Paranjpe and P. Deshpande, "Dielectric properties of some vegetable oils," in *Proceedings of the Indian Academy of Sciences-Section A*, vol. 1, no. 12. Springer, 1935, pp. 880–886.

[137] Z. Li, Y. Sun, D. Zhao, Y. Zhuang, R. Wang, F. Yang, X. Liu, and Y. Chen, "Surface tension of binary mixtures of (ionic liquid + tributyl phosphate)," *The Journal of Chemical Thermodynamics*, vol. 132, pp. 214–221, 2019.

[138] I. S. Khattab, F. Bandarkar, M. Khoubnasabjafari, and A. Jouyban, "Density, viscosity, surface tension, and molar volume of propylene glycol+water mixtures from 293 to 323K and correlations by the Jouyban–Acree model," *Arabian Journal of Chemistry*, vol. 10, pp. S71 – S75, 2017.

[139] M. Oroian and G. Gutt, "Influence of temperature on the physical properties of vegetable oils," *Food and Environment Safety Journal*, vol. 14, no. 2, 2016.

[140] R. Auerbach, "Oberflächenspannung und schallgeschwindigkeit," *Experientia*, vol. 4, no. 12, pp. 473–474, 1948.

[141] V. S. Kislik, *Liquid membranes: principles and applications in chemical separations and wastewater treatment*. Elsevier, 2009.

[142] P. Ajwani, L. Lokwani, and U. Sharma, "Bulk liquid membrane transport of alkali metal cations using non cyclic ionophores," *Proceedings of the National Academy of Sciences, India Section A: Physical Sciences*, vol. 82, pp. 91–95, 2012.

[143] N. Kocherginsky and Q. Yang, "Big carrousel mechanism of copper removal from ammoniacal wastewater through supported liquid membrane," *Separation and purification technology*, vol. 54, no. 1, pp. 104–116, 2007.

[144] L. R. de Lemos, I. J. B. Santos, G. D. Rodrigues, L. H. M. da Silva, and M. C. H. da Silva, "Copper recovery from ore by liquid–liquid extraction using aqueous two-phase system," *Journal of hazardous materials*, vol. 237, pp. 209–214, 2012.

[145] A. E. Visser, R. P. Swatloski, S. T. Griffin, D. H. Hartman, and R. D. Rogers, "Liquid/liquid extraction of metal ions in room temperature ionic liquids," *Separation Science and Technology*, vol. 36, no. 5-6, pp. 785–804, 2001.

[146] G.-T. Wei, Z. Yang, and C.-J. Chen, "Room temperature ionic liquid as a novel medium for liquid/liquid extraction of metal ions," *Analytica Chimica Acta*, vol. 488, no. 2, pp. 183–192, 2003.

[147] P. G. Mazzola, A. M. Lopes, F. A. Hasmann, A. F. Jozala, T. C. Penna, P. O. Magalhaes, C. O. Rangel-Yagui, and A. Pessoa Jr, "Liquid–liquid extraction of biomolecules: an overview and update of the main techniques," *Journal of Chemical Technology & Biotechnology: International Research in Process, Environmental & Clean Technology*, vol. 83, no. 2, pp. 143–157, 2008.

[148] N. Suzuki, K. Satoh, H. Shoji, and H. Imura, "Liquid-liquid extraction behavior of arsenic (iii), arsenic (v), methylarsonate and dimethylarsinate in various systems," *Analytica chimica acta*, vol. 185, pp. 239–248, 1986.

[149] S. J. B. e. Silva, G. M. D. Ferreira, H. P. Neves, L. R. de Lemos, G. D. Rodrigues, and A. B. Mageste, "Use of aqueous two-phase systems formed by triton x and choline chloride for extraction of organic and inorganic arsenic," *Separation and Purification Technology*, vol. 263, p. 118082, 2021.

[150] L. Iberhan and M. Wiśniewski, "Removal of arsenic (iii) and arsenic (v) from sulfuric acid solution by liquid–liquid extraction," *Journal of Chemical Technology & Biotechnology: International Research in Process, Environmental & Clean Technology*, vol. 78, no. 6, pp. 659–665, 2003.

[151] R. C. Assis, B. A. de Araujo Faria, C. L. Caldeira, A. B. Mageste, L. R. de Lemos, and G. D. Rodrigues, "Extraction of arsenic (iii) in aqueous two-phase systems: A new methodology for determination and speciation analysis of inorganic arsenic," *Microchemical Journal*, vol. 147, pp. 429–436, 2019.

[152] R. Güell, C. Fontàs, E. Anticó, V. Salvadó, J. G. Crespo, and S. Velizarov, "Transport and separation of arsenate and arsenite from aqueous media by supported liquid and anion-exchange membranes," *Separation and purification technology*, vol. 80, no. 3, pp. 428–434, 2011.

[153] C.-Y. Tsai, Y.-F. Chen, W.-C. Chen, F.-R. Yang, J.-H. Chen, and J.-C. Lin, "Separation of gallium and arsenic in wafer grinding extraction solution using a supported liquid membrane that contains pc88a as a carrier," *Journal of Environmental Science and Health*, vol. 40, no. 2, pp. 477–491, 2005.

[154] D. Y. Takigawa, "Separation of metals by supported liquid membrane," May 19 1992, uS Patent 5,114,579.

[155] K. Hylton and S. Mitra, "A microfluidic hollow fiber membrane extractor for arsenic (v) detection," *Analytica chimica acta*, vol. 607, no. 1, pp. 45–49, 2008.

[156] L. Li, P. Yan, W. Gao, and Y. Li, "Emulsion liquid membrane separation of as (III) and As (V)," *Fresenius' journal of analytical chemistry*, vol. 363, pp. 317–319, 1999.

[157] A. Kargari, T. Kaghazchi, and M. Soleimani, "Role of emulsifier in the extraction of gold (iii) ions from aqueous solutions using the emulsion liquid membrane technique," *Desalination*, vol. 162, pp. 237–247, 2004.

[158] S. M. Mousavi, S. Kiani, M. R. Farmad, A. Hemati, and B. Abbasi, "Extraction of arsenic (v) from water using emulsion liquid membrane," *Journal of dispersion science and technology*, vol. 33, no. 1, pp. 123–129, 2012.

[159] S. Kiani and S. M. Mousavi, "Ultrasound assisted preparation of water in oil emulsions and their application in arsenic (v) removal from water in an emulsion liquid membrane process," *Ultrasonics sonochemistry*, vol. 20, no. 1, pp. 373–377, 2013.

[160] K. Chakrabarty, P. Saha, and A. K. Ghoshal, "Simultaneous separation of mercury and lignosulfonate from aqueous solution using supported liquid membrane," *Journal of Membrane Science*, vol. 346, no. 1, pp. 37–44, 2010.

[161] R. N. R. Sulaiman, N. Jusoh, N. Othman, N. F. M. Noah, M. B. Rosly, and H. A. Rahman, "Supported liquid membrane extraction of nickel using stable composite speek/pvdf support impregnated with a sustainable liquid membrane," *Journal of hazardous materials*, vol. 380, p. 120895, 2019.

[162] R. N. R. Sulaiman, N. Othman, N. F. M. Noah, and N. Jusoh, "Removal of nickel from industrial effluent using a synergistic mixture of acidic and solvating carriers in palm oil-based diluent via supported liquid membrane process," *Chemical Engineering Research and Design*, vol. 137, pp. 360–375, 2018.

[163] P. Nidheesh and T. A. Singh, "Arsenic removal by electrocoagulation process: recent trends and removal mechanism," *Chemosphere*, vol. 181, pp. 418–432, 2017.

[164] A. Mudgal, "Draft review of the household arsenic removal technology options," *Rural Water Supply Network (http://www. htnweb. com)*, 2001.

[165] M. Leist, R. Casey, and D. Caridi, "The management of arsenic wastes: problems and prospects," *Journal of Hazardous Materials*, vol. 76, no. 1, pp. 125–138, 2000.

[166] C. E. Halim, R. Amal, D. Beydoun, J. A. Scott, and G. Low, "Implications of the structure of cementitious wastes containing Pb (II), Cd (II), As (V), and Cr (VI) on the leaching of metals," *Cement and Concrete Research*, vol. 34, no. 7, pp. 1093–1102, 2004.

[167] M. Y. Mollah, M. Kesmez, and D. L. Cocke, "An x-ray diffraction (XRD) and fourier transform infrared spectroscopic (FT-IR) investigation of the long-term effect on the solidification/stabilization (S/S) of arsenic (V) in Portland cement type-V," *Science of the total environment*, vol. 325, no. 1-3, pp. 255–262, 2004.

[168] P. Riveros, J. Dutrizac, and P. Spencer, "Arsenic disposal practices in the metallurgical industry," *Canadian Metallurgical Quarterly*, vol. 40, no. 4, pp. 395–420, 2001.

[169] B. Cancès, F. Juillot, G. Morin, V. Laperche, L. Alvarez, O. Proux, J.-L. Hazemann, G. Brown, and G. Calas, "XAS evidence of as (V) association with iron oxyhydroxides in a contaminated soil at a former arsenical pesticide processing plant," *Environmental Science & Technology*, vol. 39, no. 24, pp. 9398–9405, 2005.

[170] K. M. Hassan, K. Fukushi, K. Turikuzzaman, and S. Moniruzzaman, "Effects of using arsenic–iron sludge wastes in brick making," *Waste management*, vol. 34, no. 6, pp. 1072–1078, 2014.

[171] X. Savarimuthu, M. M. Hira-Smith, Y. Yuan, O. S. von Ehrenstein, S. Das, N. Ghosh, D. G. Mazumder, and A. H. Smith, "Seasonal variation of arsenic concentrations in tubewells in West Bengal, India," *Journal of health, population, and nutrition*, vol. 24, no. 3, p. 277, 2006.

[172] M. Laha, H. Arambagh, and W. Bengal, "Social implication of arsenic pollution in eastern Barddhaman," *Transactions*, vol. 35, no. 2, pp. 173–184, 2013.

[173] S. Puri, P. Kumar, S. Rana, B. K. Bansod, S. Debnath, C. Ghanshyam, and P. Kapur, "GIS-based geospatial mapping of arsenic polluted underground water in Purbasthali block in Bardhaman," in *Proceedings of the International Conference on Communication and computing (ICC 2014)*, K. R. Venugopal and S. C. Lingareddy, Eds., IEEE - Elsevier, Society of Information processing. Bangalore, India: Elsevier, June 2014, pp. 544–552.

[174] B. Biswas, "Geomorphic controls of arsenic in ground water in Purbasthali I & II blocks of Burdwan district, West Bengal, India," *International Journal of Environmental Sciences*, vol. 1, no. 4, pp. 419–439, 2010.

[175] T. Pal, P. K. Mukherjee, and S. Sengupta, "Nature of arsenic pollutants in groundwater of Bengal basin-a case study from Baruipur area, West Bengal, India," *Current Science*, vol. 82, no. 5, pp. 554–561, 2002.

[176] P. Kalita, C. Gogoi, and S. Maunash, "Hydro chemical assessment of groundwater in north-eastern region of India: a case study of western suburb of Jorhat town of Assam, India," *Current World Environment*, vol. 16, no. 1, pp. 18–33, 2021.

[177] P. Saikia, P. Kotoky, and U. Goswami, "Distribution of fluoride and arsenic contents in the ground water system, Jorhat district, Assam, India," *International Journal of Scientific Research*, vol. 6, pp. 844–847, 2017.

[178] S. Ghosh and P. Sar, "Identification and characterization of metabolic properties of bacterial populations recovered from arsenic contaminated ground water of north east India (Assam)," *Water research*, vol. 47, no. 19, pp. 6992–7005, 2013.

[179] S. Das and M. Barooah, "Characterization of siderophore producing arsenic-resistant Staphylococcus sp. strain TA6 isolated from contaminated groundwater of Jorhat, Assam and its possible role in arsenic geocycle," *BMC microbiology*, vol. 18, no. 1, pp. 1–11, 2018.

[180] L. Sailo and C. Mahanta, "Arsenic mobilization in the Brahmaputra plains of Assam: groundwater and sedimentary controls," *Environmental monitoring and assessment*, vol. 186, pp. 6805–6820, 2014.

[181] R. Nickson, C. Sengupta, P. Mitra, S. Dave, A. Banerjee, A. Bhattacharya, S. Basu, N. Kakoti, N. Moorthy, M. Wasuja *et al.*, "Current knowledge on the distribution of arsenic in groundwater in five states of India," *Journal of Environmental Science and Health, Part A*, vol. 42, no. 12, pp. 1707–1718, 2007.

[182] B. A. Shah, "Role of quaternary stratigraphy on arsenic-contaminated groundwater from parts of Barak valley, Assam, north–east India," *Environmental earth sciences*, vol. 66, pp. 2491–2501, 2012.

[183] P. K. Jha and P. Tripathi, "Arsenic and fluoride contamination in groundwater: a review of global scenarios with special reference to India," *Groundwater for Sustainable Development*, vol. 13, p. 100576, 2021.

[184] M. Sridharan and D. S. Nathan, "Chemometric tool to study the mechanism of arsenic contamination in groundwater of Puducherry region, south east coast of India," *Chemosphere*, vol. 208, pp. 303–315, 2018.

[185] C. Jain, S. Sharma, and S. Singh, "Physico-chemical characteristics and hydrogeological mechanisms in groundwater with special reference to arsenic contamination in Barpeta district, Assam (India)," *Environmental monitoring and assessment*, vol. 190, pp. 1–16, 2018.

[186] M. Buragohain, B. Bhuyan, and H. P. Sarma, "Seasonal variations of lead, arsenic, cadmium and aluminium contamination of groundwater in Dhemaji district, Assam, India," *Environmental monitoring and assessment*, vol. 170, pp. 345–351, 2010.

[187] S. P. Purkayastha, M. Choudhury, D. Deb, and C. Paul, "Arsenic contamination in ground water is a serious threat in the North Karimganj block of Karimganj district, southern part of Assam, India," *Journal of Chemical and Pharmaceutical Research*, vol. 7, no. 8, pp. 371–378, 2015.

[188] K. K. Borah, B. Bhuyan, and H. P. Sarma, "Lead, arsenic, fluoride, and iron contamination of drinking water in the tea garden belt of Darrang district, Assam, India," *Environmental monitoring and assessment*, vol. 169, pp. 347–352, 2010.

[189] J. Bayuo, M. J. Rwiza, and K. M. Mtei, "Modeling and optimization of trivalent arsenic removal from wastewater using activated carbon produced from maize plant biomass: a multivariate experimental design approach," *Biomass Conversion and Biorefinery*, pp. 1–24, 2023.

[190] A. Zialame, A. Jamshidi-Zanjani, A. K. Darban, and M. Homaee, "Arsenic removal from solution using nano-magnetic compound: optimization modeling by response surface method," *Environmental Monitoring and Assessment*, vol. 195, no. 1, p. 136, 2023.

[191] A. Theam and S. Bun, "Optimization of iron co-presence in airlift reactor for arsenic (iii) removal using respond surface methodology," in *AIP Conference Proceedings*, vol. 2785, no. 1. AIP Publishing, 2023.

[192] S. Irshad, Z. Xie, M. Qing, A. Nawaz, S. Mehmood, S. Y. Alomar, M. Faheem, and N. Walayat, "Application of BCXZM composite for arsenic removal: EPS production, biotransformation and immobilization of bacillus xzm on corn cobs biochar," *Biology*, vol. 12, no. 4, p. 611, 2023.

[193] S. Mousavi Moghanjooghi, S. Khoramnezhadian, and E. Fataei, "Quantitative modeling of arsenic removal from aqueous solution by ctab-modified zeolite using central composite design," *Applied Soil Research*, vol. 11, no. 1, pp. 87–99, 2023.

[194] J. Li, Y. Cao, J. Lu, C. Qin, W. Zhang, X. Zhang, X. Yi, and W. Yu, "Arsenate removal from water by ti electrocoagulation: Main influencing factors, response surface optimization, and potential mechanisms," *Journal of Water Process Engineering*, vol. 54, p. 104042, 2023.

[195] N. Traiwongsa, S. Suren, U. Pancharoen, K. Nootong, K. Maneeintr, W. Punyain, and A. W. Lothongkum, "Mechanisms of mercury ions separation by non-toxic organic liquid membrane via dft, thermodynamics, kinetics and mass transfer model," *Journal of Industrial and Engineering Chemistry*, vol. 117, pp. 522–537, 2023.

[196] S. Sarkar, S. Hazra, K. Chakraborty, A. Nayak, and P. Saha, "Hybrid technique for removal of arsenic from drinking water," *Chemical Engineering & Technology*, vol. 46, no. 2, pp. 242–255, 2023.

[197] K. Dunn, "Process improvement using data, 2010," *Available through download at https://learnche. org/pid/PID. pdf*, pp. 430–0461, 2019.

[198] X. Yang, E. Wen, C. Ge, A. El-Naggar, H. Yu, S. Wang, E. E. Kwon, H. Song, S. M. Shaheen, H. Wang *et al.*, "Iron-modified phosphorus-and silicon-based biochars exhibited various influences on arsenic, cadmium, and lead accumulation in rice and enzyme activities in a paddy soil," *Journal of Hazardous Materials*, vol. 443, p. 130203, 2023.

[199] L. Capobianco, F. Di Caprio, P. Altimari, M. L. Astolfi, and F. Pagnanelli, "Production of an iron-coated adsorbent for arsenic removal by hydrothermal carbonization of olive pomace: Effect of the feedwater pH," *Journal of Environmental Management*, vol. 273, p. 111164, 2020.

[200] A. J. Signes-Pastor, M. Carey, and A. A. Meharg, "Inorganic arsenic removal in rice bran by percolating cooking water," *Food Chemistry*, vol. 234, pp. 76–80, 2017.

[201] M. A. Hossain, M. K. Sengupta, S. Ahamed, M. M. Rahman, D. Mondal, D. Lodh, B. Das, B. Nayak, B. K. Roy, A. Mukherjee *et al.*, "Ineffectiveness and poor reliability of arsenic removal plants in West Bengal, India," *Environmental Science & Technology*, vol. 39, no. 11, pp. 4300–4306, 2005.

[202] S. Khan, "Ethem alpaydin. introduction to machine learning (adaptive computation and machine learning series). the mit press, 2004. isbn: 0 262 01211 1 price£ 32.95/50.00 (hardcover). xxx+ 415 pages." *Natural Language Engineering*, vol. 14, no. 1, pp. 133–137, 2008.

[203] D. Hammerstrom, "Working with neural networks," *IEEE spectrum*, vol. 30, no. 7, pp. 46–53, 1993.

[204] R. Sharma and M. Jain, "Variance based sensitivity analysis and statistical optimization of design and operating parameters of spiral wound pervaporation modules for thiophene removal from fcc gasoline," *Computers & Chemical Engineering*, vol. 141, p. 106987, 2020. [Online]. Available: https://www.sciencedirect.com/science/article/pii/S0098135420301708

[205] J. Abdi and G. Mazloom, "Machine learning approaches for predicting arsenic adsorption from water using porous metal–organic frameworks," *Scientific Reports*, vol. 12, no. 1, p. 16458, 2022.

[206] M. Al-Yaari, T. H. Aldhyani, and S. Rushd, "Prediction of arsenic removal from contaminated water using artificial neural network model," *Applied Sciences*, vol. 12, no. 3, p. 999, 2022.

[207] S. Kumar and J. Pati, "Assessment of groundwater arsenic contamination level in Jharkhand, India using machine learning," *Journal of Computational Science*, vol. 63, p. 101779, 2022.

[208] M. Mohammadi, S. A. Naghibi, A. Motevalli, and H. Hashemi, "Human-induced arsenic pollution modeling in surface waters-an integrated approach using machine learning algorithms and environmental factors," *Journal of Environmental Management*, vol. 305, p. 114347, 2022.

[209] P. Roy, N. Mondal, and K. Das, "Modeling of the adsorptive removal of arsenic: a statistical approach," *Journal of Environmental Chemical Engineering*, vol. 2, no. 1, pp. 585–597, 2014.

[210] J. Wu, N. Zhou, D. Wang, Z. Yu, R. D. Neuman, and G. Xu, "Structure and aggregation behavior of cobalt-di (2-ethylhexy1)-phosphoric acid complexes in solvent extraction systems," *Science in China Series B: Chemistry*, vol. 41, no. 1, pp. 36–44, 1998.

[211] C. Sainz-Diaz, H. Klocker, R. Marr, and H.-J. Bart, "New approach in the modelling of the extraction equilibrium of zinc with bis-(2-ethylhexyl) phosphoric acid," *Hydrometallurgy*, vol. 42, no. 1, pp. 1–11, 1996.

[212] S. J. Yoon, J. G. Lee, H. Tajima, A. Yamasaki, F. Kiyono, T. Nakazato, and H. Tao, "Extraction of lanthanide ions from aqueous solution by bis (2-ethylhexyl) phosphoric acid with room-temperature ionic liquids," *Journal of Industrial and Engineering Chemistry*, vol. 16, no. 3, pp. 350–354, 2010.

[213] M. D. L. Ballinas, E. Rodríguez de San Miguel, M. Muñoz, and J. De Gyves, "Arsenic (V) extraction from sulfuric acid media using DBBP- D2EHPA organic mixtures," *Industrial & Engineering Chemistry Research*, vol. 42, no. 3, pp. 574–581, 2003.

[214] E. Jorjani and M. Shahbazi, "The production of rare earth elements group via tributyl phosphate extraction and precipitation stripping using oxalic acid," *Arabian journal of chemistry*, vol. 9, pp. S1532–S1539, 2016.

[215] S. El Dessouky, Y. El-Nadi, I. Ahmed, E. Saad, and J. Daoud, "Solvent extraction separation of Zn (II), Fe (II), Fe (III) and Cd (II) using tributylphosphate and CYANEX 921 in kerosene from chloride medium," *Chemical Engineering and Processing: Process Intensification*, vol. 47, no. 2, pp. 177–183, 2008.

[216] S. Sarkar, S. K. Mondal, M. K. Beriya, and P. Saha, "Spectroscopic, thermodynamic and ultrasonic properties of pseudo-binary mixtures of organic extractants and vegetable oil at 25–60°c under atmospheric pressure," *Asia-Pacific Journal of Chemical Engineering*, vol. 16, no. 4, p. e2650, 2021. [Online]. Available: https://onlinelibrary.wiley.com/doi/abs/10.1002/apj.2650

[217] H. J. You and I. S. Han, "Effects of dissolved ions and natural organic matter on electrocoagulation of As (III) in groundwater," *Journal of Environmental Chemical Engineering*, vol. 4, no. 1, pp. 1008–1016, 2016.

[218] S. Sarkar, S. Hazra, K. Chakraborty, A. Nayak, and P. Saha, "Hybrid technique for removal of arsenic from drinking water," *Chemical Engineering & Technology*, vol. in press, no. 2, pp. 242–255, 2022.

[219] L. Garcia-Colin, L. Del Castillo, and P. Goldstein, "Theoretical basis for the Vogel-Fulcher-Tammann equation," *Physical Review B*, vol. 40, no. 10, pp. 7040–7044, 1989.

[220] M. J. P. Comuñas, A. Baylaucq, C. Boned, and J. Fernández, "High-pressure measurements of the viscosity and density of two polyethers and two dialkyl carbonates," *International Journal of Thermophysics*, vol. 22, no. 3, pp. 749–768, 2001.

[221] J. Safarov, F. Lesch, K. Suleymanli, A. Aliyev, A. Shahverdiyev, E. Hassel, and I. Abdulagatov, "Viscosity, density, heat capacity, speed of sound and other derived properties of 1-butyl-3-methylimidazolium tris(pentafluoroethyl) trifluorophosphate over a wide range of temperature and at atmospheric pressure," *Journal of Chemical & Engineering Data*, vol. 62, no. 10, pp. 3620–3631, 2017.

[222] T. Lech, G. Czechowski, and J. Jadżyn, "Viscosity of the series of 1,n-alkanediols," *Journal of Chemical & Engineering Data*, vol. 46, no. 3, pp. 725–727, 2001.

[223] A. Jouyban, M. Khoubnasabjafari, Z. Vaez-Gharamaleki, Z. Fekari, W. Eugene Jr *et al.*, "Calculation of the viscosity of binary liquids at various temperatures using Jouyban–Acree model," *Chemical and pharmaceutical bulletin*, vol. 53, no. 5, pp. 519–523, 2005.

[224] L. Grunberg and A. H. Nissan, "Mixture law for viscosity," *Nature*, vol. 164, pp. 799–800, 1949.

[225] A. R. Mahajan and S. R. Mirgane, "Excess molar volumes and viscosities for the binary mixtures of n-Octane, n-Decane, n-Dodecane, and n-Tetradecane with Octan-2-ol at 298.15 K," *Journal of Thermodynamics*, p. 11, 2013.

[226] R. Hind, E. McLaughlin, and A. Ubbelohde, "Structure and viscosity of liquids. camphor+ pyrene mixtures," *Transactions of the Faraday Society*, vol. 56, pp. 328–330, 1960.

[227] S. Parthasarathy and N. Bakhshi, "Relation between velocity of sound and viscosity in liquids," *Proceedings of the Physical Society. Section B*, vol. 66, no. 5, pp. 368–370, 1953.

[228] J. G. Eberhart, "The surface tension of binary liquid mixtures1," *The Journal of Physical Chemistry*, vol. 70, no. 4, pp. 1183–1186, 1966.

[229] S. Azhagiri, S. Jayakumar, R. Padmanaban, S. Gunasekaran, and S. Srinivasan, "Acoustic and thermodynamic properties of binary liquid mixtures of Benzaldehyde in Hexane and Cyclohexane," *Journal of Solution Chemistry*, vol. 38, no. 4, pp. 441–448, Apr 2009.

[230] V. A. Tabhane, S. Agarwal, and S. Ghosh, "Kalidoss-Jacobson free length theory applied to binary liquid mixtures of benzene + pyridine/piperidine/furon/tetrahydrofuron," *Indian Journal of Pure & Applied Physics*, vol. 37, pp. 583–586, 1999.

[231] B. Jacobson, "Intermolecular free lengths in liquids in relation to compressibility, surface tension and viscosity," *Acta Chemica Scandinavica*, vol. 5, pp. 1214–1216, 1951.

[232] O. Redlich and A. Kister, "Algebraic representation of thermodynamic properties and the classification of solutions," *Industrial & Engineering Chemistry*, vol. 40, no. 2, pp. 345–348, 1948.

[233] S. L. Dahire, Y. C. Morey, and P. S. Agrawal, "Excess molar volumes, intermolecular free lengths, adiabatic compressibilities and acoustic impedance of binary mixtures of anisole, toluene and ethylbenzene with dioxane at different temperatures," *International Letters of Chemistry, Physics and Astronomy*, vol. 42, pp. 72–83, 2015.

[234] A. Ali, A. Yasmin, and A. Nain, "Study of intermolecular interactions in binary liquid mixtures through ultrasonic speed measurement," *Indian Journal of Pure & Applied Physics*, vol. 40, pp. 315–322, 2002.

[235] H. Eyring, "The activated complex of chemical reactions," *Journla of Chemical Physics*, vol. 3, pp. 107–115, 1935.

[236] J. I. Weirong and D. A. Lempe, "Calculations of viscosities of liquid mixtures using eyring's theory in combination with cubic equations of state," *Chinese Journal of Chemical Engineering*, vol. 14, pp. 770–779, 2006.

[237] J. M. Matsen and E. F. Johnson, "Extension of the Andrade Equation for viscosity at the normal melting point," *Journal of Chemical and Engineering Data*, vol. 5, pp. 531–533, 1960.

[238] Z. Guo, J. Zhang, T. Zhang, C. Li, Y. Zhang, and J. Bai, "Liquid viscosities, excess properties, and viscous flow thermodynamics of triethylene glycol+water mixtures at T=(298.15, 303.15, 308.15, 313.15, and 318.15) K," *Journal of Molecular Liquids*, vol. 165, pp. 27–31, 2012.

[239] F. Corradini, A. Marchetti, M. Tagliazucchi, L. Tassi, and G. Tosi, "Viscosity data and viscous flow thermodynamics of 2-Methoxyethanol+ Water binary mixtures," *Australian Journal of Chemistry*, vol. 46, pp. 1711–1723, 1993.

[240] R. Prakash, S. Srivastava, R. Rastogi, K. Singh, and K. Bhartariya, "Ground water pollution & preventive measures in some cities of India," in *Proceedings of the Workshop on Management Techniques in Ground Water Stressed Urban Areas*, Lucknow, India, 2 2011, pp. 20–25.

[241] D. Bordoloh and P. Baruah, "Phytoplankton diversity in Digboi oil refinery effluent receiving stream of Assam, India," *Bangladesh Journal of Botany*, vol. 44, no. 2, pp. 163–175, 2015.

[242] K. Radhapyari, N. K. Jatav, and S. Datta, "Study on water quality trends in groundwater of Digboi, Assam," *Bhu-Jal News*, vol. 28, no. 1–4, pp. 38–46, 2013.

[243] M. Kobya, U. Gebologlu, F. Ulu, S. Oncel, and E. Demirbas, "Removal of arsenic from drinking water by the electrocoagulation using Fe and Al electrodes," *Electrochimica Acta*, vol. 56, no. 14, pp. 5060–5070, 2011.

[244] N. R. Council *et al.*, "Chemistry and analysis of arsenic species in water, food, urine, blood, hair, and nails," in *Arsenic in Drinking Water*. National Academies Press (US), 1999.

[245] F. Kabir and S. Chowdhury, "Arsenic removal methods for drinking water in the developing countries: technological developments and research needs," *Environmental Science and Pollution Research*, vol. 24, no. 31, pp. 24 102–24 120, 2017.

[246] S. Goldberg, "Chemical equilibrium and reaction modeling of arsenic and selenium in soils," *Dynamics and bioavailability of heavy metals in the rootzone*, pp. 65–92, 2011.

[247] J. G. Hering, P.-Y. Chen, J. A. Wilkie, and M. Elimelech, "Arsenic removal from drinking water during coagulation," *Journal of Environmental Engineering*, vol. 123, no. 8, pp. 800–807, 1997.

[248] M. B. Baskan and A. Pala, "Determination of arsenic removal efficiency by ferric ions using response surface methodology," *Journal of hazardous materials*, vol. 166, no. 2-3, pp. 796–801, 2009.

[249] D. Van Halem, S. Olivero, W. de Vet, J. Verberk, G. Amy, and J. van Dijk, "Subsurface iron and arsenic removal for shallow tube well drinking water supply in rural bangladesh," *Water Research*, vol. 44, no. 19, pp. 5761–5769, 2010.

[250] J. Farrell and B. K. Chaudhary, "Understanding arsenate reaction kinetics with ferric hydroxides," *Environmental science & technology*, vol. 47, no. 15, pp. 8342–8347, 2013.

[251] M. Kobya, E. Demirbas, and F. Ulu, "Evaluation of operating parameters with respect to charge loading on the removal efficiency of arsenic from potable water by electrocoagulation," *Journal of environmental chemical engineering*, vol. 4, no. 2, pp. 1484–1494, 2016.

[252] S. Pavón, A. Fortuny, M. Coll, M. Bertau, and A. Sastre, "Permeability dependencies on the carrier concentration and membrane viscosity for Y (III) and Eu (III) transport by using liquid membranes," *Separation and Purification Technology*, vol. 239, p. 116573, 2020.

[253] R. C. Reid, J. M. Prausnitz, and B. E. Poling, *The properties of gases and liquids*, 4th ed. New York, NY: McGraw Hill Inc., 1987.

[254] T. G. Hiss and E. L. Cussler, "Diffusion in high viscosity liquids," *AIChE Journal*, vol. 19, no. 4, pp. 698–703, 1973.

[255] K. Vijayaraghavan, T. Padmesh, K. Palanivelu, and M. Velan, "Biosorption of nickel (ii) ions onto sargassum wightii: application of two-parameter and three-parameter isotherm models," *Journal of hazardous materials*, vol. 133, no. 1-3, pp. 304–308, 2006.

[256] N. Ayawei, A. N. Ebelegi, and D. Wankasi, "Modelling and interpretation of adsorption isotherms," *Journal of chemistry*, vol. 2017, 2017.

[257] Q. Hu and Z. Zhang, "Application of dubinin–radushkevich isotherm model at the solid/solution interface: A theoretical analysis," *Journal of Molecular Liquids*, vol. 277, pp. 646–648, 2019.

[258] L. Liu, X.-B. Luo, L. Ding, and S.-L. Luo, "4 - application of nanotechnology in the removal of heavy metal from water," in *Nanomaterials for the Removal of Pollutants and Resource Reutilization*, ser. Micro and Nano Technologies, X. Luo and F. Deng, Eds. Elsevier, 2019, pp. 83–147. [Online]. Available: https://www.sciencedirect.com/science/article/pii/B9780128148372000044

[259] A. I. Adeogun and R. B. Balakrishnan, "Kinetics, isothermal and thermodynamics studies of electrocoagulation removal of basic dye rhodamine b from aqueous solution using steel electrodes," *Applied Water Science*, vol. 7, no. 4, pp. 1711–1723, 2017.

[260] D. Ringot, B. Lerzy, K. Chaplain, J.-P. Bonhoure, E. Auclair, and Y. Larondelle, "In vitro biosorption of ochratoxin a on the yeast industry by-products: comparison of isotherm models," *Bioresource technology*, vol. 98, no. 9, pp. 1812–1821, 2007.

[261] M. Samarghandi, M. Hadi, S. Moayedi, and A. F. Barjesteh, "Two-parameter isotherms of methyl orange sorption by pinecone derived activated carbon," *Iranian Journal of Environmental Health Science and Engineering*, vol. 6, no. 4, pp. 285–294, 2009.

[262] M. T. Amin, A. A. Alazba, and M. Shafiq, "Adsorptive removal of reactive black 5 from wastewater using bentonite clay: Isotherms, kinetics and thermodynamics," *Sustainability*, vol. 7, no. 11, pp. 15 302–15 318, 2015.

[263] S. Lagergren, "About the theory of so-called adsorption of soluble substances," *Kungliga Svenska Vetenskapsakademiens Handlingar*, vol. 24, pp. 1–39, 1898.

[264] J. Wang and X. Guo, "Adsorption kinetic models: Physical meanings, applications, and solving methods," *Journal of Hazardous materials*, vol. 390, p. 122156, 2020.

[265] E. D. Revellame, D. L. Fortela, W. Sharp, R. Hernandez, and M. E. Zappi, "Adsorption kinetic modeling using pseudo-first order and pseudo-second order rate laws: A review," *Cleaner Engineering and Technology*, vol. 1, p. 100032, 2020.

[266] J. O. Ojediran, A. O. Dada, S. O. Aniyi, R. O. David, and A. D. Adewumi, "Mechanism and isotherm modeling of effective adsorption of malachite green as endocrine disruptive dye using acid functionalized maize cob (AFMC)," *Scientific Reports*, vol. 11, no. 1, p. 21498, 2021.

[267] W. Weber and J. Morris, "Kinetics of adsorption on carbon from solutions," *Journal of the Sanitary Engineering Division*, vol. 89, pp. 31–39, 1963.

[268] A. Sánchez, R. Maceiras, A. Cancela, and M. Rodríguez, "Influence of n-hexane on in situ transesterification of marine macroalgae," *Energies*, vol. 5, no. 2, pp. 243–257, 2012.

[269] K. F. Akter, Z. Chen, L. Smith, D. Davey, and R. Naidu, "Speciation of arsenic in ground water samples: A comparative study of CE-UV, HG-AAS and LC-ICP-MS," *Talanta*, vol. 68, no. 2, pp. 406–415, 2005.

[270] M. Farahmandjou and F. Soflaee, "Synthesis and characterization of α-Fe_2O_3 nanoparticles by simple co-precipitation method," *Physical Chemistry Research*, vol. 3, no. 3, pp. 191–196, 2015.

[271] K. K. Bhatluri, M. S. Manna, A. K. Ghoshal, and P. Saha, "Supported liquid membrane based removal of lead (ii) and cadmium (ii) from mixed feed: conversion to solid waste by precipitation," *Journal of hazardous materials*, vol. 299, pp. 504–512, 2015.

[272] J. Haque, V. Srivastava, C. Verma, H. Lgaz, R. Salghi, and M. A. Quraishi, "N-Methyl-N,N,N-trioctylammonium chloride as a novel and green corrosion inhibitor for mild steel in an acid chloride medium: electrochemical, DFT and MD studies," *New J. Chem.*, vol. 41, pp. 13 647–13 662, 2017.

[273] Y. Li, J. Hu, M. Fu, J. Tang, L. Dong, and S. Liu, "Investigation of intermolecular interactions of mixed extractants of quaternary phosphonium or ammonium chlorides and bis (2, 4, 4-ethylhexyl) phosphoric acid for metal separation," *RSC Advances*, vol. 6, no. 62, pp. 56 772–56 779, 2016.

[274] K. Das, M. Habibullah, M. Ghosh, and N. AkberHossain, "Regression alternative to the redlich–kister equation in the determination of the excess partial molar volumes of the constituents in a binary mixture," *Physics and Chemistry of Liquids*, vol. 42, no. 1, pp. 89–94, 2004.

[275] M. Kondaiah and D. K. Rao, "Correlation of excess molar volumes with redlich-kister polynomial and evaluation of partial molar volumes, excess partial molar volumes in some binary mixtures at 308.15 K," *International Journal of Research in Pure and Applied Physics*, vol. 3, pp. 43–49, 2013.

[276] G. S. Jamieson and W. F. Baughman, "The chemical composition of sesame oil," *Journal of the American Chemical Society*, vol. 46, no. 3, pp. 775–778, 1924.

[277] T. Phaechamud and C. Savedkairop, "Contact angle and surface tension of some solvents used in pharmaceuticals," *Research Journal of Pharmaceutical, Biological and Chemical Sciences*, vol. 3, pp. 513–529, 2012.

[278] E. A. Melo-Espinosa, Y. Sánchez-Borroto, M. Errasti, R. Piloto-Rodríguez, R. Sierens, J. Roger-Riba, and A. Christopher-Hansen, "Surface tension prediction of vegetable oils using artificial neural networks and multiple linear regression," *Energy Procedia*, vol. 57, pp. 886–895, 2014, 2013 ISES Solar World Congress.

[279] N. Dutta and G. Patil, "Effect of phase transfer catalysts on the interfacial tension of water/toluene system," *The Canadian Journal of Chemical Engineering*, vol. 71, no. 5, pp. 802–804, 1993.

[280] F. Shahidi, *Bailey's industrial oil & fat products*, 6th ed. Wiley-Interscience Publications, 2005.

[281] M. Bohnet, *Ullmann's encyclopedia of industrial chemistry*. Wiley-Interscience Publications, 1995.

[282] P. Kotoky and B. Sarma, "Assessment of water quality index of the Brahmaputra river of Guwahati city of Kamrup, district of Assam, India," *Int. J. Eng. Res. Technol*, vol. 6, no. 03, pp. 536–540, 2017.

[283] D. Lakshmanan, D. A. Clifford, and G. Samanta, "Comparative study of arsenic removal by iron using electrocoagulation and chemical coagulation," *Water research*, vol. 44, no. 19, pp. 5641–5652, 2010.

[284] J. M. Kokosa, "Solvent microextraction," *Comprehensive sampling and sample preparation*, vol. 2, pp. 151–180, 2012.

[285] M. M. Perez, J. Reyes-Aguilera, T. Saucedo, M. Gonzalez, R. Navarro, and M. Avila-Rodriguez, "Study of As(V) transfer through a supported liquid membrane impregnated with trioctylphosphine oxide (Cyanex 921)," *Journal of Membrane Science*, vol. 302, no. 1, pp. 119–126, 2007.

[286] X. Yang, H. Duan, D. Shi, R. Yang, S. Wang, and H. Guo, "Facilitated transport of phenol through supported liquid membrane containing bis (2-ethylhexyl) sulfoxide (beso) as the carrier," *Chemical Engineering and Processing: Process Intensification*, vol. 93, pp. 79–86, 2015.

[287] M. Berg, S. Luzi, P. T. K. Trang, P. H. Viet, W. Giger, and D. Stüben, "Arsenic removal from groundwater by household sand filters: comparative field study, model calculations, and health benefits," *Environmental Science & Technology*, vol. 40, no. 17, pp. 5567–5573, 2006.

[288] M. Annaduzzaman, L. C. Rietveld, B. A. Hoque, M. N. Bari, and D. van Halem, "Arsenic removal from iron-containing groundwater by delayed aeration in dual-media sand filters," *Journal of Hazardous Materials*, vol. 411, p. 124823, 2021.

[289] C. L. Olson, "Comparative robustness of six tests in multivariate analysis of variance," *Journal of the American Statistical Association*, vol. 69, no. 348, pp. 894–908, 1974.

[290] A. Singh, "Arsenic contamination in groundwater of north eastern India," in *Proceedings of 11th national symposium on hydrology with focal theme on water quality, National Institute of Hydrology, Roorkee*, 2004, pp. 255–262.

[291] C. J. Izquierdo, P. Canizares, M. Rodrigo, J. Leclerc, G. Valentin, and F. Lapicque, "Effect of the nature of the supporting electrolyte on the treatment of soluble oils by electrocoagulation," *Desalination*, vol. 255, no. 1-3, pp. 15–20, 2010.

[292] S. Garcia-Segura, M. M. S. Eiband, J. V. de Melo, and C. A. Martínez-Huitle, "Electrocoagulation and advanced electrocoagulation processes: A general review about the fundamentals, emerging applications and its association with other technologies," *Journal of Electroanalytical Chemistry*, vol. 801, pp. 267–299, 2017.

[293] V. Gilhotra, L. Das, A. Sharma, T. S. Kang, P. Singh, R. S. Dhuria, and M. S. Bhatti, "Electrocoagulation technology for high strength arsenic wastewater: process optimization and mechanistic study," *Journal of cleaner production*, vol. 198, pp. 693–703, 2018.

[294] R. M. Cornell, U. Schwertmann *et al.*, *The iron oxides: structure, properties, reactions, occurrences, and uses*. Wiley-vch Weinheim, 2003, vol. 664.

[295] D. Maity and D. Agrawal, "Synthesis of iron oxide nanoparticles under oxidizing environment and their stabilization in aqueous and non-aqueous media," *Journal of Magnetism and Magnetic Materials*, vol. 308, no. 1, pp. 46–55, 2007.

[296] S. Asuha, S. Zhao, H. Wu, L. Song, and O. Tegus, "One step synthesis of maghemite nanoparticles by direct thermal decomposition of Fe–urea complex and their properties," *Journal of Alloys and Compounds*, vol. 472, no. 1-2, pp. L23–L25, 2009.

[297] S. Alibeigi and M. R. Vaezi, "Phase transformation of iron oxide nanoparticles by varying the molar ratio of fe2+:fe3+," *Chemical Engineering & Technology*, vol. 31, no. 11, pp. 1591–1596, 2008. [Online]. Available: https://onlinelibrary.wiley.com/doi/abs/10.1002/ceat.200800093

[298] M. Singh, P. Ulbrich, V. Prokopec, P. Svoboda, E. Šantavá, and F. Štěpánek, "Vapour phase approach for iron oxide nanoparticle synthesis from solid precursors," *Journal of Solid State Chemistry*, vol. 200, pp. 150–156, 2013.

[299] T. D. Glotch and G. R. Rossman, "Mid-infrared reflectance spectra and optical constants of six iron oxide/oxyhydroxide phases," *Icarus*, vol. 204, no. 2, pp. 663–671, 2009.

[300] H. Cui, W. Ren, P. Lin, and Y. Liu, "Structure control synthesis of iron oxide polymorph nanoparticles through an epoxide precipitation route," *Journal of Experimental Nanoscience*, vol. 8, p. 869–875, 11 2013.

[301] W. Salama, M. El Aref, and R. Gaupp, "Spectroscopic characterization of iron ores formed in different geological environments using FTIR, XPS, Mössbauer spectroscopy and thermoanalyses," *Spectrochimica Acta Part A: Molecular and Biomolecular Spectroscopy*, vol. 136, pp. 1816–1826, 2015.

[302] M. Farahmandjou, "Synthesis and characterization of α—Fe_2O_3 nanoparticles by simple co-precipitation method," *Physical Chemistry Research*, vol. 3, p. 193, 09 2015.

[303] I. Carabante, M. Grahn, A. Holmgren, and J. Hedlund, "In situ ATR–FTIR studies on the competitive adsorption of arsenate and phosphate on ferrihydrite," *Journal of Colloid and Interface Science*, vol. 351, no. 2, pp. 523–531, 2010.

[304] X. Zhao, B. Zhang, H. Liu, and J. Qu, "Removal of arsenite by simultaneous electro-oxidation and electro-coagulation process," *Journal of hazardous materials*, vol. 184, no. 1-3, pp. 472–476, 2010.

[305] C. Yazirin, P. Puspitasari, M. I. N. Sasongko, D. I. Tsamroh, and P. Risdanareni, "Phase identification and morphology study of hematite (Fe_2O_3) with sintering time varitions," in *AIP Conference Proceedings*, vol. 1887, no. 1. AIP Publishing LLC, 2017, p. 020038.

[306] R. Wahab, F. Khan, and A. A. Al-Khedhairy, "Hematite iron oxide nanoparticles: apoptosis of myoblast cancer cells and their arithmetical assessment," *RSC advances*, vol. 8, no. 44, pp. 24 750–24 759, 2018.

[307] H. Jiao and J. Wang, "Single crystal ellipsoidal and spherical particles of α-Fe_2O_3: hydrothermal synthesis, formation mechanism, and magnetic properties," *Journal of alloys and compounds*, vol. 577, pp. 402–408, 2013.

[308] M. Villacís-García, M. Ugalde-Arzate, K. Vaca-Escobar, M. Villalobos, R. Zanella, and N. Martínez-Villegas, "Laboratory synthesis of goethite and ferrihydrite of controlled particle sizes," *Boletín de la Sociedad Geológica Mexicana*, vol. 67, no. 3, pp. 433–446, 2015.

[309] S. Kundu and A. Gupta, "Investigations on the adsorption efficiency of iron oxide coated cement (IOCC) towards As (V)—kinetics, equilibrium and thermodynamic studies," *Colloids and Surfaces A: Physicochemical and Engineering Aspects*, vol. 273, no. 1-3, pp. 121–128, 2006.

[310] A. Dada, A. Olalekan, A. Olatunya, and O. Dada, "Langmuir, Freundlich, Temkin and Dubinin–Radushkevich isotherms studies of equilibrium sorption of Zn^{2+} unto phosphoric acid modified rice husk," *IOSR Journal of applied chemistry*, vol. 3, no. 1, pp. 38–45, 2012.

[311] K. Tan and B. Hameed, "Insight into the adsorption kinetics models for the removal of contaminants from aqueous solutions," *Journal of the Taiwan Institute of Chemical Engineers*, vol. 74, pp. 25–48, 2017.

[312] L. Al-Annaz, "Removal of sulfate ion pollutant from simulated ground water using electrocoagulation technique," Ph.D. dissertation, PhD thesis, University of Baghdad, 2014.

[313] F. Y. AlJaberi, W. T. Mohammed *et al.*, "Analyzing the removal of lead from synthesis wastewater by electrocoagulation technique using experimental design," *Desalination and Water Treatment*, vol. 111, no. 2018, pp. 286–296, 2018.

[314] C. Ucar, M. B. Baskan, and A. Pala, "Arsenic removal from drinking water by electrocoagulation using iron electrodes," *Korean Journal of Chemical Engineering*, vol. 30, pp. 1889–1895, 2013.

[315] O. J. Flores, J. L. Nava, G. Carreño, E. Elorza, and F. Martínez, "Arsenic removal from groundwater by electrocoagulation in a pre-pilot-scale continuous filter press reactor," *Chemical Engineering Science*, vol. 97, pp. 1–6, 2013.

[316] M. Kobya, E. Demirbas, U. Gebologlu, M. Oncel, and Y. Yildirim, "Optimization of arsenic removal from drinking water by electrocoagulation batch process using response surface methodology," *Desalination and Water Treatment*, vol. 51, no. 34-36, pp. 6676–6687, 2013.

[317] E. Demirbas, M. Kobya, M. S. Oncel, E. Şık, and A. Y. Goren, "Arsenite removal from groundwater in a batch electrocoagulation process: Optimization through response surface methodology," *Separation Science and Technology*, vol. 54, no. 5, pp. 775–785, 2019.

[318] D. Das and B. K. Nandi, "Arsenic removal from tap water by electrocoagulation: investigation of process parameters, kinetic analysis, and operating cost," *Journal of Dispersion Science and Technology*, vol. 42, no. 3, pp. 328–337, 2021.

[319] T. T. Q. Nguyen, P. Loganathan, B. K. Dinh, T. V. Nguyen, S. Vigneswaran, and H. H. Ngo, "Removing arsenate from water using batch and continuous-flow electrocoagulation with diverse power sources," *Journal of Water Process Engineering*, vol. 41, p. 102028, 2021.

[320] B. Ochoo, J. Valcour, and A. Sarkar, "Association between perceptions of public drinking water quality and actual drinking water quality: A community-based exploratory study in Newfoundland (Canada)," *Environmental Research*, vol. 159, pp. 435–443, 2017.

[321] M. de França Doria, "Factors influencing public perception of drinking water quality," *Water policy*, vol. 12, no. 1, pp. 1–19, 2010.

[322] F. Tarannum, A. Kansal, and P. Sharma, "Understanding public perception, knowledge and behaviour for water quality management of the river yamuna in India," *Water Policy*, vol. 20, no. 2, pp. 266–281, 2018.

[323] W. H. Organization *et al.*, *Core questions on drinking water and sanitation for household surveys*. World Health Organization, 2006.

[324] P. K. Gevera, K. Dowling, P. Gikuma-Njuru, and H. Mouri, "Public knowledge and perception of drinking water quality and its health implications: an example from the Makueni county, south-eastern Kenya," *International Journal of Environmental Research and Public Health*, vol. 19, no. 8, p. 4530, 2022.

[325] M. R. Francis, G. Nagarajan, R. Sarkar, V. R. Mohan, G. Kang, and V. Balraj, "Perception of drinking water safety and factors influencing acceptance and sustainability of a water quality intervention in rural southern India," *BMC public health*, vol. 15, pp. 1–9, 2015.

[326] D. Chakraborti, B. Das, M. M. Rahman, U. K. Chowdhury, B. Biswas, A. B. Goswami, B. Nayak, A. Pal, M. K. Sengupta, S. Ahamed *et al.*, "Status of groundwater arsenic contamination in the state of West Bengal, India: A 20-year study report," *Molecular nutrition & food research*, vol. 53, no. 5, pp. 542–551, 2009.

[327] A. Basu, P. Sen, and A. Jha, "Environmental arsenic toxicity in West Bengal, India: A brief policy review," *Indian Journal of Public Health*, vol. 59, no. 4, pp. 295–298, 2015.

[328] P. Bhattacharya, S. Frisbie, E. Smith, R. Naidu, G. Jacks, and B. Sarkar, "Arsenic in the environment: a global perspective," *Handbook of heavy metals in the environment. Marcell Dekker Inc., New York*, pp. 147–215, 2002.

[329] P. Chaudhuri, P. Aitch, and A. Dutta, "Determination of arsenic concentration in ground water and its effects on children: A case study of Sonarpur and Baruipur block, South 24 Parganas, West Bengal," *Journal of Global Resources*, vol. 6, pp. 134–140, 12 2019.

[330] S. Mooney, J. O'Dwyer, and P. Hynds, "Private groundwater management and risk awareness: A cross-sectional analysis of two age-related subsets in the Republic of Ireland," *Science of the Total Environment*, vol. 796, p. 148844, 2021.

[331] A. O. Dada, F. A. Adekola, E. O. Odebunmi, F. E. Dada, O. M. Bello, B. A. Akinyemi, O. S. Bello, and O. G. Umukoro, "Sustainable and low-cost ocimum gratissimum for biosorption of indigo carmine dye: kinetics, isotherm, and thermodynamic studies," *International Journal of Phytoremediation*, vol. 22, no. 14, pp. 1524–1537, 2020.

[332] N. V. Chukanov and A. D. Chervonnyi, *Infrared spectroscopy of minerals and related compounds*. Springer, 2016.

[333] S. J. Parikh, K. W. Goyne, A. J. Margenot, F. N. Mukome, and F. J. Calderón, "Soil chemical insights provided through vibrational spectroscopy," *Advances in agronomy*, vol. 126, pp. 1–148, 2014.

[334] C. R. Nangah, T. G. Merlain, N. J. Nsami, C. P. Tubwoh, J. Foba-Tendo, and K. J. Mbadcam, "Synthesized goethite and natural iron oxide as effective absorbents for simultaneous removal of Co (II) and Ni (II) ions from water," *Journal of Encapsulation and Adsorption Sciences*, vol. 9, no. 3, pp. 127–147, 2019.

[335] H. Swanson, H. McMurdie, M. Morris, E. Evans, and B. Paretzkin, "Standard x-ray diffraction powder patterns: Nbs monograph 25—section 5," *National Bureau of Standards Reports*, 1967.

Appendix A

Extra figures to refer

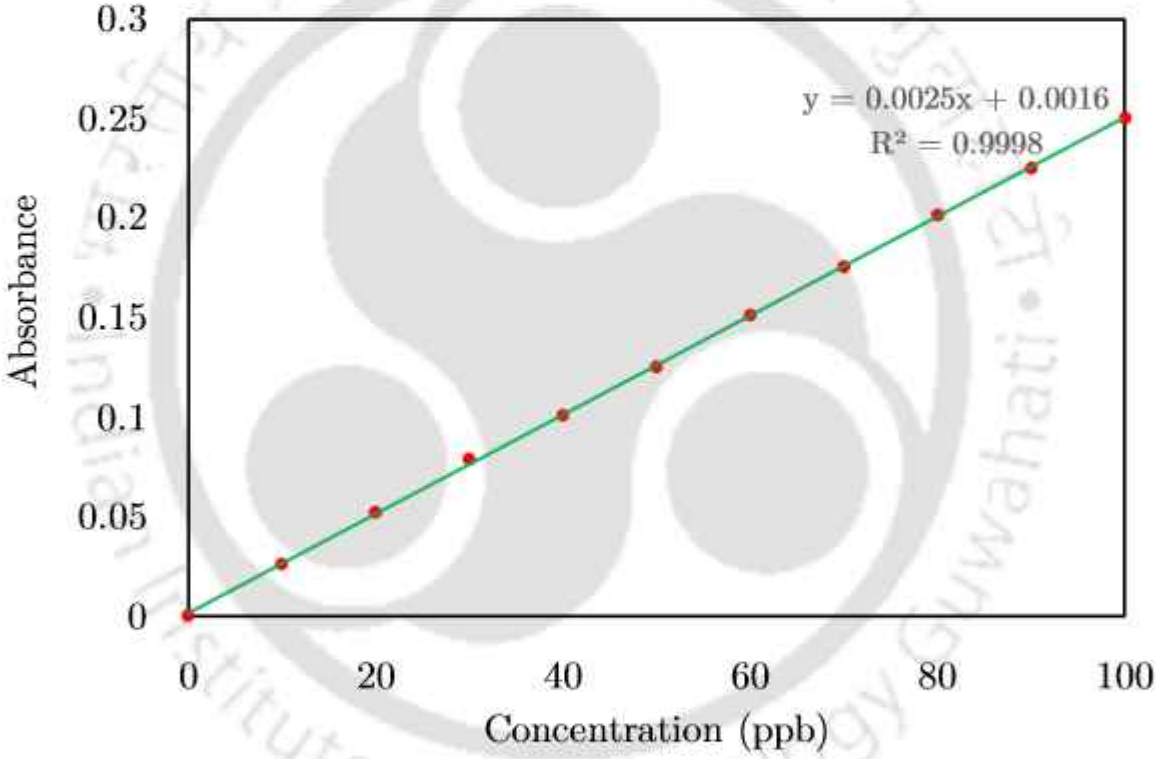

FIGURE A.1: Calibration curve for the standard arsenic solution

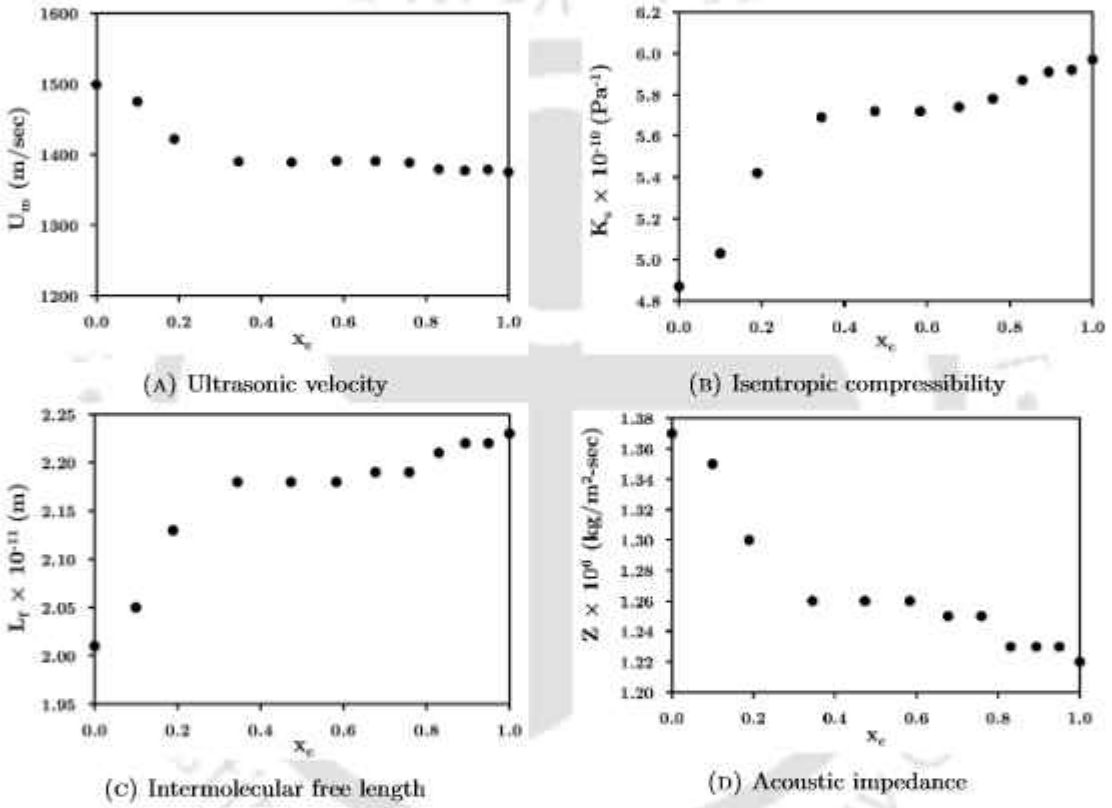

(A) Ultrasonic velocity

(B) Isentropic compressibility

(C) Intermolecular free length

(D) Acoustic impedance

FIGURE A.2: Various acoustic properties of pseudo-binary mixtures against mole fraction

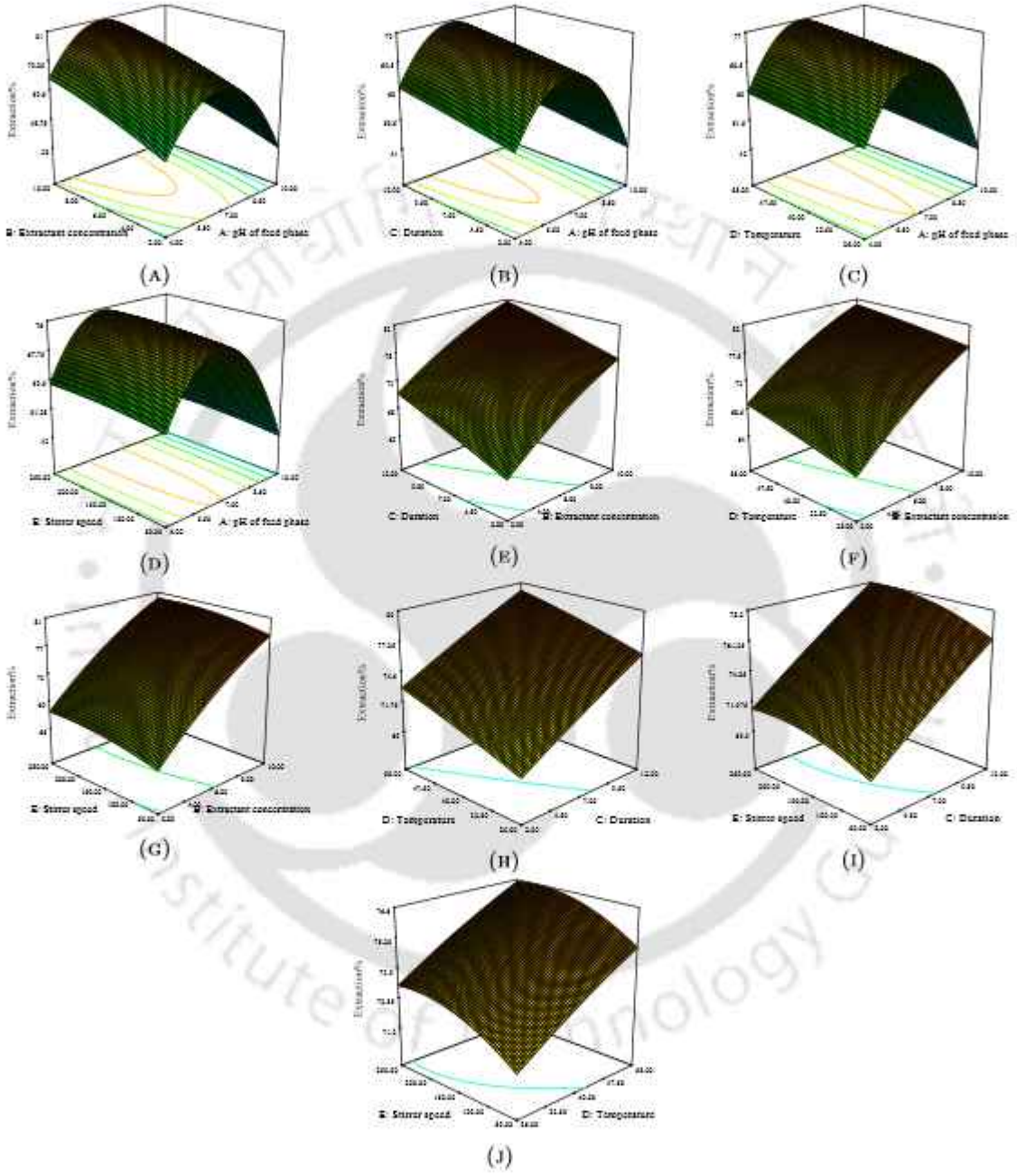

FIGURE A.3: Effect of parameters on the extraction of $As^{(V)}$in two phase study

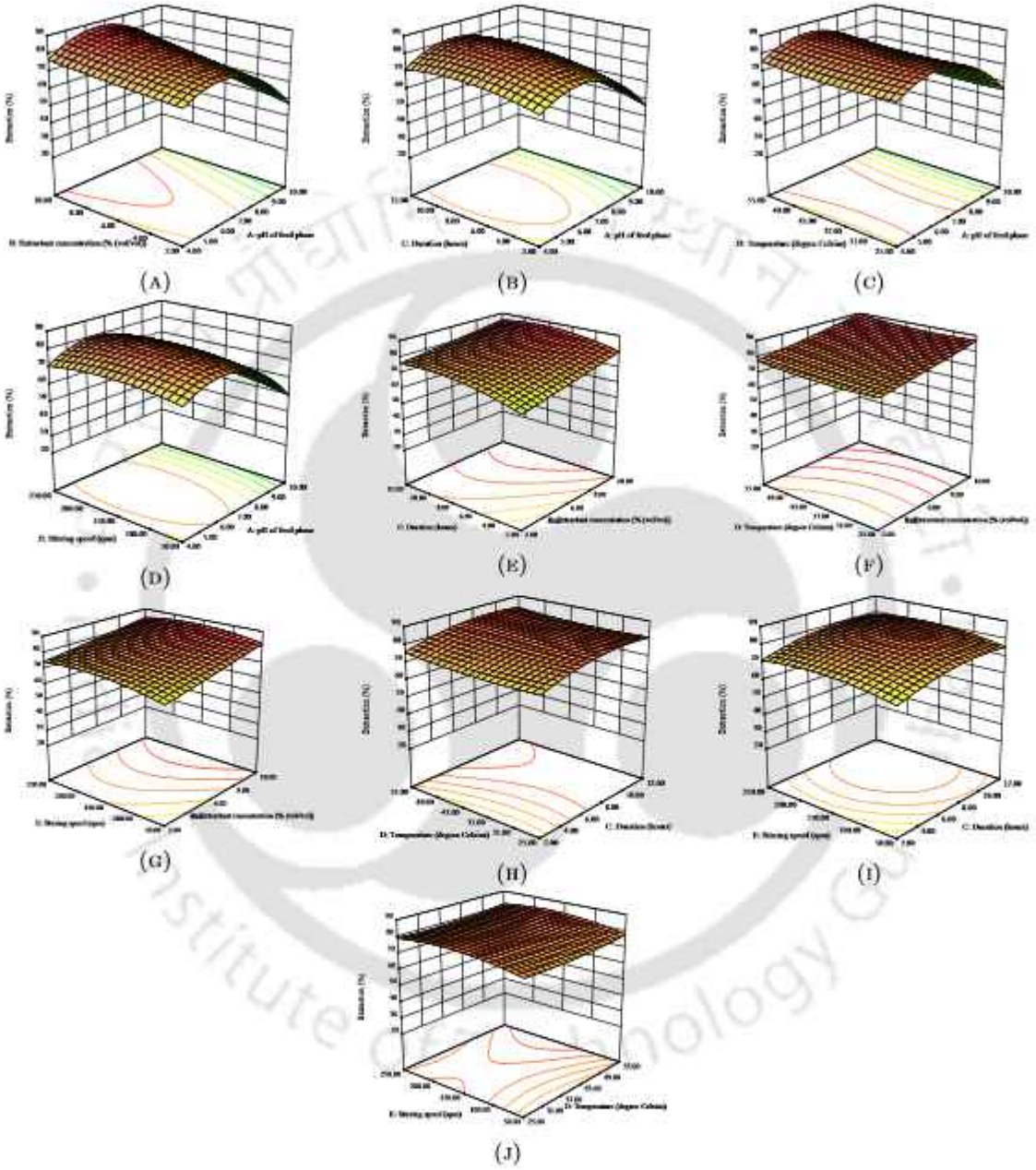

FIGURE A.4: Effect of parameters on the extraction of $As^{(III)}$:$As^{(V)}$:: 1 : 1 in two phase study

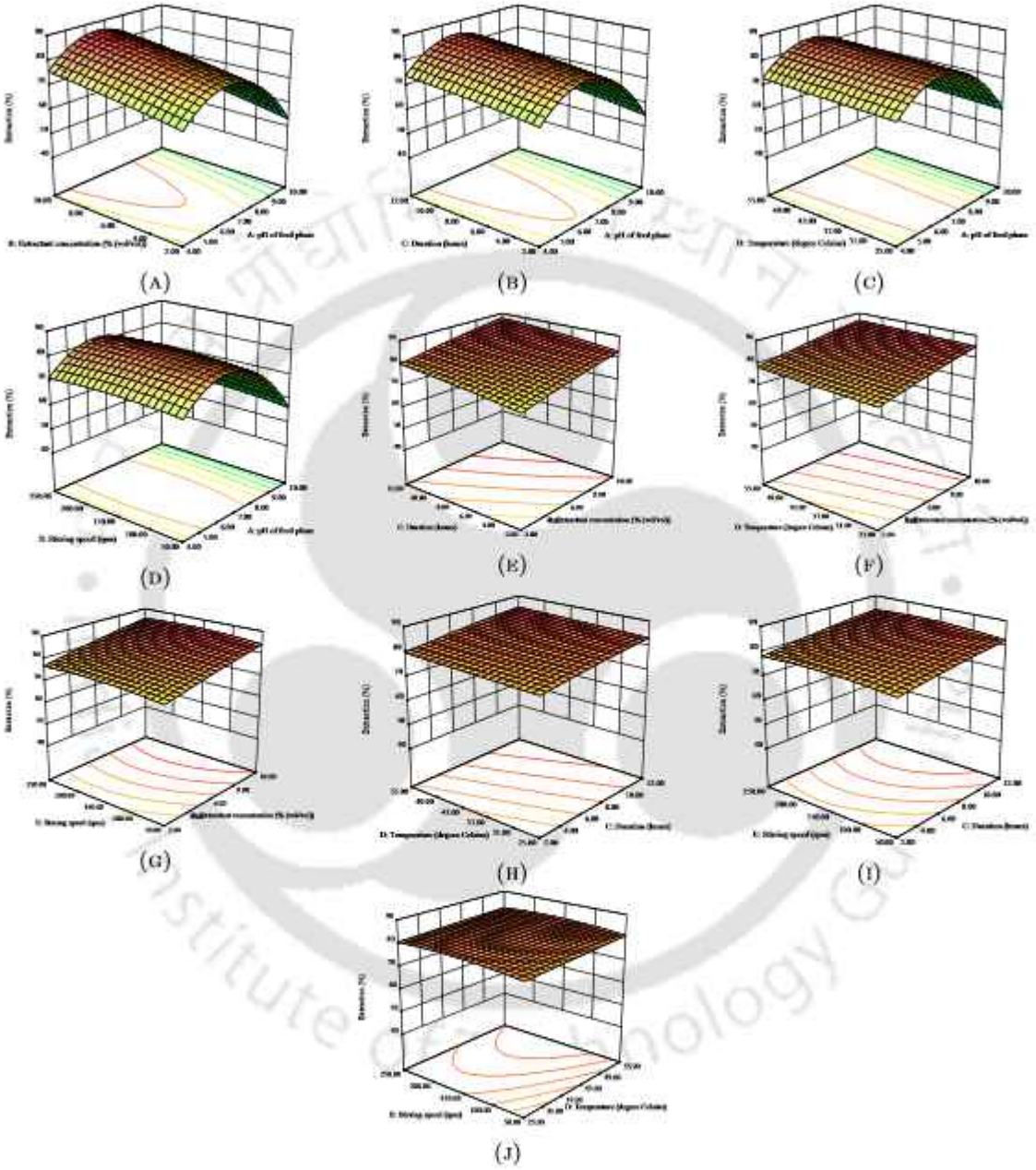

FIGURE A.5: Effect of parameters on the extraction of $As^{(III)}$:$As^{(V)}$:: 1 : 2 in two phase study

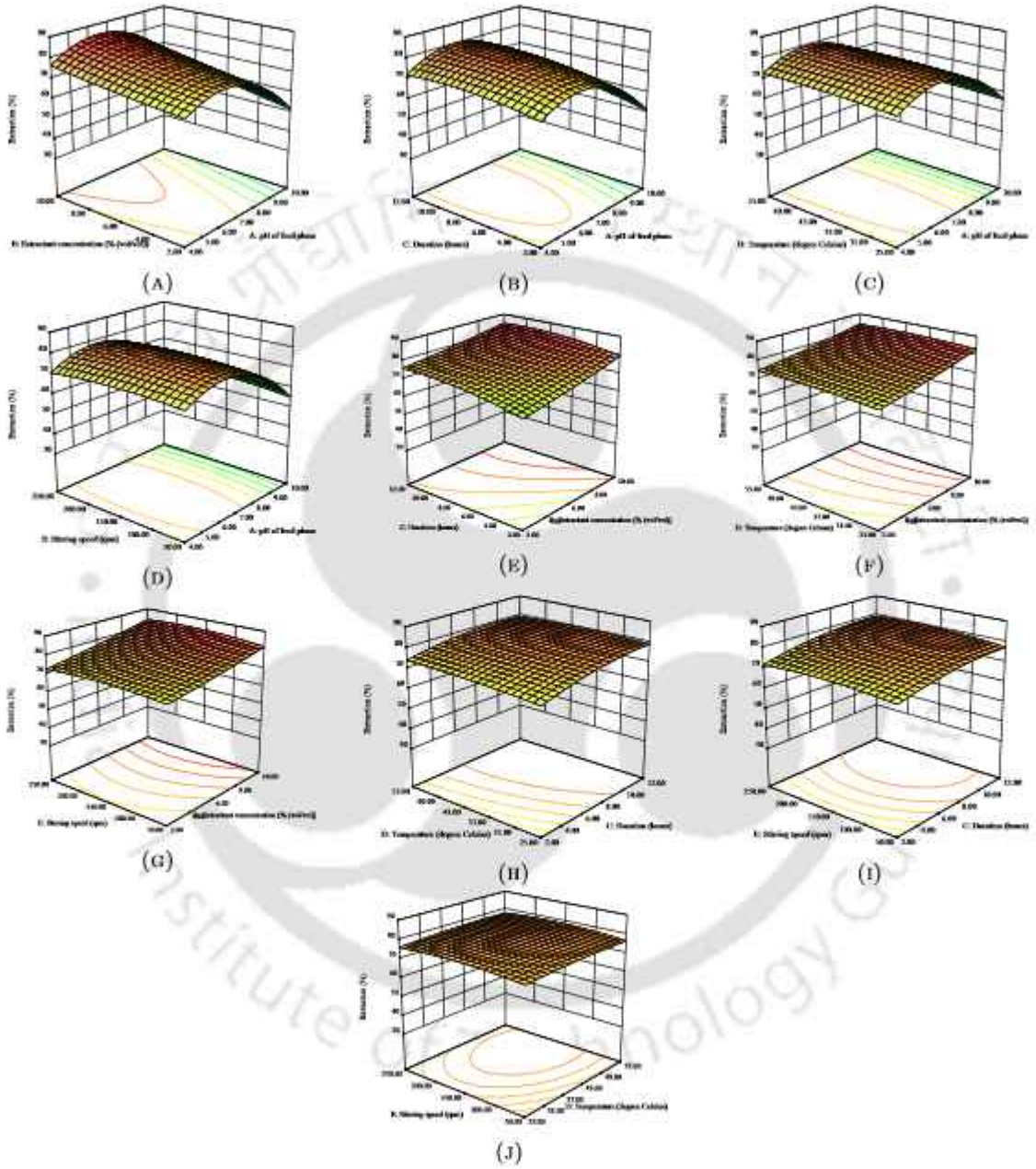

FIGURE A.6: Effect of parameters on the extraction of $As^{(III)}$:$As^{(V)}$:: 2 : 1 in two phase study

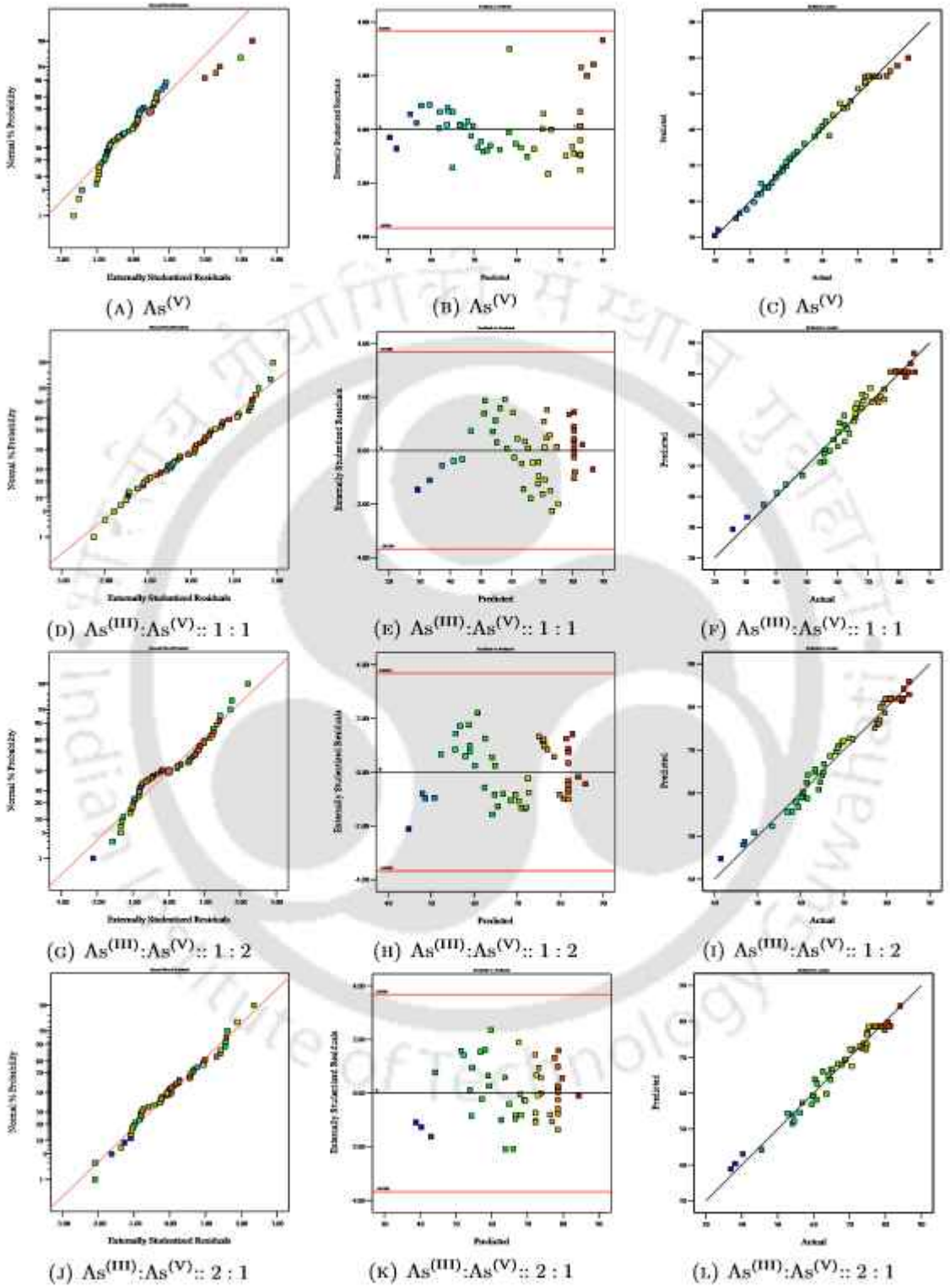

(A) $As^{(V)}$ (B) $As^{(V)}$ (C) $As^{(V)}$

(D) $As^{(III)}$:$As^{(V)}$:: 1 : 1 (E) $As^{(III)}$:$As^{(V)}$:: 1 : 1 (F) $As^{(III)}$:$As^{(V)}$:: 1 : 1

(G) $As^{(III)}$:$As^{(V)}$:: 1 : 2 (H) $As^{(III)}$:$As^{(V)}$:: 1 : 2 (I) $As^{(III)}$:$As^{(V)}$:: 1 : 2

(J) $As^{(III)}$:$As^{(V)}$:: 2 : 1 (K) $As^{(III)}$:$As^{(V)}$:: 2 : 1 (L) $As^{(III)}$:$As^{(V)}$:: 2 : 1

FIGURE A.7: Statistical analysis of the quadratic model predicted for extraction of arsenic in two phase

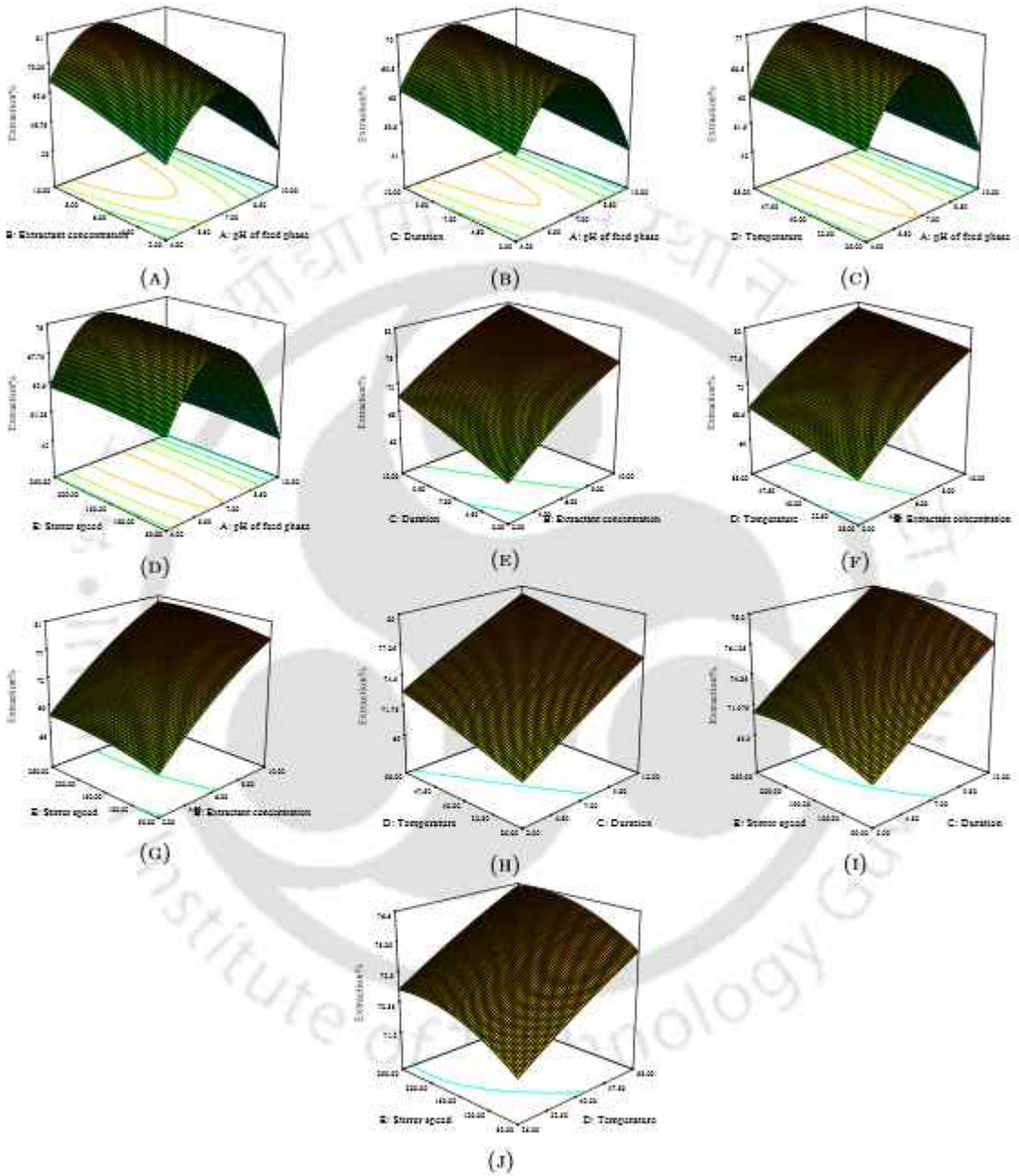

FIGURE A.8: Variation of %extraction in two phase with various combinations of factors for $As^{(V)}$using statistical model

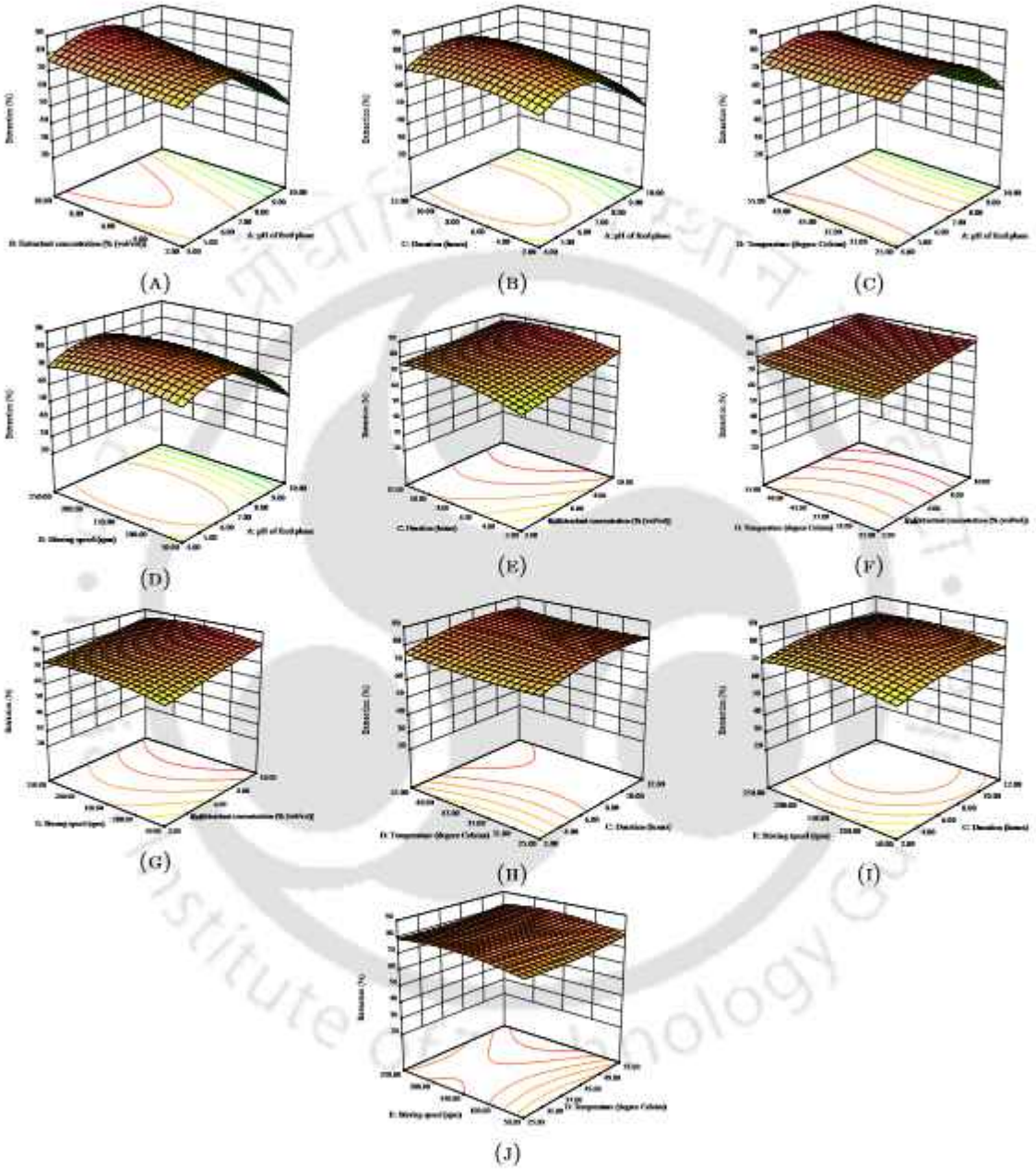

FIGURE A.9: Variation of %extraction in two phase with various combinations of factors for $As^{(III)}$:$As^{(V)}$:: 1 : 1 using statistical model

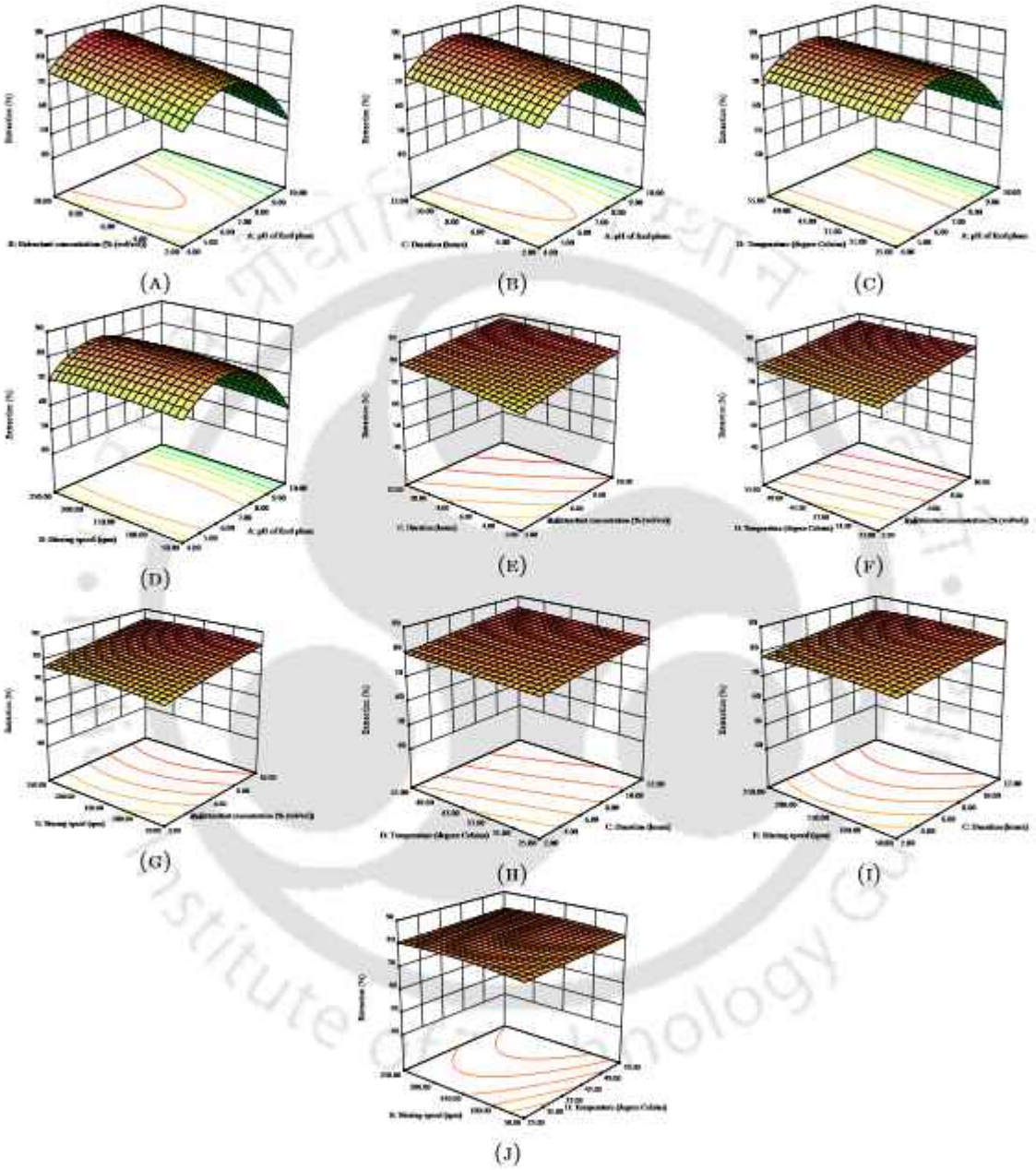

FIGURE A.10: Variation of %extraction in two phase with various combinations of factors for $As^{(III)}$:$As^{(V)}$:: 1 : 2 using statistical model

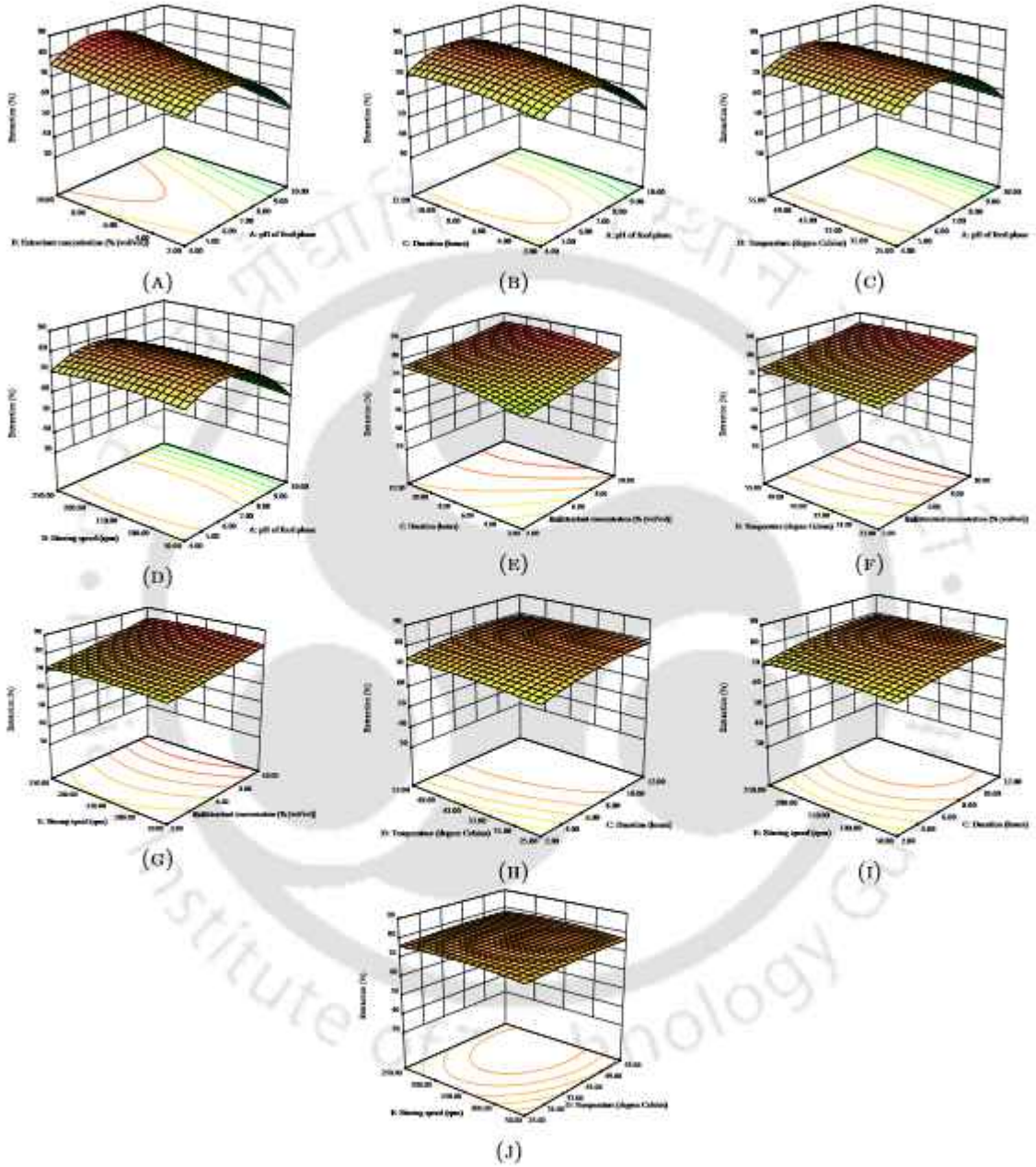

FIGURE A.11: Variation of %extraction in two phase with various combinations of factors for $As^{(III)}$:$As^{(V)}$:: 2 : 1 using statistical model

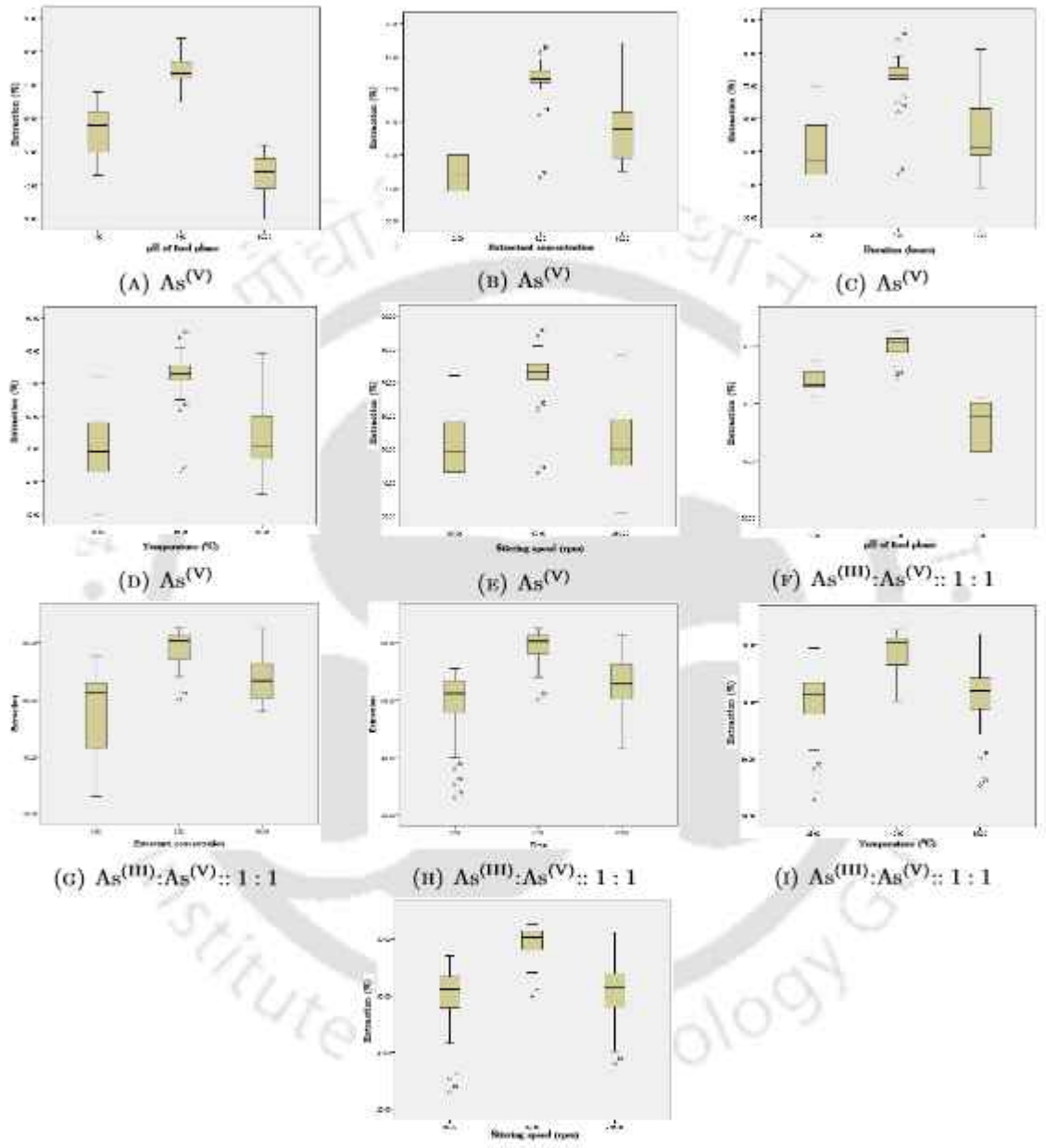

(A) $As^{(V)}$ (B) $As^{(V)}$ (C) $As^{(V)}$

(D) $As^{(V)}$ (E) $As^{(V)}$ (F) $As^{(III)}$:$As^{(V)}$:: 1 : 1

(G) $As^{(III)}$:$As^{(V)}$:: 1 : 1 (H) $As^{(III)}$:$As^{(V)}$:: 1 : 1 (I) $As^{(III)}$:$As^{(V)}$:: 1 : 1

(J) $As^{(III)}$:$As^{(V)}$:: 1 : 1

FIGURE A.12: Box plot for statistical analysis of extraction of $As^{(V)}$and $As^{(III)}$:$As^{(V)}$:: 1 : 1 in two phase

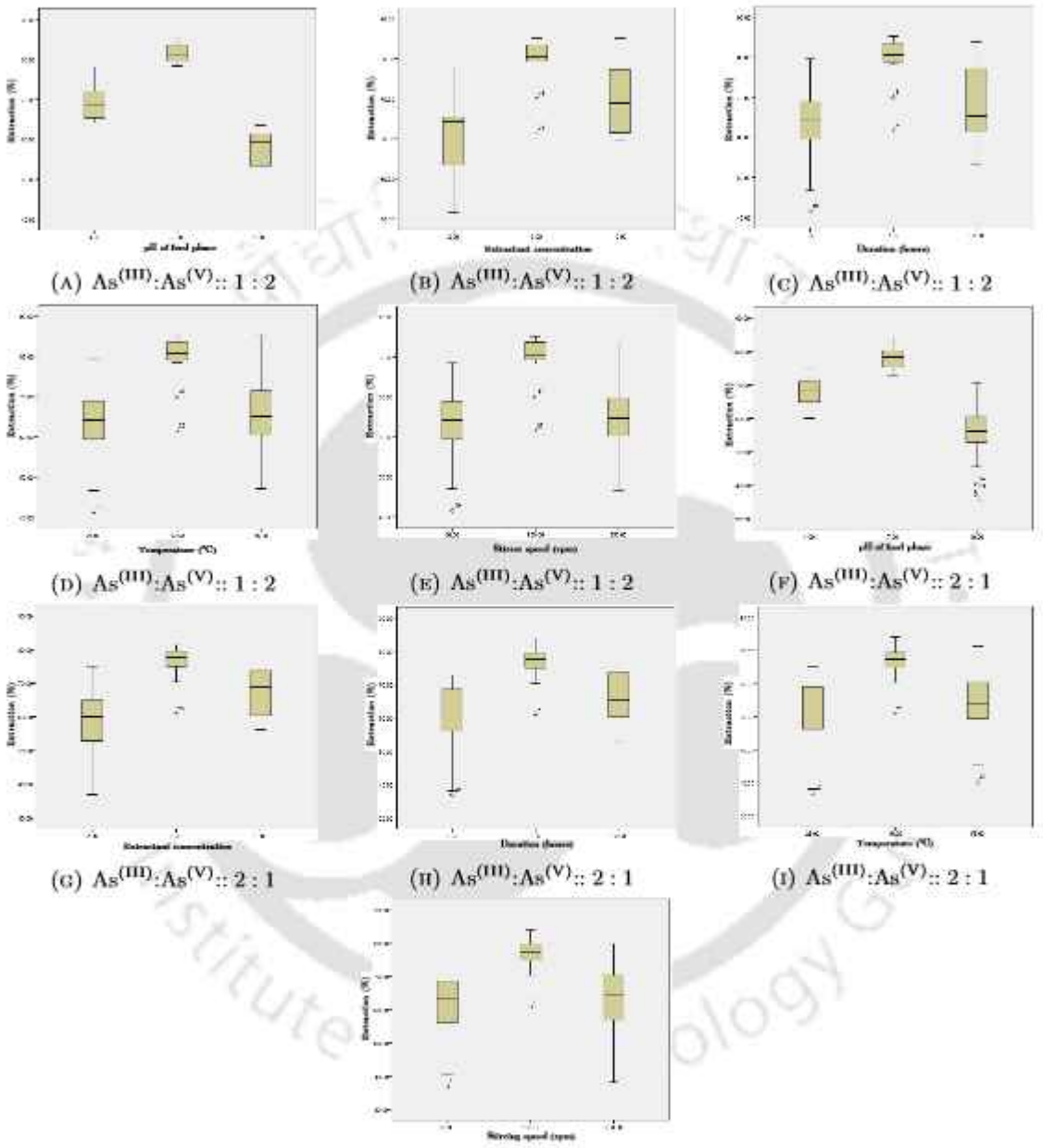

(A) $As^{(III)}$:$As^{(V)}$:: 1 : 2 (B) $As^{(III)}$:$As^{(V)}$:: 1 : 2 (C) $As^{(III)}$:$As^{(V)}$:: 1 : 2

(D) $As^{(III)}$:$As^{(V)}$:: 1 : 2 (E) $As^{(III)}$:$As^{(V)}$:: 1 : 2 (F) $As^{(III)}$:$As^{(V)}$:: 2 : 1

(G) $As^{(III)}$:$As^{(V)}$:: 2 : 1 (H) $As^{(III)}$:$As^{(V)}$:: 2 : 1 (I) $As^{(III)}$:$As^{(V)}$:: 2 : 1

(J) $As^{(III)}$:$As^{(V)}$:: 2 : 1

FIGURE A.13: Box plot for statistical analysis of extraction of $As^{(III)}$:$As^{(V)}$:: 1 : 2 and $As^{(III)}$:$As^{(V)}$:: 2 : 1 in two phase

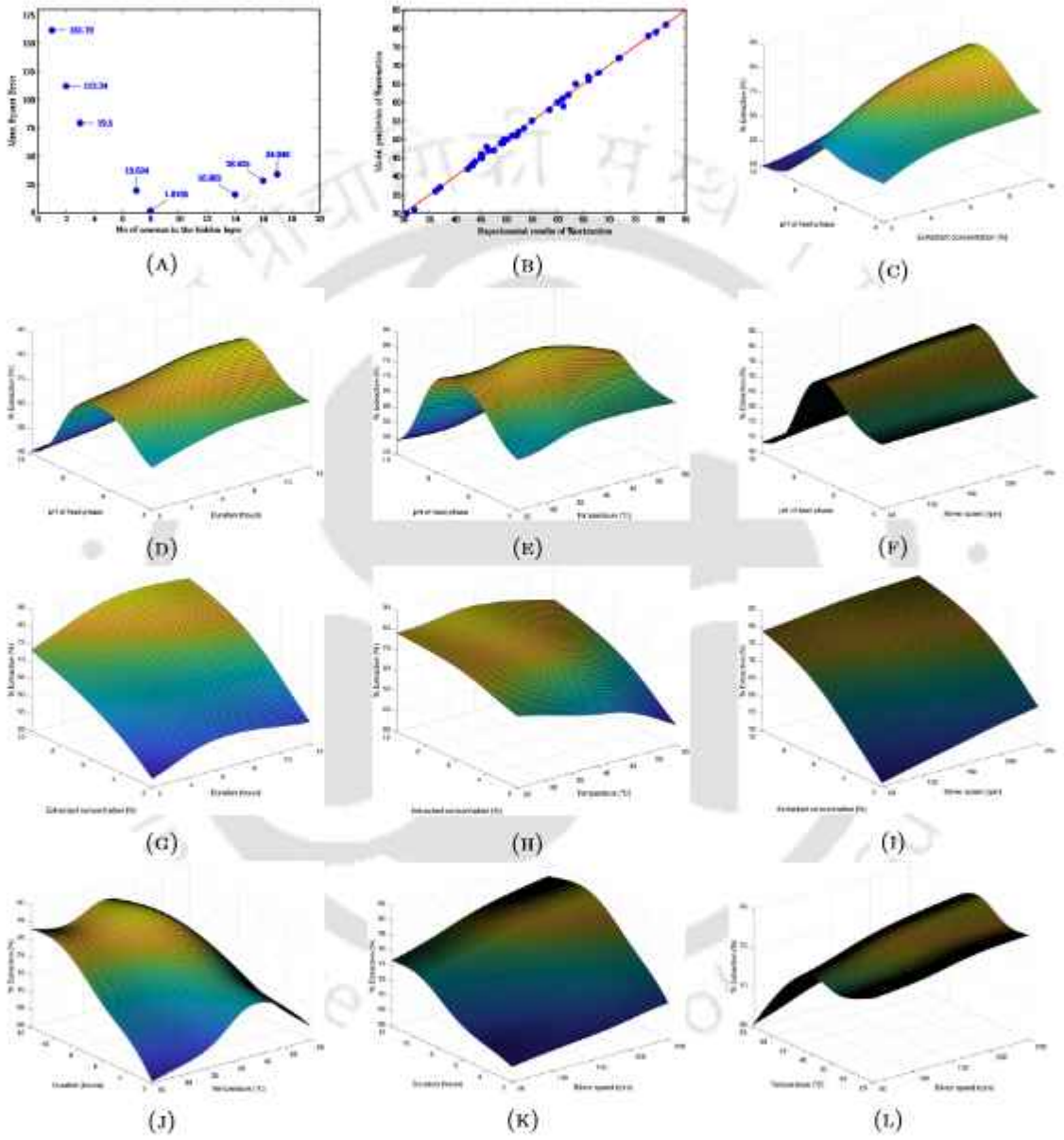

FIGURE A.14: Various plots of two phase extraction for $As^{(V)}$using machine learning

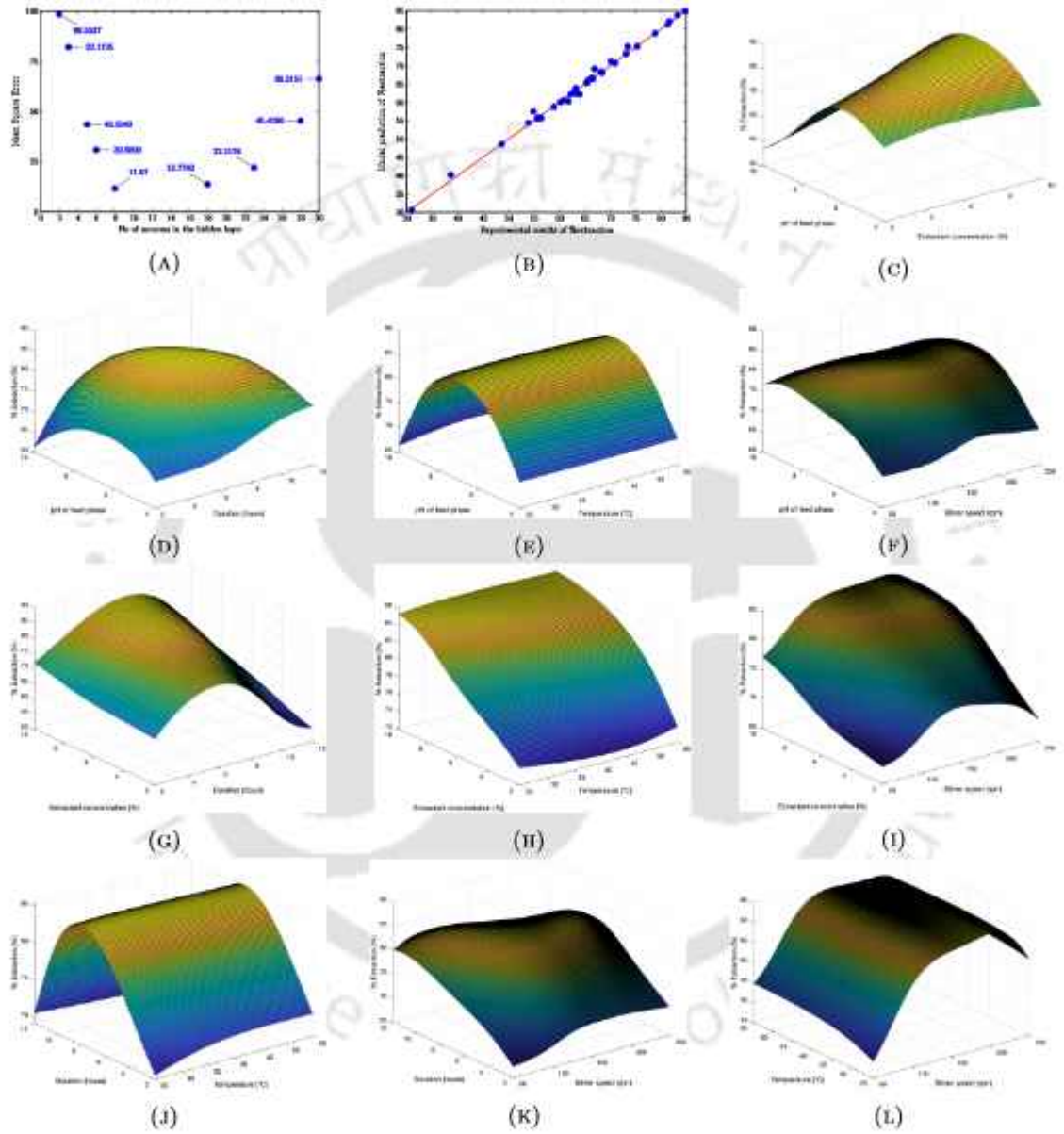

FIGURE A.15: Various plots of two phase extraction for $As^{(III)}$:$As^{(V)}$:: 1 : 1 using machine learning

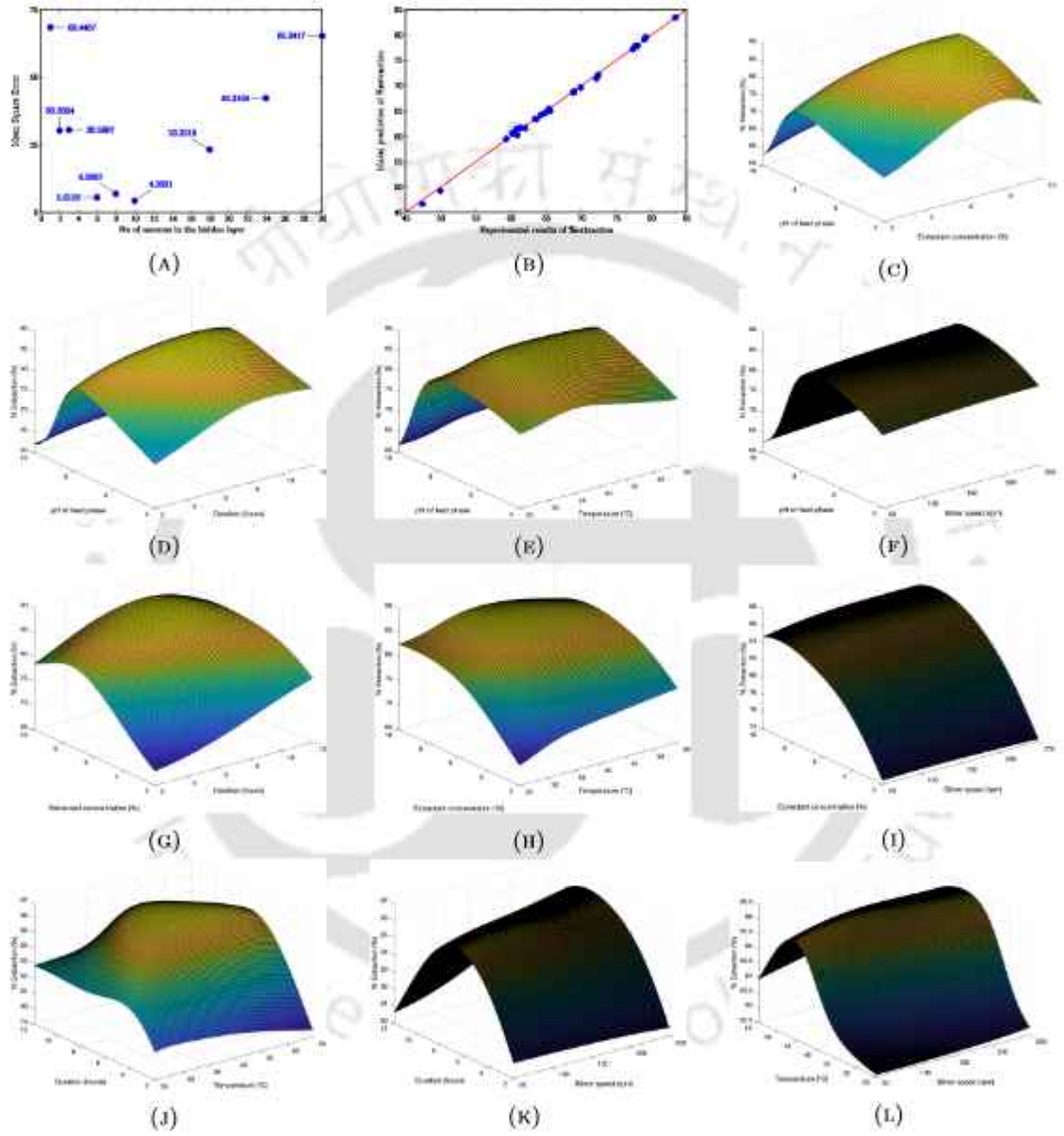

FIGURE A.16: Various plots of two phase extraction for $As^{(III)}$:$As^{(V)}$:: 1 : 2 using machine learning

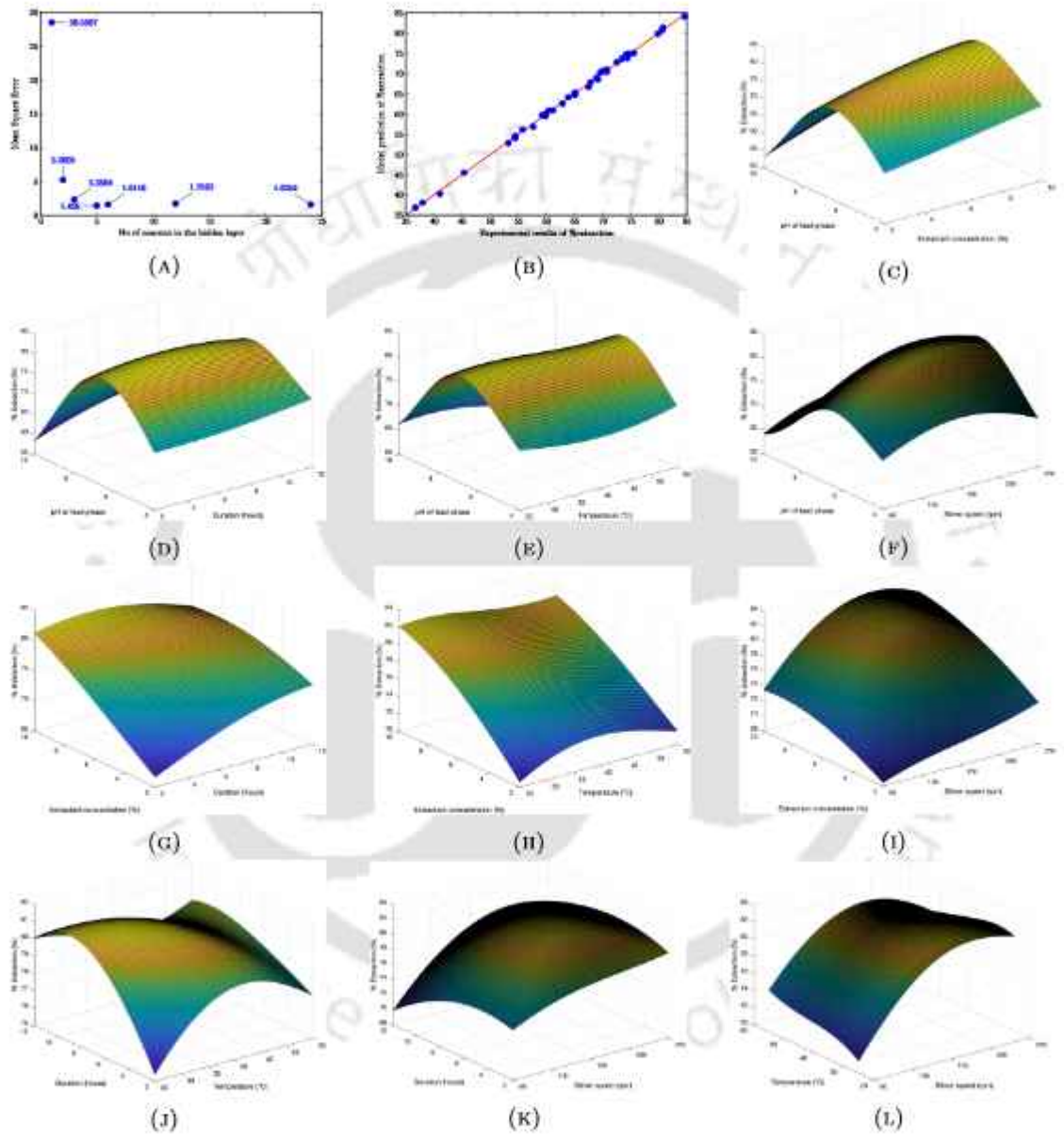

FIGURE A.17: Various plots of two phase extraction for $As^{(III)}$:$As^{(V)}$:: 2 : 1 using machine learning

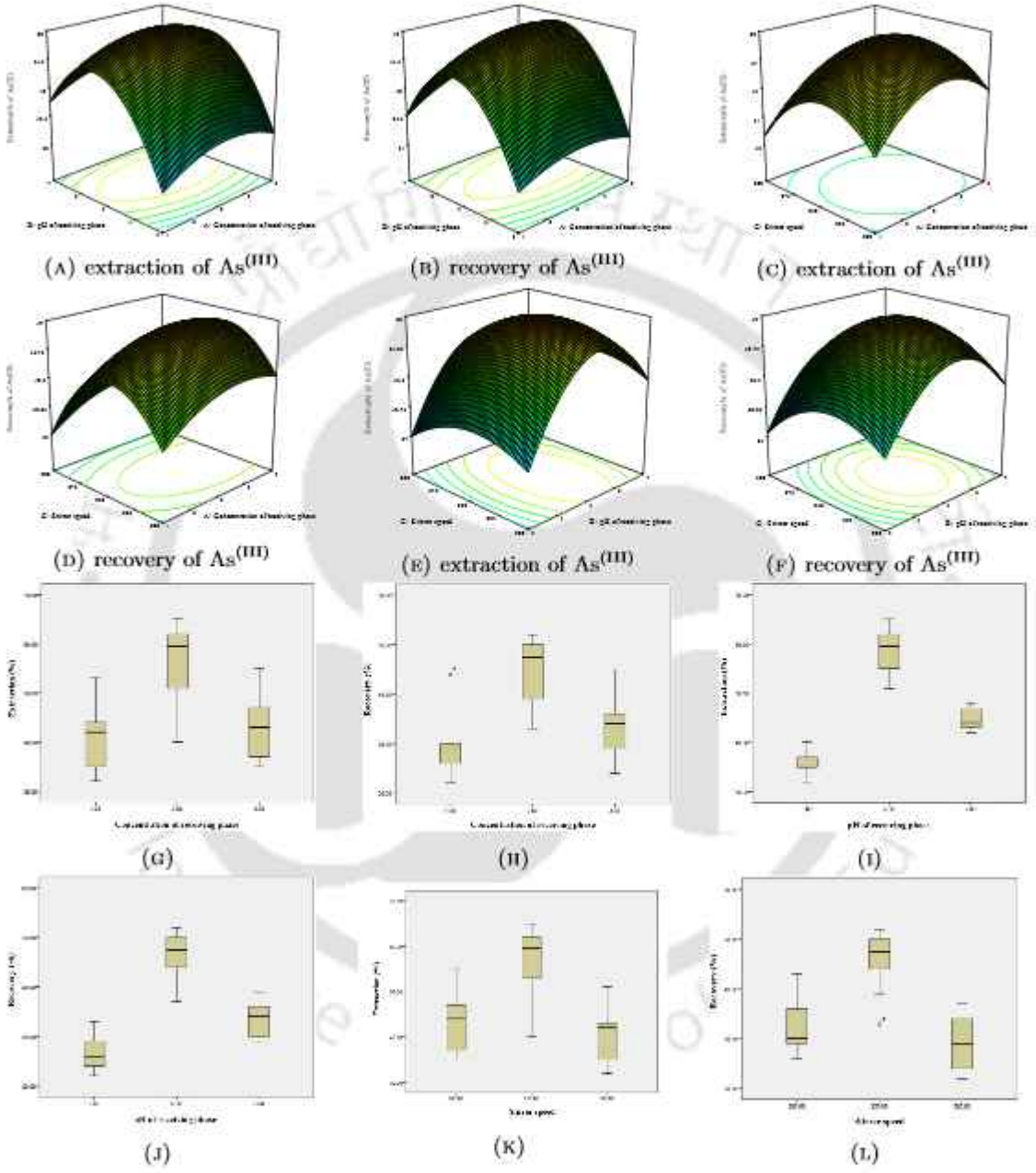

(A) extraction of $As^{(III)}$ (B) recovery of $As^{(III)}$ (C) extraction of $As^{(III)}$

(D) recovery of $As^{(III)}$ (E) extraction of $As^{(III)}$ (F) recovery of $As^{(III)}$

(G) (H) (I)

(J) (K) (L)

FIGURE A.18: Effect of interaction of parameters and box plot for statistical analysis of SLM extraction and recovery of $As^{(III)}$

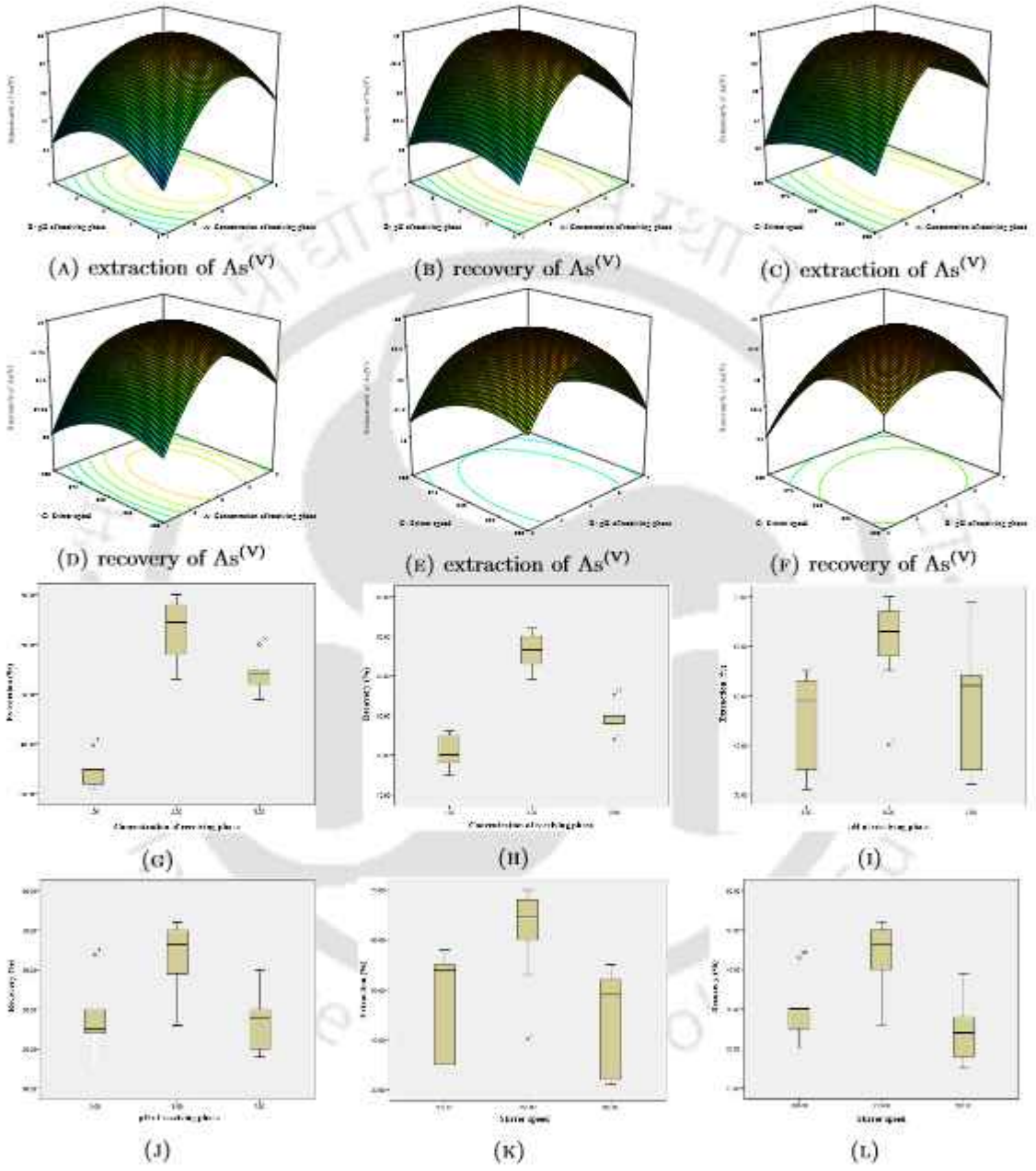

(A) extraction of $As^{(V)}$ (B) recovery of $As^{(V)}$ (C) extraction of $As^{(V)}$

(D) recovery of $As^{(V)}$ (E) extraction of $As^{(V)}$ (F) recovery of $As^{(V)}$

(G) (H) (I)

(J) (K) (L)

FIGURE A.19: Effect of interaction of parameters and box plot for statistical analysis of SLM extraction and recovery of $As^{(V)}$

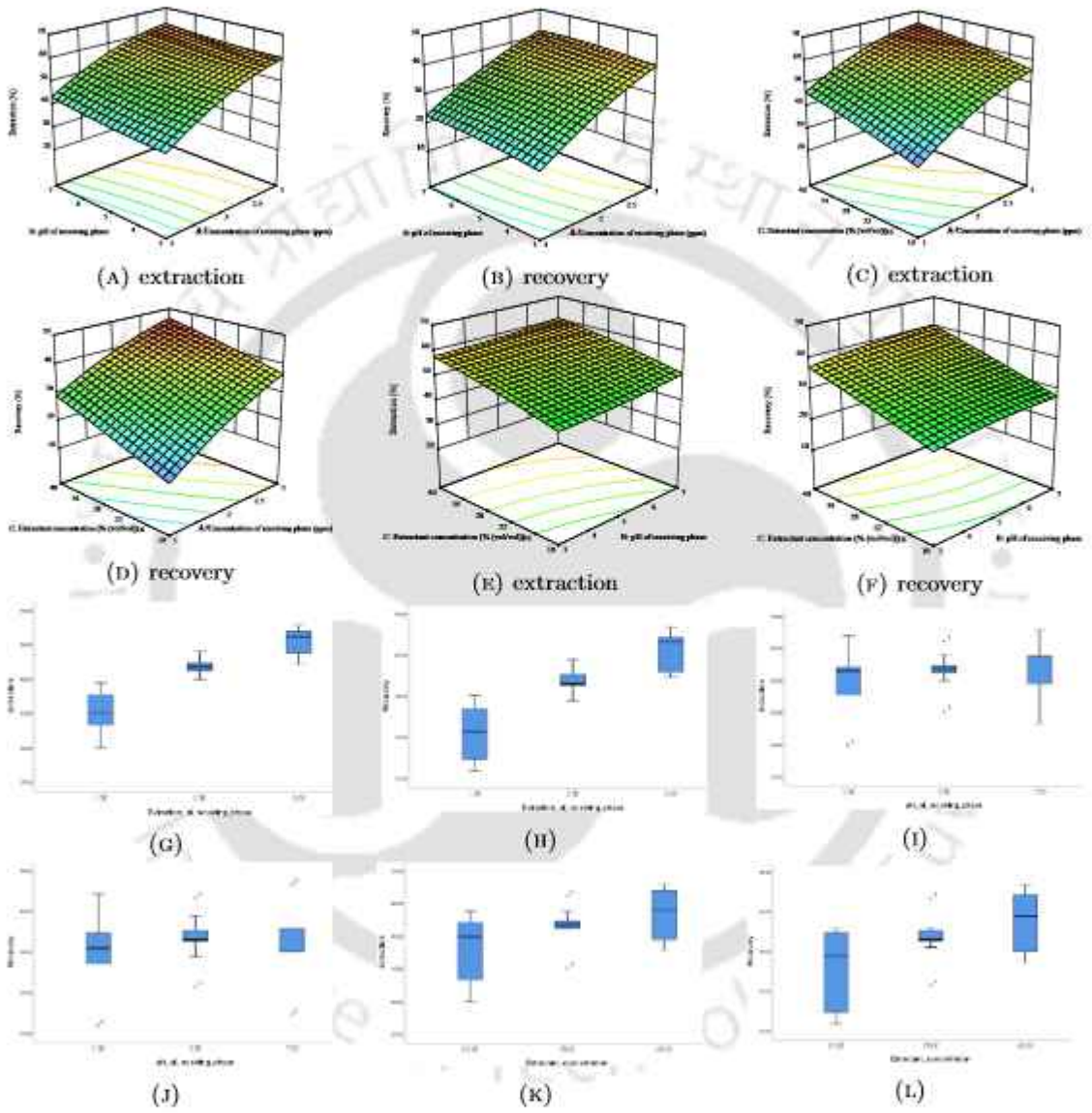

(A) extraction (B) recovery (C) extraction

(D) recovery (E) extraction (F) recovery

(G) (H) (I)

(J) (K) (L)

FIGURE A.20: Effect of interaction of parameters and box plot for statistical analysis of SLM extraction and recovery of $As^{(III)}$:$As^{(V)}$:: 1 : 1

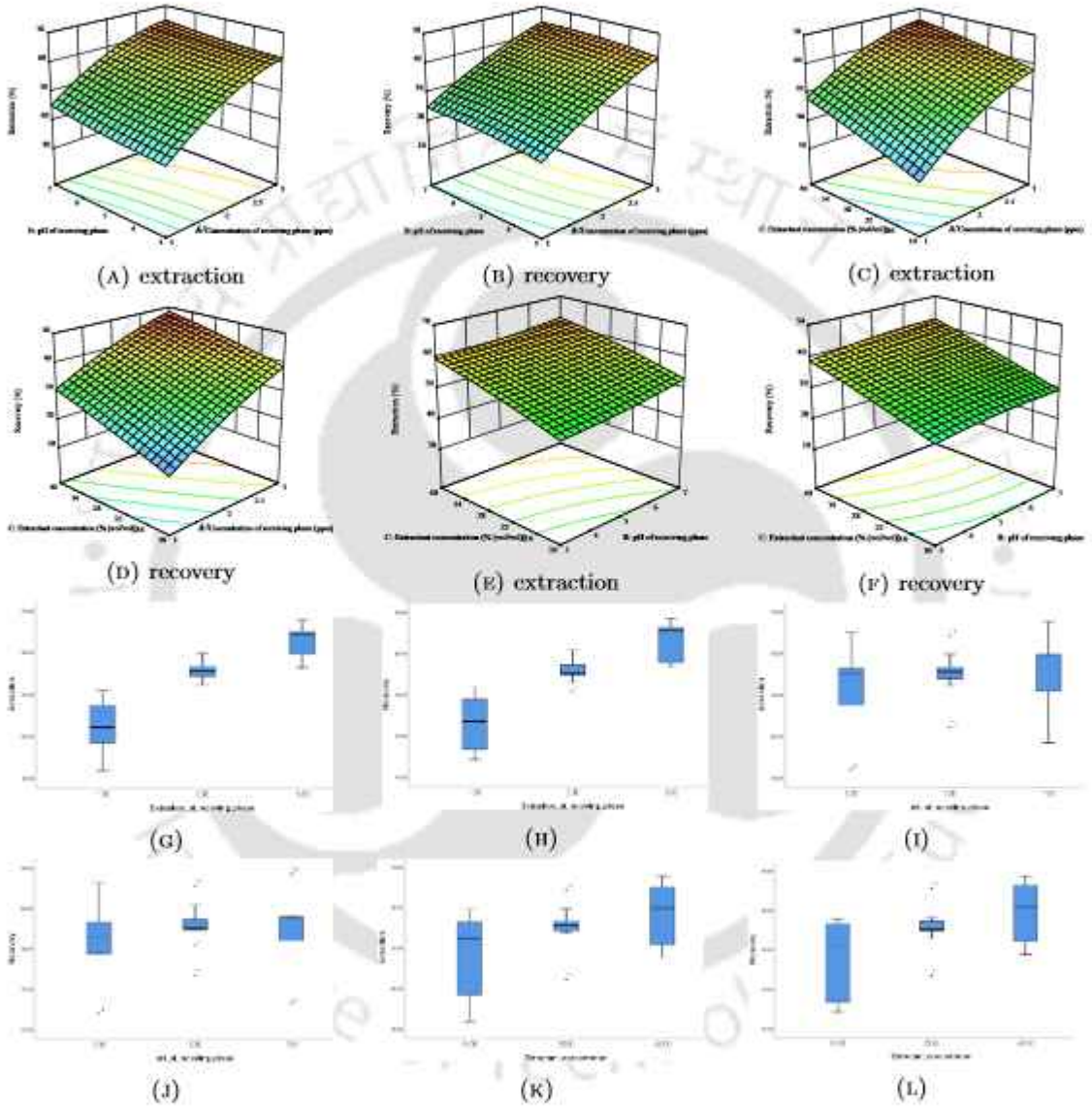

(A) extraction (B) recovery (C) extraction

(D) recovery (E) extraction (F) recovery

(G) (H) (I)

(J) (K) (L)

FIGURE A.21: Effect of interaction of parameters and box plot for statistical analysis of SLM extraction and recovery of $As^{(III)}$:$As^{(V)}$:: 1 : 2

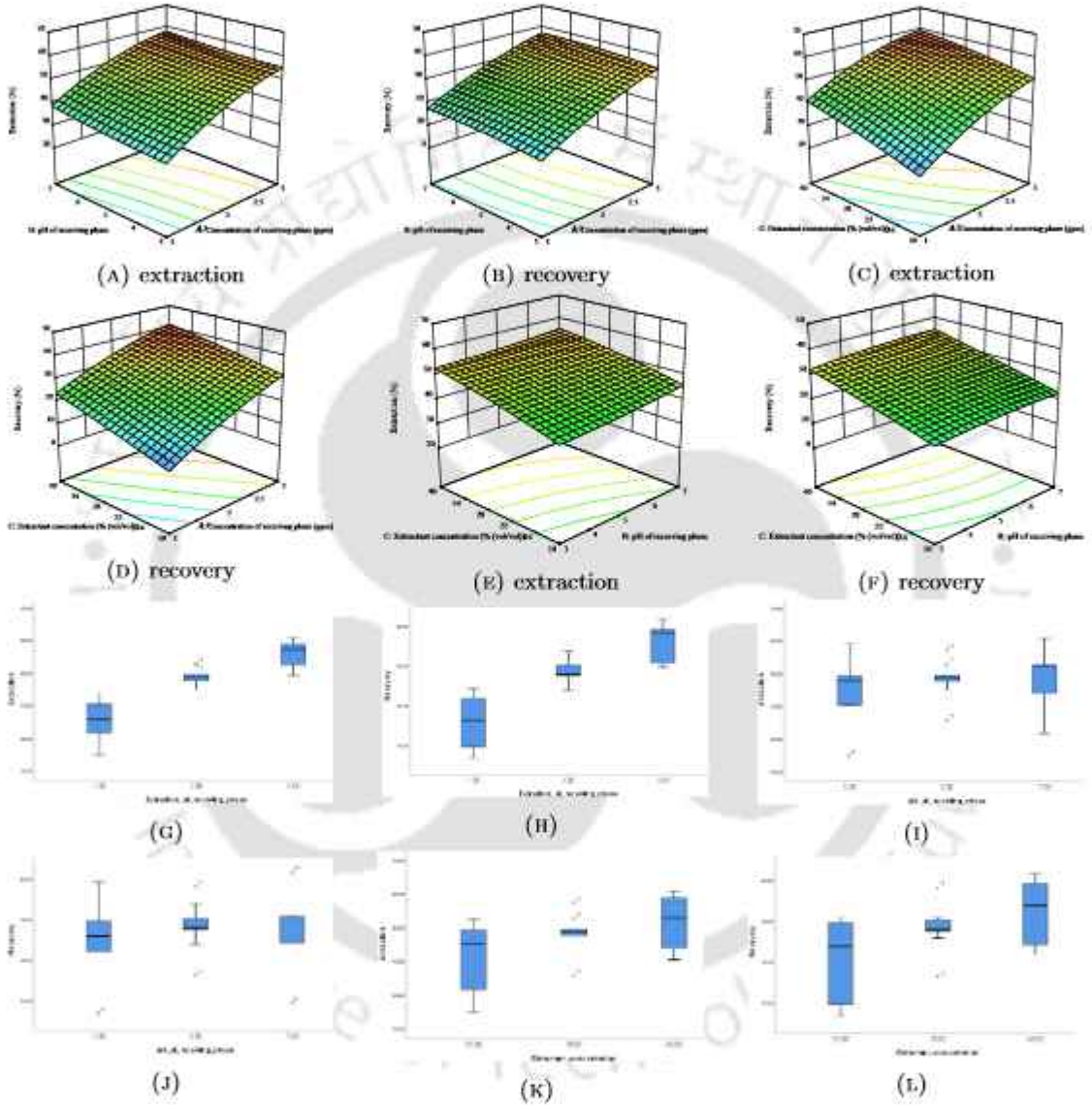

FIGURE A.22: Effect of interaction of parameters and box plot for statistical analysis of SLM extraction and recovery of $As^{(III)}$:$As^{(V)}$:: 2 : 1

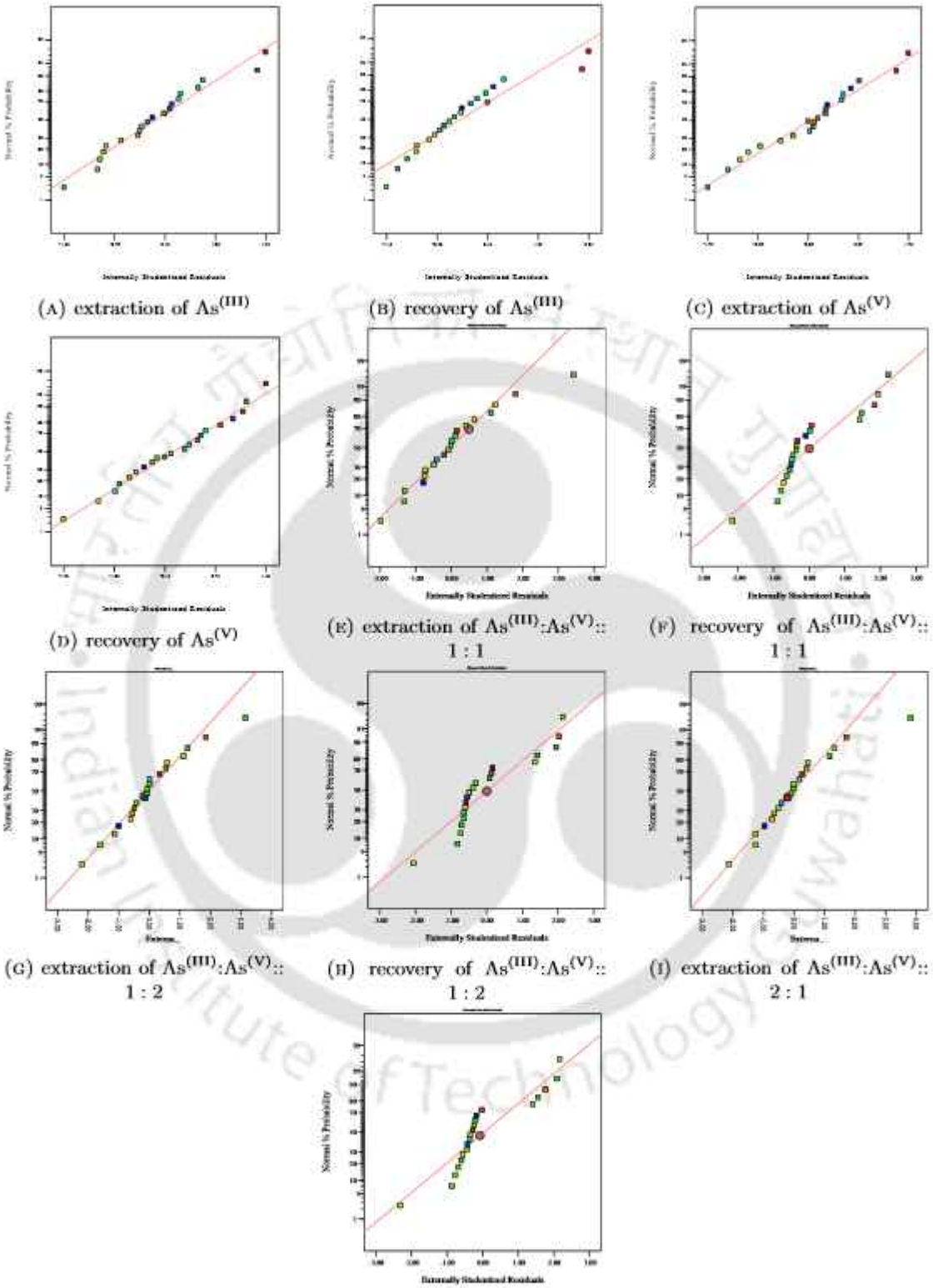

(A) extraction of $As^{(III)}$ (B) recovery of $As^{(III)}$ (C) extraction of $As^{(V)}$

(D) recovery of $As^{(V)}$ (E) extraction of $As^{(III)}$:$As^{(V)}$:: 1 : 1 (F) recovery of $As^{(III)}$:$As^{(V)}$:: 1 : 1

(G) extraction of $As^{(III)}$:$As^{(V)}$:: 1 : 2 (H) recovery of $As^{(III)}$:$As^{(V)}$:: 1 : 2 (I) extraction of $As^{(III)}$:$As^{(V)}$:: 2 : 1

(J) recovery of $As^{(III)}$:$As^{(V)}$:: 2 : 1

FIGURE A.23: Normal plot of residuals in SLM

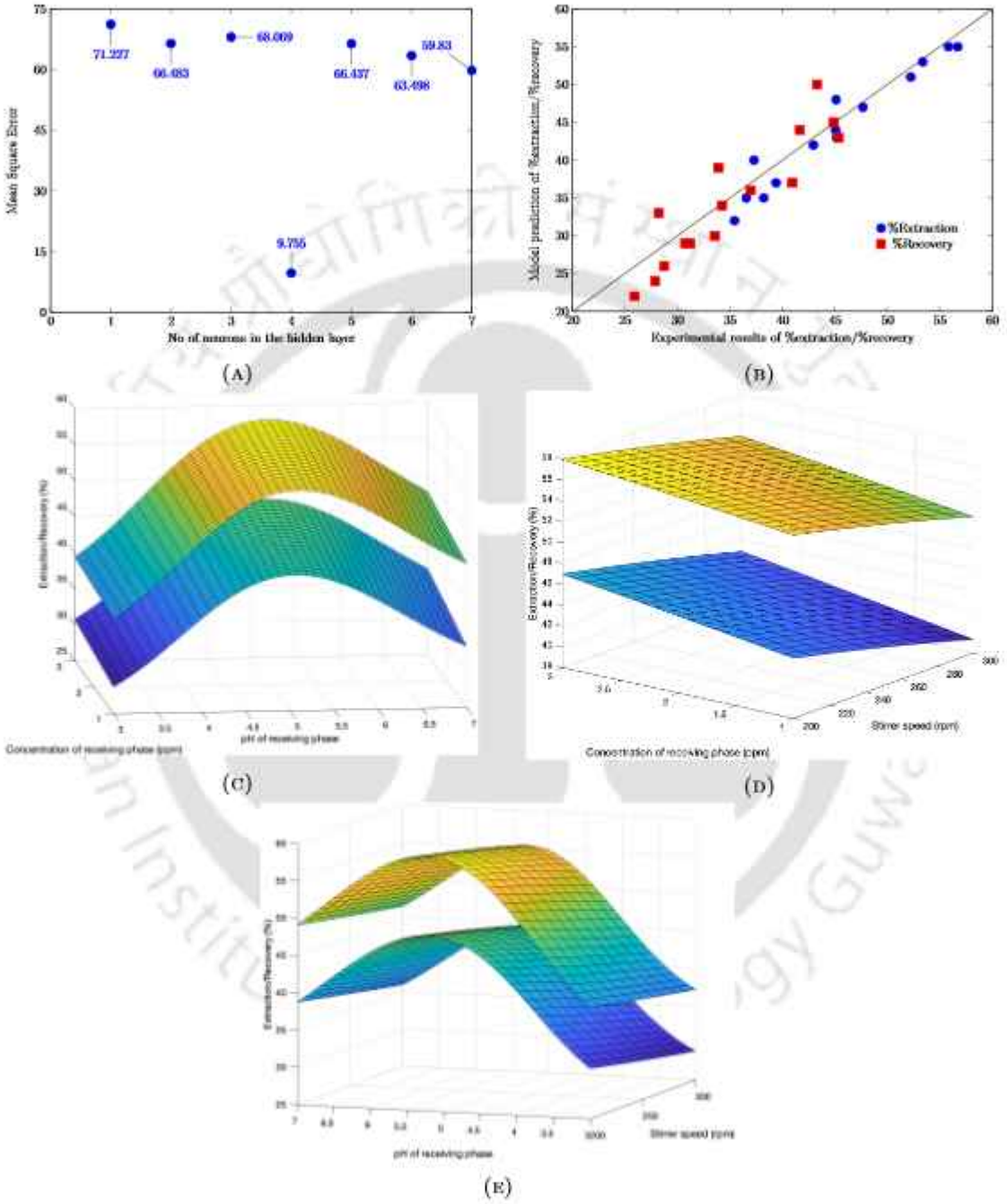

FIGURE A.24: Variation plots of three phase SLM for $As^{(III)}$using machine learning

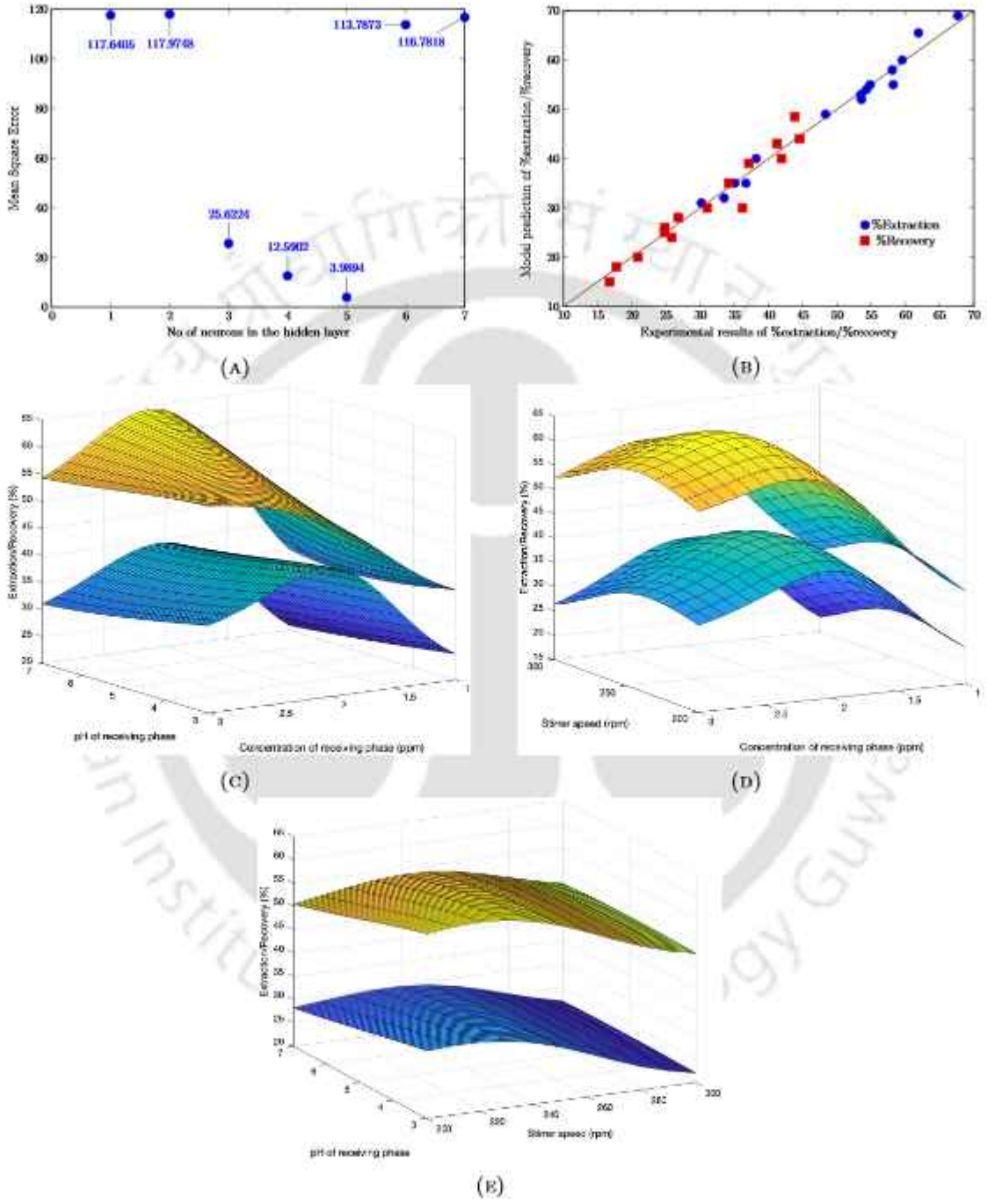

FIGURE A.25: Variation plots of three phase SLM for $As^{(V)}$using machine learning

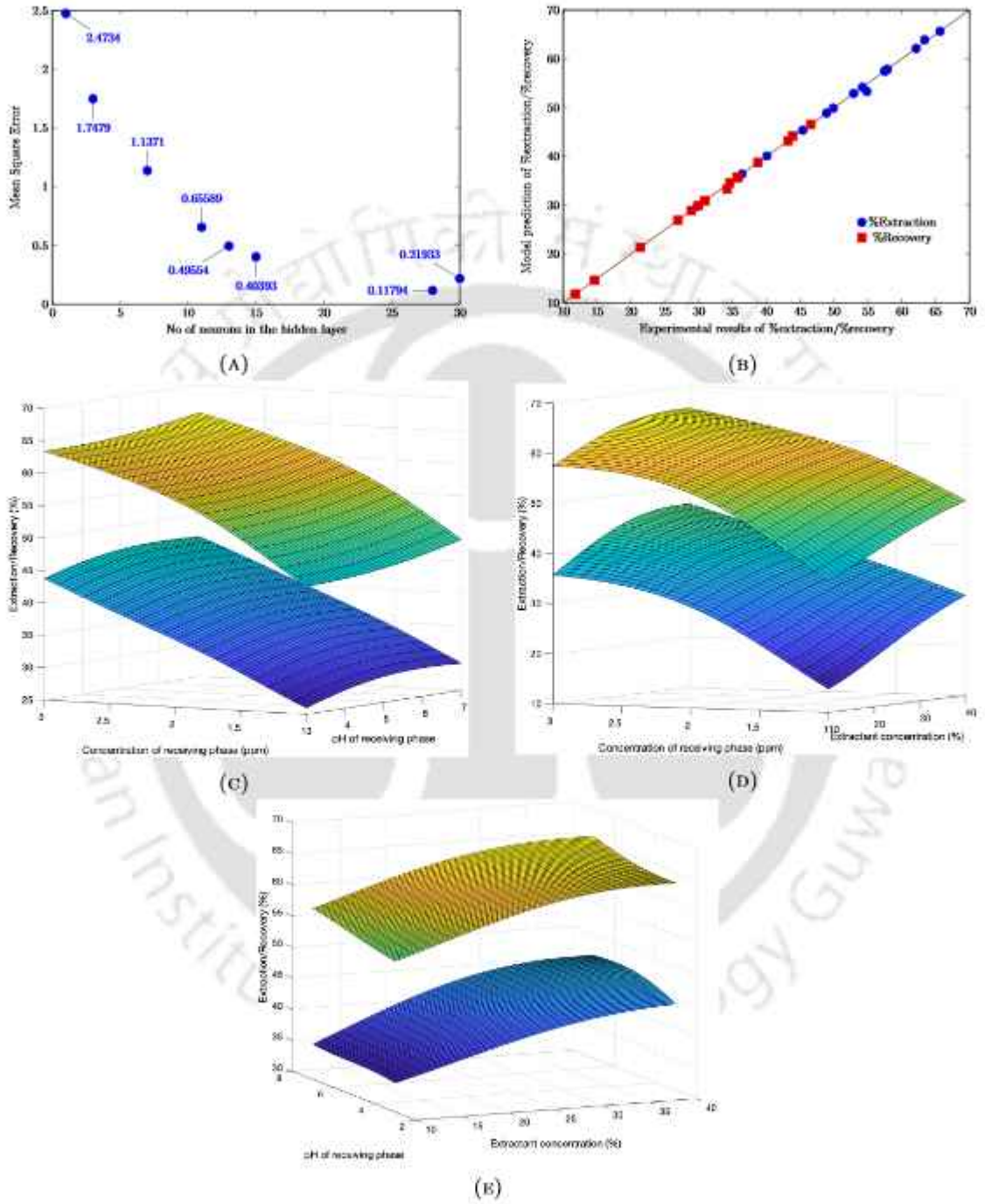

FIGURE A.26: Variation plots of three phase SLM for $As^{(III)}$:$As^{(V)}$:: 1 : 1 using machine learning

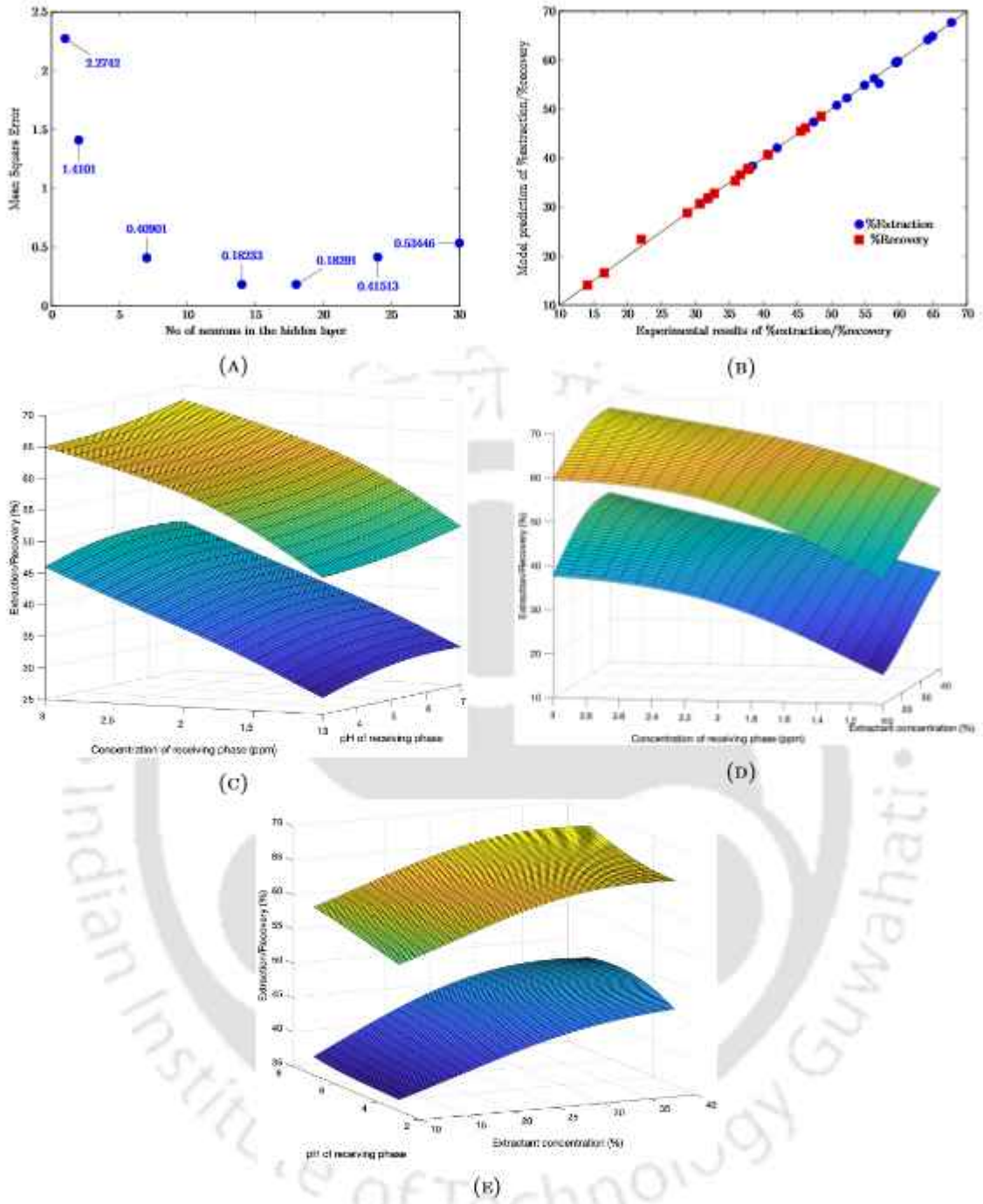

FIGURE A.27: Variation plots of three phase SLM for $As^{(III)}$:$As^{(V)}$:: 1 : 2 using machine learning

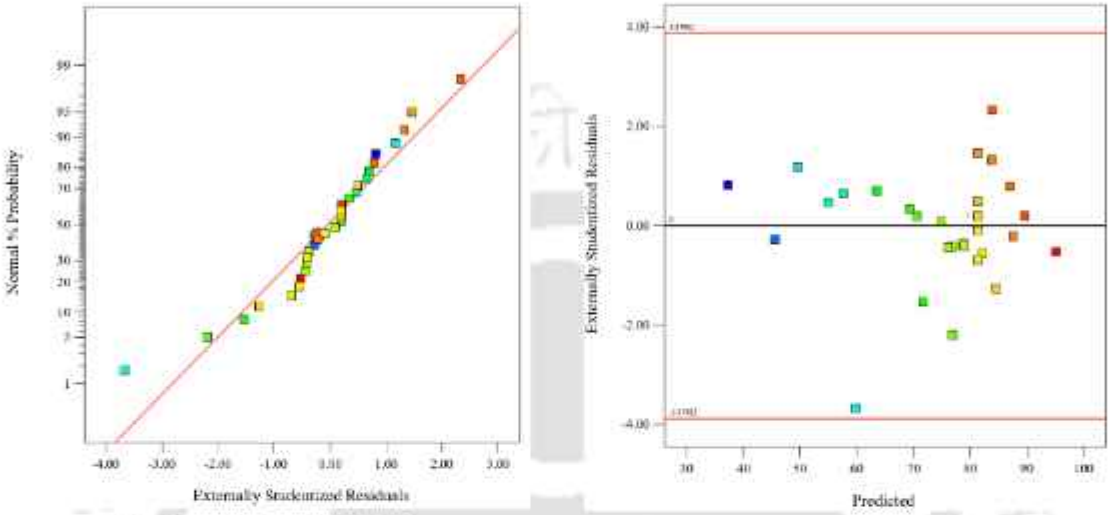

(A) Normal plot of residuals (B) Plot of residuals versus predicted

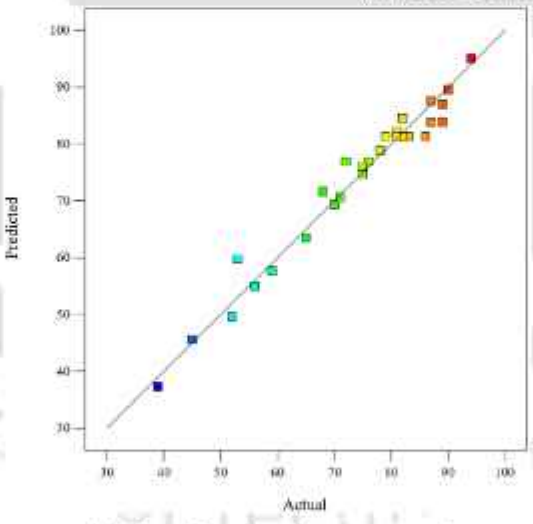

(C) Plot of predicted versus actual

FIGURE A.28: Statistical analysis of the quadratic model predicted for removal of $As^{(V)}$

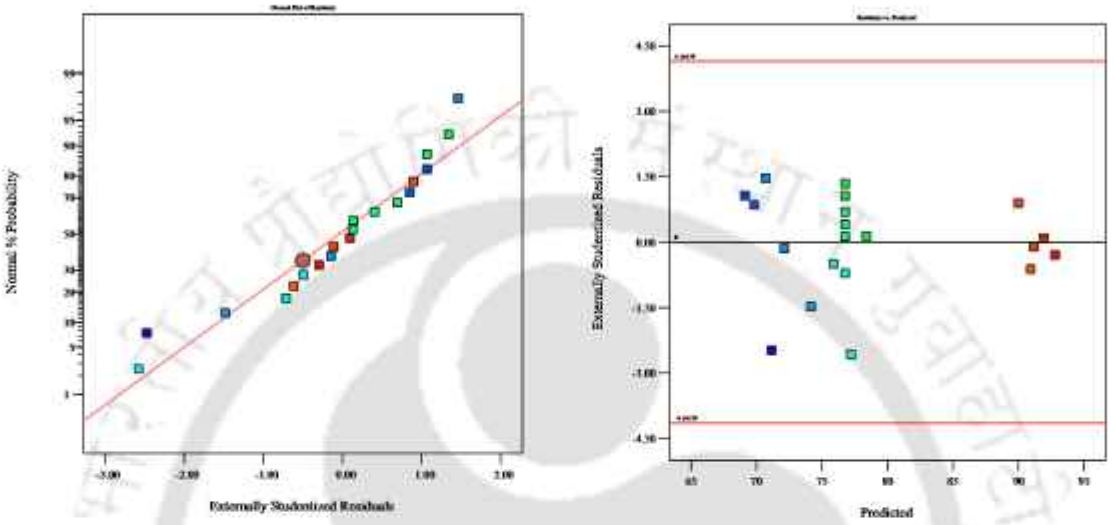

(A) Normal plot of residuals

(B) Plot of residuals versus predicted

(C) Plot of predicted versus actual

FIGURE A.29: Statistical analysis of the quadratic model predicted for removal of $As^{(III)}$

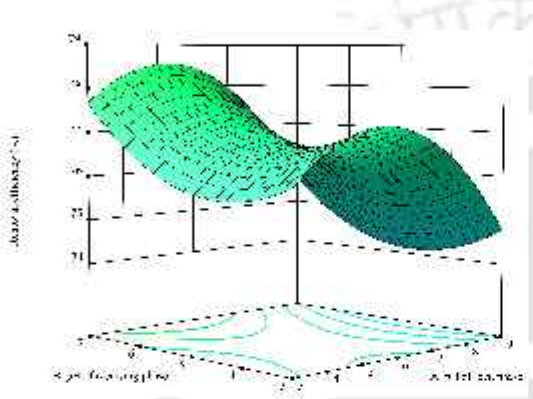

(A) pH of feed phase and receiving phase

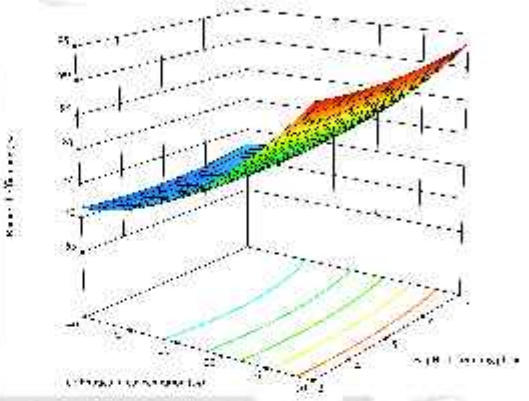

(B) receiving phase pH and extractant concentration

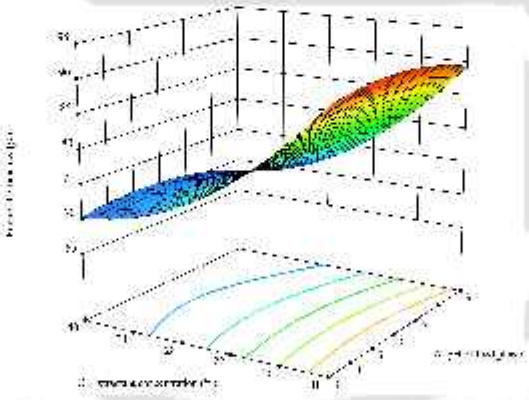

(C) pH of feed phase and extractant concentration

FIGURE A.30: Effect of the variables on the removal efficiency of $As^{(III)}$

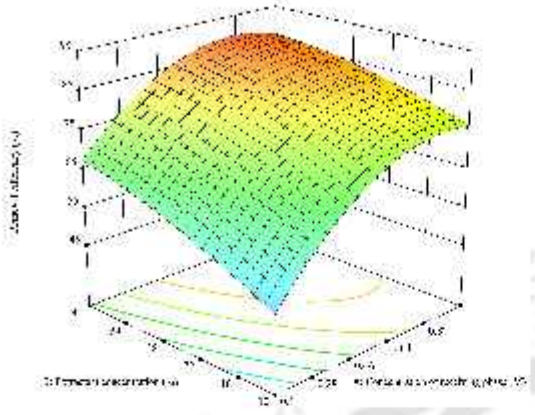

(A) concentration of receiving phase and extractant concentration

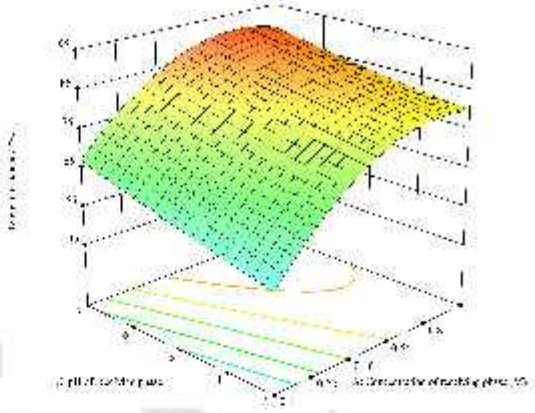

(B) concentration and pH of receiving phase

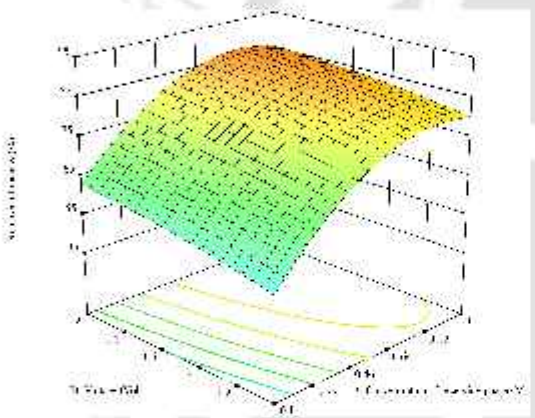

(C) concentration of receiving phase and voltage

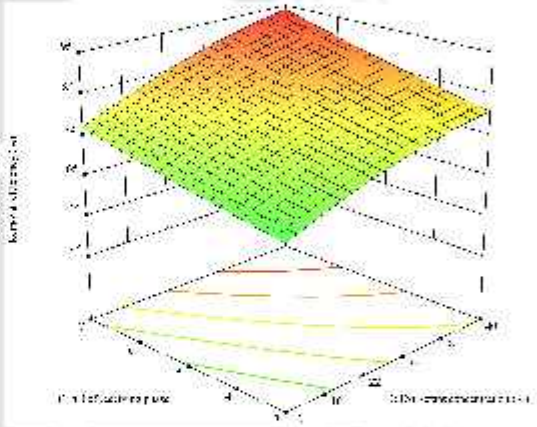

(D) extractant concentration and pH of receiving phase

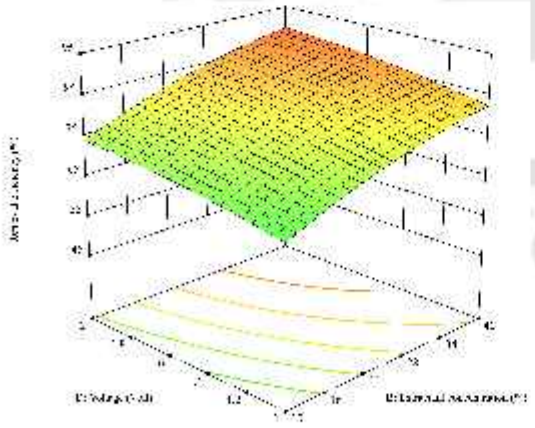

(E) extractant concnetration and voltage

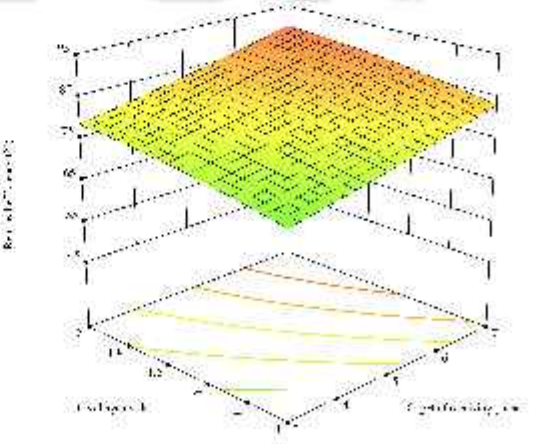

(F) pH of receiving phase and voltage

FIGURE A.31: Effect of the variables on the removal efficiency of $As^{(V)}$

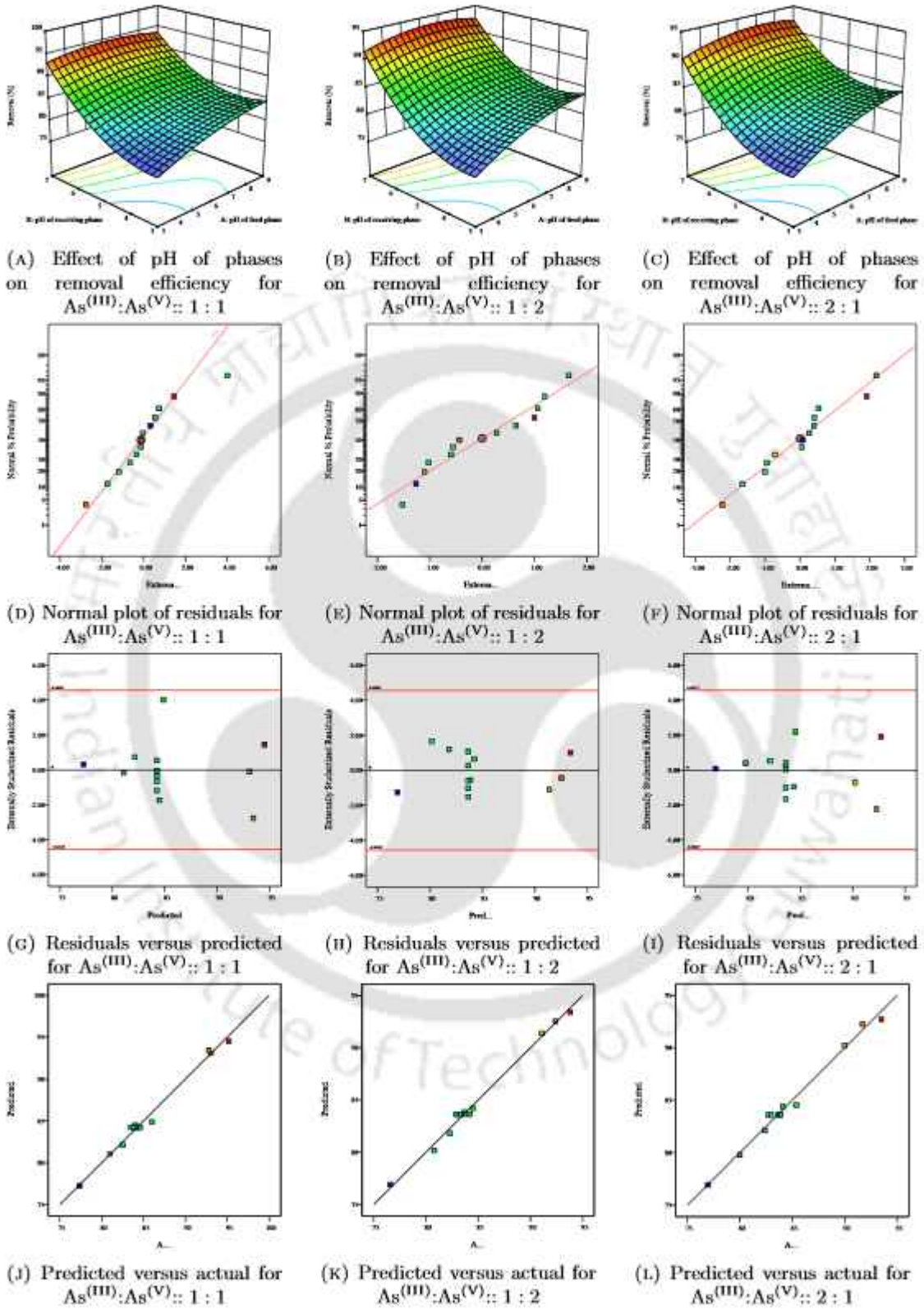

(A) Effect of pH of phases on removal efficiency for $As^{(III)}$:$As^{(V)}$:: 1 : 1

(B) Effect of pH of phases on removal efficiency for $As^{(III)}$:$As^{(V)}$:: 1 : 2

(C) Effect of pH of phases on removal efficiency for $As^{(III)}$:$As^{(V)}$:: 2 : 1

(D) Normal plot of residuals for $As^{(III)}$:$As^{(V)}$:: 1 : 1

(E) Normal plot of residuals for $As^{(III)}$:$As^{(V)}$:: 1 : 2

(F) Normal plot of residuals for $As^{(III)}$:$As^{(V)}$:: 2 : 1

(G) Residuals versus predicted for $As^{(III)}$:$As^{(V)}$:: 1 : 1

(H) Residuals versus predicted for $As^{(III)}$:$As^{(V)}$:: 1 : 2

(I) Residuals versus predicted for $As^{(III)}$:$As^{(V)}$:: 2 : 1

(J) Predicted versus actual for $As^{(III)}$:$As^{(V)}$:: 1 : 1

(K) Predicted versus actual for $As^{(III)}$:$As^{(V)}$:: 1 : 2

(L) Predicted versus actual for $As^{(III)}$:$As^{(V)}$:: 2 : 1

FIGURE A.32: Statistical plots of mixed arsenic species

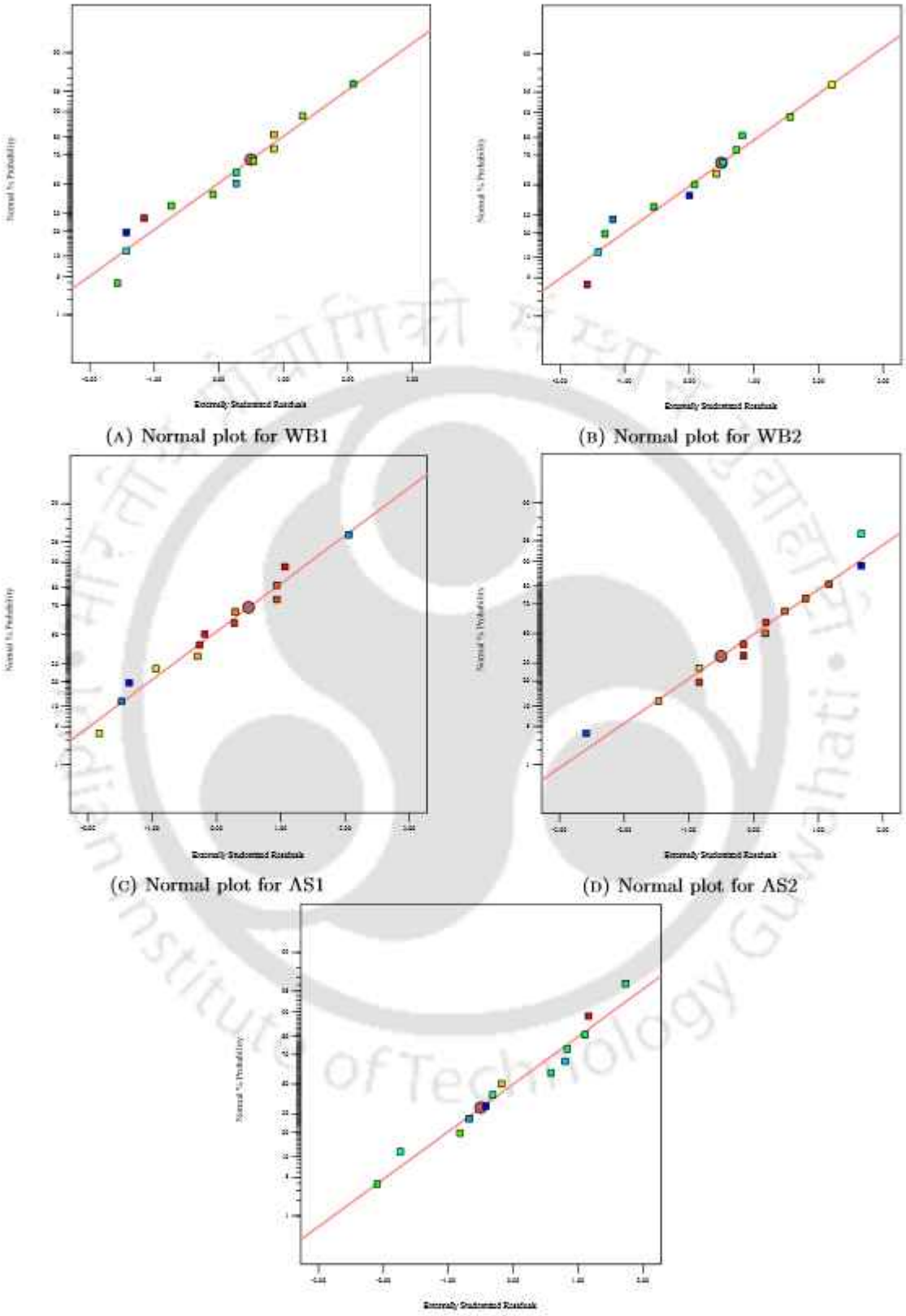

(A) Normal plot for WB1

(B) Normal plot for WB2

(C) Normal plot for AS1

(D) Normal plot for AS2

(E) Normal plot for AS3

FIGURE A.33: Normal plot of residuals of the predicted quadratic model

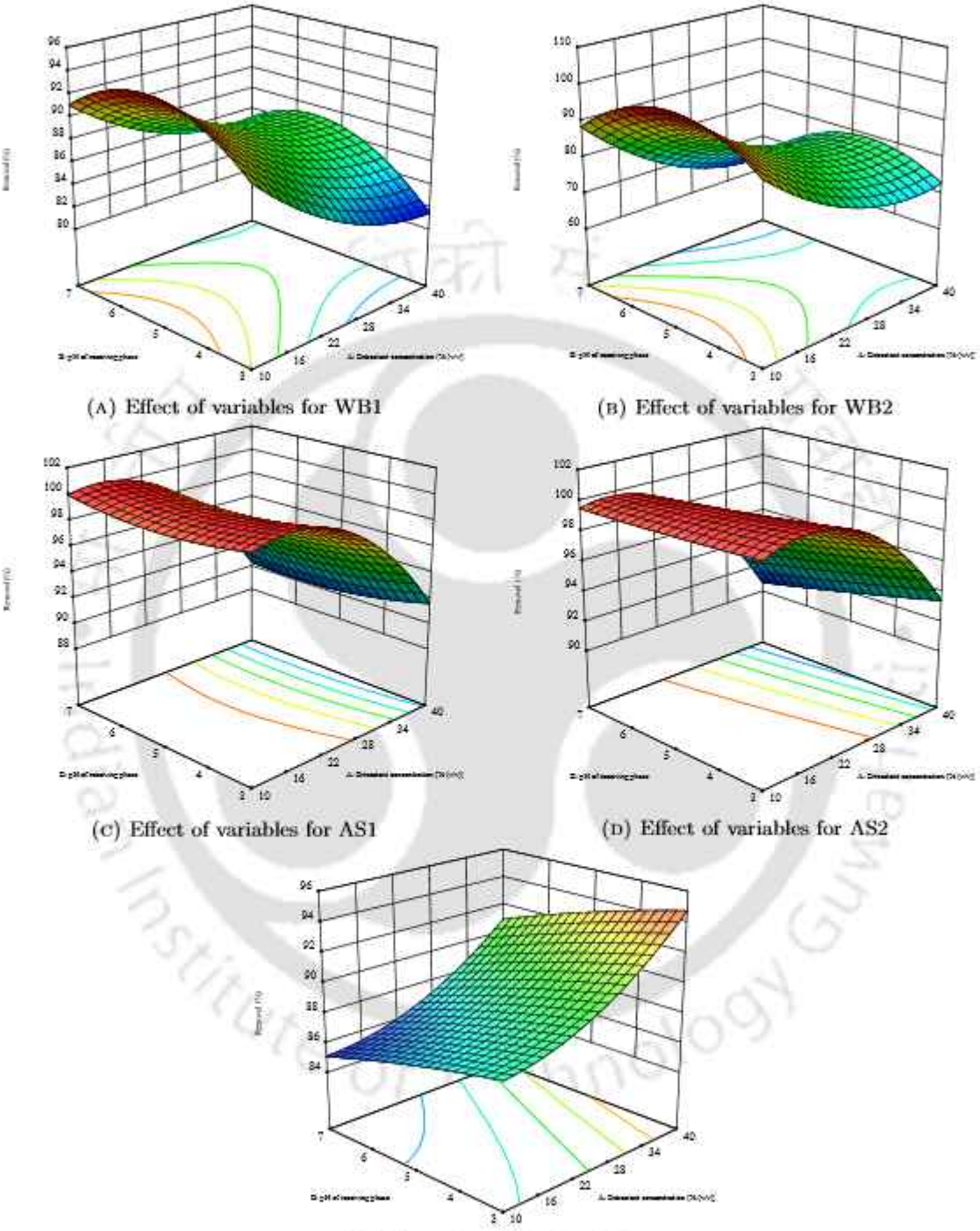

(A) Effect of variables for WB1

(B) Effect of variables for WB2

(C) Effect of variables for AS1

(D) Effect of variables for AS2

(E) Effect of variables for AS3

FIGURE A.34: Effect of the variables, viz. extractant concentration and pH of receiving phase on the removal efficiency of arsenic

INDIAN INSTITUTE OF TECHNOLOGY GUWAHATI

DEPARTMENT OF CHEMICAL ENGINEERING

WATER QUALITY BASED QUESTIONNAIRE SURVEY IN ARSENIC IMPACTED REGIONS OF BARUIPUR (WEST BENGAL, INDIA)

The survey has been conducted to gather information and gain insights into the quality and usage pattern of water in arsenic dominant regions of Baruipur, West Bengal (India). This helps to understand the perception of people residing in these areas. The survey is being conducted for research purpose only and the anonymity of the participants is maintained.

The questionnaire has been divided into four parts; first part consist of general demographic questions, second set of the questionnaire is related to water usage and organoleptic analysis of consumed water, third set of questions are linked to arsenic contamination in groundwater and the last part is specifically for people who consume water from bore well/hand pump/open well.

Part-I General demographic questions		
1.	Location	
2.	GPS coordinates	
3.	Gender	1. Male 2. Female
4.	Age	1. 18-28 years 2. 29-38 years 3. 39-48 years 4. 49-58 years 5. 59-68 years 6. Above 68 years
5.	Occupation	1. Farmer 2. Homemaker 3. Labourer 4. Carpenter 5. Unemployed 6. Others
6.	How long have you lived here?	1. Less than 5 years 2. 5-10 years 3. 10-50 years 4. More than 50 years
7.	How many members are there in your family (including yourself)?	1. One 2. Two 3. Three 4. Four 5. More than four
Part-II Water use and organoleptic related questions		

FIGURE A.35: Questionnaire for perception study Page 1

8.	What are the available sources of water in this location? (multiple choice)	1. Tap water supply 2. Open well (community) 3. Household bore well/ hand pump 4. Ponds/ lakes 5. Others
9.	What is/are the source(s) of drinking and cooking water at home? (multiple choice)	1. Tap water supply 2. Open well (community) 3. Household bore well/ hand pump 4. Ponds/ lakes 5. Others
10.	Is the water available throughout the year?	1. Yes 2. No 3. Cannot say
11.	How much water do you consume per day?	1. Less than 1 litre 2. 1-2 litres 3. 2-5 litres 4. More than 5 litres 5. Unsure
12.	How far is the source of water from your household?	1. Within the house 2. Within 50 meters 3. 50-100 meters 4. 100-500 meters 5. More than 500 meters 6. Unknown
13.	Is there any odour in the water being consumed?	1. Yes 2. No 3. Unsure
14.	If yes, please describe the odour?	1. Pleasant 2. Unpleasant 3. Other (specify)
15.	If yes, when do you notice the odour in the water?	1. Summer 2. Monsoon 3. Winter 4. Throughout the year 5. Other (specify)
16.	Is there any specific taste in your drinking/cooking water?	1. Yes 2. No 3. Unsure
17.	If yes, how is the taste of the water?	1. Salty 2. Metallic 3. Others (specify)
18.	If yes, when is the taste in water most prevalent?	1. Summer 2. Monsoon 3. Winter 4. Throughout the year 5. Others (specify)
19.	Does your drinking/cooking water have any colour?	1. Yes 2. No 3. Unsure

FIGURE A.36: Questionnaire for perception study Page 2

20.	If yes, what is the observed colour of the water?	1. Unclear 2. Murky/Muddy 3. Greyish 4. Reddish 5. Others (specify)
21.	If yes, when do you notice the change in colour in water?	1. Summer 2. Monsoon 3. Winter 4. Throughout the year 5. Other (specify)
22.	Does the food change in colour when cooked/boiled in the same water?	1. Yes 2. No 3. Unsure
23.	If yes, when do you notice the change in colour in food?	1. Summer 2. Monsoon 3. Winter 4. Throughout the year 5. Other (specify)
Part-III Water quality and arsenic related questions		
24.	Do you trust the sources of the water to be safe?	1. Yes 2. No 3. Unsure
25.	How would you rate the quality of water?	1. Very good 2. Good 3. Moderate 4. Poor 5. Very poor
26.	Do you treat your water before consumption?	1. Yes 2. No
27.	How do you treat your drinking water?	1. Boiling 2. Filtration (usage of water filters) 3. Coagulation (using alum) 4. None
28.	Do you know what arsenic is?	1. Yes 2. No 3. Unsure
29.	Do you know that arsenic is present in the groundwater?	1. Yes 2. No 3. Unsure
30.	Do you know the permissible limit of arsenic in drinking water?	1. Yes 2. No 3. Unsure
31.	Do you know the health impacts of consuming arsenic polluted water?	1. Yes 2. No 3. Unsure
32.	Do you know that people fall sick/ill by consuming arsenic contaminated water for drinking/cooking purposes?	1. Yes 2. No 3. Unsure
33.	How many member(s) is/are affected by arsenic in your family?	1. One

FIGURE A.37: Questionnaire for perception study Page 3

		2. Two 3. More than two 4. None 5. Unsure
34.	How many people have been affected by consuming arsenic contaminated water in this area?	1. Less than five 2. 5-10 3. 10-25 4. 25-50 5. More than 50 6. Unsure
35.	Other than arsenic, is there any other water related issue faced by you or others in this locality?	1. Yes 2. No 3. Unsure
36.	If yes, what is the issue?	1. Scarcity 2. Inadequacy 3. Unsafe 4. Others (specify)
37.	If yes, in which season does the water related issues occur?	1. Summer 2. Monsoon 3. Winter 4. Throughout the year 5. Others (specify)
Part-IV Bore well/hand pump/open well related questions		
38.	When was the bore well/hand pump built?	1. 0-5 years 2. 5-10 years 3. 10-25 years 4. 25-50 years 5. Unsure
39.	What is the depth of the bore well/hand pump being used?	1. <= 10 meters 2. 10-25 meters 3. 25-50 meters 4. 50-100 meters 5. Unknown
40.	What is the frequency of cleaning the open well(s)?	1. 1-3 months 2. 3-6 months 3. 6-12 months 4. >12 months 5. Not once in a year 6. Unknown

FIGURE A.38: Questionnaire for perception study Page 4

Appendix B

Extra tables to refer

TABLE B.1: Preparation of pseudo-binary mixtures

weight%	Extractant mole fraction
0	0.000
5	0.099
10	0.189
20	0.344
30	0.473
40	0.583
50	0.677
60	0.759
70	0.830
80	0.894
90	0.950
100	1.000

TABLE B.2: Analysis of variance for two-phase extraction of $As^{(V)}$

Source	Sum of squares	df	Mean square	F-value	p-value
Model	10114.76	20	505.74	134.26	<0.0001
A	1502.24	1	1502.24	398.81	<0.0001
B	1372.24	1	1372.24	364.3	<0.0001
C	355.88	1	355.88	94.48	<0.0001
D	98.94	1	98.94	26.27	<0.0001
E	24.74	1	24.74	6.57	0.0158
AB	13.78	1	13.78	3.66	0.0657
AC	0.28	1	0.28	0.075	0.7866
AD	0.031	1	0.031	8.296×10^{-3}	0.9281
AE	0.28	1	0.28	0.075	0.7866
BC	7.03	1	7.03	1.87	0.1824
BD	7.03	1	7.03	1.87	0.1824
BE	0.28	1	0.28	0.075	0.7866
CD	0.78	1	0.78	0.21	0.6522
CE	0.28	1	0.28	0.075	0.7866
DE	0.031	1	0.031	8.296×10^{-3}	0.9281
A^2	1325.23	1	1325.23	351.82	<0.0001
B^2	3.26	1	3.26	0.86	0.3602
C^2	0.054	1	0.054	0.014	0.9057
D^2	0.054	1	0.054	0.014	0.9057
E^2	1.04	1	1.04	0.28	0.6038
Residual	109.24	29	3.77		
Lack of fit	96.36	22	4.38	2.38	0.1206
Pure error	12.87	7	1.84		
Total	10224	49			

TABLE B.3: Analysis of variance for two-phase extraction of $As^{(III)}$:$As^{(V)}$:: 1 : 1

Source	Sum of squares	df	Mean square	F-value	p-value
Model	9302.02	20	465.10	40.77	<0.0001
A	2434.28	1	2434.28	213.38	<0.0001
B	1163.92	1	1163.92	102.02	<0.0001
C	497.98	1	497.98	43.65	<0.0001
D	50.78	1	50.78	4.45	0.0436
E	104.62	1	104.62	9.17	0.0051
AB	241.45	1	241.45	21.16	<0.0001
AC	98.91	1	98.91	8.67	0.0063
AD	3.77	1	3.77	0.3302	0.5699
AE	30.65	1	30.65	2.69	0.1120
BC	49.55	1	49.55	4.34	0.0461
BD	0.4656	1	0.4656	0.0408	0.8413
BE	34.20	1	34.20	3.00	0.0940
CD	2.01	1	2.01	0.1762	0.6778
CE	1.17	1	1.17	0.1026	0.7510
DE	0.0162	1	0.0162	0.0014	0.9702
A^2	610.72	1	610.72	53.53	<0.0001
B^2	0.1501	1	0.1501	0.0132	0.9095
C^2	38.37	1	38.37	3.36	0.0769
D^2	5.46	1	5.46	0.4789	0.4944
E^2	28.57	1	28.57	2.50	0.1244
Residual	330.84	29	11.41		
Lack of Fit	292.34	22	13.29	2.42	0.1167
Pure Error	38.50	7	5.50		
Cor Total	9632.86	49			

TABLE B.4: Analysis of variance for two-phase extraction of $As^{(III)}$:$As^{(V)}$:: 1 : 2

Source	Sum of squares	df	Mean square	F-value	p-value
Model	6153.11	20	307.66	58.44	<0.0001
A	1514.62	1	1514.62	287.70	<0.0001
B	668.93	1	668.93	127.06	<0.0001
C	267.57	1	267.57	50.82	<0.0001
D	35.35	1	35.35	6.72	0.0148
E	20.05	1	20.05	3.81	0.0607
AB	6.26	1	6.26	1.19	0.2846
AC	5.18	1	5.18	0.9832	0.3296
AD	0.5592	1	0.5592	0.1062	0.7468
AE	4.18	1	4.18	0.7946	0.3800
BC	6.89	1	6.89	1.31	0.2619
BD	5.32	1	5.32	1.01	0.3230
BE	1.76	1	1.76	0.3348	0.5673
CD	0.4163	1	0.4163	0.0791	0.7805
CE	0.0185	1	0.0185	0.0035	0.9531
DE	2.14	1	2.14	0.4060	0.5290
A^2	667.18	1	667.18	126.73	<0.0001
B^2	0.4877	1	0.4877	0.0926	0.7630
C^2	0.5441	1	0.5441	0.1034	0.7501
D^2	0.0029	1	0.0029	0.0005	0.9815
E^2	3.71	1	3.71	0.7039	0.4083
Residual	152.67	29	5.26		
Lack of Fit	135.20	22	6.15	2.46	0.1119
Pure Error	17.48	7	2.50		
Cor Total	6305.79	49			

TABLE B.5: Analysis of variance for two-phase extraction of $As^{(III)}$:$As^{(V)}$:: 2 : 1

Source	Sum of squares	df	Mean square	F-value	p-value
Model	6312.37	20	315.62	53.75	<0.0001
A	1682.00	1	1682.00	286.44	<0.0001
B	931.15	1	931.15	158.57	<0.0001
C	388.50	1	388.50	66.16	<0.0001
D	26.82	1	26.82	4.57	0.0411
E	13.28	1	13.28	2.26	0.1434
AB	84.34	1	84.34	14.36	0.0007
AC	69.35	1	69.35	11.81	0.0018
AD	1.42	1	1.42	0.2410	0.6272
AE	11.10	1	11.10	1.89	0.1796
BC	22.56	1	22.56	3.84	0.0596
BD	7.29	1	7.29	1.24	0.2744
BE	3.00	1	3.00	0.5101	0.4808
CD	24.48	1	24.48	4.17	0.0504
CE	1.86	1	1.86	0.3163	0.5781
DE	0.2329	1	0.2329	0.0397	0.8435
A^2	441.10	1	441.10	75.12	<0.0001
B^2	0.6448	1	0.6448	0.1098	0.7428
C^2	11.75	1	11.75	2.00	0.1679
D^2	1.37	1	1.37	0.2334	0.6326
E^2	6.17	1	6.17	1.05	0.3138
Residual	170.29	29	5.87		
Lack of Fit	150.44	22	6.84	2.41	0.1172
Pure Error	19.85	7	2.84		
Cor Total	6482.66	49			

TABLE B.6: Spearman's correlational analysis for the extraction of combined arsenic ions in two-phase system

Type	Variables	Parameters	A	B	C	D	E	%Ex
$As^{(III)}$:$As^{(V)}$:: 1 : 1	A	Correlation coefficient	1	0	0	0	0	-0.503
		Significance (two-tailed)	-	1	1	1	1	0
	B	Correlation coefficient	0	1	0	0	0	0.269
		Significance (two-tailed)	1	-	1	1	1	0.059
	C	Correlation coefficient	0	0	1	0	0	0.155
		Significance (two-tailed)	1	1	-	1	1	0.284
	D	Correlation coefficient	0	0	0	1	0	0.069
		Significance (two-tailed)	1	1	1	-	1	0.634
	E	Correlation coefficient	0	0	0	0	1	0.061
		Significance (two-tailed)	1	1	1	1	-	0.676
	%Ex	Correlation coefficient	-0.503	0.269	0.155	0.069	0.061	1
		Significance (two-tailed)	0	0.059	0.284	0.634	0.676	-
$As^{(III)}$:$As^{(V)}$:: 1 : 2	A	Correlation coefficient	1	0	0	0	0	-0.486
		Significance (two-tailed)	-	1	1	1	1	0
	B	Correlation coefficient	0	1	0	0	0	0.254
		Significance (two-tailed)	1	-	1	1	1	0.075
	C	Correlation coefficient	0	0	1	0	0	0.133
		Significance (two-tailed)	1	1	-	1	1	0.358
	D	Correlation coefficient	0	0	0	1	0	0.077
		Significance (two-tailed)	1	1	1	-	1	0.594
	E	Correlation coefficient	0	0	0	0	1	0.047
		Significance (two-tailed)	1	1	1	1	-	0.746
	%Ex	Correlation coefficient	-0.486	0.254	0.133	0.077	0.047	1
		Significance (two-tailed)	0	0.075	0.358	0.594	0.746	-
$As^{(III)}$:$As^{(V)}$:: 2 : 1	A	Correlation coefficient	1	0	0	0	0	-0.439
		Significance (two-tailed)	-	1	1	1	1	0.001
	B	Correlation coefficient	0	1	0	0	0	0.301
		Significance (two-tailed)	1	-	1	1	1	0.034
	C	Correlation coefficient	0	0	1	0	0	0.187
		Significance (two-tailed)	1	1	-	1	1	0.195
	D	Correlation coefficient	0	0	0	1	0	0.054
		Significance (two-tailed)	1	1	1	-	1	0.711
	E	Correlation coefficient	0	0	0	0	1	0.044
		Significance (two-tailed)	1	1	1	1	-	0.763
	%Ex	Correlation coefficient	-0.439	0.301	0.187	0.054	0.044	1
		Significance (two-tailed)	0.001	0.034	0.195	0.711	0.763	-

TABLE B.7: Univariate analysis of variance for extraction of $As^{(V)}$in two phase

Source	Type III Sum of Squares	df	Mean Square	F	Significance
Corrected model	10211.125	42	243.122	132.183	0.000
Intercept	68246.109	1	68246.109	37104.681	0.000
A	1934.578	2	967.289	525.905	0.000
B	1122.421	2	561.210	305.124	0.000
C	313.490	2	156.745	85.221	0.000
D	99.330	2	49.665	27.002	0.001
E	36.544	2	18.272	9.934	0.009
AB	13.781	1	13.781	7.493	0.029
AC	0.281	1	0.281	0.153	0.707
AD	0.031	1	0.031	0.017	0.900
AE	0.281	1	0.281	0.153	0.707
BC	7.031	1	7.031	3.823	0.091
BD	7.031	1	7.031	3.823	0.091
BE	0.281	1	0.281	0.153	0.707
CD	0.781	1	0.781	0.425	0.535
CE	0.281	1	0.281	0.153	0.707
DE	0.031	1	0.031	0.017	0.900
ABC	9.031	1	9.031	4.910	0.062
ABD	0.781	1	0.781	0.425	0.535
ABE	0.031	1	0.031	0.017	0.900
ACD	1.531	1	1.531	0.833	0.392
ACE	0.031	1	0.031	0.017	0.900
ADE	0.031	1	0.031	0.017	0.900
BCD	2.531	1	2.531	1.376	0.279
BCE	0.031	1	0.031	0.017	0.900
BDE	0.281	1	0.281	0.153	0.707
CDE	0.031	1	0.031	0.017	0.900
ABCD	0.281	1	0.281	0.153	0.707
ABCE	0.781	1	0.781	0.425	0.535
ABDE	0.281	1	0.281	0.153	0.707
ACDE	0.031	1	0.031	0.017	0.900
BCDE	0.281	1	0.281	0.153	0.707
ABCDE	0.281	1	0.281	0.153	0.707
Error	12.875	7	1.839		
Total	176112	50			
Corrected total	10224	49			

TABLE B.8: Univariate analysis of variance for extraction of $As^{(III)}$:$As^{(V)}$:: 1 : 1 in two phase

Source	Type III Sum of Squares	df	Mean Square	F	Significance
Corrected model	9594.356	42	228.437	41.533	0.000
Intercept	86311.733	1	86311.733	15692.716	0.000
A	1887.962	2	943.981	171.629	0.000
B	769.911	2	384.955	69.990	0.000
C	485.347	2	242.674	44.122	0.000
D	48.462	2	24.231	4.406	0.058
E	173.962	2	86.981	15.814	0.003
AB	241.450	1	241.450	43.899	0.000
AC	98.912	1	98.912	17.984	0.004
AD	3.768	1	3.768	0.685	0.435
AE	30.654	1	30.654	5.573	0.050
BC	49.551	1	49.551	9.009	0.020
BD	0.466	1	0.466	0.085	0.780
BE	34.196	1	34.196	6.217	0.041
CD	2.010	1	2.010	0.365	0.565
CE	1.170	1	1.170	0.213	0.659
DE	0.016	1	0.016	0.003	0.958
ABC	126.405	1	126.405	22.982	0.002
ABD	4.061	1	4.061	0.738	0.419
ABE	47.971	1	47.971	8.722	0.021
ACD	0.054	1	0.054	0.010	0.924
ACE	0.041	1	0.041	0.007	0.934
ADE	1.665	1	1.665	0.303	0.599
BCD	0.140	1	0.140	0.026	0.878
BCE	0.006	1	0.006	0.001	0.976
BDE	1.337	1	1.337	0.243	0.637
CDE	1.240	1	1.240	0.226	0.649
ABCD	1.25×10^{-5}	1	1.25×10^{-5}	0	0.999
ABCE	0.011	1	0.011	0.002	0.965
ABDE	0.572	1	0.572	0.104	0.756
ACDE	0.442	1	0.442	0.080	0.785
BCDE	0.120	1	0.120	0.022	0.887
ABCDE	0.308	1	0.308	0.056	0.820
Error	38.501	7	5.5		
Total	227550.353	50			
Corrected total	9632.857	49			

TABLE B.9: Univariate analysis of variance for extraction of $As^{(III)}$:$As^{(V)}$:: 1 : 2 in two phase

Source	Type III Sum of Squares	df	Mean Square	F	Significance
Corrected model	6288.312	42	149.722	59.973	0
Intercept	97072.087	1	97072.087	38883.494	0
A	1330.526	2	665.263	266.480	0
B	431.747	2	215.874	86.471	0
C	173.646	2	86.823	34.778	0
D	43.615	2	21.808	8.735	0.013
E	26.719	2	13.359	5.351	0.039
AB	6.257	1	6.257	2.506	0.157
AC	5.176	1	5.176	2.073	0.193
AD	0.559	1	0.559	0.224	0.650
AE	4.183	1	4.183	1.676	0.237
BC	6.891	1	6.891	2.760	0.141
BD	5.322	1	5.322	2.132	0.188
BE	1.763	1	1.763	0.706	0.429
CD	0.416	1	0.416	0.167	0.695
CE	0.019	1	0.019	0.007	0.934
DE	2.137	1	2.137	0.856	0.386
ABC	87.417	1	87.417	35.016	0.001
ABD	5.192	1	5.192	2.080	0.192
ABE	1.616	1	1.616	0.647	0.448
ACD	0.102	1	0.102	0.041	0.845
ACE	0.014	1	0.014	0.006	0.942
ADE	0.717	1	0.717	0.287	0.609
BCD	1.449	1	1.449	0.581	0.471
BCE	0.454	1	0.454	0.182	0.683
BDE	0.888	1	0.888	0.356	0.570
CDE	0.000	1	0.000	0.000	0.991
ABCD	1.744	1	1.744	0.698	0.431
ABCE	1.81	1	1.81	0.725	0.423
ABDE	0.493	1	0.493	0.197	0.670
ACDE	0.131	1	0.131	0.053	0.825
BCDE	0.027	1	0.027	0.011	0.920
ABCDE	0.003	1	0.003	0.001	0.973
Error	17.475	7	2.496		
Total	245909.434	50			
Corrected total	6305.788	49			

TABLE B.10: Univariate analysis of variance for extraction of $As^{(III)}$:$As^{(V)}$:: 2 : 1 in two phase

Source	Type III Sum of Squares	df	Mean Square	F	Significance
Corrected model	6462.812	42	153.876	54.263	0
Intercept	90398.897	1	90398.897	31878.403	0
A	1302.070	2	651.035	229.582	0
B	630.156	2	315.078	111.110	0
C	289.441	2	144.721	51.035	0
D	37.953	2	18.977	6.692	0.024
E	21.296	2	10.648	3.755	0.078
AB	84.338	1	84.338	29.741	0.001
AC	69.355	1	69.355	24.457	0.002
AD	1.415	1	1.415	0.499	0.503
AE	11.104	1	11.104	3.916	0.088
BC	22.562	1	22.562	7.956	0.026
BD	7.287	1	7.287	2.570	0.153
BE	2.995	1	2.995	1.056	0.338
CD	24.483	1	24.483	8.634	0.022
CE	1.858	1	1.858	0.655	0.445
DE	0.233	1	0.233	0.082	0.783
ABC	45.054	1	45.054	15.888	0.005
ABD	1.791	1	1.791	0.632	0.453
ABE	1.333	1	1.333	0.470	0.515
ACD	15.806	1	15.806	5.574	0.050
ACE	0.144	1	0.144	0.051	0.828
ADE	3.665	1	3.665	1.293	0.293
BCD	0.342	1	0.342	0.121	0.738
BCE	7.249	1	7.249	2.556	0.154
BDE	8.915	1	8.915	3.144	0.120
CDE	8.333	1	8.333	2.939	0.130
ABCD	0.029	1	0.029	0.010	0.922
ABCE	16.661	1	16.661	5.875	0.046
ABDE	1.005	1	1.005	0.354	0.570
ACDE	4.111	1	4.111	1.450	0.268
BCDE	0.100	1	0.100	0.035	0.856
ABCDE	1.324	1	1.324	0.467	0.516
Error	19.850	7	2.836		
Total	229105.954	50			
Corrected total	6482.662	49			

TABLE B.11: Analysis of variance for extraction and recovery of $As^{(III)}$in 3 phase SLM

Type	Source	Sum of squares	Degree of freedom	Mean square	F-value	p-value
Extraction of $As^{(III)}$	Model	1834.15	9	203.79	23.14	<0.0001
	F	9.25	1	9.25	1.05	0.3295
	G	162.57	1	162.57	18.46	0.0016
	H1	23.35	1	23.35	2.65	0.1345
	FG	0.40	1	0.40	0.045	0.8354
	FH1	0.47	1	0.47	0.053	0.8228
	GH1	0.20	1	0.20	0.022	0.8846
	F^2	36.06	1	36.06	4.10	0.0705
	G^2	425.67	1	425.67	48.34	<0.0001
	$H1^2$	54.49	1	54.49	6.19	0.0321
	Residual	88.06	10	8.81		
	Lack of fit	40.20	5	8.04	0.84	0.5736
	Pure error	47.87	5	9.57		
	Corrected total	1922.21	19			
Recovery of $As^{(III)}$	Model	1657.82	9	184.20	15.41	<0.0001
	F	25.34	1	25.34	2.12	0.1760
	G	109.10	1	109.10	9.13	0.0129
	H1	33.67	1	33.67	2.82	0.1242
	FG	7.84	1	7.84	0.66	0.4368
	FH1	0.29	1	0.29	0.024	0.8796
	GH1	3.10	1	3.10	0.26	0.6216
	F^2	12.82	1	12.82	1.07	0.3248
	G^2	320.41	1	320.41	26.81	0.0004
	$H1^2$	120.30	1	120.30	10.06	0.0099
	Residual	119.53	10	11.95		
	Lack of fit	27.24	5	5.45	0.30	0.8967
	Pure error	92.29	5	18.46		
	Corrected total	1777.35	19			

TABLE B.12: Analysis of variance for extraction and recovery of $As^{(V)}$ in 3 phase SLM

Type	Source	Sum of squares	Degree of freedom	Mean square	F-value	p-value
Extraction of $As^{(V)}$	Model	2444.28	9	271.59	38.85	<0.0001
	F	202.95	1	202.95	29.03	0.0003
	G	8.63	1	8.63	1.23	0.2925
	H1	28.12	1	28.12	4.02	0.0727
	FG	6.44	1	6.44	0.92	0.3597
	FH1	9.8×10^{-3}	1	9.8×10^{-3}	1.402×10^{-3}	0.9709
	GH1	0.44	1	0.44	0.063	0.8066
	F^2	528.24	1	528.24	75.56	<0.0001
	G^2	149.76	1	149.76	21.42	0.0009
	$H1^2$	17.32	1	17.32	2.48	0.1466
	Residual	69.91	10	6.99		
	Lack of fit	47.48	5	9.50	2.12	0.2151
	Pure error	22.44	5	4.49		
	Corrected total	2514.19	19			
Recovery of $As^{(V)}$	Model	2643.34	9	293.70	41.99	<0.0001
	F	182.07	1	182.07	26.03	0.0005
	G	0.40	1	0.40	0.057	0.8158
	H1	54.94	1	54.94	7.85	0.0187
	FG	4.50	1	4.50	0.64	0.4412
	FH1	2.00	1	2.00	0.29	0.6045
	GH1	18.00	1	18.00	2.57	0.1398
	F^2	651.00	1	651.00	93.06	<0.0001
	G^2	45.13	1	45.13	6.45	0.0294
	$H1^2$	74.39	1	74.39	10.63	0.0086
	Residual	69.95	10	7.00		
	Lack of fit	43.12	5	8.62	1.61	0.3077
	Pure error	26.83	5	5.37		
	Corrected total	2713.29	19			

TABLE B.13: Analysis of variance for extraction and recovery of $As^{(III)}$:$As^{(V)}$:: 1 : 1 in 3 phase SLM

Type	Source	Sum of squares	Degree of freedom	Mean square	F-value	p-value
Extraction of $As^{(III)}$:$As^{(V)}$:: 1 : 1	Model	1466.08	9	162.90	102.29	<0.0001
	F	1056.99	1	1056.99	663.72	<0.0001
	G	39.24	1	39.24	24.64	0.0006
	H2	290.74	1	290.74	182.56	<0.0001
	FG	3.19	1	3.19	2.00	0.1875
	FH2	13.03	1	13.03	8.18	0.0169
	GH2	2.70	1	2.70	1.70	0.2219
	F^2	32.42	1	32.42	20.36	0.0011
	G^2	1.30	1	1.30	0.8135	0.3883
	$H2^2$	1.19	1	1.19	0.7491	0.4070
	Residual	15.93	10	1.59		
	Lack of Fit	11.84	5	2.37	2.90	0.1341
	Pure Error	4.09	5	0.8176		
	Corrected total	1482.01	19			
Recovery of $As^{(III)}$:$As^{(V)}$:: 1 : 1	Model	1428.01	9	158.67	103.57	<0.0001
	F	990.62	1	990.62	646.60	<0.0001
	G	20.08	1	20.08	13.11	0.0047
	H2	368.93	1	368.93	240.81	<0.0001
	FG	0.7321	1	0.7321	0.4778	0.5051
	FH2	12.60	1	12.60	8.22	0.0167
	GH2	0.2888	1	0.2888	0.1885	0.6734
	F^2	9.38	1	9.38	6.13	0.0328
	G^2	1.84	1	1.84	1.20	0.2992
	$H2^2$	0.2513	1	0.2513	0.1640	0.6940
	Residual	15.32	10	1.53		
	Lack of fit	10.63	5	2.13	2.26	0.1954
	Pure error	4.69	5	0.9389		
	Corrected total	1443.33	19			

TABLE B.14: Analysis of variance for extraction and recovery of $As^{(III)}$:$As^{(V)}$:: 1 : 2 in 3 phase SLM

Type	Source	Sum of squares	Degree of freedom	Mean square	F-value	p-value
Extraction of $As^{(III)}$:$As^{(V)}$:: 1 : 2	Model	1440.46	9	160.05	78.73	<0.0001
	F	1042.44	1	1042.44	512.76	<0.0001
	G	42.85	1	42.85	21.08	0.0010
	H2	273.53	1	273.53	134.55	<0.0001
	FG	2.00	1	2.00	0.9838	0.3447
	FH2	15.68	1	15.68	7.71	0.0195
	GH2	1.62	1	1.62	0.7969	0.3930
	F^2	33.60	1	33.60	16.53	0.0023
	G^2	1.01	1	1.01	0.4944	0.4980
	$H2^2$	0.9751	1	0.9751	0.4796	0.5044
	Residual	20.33	10	2.03		
	Lack of Fit	15.00	5	3.00	2.81	0.1405
	Pure Error	5.33	5	1.07		
	Corrected total	1460.79	19			
Recovery of $As^{(III)}$:$As^{(V)}$:: 1 : 2	Model	1426.00	9	158.44	102.23	<0.0001
	F	994.01	1	994.01	641.38	<0.0001
	G	19.88	1	19.88	12.83	0.0050
	H2	364.82	1	364.82	235.39	<0.0001
	FG	0.6050	1	0.6050	0.3904	0.5461
	FH2	11.52	1	11.52	7.43	0.0213
	GH2	0.4050	1	0.4050	0.2613	0.6203
	F^2	8.12	1	8.12	5.24	0.0451
	G^2	1.84	1	1.84	1.19	0.3013
	$H2^2$	0.6028	1	0.6028	0.3889	0.5468
	Residual	15.50	10	1.55		
	Lack of fit	11.12	5	2.22	2.54	0.1644
	Pure error	4.38	5	0.8750		
	Corrected total	1441.50	19			

TABLE B.15: Analysis of variance for extraction and recovery of $As^{(III)}$:$As^{(V)}$:: 2 : 1 in 3 phase SLM

Type	Source	Sum of squares	Degree of freedom	Mean square	F-value	p-value
Extraction of $As^{(III)}$:$As^{(V)}$:: 2 : 1	Model	1453.60	9	161.51	107.09	<0.0001
	F	1048.58	1	1048.58	695.26	<0.0001
	G	40.00	1	40.00	26.52	0.0004
	H2	287.30	1	287.30	190.49	<0.0001
	FG	3.25	1	3.25	2.16	0.1728
	FH2	12.25	1	12.25	8.12	0.0172
	GH2	3.00	1	3.00	1.99	0.1887
	F^2	28.64	1	28.64	18.99	0.0014
	G^2	0.9020	1	0.9020	0.5981	0.4572
	$H2^2$	1.88	1	1.88	1.25	0.2901
	Residual	15.08	10	1.51		
	Lack of Fit	12.04	5	2.41	3.96	0.0786
	Pure Error	3.04	5	0.6080		
	Corrected total	1468.68	19			
Recovery of $As^{(III)}$:$As^{(V)}$:: 2 : 1	Model	1430.36	9	158.93	102.19	<0.0001
	F	1004.00	1	1004.00	645.56	<0.0001
	G	18.22	1	18.22	11.72	0.0065
	H2	361.20	1	361.20	232.25	<0.0001
	FG	0.3200	1	0.3200	0.2058	0.6598
	FH2	10.58	1	10.58	6.80	0.0261
	GH2	0.1250	1	0.1250	0.0804	0.7826
	F^2	9.64	1	9.64	6.20	0.0320
	G^2	1.86	1	1.86	1.20	0.2996
	$H2^2$	0.2864	1	0.2864	0.1842	0.6769
	Residual	15.55	10	1.56		
	Lack of fit	10.80	5	2.16	2.27	0.1944
	Pure error	4.75	5	0.9507		
	Corrected total	1445.91	19			

TABLE B.16: Normality test for 3 phase SLM using Shapiro-Wilk model - Individual arsenic species

Independent variables	Range	df	$As^{(III)}$				$As^{(V)}$			
			Extraction		Recovery		Extraction		Recovery	
			Statistic	Significance	Statistic	Significance	Statistic	Significance	Statistic	Significance
F	1	5	0.961	0.813	0.878	0.299	0.914	0.492	0.933	0.619
	2	10	0.9	0.22	0.898	0.209	0.917	0.334	0.947	0.631
	3	5	0.952	0.75	0.982	0.947	0.978	0.925	0.961	0.816
G	3	5	0.967	0.853	0.97	0.875	0.867	0.254	0.948	0.72
	5	10	0.949	0.652	0.934	0.492	0.856	0.069	0.88	0.131
	7	5	0.915	0.501	0.947	0.715	0.928	0.584	0.94	0.665
H1	200	5	0.952	0.75	0.923	0.549	0.776	0.051	0.928	0.582
	250	10	0.895	0.194	0.886	0.151	0.817	0.023	0.868	0.096
	300	5	0.958	0.796	0.942	0.679	0.826	0.129	0.951	0.741

TABLE B.17: Normality test for 3 phase SLM using Shapiro-Wilk model - Combined arsenic species

Independent variables	Range	df	$As^{(III)}$:$As^{(V)}$:: 1 : 1				$As^{(III)}$:$As^{(V)}$:: 1 : 2			
			Extraction		Recovery		Extraction		Recovery	
			Statistic	Significance	Statistic	Significance	Statistic	Significance	Statistic	Significance
	1	5	0.981	0.94	0.939	0.661	0.98	0.934	0.936	0.64
F	2	10	0.918	0.345	0.949	0.659	0.92	0.359	0.953	0.702
	3	5	0.939	0.661	0.869	0.264	0.949	0.727	0.857	0.219
	3	5	0.952	0.751	0.97	0.876	0.943	0.69	0.974	0.898
G	5	10	0.885	0.148	0.915	0.315	0.886	0.154	0.915	0.318
	7	5	0.94	0.666	0.94	0.665	0.941	0.673	0.941	0.676
	10	5	0.907	0.451	0.851	0.196	0.901	0.414	0.85	0.196
H2	25	10	0.818	0.024	0.849	0.057	0.834	0.037	0.852	0.061
	40	5	0.908	0.456	0.916	0.502	0.924	0.553	0.915	0.498
			$As^{(III)}$:$As^{(V)}$:: 2 : 1							
	1	5	0.979	0.93	0.929	0.587				
F	2	10	0.906	0.257	0.947	0.633				
	3	5	0.935	0.631	0.871	0.272				
	3	5	0.952	0.75	0.971	0.881				
G	5	10	0.885	0.147	0.915	0.314				
	7	5	0.942	0.682	0.947	0.718				
	10	5	0.909	0.463	0.85	0.194				
H2	25	10	0.816	0.023	0.85	0.058				
	40	5	0.908	0.456	0.903	0.428				

TABLE B.18: Pearson correlational analysis in 3 phase SLM for single species arsenic

Type	Variables	Parameters	F	G	H	%Ex	%Re
$As^{(III)}$	F	Pearson Correlation	1	0	0	0.075	0.127
		Significance (two-tailed)	-	1	1	0.752	0.593
	G	Pearson Correlation	0	1	0	0.309	0.254
		Significance (two-tailed)	1	-	1	0.185	0.279
	H	Pearson Correlation	0	0	1	-0.103	-0.135
		Significance (two-tailed)	1	1	-	0.666	0.571
	%Ex	Pearson Correlation	0.075	0.309	-0.103	1	0.976
		Significance (two-tailed)	0.752	0.185	0.666	-	0
	%Re	Pearson Correlation	0.127	0.254	-0.135	0.976	1
		Significance (two-tailed)	0.593	0.279	0.571	0	-
$As^{(V)}$	F	Pearson Correlation	1	0	0	0.547	0.26
		Significance (two-tailed)	-	1	1	0.013	0.267
	G	Pearson Correlation	0	1	0	0.107	-0.012
		Significance (two-tailed)	1	-	1	0.653	0.960
	H	Pearson Correlation	0	0	1	-0.102	-0.145
		Significance (two-tailed)	1	1	-	0.670	0.541
	%Ex	Pearson Correlation	0.547	0.107	-0.102	1	0.907
		Significance (two-tailed)	0.013	0.653	0.670	-	0
	%Re	Pearson Correlation	0.260	-0.012	-0.145	0.907	1
		Significance (two-tailed)	0.267	0.960	0.541	0	-

TABLE B.19: Pearson correlational analysis in 3 phase SLM for combined salt arsenic

Type	Variables	Parameters	F	G	H	%Ex	%Re
$As^{(III)}$:$As^{(V)}$:: 1 : 1	F	Pearson Correlation	1	0	0	0.845	0.828
		Significance (two-tailed)	-	1	1	0	0
	G	Pearson Correlation	0	1	0	0.163	-0.118
		Significance (two-tailed)	1	-	1	0.493	0.62
	H	Pearson Correlation	0	0	1	0.443	0.506
		Significance (two-tailed)	1	1	-	0.05	0.023
	%Ex	Pearson Correlation	0.845	0.163	0.443	1	0.989
		Significance (two-tailed)	0	0.493	0.05	-	0
	%Re	Pearson Correlation	0.828	0.118	0.506	0.989	1
		Significance (two-tailed)	0	0.62	0.023	0	-
$As^{(III)}$:$As^{(V)}$:: 1 : 2	F	Pearson Correlation	1	0	0	0.845	0.83
		Significance (two-tailed)	-	1	1	0	0
	G	Pearson Correlation	0	1	0	0.171	0.117
		Significance (two-tailed)	1	-	1	0.47	0.622
	H	Pearson Correlation	0	0	1	0.433	0.503
		Significance (two-tailed)	1	1	-	0.057	0.024
	%Ex	Pearson Correlation	0.845	0.171	0.433	1	0.987
		Significance (two-tailed)	0	0.47	0.057	-	0
	%Re	Pearson Correlation	0.83	0.117	0.503	0.987	1
		Significance (two-tailed)	0	0.622	0.024	0	-
$As^{(III)}$:$As^{(V)}$:: 2 : 1	F	Pearson Correlation	1	0	0	0.845	0.833
		Significance (two-tailed)	-	1	1	0	0
	G	Pearson Correlation	0	1	0	0.165	0.112
		Significance (two-tailed)	1	-	1	0.487	0.637
	H	Pearson Correlation	0	0	1	0.442	0.5
		Significance (two-tailed)	1	1	-	0.051	0.025
	%Ex	Pearson Correlation	0.845	0.165	0.442	1	0.99
		Significance (two-tailed)	0	0.487	0.051	-	0
	%Re	Pearson Correlation	0.833	0.112	0.5	0.99	1
		Significance (two-tailed)	0	0.637	0.025	0	-

TABLE B.20: Multivariate Analysis of Variance (MANOVA) test for $As^{(III)}$in three phase

Effect		Value	F	Hypothesis df	Error df	Sig.	Partial η^2
Intercept	Pillai's Trace	0.999	2859.573	2	4	0	0.999
	Wilks' Lambda	0.001	2859.573	2	4	0	0.999
	Hotelling's Trace	1429.787	2859.573	2	4	0	0.999
	Roy's Largest Root	1429.787	2859.573	2	4	0	0.999
F	Pillai's Trace	1.057	2.804	4	10	0.085	0.529
	Wilks' Lambda	0.119	3.803	4	8	0.051	0.655
	Hotelling's Trace	5.937	4.452	4	6	0.052	0.748
	Roy's Largest Root	5.675	14.188	2	5	0.009	0.850
G	Pillai's Trace	0.974	2.372	4	10	0.122	0.487
	Wilks' Lambda	0.026	10.341	4	8	0.003	0.838
	Hotelling's Trace	37.075	27.806	4	6	0.001	0.949
	Roy's Largest Root	37.075	92.688	2	5	0	0.974
H1	Pillai's Trace	0.938	2.209	4	10	0.141	0.469
	Wilks' Lambda	0.075	5.304	4	8	0.022	0.726
	Hotelling's Trace	12.159	9.119	4	6	0.010	0.859
	Roy's Largest Root	12.144	30.361	2	5	0.002	0.924
FG	Pillai's Trace	0.230	0.597	2	4	0.593	0.230
	Wilks' Lambda	0.770	0.597	2	4	0.593	0.230
	Hotelling's Trace	0.299	0.597	2	4	0.593	0.230
	Roy's Largest Root	0.299	0.597	2	4	0.593	0.230
FH1	Pillai's Trace	0.028	0.059	2	4	0.944	0.028
	Wilks' Lambda	0.972	0.059	2	4	0.944	0.028
	Hotelling's Trace	0.029	0.059	2	4	0.944	0.028
	Roy's Largest Root	0.029	0.059	2	4	0.944	0.028
GH1	Pillai's Trace	0.230	0.597	2	4	0.593	0.230
	Wilks' Lambda	0.770	0.597	2	4	0.593	0.230
	Hotelling's Trace	0.299	0.597	2	4	0.593	0.230
	Roy's Largest Root	0.299	0.597	2	4	0.593	0.230
FGH1	Pillai's Trace	0.043	0.090	2	4	0.916	0.043
	Wilks' Lambda	0.957	0.090	2	4	0.916	0.043
	Hotelling's Trace	0.045	0.090	2	4	0.916	0.043
	Roy's Largest Root	0.045	0.090	2	4	0.916	0.043

TABLE B.21: Multivariate Analysis of Variance (MANOVA) test for $As^{(V)}$in three phase

Effect		Value	F	Hypothesis df	Error df	Sig.	Partial η^2
Intercept	Pillai's Trace	0.999	1665.929	2	4	0	0.999
	Wilks' Lambda	0.001	1665.929	2	4	0	0.999
	Hotelling's Trace	832.964	1665.929	2	4	0	0.999
	Roy's Largest Root	832.964	1665.929	2	4	0	0.999
F	Pillai's Trace	1.939	79.891	4	10	0	0.970
	Wilks' Lambda	0.001	65.929	4	8	0	0.971
	Hotelling's Trace	68.008	51.006	4	6	0	0.971
	Roy's Largest Root	42.470	106.174	2	5	0	0.977
G	Pillai's Trace	1.619	10.635	4	10	0.001	0.810
	Wilks' Lambda	0.017	13.271	4	8	0.001	0.869
	Hotelling's Trace	20.195	15.146	4	6	0.003	0.910
	Roy's Largest Root	18.150	45.376	2	5	0.001	0.948
H1	Pillai's Trace	1.326	4.923	4	10	0.019	0.663
	Wilks' Lambda	0.074	5.342	4	8	0.022	0.728
	Hotelling's Trace	7.077	5.308	4	6	0.036	0.780
	Roy's Largest Root	6.207	15.518	2	5	0.007	0.861
FG	Pillai's Trace	0.468	1.757	2	4	0.283	0.468
	Wilks' Lambda	0.532	1.757	2	4	0.283	0.468
	Hotelling's Trace	0.879	1.757	2	4	0.283	0.468
	Roy's Largest Root	0.879	1.757	2	4	0.283	0.468
FH1	Pillai's Trace	0.416	1.426	2	4	0.341	0.416
	Wilks' Lambda	0.584	1.426	2	4	0.341	0.416
	Hotelling's Trace	0.713	1.426	2	4	0.341	0.416
	Roy's Largest Root	0.713	1.426	2	4	0.341	0.416
GH1	Pillai's Trace	0.693	4.516	2	4	0.094	0.693
	Wilks' Lambda	0.307	4.516	2	4	0.094	0.693
	Hotelling's Trace	2.258	4.516	2	4	0.094	0.693
	Roy's Largest Root	2.258	4.516	2	4	0.094	0.693
FGH1	Pillai's Trace	0.555	2.496	2	4	0.198	0.555
	Wilks' Lambda	0.445	2.496	2	4	0.198	0.555
	Hotelling's Trace	1.248	2.496	2	4	0.198	0.555
	Roy's Largest Root	1.248	2.496	2	4	0.198	0.555

TABLE B.22: Multivariate Analysis of Variance (MANOVA) test for $As^{(III)}$:$As^{(V)}$:: 1 : 1 in three phase

Effect		Value	F	Hypothesis df	Error df	Sig.
Intercept	Pillai's Trace	1	16685.519	2	4	0
	Wilks' Lambda	0	16685.519	2	4	0
	Hotelling's Trace	8342.76	16685.519	2	4	0
	Roy's Largest Root	8342.76	16685.519	2	4	0
F	Pillai's Trace	1.319	4.847	4	10	0.02
	Wilks' Lambda	0.002	40.181	4	8	0
	Hotelling's Trace	300.734	225.55	4	6	0
	Roy's Largest Root	300.257	750.643	2	5	0
G	Pillai's Trace	1.353	5.227	4	10	0.016
	Wilks' Lambda	0.047	7.217	4	8	0.009
	Hotelling's Trace	11.744	8.808	4	6	0.011
	Roy's Largest Root	10.969	27.423	2	5	0.002
H2	Pillai's Trace	0.992	2.461	4	10	0.113
	Wilks' Lambda	0.011	16.948	4	8	0.001
	Hotelling's Trace	88.466	66.349	4	6	0
	Roy's Largest Root	88.462	221.156	2	5	0
FG	Pillai's Trace	0.44	1.573	2	4	0.313
	Wilks' Lambda	0.56	1.573	2	4	0.313
	Hotelling's Trace	0.786	1.573	2	4	0.313
	Roy's Largest Root	0.786	1.573	2	4	0.313
FH2	Pillai's Trace	0.794	7.729	2	4	0.042
	Wilks' Lambda	0.206	7.729	2	4	0.042
	Hotelling's Trace	3.865	7.729	2	4	0.042
	Roy's Largest Root	3.865	7.729	2	4	0.042
GH2	Pillai's Trace	0.564	2.582	2	4	0.19
	Wilks' Lambda	0.436	2.582	2	4	0.19
	Hotelling's Trace	1.291	2.582	2	4	0.19
	Roy's Largest Root	1.291	2.582	2	4	0.19
FGH2	Pillai's Trace	0.07	.149	2	4	0.866
	Wilks' Lambda	0.93	.149	2	4	0.866
	Hotelling's Trace	0.075	.149	2	4	0.866
	Roy's Largest Root	0.075	.149	2	4	0.866

TABLE B.23: Multivariate Analysis of Variance (MANOVA) test for $As^{(III)}$:$As^{(V)}$:: 1 : 2 in three phase

Effect		Value	F	Hypothesis df	Error df	Sig.
Intercept	Pillai's Trace	1	14664.853	2	4	0
	Wilks' Lambda	0	14664.853	2	4	0
	Hotelling's Trace	7332.426	14664.853	2	4	0
	Roy's Largest Root	7332.426	14664.853	2	4	0
F	Pillai's Trace	1.273	4.38	4	10	0.027
	Wilks' Lambda	0.003	37.494	4	8	0
	Hotelling's Trace	281.413	211.06	4	6	0
	Roy's Largest Root	281.03	702.575	2	5	0
G	Pillai's Trace	1.343	5.115	4	10	0.017
	Wilks' Lambda	0.052	6.73	4	8	0.011
	Hotelling's Trace	10.511	7.884	4	6	0.014
	Roy's Largest Root	9.737	24.342	2	5	0.003
H2	Pillai's Trace	1.067	2.861	4	10	0.081
	Wilks' Lambda	0.011	17.341	4	8	0.001
	Hotelling's Trace	85.221	63.916	4	6	0
	Roy's Largest Root	85.135	212.837	2	5	0
FG	Pillai's Trace	0.278	0.769	2	4	0.522
	Wilks' Lambda	0.722	0.769	2	4	0.522
	Hotelling's Trace	0.385	0.769	2	4	0.522
	Roy's Largest Root	0.385	0.769	2	4	0.522
FH2	Pillai's Trace	0.792	7.614	2	4	0.043
	Wilks' Lambda	0.208	7.614	2	4	0.043
	Hotelling's Trace	3.807	7.614	2	4	0.043
	Roy's Largest Root	3.807	7.614	2	4	0.043
GH2	Pillai's Trace	0.414	1.411	2	4	0.344
	Wilks' Lambda	0.586	1.411	2	4	0.344
	Hotelling's Trace	0.706	1.411	2	4	0.344
	Roy's Largest Root	0.706	1.411	2	4	0.344
FGH2	Pillai's Trace	0.164	0.392	2	4	0.699
	Wilks' Lambda	0.836	0.392	2	4	0.699
	Hotelling's Trace	0.196	0.392	2	4	0.699
	Roy's Largest Root	0.196	0.392	2	4	0.699

TABLE B.24: Multivariate Analysis of Variance (MANOVA) test for $As^{(III)}$:$As^{(V)}$:: 2 : 1 in three phase

Effect		Value	F	Hypothesis df	Error df	Sig.
Intercept	Pillai's Trace	1	18312.672	2	4	0
	Wilks' Lambda	0	18312.672	2	4	0
	Hotelling's Trace	9156.336	18312.672	2	4	0
	Roy's Largest Root	9156.336	18312.672	2	4	0
F	Pillai's Trace	1.237	4.05	4	10	0.033
	Wilks' Lambda	0.002	42.636	4	8	0
	Hotelling's Trace	378.253	283.69	4	6	0
	Roy's Largest Root	377.939	944.846	2	5	0
G	Pillai's Trace	1.294	4.581	4	10	0.023
	Wilks' Lambda	0.041	7.899	4	8	0.007
	Hotelling's Trace	15.299	11.474	4	6	0.006
	Roy's Largest Root	14.743	36.857	2	5	0.001
H2	Pillai's Trace	0.992	2.462	4	10	0.113
	Wilks' Lambda	0.009	18.669	4	8	0
	Hotelling's Trace	105.622	79.217	4	6	0
	Roy's Largest Root	105.62	264.051	2	5	0
FG	Pillai's Trace	0.53	2.255	2	4	0.221
	Wilks' Lambda	0.47	2.255	2	4	0.221
	Hotelling's Trace	1.127	2.255	2	4	0.221
	Roy's Largest Root	1.127	2.255	2	4	0.221
FH2	Pillai's Trace	0.816	8.891	2	4	0.034
	Wilks' Lambda	0.184	8.891	2	4	0.034
	Hotelling's Trace	4.445	8.891	2	4	0.034
	Roy's Largest Root	4.445	8.891	2	4	0.034
GH2	Pillai's Trace	0.595	2.938	2	4	0.164
	Wilks' Lambda	0.405	2.938	2	4	0.164
	Hotelling's Trace	1.469	2.938	2	4	0.164
	Roy's Largest Root	1.469	2.938	2	4	0.164
FGH2	Pillai's Trace	0.136	0.314	2	4	0.747
	Wilks' Lambda	0.864	0.314	2	4	0.747
	Hotelling's Trace	0.157	0.314	2	4	0.747
	Roy's Largest Root	0.157	0.314	2	4	0.747

TABLE B.25: Tests of between-subjects effects for $As^{(III)}$in three phase

Source	Dependent Variable	Type III Sum of Squares	df	Mean Square	F	Sig.	Partial η^2
Corrected Model	Extraction	2097.967	14	149.855	27.923	0.001	0.987
	Recovery	1769.300	14	126.379	36.108	0	0.990
Intercept	Extraction	25220.511	1	25220.511	4699.474	0	0.999
	Recovery	14910.897	1	14910.897	4260.256	0	0.999
F	Extraction	103.263	2	51.631	9.621	0.019	0.794
	Recovery	60.525	2	30.262	8.646	0.024	0.776
G	Extraction	663.935	2	331.968	61.857	0	0.961
	Recovery	379.900	2	189.950	54.271	0	0.956
H1	Extraction	140.066	2	70.033	13.050	0.010	0.839
	Recovery	171.080	2	85.540	24.440	0.003	0.907
FG	Extraction	0.125	1	0.125	0.023	0.885	0.005
	Recovery	4.500	1	4.500	1.286	0.308	0.205
FH1	Extraction	0.125	1	0.125	0.023	0.885	0.005
	Recovery	0.500	1	0.500	0.143	0.721	0.028
GH1	Extraction	0.125	1	0.125	0.023	0.885	0.005
	Recovery	4.500	1	4.500	1.286	0.308	0.205
FGH1	Extraction	1.125	1	1.125	0.210	0.666	0.040
	Recovery	0	1	0	0	1	0
Error	Extraction	26.833	5	5.367			
	Recovery	17.500	5	3.500			
Total	Extraction	50932	20				
	Recovery	31278	20				
Corrected Total	Extraction	2124.800	19				
	Recovery	1786.800	19				

TABLE B.26: Tests of between-subjects effects for $As^{(V)}$ in three phase

Source	Dependent Variable	Type III Sum of Squares	df	Mean Square	F	Sig.	Partial η^2
Corrected Model	Extraction	3102.200	14	221.586	26.379	0.001	0.987
	Recovery	2697.967	14	192.712	35.909	0	0.990
Intercept	Extraction	30645.551	1	30645.551	3648.280	0	0.999
	Recovery	11881.702	1	11881.702	2213.982	0	0.998
F	Extraction	1282.041	2	641.020	76.312	0	0.968
	Recovery	699.790	2	349.895	65.198	0	0.963
G	Extraction	102.426	2	51.213	6.097	0.046	0.709
	Recovery	78.648	2	39.324	7.327	0.033	0.746
H1	Extraction	164.883	2	82.442	9.814	0.019	0.797
	Recovery	152.501	2	76.250	14.208	0.009	0.850
FG	Extraction	0.125	1	0.125	0.015	0.908	0.003
	Recovery	4.500	1	4.500	0.839	0.402	0.144
FH1	Extraction	0.125	1	0.125	0.015	0.908	0.003
	Recovery	2	1	2	0.373	0.568	0.069
GH1	Extraction	3.125	1	3.125	0.372	0.569	0.069
	Recovery	18	1	18	3.354	0.127	0.401
FGH1	Extraction	1.125	1	1.125	0.134	0.729	0.026
	Recovery	2	1	2	0.373	0.568	0.069
Error	Extraction	42	5	8.400			
	Recovery	26.833	5	5.367			
Total	Extraction	60818	20				
	Recovery	28072	20				
Corrected Total	Extraction	3144.200	19				
	Recovery	2724.800	19				

TABLE B.27: Tests of between-subjects effects for $As^{(III)}$:$As^{(V)}$:: 1 : 1 in three phase

Source	Dependent Variable	Type III Sum of Squares	df	Mean Square	F	Sig.	Partial η^2
Corrected model	Extraction	1477.918	14	105.566	129.114	0	0.997
	Recovery	1438.632	14	102.759	109.447	0	0.997
Intercept	Extraction	33996.216	1	33996.216	41579.652	0	1
	Recovery	12855.28	1	12855.28	13691.901	0	1
F	Extraction	1025.636	2	512.818	627.211	0	0.996
	Recovery	961.409	2	480.705	511.989	0	0.995
G	Extraction	44.224	2	22.112	27.044	0.002	0.915
	Recovery	22.344	2	11.172	11.899	0.013	0.826
H2	Extraction	259.312	2	129.656	158.578	0	0.984
	Recovery	334.568	2	167.284	178.171	0	0.986
FG	Extraction	3.188	1	3.188	3.899	0.105	0.438
	Recovery	0.732	1	0.732	0.78	0.418	0.135
FH2	Extraction	13.031	1	13.031	15.937	0.01	0.761
	Recovery	12.6	1	12.6	13.42	0.015	0.729
GH2	Extraction	2.703	1	2.703	3.306	0.129	0.398
	Recovery	0.289	1	0.289	0.308	0.603	0.058
FGH2	Extraction	0.3	1	0.3	0.367	0.571	0.068
	Recovery	0.14	1	0.14	0.15	0.715	0.029
Error	Extraction	4.088	5	0.818			
	Recovery	4.694	5	0.939			
Total	Extraction	55781.669	20				
	Recovery	22131.855	20				
Corrected total	Extraction	1482.006	19				
	Recovery	1443.327	19				

TABLE B.28: Tests of between-subjects effects for $As^{(III)}$:$As^{(V)}$:: 1 : 2 in three phase

Source	Dependent Variable	Type III Sum of Squares	df	Mean Square	F	Sig.	Partial η^2
Corrected model	Extraction	1455.456	14	103.961	97.464	0	0.996
	Recovery	1437.122	14	102.652	117.316	0	0.997
Intercept	Extraction	36649.508	1	36649.508	34358.914	0	1
	Recovery	14517.568	1	14517.568	16591.506	0	1
F	Extraction	1013.48	2	506.74	475.069	0	0.995
	Recovery	967.239	2	483.619	552.708	0	0.995
G	Extraction	48.004	2	24.002	22.502	0.003	0.9
	Recovery	22.592	2	11.296	12.910	0.011	0.838
H2	Extraction	243.21	2	121.605	114.005	0	0.979
	Recovery	331.999	2	165.999	189.714	0	0.987
FG	Extraction	2	1	2	1.875	0.229	0.273
	Recovery	0.605	1	0.605	0.691	0.444	0.121
FH2	Extraction	15.68	1	15.68	14.7	0.012	0.746
	Recovery	11.52	1	11.52	13.166	0.015	0.725
GH2	Extraction	1.62	1	1.62	1.519	0.273	0.233
	Recovery	0.405	1	0.405	0.463	0.527	0.085
FGH2	Extraction	0.98	1	0.98	0.919	0.382	0.155
	Recovery	0.045	1	0.045	0.051	0.830	0.010
Error	Extraction	5.333	5	1.067			
	Recovery	4.375	5	0.875			
Total	Extraction	59899.65	20				
	Recovery	24800.11	20				
Corrected total	Extraction	1460.790	19				
	Recovery	1441.497	19				

TABLE B.29: Tests of between-subjects effects for $As^{(III)}$:$As^{(V)}$:: 2 : 1 in three phase

Source	Dependent Variable	Type III Sum of Squares	df	Mean Square	F	Sig.	Partial η^2
Corrected model	Extraction	1465.642	14	104.689	172.185	0	0.998
	Recovery	1441.159	14	102.940	108.282	0	0.997
Intercept	Extraction	27835.261	1	27835.261	45781.680	0	1
	Recovery	9117.061	1	9117.061	9590.177	0	0.999
F	Extraction	1013.248	2	506.624	833.263	0	0.997
	Recovery	972.497	2	486.249	511.482	0	0.995
G	Extraction	44.612	2	22.306	36.688	0.001	0.936
	Recovery	20.749	2	10.374	10.913	0.015	0.814
H2	Extraction	255.939	2	127.970	210.477	0	0.988
	Recovery	328.707	2	164.354	172.882	0	0.986
FG	Extraction	3.251	1	3.251	5.347	0.069	0.517
	Recovery	0.32	1	0.32	0.337	0.587	0.063
FH2	Extraction	12.251	1	12.251	20.15	0.006	0.801
	Recovery	10.58	1	10.58	11.129	0.021	0.69
GH2	Extraction	3.001	1	3.001	4.936	0.077	0.497
	Recovery	0.125	1	0.125	0.131	0.732	0.026
FGH2	Extraction	0.451	1	0.451	0.742	0.428	0.129
	Recovery	0.32	1	0.32	0.337	0.587	0.063
Error	Extraction	3.04	5	0.608			
	Recovery	4.753	5	0.951			
Total	Extraction	45968.86	20				
	Recovery	16155.8	20				
Corrected total	Extraction	1468.682	19				
	Recovery	1445.912	19				

TABLE B.30: Post hoc (Tukey HSD) analyses for $As^{(III)}$in three phase

Dep. Var.	F_i	F_j	Mean Diff. (F_i−F_j)	Std. Error	Sig.	95% Confidence Interval	
						Lower bound	Upper bound
Extraction	1	2	-15.3*	1.26886	0	-19.4288	-11.1712
		3	-2.2	1.46515	0.366	-6.9675	2.5675
	2	1	15.3*	1.26886	0	11.1712	19.4288
		3	13.1*	1.26886	0	8.9712	17.2288
	3	1	2.2	1.46515	0.366	-2.5675	6.9675
		2	-13.1*	1.26886	0	-17.2288	-8.9712
Recovery	1	2	-14.7*	1.02470	0	-18.0343	-11.3657
		3	-3.4	1.18322	0.076	-7.2501	0.4501
	2	1	14.7*	1.02470	0	11.3657	18.0343
		3	11.3*	1.02470	0	7.9657	14.6343
	3	1	3.4	1.18322	0.076	-0.4501	7.2501
		2	-11.3*	1.02470	0	-14.6343	-7.9657
	G_i	G_j	(G_i−G_j)				
Extraction	3	5	-22.7*	1.26886	0	-26.8288	-18.5712
		7	-9*	1.46515	0.004	-13.7675	-4.2325
	5	3	22.7*	1.26886	0	18.5712	26.8288
		7	13.7*	1.26886	0	9.5712	17.8288
	7	3	9*	1.46515	0.004	4.2325	13.7675
		5	-13.7*	1.26886	0	-17.8288	-9.5712
Recovery	3	5	-19.8*	1.02470	0	-23.1343	-16.4657
		7	-6.8*	1.18322	0.005	-10.6501	-2.9499
	5	3	19.8*	1.02470	0	16.4657	23.1343
		7	13*	1.02470	0	9.6657	16.3343
	7	3	6.8*	1.18322	0.005	2.9499	10.6501
		5	-13*	1.02470	0	-16.3343	-9.6657
	$H1_i$	$H1_j$	($H1_i$−$H1_j$)				
Extraction	200	250	-13.1*	1.26886	0	-17.2288	-8.9712
		300	3	1.46515	0.196	-1.7675	7.7675
	250	200	13.1*	1.26886	0	8.9712	17.2288
		300	16.1*	1.26886	0	11.9712	20.2288
	300	200	-3	1.46515	0.196	-7.7675	1.7675
		250	-16.1*	1.26886	0	-20.2288	-11.9712
Recovery	200	250	-13*	1.02470	0	-16.3343	-9.6657
		300	3.6	1.18322	0.063	-0.2501	7.4501
	250	200	13*	1.02470	0	9.6657	16.3343
		300	16.6*	1.02470	0	13.2657	19.9343
	300	200	-3.6	1.18322	0.063	-7.4501	0.2501
		250	-16.6*	1.02470	0	-19.9343	-13.2657

TABLE B.31: Post hoc (Tukey HSD) analyses for $As^{(V)}$in three phase

Dep. Var.	F_i	F_j	Mean Diff. (F_i−F_j)	Std. Error	Sig.	95% Confidence Interval	
						Lower bound	Upper bound
Extraction	1	2	-28.5*	1.58745	0	-33.6654	-23.3346
		3	-19.4*	1.83303	0	-25.3645	-13.4355
	2	1	28.5*	1.58745	0	23.3346	33.6654
		3	9.1*	1.58745	0.005	3.9346	14.2654
	3	1	19.4*	1.83303	0	13.4355	25.3645
		2	-9.1*	1.58745	0.005	-14.2654	-3.9346
Recovery	1	2	-25.3*	1.26886	0	-29.4288	-21.1712
		3	-8.6*	1.46515	0.005	-13.3675	-3.8325
	2	1	25.3*	1.26886	0	21.1712	29.4288
		3	16.7*	1.26886	0	12.5712	20.8288
	3	1	8.6*	1.46515	0.005	3.8325	13.3675
		2	-16.7*	1.26886	0	-20.8288	-12.5712
	G_i	G_j	(G_i−G_j)				
Extraction	3	5	-16.3*	1.58745	0	-21.4654	-11.1346
		7	-3.8	1.83303	0.190	-9.7645	2.1645
	5	3	16.3*	1.58745	0	11.1346	21.4654
		7	12.5*	1.58745	0.001	7.3346	17.6654
	7	3	3.8	1.83303	0.190	-2.1645	9.7645
		5	-12.5*	1.58745	0.001	-17.6654	-7.3346
Recovery	3	5	-16.2*	1.26886	0	-20.3288	-12.0712
		7	0.4000	1.46515	0.960	-4.3675	5.1675
	5	3	16.2*	1.26886	0	12.0712	20.3288
		7	16.6*	1.26886	0	12.4712	20.7288
	7	3	-0.4000	1.46515	0.960	-5.1675	4.3675
		5	-16.6*	1.26886	0	-20.7288	-12.4712
	$H1_i$	$H1_j$	($H1_i$−$H1_j$)				
Extraction	200	250	-14.4*	1.58745	0.001	-19.5654	-9.2346
		300	3.6000	1.83303	0.216	-2.3645	9.5645
	250	200	14.4*	1.58745	0.001	9.2346	19.5654
		300	18.0*	1.58745	0	12.8346	23.1654
	300	200	-3.6000	1.83303	0.216	-9.5645	2.3645
		250	-18.0*	1.58745	0	-23.1654	-12.8346
Recovery	200	250	-14.4*	1.26886	0	-18.5288	-10.2712
		300	4.8*	1.46515	0.049	0.0325	9.5675
	250	200	14.4*	1.26886	0	10.2712	18.5288
		300	19.2*	1.26886	0	15.0712	23.3288
	300	200	-4.8*	1.46515	0.049	-9.5675	-0.0325
		250	-19.2*	1.26886	0	-23.3288	-15.0712

TABLE B.32: Post hoc (Tukey HSD) analyses for $As^{(III)}$:$As^{(V)}$:: 1 : 1 in three phase

Dep. Var.	F_i	F_j	Mean Diff. (F_i−F_j)	Std. Error	Sig.	95% Confidence Interval	
						Lower bound	Upper bound
Extraction	1	2	-13.6980	0.49526	0	-15.3095	-12.0865
		3	-20.5620	0.57188	0	-22.4228	-18.7012
	2	1	13.6980	0.49526	0	12.0865	15.3095
		3	-6.8640	0.49526	0	-8.4755	-5.2525
	3	1	20.5620	0.57188	0	18.7012	22.4228
		2	6.8640	0.49526	0	5.2525	8.4755
Recovery	1	2	-12.4720	0.53072	0	-14.1989	-10.7451
		3	-19.9060	0.61283	0	-21.9001	-17.9119
	2	1	12.4720	0.53072	0	10.7451	14.1989
		3	-7.4340	0.53072	0	-9.1609	-5.7071
	3	1	19.9060	0.61283	0	17.9119	21.9001
		2	7.4340	0.53072	0	5.7071	9.1609
	G_i	G_j	(G_i−G_j)				
Extraction	3	5	-3.7500	0.49526	0.001	-5.3615	-2.1385
		7	-3.9620	0.57188	0.002	-5.8228	-2.1012
	5	3	3.7500	0.49526	0.001	2.1385	5.3615
		7	-0.2120	0.49526	0.906	-1.8235	1.3995
	7	3	3.9620	0.57188	0.002	2.1012	5.8228
		5	0.2120	0.49526	0.906	-1.3995	1.8235
Recovery	3	5	-3.5240	0.53072	0.003	-5.2509	-1.7971
		7	-2.8340	0.61283	0.013	-4.8281	-0.8399
	5	3	3.5240	0.53072	0.003	1.7971	5.2509
		7	0.6900	0.53072	0.454	-1.0369	2.4169
	7	3	2.8340	0.61283	0.013	0.8399	4.8281
		5	-0.6900	0.53072	0.454	-2.4169	1.0369
	$H2_i$	$H2_j$	($H2_i$−$H2_j$)				
Extraction	10	25	-7.6990	0.49526	0	-9.3105	-6.0875
		40	-10.7840	0.57188	0	-12.6448	-8.9232
	25	10	7.6990	0.49526	0	6.0875	9.3105
		40	-3.0850	0.49526	0.004	-4.6965	-1.4735
	40	10	10.7840	0.57188	0	8.9232	12.6448
		25	3.0850	0.49526	0.004	1.4735	4.6965
Recovery	10	25	-7.9750	0.53072	0	-9.7019	-6.2481
		40	-12.1480	0.61283	0	-14.1421	-10.1539
	25	10	7.9750	0.53072	0	6.2481	9.7019
		40	-4.1730	0.53072	0.001	-5.8999	-2.4461
	40	10	12.1480	0.61283	0	10.1539	14.1421
		25	4.1730	0.53072	0.001	2.4461	5.8999

TABLE B.33: Post hoc (Tukey HSD) analyses for $As^{(III)}$:$As^{(V)}$:: 1 : 2 in three phase

Dep. Var.	F_i	F_j	Mean Diff. (F_i−F_j)	Std. Error	Sig.	95% Confidence Interval	
						Lower bound	Upper bound
Extraction	1	2	-13.7	0.56569	0	-15.5407	-11.8593
		3	-20.42	0.65320	0	-22.5454	-18.2946
	2	1	13.7	0.56569	0	11.8593	15.5407
		3	-6.72	0.56569	0	-8.5607	-4.8793
	3	1	20.42	0.65320	0	18.2946	22.5454
		2	6.72	0.56569	0	4.8793	8.5607
Recovery	1	2	-12.46	0.51235	0	-14.1271	-10.7929
		3	-19.94	0.59161	0	-21.8650	-18.0150
	2	1	12.46	0.51235	0	10.7929	14.1271
		3	-7.48	0.51235	0	-9.1471	-5.8129
	3	1	19.94	0.59161	0	18.0150	21.8650
		2	7.48	0.51235	0	5.8129	9.1471
	G_i	G_j	(G_i−G_j)				
Extraction	3	5	-3.92	0.56569	0.002	-5.7607	-2.0793
		7	-4.14	0.65320	0.003	-6.2654	-2.0146
	5	3	3.92	0.56569	0.002	2.0793	5.7607
		7	-0.22	0.56569	0.921	-2.0607	1.6207
	7	3	4.14	0.65320	0.003	2.0146	6.2654
		5	0.22	0.56569	0.921	-1.6207	2.0607
Recovery	3	5	-3.54	0.51235	0.002	-5.2071	-1.8729
		7	-2.82	0.59161	0.012	-4.7450	-0.8950
	5	3	3.54	0.51235	0.002	1.8729	5.2071
		7	0.72	0.51235	0.406	-0.9471	2.3871
	7	3	2.82	0.59161	0.012	0.8950	4.7450
		5	-0.72	0.51235	0.406	-2.3871	0.9471
	$H2_i$	$H2_j$	($H2_i$−$H2_j$)				
Extraction	10	25	-7.56	0.56569	0	-9.4007	-5.7193
		40	-10.46	0.65320	0	-12.5854	-8.3346
	25	10	7.56	0.56569	0	5.7193	9.4007
		40	-2.9	0.56569	0.008	-4.7407	-1.0593
	40	10	10.46	0.65320	0	8.3346	12.5854
		25	2.9	0.56569	0.008	1.0593	4.7407
Recovery	10	25	-8.03	0.51235	0	-9.6971	-6.3629
		40	-12.08	0.59161	0	-14.0050	-10.1550
	25	10	8.03	0.51235	0	6.3629	9.6971
		40	-4.05	0.51235	0.001	-5.7171	-2.3829
	40	10	12.08	0.59161	0	10.1550	14.0050
		25	4.05	0.51235	0.001	2.3829	5.7171

TABLE B.34: Post hoc (Tukey HSD) analyses for $As^{(III)}$:$As^{(V)}$:: 2 : 1 in three phase

Dep. Var.	F_i	F_j	Mean Diff. (F_i−F_j)	Std. Error	Sig.	95% Confidence Interval	
						Lower bound	Upper bound
Extraction	1	2	-13.62	0.42708	0	-15.0097	-12.2303
		3	-20.48	0.49315	0	-22.0847	-18.8753
	2	1	13.62	0.42708	0	12.2303	15.0097
		3	-6.86	0.42708	0	-8.2497	-5.4703
	3	1	20.48	0.49315	0	18.8753	22.0847
		2	6.86	0.42708	0	5.4703	8.2497
Recovery	1	2	-12.58	0.53404	0	-14.3177	-10.8423
		3	-20.04	0.61666	0	-22.0465	-18.0335
	2	1	12.58	0.53404	0	10.8423	14.3177
		3	-7.46	0.53404	0	-9.1977	-5.7223
	3	1	20.04	0.61666	0	18.0335	22.0465
		2	7.46	0.53404	0	5.7223	9.1977
	G_i	G_j	(G_i−G_j)				
Extraction	3	5	-3.86	0.42708	0.001	-5.2497	-2.4703
		7	-4	0.49315	0.001	-5.6047	-2.3953
	5	3	3.86	0.42708	0.001	2.4703	5.2497
		7	-0.14	0.42708	0.943	-1.5297	1.2497
	7	3	4	0.49315	0.001	2.3953	5.6047
		5	0.14	0.42708	0.943	-1.2497	1.5297
Recovery	3	5	-3.49	0.53404	0.003	-5.2277	-1.7523
		7	-2.70	0.61666	0.016	-4.7065	-0.6935
	5	3	3.49	0.53404	0.003	1.7523	5.2277
		7	0.79	0.53404	0.375	-0.9477	2.5277
	7	3	2.70	0.61666	0.016	0.6935	4.7065
		5	-0.79	0.53404	0.375	-2.5277	0.9477
	$H2_i$	$H2_j$	($H2_i$−$H2_j$)				
Extraction	10	25	-7.78	0.42708	0	-9.1697	-6.3903
		40	-10.72	0.49315	0	-12.3247	-9.1153
	25	10	7.78	0.42708	0	6.3903	9.1697
		40	-2.94	0.42708	0.002	-4.3297	-1.5503
	40	10	10.72	0.49315	0	9.1153	12.3247
		25	2.94	0.42708	0.002	1.5503	4.3297
Recovery	10	25	-7.95	0.53404	0	-9.6877	-6.2123
		40	-12.02	0.61666	0	-14.0265	-10.0135
	25	10	7.95	0.53404	0	6.2123	9.6877
		40	-4.07	0.53404	0.001	-5.8077	-2.3323
	40	10	12.02	0.61666	0	10.0135	14.0265
		25	4.07	0.53404	0.001	2.3323	5.8077

TABLE B.35: Levene's test of homogeneity of error variances in three phase

Type	Based on	F		df1		df2		Sig.	
		Ext.	Rec.	Ext.	Rec.	Ext.	Rec.	Ext.	Rec.
$As^{(III)}$	Mean	0.011	0.003	2	2	17	17	0.989	0.997
	Median	0.001	0.017	2	2	17	17	0.999	0.984
	Median and adjusted df	0.001	0.017	2	2	16.106	15.996	0.999	0.984
	Trimmed mean	0.006	0.008	2	2	17	17	0.994	0.992
$As^{(V)}$	Mean	1.683	0.354	2	2	17	17	0.215	0.707
	Median	1.139	0.345	2	2	17	17	0.344	0.713
	Median and adjusted df	1.139	0.345	2	2	14.931	16.634	0.347	0.713
	Trimmed mean	1.57	0.355	2	2	17	17	0.237	0.706
$As^{(III)}$:$As^{(V)}$:: 1 : 1	Mean	4.338	6.325	2	2	17	17	0.03	0.009
	Median	3.486	3.638	2	2	17	17	0.054	0.048
	Median and adjusted df	3.486	3.638	2	2	10.771	12.435	0.068	0.057
	Trimmed mean	4.376	6.030	2	2	17	17	0.029	0.009
$As^{(III)}$:$As^{(V)}$:: 1 : 2	Mean	4.295	6.169	2	2	17	17	0.031	0.01
	Median	3.33	3.302	2	2	17	17	0.06	0.061
	Median and adjusted df	3.33	3.302	2	2	10.737	12.288	0.075	0.071
	Trimmed mean	4.353	6.15	2	2	17	17	0.03	0.01
$As^{(III)}$:$As^{(V)}$:: 2 : 1	Mean	4.7	6.339	2	2	17	17	0.024	0.009
	Median	3.407	3.459	2	2	17	17	0.057	0.055
	Median and adjusted df	3.407	3.459	2	2	10.753	12.687	0.071	0.063
	Trimmed mean	4.56	6.289	2	2	17	17	0.026	0.009

TABLE B.36: Experimental design with factors and response for $As^{(V)}$

Std	Run	Factor 1 - A	Factor 2 - B	Factor 3 - C	Factor 4 - D	Response 1
1	16	0.1	10	3	1	39
2	29	1.0	10	3	1	70
3	30	0.1	40	3	1	56
4	20	1.0	40	3	1	78
5	2	0.1	10	7	1	52
6	15	1.0	10	7	1	76
7	7	0.1	40	7	1	71
8	9	1.0	40	7	1	90
9	27	0.1	10	3	2	45
10	10	1.0	10	3	2	75
11	5	0.1	40	3	2	65
12	18	1.0	40	3	2	82
13	26	0.1	10	7	2	59
14	12	1.0	10	7	2	81
15	22	0.1	40	7	2	78
16	14	1.0	40	7	2	94
17	24	0.1	25	5	1.5	53
18	6	1.0	25	5	1.5	89
19	13	0.55	25	5	1.5	68
20	25	0.55	40	5	1.5	89
21	19	0.55	25	3	1.5	75
22	28	0.55	25	7	1.5	87
23	21	0.55	25	5	1	72
24	17	0.55	25	5	2	87
25	9	0.55	25	5	1.5	86
26	1	0.55	25	5	1.5	81
27	11	0.55	25	5	1.5	82
28	3	0.55	25	5	1.5	79
29	8	0.55	25	5	1.5	83
30	23	0.55	25	5	1.5	82

TABLE B.37: Analysis of variance for removal of $As^{(V)}$

Source	Sum of squares	Degree of freedom	Mean square	F-value	p-value
Model	5525.67	14	394.69	32.57	<0.0001
A	2616.06	1	2616.06	215.86	<0.0001
B	1058	1	1058.00	87.3	<0.0001
C	589.39	1	589.39	48.63	<0.0001
D	213.56	1	213.56	17.62	0.0008
AB	68.06	1	68.06	5.62	0.0316
AC	22.56	1	22.56	1.86	0.1926
AD	7.56	1	7.56	0.62	0.4419
BC	10.56	1	10.56	0.87	0.3653
BD	0.063	1	0.063	5.157×10^{-3}	0.9437
CD	0.063	1	0.063	5.157×10^{-3}	0.9437
A^2	233.83	1	233.83	19.29	0.0005
B^2	10.36	1	10.36	0.86	0.3697
C^2	0.65	1	0.65	0.053	0.8203
D^2	2.59	1	2.59	0.21	0.6505
Residual	181.79	15	12.12		
Lack of fit	154.96	10	15.5	2.89	0.1267
Pure error	26.83	5	5.37		
Corrected total	5707.47	29			

TABLE B.38: Optimization results and error analysis for removal of $As^{(V)}$and $As^{(III)}$

Model parameters	Optimum conditions for removal	
	$As^{(V)}$	$As^{(III)}$
R^2	0.9724	0.9681
Adjusted R^2	0.9475	0.9384
Predicted R^2	0.8613	0.8722
Adequate precision	18.179	23.471
pH of feed phase	5	5.68
pH of receiving phase	7	7
Extractant concentration (in %)	10	31
Concentration of receiving phase (in M)	1	1
Electrical potential (in V)	2	2
Predicted removal efficiency (in %)	93.4	94
Experimental removal efficiency (in %)	92.7	92
Error (in %)	0.75	2.13

TABLE B.39: Experimental design with factors and response for $As^{(III)}$

Std	Run	Factor 1 - A pH of feed phase	Factor 2 - B pH of receiving phase	Factor 3 - C Extractant concentration (%)	Response 1 Removal of arsenic (%)
1	6	3	3	10	91.06
2	8	9	3	10	90.77
3	4	3	7	10	92.54
4	14	9	7	10	90.41
5	12	3	3	40	71.85
6	5	9	3	40	70
7	15	3	7	40	72
8	2	9	7	40	70.56
9	20	3	5	25	75.2
10	10	9	5	25	72.32
11	3	6	3	25	74.5
12	13	6	7	25	78.59
13	16	6	5	10	92.07
14	9	6	5	40	68.5
15	7	6	5	25	77.5
16	19	6	5	25	78.6
17	17	6	5	25	78
18	18	6	5	25	79
19	1	6	5	25	77
20	11	6	5	25	75.5

TABLE B.40: Analysis of variance for removal of $As^{(III)}$

Source	Sum of squares	Degree of freedom	Mean square	F-value	p-value
Model	1195.29	9	132.81	39.1	<0.0001
A	7.38	1	7.38	2.17	0.1713
B	3.5	1	3.5	1.03	0.3337
C	1080.35	1	1080.35	318.1	<0.0001
AB	0.26	1	0.26	0.075	0.7894
AC	0.095	1	0.095	0.028	0.8708
BC	0.021	1	0.021	6.19×10^{-3}	0.9389
A^2	8.38	1	8.38	2.47	0.1472
B^2	2.97	1	2.97	0.87	0.3718
C^2	62.81	1	62.81	18.49	0.0016
Residual	33.96	10	3.4		
Lack of Fit	26.06	5	5.21	3.3	0.1081
Pure Error	7.9	5	1.58		
Corrected total	1229.26	19			

TABLE B.41: List of IR bands (along with the published literature references) for goethite, hematite, lepidocrocite and maghemite phases of iron oxyhydroxides

Phases of iron oxyhydroxides	IR adsorption frequency bands (cm^{-1})	References
Maghemite	700, 640–660, 620, 580, 560, 460, 390, 305	[294]
Maghemite	628.57, 584.80, 440.87, ¡401.44	[295]
Maghemite	688, 635, 562, 446	[296]
Maghemite	634, 580, 439	[297]
Maghemite	627, 577, 444, 400	[298]
Maghemite	729, 702, 691, 645, 635, 608, 584, 552, 526, 485, 476, 465, 442, 419, 393, 366, 349, 327, 309, 288, 282, 275, 262, 258, 234, 212	[299]
Lepidocrocite	1154, 1023, 895, 748, 602, 524, 504, 467, 379, 356, 281, 269, 259, 223	[299]
Lepidocrocite	3400, 3142, 1632, 1150, 1021, 754, 616	[300]
Goethite	909, 895, 799, 674, 632, 608, 582, 466, 454, 420, 398, 374, 353, 297, 287, 276, 268	[299]
Goethite	3416, 3133, 905, 902, 899, 893, 805, 802, 799, 797, 671, 664, 459, 456	[301]
Goethite	3400, 3142, 2924, 2850, 1632, 1453, 1383, 892, 795, 635	[300]
Hematite	557, 540, 473, 471, 461	[301]
Hematite	3398.9, 2956.3, 1604.5, 1481.8, 1375, 1293, 748.2, 576.6	[302]

TABLE B.42: List of IR bands (along with the published literature references) for iron-arsenic precipitate

Peaks (cm^{-1})	Functional groups	References
From the removal of $As^{(III)}$		
523	Formation of hematite (Fe_2O_3)	[301]
587	Transformation of arsenic species from $As^{(III)}$to $As^{(V)}$	[293]
632	Formation or presence of goethite (α−FeOOH)	[301]
1000	Formation or presence of lepidocrocite (β−FeOOH)	[299]
From the removal of $As^{(V)}$		
554	Presence of hematite Fe_2O_3	[301]
659	Formation or presence of goethite (α−FeOOH)	[301]
894	Fe-O-As bending vibration in goethite (α−FeOOH)	[303]
1029	Bending vibration of Fe-O-OH bond present in lepidocrocite (β−FeOOH) due to interactions with arsenic ions	[304]
1055	Presence and interaction of arsenic ions with iron oxide in the maghemite phase	[298]
1109, 1161, 1315, 1427	Corresponds to AsV	[293]

TABLE B.43: Experimental design with factors and response for arsenic removal

Run	Factors		Removal (%) of		
	A	B	$As^{(III)}$:$As^{(V)}$::1:1	$As^{(III)}$:$As^{(V)}$::1:2	$As^{(III)}$:$As^{(V)}$::2:1
1	6	5	84.6	84.2	83.8
2	9	7	92.8	92.4	91.7
3	6	5	83.5	83.1	83
4	6	3	82.5	82.3	82.4
5	3	7	93.04	91.09	90
6	9	5	86	84.5	85.4
7	3	3	77.35	76.58	76.96
8	6	5	84	82.9	82.7
9	6	7	95.18	93.81	93.5
10	3	5	81	80.79	80
11	9	3	84	83.69	84.1
12	6	5	84.2	83.8	83.66
13	6	5	83.8	83.31	83.9

TABLE B.44: Analysis of variance for removal of combined arsenic species

Source	df	$As^{(III)}$:$As^{(V)}$:: 1 : 1				$As^{(III)}$:$As^{(V)}$:: 1 : 2				$As^{(III)}$:$As^{(V)}$:: 2 : 1			
		∑Sq.	Mean Sq.	F-value	p-value	∑Sq.	Mean Sq.	F-value	p-value	∑Sq.	Mean Sq.	F-value	p-value
Model	5	310.22	62.04	126.85	<0.0001	277.43	55.49	163.37	<0.0001	248.79	49.76	105.47	<0.0001
A	1	21.7	21.7	44.36	0.0003	24.52	24.52	72.2	<0.0001	33.8	33.8	71.64	<0.0001
B	1	230.27	230.27	470.8	<0.0001	201.03	201.03	591.89	<0.0001	167.9	167.9	355.9	<0.0001
AB	1	11.87	11.87	24.26	0.0017	8.41	8.41	24.76	0.0016	7.4	7.4	15.68	0.0055
A^2	1	4.35	4.35	8.89	0.0204	5.76	5.76	16.95	0.0045	5.88	5.88	12.47	0.0096
B^2	1	46.09	46.09	94.23	<0.0001	43.45	43.45	127.93	<0.0001	39.69	39.69	84.12	<0.0001
Residual	7	3.42	0.4891			2.38	0.3396			3.3	0.4718		
Lack of fit	3	2.74	0.9119	5.3	0.0704	1.25	0.4162	1.47	0.3483	2.18	0.7252	2.57	0.1916
Pure Error	4	0.688	0.172			1.13	0.2822			1.13	0.2817		
Cor Total	12	313.64				279.8				252.09			

TABLE B.45: Optimization results and error analysis for removal of combined arsenic species

Model parameters	$As^{(III)}$:$As^{(V)}$:: 1 : 1	$As^{(III)}$:$As^{(V)}$:: 1 : 2	$As^{(III)}$:$As^{(V)}$:: 2 : 1
R^2	0.9891	0.9915	0.9869
Adjusted R^2	0.9813	0.9854	0.9775
Predicted R^2	0.9251	0.9627	0.9277
Adequate precision	36.347	41.654	33.801
pH of feed phase	6.52	6.48	6.45
pH of receiving phase	7	7	7
Predicted Removal (%)	94.5	93.45	92.83
Experimental Removal (%)	92.5	94	93.8
Error (%)	2.12	0.58	1.04

TABLE B.46: Design of experiments with factors and responses for all the locations

Run	Factors		Removal% of arsenic in				
	A	B	WB1	WB2	AS1	AS2	AS3
1	10	3	90	92	99.9	99.9	88.5
2	25	7	86.25	68	99.2	98	87
3	25	5	88.75	84	99	99.1	89.1
4	25	5	88	85	98	99.2	89
5	25	5	88.5	83	98.5	99.3	88.9
6	10	5	93.75	99	99.5	99.7	86.6
7	10	7	91.25	90	99.9	99.5	85
8	25	3	83.75	76	99.9	99.6	89.6
9	40	3	81.25	72	91.1	93.7	95
10	40	5	87.5	80	91.4	91.5	93
11	40	7	85	64	89.9	90.9	90.8
12	25	5	88.25	81	97	99	88.5
13	25	5	89	82	97.5	98.5	88

TABLE B.47: Optimization results and error analysis for all the locations

Parameters	WB1	WB2	AS1	AS2	AS3
R^2	0.99	0.98	0.9669	0.9931	0.982
Adjusted R^2	0.98	0.97	0.9433	0.9881	0.9691
Predicted R^2	0.95	0.91	0.8463	0.9637	0.9084
Adequate precision	44.93	32.75	16.3468	38.7704	30.88
Coefficient of Variation (C.V.)	0.47	2.03	0.8973	0.3607	0.5168
Extractant concentration (%(v/v))	10	10	10	10	40
pH of receiving phase	5	5	3	3	3
Predicted removal (%)	94.1	100	100	99.9	94.8
Experimental removal (%)	95	99.99	99	98.5	96.7
Error (%)	0.95	0.01	1.01	1.42	1.96

TABLE B.48: Analysis of variance for removal of arsenic in WB1 and WB2

Source	df	WB1				WB2			
		SSE	Mean Square	F-Value	p-value	SSE	Mean Square	F-Value	p-value
Model	5	123.67	24.73	145.62	<0.0001	1101.28	220.26	81.05	<0.0001
A	1	75.26	75.26	443.10	<0.0001	704.17	704.17	259.12	<0.0001
B	1	9.37	9.37	55.20	0.0001	54.00	54.00	19.87	0.0029
AB	1	1.56	1.56	9.20	0.0190	9.00	9.00	3.31	0.1116
A2	1	11.10	11.10	65.32	<0.0001	134.67	134.67	49.55	0.0002
B2	1	36.21	36.21	213.17	<0.0001	305.50	305.50	112.42	<0.0001
Residual	7	1.19	0.17			19.02	2.72		
Lack of fit	3	0.56	0.19	1.20	0.4157	9.02	3.01	1.20	0.4157
Pure error	4	0.63	0.16			10.00	2.50		
Corr. Total	12	124.86				1102.31			

TABLE B.49: Analysis of variance for removal of arsenic in AS1, AS2 and AS3

Source	df	AS1				AS2				AS3			
		SSE	Mean Square	F-Value	p-value	SSE	Mean Square	F-Value	p-value	SSE	Mean Square	F-Value	p-value
Model	5	155.1	31.02	40.96	<0.0001	124.3	24.86	200.9	<0.0001	81.09	16.22	76.38	<0.0001
A	1	120.6	120.6	159.25	<0.0001	88.17	88.17	712.3	<0.0001	58.28	58.28	274.5	<0.0001
B	1	0.602	0.602	0.795	0.402	3.84	3.84	31.02	0.0008	17.68	17.68	83.28	<0.0001
AB	1	0.360	0.360	0.475	0.513	1.44	1.44	11.63	0.0113	0.123	0.123	0.577	0.472
A2	1	32.28	32.28	42.63	0.0003	26.9	26.9	217.3	<0.0001	4.7	4.7	22.16	0.002
B2	1	1.28	1.28	1.69	0.235	0.017	0.017	0.140	0.719	0.105	0.105	0.494	0.505
Residual	7	5.3	0.757			0.866	0.124			1.49	0.212		
Lack of fit	3	2.8	0.934	1.49	0.344	0.478	0.159	1.64	0.314	0.666	0.222	1.08	0.452
Pure error	4	2.5	0.625			0.388	0.097			0.82	0.205		
Corr. Total	12	160.4				125.2				82.57			

List of Publications

International Journals

- Soumi Sarkar and Prabirkumar Saha, (2024). "**Liquid membrane based extraction of arsenic: Part 1 - Experimental Study and Mathematical Modelling**," Physical Chemistry Research, 12(2): pp. 483-504.
- Soumi Sarkar and Prabirkumar Saha, (2024). "**Liquid membrane based extraction of arsenic: Part 2 - Optimization through statistical and machine learning approach**," Physical Chemistry Research, 12(2): pp. 525-547.
- Soumi Sarkar, Soumendu Hazra, Kaushik Chakraborty, Ananya Nayak, and Prabirkumar Saha, (2023). "**Hybrid Technique for Removal of Arsenic from Drinking Water**," Chemical Engineering & Technology, 46(2): pp. 242–255.
- Soumi Sarkar, Supriyo Kumar Mondal, Manoj Kumar Beriya, and Prabirkumar Saha, (2021). "**Spectroscopic, thermodynamic and ultrasonic properties of pseudo-binary mixtures of organic extractants and vegetable oil at 25-60°C under atmospheric pressure**," Asia-Pacific Journal of Chemical Engineering, 16(4): pp. 1–21.
- Soumi Sarkar and Prabirkumar Saha, "**Hybrid technique for removal of combined As(III)and As(V)from drinking water**," *submitted in* Chemical Engineering & Technology.
- Soumi Sarkar and Prabirkumar Saha, "**Application of SLM-electrocoagulation hybrid technique for removal of arsenic from groundwater in eastern India**," *submitted in* Membrane Water Technology.

National and International Conferences

- Soumi Sarkar and Prabirkumar Saha, "**Removal of arsenic from water by liquid membrane-based separation technology**," The 8th International Congress & Exhibition on Arsenic in the Environment (AS-2021).

- Soumi Sarkar and Prabirkumar Saha, "**Arsenic Removal from Water by Flat Sheet Supported Liquid Membrane (FSSLM) Based Separation Technique**," AIChE 2021 Spring Meeting & 17th Global Congress on Process Safety.

- Soumi Sarkar and Prabirkumar Saha, "**Supported liquid membrane based separation technique for arsenic removal from water**," ACS Spring 2021 - Current Status of Environmental Research on Water Contaminants.

- Soumi Sarkar and Prabirkumar Saha, "**Hybrid method for the removal of As(V) from water**," International Conference on Waste Management (RECYCLE).

- Soumi Sarkar and Prabirkumar Saha, "**Hybrid method for the removal of As(III) from water**," National Conference on Issues and Challenges in Water Treatment and Allied Research for Sustainable Environment (WATER).

- Soumi Sarkar and Prabirkumar Saha, "**Hybrid method for removal of arsenic from water**," DST-UKIERI supported Workshop cum Symposium on Bio-inspired Nanomaterials for Environmental Applications.

- Soumi Sarkar and Prabirkumar Saha, presented by Supriyo Kumar Mondal "**A study on thermodynamic properties of binary mixtures of sesame oil with aliquat 336 and TBP**," AIChE Annual Meeting.

- Soumi Sarkar and Prabirkumar Saha, "**Removal of arsenic using environmentally benign liquid membrane for purification of drinking water**," International Conference on Waste Management (RECYCLE).

- Soumi Sarkar and Prabirkumar Saha, "**Removal of arsenic from drinking water using liquid membrane based separation technique**," DAE-BRNS Biennial Symposium on Emerging Trends in Separation Science and Technology (SESTEC).

- Soumi Sarkar and Prabirkumar Saha, "**Two phase study for the removal of arsenic from its aqueous solution by liquid membrane based separation technique**," Indian Chemical Engineering Congress (CHEMCON).